Contents

Contents

Focus and Scope

Civil Engineering Journal (C.E.J) is a multidisciplinary, an open-access, internationally double-blind peer-reviewed journal concerned with all aspects of civil engineering, which include but are not necessarily restricted to:

- Building Materials and Structures
- Constructions Technology
- Earthquake Engineering
- Renovation of Buildings
- Highway Engineering
- Road and Bridge Engineering
- Surveying and Geo-Spatial Engineering
- Tunnel Engineering
- Water Resources Engineering

- Coastal and Harbor Engineering
- Constructions Economy and Management
- Environmental Engineering
- Geotechnical Engineering
- Hydraulic and Hydraulic Structures
- Structural Engineering
- Transportation Engineering
- Urban Engineering and Economy
- Urban Drainage

Special Issues

Special Issues deal with more focused topics with high current interest falling within the scope of the journal in which they are published. Special Issue proposals are welcome at any time during the year.

For most of the civil engineering conferences it is possible to submit papers presented at the conference for subsequent publication in special issues of the C.E.J.

- **Civil Engineering Journal (C.E.J) is published monthly.**
- **Civil Engineering Journal (C.E.J) has fast peer review process (3-4 weeks).**

Civil Engineering Journal (C.E.J) Indexing & Abstracting
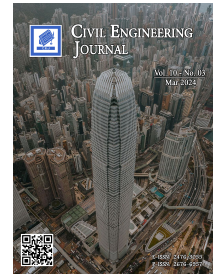
Measurement Model for Determining the Disparity Factors of Intercity Railway Transportation

Kestsirin Theerathitichaipa [1], Panuwat Wisutwattanasak [2], Chinnakrit Banyong [3], Manlika Seefong [1], Sajjakaj Jomnonkwao [1], Thanapong Champahom [4], Vatanavongs Ratanavaraha [1], Rattanaporn Kasemsri [5*]

[1] School of Transportation Engineering, Institute of Engineering, Suranaree University of Technology, Nakhon Ratchasima 30000, Thailand.

[2] Institute of Research and Development, Suranaree University of Technology, Nakhon Ratchasima 30000, Thailand.

[3] School of Industrial and Logistics Management Engineering, Institute of Engineering, Suranaree University of Technology, Nakhon Ratchasima 30000, Thailand.

[4] Department of Management, Faculty of Business Administration, Rajamangala University of Technology Isan, Nakhon Ratchasima 30000, Thailand.

[5] School of Civil Engineering, Institute of Engineering, Suranaree University of Technology, Nakhon Ratchasima 30000, Thailand.

Abstract

Countries that are still developing experience significant disparities in access to railway services, as these nations also grapple with societal inequality issues that remain unaddressed. In developed countries, railway transportation systems serve as the primary mode of transportation for both passengers and goods. However, in recent years, studies on disparities in developed countries have increased, while literature concerning developing countries remains scarce. Therefore, this study takes place in Thailand, a developing country facing significant population disparities. The objective is to examine factors contributing to these disparities in access to railway transportation systems across cities, using Exploratory Factor Analysis (EFA) and Confirmatory Factor Analysis (CFA) to identify user disparities. The sample group comprises 1,252 randomly selected railway users from various regions in Thailand, obtained through Stratified Random Sampling. The results reveal seven dimensions of disparities: cultural, spatial, societal, political, knowledge-based, economic, and environmental. The CFA results also highlight cultural disparities as a significant factor in explaining access disparities among railway users. These findings can inform relevant organizations, aiding them in better understanding the actual needs of railway users and aligning railway development plans accordingly. Ultimately, this contributes to policy development aimed at reducing access disparities and fostering a more equitable society.

Keywords: Railway Disparity Factors; Railway Accessibility; Exploratory Factor Analysis; Confirmatory Factor Analysis.

1. Introduction

The transportation system is a key component in driving the tourism and travel industry of a nation, especially the railway transportation system, which is considered a safe, cost–effective, convenient, and punctual mode of transportation [1]. When compared to other transportation systems, rail travel is widely popular in many countries. For instance, developed countries like Japan and Germany have strongly supported rail transportation as a primary intercity mode of travel [2-4]. Furthermore, railway transportation is also regarded as a sustainable mode of transport [5, 6].

However, access to railway services remains a significant issue, especially in developing countries. According to the CS Global Wealth Report 2018, Thailand, as a developing country, has the third highest inequality in the world and is the country that suffers from the greatest population inequality problem in the world [7]. The most significant challenge of inequality in Thailand is the need to manage the public transportation services, including railways, that meet the needs of the population across the country.

The current inequality situation in Thailand is related to the accessibility of train services. According to the latest statistics on intercity trains, Thailand has train stations in only 47 out of the country's 77 provinces, covering 61.04 percent. This information is based on the most recent data on railway networks, as shown in Figure 1 [8]. This means that there are still 30 provinces without railroads passing through them. Even in provinces with railroads, not every district is covered. Thailand has a total of 928 districts [9], but there are only 442 railway stations [10], covering just 48% of all districts. This lack of coverage leads to inequality in access to train services among various population groups. Access to train services is a fundamental factor in daily life, and expanding access to railway stations can provide nearby residents and those with travel needs more suitable transportation options. Wang et al. [11] have pointed out that building a railway network can help address population inequalities.
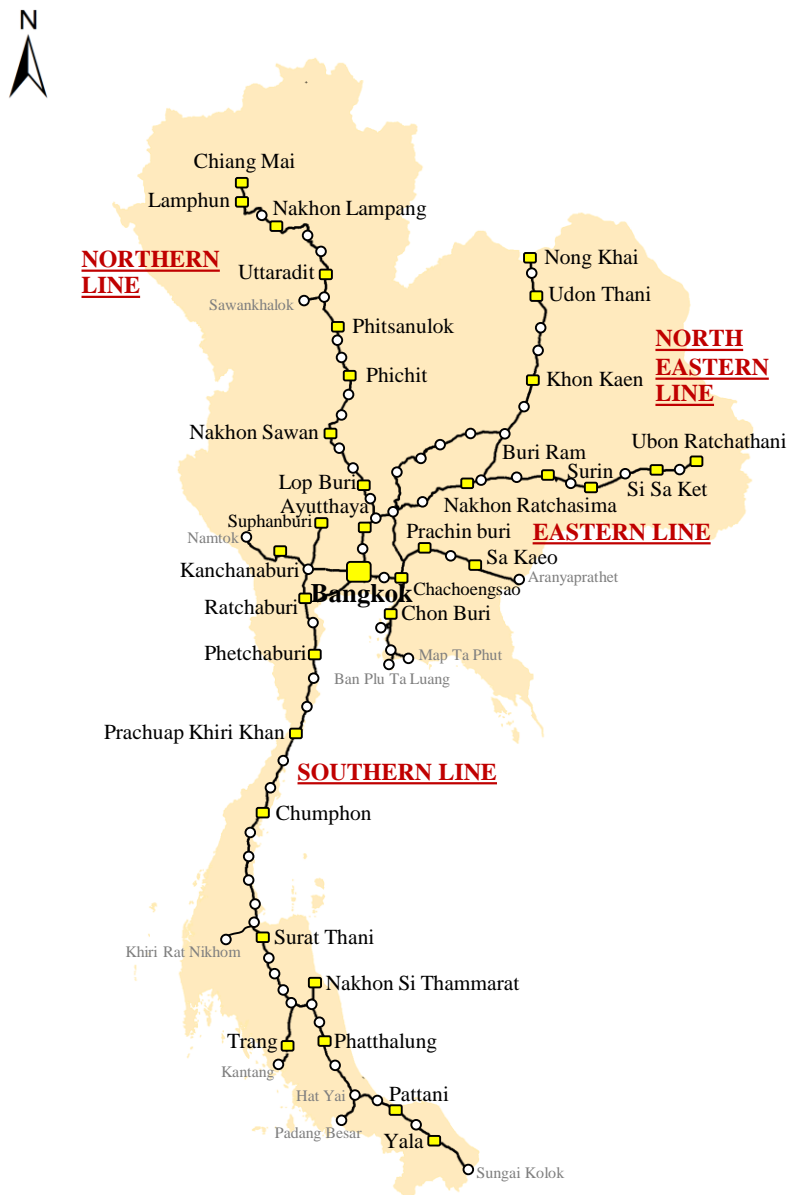
Figure 1. Railway Routes in Thailand

Furthermore, Exploratory Factor Analysis (EFA) and Confirmatory Factor Analysis (CFA) have also been applied extensively in analyzing the development of railway transportation systems. There are numerous studies that have attempted to explore factors influencing railway service usage in various dimensions. Examples include factors affecting the quality of railway services [12-14], factors influencing passenger satisfaction with railway services [15, 16], factors

affecting railway employees' job performance [17], factors influencing perceptions of railway safety [18, 19], and factors related to weather conditions affecting railway safety [19]. Although previous studies have examined the development of Thailand's rail transportation system, they have primarily focused on enhancing the quality of train services and identifying factors influencing service quality [20], as well as evaluating spatial inequality solely for analyzing accessibility to train stations [21]. However, there is currently a dearth of research on factors impacting inequality in people's utilization of train services across all dimensions. Inequality assessment can encompass various factors, including cultural, spatial, social, political, knowledge, economic, and environmental dimensions [22]. Therefore, this study aims to fill this gap by comprehensively examining all factors contributing to inequality among train users in a developing country context. By including all relevant dimensions, the study seeks to effectively address the issue of inequality in the railway transportation system.

In addition, in developed countries, there have been numerous studies attempting to examine factors contributing to inequality in various dimensions. For instance, in the United States, there has been a study investigating cultural sources of racial inequality, particularly inequality between whites and blacks. This study focused on two dimensions of explanation, or attribution: internal (regarding shortcomings in black motivation and capability); and external (regarding the socioeconomic context), using survey experiments. The results indicated the need to change public perceptions and beliefs regarding racial inequality [23]. Furthermore, studies have been conducted on inequality in accessing public transportation services and land use in the Washington, D.C. metropolitan area. This research emphasized analyzing social and spatial factors, proposing a framework that disaggregates mobility and access components to identify areas potentially affected by inadequate transportation services and limited job opportunities. The findings of this study serve as crucial data for developing regional mass transportation system plans [24]. Similarly, in France, there has been a study examining regional disparities in railway transportation investment to assess regional balance in railway line planning and financial models. The results of this study led to an analysis of data from the Ministry of Infrastructure Budgets to monitor the development of regional inequality in terms of public sector expenditure [25]. Moreover, in Italy, a study explored the impact of high-speed railways (HSR) on income inequality. This research focused on analyzing economic and social factors related to income inequality at the provincial level using the Gini index and a two-way fixed-effects model to measure relationships. The findings suggested that HSR could stimulate a reduction in household income inequality, with positive effects on GDP per capita and employment levels [26]. Lastly, in China, a study investigated intra-regional inequality and urban-rural divides using a differentiated model to examine whether high-speed railways affected intra-regional inequality. The findings indicated that high-speed rail operations expanded income gaps between urban and rural areas by promoting population aggregation, financial capital, and economic activities in urban areas adjacent to high-speed railway stations [27].

Absolutely, this research can be considered a novel study in the context of education in a developing country like Thailand. Its objectives are to study the factors influencing disparities in accessing intercity railway transportation in Thailand and to analyze the factors contributing to disparities in cultural, spatial, social, political, knowledge, economic, and environmental dimensions. This is done by considering the perspectives of current railway users through questionnaires. Subsequently, the data is analyzed using the CFA tool, which is suitable for identifying factors that can accurately confirm the nature of relationships, leading to the development of effective solutions to address disparities and meet the needs of railway users efficiently. Furthermore, this study proposes policies to reduce disparities among the Thai population for railway service providers. These policies would help relevant agencies or stakeholders involved in railway development better understand the actual needs of railway users and apply disparity indicators to create development plans that efficiently and sustainably meet the passengers' needs.

2. Literature Review

Inequality has become essential for understanding society. Frances (2016) posits that "Disparity has its roots in inequality" and "The origins of inequality in each dimension are interrelated, with inequality arising in one dimension potentially affecting another dimension of inequality in the form of an influence pathway". The framework of factors influencing inequality is depicted in Figure 2 [28].

Figure 2 illustrates that from the structure of the influence pathways of inequality in each dimension, they can be categorized into three groups of factors that influence each other. These are: Root Factors: These include cultural inequality and spatial inequality, which are the initial factors influencing housing insecurity, transportation, education, and perception [21]. Intermediate Factors: These encompass social inequality, political inequality, and knowledge inequality. This group of factors is heavily influenced by root factors, while spatial inequality influences knowledge inequality. Factors such as geographical distance from information and understanding of development discourse due to educational disparities lead to a lack of bargaining power [29, 30]. End Factors: These consist of economic inequality and environmental inequality. These factors are influenced by intermediate factors, where knowledge inequality and social inequality affect economic inequality. As the cost of living increases, economic inequality intensifies [31], while environmental inequality is influenced by political inequality and knowledge [32]. Therefore, based on this framework, the researchers conducted a literature review and compiled studies related to factors influencing inequality in each dimension, as detailed below.
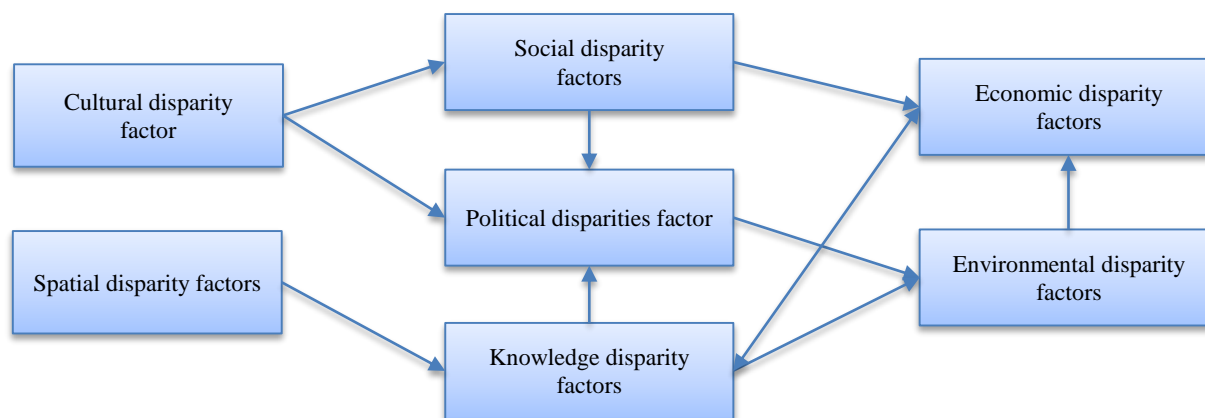
Figure 2. Framework of Factors Influencing Inequality

2.1. Cultural Inequality

For instance, O'Brien & Oakley (2015) [33] point out that there is a critical need to understand the relationship between culture and social inequality. These factors should be considered separately in both academic research and policy–making, according to customs and traditions. Furthermore, a study by Lareau (2015) [34] indicates that cultural factors affect knowledge disparities. Therefore, from the review, it can be concluded that factors related to cultural inequality include (1) ethnicity and race, (2) religion and class, and (3) gender status.

2.2. Spatial inequality

For instance, Levinson (2012) [35] points out that rail transit can have positive spatial benefits to cities near stations and has a negative impact on towns that are far from train stations. Furthermore, the studies by Cascetta et al. (2020) [31] and Luo & Zhao (2021) [36] focus on the issue of spatial access to trains. Therefore, from the review, it can be concluded that factors related to spatial inequality include (1) economic growth, (2) infrastructure and facilities, and (3) public connectivity systems.

2.3. Social inequality

For instance, Lucas et al. (2019) [37] point out that the transportation service system is unevenly distributed. It may affect different social factors. Furthermore, a study by Zhan et al. (2020) [38] emphasizes that social equality must take into account the affordability and needs of rail users. Therefore, from the review, it can be concluded that factors related to social inequality include (1) community size, (2) social roles and duties, and (3) income level.

2.4. Political inequality

For instance, Rodriguez (2018) [39] point out that political participation influences politicians in shaping policies and projects that define the quality of society. Furthermore, a study by Beaumont (2011) [40] indicates that the primary cause of political inequality stems from people's marginalization, leading to diverse political expressions. Therefore, from the review, it can be concluded that factors related to political inequality include (1) social and political participation and (2) living conditions of society.

2.5. Knowledge inequality

For instance, Wu & Zhao (2015) [41] point out that access to the education system has a positive influence on people's awareness. Furthermore, the studies by Viswanath et al. (2006) [42] and Robb et al. (2010) [43] indicate that increased knowledge development often leads to reducing the knowledge gap among groups of people. Therefore, from the review, it can be concluded that factors related to knowledge inequality include (1) awareness or perception and (2) technological systems.

2.6. Economic inequality

For instance, Di Matteo & Cardinale (2023) [26] point out that the unequal provision of rail transport services affects regional economic inequality. Studies by Knight & Song (1999) [44] also indicate that large rural–urban divides affect the economic well–being of the population. Furthermore, a study by Pokropek et al. (2015) [45] focused on studying the concept of socioeconomic conditions in a multidimensional manner through empirical investigation. Therefore, from the review, it can be concluded that factors related to economic inequality include (1) employment level, (2) wages or income, and (3) Gross Domestic Product (GDP).

2.7. Environmental inequality

For instance, Boyce (1994) [46] points out that economic activities impact environmental preservation and that power and wealth inequalities contribute to the degradation of natural resources. Furthermore, the studies by Song et al. (2016) [47] and Sun et al. (2020) [48] clearly indicate that rail transportation is the most efficient and environmentally friendly mode of transportation. Therefore, from the review, it can be concluded that factors related to environmental inequality include (1) access to natural resources and (2) environmental awareness.

From the literature review conducted previously, researchers found that studies related to factors associated with transportation inequality were considered and compiled. It was found that there were 20 studies from 13 countries, as shown in Table 1. Most research often considered inequality factors from only a few perspectives depending on the case study. However, no study was found that comprehensively assessed the inequality of railway access covering all factors. To fill this gap in the literature, researchers therefore gathered all relevant factors to examine and evaluate the inequality experienced by railway users. This would help understand the true opinions of those who genuinely require railway services. The research assumes that an appropriate model for assessing rail user inequality should have a multidimensional structure comprising seven dimensions: Cultural Inequality, Spatial Inequality, Social Inequality, Political Inequality, Knowledge Inequality, Economic Inequality, and Environmental Inequality.

Table 1. Summarizes the previous studies on factors related to inequality

Author	Country	Cultural	Spatial	Social	Political	Knowledge	Economic	Environmental	Method
Lope & Dolgun [49]	Australia		✓	✓					Gini coefficient and Lorenz curve
Sanchez [50]	US			✓			✓		Gini coefficient
Galaskiewicz et al. [51]	US	✓					✓		OLS
Clifton & Lucas [52]	UK and US		✓		✓				Empirical evidence
Zhao & Li [53]	Beijing		✓	✓			✓		Empirical evidence
Aasness & Larsen [54]	Norway						✓		Empirical evidence
Kim & Yi [55]	South Korea						✓		Transportation network analysis and Multi–regional CGE model
Chang et al. [56]	Hong Kong		✓						The gravity model
Benoussaïd et al. [57]	Paris		✓	✓				✓	OLYMPUS emissions model and the CHIMERE chemistry–transport model
Liu & Zhang [58]	China			✓			✓	✓	Hybrid MCDM Model
Wanke, et al. [59]	China				✓		✓	✓	RBSFA
Ongolo-Zogo & Epo [60]	Cameroon		✓		✓		✓		Regression function
Allen & Farber [61]	Canada			✓			✓		Simple correlation measures
Zhang et al. [62]	China					✓			SEM
Zhang & Zhang [63]	China		✓				✓	✓	SEM
Nadimi et al. [64]	Iran	✓							SEM
Wang et al. [65]	China		✓	✓	✓				SEM
Ali et al. [66]	Pakistan	✓		✓			✓		EFA, CFA and SEM
Loa et al. [67]	Canada			✓			✓		EFA and CFA
Li et al. [68]	China					✓			CFA
Present study	Thailand	✓	✓	✓	✓	✓	✓	✓	EFA and CFA

Note: OLS = Ordinary least squares regression; MCDM = Multi criteria decision making; RBSFA = Robust Bayesian Stochastic Frontier Analysis; SEM = Structural equation modelling; EFA = Exploratory factor Analysis; CFA = Confirmatory factor analysis.

3. Research Methodology

3.1. Research Framework

This study commences with a comprehensive literature review focusing on the factors contributing to inequality, with the aim of identifying gaps in previous research and introducing new findings on this aspect of inequality. Additionally, it explores potential statistical methods and theories relevant to the study. Subsequently, a questionnaire was developed based on these findings, and data were collected through face-to-face interviews with a total sample

group of 1,252 railway users. Following the completion of data collection from the railway user survey, two statistical methods were applied: EFA and CFA. Data from a subgroup of 374 participants, representing 30% of the total sample, were employed for EFA to categorize the variable components derived from users' responses to all 37 questions into 7 factors influencing inequality. The data from the remaining 878 participants, constituting 70%, were then employed for CFA to validate the factors affecting inequality identified from the EFA results. Finally, the study presents statistical results and discussion of the findings were presented along with policy recommendations for reducing inequality. The research process is illustrated in Figure 3.
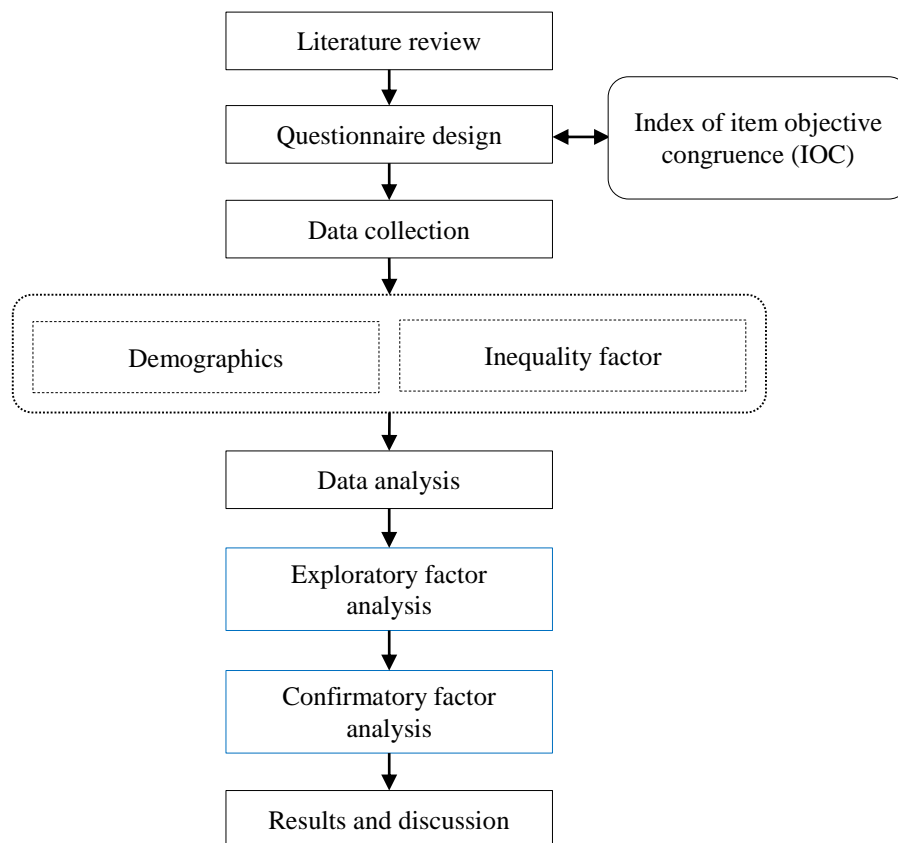
Figure 3. Research procedure

3.2. Questionnaire Structure

The questionnaire was structured into two main sections. Section 1: General Travel Behavior Information of the Survey Respondents, such as gender, age, education, occupation, income, frequency of train travel, and the purposes of train travel. Section 2: Measurement of Factors Affecting Disparities in Railway Access, consisting of 7 factors: Cultural Disparity Factor, Spatial Disparity Factor, Social Disparity Factor, Political Disparity Factor, Knowledge Disparity Factor, Economic Disparity Factor, and Environmental Disparity Factor. In this section, there are 37 questions, and the questionnaire responses are in the form of a 5–level Rating Scale [69, 70]. (Where 1 indicates strongly disagree and 5 indicates strongly agree).

We have conducted a validation of the questionnaire content using the index of item objective congruence (IOC), assessed by three experts. We considered questions with an IOC value higher than 0.50. The IOC values for the questions included in our questionnaire ranged from 0.67 to 1.00.

3.3. Participants and Data Collection

The sample group for this study consisted of railway service users within Thailand, located at 33 railway stations across four regions of the country (Northern Region, Northeastern Region, Eastern Region, and Southern Region). The sample selection was conducted using Stratified Random Sampling based on the geographical areas with railway stations to ensure that the sample represents the population effectively. Additionally, the interviews were conducted on an individual basis with respondents aged 18 and above. Furthermore, before conducting the interviews, respondents were asked for their willingness to participate. The interviews were carried out only with those who willingly agreed to participate in the survey. A total of 1,252 useful responses were obtained, which is considered sufficient for conducting CFA. According to Cangur & Ercan [71], they recommend that the sample size should be at least 15 times the number of observed variables. In this research, there are a total of 37 observed variables, so the minimum sample size required is 555. The survey received ethical approval from the Ethics Committee of Suranaree University of Technology on December 1, 2022 (COA No. 100/2565). Table 2 provides an overview of the characteristics of the survey participants.

Table 2. Participant Demographics

Characteristics	Category	Frequency	Percentage
Gender	Male	516	41
	Female	736	59
Age	18–20 years old	272	22
	21–30 years old	393	31
	31–45 years old	311	25
	46–60 years old	194	15
	Over 60 years old	82	7
Education	Primary education	88	7
	High school education	321	26
	Vocational education	277	22
	Bachelor's Degree	510	41
	Master's Degree	45	3
	Doctoral Degree	11	1
Occupation	Agriculturist/Agricultural Organization	126	10
	Entrepreneur	143	11
	Private Employee	349	28
	Government Employee	159	13
	Student	357	29
	Others	118	9
Income	Less than or equal to 10,000 Baht	447	36
	10,001–15,000 Baht	369	29
	15,001–20,000 Baht	248	20
	More than 20,000 Baht	188	15
Frequency of railway travel (per week)	Every day	108	9
	1–2 times	448	36
	3–5 times	223	18
	Occasionally	473	37
Objectives of railway travel.	Study/Work	474	38
	Rest/Travel	540	43
	Shopping	166	13
	Others	72	6

3.4. Analysis Methodology

To examine the relationship between the components derived from factors influencing inequality in railway access, covering all 7 factors, we used EFA and CFA with two main objectives:

Exploratory factor analysis (EFA) is utilized to generate indicator groups, focusing on factors. Exploratory factor analysis is a statistical method used for exploring and identifying factors to explain the relationships among observed variables. Additionally, EFA results can reduce observed variables by creating new variables in the form of common factors [72]. Therefore, researchers often employ this method when there is no well–established theory regarding the relationships among measurement components [73, 74].

Confirmatory factor analysis (CFA) is a technique used to test or confirm the relationships between observable and latent variables. CFA is employed when researchers know that the indicators are components according to theory or literature review [75, 76]. Studies have explored the components of service quality indicators for the Thai railway system [12, 20, 77]. However, there has been no research on the components of indicators of disparities in railway access in Thailand. Therefore, this study applies both EFA and CFA to analyze the indicators of disparities in railway access, considering the establishment of indicator groups and using the loadings obtained from the analysis to develop appropriate guidelines for improving disparities in railway access.

4. Research Methodology

4.1. Descriptive Statistics

The descriptive statistics of railway service users, totalling 1,252 individuals, are presented in Table 3. The preliminary statistical analysis includes measures such as mean and standard deviation. Prior to conducting CFA, it is essential to examine the descriptive statistics to confirm the appropriateness of the data for analysis. The criteria for adequacy are absolute value 2 for skewness and absolute value 7 for kurtosis [78, 79]. Table 3 illustrates that the skewness ranges from –1.367 to 0.612, and the kurtosis ranges from –1.09 to 1.385, respectively. Therefore, it can be concluded that our sample statistics follow a normal distribution and are acceptable for further analysis.

Table 3. Statistical summary: Mean, Standard deviation, Skewness and Kurtosis (N = 1252)

Variable	Description	Mean	SD	Skewness	Kurtosis
CI1	The Gender Disparities impact accessibility to railways.	2.32	1.304	0.583	–0.912
CI2	The Ethnicity Disparities impact accessibility to railways.	2.34	1.258	0.597	–0.753
CI3	The Physical Health Disparities Status of Vulnerable Groups impact accessibility to railways.	2.64	1.298	0.272	–1.090
CI4	The Religious Disparities impact accessibility to railways.	2.33	1.276	0.612	–0.798
CI5	The Cultural and Belief Differences impact accessibility to railways.	2.5	1.252	0.42	–0.915
SP1	Railway stations located within urban areas allow the population to access trains more easily compared to stations located outside urban areas.	3.83	1.181	–0.944	0.07
SP2	The Regional Income Disparities impact accessibility to railways.	3.69	1.181	–0.721	–0.282
SP3	The Spatial Resource Disparities impact accessibility to railways.	3.67	1.153	–0.705	–0.228
SP4	The Economic Growth in Specific Regions impact accessibility to railways.	3.75	1.149	–0.781	–0.175
SP5	Regional Infrastructure's impact accessibility to railways.	3.84	1.126	–0.896	0.073
SP6	The Interconnection Between Public Transportation and Railway Systems in the Area impact accessibility to railways.	3.88	1.151	–0.909	–0.008
SP7	The Physical Development of Communities impact accessibility to railways.	3.71	1.117	–0.644	–0.318
SO1	The Socioeconomic Challenges and Resilience of Communities impact accessibility to railways.	3.8	1.098	–0.897	0.233
SO2	Access to government resources (such as government agencies and community resources) impacts accessibility to railways.	3.77	1.107	–0.776	–0.029
SO3	The Social roles and responsibilities Disparities impact accessibility to railways.	3.75	1.126	–0.785	–0.057
SO4	Having a high level of social responsibility has an impact accessibility to railways.	3.66	1.129	–0.637	–0.303
SO5	Societal inequality is a crucial factor affecting access to railway routes.	3.65	1.167	–0.658	–0.415
PI1	The Socioeconomic Challenges and Resilience of Communities impact accessibility to railways.	3.9	1.08	–0.867	0.106
PI2	Access to government resources (such as government agencies and community resources) impacts accessibility to railways.	3.95	1.057	–0.876	0.126
PI3	The Social roles and responsibilities Disparities impact accessibility to railways.	4.02	1.068	–0.974	0.202
KI1	Access to educational systems and knowledge development impacts accessibility to railways.	3.82	1.127	–0.870	0.113
KI2	Access to educational resources (such as schools and universities) impacts accessibility to railways.	3.81	1.117	–0.828	–0.003
KI3	Promoting quality and beneficial knowledge impacts accessibility to railways.	4.04	1.027	–1.098	0.739
KI4	The use of modern technology and tools in daily life impacts accessibility to railways.	4.1	1.013	–1.046	0.509
KI5	Lack of information about railway routes can lead to missed opportunities to access the railway transportation system.	4.08	0.982	–1.067	0.78
KI6	Having comprehensive knowledge about railway routes enables you to access the railway transportation system.	4.09	0.995	–1.047	0.643
EC1	Unemployment or lack of job opportunities impact accessibility to railways.	3.59	1.199	–0.552	–0.645
EC2	If there are more job opportunities in your area, it will impact accessibility to railways.	3.7	1.163	–0.745	–0.197
EC3	Income or wages impact accessibility to railways.	3.76	1.185	–0.921	0.056
EC4	The difference in income levels between individuals impacts accessibility to railways.	3.74	1.185	–0.749	–0.332
EC5	The promotion of solutions to alleviate poverty impacts accessibility to railways.	3.91	1.117	–0.947	0.199
EC6	If there are solutions to alleviate poverty, it will impact accessibility to railways.	3.84	1.13	–0.893	0.132
EN1	The current pollution issues impact accessibility to railways.	3.45	1.15	–0.579	–0.431
EN2	Access to natural resources (such as tourist attractions) impacts accessibility to railways.	3.41	1.143	–0.487	–0.515
EN3	If there are current solutions to address pollution or environmental issues, it will impact accessibility to railways.	3.55	1.123	–0.500	–0.515
EN4	Maintaining a good environment impacts accessibility to railways.	4.12	1.07	–1.367	1.385
EN5	Appropriate allocation and efficient utilization of limited resources impact accessibility to railways.	4.03	1.088	–1.285	1.183

Note: SD = Standard deviation

4.2. The Exploratory Factor Analysis

We employed EFA to identify observable indicators representing each latent factor and calculate the main factors. Table 4 presents the factor analysis results. The EFA results are reliable and acceptable. We obtained a Kaiser–Meyer–Olkin (KMO) measure of 0.950, which is excellent. Additionally, Bartlett's test of sphericity yielded highly significant results, exceeding 99%. The EFA results identified 37 items, which were grouped into 7 clusters. Which can explain a total variance of 74.854%. The composite results include: (1) Cultural Disparity Factors, (2) Spatial Disparity Factors, (3) Social Disparity Factors, (4) Political Disparity Factors, (5) Knowledge Disparity Factors, (6) Economic Disparity Factors, and (7) Environmental Disparity Factors. Upon examining accuracy and reliability using Cronbach's alpha, the values for each variable ranged from 0.870 to 0.933, which surpasses the minimum threshold recommended in previous research, typically set at 0.70 [80, 81].

Table 4. Factor analysis results of exploratory factor analysis

Variable	Loading	Communalities	Eigenvalue	Item	Cronbach's α
Factor 1: Cultural disparity factor			15.873	5	0.929
CI1	0.885	0.802			
CI2	0.898	0.820			
CI3	0.849	0.746			
CI4	0.881	0.809			
CI5	0.862	0.767			
Factor 2: Spatial disparity factor			4.348	7	0.933
SP1	0.693	0.614			
SP2	0.748	0.769			
SP3	0.779	0.778			
SP4	0.788	0.789			
SP5	0.784	0.787			
SP6	0.728	0.705			
SP7	0.680	0.691			
Factor 3: Social disparity factor			2.522	5	0.907
SO1	0.670	0.728			
SO2	0.703	0.760			
SO3	0.700	0.745			
SO4	0.765	0.795			
SO5	0.717	0.698			
Factor 4: Political disparity factor			1.618	3	0.896
PI1	0.695	0.737			
PI2	0.725	0.805			
PI3	0.726	0.800			
Factor 5: Knowledge disparity factor			1.266	6	0.919
KI1	0.732	0.735			
KI2	0.698	0.722			
KI3	0.712	0.758			
KI4	0.713	0.749			
KI5	0.722	0.707			
KI6	0.704	0.682			
Factor 6: Economic disparity factor			1.102	6	0.920
EC1	0.707	0.744			
EC2	0.718	0.803			
EC3	0.686	0.811			
EC4	0.636	0.687			
EC5	0.529	0.745			
EC6	0.557	0.705			

Factor 7: Environmental disparity factor			0.967	5	0.870
EN1	0.787	0.740			
EN2	0.805	0.745			
EN3	0.798	0.753			
EN4	0.562	0.730			
EN5	0.587	0.734			
	SUM			37	**0.954**

Note: Goodness of fit for EFA: Bartlett's test approx. χ^2 = 11745.045, Degrees of freedom (df) = 666, p < 0.000.

4.3. Theoretical Confirmation

The results of the EFA will be examined in this section to verify and explain the significance of each item, confirming that the indicators can be components of each factor. The results of the CFA were analyzed using Mplus 7 software.

In Table 5, it is evident that all indicators are statistically significant as components of the latent construct of maladjustment, with factor loadings ranging between 0.687 and 0.871. All seven factors have acceptable structural reliability (CR) values between 0.8662 and 0.9319, and the average variance extracted (AVE) ranges from 0.5232 to 0.6859. The statistical values of CR are greater than 0.7, and AVE is not less than 0.5, [82-84]. Which confirms that all factors are suitable for CFA.

Table 5. Model results of Confirmatory factor analysis

Variable	Loading	S.E.	t–Stat	CR	AVE
Factor 1: Cultural disparity factor				0.9160	0.6859
CI1	0.840	0.013	63.211		
CI2	0.835	0.013	62.230		
CI3	0.818	0.015	55.147		
CI4	0.861	0.013	66.936		
CI5	0.785	0.015	52.501		
Factor 2: Spatial disparity factor				0.9319	0.6621
SP1	0.741	0.017	43.667		
SP2	0.819	0.013	65.230		
SP3	0.795	0.014	57.904		
SP4	0.849	0.011	78.286		
SP5	0.866	0.010	86.421		
SP6	0.819	0.012	68.105		
SP7	0.801	0.014	55.501		
Factor 3: Social disparity factor				0.9011	0.6461
SO1	0.830	0.012	66.569		
SO2	0.835	0.013	65.897		
SO3	0.821	0.013	63.971		
SO4	0.767	0.016	48.858		
SO5	0.763	0.017	45.859		
Factor 4: Political disparity factor				0.8662	0.6838
PI1	0.776	0.016	48.890		
PI2	0.871	0.012	74.331		
PI3	0.831	0.013	62.156		
Factor 5: Knowledge disparity factor				0.8679	0.5232
KI1	0.687	0.022	31.461		
KI2	0.710	0.021	33.927		
KI3	0.785	0.018	44.788		
KI4	0.723	0.020	35.731		
KI5	0.717	0.020	35.512		
KI6	0.714	0.020	34.987		

Factor 6: Economic disparity factor			0.9162	0.6457
EC1	0.765	0.016	47.933	
EC2	0.810	0.014	59.003	
EC3	0.812	0.014	59.078	
EC4	0.816	0.013	61.733	
EC5	0.800	0.014	55.648	
EC6	0.817	0.013	61.352	
Factor 7: Environmental disparity factor			0.8664	0.5655
EN1	0.750	0.016	46.741	
EN2	0.790	0.016	48.212	
EN3	0.807	0.016	51.603	
EN4	0.706	0.015	45.607	
EN5	0.701	0.015	45.422	

Note: CR = Composite reliability, AVE = Average variance extracted.

For the overall model fit assessment (Goodness–of–fit statistics), this study used absolute and incremental fit indices [85] and considered the following indices: Chi–square or ratio between the chi–square and the number of degrees of freedom (χ^2/df) should be less than 3 [79, 86]; Comparative fit index (CFI) should be greater than 0.95 [71, 87]; Tucker–Lewis index (TLI) should be greater than 0.95 [85, 88]; Root mean square error of approximation (RMSEA) should be less than 0.05 [89, 90]; and Standardized root mean square Residual (SRMR) should be less than 0.08 [91]. The CFA estimation results show that the model measures inequality resulting from railway access. The results were as follows: Chi–square test of model fit χ^2= 1529.267, df = 580, χ^2/df = 2.637; CFI = 0.962; TLI = 0.956; RMSEA = 0.046; and SRMR = 0.068, $p < 0.001$. From inspection, all values comply with the specified conditions. Therefore, it can be concluded that this model aligns with the empirical data.

Cultural disparity factors: The 5 variables have standardized CFA loadings ranging from 0.785 to 0.861. Specifically, CI4, "The Religious Disparities impact accessibility to railways" has the highest loading factor ($\gamma = 0.861$, t = 66.936).

Spatial disparity factors: The 7 variables have standardized CFA loadings ranging from 0.741 to 0.866. Specifically, SP5, "Regional Infrastructure's impact accessibility to railways" has the highest loading factor ($\gamma = 0.866$, t = 86.421).

Social disparity factors: The 5 variables have standardized CFA loadings ranging from 0.763 to 0.835. Specifically, SO2, "Access to government resources (such as government agencies and community resources) impacts accessibility to railways" has the highest loading factor ($\gamma = 0.835$, t = 65.897).

Political Disparities Factor: The 3 variables have standardized CFA loadings ranging from 0.776 to 0.871. Specifically, PI2, "Policies set by the government regarding railway development impact access to railway routes" has the highest loading factor ($\gamma = 0.871$, t = 74.331).

Knowledge disparity factors: The 6 variables have standardized CFA loadings ranging from 0.687 to 0.785. Specifically, KI3, "Promoting quality and beneficial knowledge impacts accessibility to railways" has the highest loading factor ($\gamma = 0.785$, t = 44.788).

Economic disparity factors: The 6 variables have standardized CFA loadings ranging from 0.765 to 0.817. Specifically, EC6, "If there are solutions to alleviate poverty, it will impact accessibility to railways" has the highest loading factor ($\gamma = 0.817$, t = 61.352).

Environmental disparity factors: The 5 variables have standardized CFA loadings ranging from 0.701 to 0.807. Specifically, EN3, "If there are current solutions to address pollution or environmental issues, it will impact accessibility to railways" has the highest loading factor ($\gamma = 0.807$, t = 51.603).

Furthermore, we have presented the results of the second-order CFA, consisting of 7 variables identified as factors influencing inequality in access to railways. The analysis revealed that all 7 exogenous latent variables have weights in the range of 0.798 to 0.988, exceeding the threshold of 0.70 [92], indicating the confirmation of the perspective of inequality concerning the use of railway station services. All exogenous latent variables are statistically significant at the 0.001 level when considering the weights of the components separated by each exogenous variable. The cultural disparity factor has the highest component weight ($\gamma = 0.988$, t = 122.927), followed by economic disparity factor ($\gamma = 0.938$, t = 87.534), social disparity factor ($\gamma = 0.885$, t = 62.811), knowledge disparity factor ($\gamma = 0.855$, t = 48.175), political disparity factor ($\gamma = 0.843$, t = 56.843), spatial disparity factor ($\gamma = 0.836$, t = 59.108), and finally, environmental disparity factor ($\gamma = 0.798$, t = 27.440). The results of the second–order CFA are illustrated in Figure 4.
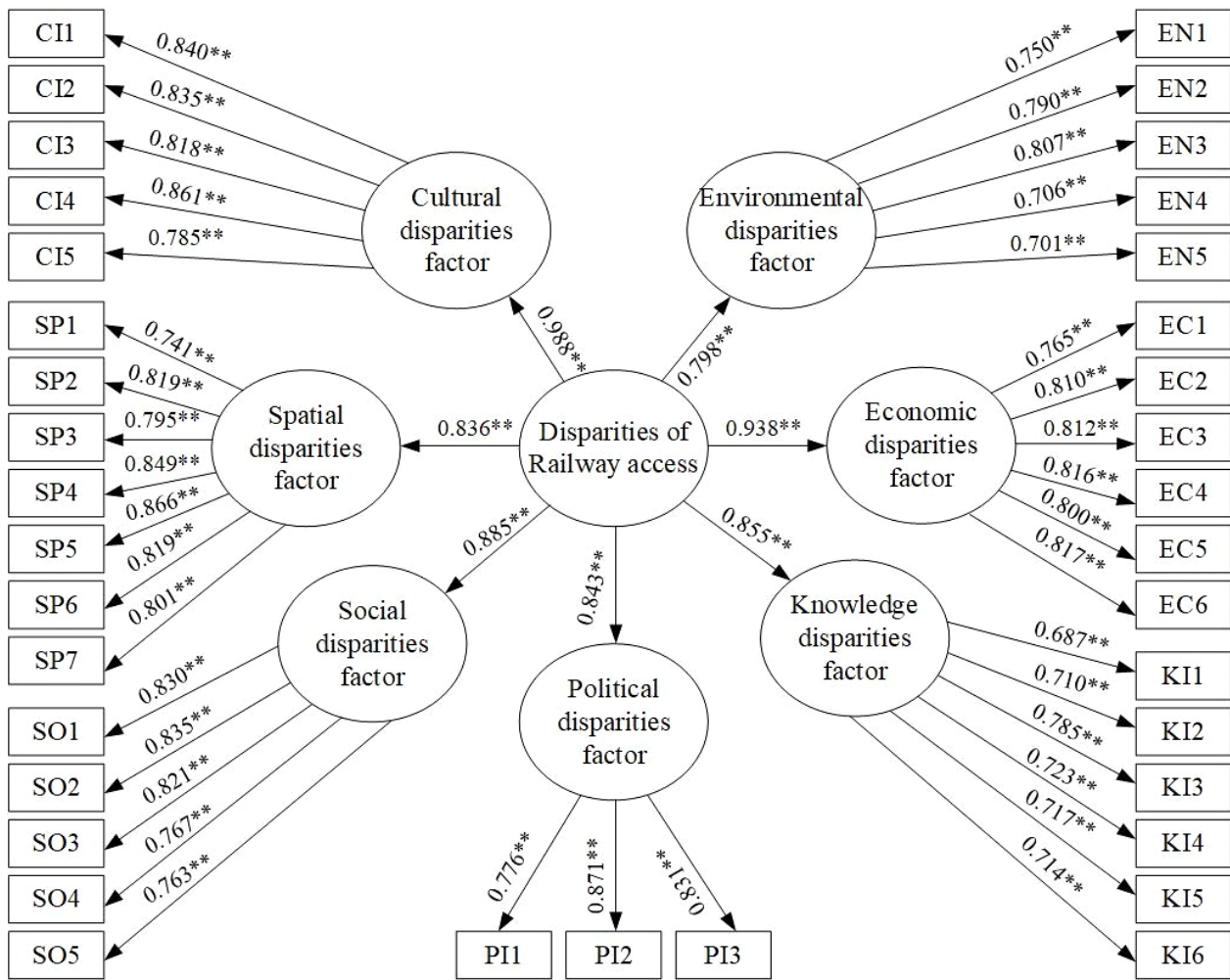
Figure 4. Results of the second–order Confirmatory factor analysis model

5. Discussion

The evaluation of the goodness-of-fit statistics for the model in this study was successful. It comprised the following indices: Chi-square or the ratio between the chi-square and the number of degrees of freedom (χ^2/df) with a value of 2.637, which is lower than 3 as per theory [79, 86]. Comparative Fit Index (CFI) with a value of 0.962, exceeding 0.95 as per theory [71, 87]. Tucker–Lewis Index (TLI) with a value of 0.956, exceeding 0.95 as per theory [85]. Root Mean Square Error of Approximation (RMSEA) with a value of 0.046, lower than 0.05 as per theory [89, 90]. Standardized Root Mean Square Residual (SRMR) with a value of 0.068, lower than 0.08 as per theory [91]. The results of all indices are consistent with the criteria and theoretically sound, confirming the consistency between the developed measurement model and both exploratory and confirmatory survey data.

When considering the results of CFA, it was found that the appropriate number of factors is 7 for assessing the factors influencing inequality in accessing railways. This study also revealed significant findings, detailed as follows:

Group 1: Cultural disparities factors have the highest composite weights, with a value of 0.988, which consists of variables from CI1 to CI5. This is related to previous studies that found cultural factors significantly influence societal changes [93, 94]. Cultural factors are also identified as a crucial strategy in addressing disparities issues [95]. Among the cultural disparity factors, the variable with the highest loading in the model is CI4, "Differences in religion affect the choice or access to railways." This finding is associated with studies indicating a strong relationship between inequality and religion, where societies with high levels of inequality have more diverse religions compared to those with low inequality [96]. Following that are CI1, "Differences in gender status affect access to railways." This finding is related to studies indicating that gender status differences influence the choice of public transportation [97]. And CI2, "Differences in race affect the choice or access to railways." This finding is related to studies indicating that inequality based on race/ethnicity affects access to public transportation [51].

Group 2: Economic disparity factor has the second composite weight, with a value of 0.938, which consists of variables from EC1 to EC6. This is related to previous studies that found railways play a crucial role in economic disparity development [58, 61, 98]. Among the economic disparity factors, the variable with the highest loading in the

model is EC6, "Having strategies to address poverty affects access to railways." This finding is associated with studies indicating that reducing addressing poverty positively impacts economic development, leading to increased utilization of railway transportation services [26]. Following that are EC4, "Differences between individuals with high income versus low income affect access to railways." This finding is related to studies indicating that railway systems affect income disparities between urban and rural residents [99]. And EC3, "Income or wages affect access to railways." This finding is related to studies indicating that income inequality affects the utilization of railway transportation services [100].

Group 3: The social disparity factor has the third composite weight, with a value of 0.885, which consists of variables from SO1 to SO5. This is related to previous studies that found social disparities influence the choice of railway transportation systems [101, 102]. Among the social disparity factors, the variable with the highest loading in the model is SO2, "Access to state resources (such as government agencies and community resources) affects access to railways." This finding is associated with studies indicating that developing state resources for railway network infrastructure expansion leads to greater equality in access [103]. Following that are SO1, "Issues of poverty and community strength affect access to the railway." This finding is related to studies indicating that the potential of communities from station-level factors and communities significantly impacts the development of railway transportation systems [104]. And SO3, "Social roles and responsibilities affect access to railways." This finding is related to studies indicating that social roles influence people's transportation service choices and travel behaviors [105].

Group 4: Knowledge disparity factor has the fourth composite weight, with a value of 0.855, which consists of variables from KI1 to KI6. This is related to previous studies that found that the development of knowledge in society influences the reduction of disparities [62, 68]. Among the knowledge disparity factors, the variable with the highest loading in the model is KI3, "Giving importance to promoting quality and beneficial knowledge affects access to railways." This finding is associated with studies indicating that advancements in providing information for transportation systems benefit reducing knowledge disparities [106]. Following that are KI4, "Utilizing modern technology and tools in daily life affects access to railways." This finding is related to studies indicating that connecting internet-enabled devices and technology tools to railway transportation services promotes significant innovations in accessing railway services [107]. And KI5, "Lack of information on train routes affects access to railways." This finding is related to studies indicating that a lack of knowledge impacts the understanding of public transportation users [62].

Group 5: Political disparity factor has the fifth composite weight, with a value of 0.843, which consists of variables from PI1 to PI3. This is related to previous studies that found factors related to political roles influence the development of disparities [108, 109]. Among the political disparity factors, the variable with the highest loading in the model is PI2, "Government policy related to trains set by the government affects access to railways." This finding is associated with studies indicating that policies benefiting certain groups in transportation contribute to disparities in accessing public transportation [108]. Following that are PI3, "Efficient train route development plans affect access to railways." This finding is related to studies indicating that strategic planning for railway route development reduces disparities in accessing railway services [109]. And PI1: "Giving importance to constructive feedback affects access to railways." This finding is related to studies indicating that genuine opinions and discussions among people enable the public to perceive the beneficial perspectives of others [110].

Group 6: Spatial disparity factor has the sixth composite weight, with a value of 0.836, which consists of variables from SP1 to SP7. This is related to previous studies that found spatial inequalities affect disparities in accessing railway transportation [36, 111]. Among the spatial disparity factors, the variable with the highest loading in the model is SP5, "Infrastructure factors in the area affect access to railways." This finding is associated with studies indicating that infrastructure networks are crucial for people's intercity travel [36]. Following that is SP4, "Economic growth in the area affects access to railways." This finding is related to studies indicating that economic growth impacts regional disparities in railway transportation development [31]. And SP6, "The connectivity pattern of the public transportation system with the rail system in the area affects access to railways." This finding is related to studies indicating that integrating bus transit systems with railways is a significant strategy for reducing disparities in accessing railway transportation [21].

Group 7: Environmental disparity factors have the lowest composite weights, with a value of 0.798, which consists of variables from EN1 to EN5. This is related to previous studies that found environmental inequalities are caused by disparities from other dimensions such as cultural, economic, and social disparities [54, 59]. Among the environmental disparity factors, the variable with the highest loading in the model is EN3, "Having strategies to address pollution and environmental issues affects access to railways." This finding is associated with studies indicating that improving environmental efficiency in cities impacts the choice of railway transportation systems [48]. Following that are EN2: "Access to resources (such as tourist attractions) affects access to railways." This finding is related to studies indicating that external resource factors, such as tourist attractions, impact travel planning and transportation system choices [112]. And EN1: "Current pollution issues affect access to railways." This finding is related to studies indicating that the risk of exposure to pollution varies by region and group, affecting environmental inequalities [113].

Furthermore, the findings of the analysis reveal that cultural disparity significantly influences the accessibility of Thailand's railway system, especially in the context of a developing nation. Through a confirmatory model evaluation

of all 37 questions, it was evident that religious differences emerged as the most influential factor affecting the choice or accessibility of railways. This finding is consistent with previous research highlighting the profound impact of religions on societal dynamics, individual behaviors, and decision-making processes related to transportation [114]. Additionally, religious considerations also shape the development of intercity railway networks [115]. Therefore, this study underscores the importance of addressing cultural disparities in railway accessibility, often rooted in religious factors. It is clear that religious differences significantly influence the decisions of railway users regarding their choice or access to railway services, particularly in the context of a developing country like Thailand. Consequently, the researchers recommend policy interventions aimed at mitigating these disparities within the study area. By doing so, valuable insights can be gained to enhance development efforts and promote equitable access to Thailand's railway system.

Therefore, based on the statistical data analysis mentioned, we have proposed a policy aimed at reducing disparities across all 7 dimensions to address and enhance the issue of disparity within the railway transportation system. The objective is to formulate policies that target the reduction of disparities and the promotion of equality in accessing railways, which is vital for fostering a sustainable society. Access to railway systems can have a significant impact on individuals' quality of life and their opportunities for advancement within communities. Additionally, the development of railway transportation systems necessitates collaborative efforts from all stakeholders, including government entities, the private sector, and the public, to ensure equitable access and utilization for all members of society. Our recommendations are derived from the critical variables identified within the model and are detailed as follows:

***Policy on Cultural Disparities*:** Based on our findings, we propose the following guidelines: (1) Policies should be in place to support train users with diverse religious backgrounds, such as providing designated seats for religious practitioners (e.g., Buddhist priests, votaries, and clergyman), having prayer rooms at train stations, and appropriate areas for prayer on trains for users of the Islamic faith. (2) Policies should address safety measures to manage concerns related to gender segregation, such as separating train carriages or seats between males and females, aligning with the findings that suggest implementing gender–segregation guidelines in public transportation policies [97], and (3) Policies should promote training on attitudes for railway staff based on the principles of fairness, such as providing service that does not discriminate based on race, disability, or gender expression [116].

***Policy on Economic Disparities*:** Based on our findings, we propose the following guidelines: (1) There should be a policy to diversify railway service fares to meet the needs of train users, and (2) there should be a policy to stimulate the economy by encouraging the public to choose rail transportation services more, such as increasing service frequency and establishing one–stop service centers [117]. These suggestions align with the results of the study that indicate transportation policies need to enhance the quality of rail services to stimulate the country's economic development [118].

***Policy on Social Disparities*:** Based on our findings, we propose the following guidelines: (1) Policies and measures should be established to reduce social gaps among people in society [119]. This can be achieved by exempting or reducing railway fares for disadvantaged groups or individuals, such as persons with disabilities and the elderly, and (2) Policies should ensure equal access to the railway transportation system, providing equitable access to services for all groups of people. For instance, railway routes should pass through educational areas like schools and universities for the convenience of students, and through employment areas like malls and industrial estates to facilitate commuting for the working population. These recommendations align with the study results, suggesting the need to enhance service coverage for various occupational groups to cater to diverse travel purposes [101].

***Policy on Knowledge Disparities*:** Based on our findings, we propose the following guidelines: (1) There should be policies for modernizing information development and information technology systems, such as developing the main website of the railway organization to serve as a tool for conveniently, rapidly, and efficiently disseminating information to railway service users. (2) Policies should be in place for providing useful knowledge to railway service users within railway stations, such as creating information dissemination points and signs with beneficial information, which should be developed to be more globally accessible (e.g., in English), and (3) Policies should promote activities related to the continuous development of knowledge for railway service personnel, such as exchanging knowledge and work experiences among employees, aligning with the study's results that suggest opening opportunities for employees to communicate, leading to the transfer of knowledge from external sources. This is important as employees may play a crucial role in exchanging valuable ideas and experiences beneficial for organizational development [120].

***Policy on Political Disparities*:** Based on our findings, we propose the following guidelines: (1) Policies should be formulated to benefit the development of railways, aiming to reduce disparities in railway accessibility at both national and local levels. These policies should ensure comprehensive railway coverage in all dimensions, and (2) Policies should promote inclusiveness in meaningful stakeholder participation for the development of collaborative railway access, involving contributions from the government, private sector, and the public. This approach aims to genuinely reduce disparities by granting equal political representation to everyone, regardless of differences or societal status [121].

***Policy on Spatial Disparities*:** Based on our findings, we propose the following guidelines: (1) Policies should focus on developing infrastructure that efficiently connects the railway transportation system (e.g., road network development) to enhance accessibility [122]. (2) Policies should emphasize the development of an integrated public transportation

system that seamlessly connects to the railway transportation system (e.g., public buses), and (3) Policies should prioritize the development of railway route networks to provide equal coverage and service across regions in Thailand. These proposals align with the government's ongoing study on the feasible development of a comprehensive and interconnected railway network covering and supporting various transportation modes across the nation [123].

Policy on Environmental Disparities: Based on our findings, we propose the following guidelines: (1) Policies should be implemented to promote environmentally friendly transportation, and (2) Policies should be introduced to enhance the environmental conditions around railway stations by increasing green areas to create a pleasant atmosphere and leave a positive impression on railway service users. These suggestions align with the study results indicating that reducing perceived disparities through environmental improvements has a positive influence on railway service users' attitudes [124].

Indeed, all the policies mentioned have been directly informed by current user feedback from railway service users in Thailand. These policies aim to engage stakeholders involved in the development of railway transportation systems, enabling them to apply these policies in setting guidelines or devising strategies to address and mitigate disparities in railway accessibility. Ultimately, these policies are geared towards fostering a new era of equality and efficiency, ultimately fostering a more equitable society.

In light of the limitations of our study, it's important to acknowledge that our research focuses exclusively on the viewpoints of railway service users, disregarding users of alternative public transportation modes. Moreover, we have omitted railway service users under the age of 18 due to their status as minors, potentially leading to a gap in understanding perspectives and attitudes towards disparities that may not be adequately addressed. Additionally, our study solely examines disparities in railway access within Thailand. To address these limitations, future research should encompass a broader range of public transportation users and involve surveying individuals under the age of 18 to ensure a more comprehensive understanding of disparities. Researchers should also consider adapting survey questions to suit different age groups appropriately. Furthermore, the findings of our study can serve as a valuable groundwork for further research and implementation in other developing nations. Addressing disparities in railway transportation access remains crucial for such countries, as it can provide deeper insights and new discoveries from various angles for future researchers.

6. Conclusions, Implications, and Research Limitations

This study aims to explore the factors contributing to disparities in accessing intercity railway systems in Thailand. We have presented findings from a combination of EFA and CFA, revealing in-depth insights into the factors influencing disparities in railway accessibility. The study surveyed 1,252 railway service users nationwide using face-to-face interviews. This study demonstrates the evaluation of the alignment between all 7 dimensions of the model and leads to the formulation of policies aimed at reducing disparities in railway accessibility in Thailand.

The results of CFA reveal that all 37 observed variables significantly contribute to indicating inequality in access to railways across the 7 factors (cultural inequality, spatial inequality, social inequality, political inequality, knowledge inequality, economic inequality, and environmental inequality) at a statistical significance level of 0.001. [125, 126]. Furthermore, in examining the standard component weights of CFA in the second order, it was found that cultural inequality was identified as the most significant indicator contributing to the highest level of inequality in accessing railway routes.

Furthermore, for the additional 6 factors, they have been ranked in the following order of importance regarding their influence on inequality in railway access: economic inequality, social inequality, knowledge inequality, political inequality, spatial inequality, and environmental inequality. Therefore, it is evident that the structural model of this study can verify the characteristics of inequality in accessing railways. Moreover, the results from both EFA and CFA can be seen as accurately representing the opinions of railway service users. These findings can effectively reflect the issue of inequality in accessing the railway transportation system. However, it's important to note that these findings can serve as suitable guidelines for policy–makers involved in the development of railways (e.g., the Department of Rail Transport and the State Railway of Thailand). They can utilize these insights to formulate policies and development plans aimed at reducing inequality and enhancing access to the rail transportation system for the population in the country efficiently.

7. Declarations

7.1. Author Contributions

7.2. Data Availability Statement

The data presented in this study are available on request from the corresponding author.

7.3. Funding

7.4. Acknowledgements

7.5. Institutional Review Board Statement

This research was approved by the Human Research Ethics Committee, Suranaree University of Technology (COA No. 100/2565, 01 December 2022).

7.6. Ethical Approval

The authors have obtained all the ethical approvals about this paper. The authors declare to obey all the academic ethical standards.

7.7. Conflicts of Interest

The authors declare no conflict of interest.

8. References

[1] Lee, W. H., Yen, L. H., & Chou, C. M. (2016). A delay root cause discovery and timetable adjustment model for enhancing the punctuality of railway services. Transportation Research Part C: Emerging Technologies, 73, 49–64. doi:10.1016/j.trc.2016.10.009.

[2] Buehler, R., & Pucher, J. (2011). Sustainable transport in Freiburg: Lessons from Germany's environmental capital. International Journal of Sustainable Transportation, 5(1), 43–70. doi:10.1080/15568311003650531.

[3] Chen, F., Shen, X., Wang, Z., & Yang, Y. (2017). An evaluation of the low-carbon effects of urban rail based on mode shifts. Sustainability (Switzerland), 9(3), 401. doi:10.3390/su9030401.

[4] Pagliara, F., Hayashi, Y., & Ram, K. S. (2022). High-Speed Rail, Equity and Inclusion. Sustainability (Switzerland), 14(11), 6710. doi:10.3390/su14116710.

[5] Dong, H., Ma, L., & Broach, J. (2016). Promoting sustainable travel modes for commute tours: A comparison of the effects of home and work locations and employer-provided incentives. International Journal of Sustainable Transportation, 10(6), 485–494. doi:10.1080/15568318.2014.1002027.

[6] Tang, S., & Lo, H. K. (2008). The impact of public transport policy on the viability and sustainability of mass railway transit - The Hong Kong experience. Transportation Research Part A: Policy and Practice, 42(4), 563–576. doi:10.1016/j.tra.2008.01.022.

[7] Credit Suisse. (2018). Global Wealth Report. Credit Suisse, Zürich, Switzerland. Available online: https://www.credit-suisse.com/media/assets/corporate/docs/about-us/research/publications/global-wealth-report-2018-en.pdf (accessed on February 2024).

[8] Thailand Trains (2023). State railway of Thailand. Railway Routes. Available online: https://www.thailandtrains.com/thailand-train-map/ (accessed on September 2023).

[9] HASC. (2023). Department of Environmental Quality Promotion. Summary of districts, sub-districts, villages of Thailand. Available online: http://www.statoids.com/yth.html (accessed on September 2023).

[10] Data Innovation and Governance Institute (2022). Open Thailand Railway Station Map User Statistics. Available online: https://data.go.th/blog/train-station (accessed on September 2023). (In Thai).

[11] Wang, L., Liu, Y., Mao, L., & Sun, C. (2018). Potential impacts of China 2030 high-speed rail network on ground transportation accessibility. Sustainability (Switzerland), 10(4), 1270. doi:10.3390/su10041270.

[12] Champahom, T., Chanpariyavatevong, K., Jomnonkwao, S., Boonyoo, T., & Ratanavaraha, V. (2022). Understanding Users' Perceived Service Quality of Railway Station: a Case Study of Nakhon Ratchasima. Suranaree Journal of Science and Technology, 29(5), 1.

[13] Jomnonkwao, S., Champahom, T., & Ratanavaraha, V. (2020). Methodologies for determining the service quality of the intercity rail service based on users' perceptions and expectations in Thailand. Sustainability (Switzerland), 12(10), 4259. doi:10.3390/su12104259.

[14] Kushwah, P. K. S., Rawat, V., Singh, A., Raje, S., Shrivastava, B., Sharma, S. K., & Shiva, A. (2018). Relationship Between Service Quality, Customer Satisfaction and Customer Perceived Value: Indian Railway Industry, 76-86.

[15] Soltanpour, A., Mesbah, M., & Habibian, M. (2020). Customer satisfaction in urban rail: a study on transferability of structural equation models. Public Transport, 12(1), 123–146. doi:10.1007/s12469-019-00223-y.

[16] Tantipanichkul, T., Boonchom, W., Suphan, K., Chiengkul, W., & Phuangpornpitak, W. (2022). Creative Tourist Satisfaction Model in Creative Community-Based Tourist Attraction along Nong Khai-Khon Kaen, Thailand Railway Route. Journal of Positive School Psychology, 2639-2648.

[17] Chu, F., Ye, L., & Guo, M. (2015). Research on the Evaluation Criteria of Railway Skilled Employees' Career Success in China. LISS 2014. Springer, Berlin, Germany. doi:10.1007/978-3-662-43871-8_141.

[18] Curcuruto, M., Griffin, M. A., Kandola, R., & Morgan, J. I. (2018). Multilevel safety climate in the UK rail industry: A cross validation of the Zohar and Luria MSC scale. Safety Science, 110, 183–194. doi:10.1016/j.ssci.2018.02.008.

[19] Derahim, N., Kadir, A., Isa, W. M. Z. W., Khairil, M., Mahfudz, M., Ciyo, M. B., Ali, M. N., Lampe, I., & Samad, M. A. (2021). Organizational safety climate factor model in the urban rail transport industry through cfa analysis. Sustainability (Switzerland), 13(5), 1–18. doi:10.3390/su13052939.

[20] Wisutwattanasak, P., Champahom, T., Jomnonkwao, S., Seefong, M., Theerathitichaipa, K., Kasemsri, R., & Ratanavaraha, V. (2023). Modeling Extended Service Quality for Public Transportation in the Post-Pandemic Period: Differentiating between Urban and Rural Areas: A Case Study of Intercity Railway, Thailand. Logistics, 7(4), 93. doi:10.3390/logistics7040093.

[21] Theerathitichaipa, K., Wisutwattanasak, P., Se, C., Seefong, M., Jomnonkwao, S., Champahom, T., Ratanavaraha, V., & Kasemsri, R. (2024). Assessment of Disparity in Accessing Railway Stations in Thailand: an Application Geographic Information System Network Analysis. Journal of Geovisualization and Spatial Analysis, 8(1), 6. doi:10.1007/s41651-023-00168-8.

[22] Suwanmolee, S. (2017). Inequality Pathway of Rawai Sea Gypsies in Phuket Province. Asia Social Issues, 10(1), 89-135.

[23] Nelson, T. E., & Joselus, D. (2023). Cultural attributions for racial inequality. Politics, Groups, and Identities, 11(4), 876–898. doi:10.1080/21565503.2022.2061361.

[24] Janatabadi, F., & Ermagun, A. (2023). Unraveling transit service and land use components of the socio-spatial inequality of access. Environment and Planning B: Urban Analytics and City Science. doi:10.1177/23998083231207534.

[25] Zhu, Y. (2023). Railroad investment and regional disparity: Public expenditure on transport infrastructure in France, 1837–57. Journal of Transport History, 44(1), 99–124. doi:10.1177/00225266221142004.

[26] Di Matteo, D., & Cardinale, B. (2023). Impact of high-speed rail on income inequalities in Italy. Journal of Transport Geography, 111. doi:10.1016/j.jtrangeo.2023.103652.

[27] Xu, Y., & Zhu, S. (2023). Transport Infrastructure, Intra-Regional Inequality and Urban-Rural Divide: Evidence from China's High-Speed Rail Construction. International Regional Science Review. doi:10.1177/01600176231177672.

[28] UNESCO. (2016). World Social Science Report, 2016. Challenging Inequalities: Pathways to a Just World. The United Nations Educational, Scientific and Cultural Organization (UNESCO), Paris, France. doi:10.54678/qtok7532.

[29] Sabnis, R., Sahu, K., Thakur, D., Surana, S., Mazhar, H., & Pandey, S. (2016). Urban and rural disparity in tobacco use and knowledge about oral cancer among adolescents: An epidemiological survey on 12 and 15-year school going students. Journal of International Society of Preventive & Community Dentistry, 6(9), S226–S231. doi:10.4103/2231-0762.197200.

[30] Wang, W., Zhang, Y., Lin, B., Mei, Y., Ping, Z., & Zhang, Z. (2020). The urban-rural disparity in the status and risk factors of health literacy: A cross-sectional survey in central China. International Journal of Environmental Research and Public Health, 17(11). doi:10.3390/ijerph17113848.

[31] Cascetta, E., Cartenì, A., Henke, I., & Pagliara, F. (2020). Economic growth, transport accessibility and regional equity impacts of high-speed railways in Italy: ten years ex post evaluation and future perspectives. Transportation Research Part A: Policy and Practice, 139, 412–428. doi:10.1016/j.tra.2020.07.008.

[32] Chakraborti, L., & Shimshack, J. P. (2022). Environmental disparities in urban Mexico: Evidence from toxic water pollution. Resource and Energy Economics, 67, 101281. doi:10.1016/j.reseneeco.2021.101281.

[33] O'Brien, D., & Oakley, K. (2015). Cultural value and inequality: A critical literature review. Arts and humanities research council. University of Leeds, Leeds, United Kingdom.

[34] Lareau, A. (2015). Cultural Knowledge and Social Inequality. American Sociological Review, 80(1), 1–27. doi:10.1177/0003122414565814.

[35] Levinson, D. M. (2012). Accessibility impacts of high-speed rail. Journal of Transport Geography, 22, 288–291. doi:10.1016/j.jtrangeo.2012.01.029.

[36] Luo, H., & Zhao, S. (2021). Impacts of high-speed rail on the inequality of intercity accessibility: A case study of Liaoning Province, China. Journal of Transport Geography, 90. doi:10.1016/j.jtrangeo.2020.102920.

[37] Lucas, K., Martens, K., Di Ciommo, F., & Dupont-Kieffer, A. (2019). Measuring transport equity (1st Ed.). Elsevier, Amsterdam, Netherlands.

[38] Zhan, S., Wong, S. C., & Lo, S. M. (2020). Social equity-based timetabling and ticket pricing for high-speed railways. Transportation Research Part A: Policy and Practice, 137, 165–186. doi:10.1016/j.tra.2020.04.018.

[39] Rodriguez, J. M. (2018). Health disparities, politics, and the maintenance of the status quo: A new theory of inequality. Social Science & Medicine, 200, 36–43. doi:10.1016/j.socscimed.2018.01.010.

[40] Beaumont, E. (2011). Promoting Political Agency, Addressing Political Inequality: A Multilevel Model of Internal Political Efficacy. The Journal of Politics, 73(1), 216–231. doi:10.1017/s0022381610000976.

[41] Wu, N., & Zhao, S. (2015). Impact of Transportation Convenience, Housing Affordability, Location, and Schooling in Residence Choice Decisions. Journal of Urban Planning and Development, 141(4). doi:10.1061/(asce)up.1943-5444.0000258.

[42] Viswanath, K., Breen, N., Meissner, H., Moser, R. P., Hesse, B., Steele, W. R., & Rakowski, W. (2006). Cancer Knowledge and Disparities in the Information Age. Journal of Health Communication, 11(sup001), 1–17. doi:10.1080/10810730600637426.

[43] Robb, K., Wardle, J., Stubbings, S., Ramirez, A., Austoker, J., MacLeod, U., Hiom, S., & Waller, J. (2010). Ethnic disparities in knowledge of Cancer Screening Programmes in the UK. Journal of Medical Screening, 17(3), 125–131. doi:10.1258/jms.2010.009112.

[44] Knight, J., & Song, L. (1999). The Rural-Urban Divide. Oxford University Press, Oxford, United Kingdom. doi:10.1093/acprof:oso/9780198293309.001.0001.

[45] Pokropek, A., Borgonovi, F., & Jakubowski, M. (2015). Socio-economic disparities in academic achievement: A comparative analysis of mechanisms and pathways. Learning and Individual Differences, 42, 10–18. doi:10.1016/j.lindif.2015.07.011.

[46] Boyce, J. K. (1994). Inequality as a cause of environmental degradation. Ecological Economics, 11(3), 169–178. doi:10.1016/0921-8009(94)90198-8.

[47] Song, M., Zhang, G., Zeng, W., Liu, J., & Fang, K. (2016). Railway transportation and environmental efficiency in China. Transportation Research Part D: Transport and Environment, 48, 488–498. doi:10.1016/j.trd.2015.07.003.

[48] Sun, X., Yan, S., Liu, T., & Wu, J. (2020). High-speed rail development and urban environmental efficiency in China: A city-level examination. Transportation Research Part D: Transport and Environment, 86. doi:10.1016/j.trd.2020.102456.

[49] Lope, D. J., & Dolgun, A. (2020). Measuring the inequality of accessible trams in Melbourne. Journal of Transport Geography, 83. doi:10.1016/j.jtrangeo.2020.102657.

[50] Sanchez, T. W. (2002). The impact of public transport on US metropolitan wage inequality. Urban Studies, 39(3), 423–436. doi:10.1080/00420980220112766.

[51] Galaskiewicz, J., Anderson, K. F., & Thompson-Dyck, K. (2021). Minority-White income inequality across metropolitan areas: The role of racial/ethnic residential segregation and transportation networks. Journal of Urban Affairs, 43(1), 16–39. doi:10.1080/07352166.2019.1660581.

[52] Clifton, K., & Lucas, K. (2004). Examining the empirical evidence of transport inequality in the US and UK. Running on Empty, 15–36, Bristol University Press, Bristol, United Kingdom. doi:10.51952/9781847426000.ch002.

[53] Zhao, P., & Li, S. (2016). Restraining transport inequality in growing cities: Can spatial planning play a role? International Journal of Sustainable Transportation, 10(10), 947–959. doi:10.1080/15568318.2016.1191693.

[54] Aasness, J., & Larsen, E. R. (2003). Distributional Effects of Environmental Taxes on Transportation. Journal of Consumer Policy, 26(3), 279–300. doi:10.1023/A:1025651404957.

[55] Kim, E., & Yi, Y. (2019). Impact analysis of high-speed rail investment on regional economic inequality: a hybrid approach using a transportation network-CGE model. Journal of Transport Economics and Policy (JTEP), 53(3), 314-333.

[56] Chang, Z., Chen, J., Li, W., & Li, X. (2019). Public transportation and the spatial inequality of urban park accessibility: New evidence from Hong Kong. Transportation Research Part D: Transport and Environment, 76, 111–122. doi:10.1016/j.trd.2019.09.012.

[57] Benoussaïd, T., Coll, I., Charreire, H., & Elessa Etuman, A. (2023). A socio-spatial analysis of air pollution exposure in the Greater Paris. EGU General Assembly 2023, Vienna, Austria, 24–28 Apr 2023, EGU23-15999. doi:10.5194/egusphere-egu23-15999.

[58] Liu, Z., & Zhang, Y. (2022). Comprehensive Sustainable Assessment and Prioritization of Different Railway Projects Based on a Hybrid MCDM Model. Sustainability (Switzerland), 14(19), 12065. doi:10.3390/su141912065.

[59] Wanke, P., Chen, Z., Zheng, X., & Antunes, J. (2020). Sustainability efficiency and carbon inequality of the Chinese transportation system: A Robust Bayesian Stochastic Frontier Analysis. Journal of Environmental Management, 260. doi:10.1016/j.jenvman.2020.110163.

[60] Ongolo-Zogo, V., & Epo, B. N. (2015). Sources of inequality in the cost of transport mobility in the city of Yaoundé, Cameroon. Development Southern Africa, 32(2), 229–239. doi:10.1080/0376835X.2014.984832.

[61] Allen, J., & Farber, S. (2019). Sizing up transport poverty: A national scale accounting of low-income households suffering from inaccessibility in Canada, and what to do about it. Transport Policy, 74, 214–223. doi:10.1016/j.tranpol.2018.11.018.

[62] Zhang, M., Zhao, P., & Qiao, S. (2020). Smartness-induced transport inequality: Privacy concern, lacking knowledge of smartphone use and unequal access to transport information. Transport Policy, 99, 175–185. doi:10.1016/j.tranpol.2020.08.016.

[63] Zhang, J., & Zhang, Y. (2021). The relationship between China's income inequality and transport infrastructure, economic growth, and carbon emissions. Growth and Change, 52(1), 243–264. doi:10.1111/grow.12472.

[64] Nadimi, N., Sangdeh, A. K., & Amiri, A. M. (2021). Deciding about the effective factors on improving public transit popularity among women in developing countries. Transportation Letters, 13(10), 707–715. doi:10.1080/19427867.2020.1801022.

[65] Wang, Y., Cao, M., Liu, Y., Ye, R., Gao, X., & Ma, L. (2022). Public transport equity in Shenyang: Using structural equation modelling. Research in Transportation Business & Management, 42. doi:10.1016/j.rtbm.2020.100555.

[66] Ali, L., Mi, J., Shah, M., Shah, S. J., Khan, S., Ullah, R., & Bibi, K. (2018). Local residents' attitude towards road and transport infrastructure (a case of China Pakistan economic corridor). Journal of Chinese Economic and Foreign Trade Studies, 11(1), 104–120. doi:10.1108/JCEFTS-08-2017-0024.

[67] Loa, P., Mashrur, S. M., & Nurul Habib, K. (2023). What influences the substitution of ride-sourcing for public transit and taxi services in Toronto? An exploratory structural equation model-based study. International Journal of Sustainable Transportation, 17(1), 15–28. doi:10.1080/15568318.2021.1978018.

[68] Li, Q., Guo, M., Chu, F., & Yang, S. (2022). Role of Knowledge Sharing in High Reliability Organizations: Take the Rail Transportation Industry as Example. SSRN Electronic Journal. doi:10.2139/ssrn.4186592.

[69] Sato, T., Yano, T., Morihara, T., & Masden, K. (2004). Relationships between rating scales, question stem wording, and community responses to railway noise. Journal of Sound and Vibration, 277(3), 609–616. doi:10.1016/j.jsv.2004.03.023.

[70] Zitrický, V., Gašparík, J., & Pečený, L. (2015). The methodology of rating quality standards in the regional passenger transport. Transport Problems, 10, 59–72. doi:10.21307/tp-2015-062.

[71] Cangur, S., & Ercan, I. (2015). Comparison of model fit indices used in structural equation modeling under multivariate normality. Journal of Modern Applied Statistical Methods, 14(1), 152–167. doi:10.22237/jmasm/1430453580.

[72] Stevens, J. P., & Stevens, J. P. (2001). Applied Multivariate Statistics for the Social Sciences. Psychology Press, New York, United States. doi:10.4324/9781410604491.

[73] Marsh, H. W., Muthén, B., Asparouhov, T., Lüdtke, O., Robitzsch, A., Morin, A. J. S., & Trautwein, U. (2009). Exploratory Structural Equation Modeling, Integrating CFA and EFA: Application to Students' Evaluations of University Teaching. Structural Equation Modeling: A Multidisciplinary Journal, 16(3), 439–476. doi:10.1080/10705510903008220.

[74] Wisutwattanasak, P., Jomnonkwao, S., Se, C., & Ratanavaraha, V. (2022). Influence of Psychological Perspectives and Demographics on Drivers' Valuation of Road Accidents: A Combination of Confirmatory Factor Analysis and Preference Heterogeneity Model. Behavioral Sciences, 12(9), 336. doi:10.3390/bs12090336.

[75] Chonsalasin, D., Jomnonkwao, S., & Ratanavaraha, V. (2021). Measurement model of passengers' expectations of airport service quality. International Journal of Transportation Science and Technology, 10(4), 342–352. doi:10.1016/j.ijtst.2020.11.001.

[76] Ratanavaraha, V., & Jomnonkwao, S. (2014). Model of users' expectations of drivers of sightseeing buses: Confirmatory factor analysis. Transport Policy, 36, 253–262. doi:10.1016/j.tranpol.2014.09.004.

[77] Jomnonkwao, S., & Ratanavaraha, V. (2016). Measurement modelling of the perceived service quality of a sightseeing bus service: An application of hierarchical confirmatory factor analysis. Transport Policy, 45, 240–252. doi:10.1016/j.tranpol.2015.04.001.

[78] Garson, G. D. (2012). Testing statistical assumptions. Statistical Associates Publishing, North Carolina State University, Raleigh, United States.

[79] Kline, R. B. (2023). Principles and practice of structural equation modeling. Guilford Publications, New York, United States.

[80] Nunnally, J. C., & Bernstein, I. H. (1994). Psychometric theory (3rd Ed.). McGraw-Hill, New York, United States.

[81] Tavakol, M., & Dennick, R. (2011). Making sense of Cronbach's alpha. International Journal of Medical Education, 2, 53–55. doi:10.5116/ijme.4dfb.8dfd.

[82] Fornell, C., & Larcker, D. F. (1981). Evaluating Structural Equation Models with Unobservable Variables and Measurement Error. Journal of Marketing Research, 18(1), 39. doi:10.2307/3151312.

[83] Hair, J. F. (2009). Multivariate Data Analysis. Kennesaw State University, Kennesaw, Georgia, United States.

[84] Kaiser, H. F. (1974). An Index of Factorial Simplicity. Psychometrika, 39(1), 31–36. doi:10.1007/BF02291575.

[85] Hooper, D., Coughlan, J., & Mullen, M. R. (2008). Structural equation modelling: Guidelines for determining model fit. Electronic Journal of Business Research Methods, 6(1), 53–60.

[86] Bagozzi, R. P., & Yi, Y. (1988). On the evaluation of structural equation models. Journal of the Academy of Marketing Science, 16(1), 74–94. doi:10.1007/BF02723327.

[87] Hu, L. T., & Bentler, P. M. (1999). Cutoff criteria for fit indexes in covariance structure analysis: Conventional criteria versus new alternatives. Structural Equation Modeling, 6(1), 1–55. doi:10.1080/10705519909540118.

[88] Hair Jr, J. F., Hult, G. T. M., Ringle, C. M., Sarstedt, M., Danks, N. P., Ray, S., ... & Ray, S. (2021). An introduction to structural equation modeling. Partial least squares structural equation modeling (PLS-SEM) using R: a workbook, 1-29. doi:10.1007/978-3-030-80519-7_1.

[89] Deb, S., & Ali Ahmed, M. (2018). Determining the service quality of the city bus service based on users' perceptions and expectations. Travel Behaviour and Society, 12, 1–10. doi:10.1016/j.tbs.2018.02.008.

[90] Marsh, H. W., & Hau, K. T. (1996). Assessing goodness of fit: Is parsimony always desirable? Journal of Experimental Education, 64(4), 364–390. doi:10.1080/00220973.1996.10806604.

[91] Schreiber, J. B., Stage, F. K., King, J., Nora, A., & Barlow, E. A. (2006). Reporting structural equation modeling and confirmatory factor analysis results: A review. Journal of Educational Research, 99(6), 323–338. doi:10.3200/JOER.99.6.323-338.

[92] Joseph, F., Hult, G. T. M., Ringle, C. M., & Sarstedt, M. (2022). A primer on partial least squares structural equation modeling (PLS-SEM). SAGE Publications, Thousand Oaks, United States.

[93] Cooper, M. (2008). Brazilian railway culture. Ph.D. Thesis, University of York, York, United Kingdom.

[94] Üblacker, J., & Lukas, T. (2023). Local cultures of control, order maintenance policing, and gentrification: A comparison of railway station districts in three German cities. Journal of Urban Affairs, 1–24. doi:10.1080/07352166.2023.2174870.

[95] Betancourt, J. R., Green, A. R., Carrillo, J. E., & Ananeh-Firempong, O. (2003). Defining cultural competence: A practical framework for addressing racial/ethnic disparities in health and health care. Public Health Reports, 118(4), 293–302. doi:10.1016/S0033-3549(04)50253-4.

[96] Jordan, J. (2014). Religion and inequality: The lasting impact of religious traditions and institutions on welfare state development. European Political Science Review, 8(1), 25–48. doi:10.1017/S1755773914000381.

[97] Goel, R., Oyebode, O., Foley, L., Tatah, L., Millett, C., & Woodcock, J. (2023). Gender differences in active travel in major cities across the world. Transportation, 50(2), 733–749. doi:10.1007/s11116-021-10259-4.

[98] Yoo, S., Kumagai, J., Kawasaki, K., Hong, S., Zhang, B., Shimamura, T., & Managi, S. (2023). Double-edged trains: Economic outcomes and regional disparity of high-speed railways. Transport Policy, 133, 120–133. doi:10.1016/j.tranpol.2023.01.016.

[99] Sun, D., Zhao, X., Zhang, G., & Chen, P. (2023). Impact of the introduction of high-speed rail on the income gap between urban and rural residents. PLOS ONE, 18(11), e0292105. doi:10.1371/journal.pone.0292105.

[100] Jiang, M., & Kim, E. (2016). Impact of high-speed railroad on regional income inequalities in China and Korea. International Journal of Urban Sciences, 20(3), 393–406. doi:10.1080/12265934.2016.1213139.

[101] Dobruszkes, F., Chen, C. L., Moyano, A., Pagliara, F., & Endemann, P. (2022). Is high-speed rail socially exclusive? An evidence-based worldwide analysis. Travel Behaviour and Society, 26, 96–107. doi:10.1016/j.tbs.2021.09.009.

[102] Fol, S., & Gallez, C. (2014). Social inequalities in urban access: Better ways of assessing transport improvements. Urban Access for the 21st Century, 46-86, Routledge, Milton Park, United Kingdom.

[103] Liu, S., Wan, Y., & Zhang, A. (2020). Does China's high-speed rail development lead to regional disparities? A network perspective. Transportation Research Part A: Policy and Practice, 138, 299–321. doi:10.1016/j.tra.2020.06.010.

[104] Borowski, E., Soria, J., Schofer, J., & Stathopoulos, A. (2023). Does ride sourcing respond to unplanned rail disruptions? A natural experiment analysis of mobility resilience and disparity. Cities, 140, 104439. doi:10.1016/j.cities.2023.104439.

[105] Zhao, P., & Li, P. (2019). Travel satisfaction inequality and the role of the urban metro system. Transport Policy, 79, 66–81. doi:10.1016/j.tranpol.2019.04.014.

[106] Gou, Y. (2023). Enhancing Producer Service Distribution through High-Speed Railways: A Knowledge Economy Perspective. Journal of the Knowledge Economy. doi:10.1007/s13132-023-01495-3.

[107] Xu, X., & Zheng, M. (2023). High-speed rail construction and urban innovation disparity in China: the role of internet development. Economic Change and Restructuring, 56(5), 3567–3599. doi:10.1007/s10644-023-09542-4.

[108] Wellman, G. C. (2014). Transportation Apartheid: The Role of Transportation Policy in Societal Inequality. Public Works Management & Policy, 19(4), 334–339. doi:10.1177/1087724X14545808.

[109] Wu, S. S., & Chong, A. (2018). Developmental rail politics: The political economy of China's high-speed rail projects in Thailand and Indonesia. Contemporary Southeast Asia, 40(3), 503–526. doi:10.1355/cs40-3g.

[110] Peacock, C. (2019). (Not) Talking Politics: Motivations and Strategies for Avoiding the Expression of Political Opinions. Western Journal of Communication, 83(5), 581–599. doi:10.1080/10570314.2019.1597157.

[111] Liu, X., Dai, L., & Derudder, B. (2017). Spatial Inequality in the Southeast Asian Intercity Transport Network. Geographical Review, 107(2), 317–335. doi:10.1111/j.1931-0846.2016.12181.x.

[112] Banerjee, I. (2023). Production of Railways cape in urban environment: Analysing railway heritage tourism potential in Siliguri City, India. Regional Sustainability, 4(1), 1–12. doi:10.1016/j.regsus.2023.02.001.

[113] Shao, S., Liu, L., & Tian, Z. (2022). Does the environmental inequality matter? A literature review. Environmental Geochemistry and Health, 44(9), 3133–3156. doi:10.1007/s10653-021-00921-2.

[114] Clark, D. C. (2012). Revolt and revival in the valleys: the influence of religion and revivalism on the politics and labour relations of the Taff Vale Railway, south Wales, 1878-1914. Ph.D. Thesis, University of Leeds, Leeds, United Kingdom.

[115] Li, B., Qizi, Z., Shahab, Y., Wu, X., & Ntim, C. G. (2024). High-speed rail network and earnings management techniques usage trade-off: the moderating effects of governance and religion. Managerial Auditing Journal, 39(1), 26–49. doi:10.1108/MAJ-01-2023-3799.

[116] ICRC. (2023). International Committee of the Red Cross. Race, fairness and Neocolonial Legacy: Identifying Pathways to Ethical Humanitarian Action. Available online: https://blogs.icrc.org/th/2020/08/06/part-1/ (accessed on February 2024).

[117] Expressway Authority of Thailand. (2023). One Stop Service Center. Available online: https://www.thaieasypass.com/en/index (accessed on September 2023).

[118] Ieda, H., Kanayama, Y., Ota, M., Yamazaki, T., & Okamura, T. (2001). How can the quality of rail services in Tokyo be further improved? Transport Policy, 8(2), 97–106. doi:10.1016/S0967-070X(01)00002-6.

[119] UNICEF (2024). UNICEF Thailand. Social Policy. UNICEF: For Every Child, Bangkok, Thailand. Available online: https://www.unicef.org/thailand/th (accessed on February 2024). (In Thai).

[120] Miwa, N., Bhatt, A., Morikawa, S., & Kato, H. (2022). High-Speed rail and the knowledge economy: Evidence from Japan. Transportation Research Part A: Policy and Practice, 159, 398–416. doi:10.1016/j.tra.2022.01.019.

[121] United Nations Thailand. (2024). Sustainable Development Goal 10: Reduce inequality, both within and between countries. United Nations Thailand, Bangkok, Thailand. Available online: https://thailand.un.org/th/sdgs/10 (accessed on February 2024).

[122] Daddow, M., Zhang, X., Qiu, H., Zhang, Z., & Liu, Y. (2020). A mathematical model for ballast tamping decision making in railway tracks. Civil Engineering Journal (Iran), 6(10), 2045–2057. doi:10.28991/cej-2020-03091601.

[123] DRT. (2023). Department of Rail Transport. Project to study the feasibility of developing a railway network to cover and connect areas throughout the country and to support multimodal transportation seamlessly (R-Map). Available online: https://www.drt.go.th/en (accessed on September 2023).

[124] Coppola, P., & Silvestri, F. (2021). Gender inequality in safety and security perceptions in railway stations. Sustainability (Switzerland), 13(7), 4007. doi:10.3390/su13074007.

[125] Hair Jr, J. F., Anderson, R. E., Tatham, R. L., & William, C. (1995). Multivariate data analysis with readings. New Jersey: Prentice Hall, New Jersey, United States.

[126] Hair, J. F., Ringle, C. M., & Sarstedt, M. (2011). PLS-SEM: Indeed a silver bullet. Journal of Marketing Theory and Practice, 19(2), 139–152. doi:10.2753/MTP1069-6679190202.
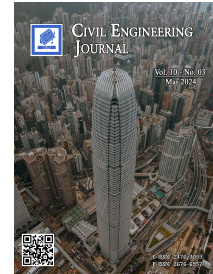
Effect of Non-Class Fly Ash on Strength Properties of Concrete

Anjeza Alaj [1] , Nexhmi Krasniqi [1*] , Tatsuya Numao [2]

[1] University for Business and Technology, Pristina, 10000, Kosovo.

[2] Graduate School of Science and Engineering, Ibaraki University, Hitachi, Japan.

Abstract

Developing of green construction and reducing CO_2 emissions in the environment is a priority for industry in the coming years. Recycling fly ash in the concrete industry is a well-known way to reduce environmental impact. Aside from this benefit, there are numerous other positive effects of incorporating fly ash into concrete; however, in this research, the objective is to replace cement with a different percentage of non-class fly ash with high CaO, more than 42%. The analyzed variables are non-class fly ash properties, the effect of fly ash presence on the main properties of concrete and examining the optimum of non-class fly ash in ordinary concrete C-25/30 and high-performance concrete C-50/60. All investigations took place in the laboratory by producing 24 different mix designs and more than 1000 specimens to examine: consistency, setting time, shrinkage, and compressive strength in the short and long terms of curing. Recycling industrial waste in new construction, especially fly ash because of its non-uniform properties, still has some obstacles and is not a practical issue, but the future must be environmentally friendly, and this research proves that the objective of producing sustainable ordinary and high-performance concrete was achieved by replacing 40% of cement with non-class high CaO content fly ash.

Keywords: Non-Class Fly Ash; Compressive Strength; Shrinkage; CO_2 Emission.

1. Introduction

A way to produce sustainable concrete is by reducing CO_2 emissions by decreasing cement production instead of incorporating industrial waste as fly ash [1, 2]. Cement as a bonding material, the basic material for concrete, causes 8% of total greenhouse gas production, which causes global warming and climate change [3, 4]. Meanwhile, fly ash does not have uniform properties and is still not specified as a quantified fly ash type for concrete mixtures. This research investigates non-class high CaO fly ash in the mass of concrete from Kosovo, its environmental impact, and its concrete properties. Furthermore, concrete is the most widely used construction material in the modern world because of its characteristics compared to other materials, which are: excellent strength, easy shape, long-lasting service, affordability, easy to obtain etc. [5, 6].

Hence, utilization of supplementary cementitious materials (SCM) such as industrial waste has been a global trend for decades. In Brazil, according to this strategy, CO_2 emissions are reduced by ~ 4.4% due to the clinker content of cement. Research institutions in Canada are pioneers in the research of using high volumes of SCM in the concrete industry [7]. India has stipulated by law the utilization of fly ash in construction materials, especially in concrete, road construction, and bricks. The Ministry of Environment and Forestry has announced the benefits of recycling this industrial waste and saving natural resources [8, 9]. Australia alone is producing more than 12 million tons of fly ash per year. 43% of this ash is re-used for various applications, including the construction industry, while the rest is being dumped as waste, causing environmental problems such as groundwater contamination, spills from bulk storage, and

ground pollution by heavy metals [10–12]. Apart from environmental benefits, fly ash contributes to other properties such as workability, expansive property [13], permeability [13], and other durability attributes [14].

The benefits of utilizing fly ash for concrete applications are threefold: savings in CO_2 emissions, reducing the disposal of fly ash into the environment, and improving concrete qualities. So, these strategies have more advantages than reducing CO_2 emissions; they also conserve natural resources, reduce the disposal of fly ash into the environment, and increase production quality. Although there is numerous research about incorporating fly ash into concrete, there still remains an important scope to analyze the utilization of different types of fly ash in concrete. Usually, studies are focused on general issues and not studding environment effects and concrete quality based on fly ash types. The impact varies completely from type of fly ash used [23], and the concrete mixture has to be designed based on the type of fly ash. Low CaO fly ash is more effectively used for concrete resistance to alkali, silica, sulphate attacks, and acid resistant [13–15]. Concrete will be more durable to aggressive environment. High CaO fly ash is better to improve the early compressive strength of concrete because of its higher reactivity.

In order to reduce the environmental impact of CO_2 emissions, the government of Kosovo should promote and develop a sustainable construction industry with the aim of reducing cement production by up to 40% and replacing it with lignite coal fly ash obtained during the burning process of coal for the production of electricity in thermal power plants. Generally, fly ash is gained from the process of burning coal to produce electrical energy in power plants, which results in a high volume of CaO content and non-class fly ash. Its properties are different based on the type of coal and the technology used for burning it, but as long as fly ash fulfills the requirements of standards (EN, ASTM, JIS, etc. based on which country is applied), it can be used in the construction and concrete industries. Basically, according to ASTM, fly ash is divided into two categories: Class C ($SiO_2 + Al_2O_3 + Fe_2O_3 \geq 50\%$) and Class F ($SiO_2 + Al_2O_3 + Fe_2O_3 \geq 70\%$) [16–18].

To date, the majority of prior research on fly ash recycling has focused on using it in concrete for different purposes; none of the studies have optimized and found the effect of different types of fly ash in the concrete industry, especially when fly ash does not meet standard requirements, does not belong to any of the above-mentioned classes, and has a high CaO content. In the present research, three goals will be explained: The first goal is to determine the mechanical properties of ordinary and high-performance concrete for short- and long-term curing when the content (10, 15, 20, 25, 30, 35, 40, 45, and 50%) of cement replacement with non-class and high CaO content of fly ash; the second goal is to find the optimum amount of this type of fly ash to produce ordinary and high-performance concrete; and the third goal is to find a reduced amount of CO_2 emissions after including this type of fly ash in concrete production in Kosovo and other environmental effects.

2. Materials and Experimental Program

2.1. Materials

The cement used was a market-available PC 20M (S-L) 42.5R, equivalent to EU standards, while fly ash was discharged from power plant Kosova B directly after the process of burning coal to produce electrical energy. The physical properties and chemical compositions of cement and fly ash are given in Tables 1 and 2.

Table 1. Chemical composition of non – class fly ash

Fineness	Non-class Fly ash
* 0.200 mm	0.1
* 0.090 mm	4.9
* 0.063 mm	8.1
* 0.043 mm	12.5
Capacity mass g/cm³	2.83
Specific surface cm²/g	6600
Flexural MPa	4.5 ± 0.3
Compressive MPa	21.1 ± 0.7

Table 2. Physical properties of non-fly ash

Materials	Compound												
	Al_2O_3	SiO_2	SO_3	K_2O	CaO	MnO	Fe_2O_3	MgO	Na_2O	LOI	Moisture 105 C°	Reactive CaO	Reactive SiO_2
Non-class Fly ash %	5.67	19.28	19.41	0.36	42.92	0.08	4.85	4.31	0.58	2.3	0.29	28.44	15.69
Cement %	6.13	19.79	2.98	0.68	63.86	-	2.73	2.42	0.19	4.14	-	-	-

To obtain high-performance concrete C 50/60, an additive based on polikarboksilat polymer was used. It contributes to meeting high demands and increasing the flow properties of fresh concrete; a constant amount of 1% cement was used in all mix designs. Conducting this experiment was used crushed-clean aggregate, which was divided into three fractions: I - (0-4) mm, II - (4-8) mm, and III - (8-16) mm. The composition of these three fractions in concrete is 45%, 22%, and 33%. The absorption value of sand was 1.1%, while for aggregate was 0.7%.

According to chemical compositions $SiO_2 + Al_2O_3 + Fe_2O_3 = 19.28 + 5.67 + 4.85 = 29.8\%$, Kosovo fly ash, which becomes from lignite coal, does not belong in class F or C based on ASTM standards. What is very important to analyze are the large specific surface of fly ash (6600 cm^2/g), spherical-shaped particles compared to angular-shaped cement particles, and the high content of CaO (42.92%). Kosovo fly ash has 19.42% of SO_3 and failed to satisfy restrictions of ASTM, BSI, and EN for SO_3 content in fly ash in order to use it in concrete. Based on standards, it should be 5%, 2.5%, and 3.0%.

2.2. Mix Designs and Details

The experimental research is divided into three parts; consequently, three mixtures were without fly ash, control concrete, while twenty-one other mixtures were designed with different percentages of fly ash content, starting from (10, 15, 20, 25, 30, 35, 40, 45, and 50%) replacing cement. In total, twenty-four mixtures with a water/binder ratio between 0.4–0.6 were cast. The material proportions remained constant, and the slump test for all mix designs conformed to curve S3, ranging between 100-150 mm. Mixture details are listed in Table 3 and Figure 1.

Table 3. Mixture proportions for 24 mix designs

Case	Mixtures	Cement (kg)	Fly ash (kg)	Sand (kg)	Gravel (kg)	Water (kg)	Additive (kg)	w/b ratio	Slump test (mm)
Case 1	M 1	290	0	868	1061	160.7	1.74	0.61	140
	M 2	261	29	864	1056	160.7	1.74	0.62	130
	M 3	246.5	43.5	862	1054	160.7	1.74	0.62	122
	M 4	232	58	860	1052	160.7	1.74	0.63	130
	M 5	217.5	72.5	827	1010	160.7	1.74	0.63	130
	M 6	203	87	856	1046	160.7	1.74	0.63	140
	M 7	174	116	860	1050	160.7	1.74	0.63	130
	M 8	145	145	859	1049	160.7	1.74	0.63	140
Case 2	M 9	340	0	791	968	211	0	0.62	122
	M 10	306	34	787	961	211.2	0	0.62	123
	M 11	298	51	784	958	211.3	0	0.62	125
	M 12	272	68	782	956	211.4	0	0.62	126
	M 13	255	85	780	953	211.5	0	0.62	130
	M 14	238	102	777	950	211.6	0	0.62	133
	M 15	204	136	781	949	211.3	0	0.62	135
	M 16	170	170	779	951	211.1	0	0.62	139
Case 3	M 17	440	0	790	965	176	4.4	0.34	137
	M 18	396	44	783	958	176	4.4	0.41	132
	M 19	374	66	780	954	176	4.4	0.41	138
	M 20	352	88	777	951	176	4.4	0.41	145
	M 21	330	110	774	946	176	4.4	0.41	141
	M 22	308	132	771	943	176	4.4	0.41	143
	M 23	264	176	775	945	176	4.4	0.41	148
	M 24	220	220	781	949	176	4.4	0.41	146

An additive based on polikarboksilat polymer was added to eight mix designs to achieve high-performance concrete C 50/60. The amount of additive was kept constant in all eight mixtures: 1% of cement + fly ash.

The fresh properties of concrete mixtures were determined through consistency and density tests. Slump values are measured in conformity standard EN 12350-2 (see Table 3). The fresh densities were determined by the quotient of their mass and the volume, with values between (2.39 – 2.45) g/cm^3 for the first part of the research, (2.22 – 2.34) gr/cm^3 for the second part, and (2.38 – 2.39) gr/cm^3 third part. The fresh densities of mixtures are also shown in Table 3. The very fine rosary shape of fly ash particles contributes to the increase in workability of fresh concrete by reducing segregation and helping to gain very sticky mass. Increasing fly ash content contributes to improving the properties of fresh concrete. Concrete specimens are molded and cured under standard conditions until testing age.
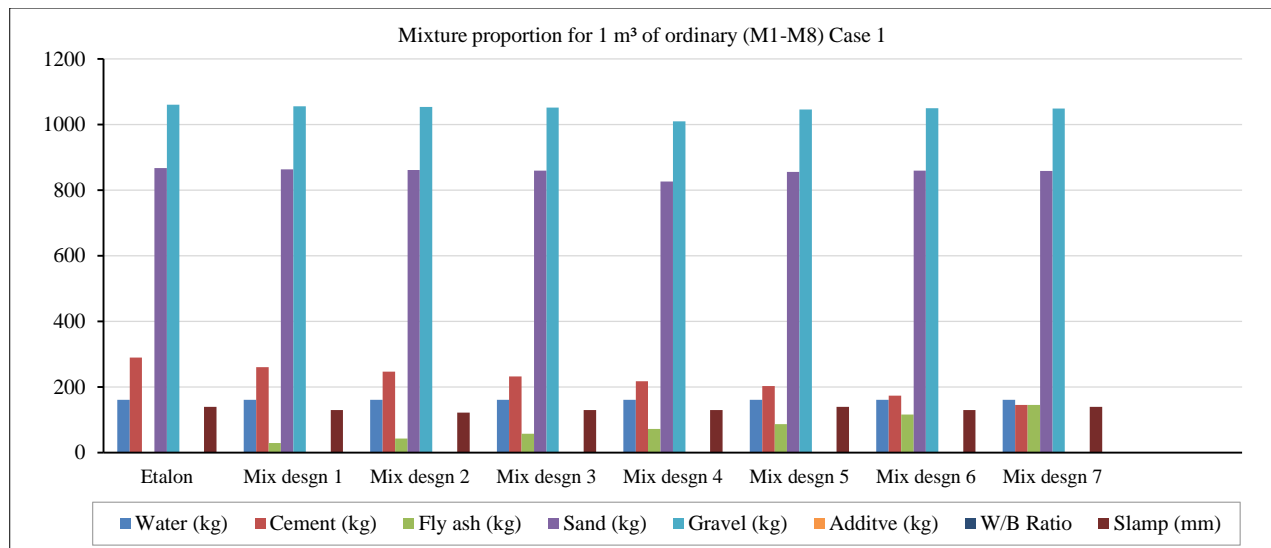
Figure 1. Components of 1 m³ of concrete for 8 different mix designs

2.3. Test Procedures

The concrete mixture was prepared in a laboratory mixer. During typical procedures, mold filling was done in two layers using a vibration table until the bubbles on the top of fresh concrete specimens disappeared. Specimens were removed from molds after 24 hours and cured in water at a constant temperature until testing after 3, 7, 21, 28, 56, 100, 180, and 365 days, then after 3, 5, 7, and 10 years. Altogether, more than 1000 specimens, 15 cm cubes, and all compressive strength results were taken as the average of three readings. For the casting shrinkage experiment, a very sensitive method was used, with 1 mm-thick empty cylinders measuring 1 cm in diameter and 10 cm in height. For this examination, in total, six mix designs were prepared according to the mix design of the first part of this research, with a difference in fly ash content of 0, 10, 15, 20, 25, and 30% of cement substitution. For preparing these very delicate specimens (in terms of dimensions and preparation method), sand was filtered and particles until 150μ were used. The material ratio was determined to be cement: sand: water = 1:2:2.1. After the samples were put on molds, they went under the oven to dry for 24 hours at 40°C. To keep specimens in a moist environment, they were clad with wet cotton rags, and to prevent humidity evaporation, specimens were put in closed plastic bags. After specimens were removed from molds for three months, they were cured in water at a constant temperature of 22±2 °C to complete the hydration process of cement + fly ash, and then 12 empty cylinders went under examination. Six of them were put on very sensitive measuring ports of the shrinkage instrument (measures were done every 10 min) and the other six were examined for weight loss. All 12 specimens during the examination were set in a chamber with a constant temperature of 22±2 °C and a relative humidity of 60±5% until the end of the examination (Figure 2).
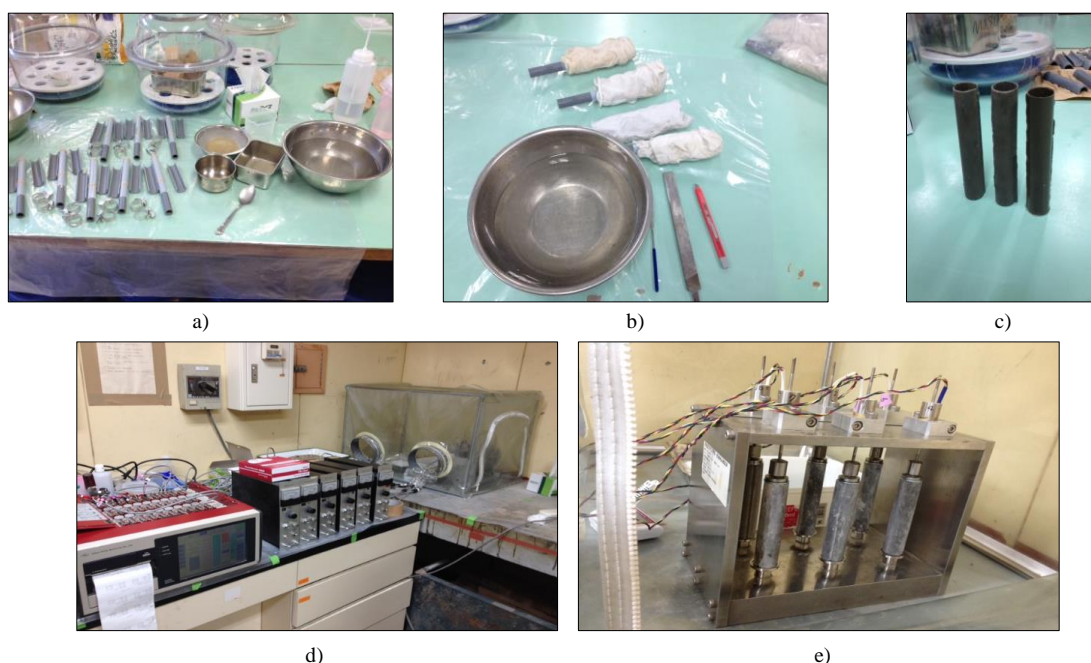

a)   b)   c)

d)   e)

Figure 2. Process of shrinkage specimen's preparation and examination: a) molds and concrete, b) specimens after 24 h, c) shrinkage empty cylinders h=10cm, D=1cm and d=1mm, d) examination process and e) empty cylinders on corresponding ports in chamber

Setting time was also in focus during the examination, which was conducted by a Vicat needle according to ASTM 191-08. Firstly, the standard consistency was determined for 10 different mix designs with 0, 10, 15, 20, 25, 30, 35, 40, 45, and 50% cement replacement with fly ash. During casting and examination, all procedures were developed according to standards and in laboratory conditions.

a)   b)

Figure 3. Examination of setting time of concrete: a) preparation of mass with standard consistency, b) examination with Vicat needle

3. Results and Discussion

3.1. Compressive Strength

The compressive strength evolution shows that the strength gain over time depends on the cement ratio replaced by fly ash. At 7 days by w/b ratio between 0.4 and 0.6, in three different cases, the gain of strength in etalon was relatively high, more than 70% for the first and second cases, and more than 85% in the third case of research on its 28-day compressive strength. In all three treated cases, when part of the cement was replaced by fly ash, the compressive strength decreased compared to reference concrete. By increasing the curing time of the specimens, compressive strength was also increased (see Figures 4 to 6). For instance, the first case, after 180 days of curing specimens with 30% fly ash content, achieved class C 25/30, and it continued to increase in strength over time. After 365 days, the mix design with 40% fly ash content gained a quality of C 25/30. Almost the same thing happened in the second case: after one year of curing, the mix design with 40% fly ash achieved quality C 25/30. Based on these dates, the different content of cement does not play any role in curing specimens for a long time. According to the third case, dates show better results; in 100 days, class C 50/60 of concrete was obtained, a mixture with 40% cement replaced with fly ash.
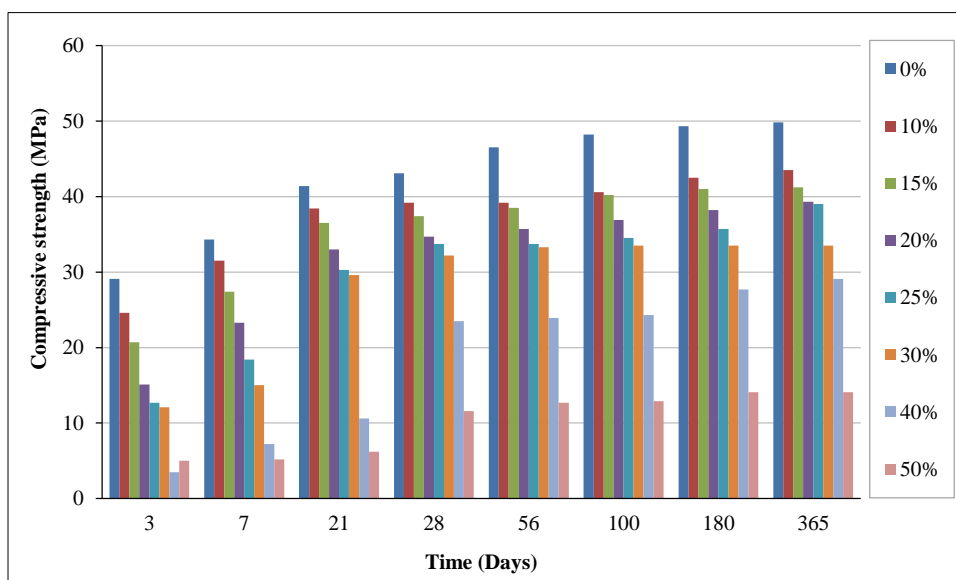
Figure 4. Relation between compressive strength and fly ash content - concrete C 25/30 - Kosovo case. With only 290 kg/m³ of cement content on etalon and adding additive

Analyzing Compressive strength progress vs. curing time is mainly dependent on the hydration rate of cement for etalon, while in the other 21 mixtures, it depends on the combination of hydration of cement + pozzolanic reaction of fly ash, which during this examination, differently from other fly ash types, started in the early ages. So, the progress of strength development in three cases has been continuous and constant since the beginning, while the intensity of strength

increase has decreased continually over time. Indeed, at mixtures with a high content of fly ash (40 and 50%), strength improvement was delayed, but based on the results, the requested quality of concrete was achieved and exceeded in time. While mix design with 30% low CaO fly ash content was achieved for ordinary concrete C 25/30 and high-performance concrete C 50/60 for 180 days, the intensity of strength increase was too low for considering improving strength during a long time of curing [19].
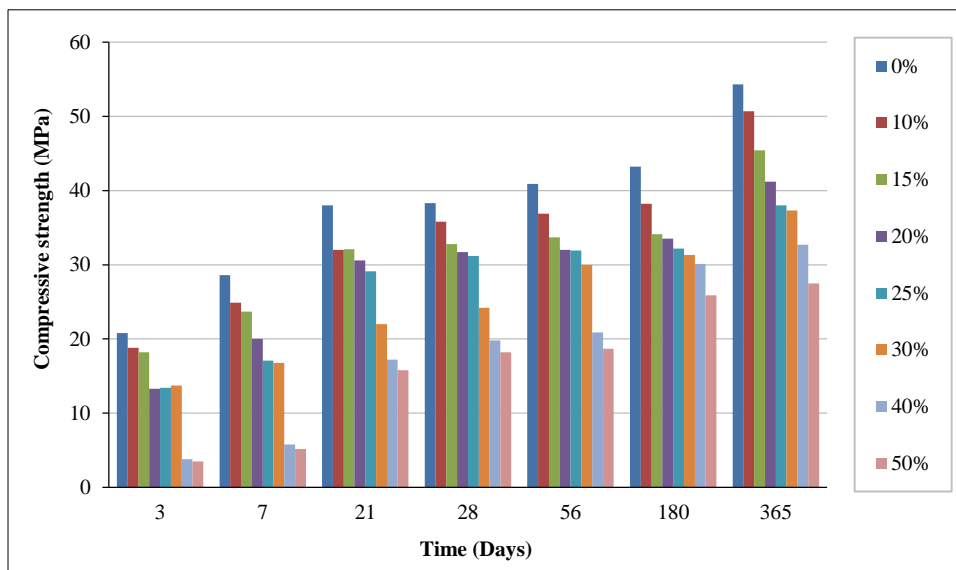
Figure 5. Relation between compressive strength and fly ash content - concrete C 25/30 - Kosovo case
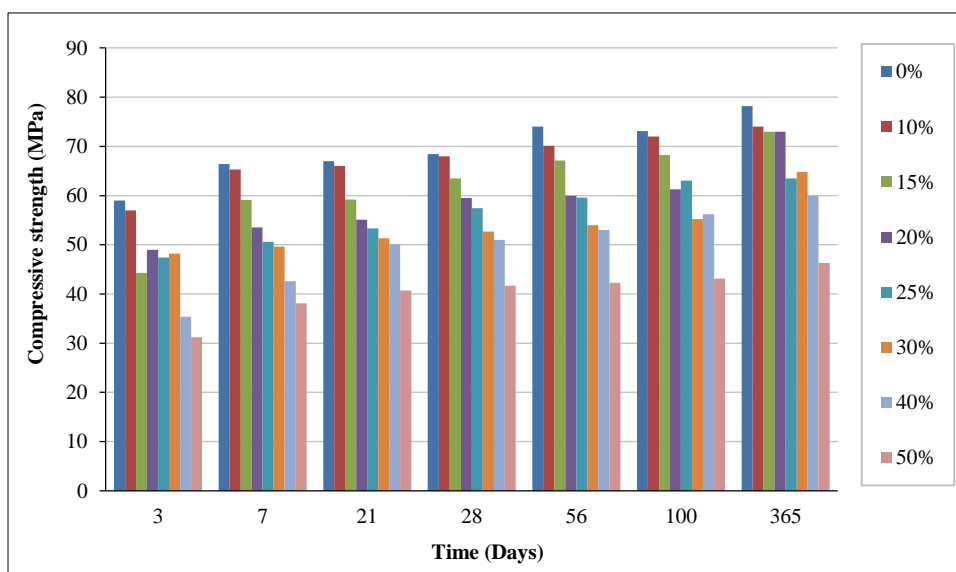
Figure 6. Relation between compressive strength and fly ash content - concrete C 50/60 - Kosovo case

3.2. Standard Consistency and Setting Time

To examine standard consistency, we designed 10 different mixtures of cement and fly ash pastes, starting with (0, 10, 15, 20, 25, 30, 35, 40, 45, and 50%) of the high CaO content of fly ash. Related to the very fine particles of non-class fly ash content, the water requirement was increased. Consequently, increasing fly ash content will also increase water content.

Figure 8 shows that the initial setting time and final setting time are prolonged due to increased water. Differently from expectations and other research, using high CaO fly ash contributes to prolonging the initial setting time more than the final setting time. For instance, in a mixture with 50% fly ash content, the initial setting time was prolonged for 94 minutes, while the final setting time was prolonged for 105 minutes. This is regarding the very high content of CaO as a reactive part of the non-class fly ash content. The very large specific surface of this non-class fly ash helps to develop the hydration process since it is in its early stages. Compared to setting time with low CaO content, where the final setting time was 87 minutes due to the little water requirement and the final setting time was 168 minutes because of the little content of the reactivity substance [19].
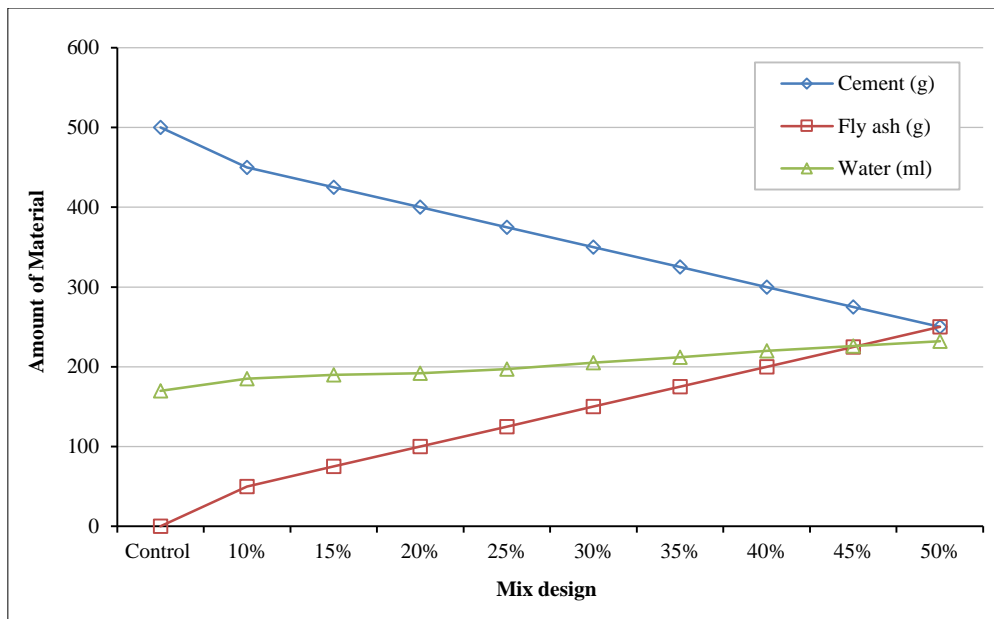
Figure 7. Material used in different mix designs during testing
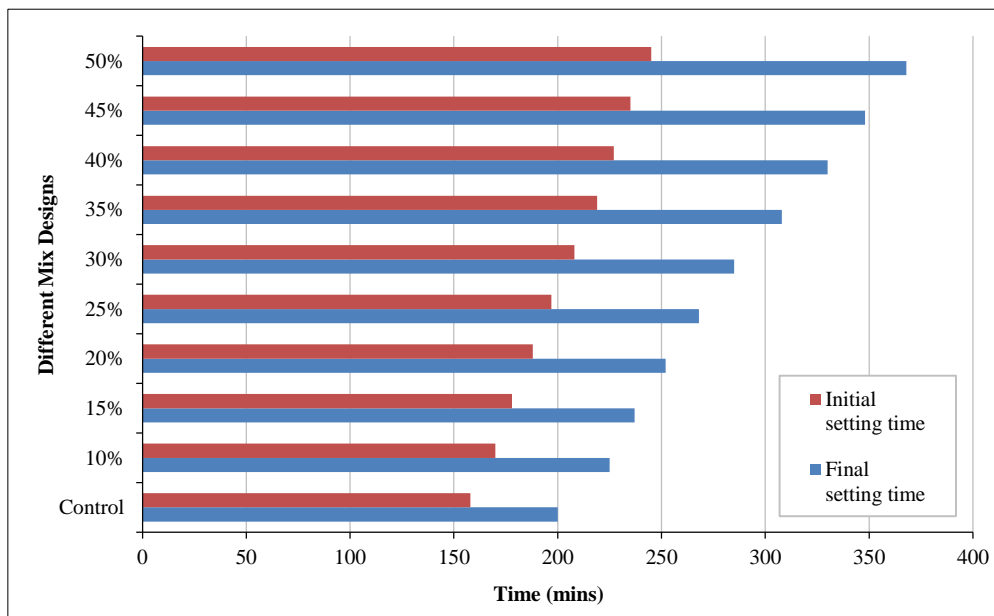
Figure 8. Setting time of fly ash-cement mortar

3.3. Shrinkage

To measure shrinkage, a very sensitive method was established called QUICK for concrete shrinkage examination. Figures 5 and 6 show that weight loss and shrinkage increase as ages increase for control concrete. Fly ash content helps to improve the pore structure of concrete, and this causes fly ash mixtures to shrink less at all ages, and the difference is considerable. Fly ash contributes to closing big pores, so the water is removed very slowly from small pores. During this process, according to capillary stress theory, an increasing internal hydrostatic stress was developed as the capillary pores became smaller. For instance, in a mixture with 10% weight loss, shrinkage was $1700mm \times 10^{-4}$ mixture with 20% fly ash content. And in mix designs with low CaO fly ash content, big pores were not closed, and as a result, water evaporated soon and the stress on capillary pores was very low. So, the examination was short, and the shrinkage was $1150mm \times 10^{-4}$ for the mix design with 20% fly ash; the difference is $550 mm \times 10^{-4}$ [19].

A higher amount of cement content increases the heat of hydration and consequently causes shrinkage. As the amount of fly ash content increases, the shrinkage decreases, and concrete will become compact as a result of improving pore structure by expansive properties of fly ash and the pozzolanic reaction [20, 21].
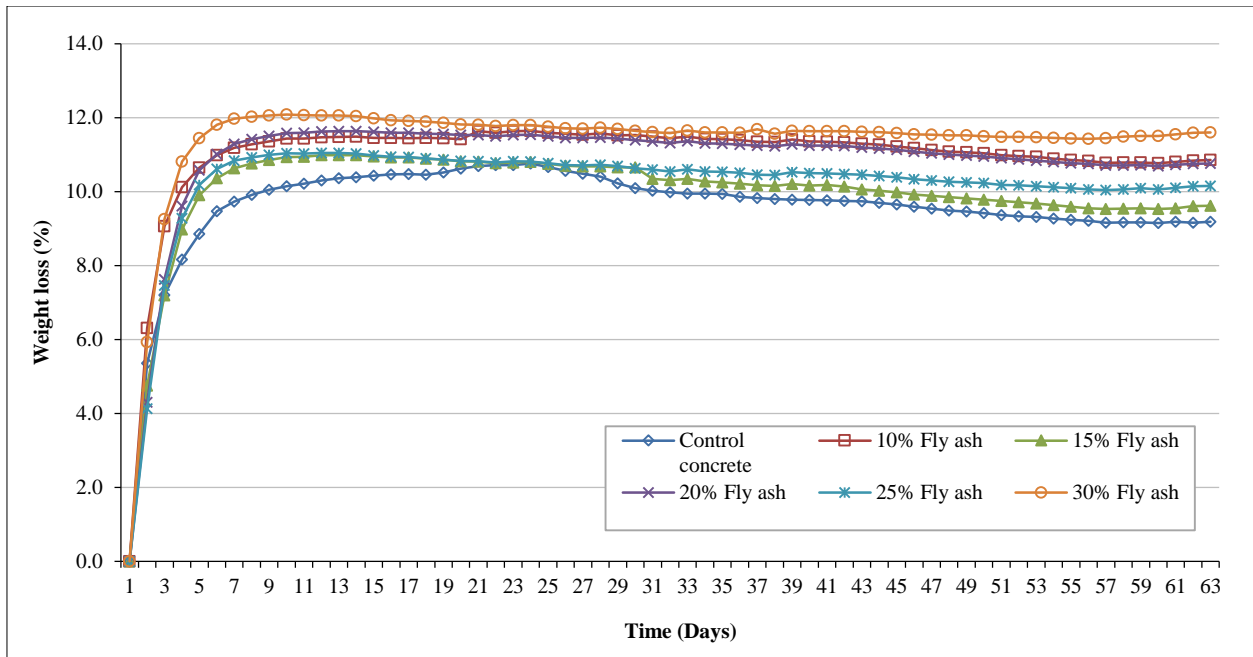
Figure 9. Weight loss of concrete specimens versus time
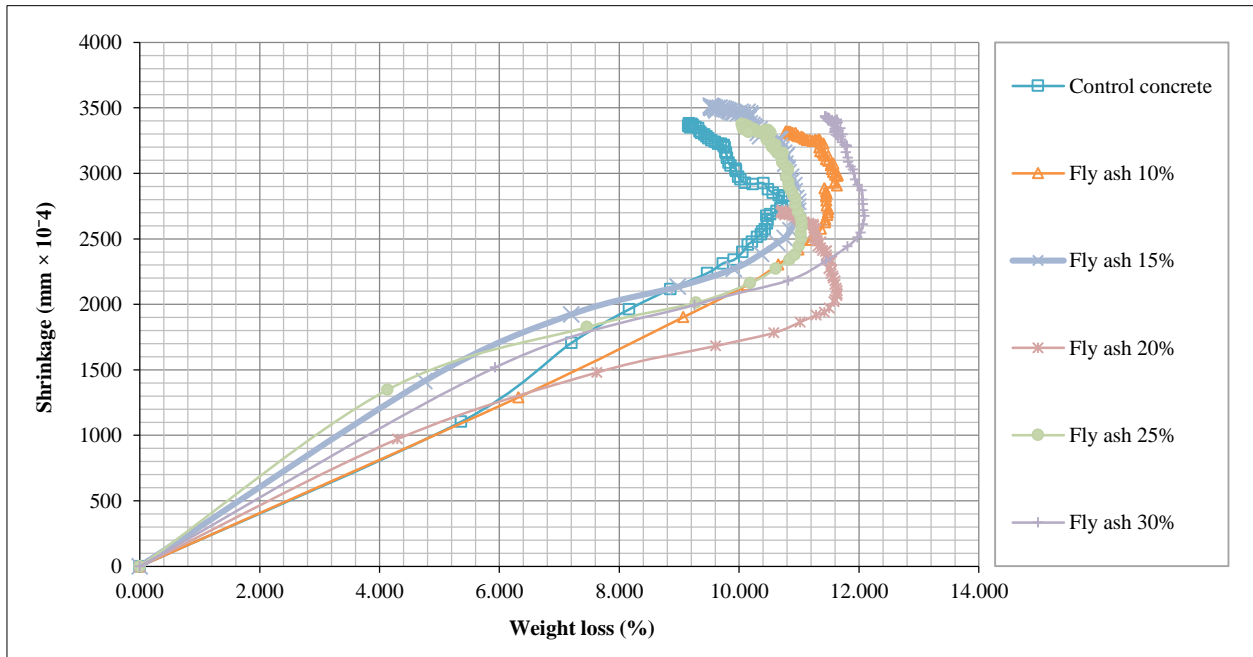
Figure 10. Shrinkage of concrete specimens versus weight loss

4. Conclusion

Developing a sustainable construction industry is very important based on the EPA's agenda to reduce environmental effects and CO_2 emissions. Concrete is the most widely used construction material, and it is still irreplaceable. Using fly ash to decrease cement production until 35–40% means reducing CO_2 release from 8% to 5.2–4.8%, reducing the price of concrete by 40% of its value, and improving the mechanical properties of the product. It is also important to consider the transport distance from the power plant to the construction site. In this case, Kosovo is a small country, and at the same time, 93% of electricity is produced from burning lignite coal in Obiliq, so the amount of fly ash is going to increase in the coming years. Increasing fly ash content implicates increasing water content. It happens with very fine particles of fly ash; that's why the strength progress of concrete takes more time than control concrete, but it is compensated by the high reactivity of the CaO content. The same effect was observed at compressive strength and shrinkage examinations. Due to the very fine particles of fly ash, the rosary shape helps to increase workability by increasing fly ash content, and the mass was sticky without segregation. The high content of CaO in fly ash is a very important component for using it to produce concrete. This contributes to speeding up the hardening process and the properties of the final product.

During the examination of the initial and final setting times, it was observed that the final setting time was prolonged only 10.5% longer than the initial one for a mixture with 50% fly ash content. This effect happened for two reasons: 1) the initial setting time was prolonged regarding the amount of water required to design standard consistency; and 2) the final setting time was fast regarding high pozzolanic activity and the hydration process as a result of the high amount of CaO content. Regarding compressive strength, high CaO content in non-class fly ash has the same effect in three investigated cases. Compressive strength is related to many factors, but according to this examination, incorporating fly ash with very high pozzolanic activity will increase continuously with time. The intensity of the strength increase will decrease with time, but it will not stop, and very good results can be achieved in the long term even with a high content of this industrial waste, up to 40%. The high specific surface area of non-class fly ash particles contributes to improving the pore structure of concrete, and to reduce concrete shrinkage, it can be used as a reducing shrinkage agent. Because of the expansive property, it helps to close the large porosity of the concrete mass, so the water is removed very slowly from small pores, and the amount is very small by inducing high stress. The examination lasted for 61 days, two times longer than in the case of fly ash with low CaO content.

5. Declarations

5.1. Author Contributions

5.2. Data Availability Statement

The data presented in this study are available in the article.

5.3. Funding

5.4. Conflicts of Interest

The authors declare no conflict of interest.

6. References

[1] Thomas, M. D. A. (2007). Optimizing the use of fly ash in concrete. Portland Cement Association, New Jersey, United States

[2] Attarde, S., Marathe, S., & Sil, A. (2014). Utilization of fly ash in construction industries for environment management. International Journal of Environmental, 3(2), 117-121.

[3] Lee, S. H., Sakai, E., Daimon, M., & Bang, W. K. (1999). Characterization of fly ash directly collected from electrostatic precipitator. Cement and Concrete Research, 29(11), 1791–1797. doi:10.1016/S0008-8846(99)00169-6.

[4] Das, B. B., & Pandey, S. P. (2011). Influence of Fineness of Fly Ash on the Carbonation and Electrical Conductivity of Concrete. Journal of Materials in Civil Engineering, 23(9), 1365–1368. doi:10.1061/(asce)mt.1943-5533.0000298.

[5] Sun, Y., & Lee, H. (2020). Research on properties evolution of ultrafine fly ash and cement composite. Construction and Building Materials, 261. doi:10.1016/j.conbuildmat.2020.119935.

[6] Amran, M., Debbarma, S., & Ozbakkaloglu, T. (2021). Fly ash-based eco-friendly geopolymer concrete: A critical review of the long-term durability properties. Construction and Building Materials, 270, 121857. doi:10.1016/j.conbuildmat.2020.121857.

[7] Herath, C., Gunasekara, C., Law, D. W., & Setunge, S. (2020). Performance of high volume fly ash concrete incorporating additives: A systematic literature review. Construction and Building Materials, 258, 120606. doi:10.1016/j.conbuildmat.2020.120606.

[8] Hino Junior, J. R., Balestra, C. E. T., & Medeiros-Junior, R. A. (2021). Comparison of test methods to determine resistance to chloride penetration in concrete: Sensitivity to the effect of fly ash. Construction and Building Materials, 277, 122265. doi:10.1016/j.conbuildmat.2021.122265.

[9] Singh, N. B., & Middendorf, B. (2020). Geopolymers as an alternative to Portland cement: An overview. Construction and Building Materials, 237, 117455. doi:10.1016/j.conbuildmat.2019.117455.

[10] da Silva Magalhães, M., Cezar, B. F., & Lustosa, P. R. (2023). Influence of Brazilian fly ash fineness on the cementing efficiency factor, compressive strength and Young's modulus of concrete. Developments in the Built Environment, 14, 100147. doi:10.1016/j.dibe.2023.100147.

[11] Felix, E. F., Carrazedo, R., & Possan, E. (2021). Carbonation model for fly ash concrete based on artificial neural network: Development and parametric analysis. Construction and Building Materials, 266, 121050. doi:10.1016/j.conbuildmat.2020.121050.

[12] Zhang, C., Fu, J., & Song, W. (2023). Mechanical model and strength development evolution of high content fly ash–cement grouting material. Construction and Building Materials, 398. doi:10.1016/j.conbuildmat.2023.132492.

[13] Nguyen, T. B. T., Saengsoy, W., & Tangtermsirikul, S. (2018). Effect of initial moisture of wet fly ash on the workability and compressive strength of mortar and concrete. Construction and Building Materials, 183, 408–416. doi:10.1016/j.conbuildmat.2018.06.192.

[14] Fernando, S., Gunasekara, C., Law, D. W., Nasvi, M. C. M., Setunge, S., & Dissanayake, R. (2023). Assessment of long term durability properties of blended fly ash-Rice husk ash alkali activated concrete. Construction and Building Materials, 369, 130449. doi:10.1016/j.conbuildmat.2023.130449.

[15] Kasaniya, M., Thomas, M. D. A., & Moffatt, E. G. (2021). Efficiency of natural pozzolans, ground glasses and coal bottom ashes in mitigating sulfate attack and alkali-silica reaction. Cement and Concrete Research, 149. doi:10.1016/j.cemconres.2021.106551.

[16] Andrew, R. M. (2018). Global CO2 emissions from cement production. Earth System Science Data, 10(1), 195–217. doi:10.5194/essd-10-195-2018.

[17] Hossain, M. M., Karim, M. R., Hasan, M., Hossain, M. K., & Zain, M. F. M. (2016). Durability of mortar and concrete made up of pozzolans as a partial replacement of cement: A review. Construction and Building Materials, 116, 128–140. doi:10.1016/j.conbuildmat.2016.04.147.

[18] ASTM C595/C595M-21. (2023). Standard Specification for Blended Hydraulic Cements. ASTM International, Pennsylvania, United States. doi:10.1520/C0595_C0595M-21.

[19] Alaj, A., Krelani, V., & Numao, T. (2023). Effect of Class F Fly Ash on Strength Properties of Concrete. Civil Engineering Journal (Iran), 9(9), 2249–2258. doi:10.28991/CEJ-2023-09-09-011.

[20] Wang, Z. (2011). Influence of fly ash on the mechanical properties of frame concrete. Sustainable Cities and Society, 1(3), 164–169. doi:10.1016/j.scs.2011.06.001.

[21] Aslani, A., Hachem-Vermette, C., & Zahedi, R. (2023). Environmental impact assessment and potentials of material efficiency using by-products and waste materials. Construction and Building Materials, 378. doi:10.1016/j.conbuildmat.2023.131197.
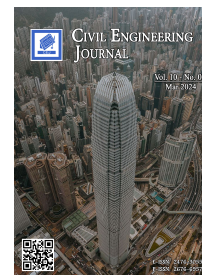
Evaluating Groundwater Quality Using Multivariate Statistical Analysis and Groundwater Quality Index

Nguyen Quoc Pham [1], Giao Thanh Nguyen [2*]

[1] Faculty of Agriculture and Environmental Resources, Dong Thap University, Dong Thap, 81000, Vietnam.

[2] College of Environment and Natural Resources, Can Tho University, Can Tho 900000, Vietnam.

Abstract

Under pressure from surface water pollution and climate change, groundwater becomes a critical water source. Information on groundwater quality could contribute to effective groundwater management. This study was carried out to utilize multivariate statistical analysis and the groundwater quality index (GWQI) to evaluate groundwater quality in Ca Mau Province, Vietnam. Twenty-five groundwater samples from residential-urban areas, cemetery areas, landfill areas, and saline intrusion areas were collected for this study. Groundwater quality was evaluated using the National Technical Regulation on Groundwater Quality (QCVN 09-MT:2015/BTNMT) and GWQI. Principal component analysis (PCA) was used to identify potential polluting sources and key variables influencing groundwater quality. Cluster analysis (CA) was applied to cluster groundwater quality, and the sites were recommended for future monitoring. The results revealed that NH_4^+-N contaminated groundwater in the landfill area, while the saline intrusion area was polluted by TDS and NH_4^+-N. The groundwater quality classified as excellent, good, poor, and very poor accounted for 44, 40%, 12%, and 4%, respectively. Cluster analysis divided groundwater quality into four groups, mainly based on the presence of NH_4^+-N and TDS. Nine groundwater sampling locations could be removed from the current groundwater quality program but still ensuring representativeness as a result of CA. PCA proposed two main sources of variation in groundwater quality at each residential-urban area: the cemetery area, the landfilling area, and the saline intrusion area. The groundwater parameters (i.e., pH, TDS, permanganate index, NH_4^+-N, NO_3^--N, and Fe) should be continued to monitor. Domestic and industrial wastewater discharge, leachate from cemeteries and landfills, the nature of groundwater aquifers, and seawater intrusion could be potential sources of groundwater variation. The current findings provide scientific information for local environmental authorities to manage and monitor groundwater quality in the study area.

Keywords: Ammonium; Ca Mau Peninsula; Groundwater Quality Index (GWQI); Multivariate Analysis.

1. Introduction

Surface water pollution, climate change-induced drought, and sea level rise lead to groundwater become more important for human beings and ecosystems [1–5]. Groundwater has been used for various purposes, such as domesticity, irrigation, transportation, and industry [6–9]. The benefit of groundwater use to ecosystems and human beings is very huge [10, 11]. However, groundwater quality has been influenced by both natural and anthropogenic activities [8, 9, 12]. The natural processes influencing groundwater quality include groundwater recharge, rock-water interactions, mineral weathering, and contaminated water from the adjoining aquifer [8, 9, 13]. Anthropogenic activities include improper groundwater exploitation, intensive applications of agrochemicals, industrial production,

waste and wastewater discharge, and urbanization [8, 12, 14]. Former studies presented that groundwater quality is polluted. For instance, Giao and Nhien (2023) [15] reported that groundwater quality in the Vietnamese Mekong Delta has been polluted by heavy metals and coliforms, and the causes of pollution may be from improper treatment of waste in domestic activities, agricultural and industrial production. The study by Laonamsai et al. (2023) [8] also found that Zn, Hg, Pd, Fe, and Mn contaminated groundwater quality in Thailand. The potential sources of groundwater pollution in Thailand were identified as untreated sewage discharge and fertilizer usage, in addition to the characteristics of geological formations. The other study found that groundwater was contaminated by iron, manganese, aluminium, and organic matter, and the significant origins of contaminants are from agriculture (the use of fertilizers and pesticides), urban waste, and industry [12]. Consumption of contaminated groundwater may pose many risks to human health, such as diarrhea, vomiting, shortness of breath, splenic hemorrhage, blue baby syndrome, or methemoglobinemia [16, 17].

Groundwater quality monitoring plays a crucial role in pollution prevention. The monitoring data (including sampling sites, parameters, and frequencies) could provide useful information for the identification of sources of groundwater variations. This information is required for the planning of groundwater usage. One of the basic ways to evaluate the characteristics of groundwater quality is to compare individual measured concentrations of groundwater parameters to corresponding values regulated by national or international standards [15, 18]. For the overall groundwater quality that is presented for a well or an aquifer, the groundwater quality index (GWQI) is used. GWQI calculation requires the use of a set of preidentified groundwater quality data, so the groundwater quality between space and time is easily compared and ranked [8, 9, 15, 19]. GWQI has been widely applied in several former studies [3, 8, 9, 12, 13, 15]. Recently, multivariate statistical methods, including principal component analysis (PCA) and cluster analysis (CA), have also been widely applied in studying groundwater quality [3, 18, 19]. PCA is used to reduce data size, providing information on potential polluting sources and key variables influencing groundwater quality [3, 20]. CA is utilized to cluster groundwater quality parameters into various groups based on the similarities or dissimilarities between space and time of the identified groundwater quality variables [3, 13, 15, 18]. PCA and CA could be used simultaneously to recommend the site, the parameters, and the frequencies of environmental quality monitoring, including groundwater.

Ca Mau Peninsula, a coastal province, is one of the five major regions of the Mekong Delta of Vietnam (1.6 million hectares, accounting for 43% of the total area of the Mekong Delta), playing an important role in the economic and social development of the region. With rapid social and economic growth, the demand for water use significantly increases. However, surface water in Ca Mau has been seriously polluted by waste discharge from industrial zones, aquaculture, agricultural, residential, and landfills [21, 22]. Therefore, groundwater has been becoming more important for water sources for the production and daily activities in Ca Mau province. Several studies have been carried out to evaluate groundwater quality in the Vietnamese Mekong Delta [15, 18, 23, 24]; however, information on groundwater quality in Ca Mau is limited. This study is conducted to evaluate groundwater quality in Ca Mau province using national technical regulations on groundwater quality and the groundwater quality index (GWQI). In addition, CA and PCA were also utilized to cluster groundwater quality and identify potential polluting sources affecting groundwater quality in the study area. The findings of the current study could contribute to groundwater quality monitoring and pollution prevention. The structure of this article comprises of the abstract, introduction, materials and methods, results and discussion, conclusion, and references.

2. Research Methodology

2.1. Description of the Study Areas

Ca Mau Peninsula is the southernmost land in the Mekong Delta region, with an area of about 1.6 million hectares, surrounded by the East and West seas. The region has an interlaced and interwoven system of rivers and canals, accounting for about 3.02% of the natural area, in which there are many large rivers with deep water levels, leading to alluvial deposits inland such as the Cua Lon River, Ganh Hao, Bay Hap, Song Doc, and Cai Tau [25]. With an average elevation of 0.5–1.5 m above sea level and a 254 km-long coastal area, there are three sides of the East, South, and Southwest, which are influenced by two tidal regimes of the West Sea (irregular tides) and the sea. In the winter, Ca Mau is considered to be the most severely affected area by saline intrusion. Along with the process of socio-economic development, the surface water of the region has been significantly polluted since groundwater sources have become an important source of clean water for daily life and industrial activities. According to the survey results of the Vietnam Geological Map Federation, the area's groundwater has relatively large reserves. The potential exploitation reserve of groundwater on the Ca Mau Peninsula is about 11,456,479 m^3 per day. In addition, according to the statistics of the whole Ca Mau Peninsula, the area that can be exploited for pale groundwater is 13,901.9 km^2 (accounting for 83.4%), and the area of saline aquifers is 2,758.1 km^2 (accounting for 15.6%). According to hydrogeological characteristics of the area, there are all 7 aquifers, including Holocene aquifer (qh), Upper Pleistocene (qp_3), Upper Middle Pleistocene (qp_{2-3}), Lower Pleistocene (qp_1), Middle Pliocene (n_2^2), Lower Pliocene (n_2^1), and Upper Miocene (n_1^3) [25].

2.2. Description of Groundwater Sampling and Analysis

Groundwater quality data were collected from the Department of Environment and Natural Resources, Ca Mau Province, Vietnam. Twenty-five groundwater samples (GW1-GW25) were collected at 9 districts, with a frequency of monitoring 3 times per year (June, September, and December) in 2022. The monitoring period for the first phase was from June 21 to 24, 2022. Four areas are subjected to groundwater sampling, including residential-urban areas (GW1-GW8), cemetery areas (GW9-GW17), landfills (GW18-GW22), and areas affected by saline intrusion (GW23-GW24). Groundwater samples were collected and stored in PE plastic bottles, refrigerated or preserved with chemicals to be transported to the laboratory as soon as possible, ensuring the method of sampling and preserving samples according to TCVN 6663-1:2011, TCVN 6663-3:2016, and TCVN 6663-11:2011. The locations of groundwater samples are detailed in Figure 1 and Table 1. Six physical and chemical parameters of groundwater, including pH, total dissolved solids (TDS), permanganate index (PI), ammonium (NH_4^+-N), nitrate (NO_3^--N), and iron (Fe), were examined. The pH parameters were measured directly in the field according to TCVN 6492:2011 (ISO 10523:2008) and SMEMW 4500.B:2012. The parameters comprising TDS, permanganate index, NH_4^+-N, NO_3^--N, and Fe were analyzed in the laboratory according to standard methods [26]. Specifically, the TDS was determined by the drying method at 180ºC according to the SMEWW 2540.C:2012 standard. The permanganate index is determined according to TCVN 6186:1996 (ISO 8467:1993 (E)). Determination of NH_4^+-N concentration by manual spectrometric method according to TCVN 6179-1:1996 (ISO 7150-1:1984E). NO_3^--N was determined by the spectrophotometric method using 2.6-dimethylphenol (TCVN 7323-1:2004, ISO 7890-1:1986). Determination of iron by spectrometric method using 1.10-phenanthroline reagent (TCVN 6177:1996, ISO 6332:1988). The analysis of groundwater samples was carried out by the Southern Environment and Natural Resources One Member Limited Liability Company.
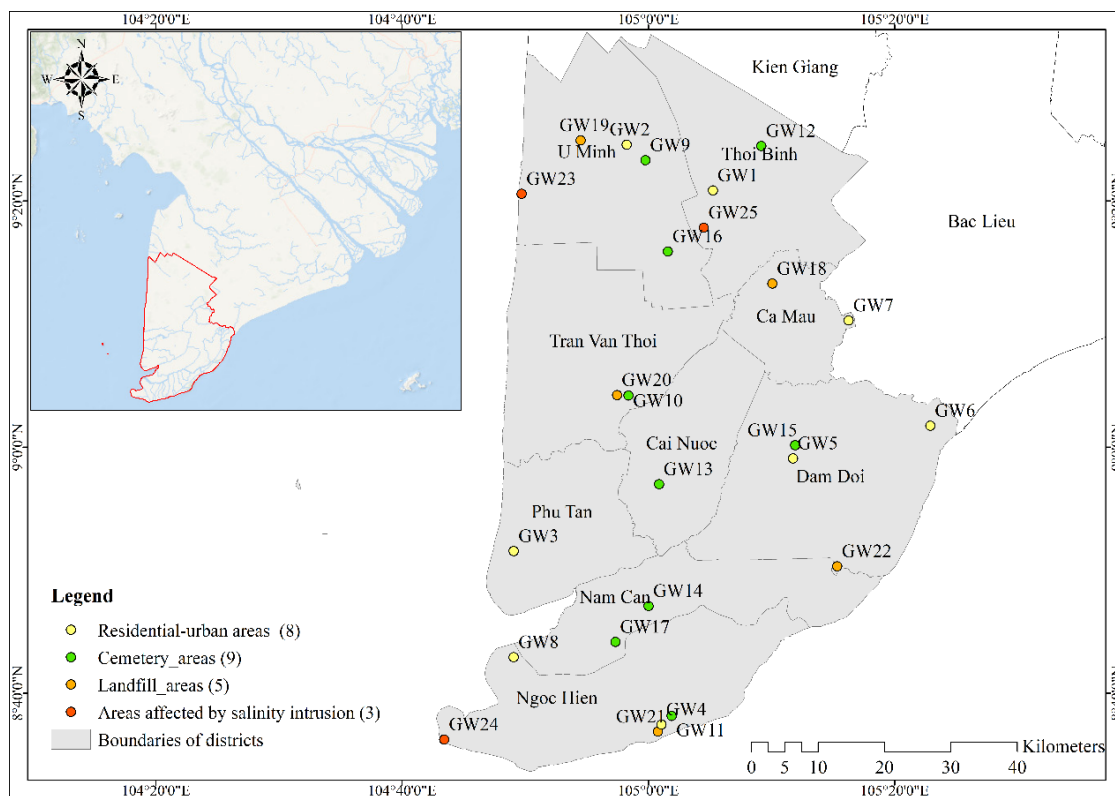
Figure 1. Map of the sampling locations in the study area

Table 1. Brief description of the sampling locations

Areas	Code	Location
	GW1	Area 4, Thoi Binh town, Thoi Binh district
	GW2	Area 2, U Minh town, U Minh district
	GW3	Area 7, Cai Doi Vam town, Phu Tan district
	GW4	Area 1, Thi Trac Rach Goc, Ngoc Hien District
Residential and urban	GW5	Dam Doi town, Dam Doi district
	GW6	Ganh Hao estuary area, Tan Thuan commune, Dam Doi district
	GW7	Tac Van Market, Tac Van Commune, Ca Mau City
	GW8	Residential Area 1, Cai Doi Vam Town, Phu Tan District

	GW9	Cemetery area in Hamlet 1, Nguyen Phich Commune, U Minh District
	GW10	Cemetery area of Tran Van Thoi district
	GW11	Cemetery area cluster 6, TT. Rach Goc, Ngoc Hien district
	GW12	Nha Dao - the land of the Holy Family of Huyen Su in Hamlet 3, Tri Phai Commune, Thoi Binh District
Cemetery	GW13	Cemetery area of Cai Nuoc district
	GW14	Cemetery area of Nam Can district
	GW15	Area near Dam Doi district cemetery
	GW16	The area of people's cemetery in Tan Phu hamlet, Khanh An commune, U Minh district
	GW17	Area of Truong Duc cemetery, Lam Hai commune, Nam Can district
	GW18	The concentrated landfill area of Ca Mau province, Tan Xuyen ward, City. Ca Mau
	GW19	The area of the cluster landfill site 2. U Minh town, U Minh district
Landfill	GW20	The landfill area of cluster 5, Tran Van Thoi town, Tran Van Thoi district
	GW21	The landfill area of cluster 1, Rach Goc town, Ngoc Hien district
	GW22	Landfill area in Hai An hamlet, Nguyen Huan commune, Dam Doi district
Areas affected by salinity intrusion	GW23	Hamlet 3, Khanh Hoi Commune, U Minh District
	GW24	Mui Hamlet, Dat Mui Commune, Ngoc Hien District
	GW25	Hamlet 2, Hang Vinh commune, Nam Can district

2.3. Data Analysis

The difference in groundwater quality parameters (pH, TDS, permanganate index, NH_4^+-N, NO_3^--N, and Fe) at various subject areas was examined using one-way analysis of variance (One-way ANOVA), followed by Duncan's test at a significant level of 5% ($p<0.05$) using SPSS software version 20.0. The groundwater quality was evaluated by comparing the measured data to the one that is being regulated in the National Technical Regulation on Groundwater Quality (QCVN 09-MT:2015/BTNMT) [27]. The limit values of groundwater parameters according to QCVN 09-MT:2015/BTNMT are detailed in Table 2.

Table 2. Limit values of the used groundwater parameters in this study

No.	Groundwater parameters	Limit values
1	pH	5.5-8.5
2	TDS	1500
3	Permanganate index	4
4	NH_4^+-N	1
5	NO_3^--N	15
6	Fe	5

Overall groundwater quality in the study area was assessed using groundwater quality index (GWQI). GWQI was calculated using Equation 1. In this study, the GWQI index was calculated from six parameters, including pH, TDS, permanganate index, NH_4^+-N, NO_3^--N and F.

$$GWQI = \sum_n^{i=1} \left[\left(\frac{W_i}{\sum_n^{i=1} W_i} \right) \times \left(\frac{C_i}{S_i} \times 100 \right) \right] \tag{1}$$

where: C_i is the concentration of each parameter, S_i is the limit value of each parameter specified in QCVN 09-MT:2015/BTNMT, Wi is the weight of each parameter calculated by Equation 2.

$$W_i = \frac{\frac{1}{\sum_n^{i=1} \left(\frac{1}{S_i} \right)}}{S_i} \tag{2}$$

GWQI classifies groundwater quality into five levels, which are presented in Table 3.

Table 3. Classification of groundwater quality based on GWQI

No.	Values	Groundwater quality	Colour
1	GWQI < 50	Excellent	
2	50 < GWQI < 100	Good	
3	100 < GWQI < 200	Poor	
4	200 < GWQI < 300	Very poor	
5	GWQI > 300	Unsuitable for drinking	

In this study, principal component analysis (PCA) was used to analyze 6 observed chemical and physical variables related to groundwater quality in Ca Mau. PCA is one of the widely used multivariate statistical techniques in environmental quality assessment and description. This method allows us to reduce the initial large data set into exploratory principal components (PCs) containing the most critical parameters affecting environmental quality [3]. When analyzing PCA, the number of PCs retained to explain the change in groundwater quality is mainly based on Eigenvalues, and the larger the PC value, the greater the contribution to the change in environmental quality and a collection of the main pollution sources for water bodies. Usually, principal components with Eigenvalues greater than 1 will be retained for evaluation [3, 28, 29]. The main components in this study were determined by varimax rotation. When choosing environmental variables correlated with each PC, the factor load is divided into 3 levels: (1) strong when > 0.75; (2) medium when fluctuating in the range of 0.75–0.5; and (3) weak when fluctuating in the range of 0.5–0.3 [3]. Cluster analysis (CA) is one of the multivariate statistical methods that group monitoring objects based on their attributes [29]. In this study, CA is applied to assess the level of groundwater pollution and group monitoring sites with the same physio-chemical characteristics in one group and different physio-chemical characteristics in different groups. Cluster analysis was performed on normalized data using the Ward method, and Euclidean distance was used to measure the similarity between groundwater quality variables [14, 29]. The resulting clusters of CA are presented in the form of dendrograms, clearly reflecting the level of water pollution and the similarity between monitoring locations. PCA and CA in this study were performed using PRIMER software version 5.2.
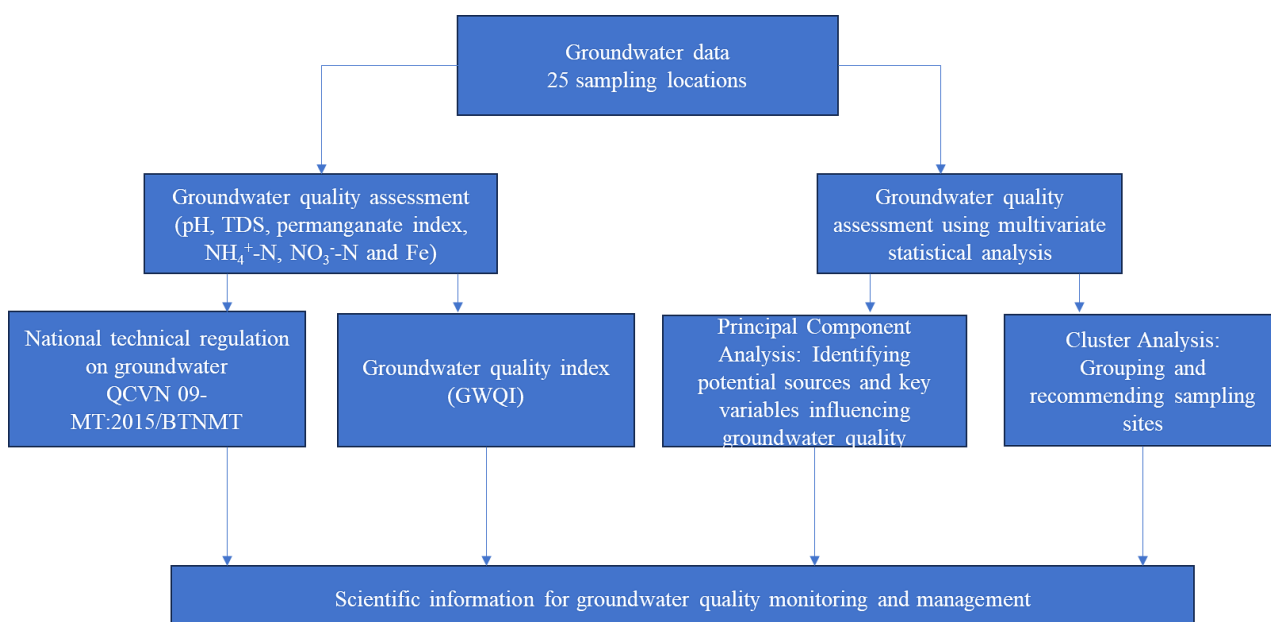
Figure 2. Flow chart of the study

3. Results and Discussion

3.1. Physical and Chemical Characteristics of Groundwater in the Ca Mau Peninsula

pH is one of the important water quality parameters that determines the alkalinity or acidity of groundwater [30]. The results showed that the average pH value in groundwater at four impact areas fluctuated in the range of 7.64 ± 0.45-8.04 ± 0.36, reaching an average of 7.81 ± 0.46. As can be seen, the groundwater in the study area was slightly alkaline (Figure 3). pH in groundwater at the landfill area was the lowest and had a statistically significant difference ($p<0.05$) with that at the cemetery area. Low pH in groundwater at landfill sites may be due to groundwater acidification by low-pH leachate from landfills [31]. Compared to the national technical regulation on groundwater quality, the pH in groundwater in the study areas was acceptable. In addition, the pH in groundwater in Ca Mau is also within the permissible level in drinking water prescribed by the Ministry of Health (2018) [32]. Former studies also measured pH values in groundwater. For example, pH in groundwater wells in the Ho Chi Minh City area was in the range of 3.4–7.4 [28], in the areas of Ba Ria – Vung Tau, it was 4.30–7.80 [19], and in the areas of Ha Nam Province, it was 6.19–7.33 [33]. A previous study also found that groundwater pH in the Mekong Delta of Vietnam was in the range of 6.54–7.76 [15]. Other studies from outside Vietnam found pH values in groundwater from 5.91 to 7.24 [3], between 7.03 and 8.50 [9], and in the range of 6.76–9.56 [34]. pH in groundwater may be acidic or alkaline, depending on the presence of chemical composition. The age of groundwater, mineralogy of aquifer materials, and geochemistry of groundwater systems have a strong influence on pH in groundwater [35].
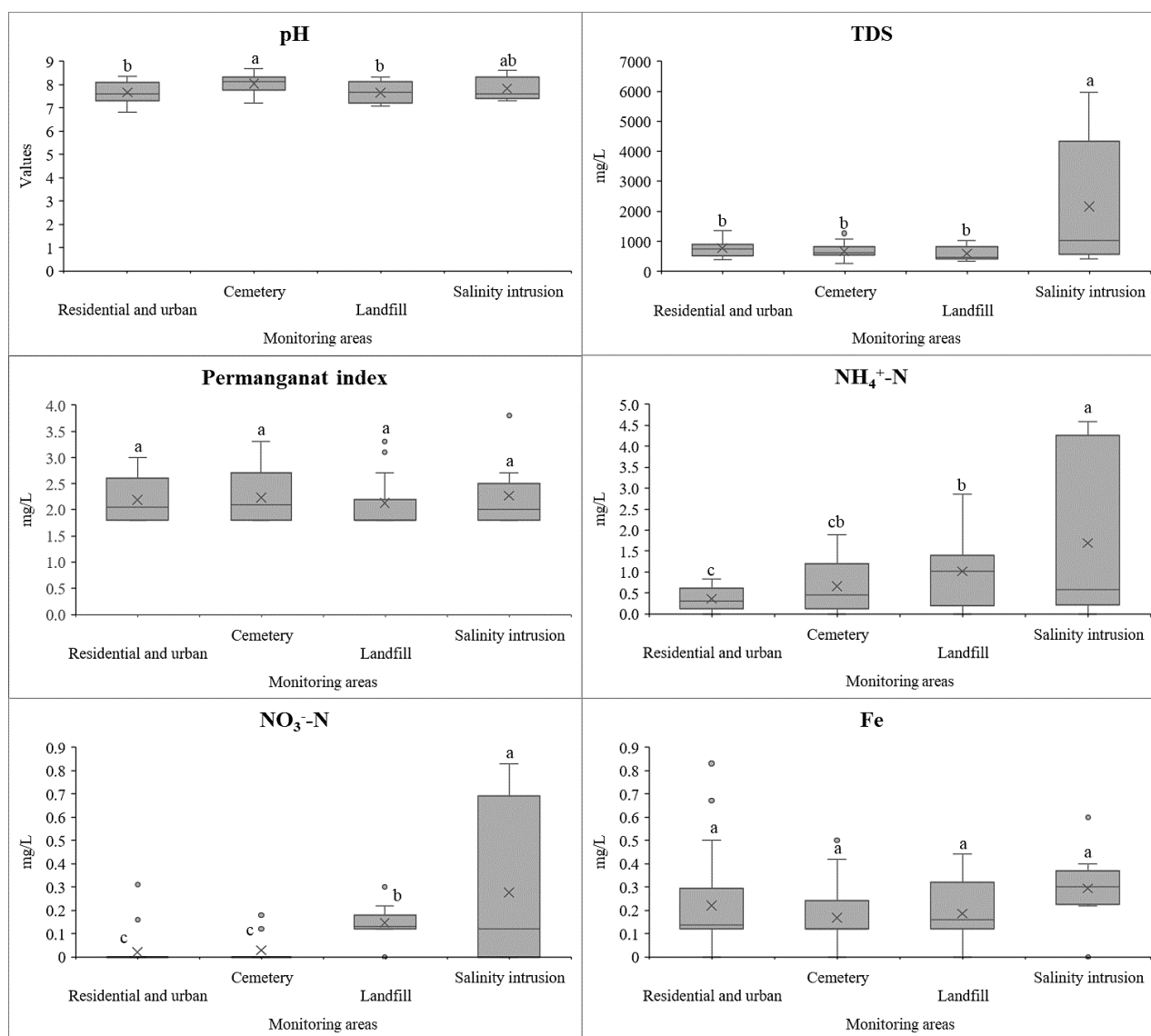
Figure 3. Spatial variations of groundwater parameters in the study areas

The total dissolved solids (TDS) concentration in groundwater in the study area was relatively high; there was a large variation between the sampling areas. The TDS concentration reached the minimum value of 588.07±227.38 mg/L at the landfill area and reached the maximum value of 2153.11±2113.31 mg/L in the area affected by saline intrusion (Figure 3). Statistical analysis results showed that TDS concentration in groundwater in areas affected by salinity intrusion was significantly different ($p<0.05$) than that from the remaining areas (Figure 3). This result indicated that groundwater in certain areas of Ca Mau Province is influenced by salt concentration. A former study found that coastal aquifers could be influenced by seawater intrusion and the horizontal movement of saline water [36]. A former study found that groundwater in the Mekong Delta had TDS values of 544–4194 mg/L [15]. In coastal areas, TDS in groundwater was found at 281–8055 mg/L in Soc Trang province [18, 37] and 286-715 mg/L in Bac Lieu province [38]. In the Mekong Delta of Vietnam, high TDS could be associated with the impact of agrochemicals, wastewater leachate, and saline intrusion. Outside Vietnam, TDS in groundwater was measured at concentrations of 149.76±132.66-202.33±211.60 mg/L [3], 223-1372 mg/L [13]. As can be seen, TD varies spatially. TDS concentrations depend on groundwater aquifer characteristics, pollution sources, and saline water intrusion. TDS is used as a factor for the classification of groundwater into fresh hard water and medium salt hard water [39]. Compared with QCVN 09-MT:2015/BTNMT [27], TDS concentrations in groundwater in residential-urban areas, cemeteries, and landfilling sites were still within the allowable limits, while the TDS in the area affected by saline intrusion exceeded the allowable limit by 1.4 times.

Permanganate index (PI) is often used as an indicator to assess the pollution level of dissolved organic compounds in water. A high permanganate index indicates that the water has been contaminated with organic substances [40]. In this study, PI ranged from 2.13±0.5 to 2.27±0.65 mg/L, averaged at 2.2±0.47 mg/L (Figure 3). The values of PI in groundwater in all sampling areas were not statistically significant ($p>0.05$) (Figure 3). Compared with QCVN 09-MT:2015/BTBMT [27], PI in all groundwater samples was less than 4 mg/L, within the allowable limit. However, PI in

groundwater in the study area exceeded the limit value in the regulation of QCVN 01-1:2018/BYT (PI = 2 mg/L) [32]. This could mean that the groundwater in the study area is organically contaminated and unsuitable for drinking. The former study measured PI in groundwater, and it was found to be lower than that of the present study. Hung et al. (2018) [41] found PI of 0.17±0.0058-2.63±0.058 mg/L in groundwater in Trang Bang district, Tay Ninh province, while PI measured at 0.47±0.15-0.63±0.25 mg/L in groundwater in Pleiku city, Gia Lai province [42]. The variation of PI in groundwater could be attributed to the presence of microorganisms due to the occurrence of nutrients [43]. The death of microorganisms could consequently release organic matter, resulting in PI variation. In addition, dissolved organic matter from agricultural and landfill areas could also percolate into groundwater, resulting in high PI [44, 45].

Figure 3 shows that NH_4^+-N concentrations in groundwater in the study areas in the range of 0.36±0.26 to 1.69±2.03 mg/L and averaged 0.76±0.94 mg/L. The highest NH_4^+-N concentrations in groundwater were found in areas influenced by saline intrusion, while the lowest were found in residential-urban areas. NH_4^+-N concentrations in the areas of landfill and saline intrusion exceeded the limit of QCVN 09-MT:2015/BTNMT [27] by 1.01 and 1.69, respectively. Notably, the concentration of NH_4^+-N in all monitored impact areas exceeded the allowable limit of QCVN 01-1:2018/BYT [32] by 1.2 to 5.6 times on the quality of clean water used for domestic purposes. Sources of NH_4^+-N contaminating groundwater could be inappropriate discharges of waste and wastewater from domestic and industrial activities, landfill leachate, and the application of fertilizers in agriculture [15, 20, 23, 28, 37, 46]. NH_4^+-N in groundwater was found up to 28.2 mg/L in Duy Tien district in Ha Nam province [33], at 16,086 mg/L at Xuan Mai town in Hanoi [47], and at 57.3 mg/L at Valley Kathmandu in Nepal [48]. Other studies found NH_4^+-N concentrations in groundwater in the Mekong Delta, Vietnam, at 0.24–10.8 mg/L [18], 0.07–2.55 mg/L in An Giang groundwater [24], and 0–7 mg/L in Tra Vinh groundwater [23]. High concentrations of NH_4^+-N in groundwater cause an unpleasant taste and odour, reduce the chlorination effect, and increase the likelihood of pathogen contamination during water distribution [7]. High levels of NH_4^+-N in the human body could lead to blue baby syndrome, liver damage, and stomach cancer [46].

The concentrations of NO_3^--N ranged from 0.02±0.07 mg/L to 0.28±0.35 mg/L, and the average value was 0.08±0.16 mg/L (Figure 3). The highest concentration of NO_3^--N was found in groundwater samples influenced by saline intrusion. Meanwhile, the lowest concentration of NO_3^--N was found in the saline intrusion areas. NO_3^--N was also found in groundwater in the Vietnamese Mekong Delta in several former studies. The mean in NO_3^--N in the provinces of An Giang, Dong Thap, and Kien Giang were 0-1.32 mg/L, 0.73-2.23 mg/L, and 0-0.60 mg/L, respectively [15], in groundwater in Soc Trang province was 0.1-0.260 mg/L. This study found that NO_3^--N concentrations in all sampling wells are within the limits of QCVN 09-MT:2015/BTNMT (15 mg/L) [27] and QCVN 01-1:2018/BYT (2 mg/L) [32]. Sources of NO_3^--N variation in groundwater may be from nitrogen fertilizer application, livestock waste, landfill leachate, and industrial waste [20, 23, 49]. The nitrate concentration in groundwater found in this study was lower than in other studies. However, some other studies have found that nitrate is very high in groundwater. NO_3^--N concentrations were found at 1.94 to 5.89 mg/L in the northeast part of Chengdu Plain in the Sichuan Basin [20] and at 0.12–11.51 mg/L in Uva province, Sri Lanka [30]. Groundwater with a high concentration of nitrate could result in health issues such as gastric cancer, birth malformation, hypertension, and methemoglobinemia [23, 50].

Iron is often dissolved in groundwater, causing the water to have scale, color, and an unpleasant taste [51]. In the Ca Mau peninsula, the Fe concentration in groundwater was very low, ranging from 0.17±0.13 mg/L to 0.29±0.16 mg/L, with an average of 0.2±0.17 mg/L. The statistical analysis showed that the Fe concentration at four different impact areas was not statistically significant (p>0.05) (Figure 3). The former study reported that Fe in groundwater in some provinces in the Mekong Delta, Vietnam, was 0.02±0.02 to 3.38±1.09 mg/L [15]. Groundwater in Soc Trang province had a significant concentration of Fe (0.04–19.8 mg/L, averaged at 2.17 mg/L) [37]. Other studies also found high Fe concentrations in groundwater [28, 33, 51]. The Fe concentration in groundwater in the former study was higher than that in the current study. The source of Fe formation in groundwater is mainly natural, such as the weathering of iron-rich minerals (hematite, goethite, magnetite, and siderite) [52]. However, the hydroxylation of iron ions occurs under anaerobic conditions, leading to iron formation in water [53]. Fe concentrations in groundwater in the study area were still within the allowable limit of QCVN 09-MT:2015/BTNMT [27]. However, Fe at the saline intrusion areas was exceeding the limit of QCVN 01-1:2018/BYT (0.3 mg/L) [32]. Fe at high concentrations (> 0.3 mg/L) causes human health risks such as hemochromatosis, leading to organ damage, cirrhosis, hepatocellular carcinoma, and hemosiderosis [53].

3.2. Potential Sources of Groundwater Quality Change

Principal component analysis showed that two main sources have an influence on groundwater in the study area (Figure 4 and Table 4). In this study, the retained PCs to explain the groundwater quality change had Eigenvalues greater than 1 [14, 53]. Two PCs were formed in residential-urban areas, cemeteries, landfills, and areas affected by the saline intrusion, explaining 79.6%, 85.2%, 89.2%, and 100% of the total variance, respectively. According to Elemile et al. (2021) [3], a total variance of PCs greater than 70% is acceptable. At the same time, the study examined the relevance of PCA through the Kaiser-Meyer-Olkin index (KMO) and Bartlett test. The significant KMO value means that the factor analysis is appropriate and the Bartlett test is statistically significant (p < 0.05); the observed variables are

correlated with each other in the population. Analysis results at each impact area, including residential-urban areas (KMO = 0.633; p = 0.01), cemetery (KMO = 0.5; p = 0.00), landfills (KMO = 0.544; p = 0.00), and areas affected by saline intrusion (KMO = 0.5; p = 0.00), indicated that all the values of KMO were equal to or greater than 0.5 and the p-value was less than 0.05. So, the results of the PCA analysis were suitable.
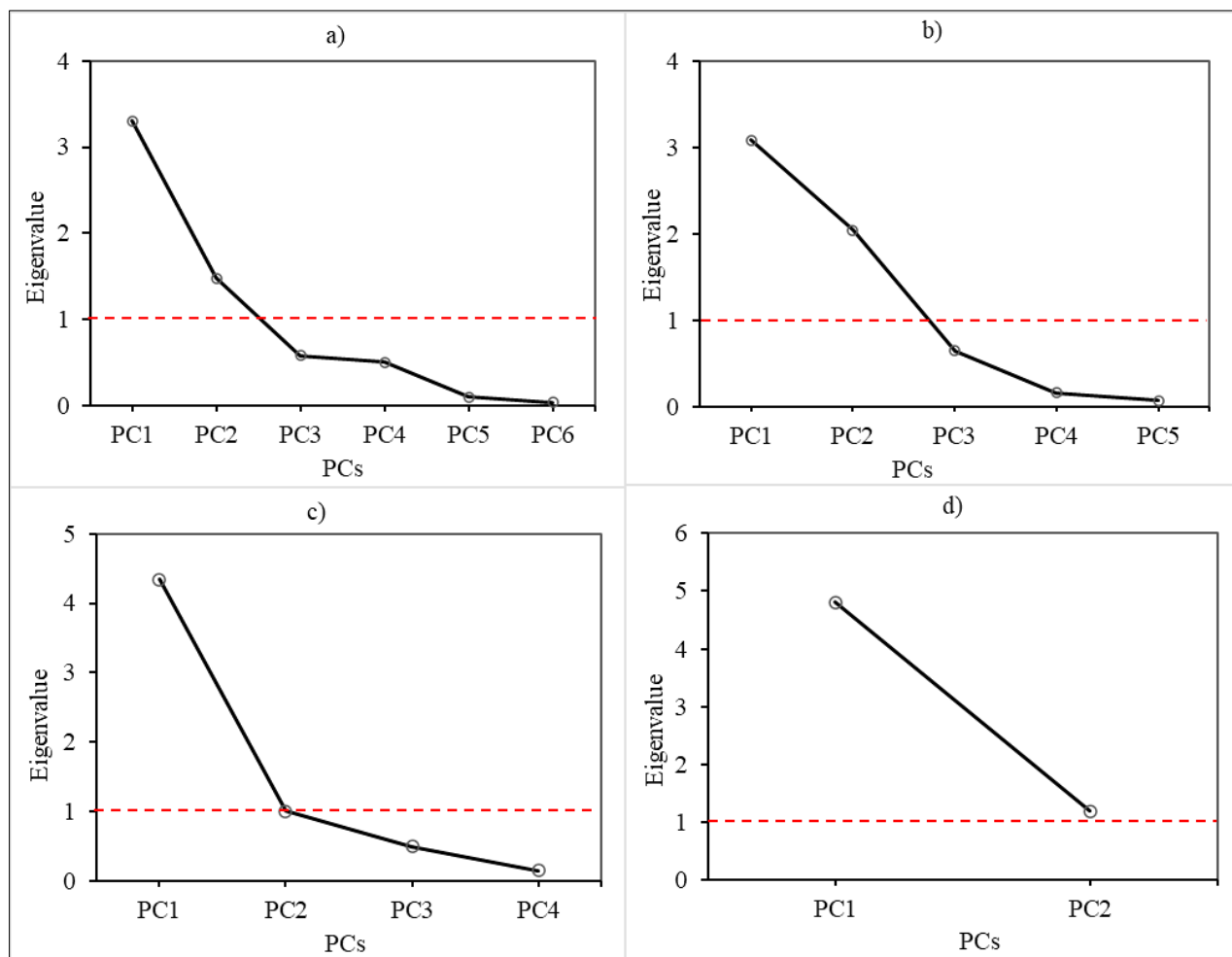
Figure 4. Scree plots for the principal component analysis

Table 4. Key variables influencing groundwater quality in the study area

Parameter	Residential and urban		Cemetery		Landfill		Salinity intrusion	
	PC1	PC2	PC1	PC2	PC1	PC2	PC1	PC2
pH	-0.396	-0.203	0.515	-0.243	-0.410	0.149	0.261	-0.753
TDS	0.433	-0.417	0.436	0.387	-0.452	0.160	-0.433	-0.286
PI	0.450	0.222	0.420	0.343	-0.451	-0.079	-0.415	-0.381
NH_4^+-N	0.501	0.080	-0.453	0.180	-0.410	-0.479	-0.452	-0.116
NO_3^--N	0.332	-0.638	0.110	0.657	-0.446	-0.215	-0.454	-0.077
Fe	0.303	0.567	-0.389	0.458	0.238	-0.819	-0.402	0.431
Eigenvalues	3.30	1.48	3.08	2.04	4.34	1.01	4.81	1.19
% Variation	55.00	24.60	51.30	34.00	72.40	16.90	80.20	19.80
Cum. % Variation	55.00	79.60	51.30	85.20	72.40	89.20	80.20	100

In the residential-urban area, the first principal component (PC1) is the most crucial component, explaining 55% of the total variance of six groundwater quality variables, with moderate loading values to NH_4^+-N (0.501) and weak to pH (-0.396), TDS (0.433), PI (0.450), NO_3^--N (0.332), and Fe (0.303). The possible source of pollution can be domestic wastewater since it contains high concentrations of TDS, C, N, and P [54, 55]. Iron oxides in the soil layer can be leached and reduced by organic matter under anaerobic conditions, leading to the formation of Fe in groundwater [28]. Therefore, PC1 could be from internal and external causes of groundwater pollution. The second component (PC2), which

explained 24.60% of the total variance of the groundwater quality dataset, had a mean loading factor of NO_3^--N (-0.638) and Fe (0.567). The concentration of Fe in groundwater in urban residential areas was relatively low, possibly due to natural causes such as the weathering of iron-rich minerals in rocks [52]. Similarly, the concentration of NO_3^--N was only recorded to be very low at GW3 and GW8, possibly because nitrogen metabolism occurred in suitable environmental conditions, which converted NH_4^+-N into NO_3^--N.

In the cemetery area, PC1 formed a moderate correlation to pH (0.515), weak to TDS (0.436), PI (0.420), NH_4^+-N (-0.453), and Fe (-0.389). PC1 explained more than 51% of the total variance of the groundwater quality parameters. Pollutants generated from old cemeteries could contaminate the soil and seep into groundwater [56]. PC2 explained 34% of the total variance and was positively related to NO_3^--N (0.657). Nitrogen, especially in the form of nitrate, is one of the main pollutants from decomposing corpses and can have a negative impact on the environment [57]. Nitrogen is one of the main components of protein in the human body, so nitrogen can enter groundwater through leachate generated after human body decomposition [58]. In addition, the groundwater affected by the cemetery area also has high pH and TDS values [58]. At the same time, PC2 also explained that it had a weak correlation with TDS (0.387), permanganate index (0.343), and Fe (0.458). This result showed that natural sources also contributed to the TDS and Fe concentrations.

At the landfill site, the first PC was correlated with most groundwater quality parameters, explaining more than 72% of the total variance. PC1 formed a weak correlation with pH (-0.410), TDS (-0.452), permanganate index (-0.451), NH_4^+-N (-0.410), and NO_3^--N (-0.446). While the second PC explained almost 17% of the total variance, it was mainly strongly correlated with Fe (-0.819). The source of groundwater pollution in this area may come from leachate, the decomposition of organic matter in waste streams. Open-air, unsorted, and uncoated landfills could lead to leachate seeping directly into the soil and entering groundwater vertically. Leachate from landfills represents a serious threat to groundwater quality as it contains a wide range of contaminants. Typically, very high and fluctuating concentrations of BOD, COD, NH_4^+-N, Fe^{2+}, and TDS were in the range of 10,000–25,000 mg/L, 15,000–40,000 mg/L, 1500–4250 mg/L, 500–1500 mg/L, and 10,000–25,000 mg/L, respectively [59]. In this study, the concentration of NH_4^+-N in groundwater in the area affected by the landfill exceeded the allowable limit of QCVN 09-MT:2015/BTNMT. The status of leachate contaminating groundwater has been reported in several areas [59–61]. In addition, unclassified waste burying could contribute to Fe accumulation in the soil and negatively affect groundwater quality in the study area.

In the area affected by saline intrusion, PC1 was the most important component, explaining more than 80% of the total variance of the groundwater quality parameters. PC1 formed correlations with most groundwater variables, such as TDS (-0.433), permanganate index (-0.415), NH_4^+-N (0.452), NO_3^--N (0.454), and Fe (-0.402), at weak levels. The high TDS concentration in groundwater samples in coastal areas is mainly derived from intrusive seawater [36]. TDS pollution can be caused by domestic and industrial wastewater, sewage pipe leaks, and the dissolution of mineral-bearing rocks. High concentrations of TDS and exceeding the allowable limit of QCVN 09-MT:2015/BTNMT were recorded in this area. In addition, this area had the highest concentrations of NH_4^+-N, NO_3^--N, permanganate, and Fe. Sources of pollution could come from domestic and industrial wastewater. Meanwhile, PC2 strongly correlated with the pH parameter (-0.753), explaining about 20% of the total variance. The pH value was greater than 7 in most of the groundwater monitoring stations, which was caused by saline intrusion in the coastal area, which increases strong basic salts and weak acids in aquifers.

PCA results indicated that two main sources are causing groundwater variation in the residential-urban area: the cemetery area, the landfilling area, and the saline intrusion area. All the observed groundwater parameters (pH, TDS, permanganate index, NH_4^+-N, NO_3^--N, and Fe) play key roles in representing groundwater quality in the study area and thus should be monitored. Potential polluting sources of groundwater in the study areas could be domestic and industrial wastewater discharge, leachate from cemeteries and landfills, the nature of groundwater aquifers, and seawater intrusion.

3.3. Classification of Groundwater Quality in the Study Area

In the study, the groundwater quality index (GWQI) was calculated from six variables (pH, TDS, permanganate index, NH_4^+-N, NO_3^--N, and Fe) to provide information regarding the overall quality of the groundwater (Figure 5). Groundwater quality in the study area was divided into four categories: (1) excellent, (2) good, (3) poor, and (4) very poor. In which, groundwater samples with excellent and good water quality accounted for the majority, with GWQI index values ranging from 31–40 and 50–86, respectively. There were a total of 21 groundwater samples with excellent water quality (accounting for 44% of the total) and good water quality (accounting for 40% of the total), including 8 groundwater samples (GW1-GW8) in residential-urban areas, 7 groundwater samples (GW9, GW10, GW11, GW13, GW15, GW16, and GW17) in the cemetery area, 4 samples of groundwater (GW18-GW22) at the landfill site, and 2 samples of groundwater (GW23 and GW24) in the affected area. At these locations, most of the groundwater parameters reached the allowable limit of QCVN 09-MT:2015/BTNMT [27]. Groundwater quality at these locations can be used for drinking purposes, but it must be treated accordingly. For poor water quality, there were three locations (accounting for 12% of the total), including GW12, GW14 in the cemetery area, and GW21 in the landfill area. These three locations had NH_4^+-N concentrations that exceeded the limit of QCVN 09-MT:2015/BTNMT by 1.3–2.3 times. The groundwater quality at the location GW24 (in the saltwater intrusion area) was very poor and not recommended for drinking purposes.

TDS and NH_4^+-N exceeded the limits of QCVN 09-MT:2015/BTNMT by 3.3 times and 4.4 times, respectively. The causes of groundwater pollution at the GW24 site may be due to seawater intrusion and improper wastewater and waste management. Compared with other studies, the overall groundwater quality in Ca Mau was better than that in Ha Nam province (GWQI 67–369) [33], but it was worse than the groundwater quality in Ba Ria – Vung Tau [19] and the groundwater quality in Dong Thap, An Giang, Hau Giang, and Kien Giang [15]. The difference in results of GWQI in various areas in the current and former studies could be from the input data. More groundwater quality parameters should be added to the calculation of the GWQI in the future at the study areas for groundwater quality evaluation.
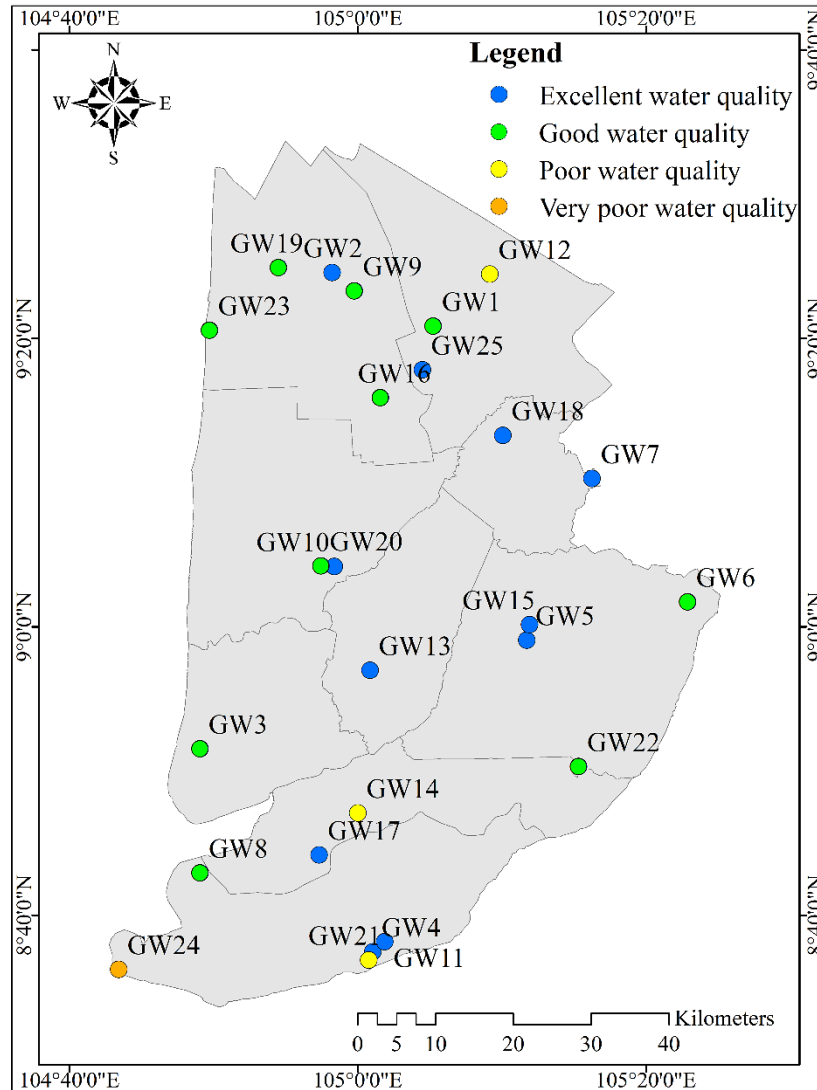
Figure 5. Map of groundwater quality classification

Four groups of groundwater quality were formed as the result of cluster analysis (Figure 6). Group I represented groundwater with the worst water quality, including site GW24 (4% of the total). This result is similar to the GWQI index result; this is a location with "very bad" water quality with TDS and NH_4^+-N concentrations exceeding the permissible limit of QCVN 09-MT:2015/BTNMT 3.3 times and 4.4 times, respectively. Group II represented groundwater of medium quality, including site GW12 (4% of the total). Group II groundwater quality had a high ammonium concentration (1.6 times higher than the limit of QCVN 09-MT:2015/BTNMT). Group III gathered several locations with the most similar groundwater characteristics, with 14 sites (56% of the total) in residential areas, urban areas, cemeteries, and areas affected by saline intrusion (GW1, GW2, GW3, GW4, GW5, GW6, GW7, GW8, GW10, GW11, GW13, GW15, GW17, and GW25). Group III was the group with the lowest concentration of groundwater pollutants and was within the allowable limits of QCVN 09-MT:2015/BTNMT. Similarly, the groundwater quality of Group IV was still unpolluted, and the concentrations of groundwater pollutants were still within the allowable limits of QCVN 09-MT:2015/BTNMT. However, the concentration of NH_4^+-N in groundwater was at an alarming level, close to 1 mg/L. Group IV gathered 9 locations, including GW9, GW14, GW16, GW18, GW19, GW20, GW21, GW22, and GW23, belonging to cemeteries, landfills, and areas affected by saline intrusion. CA results revealed that there is possible to reduce sampling sites in residential-urban areas, cemetery areas, and landfill areas. Cluster III comprised eight sites in residential-urban areas, which could mean that the groundwater quality in this area is relatively uniform. The study

result suggests reducing 4 out of 8 sites from residential-urban areas but still remaining representative of groundwater quality monitoring. In addition, there were four sites (GW10, GW11, GW13, and GW17) in the cemetery grouped in the same Cluster III, and two of these four sites could be considered to be removed from the current monitoring program. For the landfill area, the five sites of GW18, GW19, GW20, GW21, and GW22 were clustered in Group IV, and these sites could be reduced by three sites (GW20, GW21, and GW22). CA recommends reducing 9 out of 25 sites from the current monitoring program.
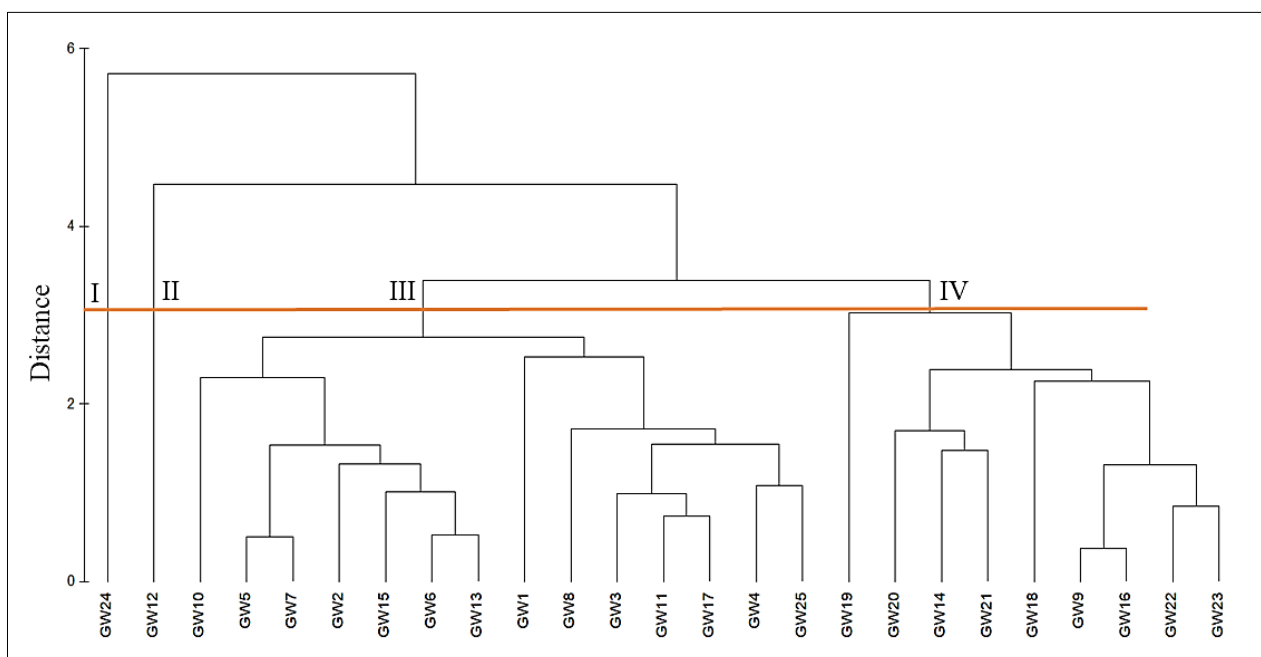
Figure 6. Clustering groundwater quality in the study area

4. Conclusion

The present study examined groundwater quality in residential-urban areas, cemetery areas, landfilling areas, and saline intrusion areas in Ca Mau Province, Vietnam. The results revealed that groundwater in the landfilling area was contaminated by NH_4^+-N, and the groundwater quality in the saline intrusion area was polluted by TDS and NH_4^+-N. The groundwater quality index classified groundwater into four categories (i.e., excellent, good, poor, and very poor water quality), accounting for 44%, 40%, 12%, and 4% of the total samples, respectively. NH_4^+-N and TDS represented groundwater parameters that contribute to poor and very poor quality. Cluster analysis divided groundwater quality into four groups, of which Group I had the lowest quality. PCA results indicated two main sources causing groundwater variation in each residential-urban area: the cemetery, landfilling, and saline intrusion areas. All the observed groundwater parameters (pH, TDS, permanganate index, NH_4^+-N, NO_3^--N, and Fe) play key roles in representing groundwater quality in the study area and, thus, should be monitored in the future. However, more groundwater quality parameters (for examples, chloride, arsenic, hardness, bicarbonate, etc.) should be added to the monitoring program. Potential polluting sources of groundwater in the study areas could be domestic and industrial wastewater discharge, leachate from cemeteries and landfills, the nature of groundwater aquifers, and seawater intrusion. The current study's results suggest reducing 9 groundwater sampling locations while still ensuring groundwater quality monitoring representative. The current findings provide scientific information for local environmental authorities to manage and monitor groundwater quality in the study area.

5. Declarations

5.1. Author Contributions

Conceptualization, N.T.G. and P.Q.N.; methodology, N.T.G. and P.Q.N.; software, N.T.G.; validation, P.Q.N.; formal analysis, N.T.G. and P.Q.N.; investigation, N.T.G.; resources, N.T.G. and P.Q.N.; data curation, N.T.G. and P.Q.N.; writing—original draft preparation, N.T.G. and P.Q.N.; writing—review and editing, N.T.G. and P.Q.N.; visualization, N.T.G. and P.Q.N.; supervision, N.T.G. and P.Q.N.; project administration, N.T.G. and P.Q.N.; funding acquisition, N.T.G. and P.Q.N. All authors have read and agreed to the published version of the manuscript.

5.2. Data Availability Statement

The data presented in this study are available in the article.

6. References

[1] Earman, S., & Dettinger, M. (2011). Potential impacts of climate change on groundwater resources - A global review. Journal of Water and Climate Change, 2(4), 213–229. doi:10.2166/wcc.2011.034.

[2] Amanambu, A. C., Obarein, O. A., Mossa, J., Li, L., Ayeni, S. S., Balogun, O., Oyebamiji, A., & Ochege, F. U. (2020). Groundwater system and climate change: Present status and future considerations. Journal of Hydrology, 589, 125163. doi:10.1016/j.jhydrol.2020.125163.

[3] Elemile, O. O., Ibitogbe, E. M., Folorunso, O. P., Ejiboye, P. O., & Adewumi, J. R. (2021). Principal component analysis of groundwater sources pollution in Omu-Aran Community, Nigeria. Environmental Earth Sciences, 80(20), 690–707. doi:10.1007/s12665-021-09975-y.

[4] Barbieri, M., Barberio, M. D., Banzato, F., Billi, A., Boschetti, T., Franchini, S., Gori, F., & Petitta, M. (2023). Climate change and its effect on groundwater quality. Environmental Geochemistry and Health, 45(4), 1133–1144. doi:10.1007/s10653-021-01140-5.

[5] Liu, Q., Wang, G., Gui, D., Liu, Y., Kotb Abd-Elmabod, S., & Wei, G. (2024). Precise ecological restoration under water diversions-groundwater-ecosystem interactions in drylands. Journal of Hydrology, 628, 130601. doi:10.1016/j.jhydrol.2023.130601.

[6] Wada, Y., Van Beek, L. P. H., Van Kempen, C. M., Reckman, J. W. T. M., Vasak, S., & Bierkens, M. F. P. (2010). Global depletion of groundwater resources. Geophysical Research Letters, 37(20), 20402. doi:10.1029/2010GL044571.

[7] Maharjan, A. K., Mori, K., & Toyama, T. (2020). Nitrogen removal ability and characteristics of the laboratory-scale tidal flow constructed wetlands for treating ammonium-nitrogen contaminated groundwater. Water (Switzerland), 12(5), 1326. doi:10.3390/W12051326.

[8] Laonamsai, J., Pawana, V., Chipthamlong, P., Chomcheawchan, P., Kamdee, K., Kimmany, B., & Julphunthong, P. (2023). Groundwater Quality Variations in Multiple Aquifers: A Comprehensive Evaluation for Public Health and Agricultural Use. Geosciences (Switzerland), 13(7), 195. doi:10.3390/geosciences13070195.

[9] Abdessamed, D., Jodar-Abellan, A., Ghoneim, S. S. M., Almaliki, A., Hussein, E. E., & Pardo, M. Á. (2023). Groundwater quality assessment for sustainable human consumption in arid areas based on GIS and water quality index in the watershed of Ain Sefra (SW of Algeria). Environmental Earth Sciences, 82(21), 510. doi:10.1007/s12665-023-11183-9.

[10] UNESCO. (2022). Groundwater: Making the invisible visible. The United Nations Educational, Scientific and Cultural Organization (UNESCO), Paris, France. Available online: https://www.unesco.org/reports/wwdr/2022/en (accessed on February 2024).

[11] Scanlon, B. R., Fakhreddine, S., Rateb, A., de Graaf, I., Famiglietti, J., Gleeson, T., Grafton, R. Q., Jobbagy, E., Kebede, S., Kolusu, S. R., Konikow, L. F., Long, D., Mekonnen, M., Schmied, H. M., Mukherjee, A., MacDonald, A., Reedy, R. C., Shamsudduha, M., Simmons, C. T., … Zheng, C. (2023). Global water resources and the role of groundwater in a resilient water future. Nature Reviews Earth & Environment, 4(2), 87–101. doi:10.1038/s43017-022-00378-6.

[12] Lu, X., Fan, Y., Hu, Y., Zhang, H., Wei, Y., & Yan, Z. (2024). Spatial distribution characteristics and source analysis of shallow groundwater pollution in typical areas of Yangtze River Delta. Science of the Total Environment, 906, 167369. doi:10.1016/j.scitotenv.2023.167369.

[13] Obeidat, M., & Awawdeh, M. (2021). Assessment of groundwater quality in the area surrounding Al-Zaatari Camp, Jordan, using cluster analysis and water quality index (WQI). Jordan Journal of Earth & Environmental Sciences, 12(3), 187-197.

[14] Ferhati, A., Kettab, R. M., Belazreg, N. E. H., Khodja, H. D., Djerbouai, S., & Hasbaia, M. (2023). Hydrochemical analysis of groundwater quality in central Hodna Basin, Algeria: a case study. International Journal of Hydrology Science and Technology, 15(1), 22. doi:10.1504/ijhst.2023.127889.

[15] Nguyen, T. G., & Huynh, N. T. H. (2023). Characterization of Groundwater Quality and Human Health Risk Assessment. Civil Engineering Journal (Iran), 9(3), 618–628. doi:10.28991/CEJ-2023-09-03-09.

[16] Zohud, A., & Alam, L. (2022). A Review of Groundwater Contamination in West Bank, Palestine: Quality, Sources, Risks, and Management. Water (Switzerland), 14(21), 3417. doi:10.3390/w14213417.

[17] Khezami, F., Gómez-Navarro, O., Barbieri, M. V., Khiari, N., Chkirbene, A., Chiron, S., Khadhar, S., & Pérez, S. (2024). Occurrence of contaminants of emerging concern and pesticides and relative risk assessment in Tunisian groundwater. Science of the Total Environment, 906, 167319. doi:10.1016/j.scitotenv.2023.167319.

[18] Giao, N. T., Anh, P. K., & Nhien, H. T. H. (2022). Groundwater Quality Assessment Using Groundwater Quality Index and Multivariate Statistical Methods and Human Health Risk Assessment in a Coastal Region of the Vietnamese Mekong Delta. Applied Environmental Research, 44(2), 68–85. doi:10.35762/AER.2022.44.2.6.

[19] Nguyen, A. H., Pham, N. T. T., Tat, V. H. M., Truong, H. T., Tran, H. N., Luu, L. K., Tran, B. M., & Luong, H. T. H. (2020). Application of groundwater quality index (GWQI) and GIS in groundwater quality zoing in Pleistocene aquifer in Phu My town, Ba Ria – Vung Tau province. Science & Technology Development Journal - Science of the Earth & Environment, 4(1), 149-161. doi:10.32508/stdjsee.v4i1.525.

[20] Li, Q., Zhang, H., Guo, S., Fu, K., Liao, L., Xu, Y., & Cheng, S. (2020). Groundwater pollution source apportionment using principal component analysis in a multiple land-use area in southwestern China. Environmental Science and Pollution Research, 27(9), 9000–9011. doi:10.1007/s11356-019-06126-6.

[21] Le, Q. T., Nguyen, K. V., & Nguyen, V. D. T. (2022). Assessment of surface water quality and some main rivers' capacity of receiving wastewater in Ca Mau province, Vietnam. The Journal of Agriculture and Development, 21(3), 53-66. doi:10.52997/jad.7.03.2022.

[22] Giao, N. T. (2022). Analysis of Surface Water Quality using Multivariate Statistical Approaches: A case study in Ca Mau Peninsula, Vietnam. Pollution, 8(2), 463–477. doi:10.22059/POLL.2021.329252.1165.

[23] Be, N. V., & Tuyen, T. T. (2007). Status of exploitation, management and quality of sand dune groundwater in Tra Vinh Province. Journal of Science Can Tho University, 8, 95-104.

[24] Giao, N. T. (2021). Chemical and microbial characteristics of surface and ground water in the areas burying swine infected with African swine fever, An Giang province, Vietnam. Journal of Energy Technology and Environment, 3(3), 9–20. doi:10.37933/nipes.e/3.3.2021.2.

[25] DoENR (2022). Environmental Report in Ca Mau Province. Department of Environment and Natural Resources (DoENR), Ca Mau, Vietnam. Available online: https://documents1.worldbank.org/curated/ru/660481568009638284/pdf/Environmental-and-Social-Impact-Assessment-for-Ca-Mau-Province.pdf (accessed on January 2024).

[26] Rice, W. E., Baird, R. B. & Eaton, A. D. (2017). Standard Methods of for the Examination of Water and Wastewater (23rd Ed.). American Public Health Association, Washington, United States.

[27] QCVN 09-MT:2015/BTNMT. (2015). National technical regulation on groundwater quality. Ministry of Natural Resources and Environment (MONRE), Hanoi, Vietnam. (In Vietnamese).

[28] Nguyen, B. T., Nguyen, T. M. T., & Bach, Q. V. (2020). Assessment of groundwater quality based on principal component analysis and pollution source-based examination: a case study in Ho Chi Minh City, Vietnam. Environmental Monitoring and Assessment, 192(6), 395. doi:10.1007/s10661-020-08331-0.

[29] Taşan, M., Demir, Y., & Taşan, S. (2022). Groundwater quality assessment using principal component analysis and hierarchical cluster analysis in Alaçam, Turkey. Water Supply, 22(3), 3431–3447. doi:10.2166/WS.2021.390.

[30] Piyathilake, I. D. U. H., Ranaweera, L. V., Udayakumara, E. P. N., Gunatilake, S. K., & Dissanayake, C. B. (2022). Assessing groundwater quality using the Water Quality Index (WQI) and GIS in the Uva Province, Sri Lanka. Applied Water Science, 12(4), 72–90. doi:10.1007/s13201-022-01600-y.

[31] Talalaj, I. A., & Biedka, P. (2016). Use of the landfill water pollution index (LWPI) for groundwater quality assessment near the landfill sites. Environmental Science and Pollution Research, 23(24), 24601–24613. doi:10.1007/s11356-016-7622-0.

[32] QCVN 01-1:2018/BYT. (2018). National technical regulation on quality of clean water used for domestic purposes. Ministry of Natural Resources and Environment (MONRE), Hanoi, Vietnam. (In Vietnamese).

[33] Tham, T. T., Thi Hien, D., Thuy Chung, N., & Tra Mai, N. (2022). Assessment of Groundwater Quality in the Holocene Aquifer in Duy Tien District, Ha Nam Province using Groundwater Quality Index (GWQI). VNU Journal of Science: Earth and Environmental Sciences, 38(1), 95–104. doi:10.25073/2588-1094/vnuees.4781.

[34] Singh, G., Singh, J., Wani, O. A., Egbueri, J. C., & Agbasi, J. C. (2024). Assessment of groundwater suitability for sustainable irrigation: A comprehensive study using indexical, statistical, and machine learning approaches. Groundwater for Sustainable Development, 24, 101059. doi:10.1016/j.gsd.2023.101059.

[35] Ayotte, J. D., Montgomery, D. L., Flanagan, S. M., & Robinson, K. W. (2003). Arsenic in groundwater in eastern New England: Occurrence, controls, and human health implications. Environmental Science and Technology, 37(10), 2075–2083. doi:10.1021/es026211g.

[36] Meyer, R., Engesgaard, P., & Sonnenborg, T. O. (2019). Origin and Dynamics of Saltwater Intrusion in a Regional Aquifer: Combining 3-D Saltwater Modeling with Geophysical and Geochemical Data. Water Resources Research, 55(3), 1792–1813. doi:10.1029/2018WR023624.

[37] Nguyen, T. G., & Huynh, T. H. N. (2022). Assessment of surface water quality and monitoring in southern Vietnam using multicriteria statistical approaches. Sustainable Environment Research, 32(1), 20. doi:10.1186/s42834-022-00133-y.

[38] Giao, N. T., Anh, P. K., & Nhien, H. T. H. (2021). Evaluating groundwater quality in Bac Lieu province using multivariate statistical method and groundwater quality index. Indonesian Journal of Environmental Management and Sustainability, 5(4), 129–135.

[39] USGS. (2000). Classification of Natural Ponds and Lakes. United States Department of the Interior, Washington, United States.

[40] Phuong, N. L., & Duong, M. T. (2018). Assessing the status of groundwater source in Thanh Khe district, Da Nang city. Journal of Science and Technology - University of Danang, 56-60. (In Vietnamese).

[41] Hung, N. T. Q., Ky, N. M., Danh, D. H., Vu, T. P., & Tuan, H. N. A. (2018). Research on status of water use and quality of domestic supply water in Trang Bang district, Tay Ninh province. VNU Journal of Science: Earth and Environmental Sciences, 34(4), 10–21. doi:10.25073/2588-1094/vnuees.4251.

[42] Anh, N. T., Ky, N. M., Hai, N. N., & Dung, B. Q. (2021). Assessment of the current status and risks caused by microorganisms in domestic water in peri-urban areas: A case study in Pleiku, Gia Lai province, Vietnam. Journal of Meteorology and Hydrology, 726, 12–24.

[43] Trung, L. A. (2020). Evaluation of the change of permanganate index in domestic water stored in households. Journal of Science of Natural Resources and Environment, 30, 41–46. (In Vietnamese).

[44] Nam, N. D. G., Akira, G., Kazutoshi, O., Trung, N. H., & Ngan, N. V. C. (2019). Assessment of Groundwater Quality and Its Suitability for Domestic and Irrigation Use in the Coastal Zone of the Mekong Delta, Vietnam. Advances in Global Change Research, 64, Springer, Cham, Switzerland. doi:10.1007/978-3-319-90400-9_10.

[45] Cuong, L. P., & Thang, N. V. (2022). Application of machine learning model to predict groundwater quality: typical in Hoi An city, Quang Nam province. . Journal of Science and Technology - University of Danang, 20(5), 106–110.

[46] Shu, J., Chen, M., Wu, H., Li, B., Wang, B., Li, B., Liu, R., & Liu, Z. (2019). An innovative method for synergistic stabilization/solidification of Mn2+, NH4+-N, PO43− and F− in electrolytic manganese residue and phosphogypsum. Journal of Hazardous Materials, 376, 212–222. doi:10.1016/j.jhazmat.2019.05.017.

[47] Dung, B. X., Thanh, D. T. K., Quynh, K. T., & Phuc, D. T. T. (2020). Seasonal variation of groundwater level and quality in Xuan Mai, HaNoi, Vietnam. Journal of Forestry Science and Technology, 9, 80–90.

[48] Shakya, B. M., Nakamura, T., Kamei, T., Shrestha, S. D., & Nishida, K. (2019). Seasonal groundwater quality status and nitrogen contamination in the shallow aquifer system of the Kathmandu Valley, Nepal. Water, 11(10), 2184. doi:10.3390/w11102184.

[49] Wu, J., Zhang, Y., & Zhou, H. (2020). Groundwater chemistry and groundwater quality index incorporating health risk weighting in Dingbian County, Ordos basin of northwest China. Geochemistry, 80(4), 125607. doi:10.1016/j.chemer.2020.125607.

[50] Majumdar, D., & Gupta, N. (2000). Nitrate pollution of groundwater and associated human health disorders. Indian journal of environmental health, 42(1), 28-39.

[51] Podgorski, J., Araya, D., & Berg, M. (2022). Geogenic manganese and iron in groundwater of Southeast Asia and Bangladesh – Machine learning spatial prediction modeling and comparison with arsenic. Science of the Total Environment, 833, 155131. doi:10.1016/j.scitotenv.2022.155131.

[52] Ullah, Z., Rashid, A., Ghani, J., Nawab, J., Zeng, X.-C., Shah, M., Alrefaei, A. F., Kamel, M., Aleya, L., Abdel-Daim, M. M., & Iqbal, J. (2022). Groundwater contamination through potentially harmful metals and its implications in groundwater management. Frontiers in Environmental Science, 10. doi:10.3389/fenvs.2022.1021596.

[53] Sharma, G. K., Jena, R. K., Ray, P., Yadav, K. K., Moharana, P. C., Cabral-Pinto, M. M. S., & Bordoloi, G. (2021). Evaluating the geochemistry of groundwater contamination with iron and manganese and probabilistic human health risk assessment in endemic areas of the world's largest River Island, India. Environmental Toxicology and Pharmacology, 87, 103690. doi:10.1016/j.etap.2021.103690.

[54] Ha, N. T. T., Hang, H. T. T., Chi, D. P., Dung, D. T., & Huy, T. Q. (2019). Treatment of domestic wastewater and livestock wastewater by algae on the filter material. Vietnam Journal of Agricultural Science, 17(10), 826–834. (In Vietnamese).

[55] Al-Hiyaly, S. A. K., Ali, Z. H., & Alobiady, A. A.-H. M. J. (2021). Removing of fat residues from domestic kitchen wastewater by synthetic filter of saw dust. IOP Conference Series: Earth and Environmental Science, 779(1), 012095. doi:10.1088/1755-1315/779/1/012095.

[56] Nguyen, T., & Nguyen, L. (2018). Groundwater pollution by longstanding cemetery and solutions for urban cemetery planning in Ho Chi Minh City – from reality to solutions. MATEC Web of Conferences, 193, 02008. doi:10.1051/matecconf/201819302008.

[57] Vaezihir, A., & Mohammadi, S. (2016). Groundwater contamination sourced from the main cemetery of Tabriz, Iran. Environmental Forensics, 17(2), 172–182. doi:10.1080/15275922.2016.1163621.

[58] Jafarpoor Kandoli, S., Alidadi, H., Najafpoor, A. A., Mehrabpour, M., Hosseinzadeh, A., & Momeni, F. (2019). Assessment of cemetery effects on groundwater quality using GIS. Desalination and Water Treatment, 168, 235–242. doi:10.5004/dwt.2019.24622.

[59] Costa, A. M., Alfaia, R. G. de S. M., & Campos, J. C. (2019). Landfill leachate treatment in Brazil – An overview. Journal of Environmental Management, 232, 110–116. doi:10.1016/j.jenvman.2018.11.006.

[60] Stefania, G. A., Rotiroti, M., Buerge, I. J., Zanotti, C., Nava, V., Leoni, B., Fumagalli, L., & Bonomi, T. (2019). Identification of groundwater pollution sources in a landfill site using artificial sweeteners, multivariate analysis and transport modeling. Waste Management, 95, 116–128. doi:10.1016/j.wasman.2019.06.010.

[61] Kumari, P., Gupta, N. C., Kaur, A., & Singh, K. (2019). Application of Principal Component Analysis and Correlation for Assessing Groundwater Contamination in and around Municipal Solid Waste Landfill of Ghazipur, Delhi. Journal of the Geological Society of India, 94(6), 595–604. doi:10.1007/s12594-019-1366-7.
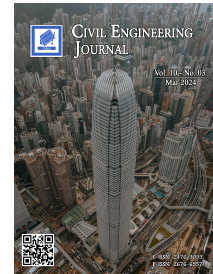
Cost Efficiency of Retrofitting Green Chemical Industrial Buildings

Albert Eddy Husin [1]*, Lastarida Sinaga [1], Mawardi Amin [1], Kristiyanto [1], Eka Juni Arif [1], Bernadette D. Kussumardianadewi [1], Wyllem T. Ator [1]

[1] *Department of Civil Engineering, Mercu Buana University, Jakarta, Indonesia.*

Abstract

Climate change is a threat and crisis that hit the world today. The green industry is widely implemented in the manufacturing sector as an effort to reduce negative impacts on the environment. The implementation of the green industry is influenced by various factors. The Chemical Industry is one sector that faces challenges in implementing green industry practices. The objective of this paper is to create an innovative conceptual framework that combines blockchain technology and building information modeling. This research examines the concept of green retrofitting in the chemical industry using an assessment based on the Ministry of Public Works and Housing Regulation No. 21 of 2021. The study was conducted in a chemical industry located in Cilegon, Banten, Indonesia. The research method combines Blockchain-Building Information Modeling (BIM) to analyze the cost efficiency of green retrofitting and Structural Equation Modeling-Partial Least Squares (SEM-PLS) as a tool to process data from questionnaires and identify influential factors. The results indicate that the use of Blockchain-BIM can reduce retrofitting costs by 4.42% for low-level, 4.45% for medium-level, and 4.40% for high-level categories. This demonstrates that Blockchain-BIM has a significant impact on improving cost performance in the retrofitting process.

Keywords: Green Retrofit; Green Chemical Industry; Blockchain-BIM; SEM-PLS; Cost Efficiency.

1. Introduction

The awareness of the worldwide consequences of climate change, energy depletion, and the increase in greenhouse gas emissions has intensified public concern about the current trends in energy consumption [1–3]. Approximately 30% of the world's total CO2 emissions can be attributed to buildings [4–6]. The progression of climate change and increasing temperatures amplifies the occurrence and intensity of droughts. In arid and semi-arid areas, climate change has resulted in more frequent and severe droughts, diminishing the accessibility of water for diverse purposes [7]. As part of the Coordinated Regional Climate Downscaling Experiment, Ozturk et al. [8] conducted a study investigating the impact of climate change on the seasonal fluctuations of precipitation and temperature in an Asian region. The results indicated a notable warming trend in surface temperatures in the southeastern Pacific. Due to the significant challenge of global warming faced by the world, climate change is an important environmental issue [9], impacting both private sector institutions and governments. It has become essential for all communities to develop new business plans that prioritize finding environmental solutions. The construction industry plays an important role in various industrial impacts on the natural environment. The industry is characterized by high energy and resource consumption and high environmental pollution [10]. The construction sector bears responsibility for the excessive utilization of natural resources and energy consumption [11, 12]. The concept of Green Buildings offers several advantages in terms of economics, social aspects,

and the environment, which incorporate principles of sustainable resource conservation (energy, water, land, and nature), resource efficiency (energy, water, land, and materials), and resource sharing (public facilities for transportation and work) [13]. The Technical Guidelines of the Ministry of Public Works and Housing No. 1 of 2022 provide the latest guidelines for green building construction in Indonesia. According to this regulation, there are three rating levels: Green Building Main (80%−100%), Middle (65%−80%), and Primary (45%−65%), with a maximum total score of 165 points [14]. Generally, retrofitting existing buildings tends to be more expensive compared to integrating Green Building concepts into new construction. The cost to upgrade existing buildings into Green Buildings can reach around 10.77% of the initial cost [15].

The green building chemical industry plays a crucial role in promoting the development of environmentally sustainable buildings through the integration of design strategies that minimize the adverse effects of buildings on the environment and their occupants [16]. The chemical industry catalyzes the development and progress of modern society [16]. The issue of global warming is a significant global concern that affects both private enterprises and governmental organizations, necessitating the need for everyone to devise innovative business plans that prioritize environmental solutions [17]. Draft Building Green has multiple advantages in terms of economics, social aspects, and the establishment of environmentally friendly structures through the utilization of sustainable conservation sources (energy, water, land, and nature), efficient power sources (such as geothermal energy and eco-friendly materials), and the ability to share resources (including general facilities, transportation, and workspace) [1, 18].

Identifying critical success factors (CSFs) is crucial for the successful implementation of a project and the attainment of specified objectives [19]. In the context of green concept development, understanding the CSFs is vital for ensuring optimal project performance, as suggested by the existing literature and proposed methodology [20]. Based on the reviewed literature, the three most significant factors are management support, financial capability, and design specifications [21]. Furthermore, the literature indicates that project cost is a more critical factor compared to project schedule and quality. Green buildings offer tangible benefits such as 30-50% water savings and 20-30% energy savings. Additionally, there are intangible benefits such as enhanced air quality, natural light, and improved health, comfort, and well-being for occupants [22].

Blockchain operates as a decentralized framework for handling transactions and information [23]. Blockchain is a technology that enables the secure and immutable exchange of information and transactions between two or more participants through complete encryption [24]. Blockchain technology relies on distributed ledger technology—a shared ledger among all participants in the network [25, 26]. Transfers do not require a centralized intermediary to identify and authenticate information but are distributed among multiple independent participants in the blockchain network (nodes) who register and validate it [27]. Each participant has an exact copy of the information, enabling traceable and tamper-proof transactions. This transparency can be extended to every change made to the project model [28]. The identification has been made that Blockchain possesses the capability to overcome obstacles hindering industries from embracing BIM for sustainable design [29].

Building Information Modeling (BIM) represents a paradigm shift that offers numerous benefits, not only for those involved in the construction industry but also for the wider community [30]. A superior building requires less energy, labor, and capital during its construction phase [31]. Through BIM models that create realistic prototypes of building design and construction, it generates sufficient information that meets the needs of users [25, 28, 31]. BIM provides all the necessary tools and automation to achieve end-to-end communication, data exchange, and information sharing among collaborators [32]. A Building Information Modeling (BIM) model, which serves as a prototype for the visual representation of genuine building design and construction, is capable of producing substantial information for users [33]. Lessons learned include the fact that, while BIM can provide certain benefits to a project, it also extends the project duration and increases project costs [34, 35]. The first integrated application of Blockchain and BIM aimed at productivity has been tested at the research and technology development site of the Spanish DELFOS project [36]. The integrated technology of BIM and Blockchain promises an increasingly secure and private environment for conducting business with full control over processes [37]. Blockchain enables features such as proof of ownership, for example, addressing rights; proof-of-provenance, for example, recording through a traceable and immutable ledger; and reduction of human errors and deviations [38]. Blockchain smart contracts have emerged as a new value proposition for enhancing specific sustainability aspects within projects [39].

This research utilizes an Action Research approach to transform the building's status into a green industry and address the environmental impacts generated by the chemical industry [40]. To obtain a better analysis of cost efficiency using Blockchain-BIM in the green retrofit-based chemical industry, a research framework was employed, consisting of variables formulated to compare the resulting impacts. The collected data was then analyzed to gather preliminary information. This initial information was subsequently discussed and reviewed to draw conclusions regarding the effective payment process and provide a descriptive account to enhance cost efficiency using Blockchain-BIM in the green retrofit-based industry.

2. Methodological Framework

2.1. Data Collection

In this study, primary data was collected through an audit or verification process to evaluate the compliance of existing buildings with green building requirements [41]. The primary data reflects the level of compliance with the Technical Guidelines of the Ministry of Public Works and Housing Regulation No. 01 of 2022. In this stage, the use of data begins with available secondary data within the company, such as energy production and consumption data. Additionally, secondary data in the form of project documents, such as planning drawings, Bill of Quantity, and operational data of the facility, will also be utilized. During the development of the questionnaire, the author sought indicators that had the most significant influence. When formulating the questionnaire, we referred to the indicators that had been identified and presented by previous researchers. This questionnaire will be distributed to project stakeholders, including those directly and indirectly involved. In analyzing the data, we will utilize a simulation tool called Structural Equation Modeling (SEM) using the SMART PLS (Partial Least Squares) 3.0 software. Additionally, we will conduct interviews to gain a deeper understanding. With the use of this tool, we aim to identify the main factors and dominant subfactors that influence the cost efficiency we are examining. SMART PLS is a widely used and renowned software for data analysis in scientific research.

2.2. Research Methodology

The objective of this research is to identify the significant factors influencing the implementation of cost efficiency in green retrofitting of the chemical industry based on Blockchain-Building Information Modeling (BIM). Below is a flowchart diagram (Figure 1) illustrating the process of discovering the most significant influencing factors. In the initial stage of this research, the identification of relevant factors and subfactors was conducted. Subsequently, data collection was carried out using the research instrument. These steps have been completed before the current discussion. The research involved a literature review to gather influential factors related to the Chemical Industry (X1), Green Retrofitting (X2), Blockchain-BIM (X3), and Cost Variable (Y).
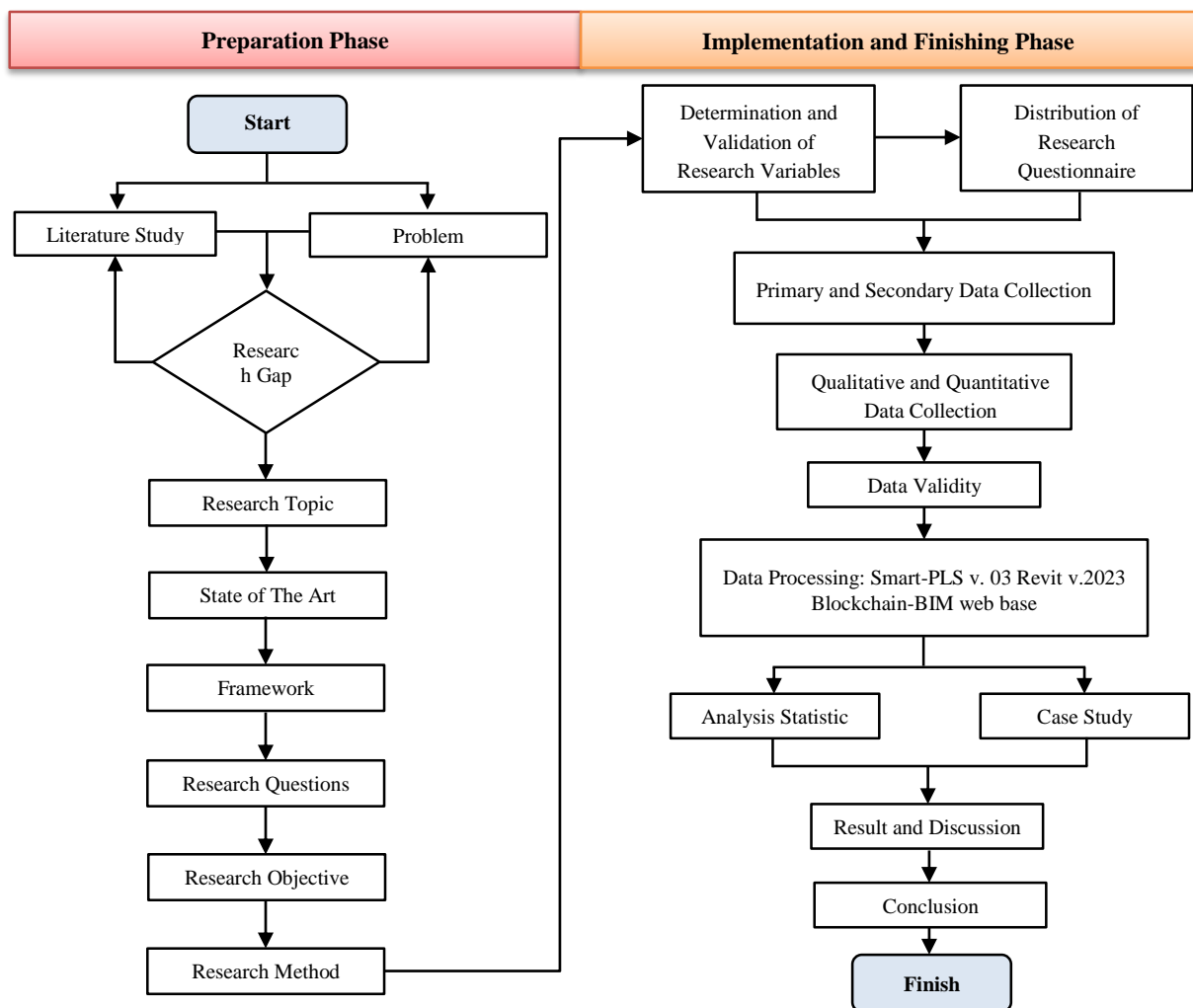
Figure 1. Research Framework [5, 42]

The questionnaire provided to selected respondents involves a rating scale from 1 to 6, where each answer choice represents a different criterion. The scale is designed in such a way that a score of 1 indicates the least expected answer, while a score of 6 indicates the most expected answer. The processed and tabulated data in Excel format will be securely stored as an archive. This is done to ensure that the data can serve as easily accessible evidence if needed. Following data collection, the data will be examined and categorized based on respondents' highest education level, position, and work experience. This process is crucial to ensure the targeted distribution of the questionnaire and to ensure the obtained data has good validity. The research instruments used, including the questionnaire, have been thoroughly prepared and are available in a comprehensive appendix that also includes a summary of respondent data.

The PLS (Partial Least Squares) method follows a three-stage approach, which includes the principal component approach, the projection or regression approach, and the measurement approach. In SEM-PLS analysis, several factors need to be considered when determining the appropriate sample size, such as missing values, data distribution, and measurement scales [43]. Researchers should pay attention to whether the data used meets the requirements for SEM-PLS modeling. Researchers should also consider the presence of incomplete observations (missing values) in their data. Additionally, it is advisable to use a better measurement scale than a nominal scale when measuring endogenous latent variables to ensure a well-identified model. In SEM-PLS testing, factors under consideration encompass model properties, sample size, the distribution shape of data, missing values, and the measurement scale. The determination of the minimum sample size arises from the path factor (p-min) and the variation observed during the 80% statistical stress test [44]. To accomplish the research objectives, the subsequent phase involves formulating a research plan for each step to obtain statistical analysis and outlining the steps for implementing the research in the case studies.

Revit is renowned across various engineering domains due to its versatility, exceptional precision, and rapidity. It functions as a Building Information Modeling (BIM) software, commonly referred to as Revit. The evolution of information modeling streamlines the storage of data, facts, and analyses. The results of the project will be amalgamated with a supportive framework to generate a realistic depiction. For enhanced accuracy in translation, additional details from the source text are necessary. Panels are present on both opposing sides. The assessment of project time and cost management principles, coupled with existing methodologies, aims to provide actionable suggestions.

According to Figure 2, the execution of the research involves 4 main variables, which are subsequently investigated and analyzed to ensure the precision of the research. Subsequently, the researcher details the stages involved in exploring, developing, and analyzing the key factors in the research process to attain the research objectives.
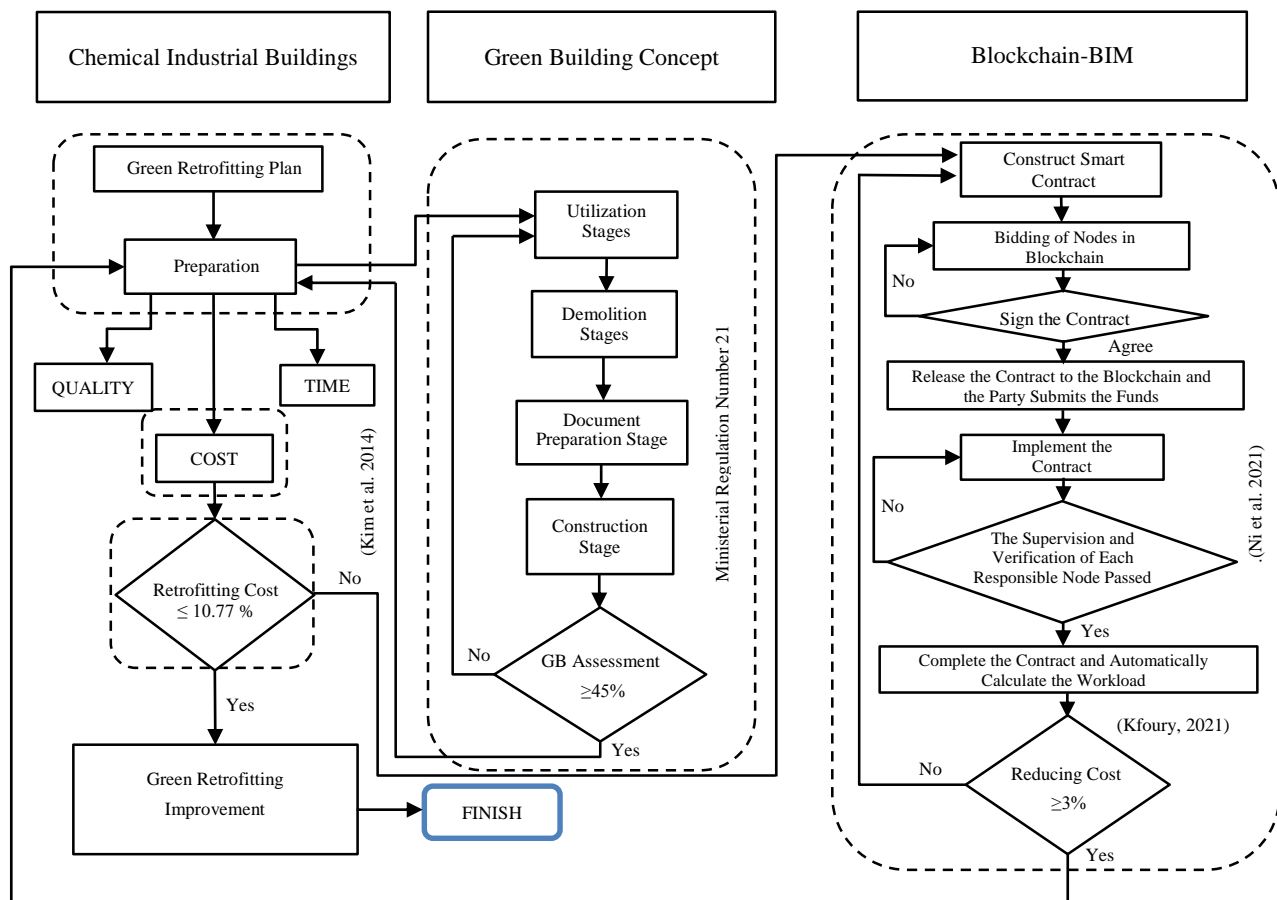
Figure 2. Research Implementation of GB Concept on Chemical Industrial Building, Configured of [42, 45, 46] and Flow Adoption of Yuliatti et al. (2022) [47]

3. Result and Discussion

3.1. Data Processing Result

The study was conducted at a Chemical Industry Building Project located in Cilegon-Banten, Indonesia. This project, spanning approximately ± 50,000 m², is intricate and aligns with all the stipulated parameters outlined in the Technical Guidelines for implementing the latest Green Building regulations mandated by the Indonesian government. Research questionnaires were distributed to 120 participants, which meets the minimum requirement of 118 respondents for statistical analysis (Figure 3). The respondent data consists of the information collected from the participants:
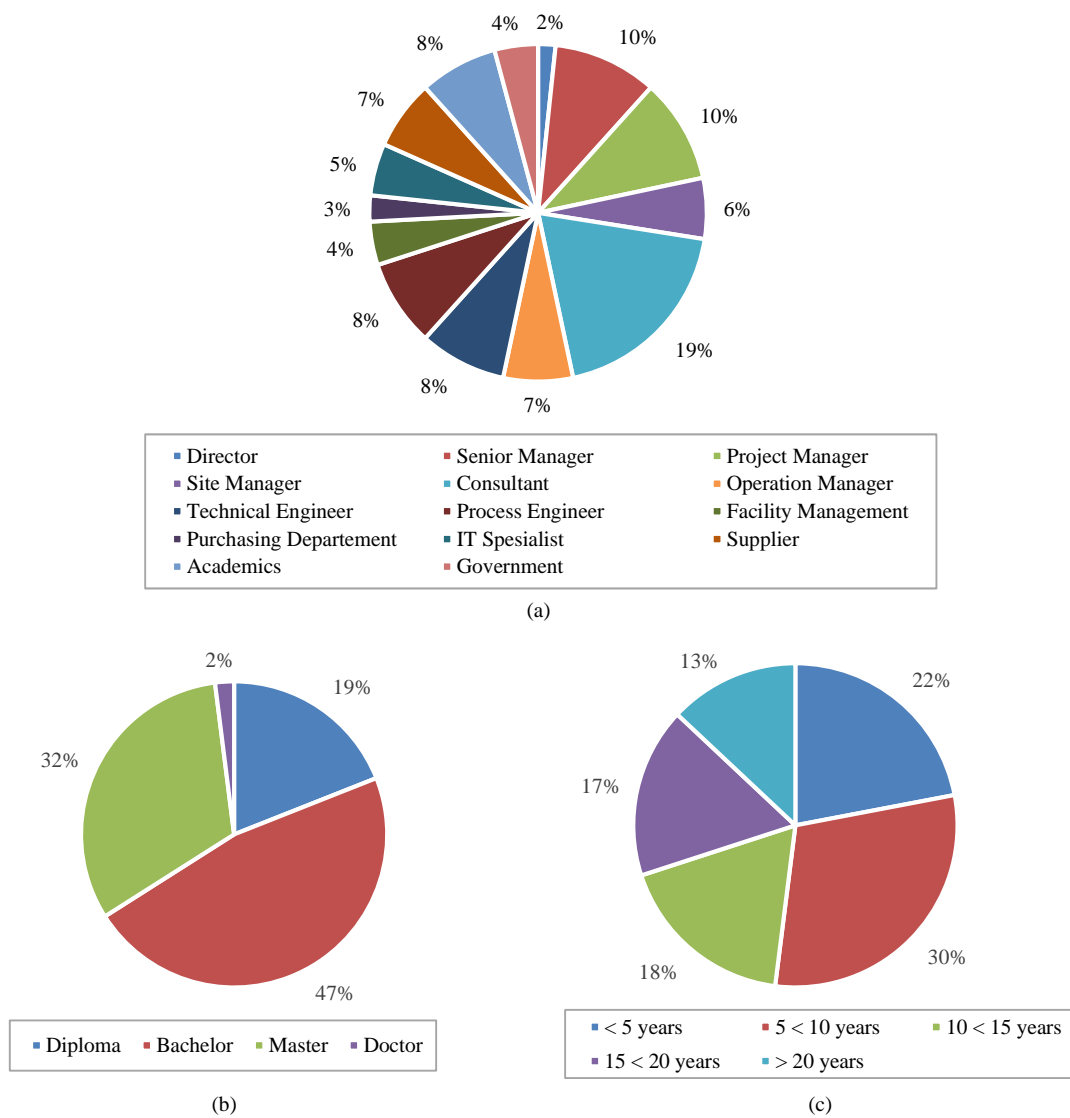
Figure 1. Respondent data, (a) position, (b) education, (c) work experience

To ensure that the data population is accurately targeted, determining the population is not solely based on the population size but also involves validation from experts. This is done to ensure that the targeted population aligns with the research objectives. After data collection, the gathered data is examined and grouped based on variables such as education, job position, and project experience. This is crucial to appropriately direct the questionnaire to relevant respondents, thereby obtaining valid data (Table 1). By the latest Green Building regulations established by the Indonesian government, it is mandatory for this building to meet the specified Green Building criteria. However, the evaluation results reveal a score of 62.3 points in the planning stage, indicating the need for improvements across various aspects to achieve a minimum Basic rating of 74.25 points. Of particular significance is the role of energy-related points in reaching this goal.

Table 1. Performance Assessment of Utilization Stage in Green Building based on Technical Guidelines of the Ministry of PUPR No.1 Year 2022 [14, 48]

No.	Criteria	Point	No.	Criteria	Point
1	Public Transportation	1	57	Do not use materials that affect health	2
2	Vehicle electric battery charging	1	58	Construction does not interfere with activities	2
3	Bicycle parking lots	1	59	Project innovation toward 'green' area improvement	2
4	Environmental Management Documents	1	60	Efficient construction equipment	1
5	Document on water-saving efforts	1	61	Safety against tool use	1
6	Document on energy-saving efforts	1	62	Management of construction waste piles	1
7	Area improvement effort document	1	63	Green construction process document	1
8	Document on waste management efforts	1	64	Work handover document	1
9	Document on waste management efforts	1	65	Government spatial plant drawing document	1
10	Opr. & Standard Operating Procedure (SOP) Document	1	66	Evaluation of waste management utilization	3
11	Master plan area	1	67	Evaluation of water consumption utilization	3
12	Performance management area	1	68	Evaluation of local material utilization	3
13	Inspection of area infrastructure and facilities	1	69	Evaluation of electricity consumption utilization	3
14	SOP emergency response	1	70	Evaluation of Outdoor Space Function Utilization	3
15	Maintenance manager training	2	71	Maintenance and care according to evaluation	4
16	Soft skills training	1	72	Improvements to increase tenant satisfaction	4
17	Local architecture design	2	73	Local architecture for building and area design	2
18	Preservation of heritage areas and buildings	2	74	Preservation of cultural heritage buildings	2
19	20% local raw materials (0-20 km radius)	3	75	20% local materials	2
20	Consumption plants (min. 10% of green space area)	1	76	Planting of consumption of crops min. 10%	2
21	Drainage with flood ≤ 30cm, receding ≤ 2 hours	1	77	Drainage reliability to manage water logging	2
22	Periodic blackout-free power grid	2	78	Regional power grid free of periodic blackouts	2
23	Information and communication networks.	2	79	Disruption-free information. and comm. networks	2
24	Facilities are in good condition.	2	80	Vehicle electric battery charging	2
25	Min. 10% of the area of the facility	1	81	Min. 10% of the area for MSEs	1
26	Maintenance of regional road facilities and infrastructure	1	82	There are road operations within the area	1
27	Green lanes on-road facilities and infrastructure	1	83	Green lanes on-road facilities and infrastructure as required	1
28	Path of Sharing in a Residential Environment	1	84	Roads in residential neighborhoods	1
29	Shared beneficial path	1	85	Sharing the road with speed bumps	1
30	Sharing road equipped with speed bumps	1	86	There are road signs	1
31	Road signs or markers	1	87	Min. 50 street trees per 10 meters	1
32	Min. 50% of road sections share trees	1	88	There is >30% green space from the total area of the whole area	3
33	Outdoor Space > 30% of the total area	3	89	Land area according to the Government Spatial Plan	2
34	Land by Government Spatial Plan	3	90	Not using productive land	1
35	Development of areas not on productive land	2	91	There is a soil pollution investigation	1
36	Area soil pollution investigation	1	92	Negative value land revitalization	2
37	Land revitalization is negative.	2	93	Min. 50% natural terrain	2
38	Retain min. 50% natural landforms.	2	94	Min. 30% infiltration surface area	1
39	Min. 30% of the area's surface for rainwater.	2	95	Min. 10% porous land cover	2
40	Min. 10% using porous covers	1	96	There is green vegetation with a canopy area of min. 20% of the area	2
41	Green vegetation min. 20% area	2	97	There is a use of alternative water sources of at least 10%.	1
42	Alternative water sources min. 10%	1	98	Note of work application	1
43	Whole area water meters	1	99	The entire area uses water meters	1
44	Min. 1% catchment area	1	100	Min. 1% water catchment area	1
45	Min. 1 communal wastewater treatment	1	101	There is a communal wastewater treatment plant	1

46	Min. 1 communal garbage	1	102	There is at least 1 communal waste disposal facility	1
47	Min. 1 communal waste composter	1	103	Min. 1 waste composter facility	1
48	Min. 1 waste collection device	1	104	There is at least 1 polling station	1
49	Min. 1 temporary waste storage	1	105	There is 1 waste recycling building	1
50	Min. 1 Waste recycling	1	106	There is an organization that manages the waste in the area	1
51	Waste management organization	1	107	There is the use of renewable electricity sources	2
52	Infrastructure lighting area	2	108	Project implementation record	1
53	Facility lighting area	1	109	If only 50% of the lights are illuminated, the score is 1 point.	2
54	Facilities and infrastructure meet the law	2	110	There is the use of renewable electrical energy sources	2
55	Reuse of used materials min. 10% of the total cost	2	111	Facilities and infrastructure comply with laws and regulations	2
56	Renewable materials min. 10% of material costs	2	112	Use of 10% reused materials	2

3.2. Implementation of SEM-PLS for Identifying the Dominant Factor of Influence

In this research project, the questionnaire data gathered by the researchers will undergo processing and analysis using "structural equation modeling" (SEM). The p-values of the loading factor and path coefficient, along with the diagram corresponding to Figure 4, can demonstrate the relationship between p-value and path coefficient. SEM allows for a thorough examination of latent variables, factors, and procedural issues, which can be analyzed as subfactors of observed or latent variables. The researchers utilized the SEM SMART-PLS software version 3.0 for this analysis. Figure 5 shows that the R-Square value of the collective influence on the Cost (Y) variable is 0.825, with an adjusted R-Square value of 0.824. This indicates that all independent variables collectively influence the Cost (Y) variable by 0.825, or 82.5%. Since the adjusted R-Square value of 82.5% is greater than 50%, it can be concluded that the influence of all independent variables on the Cost (Y) variable is considered strong.
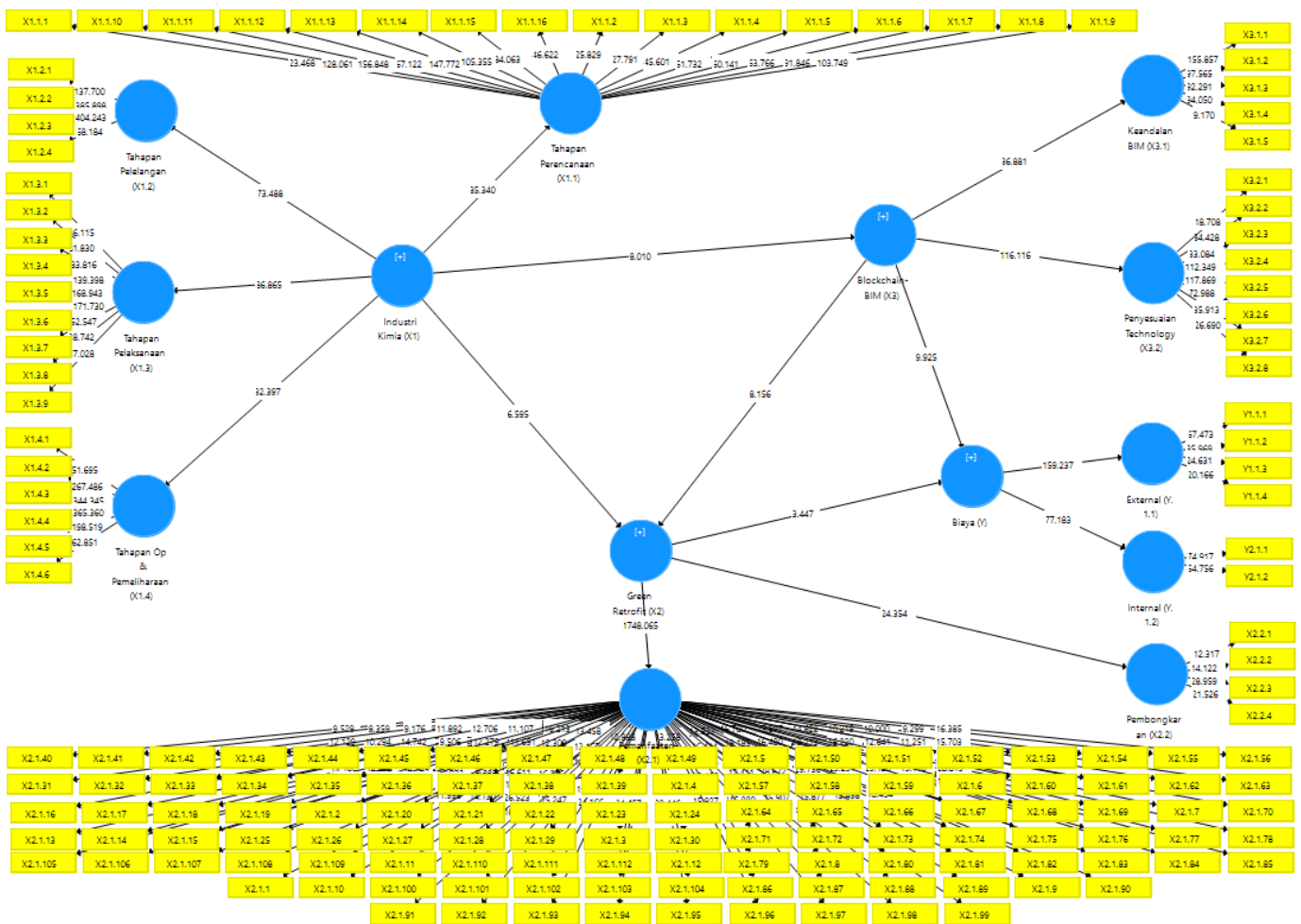
Figure 2. The Diagram of P-values and Partial Coefficients

R Square
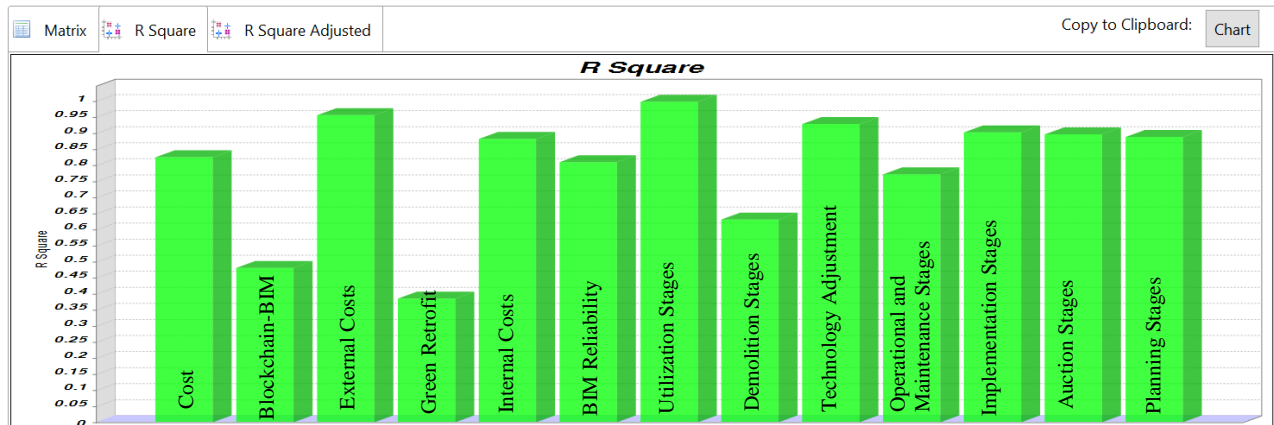
Figure 3. The diagram of R-Square values

Based on the analysis conducted on 170 factors, it was found that there are 10 factors in Table 2, that have the most significant influence in improving the cost performance of Green Building retrofit in Industrial Buildings using Blockchain-BIM Table 3. The most influential factor, in descending order, is the evaluation of electricity consumption utilization Table 4.

Table 1. The Most Influential Main Factor

No	Factor	R Square
1	Utilization Stages (X2.1)	0.998
2	External Costs (Y1.1)	0.956
3	Technology Adjustment (X3.2)	0.928
4	Implementation Stages (X1.3)	0.902
5	Auction Stages (X1.2)	0.896
6	Planning Stages (X1.1)	0.888
7	Internal Costs (Y2.1)	0.882
8	BIM Reliability (X3.1)	0.810
9	Operational and Maintenance Stages (X1.4)	0.772
10	Demolition Stages (X2.2)	0.631

Table 2. Results of Construct Reliability Examination based on Convergent Validity

Main Factor	Cronbach's Alpha	rho_A	Composite Reliability	Average Variance Extracted (AVE)
Green Retrofit (X2)	0.992	0.992	0.992	0.514
Chemical Industry (X1)	0.993	0.993	0.993	0.807
External Costs (Y2)	0.900	0.904	0.952	0.909
Internal Costs (Y1)	0.901	0.904	0.931	0.773
Costs (Y)	0.935	0.940	0.949	0.757
Blockchain-BIM (X3)	0.973	0.974	0.976	0.760
BIM Reliability (X3.1)	0.949	0.950	0.964	0.844
Auction Stage (X1.2)	0.992	0.992	0.994	0.977
Implementation Stages (X1.3)	0.992	0.992	0.993	0.938
Utilization Stages (X2.1)	0.991	0.992	0.992	0.517
Demolition Stages (X2.2)	0.871	0.883	0.912	0.721
Technology Adjustment (X3.2)	0.979	0.980	0.983	0.876
Planning Stages (X1.1)	0.991	0.992	0.992	0.887
Operational and Maintenance Stages (X1.4)	0.995	0.995	0.996	0.977

Table 3. The Most Influential Sub Factor (Significant)

No	Sub Factor	Original Sample Value	Mean	t. statistic > 1.96 (p < 0.05)	R Square
1	Waste management	X2.1.66	0.831	0.831	32.617	
2	Blockchain Transactions	X3.2.3	0.920	0.920	32.344	
3	Demolition Material Disposal Locations	X2.2.3	0.866	0.865	27.238	
4	Planting consumption crops min. 10% of the industrial open space area	X2.1.76	0.815	0.815	27.612	
5	Min. 30% of the surface area absorbs rainwater	X2.1.94	0.812	0.811	25.279	0.998
6	Documents efforts to save energy	X2.1.6	0.686	0.686	12.958	
7	The reliability of the drainage network manages stagnant water	X2.1.77	0.715	0.717	15.756	
8	The use of renewable sources of electrical energy for lighting industrial facilities	X2.1.108	0.709	0.709	12.599	
9	Evaluation of water consumption utilization	X2.1.67	0.680	0.681	12.571	
10	Evaluation of the utilization of electricity consumption	X2.1.69	0.653	0.653	9.735	

The suggested optimization and decision support techniques are subjected to simulation for validation purposes. All simulations were and 12 GB of RAM, using BIM Revit 2023. The results of the retrofit simulation conducted with the addition of natural lighting in the warehouse building have proven to be very successful. From the lighting lux measurement results, before the retrofit, it was below 200 lux Figure 6, and after the retrofit, the luminance value increased to above 200 lux Figure 7.
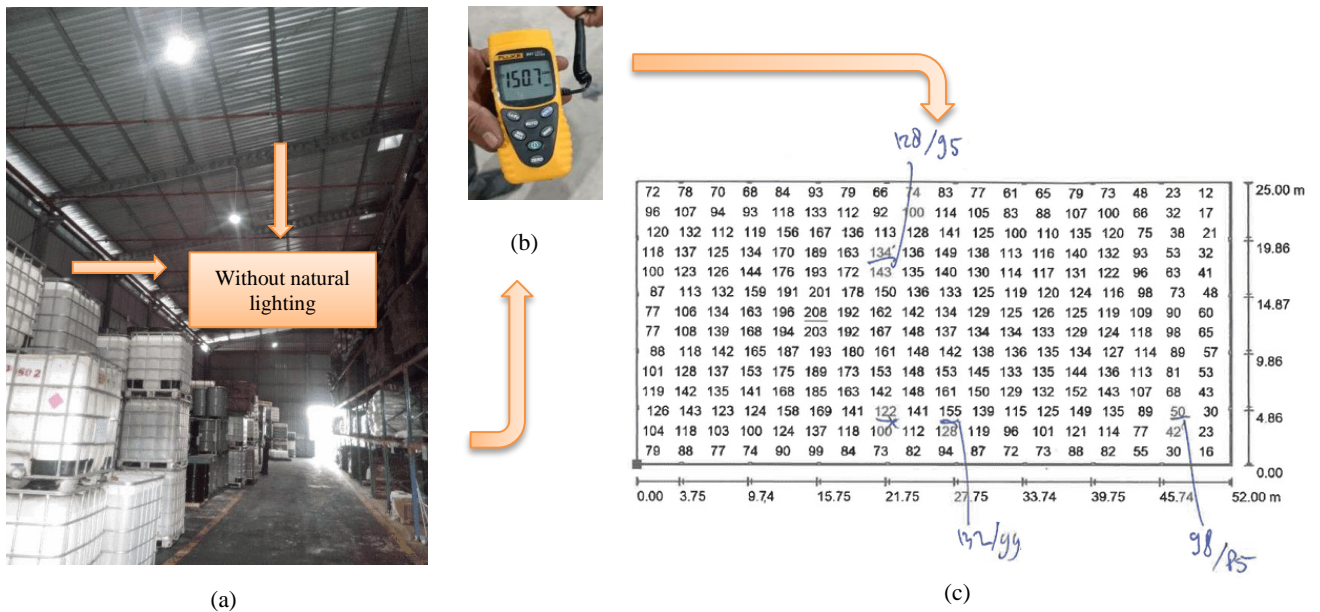
Figure 4. Lumination check before retrofitting, (a) building condition without natural lighting, (b) lux meter measurement value, (c) values chart in lux
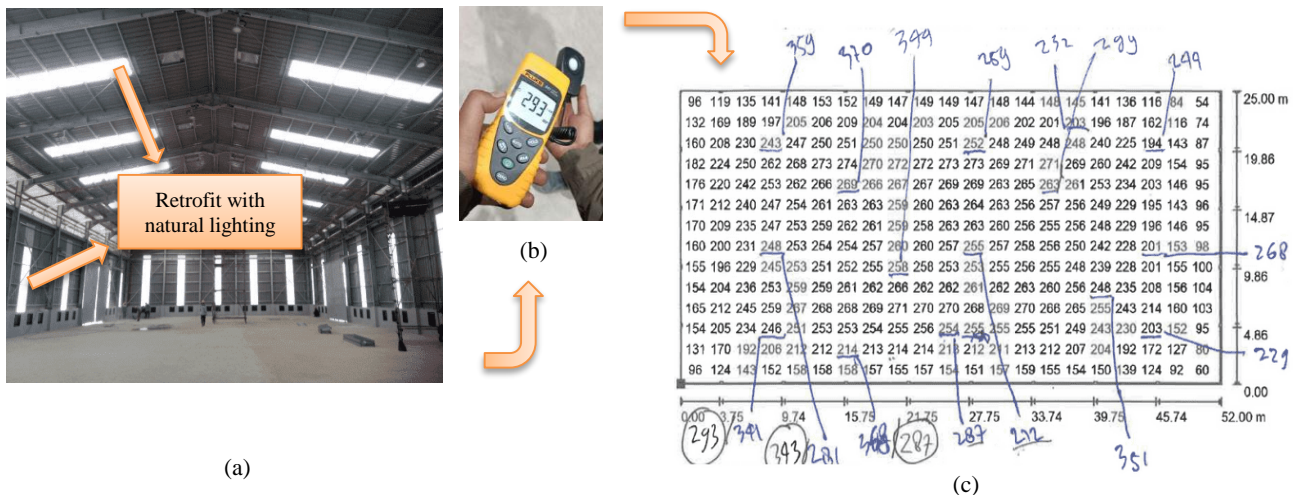
Figure 5. Lumination check after retrofitting, (a) building condition with natural lighting, (b) lux meter measurement value, (c) values chart in lux

Utilizing BIM enabled the creation of highly efficient building models for overseeing low-carbon construction initiatives. This approach ensures a thorough analysis of the entire lifecycle, encompassing service life planning and the optimization of building design and usage throughout its lifecycle. Before the retrofitting of the existing building, the monthly electricity consumption can be observed in Table 5, and the electricity consumption versus the kWh meter graph is shown in Figure 8.

Table 4. Monthly electricity consumption of case study, 2023

Month	KWh			Cost/KWh (IDR)	Total Cost (IDR)
	LWBP	**WBP**	**Total**		
Jan-22	625,350	130,950	756,300	IDR 1,035.78	IDR 783,360,414
Feb-22	625,460	130,810	756,270	IDR 1,035.78	IDR 783,329,341
Mar-22	624,300	131,990	756,290	IDR 1,035.78	IDR 783,350,056
Apr-22	628,890	127,360	756,250	IDR 1,035.78	IDR 783,308,625
May-22	624,980	130,860	755,840	IDR 1,035.78	IDR 782,883,955
Jun-22	624,340	132,020	756,360	IDR 1,035.78	IDR 783,422,561
Jul-22	626,450	129,900	756,350	IDR 1,035.78	IDR 783,412,203
Aug-22	624,580	131,780	756,360	IDR 1,035.78	IDR 783,422,561
Sep-22	624,390	131,940	756,330	IDR 1,035.78	IDR 783,391,487
Oct-22	622,990	133,350	756,340	IDR 1,035.78	IDR 783,401,845
Nov-22	624,640	131,670	756,310	IDR 1,035.78	IDR 783,370,772
Dec-22	625,680	130,670	756,350	IDR 1,035.78	IDR 783,412,203
Total (IDR)	**7,502,050**	**1,573,300**	**9,075,350**	**IDR 12,429.36**	**IDR9,400,066,023**
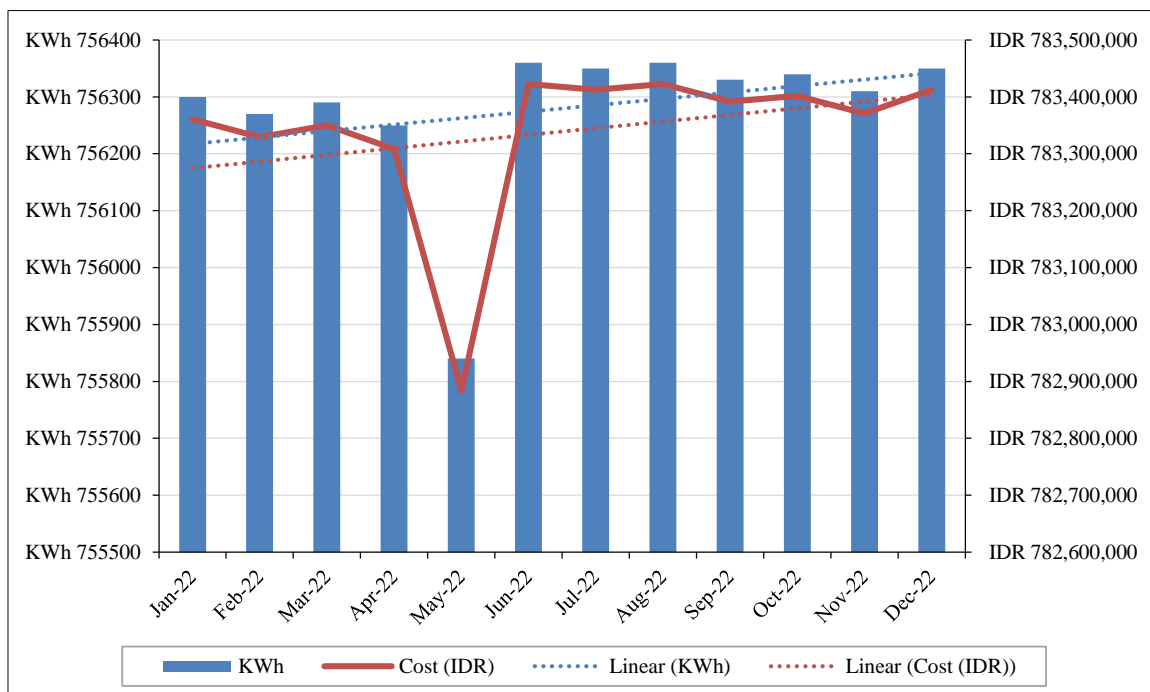
Figure 6. Monthly electricity consumption of case study, 2023

Table 6 and Figure 9 below illustrate the reduction in electricity consumption measured in kWh meters, resulting in reduced electricity usage costs from March 2024 to August 2024 after the green retrofitting of the chemical industry building.

Table 5. Monthly electricity consumption of case study, 2024

Month	KWh			Cost/KWh (IDR)	Total Cost (IDR)
	LWBP	WBP	Total		
Jan-23	625,456	130,975	756,431	IDR 1,035.78	IDR 783,496,101
Feb-23	625,468	130,828	756,296	IDR 1,035.78	IDR 783,356,271
Mar-23	622,200	126,990	749,190	IDR 1,035.78	IDR 775,996,018
Apr-23	621,890	126,360	748,250	IDR 1,035.78	IDR 775,022,385
May-23	620,980	125,860	746,840	IDR 1,035.78	IDR 773,561,935
Jun-23	620,340	125,020	745,360	IDR 1,035.78	IDR 772,028,981
Jul-23	619,850	124,900	744,750	IDR 1,035.78	IDR 771,397,155
Aug-23	620,180	125,180	745,360	IDR 1,035.78	IDR 772,028,981
Total (IDR)	**4,976,364**	**1,016,113**	**5,992,477**	**IDR 8,286.24**	**IDR6,206,887,827**
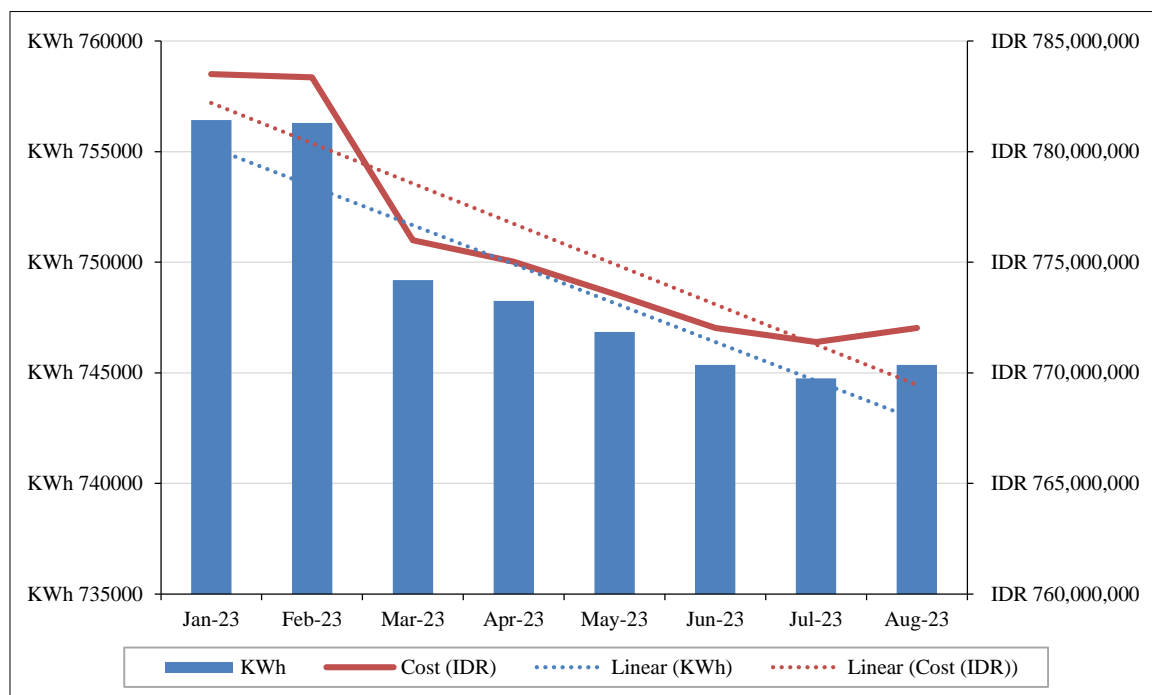
Figure 7. Monthly electricity consumption of case study, 2024

The analysis of the implementation of Blockchain-Building Information Modeling (BIM) on retrofitting works through modeling and input of unit price parameters resulted in the investment value of chemical industry retrofitting works and the analysis results as shown in Table 7, cost savings of 4.42% for Primary, 4.45% for Middle, and 4.40% for Main were obtained.

Table 6. Budget Plan for Green Retrofitting with Blockchain-BIM

NO	DESCRIPTION	Initial Budget Plan	Green Building Improvement Budget Plan			Green Building Improvement Budget Plan Using Blockchain-BIM		
			PRIMARY	MIDDLE	MAIN	PRIMARY	MIDDLE	MAIN
1	Preliminary, Legal, and Safety Work	4,539,606,575	4,539,606,575	4,539,606,575	4,539,606,575	4,539,606,575	4,539,606,575	4,539,606,575
2	Structure Office Building	19,395,000,000	19,395,000,000	19,395,000,000	19,395,000,000	19,395,000,000	19,395,000,000	19,395,000,000
3	Laboratory Building	1,320,763,000	1,320,763,000	1,320,763,000	1,320,763,000	1,320,763,000	1,320,763,000	1,320,763,000
4	Utility Facility	24,937,500,000	24,937,500,000	24,937,500,000	24,937,500,000	24,937,500,000	24,937,500,000	24,937,500,000
5	Plant Production Facility	106,816,000,000	106,816,000,000	106,816,000,000	106,816,000,000	106,816,000,000	106,816,000,000	106,816,000,000
6	Infrastructure Facility	10,500,000,000	10,500,000,000	10,500,000,000	10,500,000,000	10,500,000,000	10,500,000,000	10,500,000,000
7	Provision of Green Building Handbook (BGH) SOP & Governance Documents.		260,000,000	364,000,000	572,000,000	260,000,000	364,000,000	572,000,000
8	Planning for Renovation Work		416,000,000	468,000,000	577,200,000	416,000,000	468,000,000	577,200,000
9	Retrofitting Works							
	- Bus Stop		-	385,000,000	385,000,000	-	367,290,000	367,290,000
	- Solar panel		8,586,070,577	8,586,070,577	8,586,070,577	8,191,111,330	8,191,111,330	8,191,111,330
	- Replacement of Water-Efficient Sanitary Fixtures		-	445,769,222	445,769,222	-	425,263,837	425,263,837
	- Provision of Outdoor Smoking Area Outside the Building		-	-	175,000,000	-	-	166,950,000
	- Temporary Waste Storage Area		2,026,061,613	2,026,061,613	2,026,061,613	1,932,862,779	1,932,862,779	1,932,862,779
	- Organic Waste Composting Machine		-	-	397,612,378	-	-	379,322,209
	- Inorganic Waste Recycling Machine		-	-	357,500,000	-	-	341,055,000
	- Provision of Biopores and Infiltration		489,750,000	489,750,000	489,750,000	467,221,500	467,221,500	467,221,500
	- Natural Lighting Fixtures inside the Building		995,766,611	995,766,611	995,766,611	949,961,347	949,961,347	949,961,347
	- Public Street Lighting and Garden Lamps Using Solar Cells		-	3,668,836,563	3,668,836,563	-	3,500,070,081	3,500,070,081
	- Sewage Treatment Plant (STP)		-	2,391,214,509	2,391,214,509	-	2,281,218,642	2,281,218,642
	- Improvement cooling tower system		2,928,913,800	2,928,913,800	2,928,913,800	2,794,183,765	2,794,183,765	2,794,183,765
10	Maintenance Work During Utilization Period		1,361,881,973	1,702,352,466	2,213,058,205	1,299,235,402	1,624,044,252	2,111,257,528
11	Socialization and Empowerment Work for Green Building Occupants/Users		453,960,658	453,960,658	453,960,658	433,078,467	433,078,467	433,078,467
	TOTAL (IDR)	167,508,869,575	185,027,274,806	192,414,565,592	194,172,583,710	184,252,524,165	191,307,175,575	192,998,916,060
	Difference between Non-Green Building Cost Estimate (RAB) and Green Building Improvement Cost Estimate (RAB) (IDR)		17,518,405,231	24,905,696,017	26,663,714,135	16,743,654,590	23,798,306,000	25,490,046,485
	Difference (%)		10.46%	14.87%	15.92%	774,750,641	1,107,390,017	1,173,667,650
	Percentage Reduction in Cost Difference					4.42%	4.45%	4.40%

4. Conclusion

The implementation of green initiatives like energy-efficient systems, improved lighting, water conservation, and recycling results in a 10.77% increase in green construction costs, often referred to as retrofitting costs. Considering that all assessment results indicate a rating exceeding 10.77%, it implies the need for retrofitting. To mitigate these retrofitting expenses, the blockchain-BIM approach can be employed. The flow diagram for implementing cost efficiency in Green Industrial Buildings using Blockchain-BIM has proven to be effective in improving the cost efficiency of Green buildings. The research results showed cost savings of 4.42% at the Primary level, 4.45% at the Middle level, and 4.40% at the Main level for Chemical Industry Buildings with Blockchain-BIM implementation. Based on the analysis results, the hypothesis was confirmed that the Blockchain-BIM method in the Green Industry can effectively improve the cost efficiency of Chemical Industrial Buildings.

In this research, assistance is required for initiating the development of intelligent smart contracts on the Blockchain network due to limitations that impact the technological aspect of the study. The researchers have encountered setbacks multiple times while attempting to create applications based on Blockchain. Consequently, future studies should involve collaborative efforts with Blockchain practitioners to streamline and facilitate the implementation of this method. The associated expenses, conversely, will be in direct correlation with the electrical energy generated, depending on the stakeholders in question. Evaluating the profitability of a technology necessitates considering both its cost and energy demands. Moreover, governmental policies, regulations, and incentives are pivotal and can drive the widespread adoption of the Green Building (GB) concept, particularly in retail structures. This strategy is crucial for attaining the objectives of sustainable development in Indonesia.

5. Declarations

5.1. Author Contributions

5.2. Data Availability Statement

The data presented in this study are available in the article.

5.3. Funding

5.4. Acknowledgments

5.5. Conflicts of Interest

The authors declare no conflict of interest.

6. References

[1] Huo, T., Ren, H., Zhang, X., Cai, W., Feng, W., Zhou, N., & Wang, X. (2018). China's energy consumption in the building sector: A Statistical Yearbook-Energy Balance Sheet based splitting method. Journal of Cleaner Production, 185(2018), 665–679. doi:10.1016/j.jclepro.2018.02.283.

[2] Mi, Z. F., Pan, S. Y., Yu, H., & Wei, Y. M. (2015). Potential impacts of industrial structure on energy consumption and CO_2 emission: A case study of Beijing. Journal of Cleaner Production, 103, 455–462. doi:10.1016/j.jclepro.2014.06.011.

[3] Zhang, Y. J., Hao, J. F., & Song, J. (2016). The CO_2 emission efficiency, reduction potential and spatial clustering in China's industry: Evidence from the regional level. Applied Energy, 174(2016), 213–223. doi:10.1016/j.apenergy.2016.04.109.

[4] Li, D., Cui, P., & Lu, Y. (2016). Development of an automated estimator of life-cycle carbon emissions for residential buildings: A case study in Nanjing, China. Habitat International, 57, 154–163. doi:10.1016/j.habitatint.2016.07.003.

[5] Le, D.-L., Nguyen, T.-Q., & Huu, K. D. (2021). Life Cycle Carbon Dioxide Emissions Assessment in the Design Phase: A Case of a Green Building in Vietnam. Engineering Journal, 25(7), 121–133. doi:10.4186/ej.2021.25.7.121.

[6] Li, H., Deng, Q., Zhang, J., Xia, B., & Skitmore, M. (2019). Assessing the life cycle CO_2 emissions of reinforced concrete structures: Four cases from China. Journal of Cleaner Production, 210(38), 1496–1506. doi:10.1016/j.jclepro.2018.11.102.

[7] Javan, K., Mirabi, M., Hamidi, S. A., Darestani, M., Altaee, A., & Zhou, J. (2023). Enhancing Environmental Sustainability in a Critical Region: Climate Change Impacts on Agriculture and Tourism. Civil Engineering Journal, 9(11), 2630–2648. doi:10.28991/cej-2023-09-11-01.

[8] Ozturk, T., Altinsoy, H., Türkeş, M., & Kurnaz, M. (2012). Simulation of temperature and precipitation climatology for the Central Asia CORDEX domain using RegCM 4.0. Climate Research, 52, 63–76. doi:10.3354/cr01082.

[9] Nukusheva, A., Ilyassova, G., Rustembekova, D., Zhamiyeva, R., & Arenova, L. (2021). Global warming problem faced by the international community: international legal aspect. International Environmental Agreements: Politics, Law and Economics, 21, 219-233. doi:10.1007/s10784-020-09500-9.

[10] Tong, Z., Chen, Y., Malkawi, A., Liu, Z., & Freeman, R. B. (2016). Energy saving potential of natural ventilation in China: The impact of ambient air pollution. Applied Energy, 179, 660–668. doi:10.1016/j.apenergy.2016.07.019.

[11] Atabay, S., Pelin Gurgun, A., & Koc, K. (2020). Incorporating BIM and Green Building in Engineering Education: Assessment of a School Building for LEED Certification. Practice Periodical on Structural Design and Construction, 25(4), 1–11. doi:10.1061/(asce)sc.1943-5576.0000528.

[12] Liang, X., Shen, G. Q., & Guo, L. (2015). Improving management of green retrofits from a stakeholder perspective: A case study in China. International Journal of Environmental Research and Public Health, 12(11), 13823–13842. doi:10.3390/ijerph121113823.

[13] Laudeman, S. M., Raja, T., & Bansal, N. (2022). Early-Stage Structural Steel Estimation for Embodied Carbon Decision Making. ASHRAE Building Decarbonization 2022 Conference, 5-7 October, 2022, Athens, Greece.

[14] BPK (2024). Regulation of the Minister of Public Works and Public Housing of the Republic of Indonesia. (2021). Number 21 of 2021 concerning Green Building Performance Assessment. Tentang Database Peraturan, Jakarta, Indonesia. Available online: https://peraturan.bpk.go.id/Download/211361/Permen%20PUPR_21_2021.pdf (accessed on February 2024).

[15] Sun, C. Y., Chen, Y. G., Wang, R. J., Lo, S. C., Yau, J. T., & Wu, Y. W. (2019). Construction cost of green building certified residence: A case study in Taiwan. Sustainability (Switzerland), 11(8), 2195. doi:10.3390/su11082195.

[16] Colberg, J., Kuok, K., Hii, M., & Koenig, S. G. (2022). Importance of Green and Sustainable Chemistry in the Chemical Industry. ACS Sustainable Chemistry and Engineering, 10(26), 8239–8241. doi:10.1021/acssuschemeng.2c03306.

[17] Homod, R. Z., & Sahari, K. S. M. (2013). Energy savings by smart utilization of mechanical and natural ventilation for hybrid residential building model in passive climate. Energy and Buildings, 60, 310-329. doi:10.1016/j.enbuild.2012.10.034.

[18] Tang, B., Zou, Y., Yu, B., Guo, Y., & Zhao, G. (2021). Clean heating transition in the building sector: The case of Northern China. Journal of Cleaner Production, 307, 127206. doi:10.1016/j.jclepro.2021.127206.

[19] Srivanit, M., & Jareemit, D. (2020). Modeling the influences of layouts of residential townhouses and tree-planting patterns on outdoor thermal comfort in Bangkok suburbs. Journal of Building Engineering, 30, 101262. doi:10.1016/j.jobe.2020.101262.

[20] Darko, A., Zhang, C., & Chan, A. P. C. (2017). Drivers for green building: A review of empirical studies. Habitat International, 60, 34–49. doi:10.1016/j.habitatint.2016.12.007.

[21] Hwang, B. G., Zhu, L., Wang, Y., & Cheong, X. (2017). Green building construction projects in Singapore: Cost premiums and cost performance. Project Management Journal, 48(4), 67-79. doi:10.1177/875697281704800406.

[22] Shiekh, A. El, & Barsoum, J. (2021). Determining Building Sustainability using BIM applications: Review. IJISET-International Journal of Innovative Science, Engineering & Technology, 8(6), 86-98.

[23] Gunjan, V. K., Singh, S. N., Duc-Tan, T., Aponte, G. J. R., & Kumar, A. (Eds.). (2020). ICRRM 2019-System Reliability, Quality Control, Safety, Maintenance and Management: Applications to Civil, Mechanical and Chemical Engineering. Springer Singapore. doi:10.1007/978-981-13-8507-0.

[24] Al-Jaroodi, J., & Mohamed, N. (2019). Blockchain in Industries: A Survey. IEEE Access, 7, 36500–36515. doi:10.1109/access.2019.2903554.

[25] Nawari, N., & Ravindran, S. (2019). Blockchain and Building Information Modeling (BIM): Review and Applications in Post-Disaster Recovery. Buildings, 9(6), 149. doi:10.3390/buildings9060149.

[26] Abeyratne, S. A., & Monfared, R. P. (2016). Blockchain-ready manufacturing supply chain using distributed ledger. International Journal of Research in Engineering and Technology, 5(9), 1-10.

[27] Brandão, A., Mamede, H. S., & Gonçalves, R. (2018). Systematic Review of the Literature, Research on Blockchain Technology as Support to the Trust Model Proposed Applied to Smart Places. Trends and Advances in Information Systems and Technologies, 27-29 March 2018, Naples, Italy.

[28] Celik, Y., Petri, I., & Barati, M. (2023). Blockchain-supported BIM data provenance for construction projects. Computers in Industry, 144, 103768. doi:10.1016/j.compind.2022.103768.

[29] Liu, Z., Jiang, L., Osmani, M., & Demian, P. (2019). Building information management (BIM) and blockchain (BC) for sustainable building design information management framework. Electronics, 8(7), 724. doi:10.3390/electronics8070724.

[30] Amhaimedi, S., Naimi, S., & Alsallami, S. (2023). Assessment of a Decision-Making Model for Monitoring the Success of a Project for Smart Buildings. Civil Engineering Journal, 9(1), 127–142. doi:10.28991/cej-2023-09-01-010.

[31] Ye, X., Sigalov, K., & König, M. (2020). Integrating BIM and cost-included information container with Blockchain for construction automated payment using billing model and smart contracts. Proceedings of the International Symposium on Automation and Robotics in Construction. doi:10.22260/isarc2020/0192.

[32] Heaton, J., Parlikad, A. K., & Schooling, J. (2019). A Building Information Modelling approach to the alignment of organizational objectives to Asset Information Requirements. Automation in Construction, 104, 14–26. doi:10.1016/j.autcon.2019.03.022.

[33] Du, X., Zhang, Y., & Lv, Z. (2020). Investigations and analysis of indoor environment quality of green and conventional shopping mall buildings based on customers' perception. Building and Environment, 177, 106851. doi:10.1016/j.buildenv.2020.106851.

[34] Fialho, B. C., Codinhoto, R., & Fabricio, M. M. (2020). BIM and IoT for the AEC Industry: A systematic literature mapping. Procedia Engineering, 2(4), 392-399.

[35] Changsaar, C., Abidin, N. I., Khoso, A. R., Luenhui, L., Yaoli, X., & Hunchuen, G. (2022). Optimizing energy performance of an Eco-Home using Building Information Modelling (BIM). Innovative Infrastructure Solutions, 7(2), 140. doi:10.1007/s41062-022-00747-6.

[36] Mathews, M., Robles, D., & Bowe, B. (2017). BIM+ blockchain: A solution to the trust problem in collaboration? CITA BIM Gathering 2017, November 23rd-24th November 2017, Dublin, Ireland. doi:10.21427/D73N5K.

[37] Zia, I., Singh, P., Tiwari, A. K., & Pandey, A. (2022). Integration Blockchain for Data Sharing and Collaboration in Mobile Healthcare Applications. Lecture Notes in Electrical Engineering, 8-13 October, 2022, Montreal, Canada.

[38] Kfoury, B. (2021). The role of blockchain in reducing the cost of financial transactions in the retail industry. WCNC-2021: Workshop on Computer Networks & Communications, 01 May 2021, Chennai, India.

[39] Sreckovic, M., Sibenik, G., Breitfuß, D., & Preindl, T. (2020). Analysis of Design Phase Processes with BIM for Blockchain Implementation. SSRN Electronic Journal, 1-7. doi:10.2139/ssrn.3577529.

[40] Crawley, D. B., Lawrie, L. K., Winkelmann, F. C., Buhl, W. F., Huang, Y. J., Pedersen, C. O., Strand, R. K., Liesen, R. J., Fisher, D. E., Witte, M. J., & Glazer, J. (2001). EnergyPlus: creating a new-generation building energy simulation program. Energy and Buildings, 33(4), 319–331. doi:10.1016/s0378-7788(00)00114-6.

[41] Al-Abbas, B., Abdul Rasoul, Z. M. R., Hasan, D., & Rasheed, S. E. (2023). Experimental Study on Ultimate Strength of Steel Tube Column Filled with Reactive Powder Concrete. Civil Engineering Journal (Iran), 9(6), 1344–1355. doi:10.28991/CEJ-2023-09-06-04.

[42] Husin, A. E., & Priyawan, P. (2023). Implementation of the Last Indonesian Minister Regulation of 2022 uses SEM-PLS and Blockchain-BIM to Green Cost Efficiency. Journal of Sustainable Architecture and Civil Engineering, 33(2), 96–112. doi:10.5755/j01.sace.33.2.34229.

[43] Sutikno, S., Husin, A. E., & Yuliati, M. M. E. (2022). Using PLS-SEM to analyze the criteria for the optimum cost of green MICE projects in Indonesia based on value engineering and lifecycle cost analysis. Archives of Civil Engineering, 68(4), 555–570. doi:10.24425/ace.2022.143054.

[44] Sarstedt, M., Ringle, C. M., & Hair, J. F. (2022). Partial Least Squares Structural Equation Modeling. Handbook of Market Research. Springer, Cham, Switzerland. doi:10.1007/978-3-319-57413-4_15.

[45] Husin, A. E., Ardiansyah, M. K., Kussumardianadewi, B. D., & Kurniawan, I. (2023). A Study on the Application of Green Retrofitting in the Ready-Mix Concrete (RMC) Industry in Indonesia to Improve Cost Retrofitting Performance. Civil Engineering and Architecture, 11(5), 2958–2973. doi:10.13189/cea.2023.110812.

[46] Husin, A. E., Priyawan, P., Kussumardianadewi, B. D., Pangestu, R., Prawina, R. S., Kristiyanto, K., & Arif, E. J. (2023). Renewable Energy Approach with Indonesian Regulation Guide Uses Blockchain-BIM to Green Cost Performance. Civil Engineering Journal (Iran), 9(10), 2486–2502. doi:10.28991/CEJ-2023-09-10-09.

[47] Yuliatti, M. M. E., Husin, A. E., & Sutikno, S. (2022). Improved Performance of Toll Road Projects Based on System Dynamics Integrated Life Cycle Cost Analysis Green Retrofitting. Civil Engineering and Architecture, 10(6), 2713–2730. doi:10.13189/cea.2022.100635.

[48] PUPR. (2022). Regulation of the Minister of Public Works and Public Housing Number 21 of 2021 concerning Green Building Performance Assessment. Ministerial Regulation Number 21: PUPR Ministry Legal Bureau, Jakarta, Indonesia. Available online: https://jdih.pu.go.id/detail-dokumen/2881/1#div_cari_detail (accessed on April 2023).
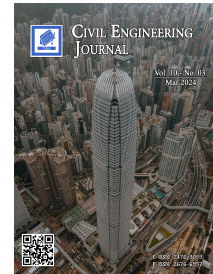
Assessment of Ground Penetrating Radar for Pyrite Swelling Detection in Soils

Nabil KhoderAgha [1]*, Gabriel Assaf [1]

[1] Faculty of Construction Engineering, École de Technologie Supérieure, 1100 Notre-Dame St. W, Montreal, QC H3C 1K3, Canada.

Abstract

Pyrite swelling in soils below buildings is a major issue. It leads to severe deformations in floor foundations. A survey is carried out at a selected site in the city of Laval, Quebec, to assess the usefulness of ground-penetrating radar (GPR) to detect deformations that may be indicative of the presence of pyrite. Four soil samples are taken from the aforementioned site to determine the soil type below the concrete slab. The results indicate the presence of limestone, moor clay, and shale sediments, which are prone to pyrite swelling. The GPR data were collected using the GSSI SIR 4000 with a high frequency antenna and processed using RADAN software. The GPR data indicate the presence of severe deformation in many locations of the concrete slab. The most important wave reflections indicative of pyrite swelling are the rebar reflections, showing interesting pushed-up and dropped-down reflections. These reflections appear in two forms. The first is the attenuated reflections that may occur due to pyrite-rich materials. The second is the high amplitude reflections that occur because of the air void, which can be formed due to heaving the concrete slab because of pyrite swelling. As a result, GPR appears to be an effective method for assessing and mapping the effect of pyrite swelling below concrete slabs.

Keywords: Assessment; Ground Penetrating Radar; Radan; Pyrite.

1. Introduction

Major issues with concrete slabs occur in buildings that are constructed on compact rock fills containing pyrite, particularly black shale and mudstone. Pyrite oxides when shale is excavated or used as a foundation material. Pyrite is very sensitive to humidity, whereas even a very small amount of water can lead to the Pyrite reaction [1]. Pyrite problems are observed as swelling shale bedrock affects the foundations and concrete slab on grade of buildings. The first documented case of pyrite swelling in bedrock was reported in Canada in the late 1960s [2]. Such swelling issues often take a considerable amount of time to become evident. For instance, it took approximately 20 years to diagnose that the swelling problems in Quebec City were caused by pyrite [3]. Similarly, numerous cases of concrete heaving due to pyrite swelling have been reported in the UK [4], Ireland [2], the USA [1], and Japan [5].

The effect of pyrite on building foundations is well discussed and documented in the literature. Hawkins and John report that oxygen and moisture are key factors that help pyrite crystallisation within most rock types, leading to swelling and thereby extensive damage to the concrete slab [6, 7]. This damage may be observed either in the concrete itself as result of pyrite presence in the aggregate within the mix or in the soil underneath the slab. Maher & Gray report that serious pyrite swelling problems in the concrete slabs that occurred in a large number of buildings in Ireland and Canada were due to the use of mudstone aggregation, which contains pyrite crystals [2]. Hoover et al. report severe cracks in concrete slabs in the Evangelical Hospital in Pennsylvania, USA, due to swelling of the underlying soil, which consists

of weathered shale fragments [8]. They suggested additional laboratory research to produce better identification tools for geotechnical engineers unfamiliar with pyrite's expansive nature. Maher et al. describe a large-scale laboratory study involving pyrite-swelling tests conducted over two years [9]. The results demonstrate that mudstone swelling continues at a rate of 0.6% of the fill thickness per year, leading to significant building damage. Mckeon et al. proposed a novel physical model that provides a valuable framework for predicting the time required to generate specific amounts of floor movement in residential dwellings [10].

GPR has been widely used for various applications, including archaeology, geology, engineering, and environmental studies [11–15]. It provides high-resolution two-dimensional (2D) and three-dimensional (3D) images of the subsurface [11]. Furthermore, it is an economical, fast, and effective method compared with the traditional methods [16, 17].

Ground-penetrating radar (GPR) is a non-invasive, non-destructive method that offers precise imaging capabilities. It helps researchers and surveyors accurately locate and determine the depth of buried objects. It depends on emitting electromagnetic (EM) waves through the ground by a transmitting antenna. These EM waves will propagate and intersect any geological interface between two different materials that occurs due to any difference in the physical and chemical properties. As a result, the propagation velocity of the EM waves will change, and part of these waves will reflect back to the surface [18]. As such, the receiving antenna will record wavelength, amplitude, and the two-way travel time as shown in Figure 1.
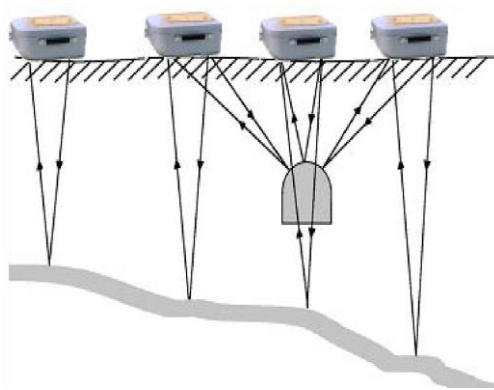
Figure 1. Illustrates the principle of ground penetrating radar detection

Many research studies discuss the effectiveness of the GPR to assess concrete slab conditions and to detect rebar, cracks, voids, and other issues in concrete. Oikonomopoulou et al. report a laboratory application of GPR on six concrete slabs, where several objects made of different materials are embedded within [19]. They concluded that the GPR is effective in the identification the embedded objects. They also found that the cross-polarization GPR antennas can detect different rebar diameters. Liu et al. propose a rebar detection method using deep learning and migration [20]. The results suggest that this method can automatically detect the rebar from the GPR image in real-time. Tian et al. detect and identify three major defects in concrete structures, including delamination, air void, and moisture by analyzing their reflection polarity [21]. Perez-Garcia el at. investigate cracks in concrete slab on grade with GPR [22]. Rahman M, et al. use a controlled laboratory environment to analyze the attenuation of GPR signals in concrete due to various subsurface defects and rebar [23]. The results show a variation in the measured reflected amplitudes for different materials due to differing dielectric constants. Dinh & Gucunski explore various factors that may affect the detectability of concrete delamination in GPR images [24]. They conclude that there is always a signal reflected whenever there is delamination or solid-air interface, with increasing signal strength with the thickness of the delamination. Rasol et al. reports a laboratory investigation to assess the ability of the GPR to detect and quantify cracks in concrete samples covered with asphalt [25]. The results showed that crack's width was detected in most cases with cross-polarisation.

No literature reports the use of GPR to detect the effect of pyrite swelling in concrete slabs. This paper reports research organized in two parts. The first part is to assess the soil composition beneath the slab to verify any evidence of pyrite existence in the soil. The second part is to delimitate the impacted pyrite swelling underneath the slab using a high-frequency GPR antenna, offering maximum resolution for targets within or just below the concrete slab.

2. Site Description and Fieldwork

The investigated site in a commercial building is located in the city of Laval, Canada, at latitude 45°33'12.96" N and Longitude 73°45'24.08" W, severe cracks and heaving are observed on concrete slabs on grade as presented in Figure 2. The fill materials beneath the concrete slab predominantly consist of clayey materials. Before collecting GPR data, Figure 3 shows that four soil samples were extracted directly from the area beneath the concrete slab. These samples were selected from the corners of the slab to identify and characterize the soil type underneath the slabs.
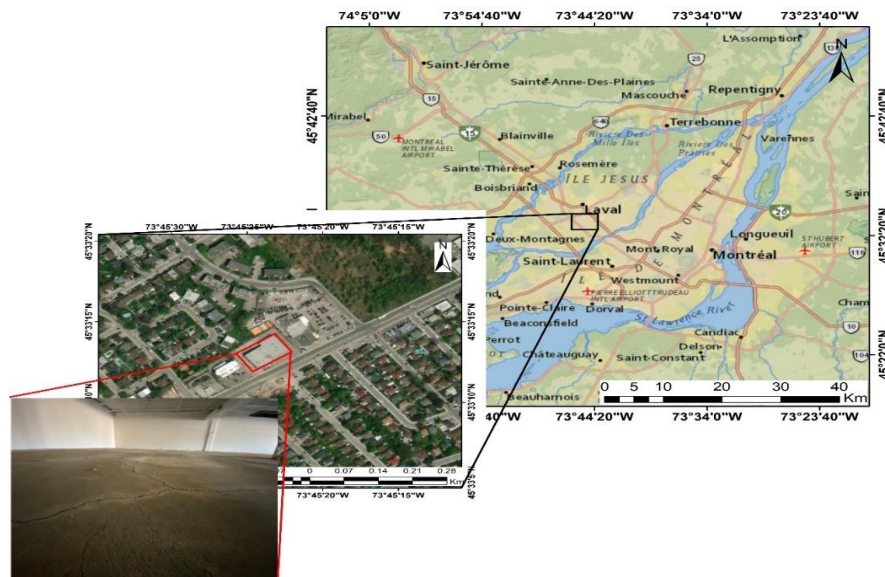
Figure 2. Location of the investigated site, the concrete slab is characterized by the presence of cracks and heaves that distributed along it
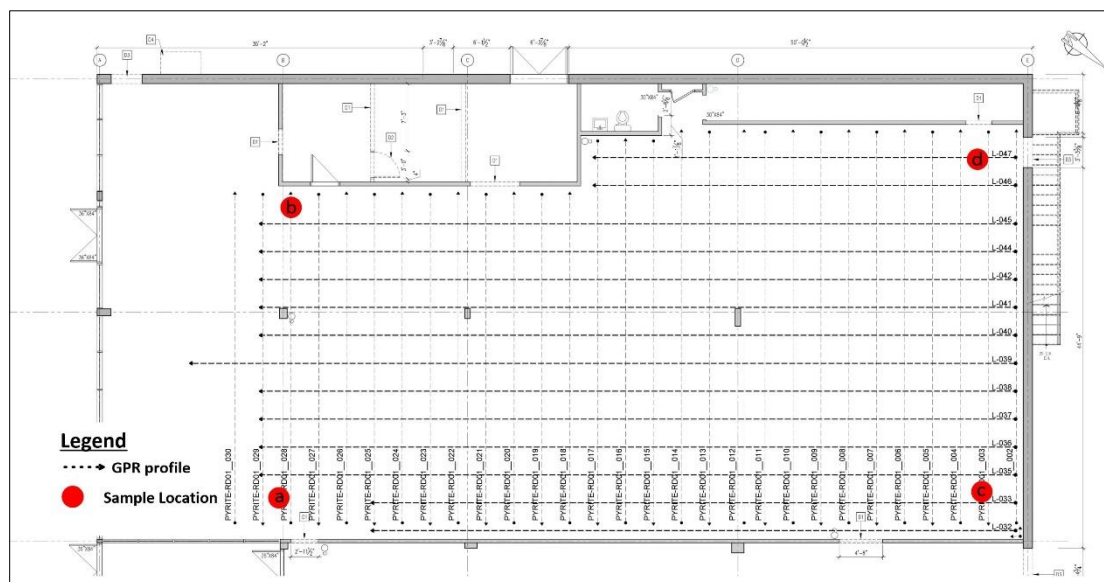
Figure 3. GPR profiles within the investigated site. Red dots represent the locations of the soil samples

The GPR data were collected using a Geophysical Survey Systems, Inc. (GSSI) SIR4000 pro console coupled with a 1600 MHz antenna [26]. The GPR data is collected within a grid measuring 14 x 28 m. This grid comprised 14 GPR profiles in the X-direction and 29 profiles in the Y-direction, with a 1-meter spacing between every two profiles as shown in Figure 3. The length of the profiles in the X-direction ranged between 23 m to 28 m, but most of the profiles were within 26 m long, while in the Y-direction, the profiles varied between 12 m and 14 m. The variation in profile lengths was adjusted by the presence of obstacles within the investigated site.

3. Data Processing and Interpretation

The processing and interpretation of the data are divided into two steps as shown in Figure 4. The first step is to identify and characterize the soil samples, while the second step collects, processes and interprets the GPR data.

The soil samples were analyzed using the CTQM200 protocol to determine the Petrographic Swelling Potential Index (PSPI) as tabulated in Table 1 [27]. This analysis involved testing of weighted soil groups extracted from various depths for each sample, Figure 3 presents the locations of the samples. Each weighted soil is treated to classify its components. Here, the components consist of twelve items and each item represents a soil type. However, only two main components respond to the PSPI. These components are Dolo Limestone/Clayey Dolomite and Shale. For each sample, the percentage of the practical fraction size (RF%) of the components was measured, and the PSPI was

subsequently calculated. The PSPI values are varied between 3.4 to 5.4 reflecting aggregates deemed to come from the right and left sides of the site. Consequently, the soil type can be classified as Ordovician limestone, more clayey in places, which probably intersects thin clayey beds and shale sediments. The Shale and clayey materials on the site are more likely to contain pyrite within their particles, which can react with air and moisture. Then pyrite swelling is probably the reason for the concrete slab deformation in the investigated site.
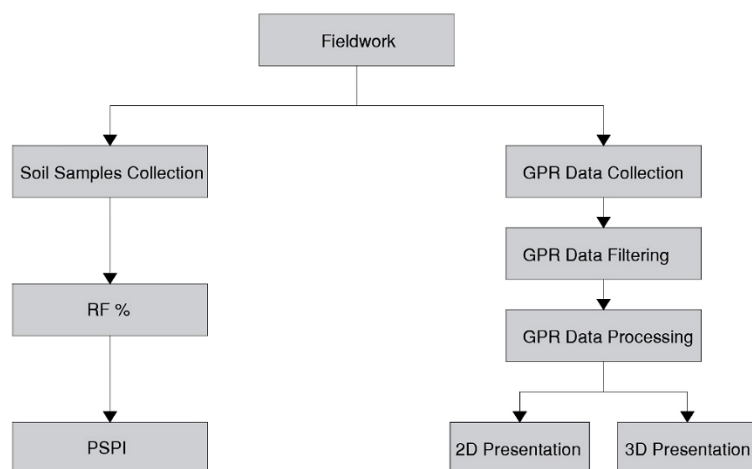
Figure 4. Flowchart of the research methodology

Table 1. PSPI test results

Sample (a)		Shale	Dolo limestone/ Clayey Dolomite
	RF%*	2.10	13.0
	PSPI Coefficient	1.00	0.10
	PSPI**	2.10	1.30
PSPI (Shale+Dololimstone)***			3.4
Sample (b)		**Shale**	**Dololimestone/ Clayey Dolomite**
	RF%*	3.00	18.1
	PSPI Coefficient	1.00	0.10
	PSPI**	3.00	1.81
PSPI (Shale+Dololimstone)***			4.81
Sample (c)		**Shale**	**Dololimestone/ Clayey Dolomite**
	RF%*	3.40	20.0
	PSPI Coefficient	1.00	0.10
	PSPI**	3.40	2.00
PSPI (Shale+Dololimstone)***			5.40
Sample (d)		**Shale**	**Dololimestone/ Clayey Dolomite**
	RF%*	2.40	17.2
	PSPI Coefficient	1.00	0.10
	PSPI**	2.40	1.72
PSPI (Shale+Dololimstone)***			4.12

* %RF = % compared to the % of the particle size fraction without debris;

** PSPI= Petrographic Swelling Potential Index;

*** PSPI Cumulative of the sample.

The GPR profiles were processed using RADAN software from the GSSI manufacturer. The processing involved several basic steps to enhance the quality of the 2D GPR profiles. These steps included time zero correction (0.703 ns), background removal, and Bandpass filter (500 MHz for high pass and 3000 MHz for low pass). These processing steps improve the clarity and accuracy of the GPR data. For the 3D GPR model, all the GPR profiles are migrated with a velocity of 0.09 m/ns and then the Hilbert transform is used as the final processing step. However, three main reflections are observed within the processed GPR profiles. These reflections correspond to the presence of rebar, voids, and utility lines presented Figure 5. These reflections provide valuable information about the subsurface conditions and can help in identifying potential areas of concern related to pyrite swelling and concrete slab deformation.
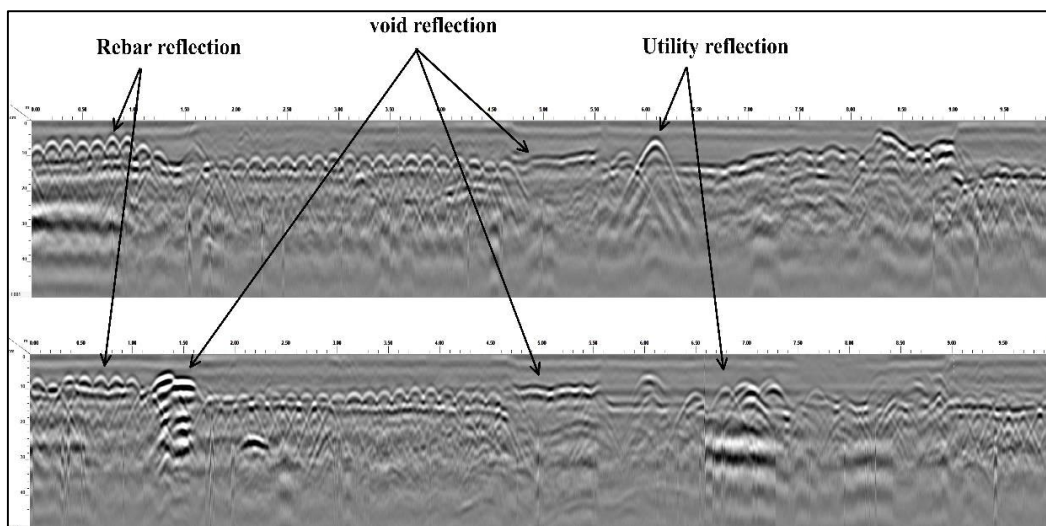
Figure 5. GPR profiles no. 10 and 12, showing rebar, void, and utility reflections

The rebar reflections in all the GPR profiles show clear deformation in their shapes and locations, indicating significant distortion of the concrete slab. This distortion is attributed to the swelling of the underlying soil that is caused by the reaction of pyrite with the surrounding materials shown in Figure 6. Normally, when the concrete slab is in good condition, the rebar mesh should appear at a consistent level. However, due to the severe impact of the swelling on the concrete slab, the rebar mesh is distorted. This deformation can therefore be considered as evidence of the presence of pyrite in the subsurface material.
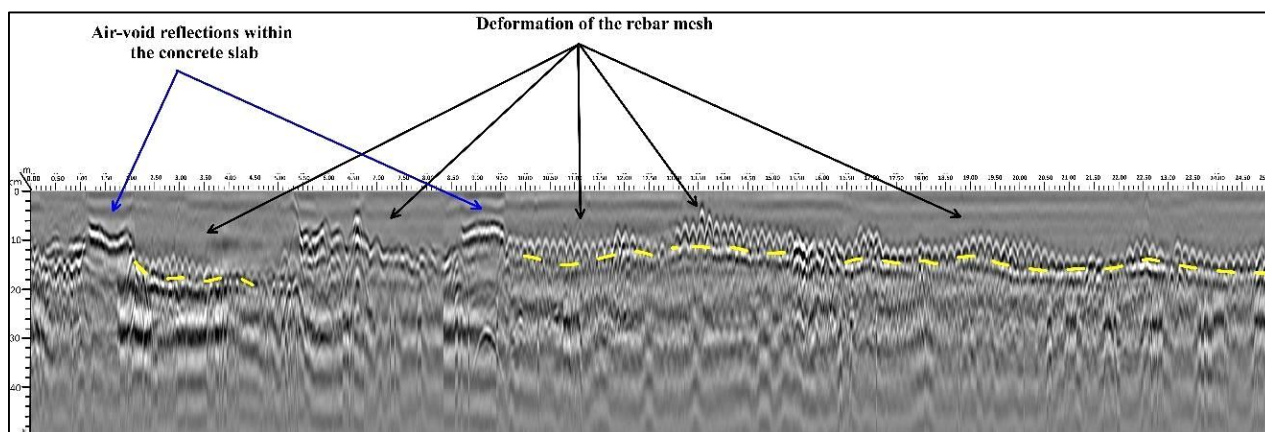
Figure 6. GPR profile no. 38, showing the rebar reflections are distorted due to the swelling, which severely effect the concrete slab

Figure 6 is a good example that shows the deformations in the slab where some parts of the rebar are slightly up and others are slightly down. The GPR profile no. 38 in Figure 6 shows that the thickness of the slab varies between 12 to 18 cm in depth. Furthermore, two distinctive reflections observed as a result of air voids inside or just beneath the concrete slab appear clearly in this profile. An interesting reflection is also shown in some GPR profiles, which indicates that part of the concrete slab is pushed up while the other parts remain at their locations, as shown in Figure 7. This reflection appears clearly at a depth of 8cm, while the other reflections appear at a depth of 16cm. This uplifted part of reflection may indicate two things. The first is an air void that is created just below the concrete slab. The second is that the reflections from the rebar are too weak. This phenomenon may occur for two reasons. The first reason is the high amplitude reflection of the air void, where the GPR waves speed up when traveling through the air void to reach airspeed, then severely slow down when hitting the underlying layer. Therefore, this high-amplitude reflection will cover the weaker reflections of the rebar. The second reason is the high attenuation that occurs due to the high conductivity of pyrite-rich materials [16] and their reaction with moisture [7]. It seems that the concentration of pyrite and moisture in this part of the slab is higher than in the other parts. Therefore, the reaction of pyrite with its surrounding materials may lead to attenuate the GPR wave and produce weak reflections. On the other hand, the other parts of reflection appear approximately at the same level as shown in Figure 7. This may indicate that this part of the concrete slab is intact, and mainly no pyrite swelling occurs at these parts.
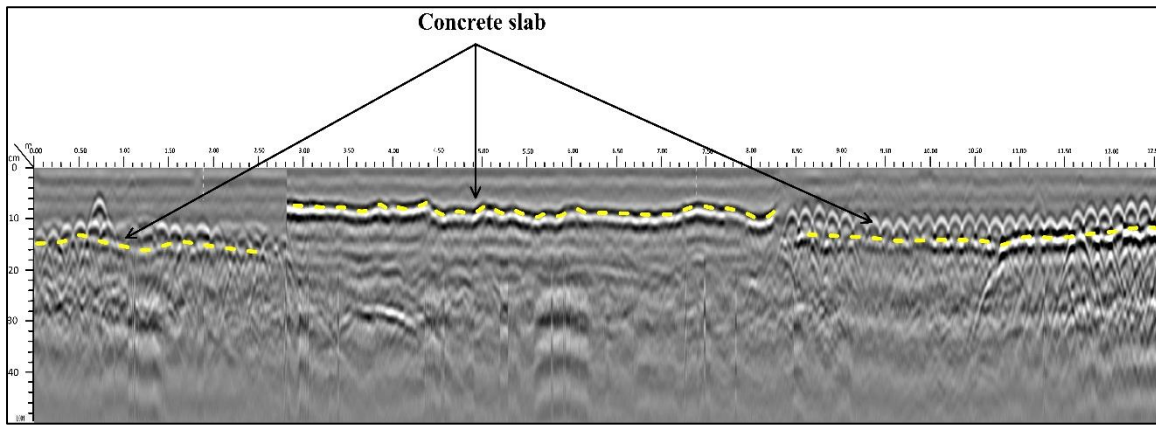
Figure 7. GPR profile no. 13, showing that the bottom of the concrete slab is pushed up due to swelling of underying materials. The other parts of the slab remain at the same level

The 3D presentation shows how the high attenuation of the GPR waves, and the swelling of the underneath materials affect the GPR reflections. For instance, the cross-section of the GPR profiles No. 11 (in the Y-direction) and No. 45 (in the X-direction) reveals distinct zones of attenuation, as shown in Figure 8a. The effect of the swelling can also be seen along the cross-section, where some parts of the concrete slab are pushed up and others are dropped down. Additionally, multiple distinct reflections from air voids are observed on both GPR profiles at approximately the same level. These reflections collectively indicate that the deformation of the concrete slab is severe due to the reaction of pyrite with other materials. Another good example is shown in Figure 8b, where a cross-section of the GPR profiles No. 8 (in the Y-direction) and No. 37 (in the X-direction) is presented. Again, the zones of low and high amplitude reflections, as well as the upward and downward reflected parts, indicate the indirect impact of pyrite when it reacts with moisture and the surrounding materials. These sections effectively highlight the effect of pyrite swelling, which significantly attenuates the GPR reflections and leads to severe deformation in the concrete slab.
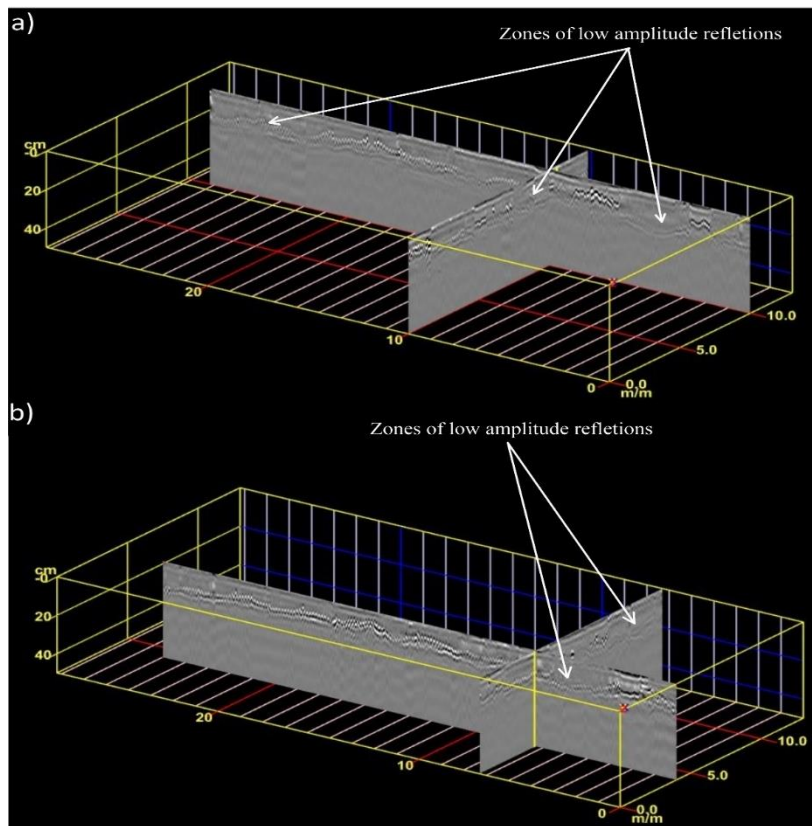
Figure 8. Low and high amplitude reflections zones

To obtain a more detailed understanding of the condition of the concrete slab and the underlying materials, a 3D Iso-surface map is derived from the grid of the GPR profiles at a depth of about 12 cm beneath the ground surface presented in Figure 9. Within this map, two significant areas are observed. The first area corresponds to the rebar mesh, which is visible in some locations. The amplitude strength of the rebar reflections on the map varies, ranging

from very high to low amplitude reflections. This variation is expected since the level of the rebar mesh is not uniform due to the swelling of the underlying soil. The second area looks vanished with no reflections. It seems that this area is the most affected by the attenuations and/or swelling of the underneath materials. This suggests that the concrete slab is severely affected in these regions of vanished reflections. However, this does not imply that the other rebar mesh areas are not affected by attenuation or swelling, but it seems that the concentration of pyrite in rebar mesh areas is relatively lower than in other areas.
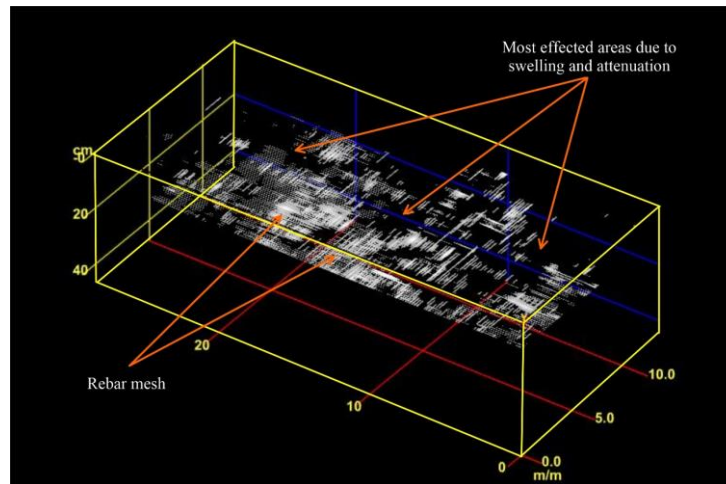
Figure 9. Iso-surface map. Two main areas are present, the rebar mesh area and the area with no reflections

Based on the above results, the GPR method successfully addressed the effect of the pyrite reaction with moisture and other surrounding materials on the concrete slab. This reaction is shown on the GPR profiles as air-void reflections, pushed-up reflections, and dropped-down reflections. Further, the pyrite reaction also appeared as an attenuation that affects the GPR waves to produce very weak reflections. These results provide valuable information about the condition of the concrete slab and the underlying materials, which highlights the extent of deformation in the concrete slab due to the influence of the pyrite swelling effect.

4. Conclusion

Pyrite swelling in concrete slabs is a major issue. Many cases have been registered in Quebec since the 1960s. The use of the GPR method to trace pyrite swelling in concrete slabs is investigated in this paper. In order to detect pyrite swelling in slabs on grade, an extensive assessment is applied using the GPR method in a selected site that occurs in the city of Laval, Quebec. Before the GPR survey, soil samples were collected to determine the soil composition behind the concrete slab. The analysis revealed the presence of limestone, which is more clayey in places and probably intersects thin clayey beds, severe and shale sediments. These sediments are known to have a higher tendency to produce pyrite swelling. The GPR investigation identified three types of reflections: rebar, air-void, and utility reflections. The most important reflections that indicate the pyrite swelling are the rebar reflections. These reflections show a clear deformation in their shapes and places, indicating that the concrete slab is exposed to severe distortion due to pyrite swelling. This deformation is presented on the GPR profiles in the form of pushed-up and dropped-down reflections. The effect of the pyrite swelling on GPR reflections can be recognized in two means. Firstly, the attenuated reflections that may occur as a result of pyrite-rich materials. Secondly, the high-amplitude reflections that may occur due to the presence of air voids. These air voids can be caused due to pushing the concrete slab as a result of pyrite swelling. The 3D Iso-surface map provided valuable information about the most affected areas of the concrete slab. The deformed locations can be recognized easily compared with intact locations. In conclusion, the results indicate that GPR is an effective and reliable method for assessing and mapping the deformations in concrete slabs. It has the capability to locate areas of deformation without the need for extensive excavation work. This makes GPR a valuable tool for addressing the pyrite swelling issues in concrete slabs and ensuring the structural integrity of buildings.

5. Declarations

5.1. Author Contributions

Conceptualization, N.K.A. and G.J.A.; methodology, N.K.A. and G.J.A.; formal analysis, N.K.A.; writing—original draft preparation, N.K.A. and G.J.A.; writing—review and editing, N.K.A. and G.J.A. All authors have read and agreed to the published version of the manuscript.

5.2. Data Availability Statement

The data presented in this study are available on request from the corresponding author.

5.4. Conflicts of Interest

The authors declare no conflict of interest.

6. References

[1] Anderson, W. H. (2008). Foundation problems and pyrite oxidation in the Chattanooga Shale, University of Kentucky, Estill County, Kentucky. Report of Investigations--KGS. University of Kentucky, Lexington, United States. doi:10.13023/kgs.ri18.12.

[2] Maher, M., & Gray, C. (2014). Aggregates prone to causing pyrite-induced heave: How they can be avoided. Proceedings of the 17th Extractive Industry Geology Conference, September 2014, Ormskirk, United Kingdom.

[3] ACQC. 1999. Pyrite and Your House. Association des Consommateurs pour la Qualité Dans la Construction, Montréal, Canada. (In French).

[4] Nixon, P. J. (1978). Floor heave in buildings due to the use of pyritic shales as fill material. Chemistry and Industry, March, 160-164.

[5] Yamanaka, T., Miyasaka, H., Aso, I., Tanigawa, M., Shoji, K., & Yohta, H. (2002). Involvement of sulfur- and iron-transforming bacteria in heaving of house foundations. Geomicrobiology Journal, 19(5), 519–528. doi:10.1080/01490450290098487.

[6] Hawkins, A. B. (2014). Implications of pyrite oxidation for engineering works. In Implications of Pyrite Oxidation for Engineering Works. Springer International Publishing, Cham, Switzerland, doi:10.1007/978-3-319-00221-7.

[7] Cripps, J. C., Reid, J. M., Czerewko, M. A., & Longworth, I. (2019). Tackling problems in civil engineering caused by the presence of pyrite. Quarterly Journal of Engineering Geology and Hydrogeology, 52(4), 481–500. doi:10.1144/qjegh2019-024.

[8] Hoover, S. E., Wang, M. C., & Dempsey, B. (2004). Structural damage induced by pyritic shale. International Conference on Case Histories in Geotechnical Engineering, 13-17 April, 2004, Missouri, United states.

[9] Maher, M. L. J., Azzie, B., Gray, C., & Hunt, J. (2011). A large scale laboratory swell test to establish the susceptibility to expansion of crushed rock containing pyrite. Proceedings of the 14th Pan-Am CGS Geotechnical Conference, 1-7 October, 2011, Toronto, Canada.

[10] McKeon, É. P., O'Connell, A. M., & McCabe, B. A. (2017). Laboratory foundation model with pyrite-bearing mudstone fill. International Journal of Physical Modelling in Geotechnics, 17(4), 204–219. doi:10.1680/jphmg.16.00001.

[11] Conyers, L. B. (2004). Ground-penetrating Radar for Archaeology. AltaMira Press, California, United States.

[12] AL-Hameedawi, M. M., Thabit, J. M., & AL-Menshed, F. H. (2023). Electrical resistivity tomography and ground-penetrating radar methods to detect archaeological walls of Babylonian houses near Ishtar temple, ancient Babylon city, Iraq. Geophysical Prospecting, 71(9), 1792–1806. doi:10.1111/1365-2478.13293.

[13] Pajewski, L., Benedetto, A., Derobert, X., Giannopoulos, A., Loizos, A., Manacorda, G., Marciniak, M., Plati, C., Schettini, G., & Trinks, I. (2013). Applications of Ground Penetrating Radar in civil engineering - COST action TU1208. 2013 7th International Workshop on Advanced Ground Penetrating Radar. doi:10.1109/iwagpr.2013.6601528

[14] Knight, R. (2001). Ground penetrating radar for environmental applications. Annual Review of Earth and Planetary Sciences, 29(1), 229–255. doi:10.1146/annurev.earth.29.1.229.

[15] Busby, J., Cuss, R., Raines, M., & Beamish, D. (2004). Application of ground penetrating radar geological investigations. British Geological Survey, Keyworth, United Kingdom.

[16] Mellett, J. S. (1995). Ground penetrating radar applications in engineering, environmental management, and geology. Journal of Applied Geophysics, 33(1–3), 157–166. doi:10.1016/0926-9851(95)90038-1.

[17] Balkaya, Ç., Kalyoncuoğlu, Ü. Y., Özhanlı, M., Merter, G., Çakmak, O., & Talih Güven. (2018). Ground-penetrating radar and electrical resistivity tomography studies in the biblical Pisidian Antioch city, southwest Anatolia. Archaeological Prospection, 25(4), 285–300. doi:10.1002/arp.1708.

[18] Neal, A. (2004). Ground-penetrating radar and its use in sedimentology: Principles, problems and progress. Earth-Science Reviews, 66(3–4), 261–330. doi:10.1016/j.earscirev.2004.01.004.

[19] Oikonomopoulou, E. C., Palieraki, V. A., Sfikas, I. P., & Trezos, C. G. (2022). Reliability and limitations of GPR for identifying objects embedded in concrete – Experience from the lab. Case Studies in Construction Materials, 16, 898. doi:10.1016/j.cscm.2022.e00898.

[20] Liu, H., Lin, C., Cui, J., Fan, L., Xie, X., & Spencer, B. F. (2020). Detection and localization of rebar in concrete by deep learning using ground penetrating radar. Automation in Construction, 118, 103279. doi:10.1016/j.autcon.2020.103279.

[21] Tian, H., Zhou, Z., Zhang, Y., & Wei, Y. (2020). Axial behavior of reinforced concrete column with ultra-high performance concrete stay-in-place formwork. Engineering Structures, 210, 110403. doi:10.1016/j.engstruct.2020.110403.

[22] Pérez-Gracia, V., González-Drigo, R., & Di Capua, D. (2008). Horizontal resolution in a non-destructive shallow GPR survey: An experimental evaluation. NDT and E International, 41(8), 611–620. doi:10.1016/j.ndteint.2008.06.002.

[23] Abdul Rahman, M., Donda, D., Latosh, F., Tarussov, A., & Bagchi, A. (2022). Entropy evaluation of subsurface materials and defects in Concrete Slabs using GPR. 11th International Conference on Structural Health Monitoring of Intelligent Infrastructure, 8-12 August, 2022, Montreal, Canada.

[24] Dinh, K., & Gucunski, N. (2021). Factors affecting the detectability of concrete delamination in GPR images. Construction and Building Materials, 274, 121837. doi:10.1016/j.conbuildmat.2020.121837.

[25] Rasol, M. A., Pérez-Gracia, V., Fernandes, F. M., Pais, J. C., Santos-Assunçao, S., Santos, C., & Sossa, V. (2020). GPR laboratory tests and numerical models to characterize cracks in cement concrete specimens, exemplifying damage in rigid pavement. Measurement, 158, 107662. doi:10.1016/j.measurement.2020.107662.

[26] GSSI Handbook. (2003). Geophysical Survey Systems, Inc., North Salem, United States. Available online: www.geophysical.com (accessed on February 2024).

[27] Procedure CTQ-M200. (2001). Appraisal procedure for existing residential buildings. Quebec Technical Committee for the Study of Swelling, Quebec City, Canada.
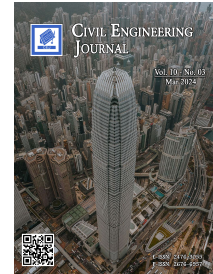
Integration of Artificial Intelligence Applications and Knowledge Management Processes for Construction Projects Management

Meervat R. Altaie [1*] , Marwa M. Dishar [1]

[1] *Department of Civil Engineering, Faculty of Engineering, University of Baghdad, Baghdad, Baghdad, Iraq.*

Abstract

Artificial intelligence systems have gained access to various scientific and research fields, especially in the construction industry. The study seeks to confirm the vital role of introducing Knowledge Management (KM) integrated with Artificial intelligence (AI) applications in the projects. It requires qualifying engineers and imposing their current qualifications to achieve the benefits of Integration of AI Applications based on KM processes to perform their professional roles and recognize the need to develop their capabilities through training and development. The field survey was intended only for 85 engineers working on construction projects (public and private sectors). Three axes were clarified to allocate the extent of the sample response and determine the benefits of using the KM process and AI applications for the success of construction projects. The results showed a positive relationship between the demographic variables of the response and the benefit of using the KM process and AI applications and explaining the variance in the regression relationships. Therefore, the study suggests integrating AI applications based on the KM process to achieve business goals and effectively benefit and exchange management, as its use leads to faster and more effective decision-making, especially if the project strategy approves it.

Keywords: Knowledge Management; Artificial Intelligence; construction; Correlation; Regression.

1. Introduction

Knowledge is vital in our daily lives, whether at the personal level or within institutions; knowledge enables us to understand the world around us and make the right decisions effectively. It is luxurious, as the information, experiences, skills, and capabilities of the individual or organization enable them to make the correct decisions and behaviors promptly. It includes scientific, experimental, cultural, social, technical, administrative, and other knowledge. Knowledge is constantly changing and evolving due to updates, innovations, and changes in society, culture, technology, economics, science, and modern technologies. So, knowledge management is the process of identifying, collecting, organizing, analyzing, distributing, and using knowledge in an organization and includes the creation and improvement of systems, methods, and operations to collect, share, and use knowledge within the organization [1].

The use of information, data, knowledge, skills, and abilities inherent within organizations is one of the most important reasons for their success, in addition to the organization's ideas, commitment, and motives in making good decisions, which is evidence of this organization's distinctive environment. Therefore, organizations are interested in implementing KM processes and techniques as an integral part of comprehensive development strategies for their increasingly important role in global economic development [2].

In our current era, AI applications are assuming increasing importance due to their possession of the keys to the fundamental processes of explicit knowledge in attracting, storing, sharing, and spreading, doubling the value of data and information, and employing them in supporting knowledge management, which has exceptionally increased in importance and area in recent years thanks to unlimited capabilities in construction projects [3].

Applying AI techniques to construction projects gives the project manager more control and better management of all project phases. Human error by project managers is one of the inherent problems facing project management, which leads to project failure. The application of AI techniques in any project phase can lead to improving accuracy, forecasting, and addressing administrative and technical errors in projects whose benefits have become apparent, especially in dealing with uncertainty, improving efficiency, scheduling, stakeholder management, and improving cost management in engineering, procurement, and construction (EPC) projects [4].

However, the problem of integrating the use of AI applications with the concept of KM faces many challenges, and this is clear from the different percentages of variation between workers in the construction industry sector, especially engineers, in how to apply it in the project work.

The engineers need to be able to use AI applications to complement their experience in KM. It requires studying a set of demographic characteristics for engineers and knowing the extent to which these characteristics affect the ability of engineers to use artificial intelligence applications with knowledge management to achieve the goals required for the success of projects. It is what the current study is seeking to find out.

2. Literature Review

Many scientific studies have reviewed the discovery of AI and its role in enhancing KM systems and practices through various methods that support appropriate decision-making. Some studies have focused on the overall benefits and available opportunities that can significantly facilitate the work of construction sector organizations.

The study referred to many scientific publications in the past century that studied the topic of AI-PM, indicating that the construction sector is the sector most affected by AI due to the nature of massive projects in this sector, which are characterized by their complexity. Multiple studies have dealt with artificial intelligence significantly in planning and measurement processes, predicting project time, studying uncertainty, studying safety issues, project delivery, predicting project status, and many other applications and fields in various project phases and within multiple scenarios supported by artificial intelligence.

Anumba & Khallaf's study reported the benefits of using AI-based knowledge management through different vital technologies that facilitate knowledge management in the construction field by classifying some artificial intelligence techniques for organizational knowledge management processes and systems. The most important benefits are the ease of matching knowledge with problems, retrieving data quickly, increasing the ability to create new knowledge, improving knowledge evaluation, increasing capital, greater flexibility in representing knowledge, ease of participation, and improving the decision-making process [5]. Igbinovia & Ikenwe's study recommended the need to encourage organizations to create knowledge through scientific methods supported by artificial intelligence, with the need to support research activities and encourage cooperation and teamwork between individuals and institutions [6].

Ramaj & Pjero's study also recommended deepening knowledge about information technology through training or special courses. Especially in light of the increasing use of information systems in all sectors and different industries in which there is business through mutual interaction between professional bodies and universities [7]. Karki & Hadikusumo's study was conducted to find the competency factors of project managers in Nepal by developing a predictive model of project manager performance using a machine learning approach in medium-sized construction projects. The study determined that project managers must have high competence in leadership skills, personal characteristics, team development and delegation, communication, technical, problem-solving, and relationship management skills [8].

The workers must connect with knowledge management while developing their abilities to use artificial intelligence, which requires new skills, competencies, and capabilities. It calls for enhancing perceptions, skills, and work practices so that workers can benefit from their knowledge management partners while avoiding risks. These early preparations by organizations help apply the capabilities of artificial intelligence based on knowledge management processes, which is only achieved through an effective symbiotic partnership between workers in knowledge management and intelligent systems [9].

Therefore, our study seeks to clarify the impact of applying knowledge management based on artificial intelligence and to reveal the various goals that must be met for the success of investment projects by shedding light on scientific methods for managing investment construction projects and arriving at methods that help control projects. Successful application can only be achieved after providing a qualified cadre of engineers who can develop their skills using artificial intelligence in the stages of knowledge management. It requires knowing the biographical characteristics of engineers and their relationship with the success of the integration method to achieve the project goals.

3. Methodological Framework

The flow chart in Figure 1 explains the methodology of the study, which consists mainly of the Conceptual Framework for the theoretical application and the practical study to finalize the test of the two hypotheses for the study. As mentioned below:
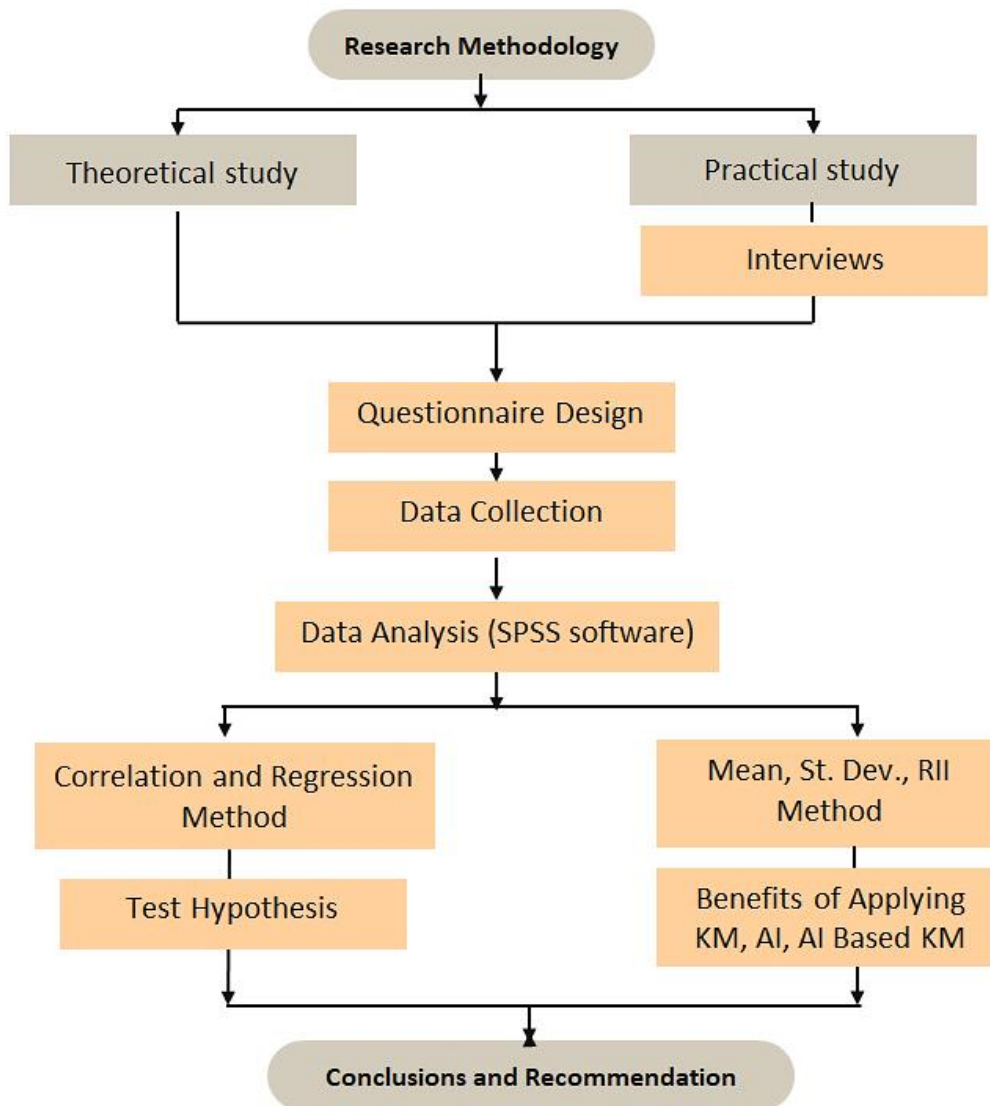
Figure 1. Flow chart of the study

3.1. Problem, Justification and Objectives of the Study

Investment projects must improve using AI applications based on KM processes at all project stages. The different demographic characteristics of engineers may contribute to significant skills and abilities to use AI integrated with the KM process, in addition to determining the level of training necessary to improve engineers' skills and professional capabilities.

After recent technological development, the construction industry has flourished in Iraq to carry out and develop the construction industry in a way that serves the country's interests, especially after the disclosure of the strategic Iraqi plan for the year 2030 and the beginning of the work to reconstruct the liberated cities. Various construction projects have worked on the inclusion and application of all modern technologies in the rehabilitation and implementation of construction projects, which will inevitably lead to an upgrade in the performance of construction projects and identify the main obstacles facing the management of construction projects and address their causes.

Determine the relationship type between the applying AI applications based on KM with the performance and qualifications of engineers. This can help to address the project problems, especially delays in cost and time overruns, treat the challenges, and help in completing the project activities in a shorter time with a lower cost within the required quality. The correlation type will also determine the qualifications required for engineers to work for construction companies seeking unique distinctions within the current competition in the construction industry.

The following are the main objectives can be clarified:

a) Detecting the benefits of applying the KM process in construction project management in Iraq.

b) Detecting the benefits of applying AI applications in construction project management in Iraq.

c) Detecting the benefits of integrating AI Applications and KM processes for construction project management in Iraq.

d) Recognizing the correlation between demographic variables and the integration of AI Applications and KM processes for construction project management in Iraq from the engineers' point of view.

e) Interpreting the variation in the regression relationships between demographic variables and the integration of AI Applications and KM processes for construction project management in Iraq from the engineers' point of view.

3.2. Hypotheses of the Study

The study states two hypotheses:

1st Hypothesis: There is a positive correlation between the demographic variables for engineers (Age, Qualification, Current Position, and Years of Experience) and:

  a) The Benefits of applying the KM process in the construction projects management.

  b) The Benefits of applyingAI applications in the construction projects management.

2nd Hypothesis: There is a statistically significant effect for the demographic characteristics of the engineers (Age, Qualification, Current Position, and Years of Experience) and:

  a) The Benefits of applying the KM process in the construction projects management.

  b) The Benefits of applyingAI applications in the construction projects management.

3.3. Methodology of the Study

The analytical descriptive approach and the deductive approach were adopted to address the impact of the application for integrating AI applications and KM processes for construction project management in Iraq from the engineers' point of view in Iraq.

The practical study was applied to a random sample of public and private sectors in Iraq from a selected sample of engineers; the study clarifies various benefits from statistical results to link various factors and influences that led to the integrated relationship results. Statistical Package for the Social Sciences (SPSS-version 25) was used to analyze and process the data contained and test the hypotheses' validity.

4. Conceptual Framework

The study's conceptual framework will focus on two crucial axes, knowledge management (KM) and Artificial Intelligence (AI), by focusing on various theoretical foundations and concepts.

4.1. Knowledge Management (KM) Concepts

KM is a multidisciplinary business model that deals with all aspects of knowledge in all companies, including knowledge creation, codification, sharing, and imparting to enhance learning and innovation. All technological tools and organizational procedures that can contribute to the success of organizations must be included [10].

4.1.1. Definition of KM

KM is defined as "planning, organizing, controlling, coordinating, and synthesizing knowledge and assets related to intellectual capital, operations, personal and organizational capabilities, and capabilities, so that the greatest possible positive impact on the results of competitive advantage is achieved, and KM includes achieving the process of sustainability of knowledge and capital intellectual money and its exploitation [11]. It is also defined as the ability of knowledge to create new knowledge, disseminate it throughout the organization, and embody it in products and services [12].

4.1.2.KM Processes

KM has several processes that differ according to their inputs. The researchers unanimously agreed that there are six essential processes for KM, namely: diagnosing knowledge, defining knowledge goals, generating knowledge, storing knowledge, distributing it, and finally applying it, which can be explained in detail as follows [13].

A) Knowledge Acquisition and Generation

The process of acquiring knowledge can be defined as obtaining knowledge from various sources (experts, specialists, competitors, customers, databases, or through the archives of the organization) using performance measurement methods, attending conferences and workshops, using experts, periodicals, publications, email, and individual learning [14]. It is possible to obtain knowledge sometimes by chance, provided that the importance of this knowledge is realized through various methods such as storage and retrieval in a better way to achieve the desired benefit, and this method differs from one organization to another, provided that it is understood in its way because it has a substantial impact on the culture of the organization and its style in managing the approach to knowledge acquisition that is required to achieve the success of the organization [15].

B) Knowledge Storage

After the Knowledge Acquisition process, it is stored in many ways; the most essential storing ways are:

1) Organizations can record everything that happens for all information in a specific place as individual records, like regular files or on a computer network. It is available for all organization members to view the information if they want it in the needed time [16].

2) A responsible person stores information accurately by collecting it in a manner that is easy to use by everyone if they want to view it, without caring about analyzing knowledge and being able to disseminate and circulate it effectively. All individuals can provide their knowledge to any person or department if they want to view it in time. Nevertheless, this entity should analyze and purify the knowledge, then store it in the best and most accurate manner so the organization or a specific responsible person can easily circulate it.

3) Collect knowledge in an organized manner, analyzed and purified. It is arranged, coordinated, and fragmented to be stored in the best way, but taking this into account, it must be quickly circulated, published, and extracted accurately and efficiently by any individual working in the organization [17].

C) Knowledge Sharing

The third loop in KM circles is knowledge transfer; it depends on the presence of formal and informal methods and applicable mechanisms. "Informal methods may include job changes inside or outside the organization, personal relationships that bind workers to each other, and work teams [18]. Many factors affect the transfer of knowledge in the organization, like cost "when purchasing devices, using technology, holding conferences and seminars, and the transfer of knowledge can be affected by the potential of content change in light of the structure of the hierarchical organizational structure [6].

D) Knowledge Application

The application of knowledge is the primary goal of the KM process. This application requires organizing knowledge (through classification, indexing, or appropriate tabulation of knowledge), knowledge retrieval (by enabling employees in the organization to access it quickly and in the shortest time) and making knowledge ready for use (deleting some inconsistent parts, re-correcting and constantly examining knowledge, introducing new and appropriate ones, and excluding obsolete ones [18]. That is, the knowledge must be used functionally and effectively to fill a void or need. KM has proven through its practical applications and, in many situations, that it is the fastest and easiest way to add value to the organization and individuals [19, 20].

4.2. Artificial Inelegant (AI) and Its Conditions

AI is the product of 2,000 years of traditions of philosophy, perception, and learning theories and 400 years of mathematics that led to the possession of theories in logic, probabilities, and computing, in addition to a long history of the development of psychology and what revealed the capabilities and workings of the human brain [21].

4.2.1. Definition of AI

AI is defined as computing systems that can participate in human-like processes such as learning, adaptation, synthesis, self-correction, and the use of data to process complex tasks. It has become clear how AI has changed the performance of jobs and tasks in various fields, and many experts predict that by 2030, more than 80% of repetitive tasks will be eliminated by intelligent machines. The application of AI in the construction industry, based on previous knowledge, is nothing new and has proven successful in various fields [22].

Artificial intelligence aims to solve problems in various disciplines in a manner similar to human methods by creating images and texts and making decisions based on stored data. This means that any organization can integrate artificial intelligence capabilities into various applications to improve business, accelerate decision-making, and stimulate innovation [23].

4.2.2. AI Terms

There must be three main elements of AI are implemented correctly, and they are mainly represented in the following:

a) The ability to learn this information from statement to information to knowledge, after the growth of his intelligence abilities in analysis and deduction, then the ability to maneuver and choose from among the available alternatives [24].

b) The possibility of collecting and analyzing data and information is the ability to visualize relationships between this information and data, especially in light of the increasing spread of giant data available on databases [25].

c) Making decisions based on analyzing information is the stage of making intelligent decisions among several options and not relying on just one algorithm to achieve a specific goal [26].

5. Field of the Study

Field study consists from the following procedures:

5.1. Design the Study Questionnaire

To facilitate field study procedures and collect and analyze data to complete the field side of the study, a questionnaire was prepared in a way that helps collect data and obtain accuracy in its design with what was covered in the theoretical side as well as previous studies and the clarity of the questions and phrases of the questionnaire to enable the sample members to answer them objectively.

The current study relied on a structure similar in design to a previous study conducted to reveal the impact of knowledge management processes based on artificial intelligence software when applied to construction projects in the Kingdom of Saudi Arabia and on a group of study factors that were added to the axes of the questionnaire. It is worth noting that the Alghamdi & Al-Dirman study recommended enhancing the application of knowledge management based on artificial intelligence software to solve the problems of delayed completion of construction projects, as well as the need for financial attention, and striving to improve project efficiency while sharing and applying knowledge that supports knowledge management processes [27]. That is what our current study is trying to prove, but from the point of view of engineers working on Iraqi construction projects. It concluded by constructing a questionnaire that includes two parts, as follows:

- The first part includes personal data related to the general characteristics of the study sample members, including age, qualification, current position, and years of experience.

- The second part is divided into three dimensions, as follows:

  a) The Benefits of applying the KM process (15 elements).

  b) The Benefits of applyingAI applications (17 elements).

  c) The Benefits of applying an integrated combination of KM and AI applications (18 elements).

5.2. Select Sample of the Study

The study depended on a deliberate sample, including a group of engineers working in various construction companies in the public and private sectors in various construction sectors in Iraq. The study sample was distributed to 100 questionnaires for engineers characterized by high professionalism and efficiency. After retrieving and sorting them, it was found that 85 questionnaires were suitable for statistical processing.

5.3. Internal Consistency

Internal consistency, or the study's validity, is that the questionnaire questions perform and measure what they were designed to measure [28]. It means the clarity of the questionnaire, its vocabulary, the questionnaire paragraphs, and its comprehensibility to the members of the study sample who will be included in the questionnaire, as well as the questionnaire paragraphs being for statistical analysis. Internal consistency can also be defined as the degree of interconnection of each scale factor with the total result of the total scale to which the phrase belongs [29, 30].

The questionnaire was distributed to ten (10) experts from academics and engineers in the public and private sectors to perform and measure what the questionnaire was designed to measure, the clarity of the questionnaire, vocabulary, elements of a questionnaire, and its concept for the study.

Tables 1 to 3 show a summary of the results, which showed a statistically significant relationship between the elements of each axis. The questionnaire designed for the study has a high degree of internal consistency.

Table 1. Validity of the internal consistency for KM Process Benefits

No.	Dimensions and axes of the study	Correlation with the total	
		Pearson Correlation	Sig
1	Improve the decision-making process	0.923**	0.000
2	Follow up on the implementation of the project plan	0.931**	0.000
3	Continuous improvement of operations	0.911**	0.000
4	Improve the efficiency of tasks or activities	0.949**	0.000
5	Contribute to improving teamwork	0.960**	0.000
6	Reduce the company's costs and prepare the project budget	0 .962**	0.000
7	Control project time planning	0 .948**	0.000
8	Improve the quality of products and services	0.949**	0.000
9	Exchange experiences between employees and communication	0.903**	0.000
10	Share information among stakeholders	0.951**	0.000
11	Reduce the risks of tasks/activities	0.940**	0.000
12	Describe procedures within the organisation	0.949**	0.000
13	Prove methods to feature KM in construction projects	0.923**	0.000
14	Recourse allocation and analysis	0.947**	0.000
15	Develop quality control on the spot	0.965**	0.000

**: A significant relationship between the statement and the total score of its axis.

Table 2. Validity of the internal consistency for AI Applications Benefits

No.	Dimensions and axes of the study	Correlation with the total	
		Pearson Correlation	Sig
1	Learn the best practices	0.913**	0.000
2	Prepare and issue the predictive reports	0.961**	0.000
3	Provide recommendations to address the causes of the delay	0.912**	0.000
4	Prepare purchasing management automatically	0.936**	0.000
5	Link resources with project activities	0.901**	0.000
6	provide a project uncertainty assessment	0 .953**	0.000
7	provide a project risk management and analysis	0 .948**	0.000
8	Plan performance and analysis for projects	0.946**	0.000
9	provide a project time management and analysis	0.913**	0.000
10	Issue alerts when the project deviation	0.937**	0.000
11	Introduce safety oversight for construction tasks	0.942**	0.000
12	Introduce cost estimation and management	0.944**	0.000
13	learn to develop local practices	0.925**	0.000
14	Prepare the budget for bidding properly	0.938**	0.000
15	Familiarise the relevant legislation for the project	0.928**	0.000
16	Selecting the materials or equipment	0.897**	0.000
17	Develop quality control on the spot	0.902**	0.000

**: A significant relationship between the statement and the total score of its axis.

Table 3. Validity of the internal consistency for Integrated AI & KM Benefits

No.	Dimensions and axes of the study	Pearson Correlation	Sig
		Correlation with the total	
1	Compliance with the project implementation plan	0.913**	0.000
2	Match the contractor's capabilities to the requirements of the project	0.814**	0.000
3	Improve the implementation of the KM system	0.771**	0.000
4	Enhance the significant amount of project time	0.681**	0.000
5	Resolve expected risks in projects for all parties	0.823**	0.000
6	Match the achieved costs with the estimated cost	0.842**	0.000
7	Facilitate the difficulties in the contractor's financial	0.815**	0.000
8	Enhance site supervision	0.789**	0.000
9	Improve the competence of the project manager	0.698**	0.000
10	Improve communication between project parties	0.814**	0.000
11	Set up the Violations with subcontracting parties	0.791**	0.000
12	Prove methods to feature KM in construction projects	0.781**	0.000
13	Focus on the individual level rather than the team level	0.845**	0.000
14	Enhance sharing knowledge	0.872**	0.000
15	Apply the necessary technological infrastructure to implement it	0.865**	0.000
16	Gather scattered information systems and various technological means	0.799**	0.000
17	Improve time and extra workload	0.812**	0.000
18	Clarify unknown concepts to the contractor and the engineers	0.0903**	0.000

**: A significant relationship between the statement and the total score of its axis.

The correlation coefficients shown in the tables above on the three axes are characterized by internal consistency, as the correlation relationship is statistically significant. The Sig. value (the significance level) of the statistical values of the Pearson correlation coefficients calculated in each dimension is less than the 0.05 significance level, indicating a relationship between the study axes for each axis.

5.4. Reliability of the Study

The concept of reliability refers to the ability of an instrument to measure what it is designed to measure over different periods. Cronbach's alpha coefficient was used to determine the stability of the study tool [31, 32].

Table 4 indicates the results of Cronbach's alpha coefficient values for all study axes, which were more significant than 0.7; this indicates that the study tool has high stability and reliability [33]. The questionnaire for the study has reliability.

Table 4. coefficients of Cronbach's alpha

Dimensions and axes of the study	No. of elements	Cronbach's alpha coefficient
Benefits of applying the KM process	15	0.923
Benefits of applying AI applications	17	0.907
Benefits of applying an integrated combination of KM and AI	18	0.929

5.5. Statistical Methods

SPSS was used to collect and analyze the data from the study. Many statistical methods commensurate with the nature of the data were used [34]. These methods are Arithmetic Mean, Standard Deviation, Relative Important Index, Correlations between the Variables, and Multiple Regressions Analysis.

6. Statistical Results

The following are the final results that will be adopted to verify the research hypotheses.

6.1. Demographic Characteristics

Table 5 reviews the different characteristics of the sample distribution stated in the questionnaire under study. It includes (Age, Qualification, Current Position, and Years of Experience) and they represent in Figure 2.

Table 5. Demographic characteristics

Variable	Category	frequency	%	Accumulative per cent
Age	21-30	16	18.82	18.82
	31-40	17	20	38.82
	41-50	20	23.53	62.35
	More than 51	32	37.65	100
Qualification	Diploma	14	16.47	16.47
	Bachelor's	33	38.82	55.29
	Master's	24	28.24	83.53
	PhD	14	16.47	100
Current position	Director general	6	7.06	7.06
	Project manager	17	20	27.06
	Advisor	20	23.53	50.59
	Site engineer	42	49.41	100
Years of Experience	Less than 5 yr.	21	24.71	24.71
	6-10	19	22.35	47.06
	11-15	18	21.18	68.24
	16-20	15	17.65	85.89
	More than 20	12	14.12	100
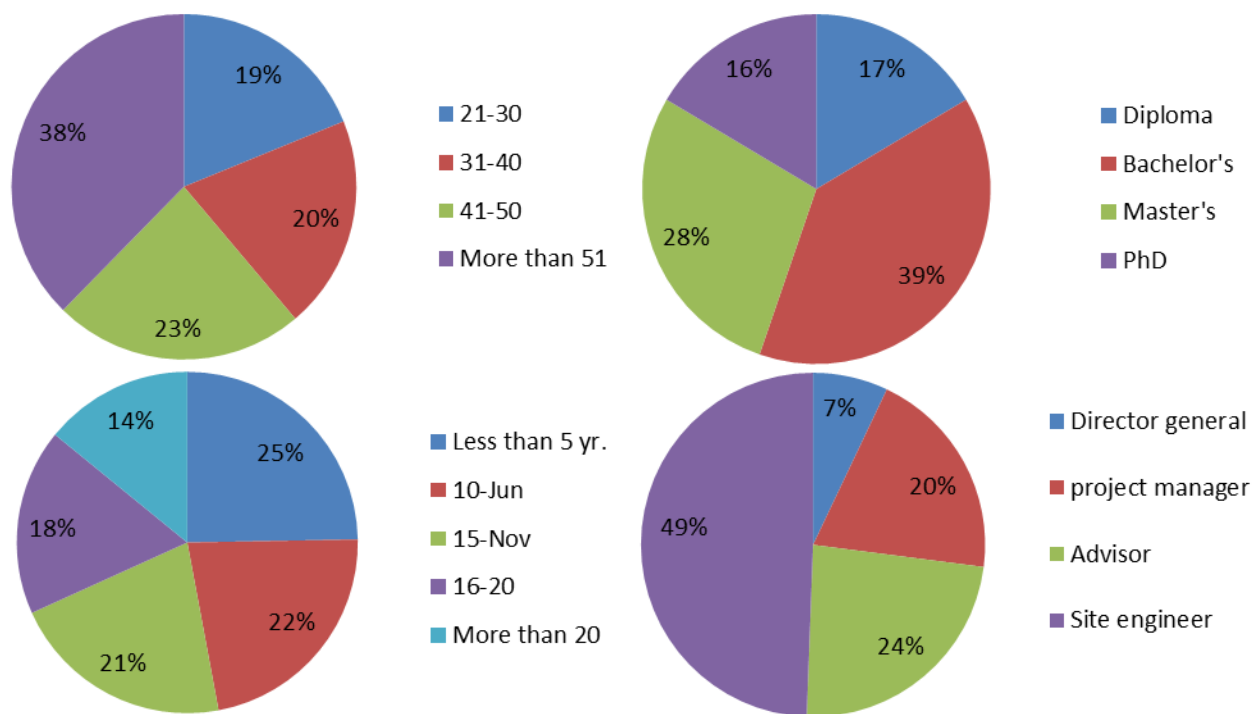
Figure 2. Demographic characteristics

6.2. Results and Descriptions

6.2.1. Mean, Standard Deviation, and Relative Important Index Results

A. Benefits of applying the KM process in construction project management:

This axis dealt with 15 objectives to determine how the sample used the KM process in the construction work. Table 6 refers to the Arithmetic Mean, Standard Deviation, Variance, and Relative Important Index (RII) results. There was high agreement among the respondents to all objectives of this axis, as the percentage reached the axis (77.64%). The five most essential percentages of the sample's responses to the objectives of this axis are: contribute to improving teamwork (85%), improve the efficiency of tasks or activities (82.8%), exchange experiences between employees and communication (82.6%), continuous improvement of operations (82.4%), and follow up on the implementation of the project plan (82.4%).

Table 6. Statistical Results for the Benefits of Applying KM Process

No.	Objective	Std. Deviation	Mean	RII%	Ranking
1	Improve the decision-making process	1.28	4.07	81.4	7
2	Follow up on the implementation of the project plan	1.349	4.12	82.4	5
3	Continuous improvement of operations	1.051	4.12	82.4	4
4	Improve the efficiency of tasks or activities	1.002	4.14	82.8	2
5	Contribute to improving teamwork	0.937	4.25	85	1
6	Reduce the company's costs and prepare the project budget	0.988	4	80	9
7	Control project time planning	0.919	4.01	80.2	8
8	Improve the quality of products and services	1.156	3.79	75.8	11
9	Exchange experiences between employees and communication	0.997	4.13	82.6	3
10	Share information among stakeholders	1.128	3.88	77.6	10
11	Reduce the risks of tasks/activities	1.128	4.12	82.4	6
12	Describe procedures within the organisation	1.106	3.78	75.6	12
13	Prove methods to feature KM in construction projects	1.020	3.11	62.2	15
14	Recourse allocation and analysis	0.989	3.50	70.0	13
15	Develop quality control on the spot	1.012	3.21	64.2	14
	Total		**3.882**	**77.64**	**High**

B. Benefits of Applying AI applications in construction projects management:

This axis dealt with 17 different objectives to determine the percentages of AI applications used in the management and follow-up of projects. Table 7 refers to the Arithmetic Mean, Standard Deviation, Variance, and Relative Important Index (RII) results. There was high agreement among the respondents to all objectives of this axis, as the percentage reached the axis (80.44%). The five most essential percentages of the sample's responses to the objectives of this axis are: prepare and issue the predictive reports (92.4%); learn the best practices (87.6%); link resources with project activities (85.6%); introduce safety oversight for construction tasks (84%); and prepare purchasing management automatically (83.8%).

Table 7. Statistical Results for the Benefits of Applying AI Applications

No.	Objective	Std. Deviation	Mean	RII%	Ranking
1	Learn the best practices	0.899	4.38	87.6	2
2	Prepare and issue the predictive reports	0.723	4.62	92.4	1
3	Provide recommendations to address the causes of the delay	1.028	4.12	82.4	8
4	Prepare purchasing management automatically	0.945	4.19	83.8	5
5	Link resources with project activities	0.881	4.28	85.6	3
6	provide a project uncertainty assessment	0.957	4.01	80.2	10
7	provide a project risk management and analysis	0.926	4.02	80.4	9
8	Plan performance and analysis for projects	0.957	4.01	80.2	11
9	provide a project time management and analysis	0.937	4.16	83.2	7
10	Issue alerts when the project deviation	1.067	3.93	78.6	12
11	Introduce safety oversight for construction tasks	1.021	4.2	84.0	4
12	Introduce cost estimation and management	1.091	3.8	76.0	15
13	learn to develop local practices	1.082	3.92	78.4	13
14	Prepare the budget for bidding properly	1.045	4.16	83.2	6
15	Familiarise the relevant legislation for the project	1.067	3.80	76.0	14
16	Selecting the materials or equipment	1.102	3.50	70.9	16
17	Develop quality control on the spot	1.072	3.23	64.6	17
	Total		**4.02**	**80.44**	**High**

C. Benefits of applying an integrated combination of KM and AI in construction projects management:

This axis dealt with 18 different objectives to determine the benefits and impacts of using the integrated combination of KM and AI in construction projects related to the engineers' view. Table 8 refers to the Arithmetic Mean, Standard Deviation, Variance, and Relative Important Index (RII) results. The respondents agreed highly to all reasons for this axis, as the percentage reached the axis (77.37%). The results were arranged in ascending order, depending on the five most essential percentages of the sample's responses to the objectives of this axis are: "Compliance with the project implementation plan (92.5%), Resolve expected risks in projects for all parties (89.9%), Gather scattered information systems and various technological means (85.3%), Enhance the significant amount of project time (85.1%), and Apply the necessary technological infrastructure to implement it (83.5%)".

Table 8. Statistical Results for the Benefits of the Integration of AI Applications based on KM

No.	Objective	Std. Deviation	Mean	RII%	Ranking
1	Compliance with the project implementation plan	0.676	4.627	92.5	1
2	Match the contractor's capabilities to the requirements of the project	0.885	3.675	73.5	12
3	Improve the implementation of the KM system	0.866	3.928	78.6	9
4	Enhance the significant amount of project time	0.895	4.253	85.1	4
5	Resolve expected risks in projects for all parties	0.846	4.494	89.9	2
6	Match the achieved costs with the estimated cost	0.970	3.6386	72.8	13
7	Facilitate the difficulties in the contractor's financial	0.997	3.699	74.0	11
8	Enhance site supervision	0.934	4.072	81.4	7
9	Improve the competence of the project manager	1.025	3.59	71.8	14
10	Improve communication between project parties	0.989	3.29	65.8	17
11	Set up the Violations with subcontracting parties	1.045	3.41	68.2	15
12	Prove methods to feature KM in construction projects	0.926	3.26	65.2	18
13	Focus on the individual level rather than the team level	0.981	3.988	79.8	8
14	Enhance sharing knowledge	0.872	4.084	81.7	6
15	Apply the necessary technological infrastructure to implement it	0.885	4.181	83.6	5
16	Gather scattered information systems and various technological means	0.938	4.265	85.3	3
17	Improve time and extra workload	0.857	3.855	77.1	10
18	Clarify unknown concepts to the contractor and the engineers	1.012	3.32	66.4	16
	Total		**3.868**	**77.37**	**High**

The results also indicate how the demographic characteristics of the sample affect achieving the benefits of applying knowledge management and artificial intelligence applications. There are clear variations and differences depending on the category of the sample. Figure 3 indicates that the current generation of engineers (age from 21 to 30) excels in using artificial intelligence in their work in parallel with the use of knowledge management. This will lead to a huge stimulation of integration between the two axes. Therefore, age has an inverse relationship with the axes of the study.
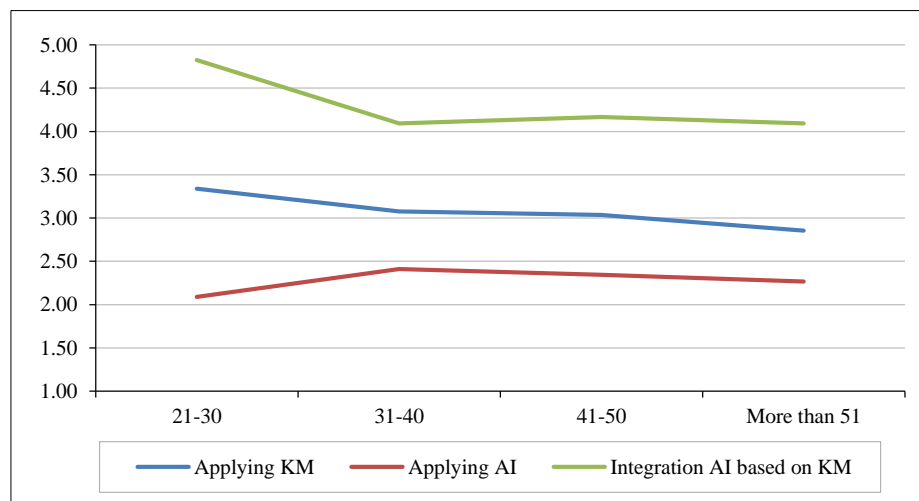
Figure 3. Effect of age category

As for Figure 4, academic achievement has an important role in achieving the goal; the relationship is linear with the study axes.
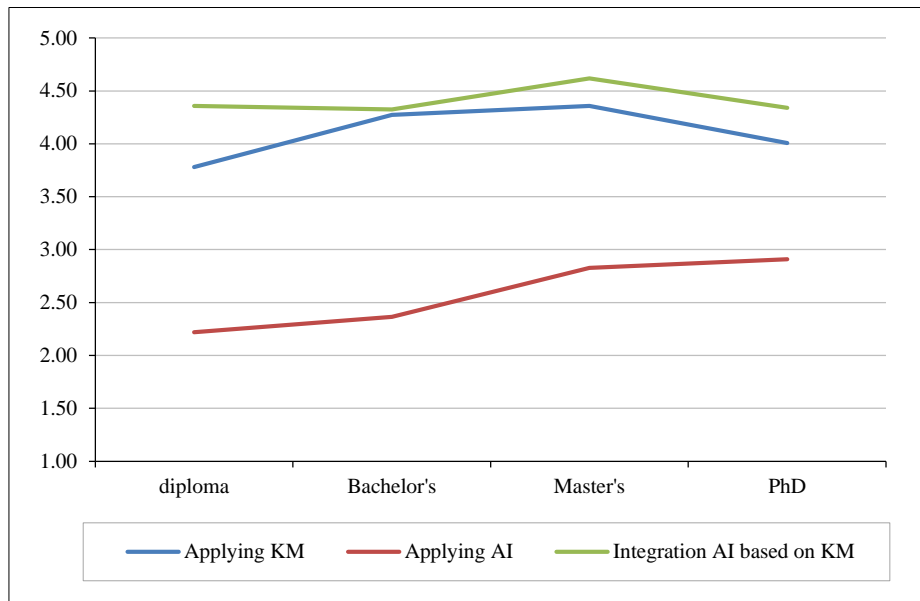
Figure 4. Effect of Qualification category

However, Figure 5 notices a diverse relationship with the current job position of the engineer, and this is good and fits with their responsibilities for managing construction tasks. But the project manager has an important role in achieving high points for the three axes under study.
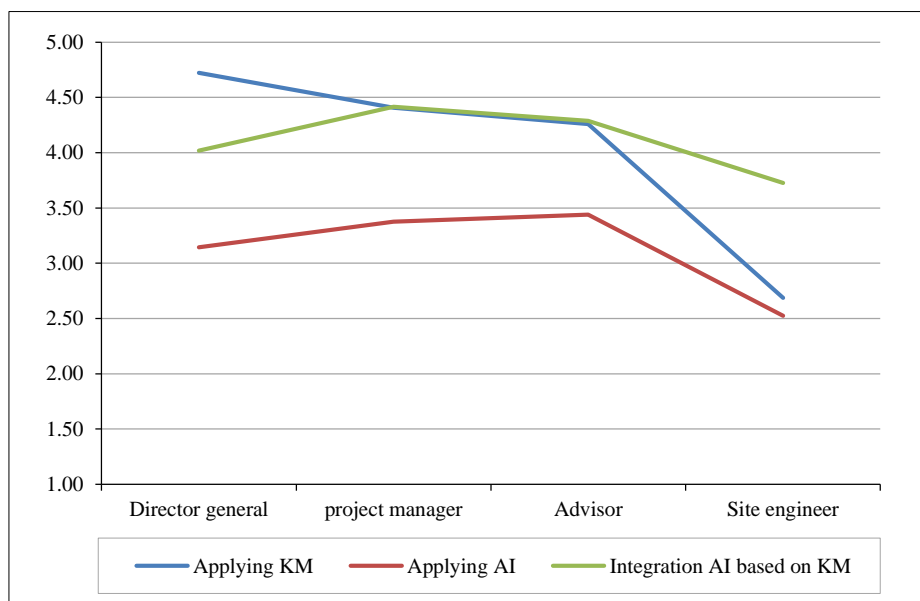
Figure 5. Effect of Current position category

Figure 6 shows the effect of experience with the use of KM processes and AI applications. Although it is not possible for those with great experience to be compatible with the uses of AI in their work, they received a high rating in knowledge management despite their reliance on the manual method in implementing activities. The results show that the respondents who have experience (10–20) have experienced most of the different applications in AI and have become experienced in their field of work by using AI applications. As for those who have little experience, they need higher training to compete with those with greater experience due to their ability to understand the basics and applications of artificial intelligence.
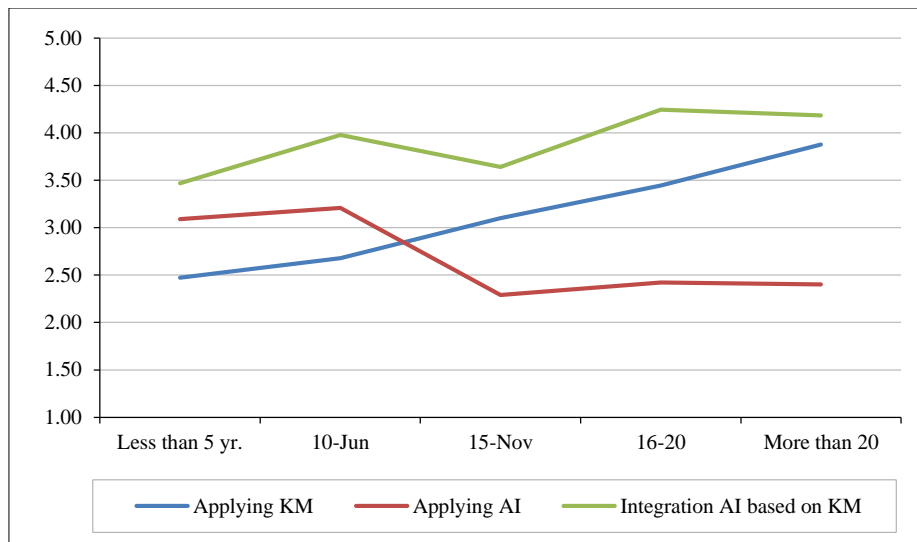
Figure 6. Effect of Years of Experience category

6.2.2. Test of Hypothesis

1st Hypothesis: The statistical hypothesis adopted a positive correlation between the demographic variables of the selected sample, including (Age, Qualification, Current Position, and Years of Experience) and the two axes (The Benefits of applying the KM process and AI applications in construction project management). Table 9 indicates the results of hypothesis testing according to the simple correlation coefficient between the variables.

Table 9. Simple correlation coefficient between variables

Category		Applying AI applications	Applying KM process
Age	Pearson Correlation	**-0.196**	**-0.152**
	Sig. (2-tailed)	0.072	0.164
Qualification	Pearson Correlation	**-0.238***	**-0.259***
	Sig. (2-tailed)	0.028	0.017
Current position	Pearson Correlation	**0.395****	**0.372****
	Sig. (2-tailed)	<0.001	<0.001
Years of experience	Pearson Correlation	**0.328****	**0.302****
	Sig. (2-tailed)	0.02	0.03

**. Correlation is significant at the 0.05 level (2-tailed).

*. Correlation is significant at the 0.01 level (2-tailed).

1) There is a negative statistically significant correlation between Age and the two axes (Applying KM processes and AI applications), and the values of the simple correlation coefficient between them are -0.196 and -0.152, respectively, which are out of a statistically significant value at the probabilistic level of 0.05.

2) Statistically significant correlation between qualification and the two axes (Applying KM processes and AI applications), the values of the simple correlation coefficient between the variables are (-0.238 and -0.259), respectively, which are two statistically significant values at the level of probability 0.05.

3) A positive statistically significant correlation between the current position and the two axes (using KM processes and AI applications in the management of investment projects), as the value of the correlation coefficient between the two variables, reached (0.395 and 0.372), respectively, which is a statistically significant value at the probabilistic level of 0.05.

4) There is a positive statistically significant correlation between years of experience and (Applying KM processes and AI applications in construction project management; the values of the simple correlation coefficient between them reached 0.328 and 0.302, respectively, which is a statistically significant value at the probabilistic level of 0.05.

2nd Hypothesis: Regression analysis was used to determine the relationships between the variables. Linear regression approximates the causal relationship between two or more variables. Regression models are considered highly valuable because they are one of the most common ways to make predictions and inferences [35].

Simple linear regression occurs when there is only one response variable or when studying and analyzing the effect of one variable on another variable. It is concerned with studying the dependence of one variable, known as the dependent variable or dependent variable on one or more variables defined as explanatory variables or independent variables to estimate or predict the average values of the dependent variable with the information of the explanatory variables. Regression analysis is used for three primary purposes [36]. The study explains the variation in the application of the KM process in construction project management and then for AI applications in construction project management with the demographic variables of the samples.

A. Interpretation of variance for applying the KM process in construction project management:

The research hypothesis developed was that there is an impact of all demographic variables on the use of the KM process. This hypothesis was tested according to the linear regression coefficient, as its results are shown in Table 10.

Table 10. Correlation coefficient of determination

Model	R	R Square	Adjusted R Square	Std. Error of the Estimate
1	0.579 [a]	0.378	0.290	0.76460

a. Predictors: (Constant), Age, Qualification, Current Position, Years of Experience.

The results indicate that the value of the multiple correlation coefficient between all demographic variables and the use of the KM process in construction projects amounted to the values of the three correlation coefficients, the simple correlation coefficient R (0.579). The coefficient of determination, square R, was (0.378), while the adjusted coefficient of determination was (0.290), which means that the independent explanatory variables (Age, Qualification, current position, Years of experience) were able to explain the changes that occurred in the interpretation of variance in the application of the KM process in construction project management. The rest is attributed to other factors. State the following hypothesis to test the significance of the regression:

$$H_0: B_1 = B_2 = B_3 = B_4 \tag{1}$$

where H_1 is At least one parameter is not equal to zero.

From Tables 11 and 12, the value of (Sig<0.001) is less than the value ($\alpha = 0.05$), so reject the null hypothesis and accept the alternative hypothesis; the regression is significant. That means there is an effect of the independent variables on the dependent variables, and predict the dependent variable by independent variables.

Table 11. Analysis of variance in a multiple linear regression model

	Model	Sum of Squares	Mean Square	F	Sig.
	Regression	22.443	5.611	9.597	<0.001[a]
1	Residual	46.769	0.585		
	Total	69.212			

a. Predictors: (Constant), Age, Qualification, Current Position, Years of Experience.

Table 12. Model summary

Model	Unstandardised Coefficients		Standardised Coefficients	t	Sig.	Correlations		
	B	Std. Error	Beta			Zero-order	Partial	Part
(Constant)	5.775	0.329		17.579	<.001			
Age	0.696	0.229	0.875	3.031	0.003	-0.196	0.321	0.279
Qualification	-0.306	0.246	-0.323	-1.244	0.217	-0.238	-0.138	-0.114
Current position	-1.150	0.207	-1.244	-5.563	<0.001	-0.395	-0.528	-0.511
Years of Experience	0.246	0.197	0.376	1.249	0.215	-0.193	0.138	0.115

To determine which of the coefficients is significant and causes significant analysis of variance for the multiple linear regression test for the significance of each parameter separately, it was found that two factors (Qualification and Years of Experience) are not significant, which means they have no significant effect on the significance of the analysis of variance regression. However, in the case of the variables (Age and current position), these coefficients are significant and impact the use of knowledge applications. The significance of the analysis of variance is due to the multiple linear regressions. To find out the percentage for each variable that contributes to explaining the variation in the applying KM process in construction project management, correlational analysis and stepwise multiple regression were performed, as

shown in Tables 13 to 15, where the results indicate a multiple linear regression equation that includes two variables: Age and current position. The results of the coefficient of determination indicate that the two variables explain 29.1% of the variance in the applying KM process.

Table 13. Adjusted model summary (KM process)

Model	R	R Square	Adjusted R Square	Std. The error of the Estimate	Change statistics		
					R Square Change	F Change	Sig. F Change
1	0.555[a]	0.308	0.291	0.76420	0.308	18.257	<0.001

a. Predictors: (Constant), Age, Current Position.

Table 14. Adjusted Analysis of Variance in a multiple linear regression model

	Model	Sum of Squares	df	Mean Square	F	Sig.
1	Regression	21.324	2	10.662	18.257	<0.001[a]
	Residual	47.888	82	0.584		
	Total	69.212	84			

a. Predictors: (Constant), Age, Current Position.

Table 15. An adjusted model summary

Model	Unstandardised Coefficients		Standardised Coefficients	t	Sig.
	B	Std. Error	Beta		
(Constant)	5.579	0.295		18.899	<0.001
Age	0.741	0.175	.932	4.242	<0.001
Current Position	-1.148	0.203	-1.242	-5.652	<0.001

B. An explanation of the variation in AI applications in construction project management:

The research hypothesis developed was that there is an impact of all demographic variables on the use of AI applications in investment projects. This hypothesis was tested using the linear regression coefficient, as shown in Table 16.

Table 16. Correlation coefficient of determination

Model	R	R Square	Adjusted R Square	Std. An error in the Estimate
1	0.611[a]	0.373	0.342	0.64814

a. Predictors: (Constant), Age, Qualification, Current Position, Years of Experience.

The results indicate that the multiple correlation coefficient between all demographic variables and the use of AI applications in construction projects amounted to the values of the three correlation coefficients, including the simple correlation coefficient R, which was 0.611. The coefficient of determination, square R, was (0.373), while the adjusted coefficient of determination was (0.342), which means that the independent explanatory variables (Age, Qualification, current position, Years of experience) were able to explain the changes that occurred in the interpretation of variance in the use of AI applications in investment construction projects. The rest is attributed to other factors. State the following hypothesis to test the significance of the regression:

$$H_0: B_1 = B_2 = B_3 = B_4 \qquad\qquad (2)$$

where H_1 is At least one parameter is not equal to zero

From Tables 17 and 18, the value of (Sig<0.001) is less than the value ($\alpha = 0.05$), so reject the null hypothesis and accept the alternative hypothesis; the regression is significant. That means there is an effect of the independent variables on the dependent variables, and predict the dependent variable by independent variables.

Table 17. Analysis of variance in a multiple linear regression model

	Model	Sum of Squares	Mean Square	F	Sig.
1	Regression	20.028	5.007	11.919	<0.001[a]
	Residual	33.607	0.420		
	Total	53.635			

a. Predictors: (Constant), Age, Qualification, Current Position, Years of Experience.

Table 18. Model summary

Model	Unstandardised Coefficients		Standardised Coefficients	t	Sig.	Correlations		
	B	Std. Error	Beta			Zero-order	Partial	Part
(Constant)	5.608	0.278		20.139	<0.001			
Age	0.891	0.194	1.274	4.583	<0.001	-0.152	0.456	0.406
Qualification	-0.428	0.209	-0.513	-2.052	0.043	-0.259	-0.224	-0.182
Current position	-1.042	0.175	-1.280	-5.948	<0.001	-0.372	-0.554	-0.526
Years of Experience	0.120	0.167	0.209	0.722	0.472	-0.202	0.080	0.064

To determine which of the coefficients is significant and causes significant ANOVA for multiple linear regression, test the significance of each parameter separately. It was found that factors (Years of Experience) are not significant, and this means they have no significant effect on the significance of the analysis of variance regression. However, in the case of the variables (Age, Qualification, current position), these coefficients are significant and impact the use of AI applications. The reason for the significance of the analysis of variance is the multiple linear regression. To find out the percentage for each variable that contributes to explaining the variation in the use of AI applications in investment projects, correlational analysis and stepwise multiple regression were performed, as shown in Tables 19 to 21, where the results indicate a multiple linear regression equation that includes three variables: Age, Qualification and Current position. The results of the coefficient of the determination indicate that the three variables explain 34.6 % of the variance in the use of AI applications.

Table 19. Adjusted model summary (Applying AI Application)

Model	R	R Square	Adjusted R Square	Std. An error in the Estimate	Change statistics		
					R Square Change	F Change	Sig. F Change
1	0.608	0.369	0.346	0.64622	0.369	15.812	<0.001

a. Predictors: (Constant), Age, Qualification, Current Position.

Table 20. Analysis of variance in a multiple linear regression model

Model		Sum of Squares	df	Mean Square	F	Sig.
	Regression	19.809	3	6.603	15.903	<0.001[a]
1	Residual	33.216	81	0.4152		
	Total	53.025	84			

a. Predictors: (Constant), Age, Qualification, Current Position.

Table 20. An adjusted model summary (AI Application)

Model	Unstandardised Coefficients		Standardised Coefficients	t	Sig.
	B	Std. Error	Beta		
(Constant)	5.523	0.252		21.950	<0.001
Age	0.948	0.178	1.354	5.331	<0.001
Qualification	-0.334	0.162	-0.400	-2.056	0.043
Years of experience	-1.031	0.174	-1.268	-5.926	<0.001

7. Conclusions

The study seeks to find new advantages to enhance the success of the implementation of construction projects in different regions of the governorates of Iraq depending on the type of applied characteristics, like the work of management and facilities used. The study dealt with enhancing the KM process based on AI applications. The study reached several results, the most important of which are:

- The percentage of engineers' responses on the axis of the benefits of applying the KM process to construction projects (77.64%) is relatively high.

- The percentage of engineers' responses for the benefits of using AI applications in project management and follow-up is very high, amounting to 82.13%.

- The percentage of engineers' responses for the benefits of integrating AI applications based on the KM process in project management is very high, amounting to 77.37%.

- The percentage of engineers' benefits about using the integration of KM and AI in construction projects related to the view of engineers in descending order to include (Compliance with the project implementation plan, Resolving expected risks in projects for all parties, gathering scattered information systems and various technological means, enhancing the significant amount of project time, and applying the necessary technological infrastructure to implement it).

- The impact of two variables (Qualification and Years of Experience) on the application of the KM process in construction projects is not significant; they have no significant effect on the significance of the analysis of variance regression.

- The impact of two variables (Age and current position) is significant and impacts the application of the KM process for the significance of the analysis of variance.

- There is a negative statistically significant correlation between the age and the two axes (KM processes and AI applications in construction projects); the values of the simple correlation coefficient between them reached 0.196 and 0.152, respectively, which are two statistically significant values at the probability level of 0.05.

- There is a negative statistically significant correlation between the age and the two axes (using the KM process and AI applications in the management of investment projects); the values of the simple correlation coefficient between the variables reached 0.283 and 0.259, respectively, which are two statistically significant values at the level of probability 0.05, which is a statistically significant value at the probabilistic level of 0.05.

- There was a positive statistically significant correlation between the current position and the two axes (using the KM process and AI applications in the management of investment projects), as the value of the correlation coefficient between the two variables reached 0.395 and 0.372, respectively, which is a statistically significant value at the probabilistic level of 0.05.

- There was a positive statistically significant correlation between years of experience and the two axes (using the KM process and AI applications in the management of investment projects); the values of the simple correlation coefficient between them reached 0.328 and 0.302, respectively, which is a statistically significant value at the probabilistic level of 0.05.

7.1. Recommendations

KM is a fundamental philosophical principle in the new information era. Because it has a considerable impact on the value-added benefits if it is implemented correctly and integrated with AI software to enhance a practical path for the parties involved in the implementation process, access to knowledge and information in a faster time, and passing many of the required modifications and changes. However, AI software can assist in various KM processes by different construction companies, regardless of the type of construction project.

The study showed that the success of many investment companies in adopting AI applications is due to solid reasons, such as the huge investments at the beginning, their awareness of its full benefits, or how it can enhance KM within the company and during the various stages of the project. So, there is ample space for research and development in the future, mainly if the user focuses directly on his ability to use these systems and develop them to serve the construction process. The role of the expanded value of knowledge gives importance to KM in building a structure for the technological approach within the company, and this work takes the form of qualitative research to assess the level of the categories of AI software currently used or required to be used in the KM process. For this, future research must be done extensively to introduce new concepts to most investment companies that desire to apply and expand AI applications based on KM. Provide that the user's demographic characteristics are essential for the correct application and appropriate development of KM integration in all construction project phases.

The study recommends the need to strengthen the adoption of the application of KM based on AI applications to resolve all problems of delayed completion of investment construction projects in Iraq, in addition to the need to pay attention to the financial aspect and improve the efficiency of these projects by sharing and applying KM in integration with the application of intelligent applications, which is the basis of KM operations.

Adopting the demographic characteristics of engineers (years of experience, current position) can help organizations choose the appropriate engineers to perform their professional work to help complete projects with high quality. It can also be adopted for the purpose of training and development to raise the skills of engineers in light of the great development witnessed by the construction industry after the tremendous developments in most applications of artificial intelligence.

8. Declarations

8.1. Author Contributions

Conceptualization, M.R.A. and M.M.D.; methodology M.R.A.; validation, M.R.A. and M.M.D.; formal analysis, M.R.A.; investigation, M.M.D.; resources, M.R.A.; data curation, M.R.A.; writing—original draft preparation, M.R.A.; writing—review and editing, M.R.A.; visualization, M.R.A.; supervision, M.R.A.; project administration, M.R.A.; funding acquisition, M.R.A. All authors have read and agreed to the published version of the manuscript.

8.2. Data Availability Statement

The data presented in this study are available on request from the corresponding author.

8.3. Funding

8.4. Conflicts of Interest

The authors declare no conflict of interest.

9. References

[1] Travis, M. L., Aruldoss, A., Kowalski, K. B., & Parayitam, S. (2023). The effect of knowledge conversion on innovation and performance: A multi-layered moderated-mediation model. Knowledge and Process Management, 30(4), 409–433. doi:10.1002/kpm.1748.

[2] Tiwari, S. P. (2022). Knowledge Enhancement and Mobile Technology: Improving Effectiveness and Efficiency. International Journal of Social Science Research and Review, 5(7), 127–134. doi:10.47814/ijssrr.v5i7.338.

[3] Ahmad, K., Iqbal, W., El-Hassan, A., Qadir, J., Benhaddou, D., Ayyash, M., & Al-Fuqaha, A. (2024). Data-Driven Artificial Intelligence in Education: A Comprehensive Review. IEEE Transactions on Learning Technologies, 17, 12–31. doi:10.1109/TLT.2023.3314610.

[4] Maphosa, V., & Maphosa, M. (2022). AI In Project Management Research: A Bibliometric Analysis". Journal of Theoretical and Applied Information Technology, 100(16), 5000–5012. doi:10.5281/zenodo.7134074.

[5] Anumba, C., & Khallaf, R. (2022). Use of Artificial Intelligence to Improve Knowledge Management in Construction. IOP Conference Series: Earth and Environmental Science, 1101(3), 032004. doi:10.1088/1755-1315/1101/3/032004.

[6] Igbinovia, M. O., & Ikenwe, I. J. (2018). Knowledge management: processes and systems. Information Impact: Journal of Information and Knowledge Management, 8(3), 26. doi:10.4314/iijikm.v8i3.3

[7] Ramaj, B. Z., & Pjero, E. (2023). The Implementation of Accounting Information Systems for its Role in Marketing and Management Processes. European Journal of Marketing and Economics, 6(1), 28–38. doi:10.2478/ejme-2023-0003.

[8] Karki, S., & Hadikusumo, B. (2023). Machine learning for the identification of competent project managers for construction projects in Nepal. Construction Innovation, 23(1), 1–18. doi:10.1108/CI-08-2020-0139.

[9] Jarrahi, M. H., Askay, D., Eshraghi, A., & Smith, P. (2023). Artificial intelligence and knowledge management: A partnership between human and AI. Business Horizons, 66(1), 87–99. doi:10.1016/j.bushor.2022.03.002.

[10] Rane, N. (2023). Integrating Building Information Modelling (BIM) and Artificial Intelligence (AI) for Smart Construction Schedule, Cost, Quality, and Safety Management: Challenges and Opportunities. SSRN Electronic Journal, 1-20. doi:10.2139/ssrn.4616055.

[11] Nanjundeswaraswamy, T., & Swamy, D. (2022). Knowledge management processes and organizational culture in the higher educational technical institutions. Journal of Economic and Administrative Sciences, 38(2), 270–286. doi:10.1108/jeas-07-2020-0134.

[12] Lam, L., Nguyen, P., Le, N., & Tran, K. (2021). The relation among organizational culture, knowledge management, and innovation capability: Its implication for open innovation. Journal of Open Innovation: Technology, Market, and Complexity, 7(1), 1–16. doi:10.3390/joitmc7010066.

[13] Hsu, H. C., Chang, S., Chen, C. C., & Wu, I. C. (2020). Knowledge-based system for resolving design clashes in building information models. Automation in Construction, 110. doi:10.1016/j.autcon.2019.103001.

[14] Ugwu, C. I., & Ekere, J. N. (2019). Knowledge management for improving services in federal university libraries in Nigeria. Journal of Librarianship and Information Science, 51(2), 356–369. doi:10.1177/0961000617742446.

[15] Abubakar, A. M., Elrehail, H., Alatailat, M. A., & Elçi, A. (2019). Knowledge management, decision-making style and organizational performance. Journal of Innovation and Knowledge, 4(2), 104–114. doi:10.1016/j.jik.2017.07.003.

[16] Alavi, M., & Leidner, D. E. (2001). Review: Knowledge Management and Knowledge Management Systems: Conceptual Foundations and Research Issues. MIS Quarterly, 25(1), 107. doi:10.2307/3250961.

[17] Bem, R. M. de, & Coelho, CCSR. (2013). Applications of knowledge management in the area of Librarianship and Information Science. Brazilian Journal of Information Science: Research Trends, 7(1), 69–97. doi:10.36311/1981-1640.2013.v7n1.06.p67.

[18] Galgotia, D., & Lakshmi, N. (2022). Implementation of Knowledge Management in Higher Education: A Comparative Study of Private and Government Universities in India and Abroad. Frontiers in Psychology, 13. doi:10.3389/fpsyg.2022.944153.

[19] Galgotia, D., & Lakshmi, N. (2022). Implementation of Knowledge Management in Higher Education: A Comparative Study of Private and Government Universities in India and Abroad. Frontiers in Psychology, 13. doi:10.3389/fpsyg.2022.944153.

[20] Tiwari, S. P. (2022). Knowledge Management Strategies and Emerging Technologies - An Overview of The Underpinning Concepts. International Journal of Innovative Technologies in Economy, 1(37), 1-3. doi:10.31435/rsglobal_ijite/30032022/7791.

[21] Al-Hawamdeh, M. M., & Alshaer, S. A. (2022). Artificial Intelligence Applications as a Modern Trend to Achieve Organizational Innovation in Jordanian Commercial Banks. The Journal of Asian Finance, Economics and Business, 9(3), 257-263.

[22] Bahroun, Z., Tanash, M., As'ad, R., & Alnajar, M. (2023). Artificial Intelligence Applications in Project Scheduling: a Systematic Review, Bibliometric Analysis, and Prospects for Future Research. Management Systems in Production Engineering, 31(2), 144–161. doi:10.2478/mspe-2023-0017.

[23] Svetlova, E. (2022). AI meets narratives: the state and future of research on expectation formation in economics and sociology. Socio-Economic Review, 20(2), 841–861. doi:10.1093/ser/mwab033.

[24] Emad, A., Naimi, S., Altaie, M. R. (2023). Artificial intelligence based statistical process control for monitoring and quality control of water resources: a complete digital solution. International Journal of Intelligent Systems and Applications in Engineering, 11(5s), 314-324.

[25] Narayanan, V. K. (2019). Using institutional knowledge to answer puzzling questions about novel challenges and opportunities. Strategy and Leadership, 47(6), 15–23. doi:10.1108/SL-08-2019-0116.

[26] Nabizadeh R., H., & Nabizadeh, A. H. (2023). Towards human-centered artificial intelligence (AI) in architecture, engineering, and construction (AEC) industry. Computers in Human Behavior Reports, 11(8), 100319. doi:10.1016/j.chbr.2023.100319.

[27] Alghamdi, S. E. K., & Al-dirman, F. (2022). Knowledge Management Applications Based on Artificial Intelligence: A Systematic Review. International Transaction Journal of Engineering, Management, & Applied Sciences & Technologies, 12(13), 12A13O, 1-16. doi:10.14456/ITJEMAST.2021.267.

[28] Ahmed, G. A., & Altaie, M. R. (2021). Investigation the Opportunity of BIM with Agile Management Approach in Iraqi Construction Projects. E3S Web of Conferences, 318, 02001. doi:10.1051/e3sconf/202131802001.

[29] Khameesa, A. S., & Altaay, M. R. (2022). Evaluating the Efficiency of Finance Methods in Residential Complex Projects in Iraq. Engineering, Technology and Applied Science Research, 12(1), 8080–8084. doi:10.48084/etasr.4663.

[30] Altaie, M. R., Muhsin, I. F., & Dishar, M. M. (2023). Managing the Utilization of Preventive Measures for Fire Resistance in the Hospitals. Civil and Environmental Engineering, 19(2), 520–531. doi:10.2478/cee-2023-0047.

[31] Kadhom, A., & Altaie, M. (2023). Impact of project delivery method on geotechnical site conditions for implementing water treatment plants in Iraq. AIP Conference Proceedings, 2651(1), 20018. doi:10.1063/5.0106524.

[32] Altaie, M. R., Dishar, M. M., & Muhsin, I. F. (2023). Fundamental Challenges and Management Opportunities in Post Disaster Reconstruction Project. Civil Engineering Journal, 9(9), 2161–2174. doi:10.28991/cej-2023-09-09-05.

[33] Obead, K. R., & Wali, M. R. (2020). Developing Systems Engineering for Sustainable Infrastructure Projects. IOP Conference Series: Materials Science and Engineering, 901(1), 012026. doi:10.1088/1757-899x/901/1/012026.

[34] Khamees, A. S., & Altaay, M. R. (2022). Optimizing Methods of Funding Residential Complexes Projects. International Journal of Intelligent Systems and Applications in Engineering, 10(3), 57-63.

[35] Tsukuma, H., & Kubokawa, T. (2020). Multivariate Linear Model and Group Invariance. Shrinkage Estimation for Mean and Covariance Matrices, 27–33. doi:10.1007/978-981-15-1596-5_4.

[36] Saleh, A. K. M. E., & Shalabh. (2014). A ridge regression estimation approach to the measurement error model. Journal of Multivariate Analysis, 123, 68–84. doi:10.1016/j.jmva.2013.08.014.
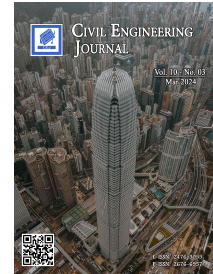
Response Reduction Factor for Structures with Significant Irregularities on Different Soil Stratum

Shorouk M. Elsadany [1*], M. N. Fayed [2], Tamer M. Sorour [2],
A. M. Anwar [3], Nasr E. Nasr [1, 2]

[1] Teaching Assistant of Structural Engineering, 6 October University, Cairo, Egypt.

[2] Structural Engineering Department, Ain Sham University, Cairo 11757, Egypt.

[3] Head of Hydraulic Structures Department, National Water Research Center, Egypt.

Abstract

The ability of a structure to dissipate energy through inelastic behavior is reflected in the response reduction factor (R), which is influenced by redundancy, ductility, and overstrength. Accurate determination of R is crucial for seismic design. This study focuses on determining the response factor for reinforced concrete (RC) structures with various irregularities. Non-linear static pushover analysis using SAP2000 was employed for numerical simulations to assess the impact of soil-structure interaction (SSI). The analysis included elevational and in-plan irregularities, revealing that buildings with irregular vertical geometries have lower inelastic seismic capacities compared to regular buildings. Consequently, R should be reduced by 15–40% from the ECP 2020 standard before the design phase for such structures. Irregularity was found to have a significant impact on weak soil conditions (C), leading to a reduction in R of 20.3% and 13.1% for fixed and isolated supports, respectively, on loose soil. Additionally, stiffer base soils were associated with higher R values for the same structure.

Keywords: Irregular RC Buildings; Elevation Irregularity; Plan Irregularity; Nonlinear Static Pushover Analysis; Response Reduction Factor; Soil Structure Interaction.

1. Introduction

A structure must be able to withstand intense seismic events without collapsing suddenly, even though it may suffer some structural and nonstructural damage. This is the core principle of earthquake-resistant design, which involves constructing a structure to withstand seismic forces by dissipating energy and exhibiting inelastic behavior [1-3]. Recent earthquakes have shown that elastic analysis is inadequate for assessing the true seismic performance of reinforced concrete buildings. Nonlinear time history analysis (NTHA), although challenging and dependent on ground motion data, can predict the likely inelastic response of structures [4]. To ensure safe and cost-effective designs, elastic analysis techniques are used to account for a structure's inelastic response by amplifying deformations and reducing seismic forces. Therefore, seismic design response elements are essential for both safety and cost-effectiveness [5]. Many seismic codes include response reduction or behavior factor (R) in their seismic analysis studies. NTHA is being replaced by other performance-based seismic evaluation techniques, such as nonlinear pushover analysis (NPA).

Several methods, including the FEMA440 displacement coefficient technique [6], the capacity spectrum technique of ATC-40 [7], the N2 method by Fajfar & Fischinger [8], and modal pushover analysis (MPA) [9], are considered as part of nonlinear pushover analysis (NPA) to determine a structure's inelastic performance. The response factor (R) is a crucial element in earthquake design, representing a structure's ability to dissipate energy through inelastic deformations [2]. Most structures use reduction factors to reduce seismic loads and bring the building closer to the inelastic range. Therefore, more deformation is required to dissipate energy from the structure. It is essential to consider both the economy and the performance and safety of constructions during earthquakes, highlighting the significance of the behavior factor in the seismic design process. The behavior factor (R) is a key component in the seismic design of new construction materials and is also used in equivalent static analysis as a seismic design parameter. It determines the nonlinear behavior of structural buildings during intense earthquakes. R is determined by engineering judgment and experimental testing; however, there is no standard method to calculate this value under various circumstances. Building response characteristics, which significantly impact the rates assigned to R, must be systematically assessed to enhance the reliability of modern earthquake-resistant buildings [10].

Accurate estimation of R is essential for assessing a structure's seismic response effectively. If the modification factor is overestimated, it can lead to a reduction in base shear and potentially result in more economical design solutions. However, precautions should be taken to ensure the structure's ductility performance [2-4]. Conversely, underestimating R could lead to uneconomical structural designs. Design codes implicitly account for structural non-linearity by reducing the seismic base shear of structures by the value of R.

The structural systems of buildings often need to incorporate various geometric irregularities, either in the horizontal or vertical plane, as specified by architectural requirements. Many existing structures exhibit severe irregularities that may not be addressed by current design codes, necessitating thorough research for their proper design [3]. Past experiences have shown that irregular constructions are more prone to catastrophic damage during earthquakes compared to regular structures [11]. In reality, most existing structures are asymmetrical, some intentionally designed that way for reasons such as creating commercial basements by removing central columns. Moreover, smaller beams and columns were added to the upper stories to meet functional requirements and for additional commercial purposes, such as storing large mechanical appliances. This variation in usage along a floor's length compared to neighboring floors results in irregularities in mass, stiffness, and strength distribution. Other structures may unintentionally become irregular due to factors like inconsistent building techniques and materials. The irregular distribution of mass, strength, and stiffness along a building's height can also occur [2]. Previous experiences demonstrate that structures with vertical irregularities perform poorly inelastically when located in seismically active areas. Hence, reliable design requirements are crucial for earthquake-prone areas. Regarding the impact of these irregularities [12], Brahmavrathan & Arunkumar [2] noted that the number of stories greatly influences the reduction of R for non-regular structures. Their research showed that the R factor value decreased by 37.53% and 31.04% for ordinary moment resisting frames (OMRF) and stiff moment resisting frames (SMRF) structures, respectively.

ECP-201 (2012) [13] sets values for R ranging from 3 to 5 for framed structures with sufficient to limited ductility. These values need to be adjusted to accommodate severe irregularities. Fayed et al. [3] calculated behavior factor values at failure for idealized multistory frame systems with moment resistance made of RC and developed in compliance with ECP-201 (2012) [13]. A decrease in the stated R values was observed. The structure's fundamental TP and seismic zone significantly impact the reduction factor. It decreases as the seismic zone becomes larger and increases with a longer basic TP. Hussein et al. [1] assessed how irregularities in floor heights and span lengths affect the behavior factor for common RC frames used in various structures. The outcomes showed inconsistent R values compared to structures with uniform bay length and floor height. El-Mahdy et al. [14] noted that R values differ in the X- and Y-directions for the cases covered in their research, which is more realistic than the design code-specified constant value. The lowest R values were determined for constructions with a loose ground story and a coupled asymmetric setback. Additionally, R's sensitivity to the vertical irregularity index (Vtm) was found to have an R-squared value of 80%, as demonstrated by Ahmed et al. [15].

Moreover, this article addresses the impact of SSI. The interaction between soil and foundation significantly affects the structure's response [16, 17]. The behavior of a structure during an earthquake is influenced by three interconnected systems: the construction, the foundation, and the soil surrounding the foundation. SSI is the process through which the soil's response affects the structure's motion, and the motion of the structure affects the soil's response [16, 18]. Design codes do not provide sufficient guidance on incorporating SSI effects on structures. A well-defined computational technique is necessary to encourage practical engineers to include SSI in the design process [19]. For ensuring the safety and earthquake resilience of non-regular RC buildings, it is important to conduct a thorough seismic risk evaluation considering both site selection and geometric irregularity. Proper consideration of these issues during design and strengthening stages will result in safer structures and more effective mitigation measures [20]. According to some studies, the flexible base condition affects the building's response differently than the fixed base condition, reducing the structure's stiffness and altering the response spectrum [21].

The structure's response is dependent on various factors, including the stiffness of the soil, the structure's dynamic characteristics, damping factor, natural period, mass, and stiffness [22-25]. In the United States, the amount of scientific investigation considering SSI increased towards the end of the 2000s, with some studies summarized in the FEMA-440 report [6], which considered nonlinear analysis. The findings of this research were incorporated into US code requirements [26]. However, the provisions in FEMA-440 and ASCE 2013 standards are not recommended for NLT assessments, highlighting the need for new studies. In 2012, additional research on SSI in performance-based seismic engineering was compiled, suggesting an approach that could be applied to NLT analysis [27, 18]. Research investigated the impact of soil-structure interaction and found a significant decrease in R due to SSI for 3, 6, and 9-story buildings, with a 16% reduction in loose soils (R fixed support vs. R isolated footing type D). ECP-201 (2012) suggests a value of 3.9 for the response reduction factor R for limited ductility reinforced concrete moment frame buildings in multi-story multi-bay frames. Building on soft soil increases displacement, while increasing soil rigidity decreases lateral displacement [28]. The natural period becomes longer when considering the soil's flexibility, and the characteristics of the footings affect the building's performance [22, 7]. Many researchers have studied the influence of irregularities on RC structures' seismic performance, finding that regular buildings have larger roof displacement values than irregular buildings, while non-regular buildings were the first to achieve life safety and collapse prevention [23].

The influence of plan irregularity, specifically L-shaped structures, was illustrated by determining the actual overturning moment response from seismic analysis of L-shaped models. Improper layout of building elements could compromise the building's stability [29]. The increased total mass and rigidity of the building caused more displacement in the structure. Top displacement is greater in irregular building models than in standard frames. Additionally, the model of vertical irregularities included in the bottom story displayed the maximum value of the story drift ratio [24]. Allena & Chowdary [25] investigated how irregularities affected the seismic performance of high-rise buildings. They found that when the center of gravity and center of mass were aligned, mass irregularity did not significantly affect the reduction in frequency. The model with lumped mass at lower stories was substantially stiffer and showed more resistance [30]. It is evident that base shear and lateral displacement increase as seismic energy rises, indicating greater seismic demand for the structure. Nonlinear static pushover analysis (POA) has gained significant attention among researchers in recent years, providing a review of various pushover analysis approaches for vertical and horizontal irregularities of structures [31]. The factor R is affected by the hysteresis loop's shape, ductility, natural period, structural system, and construction materials. Only 8% of previous research attempts were dedicated to assessing the seismic response of irregular buildings [5].

This study focused on three main branches: evaluating the modification factor for irregular RC structures, employing nonlinear seismic analysis using the pushover analysis (POA) method to assess the seismic performance of irregular buildings, and incorporating soil-structure interaction (SSI) to evaluate the influence of soil and foundation type on assessing R. Nonlinear POA was used to evaluate the modification factor R for three RC structures with structural plan and elevation irregularities. Changes in floor plan geometry were made for each structure, which had different areas and heights. The study also considered the influence of various soil types on various subgrade response moduli (ks), as well as various seismic regions with ground accelerations of 0.15g, 0.20g, and 0.25g. Finally, the two response spectra identified by ECP were considered and investigated.

2. Response Modification Factor

The concept behind the response factor is to integrate nonlinearity with the overstrength, redundancy, and ductility of a structure to accurately assess the seismic force. Figure 1 illustrates the relationship between a structure's base shear (total horizontal load) and its roof displacement, as described by [1-3] for nonlinear static analysis. The reduction factor is typically expressed as a function of various structural system factors, including strength, ductility, damping, and redundancy. This factor is referred to as the response modification factor (R-factor) in the Egyptian code (ECP 2020), the behavior factor in the Eurocode, and the response modification coefficient in ASCE/SEI 7-22 [26, 32-34]. Therefore, the response factor (R) is calculated as follows:

$$R = R_S \cdot R_\mu \cdot R_{\mathrm{z}} \cdot R_R \tag{1}$$

where, R_S is the over strength that is defined as the ratio of the base shear at yielding to the design lateral strength.

$$Rs = Vy/Vd \tag{2}$$

where R_R intended to quantify the improved reliability of seismic framing system that uses multiple lines of vertical seismic framing in each principal direction of the building. The higher of the redundancy factor R_R Cannot be larger than one. Therefore, R_R was taken equal to unity, R_{z} is the damping factor used to account for the influence of additional viscous damping in constructions that have additional energy dissipation devices. If such devices are not provided, the damping factor is normally set at 1.0, and R_μ of the displacement at yield to the allowable displacement or maximum considered displacement.
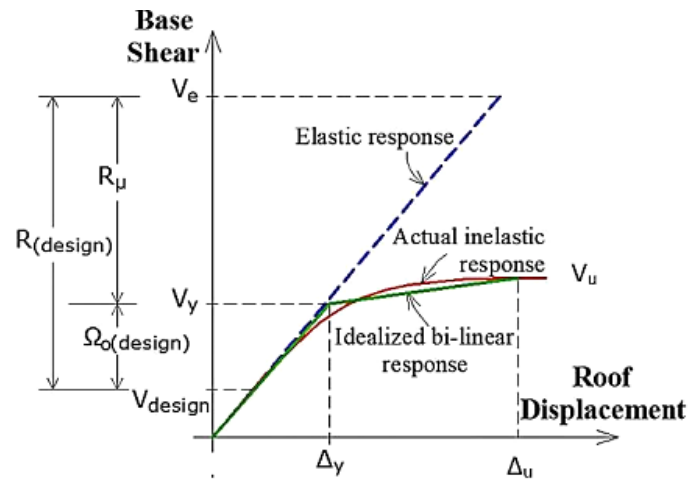
Figure 1. Relationship between applied base shear and roof horizontal deformation for regular buildings [3]

Factor that reduces ductility $R\mu$ based on the properties of earthquake ground motion additionally features of structure including ductility and basic period of vibration (T) [11, 35-42]. In this study, the formulation recommended by Priestley & Paulay (1992) [38] is used:

Rμ = 1.0	for zero-period structures	(3-a)
$R\mu = \sqrt{2\mu - 1}$	for short-period structure	(3-b)
Rμ = μ	for long-period structure	(3-c)
Rμ = 1+ (μ-1) T/0.70	(0.70 < T < 0.30)	(3-d)

where, $R\mu$ is the ductility reduction factor and μ is the displacement ductility.

Many codes and standards had addressed ranges for R, UBC97 has set values for (R) ranges between 3.5–8.5 while IBC (2012) [43] and ASCE7 uses near values ranges from 3.0–8.0 for ordinary to special moment resisting frames, respectively. ECP 2012 and IS 1893 have set values ranges from 5.0–7.0 and 3.0–5.0 for limited (ordinary) to Sufficient ductility frames, respectively. Moreover, Eurocode related the value of (R) to the ratio (Vu/Vy) based on the structure configuration.

3. Nonlinear Static Analysis (Pushover Analysis (POA))

Nonlinear Dynamic Time History (NDTH) analysis is widely recognized as the most accurate method for seismic evaluation in structural nonlinear analysis. However, due to its extensive computational requirements and the complexity of interpreting the responses for design purposes, it is considered impractical for routine use in structural design. Another significant challenge is the selection of suitable acceleration records for the numerical analysis, along with the need to account for torsional effects in the nonlinear static responses of irregular buildings.

The findings of nonlinear static analyses on irregular multi-story RC buildings were deemed appropriate [10]. Previous studies [44-47] have developed a 3D pushover approach for investigating non-regular building structures. So, it can be concluded that nonlinear static pushover analysis (POA) yields satisfactory results when applied to the analysis of irregular buildings. Consequently, nonlinear static POA has been utilized to compute the response factor for a building model.

Pushover Analysis (POA) is a method used for conducting non-linear static structural analysis. It determines the capacity curve by comparing base shear with displacement and evaluates the formation of plastic hinges at different stages beyond the elastic limit. In this analysis, the increasing load is represented by horizontal forces or displacements applied to a mathematical model of the building. The analysis concludes when it reaches a critical condition or target displacement. This target displacement or drift represents the maximum displacement or drift experienced by the building during the earthquake.
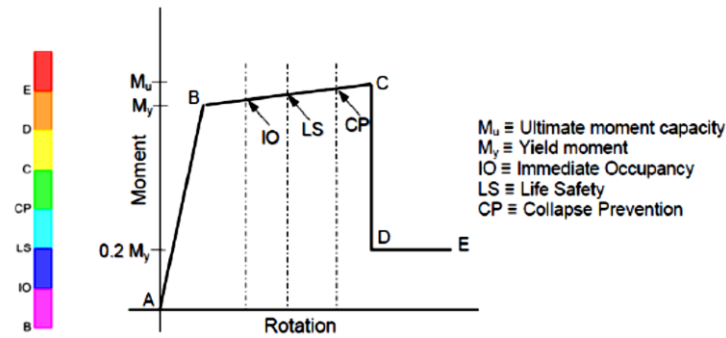
Figure 2. Moment - rotation graph for pushover analysis

4. Research Methodology

In this comparative analysis, we employed the equivalent static approach to seismic analysis for buildings with 6, 7, and 10 stories. Finite Element Models were created using the widely used software SAP2000 [46], with frame elements used to model beams and columns, and shell elements for simulating slabs. A parametric study was conducted, varying soil type, seismic zone, building irregularity, and using different spectra (I and II) as the main parameters. The design and comparison were guided by ECP-203. Figure 3 outlines the test procedures and estimates the number of trials needed for the study. Initially, the focus was on three models of structures with irregularities, labeled A, B, and C, with irregularity percentages of 28.6%, 30%, and 21%, respectively. Irregularity percentage was calculated as the total surface area of the cut floors of a building compared to the total surface area of all floors of the corresponding regular building. Corresponding regular models, named A', B', and C', were also created for control. These six models were constructed on different soil strata, categorized as per ECP-203 classification. This resulted in twelve models subjected to two types of response spectrum, each simulated at different seismic zones, totaling 144 models. Nonlinear pushover static analysis was utilized to determine the status of plastic hinges at yield and ultimate states. The structures were horizontally displaced until reaching predetermined failure conditions.
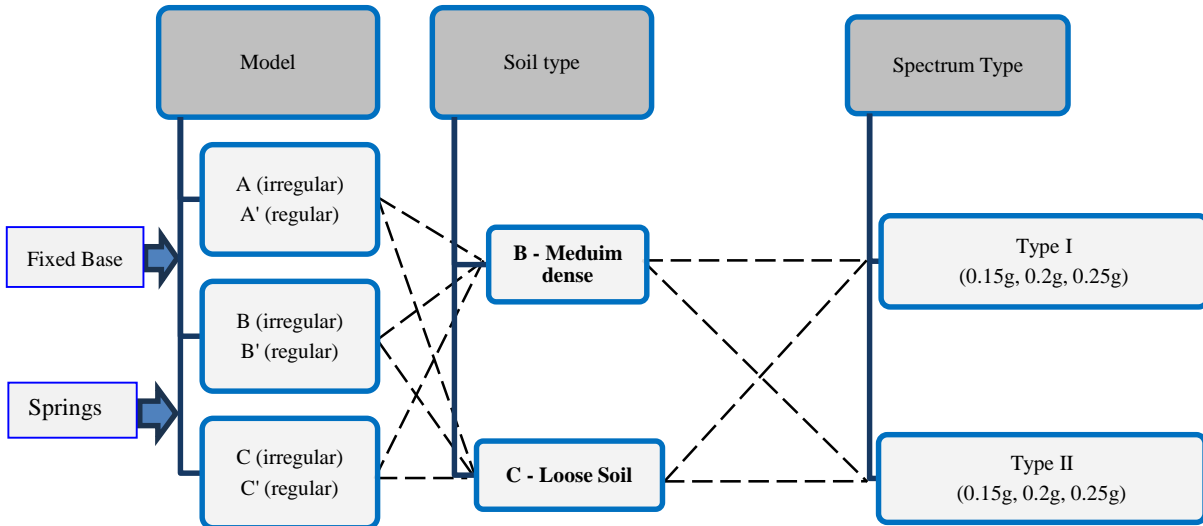
Figure 3. Sequence of numerical trails

5. Models Description

In this section, three different categories of structures were numerically simulated. The first category was denoted as Model (A) and Model (A'), representing relatively short buildings with 7 floors and a stepped reduction in floor area in one direction only. The second category was denoted as Model (B) and Model (B'), representing relatively taller buildings with 10 stories. The third category, named Model (C) and Model (C'), represented buildings with a random reduction in floor areas, each with 6 stories. Figure 4 illustrates different cross-sectional views for the three models, while Figure 5 shows 3D views of all structures. The irregularity percentage of each structure was determined by calculating the total surface area of the regular structure and subtracting the missing area until the irregularity percentage of buildings A, B, and C reached 28.6%, 30%, and 21%, respectively.
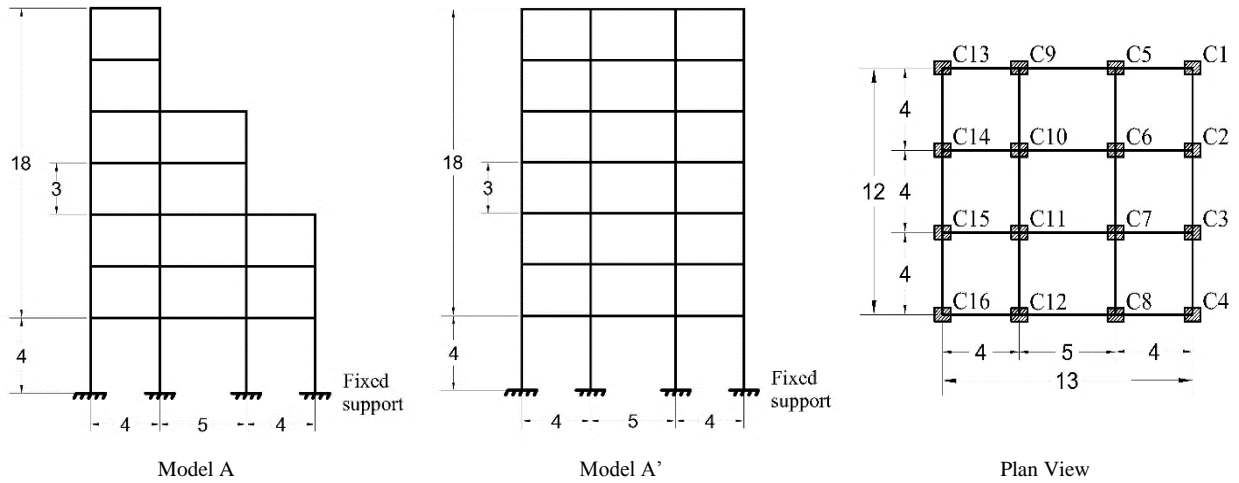
Model A   Model A'   Plan View

Typical Floor Elevation View -irregularity percentage (28.6%)

Model B   Model B'   Plan View
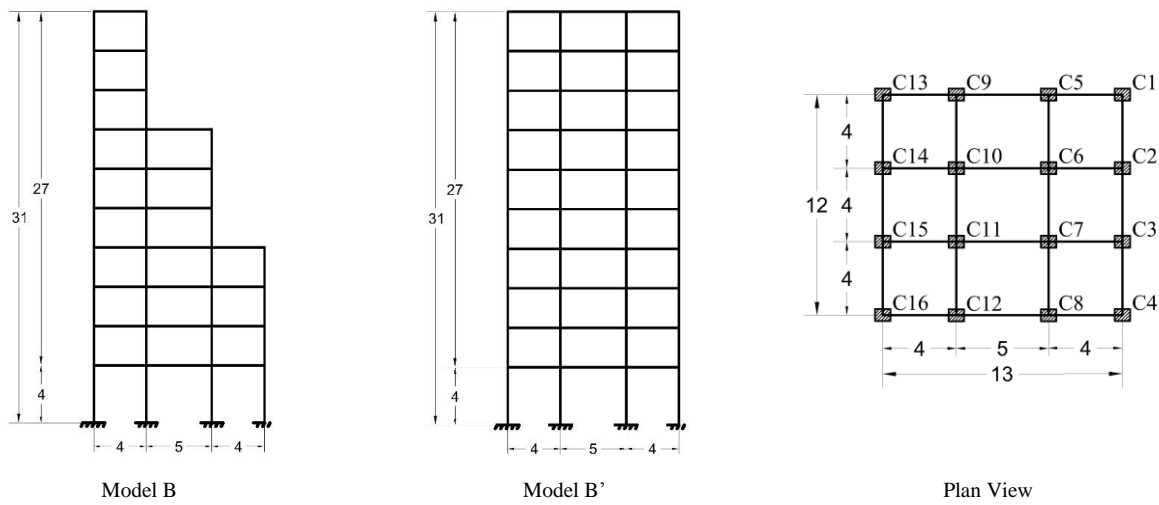
Typical Floor Elevation View- irregularity percentage (30%)

Model C   Model C'   Plan View
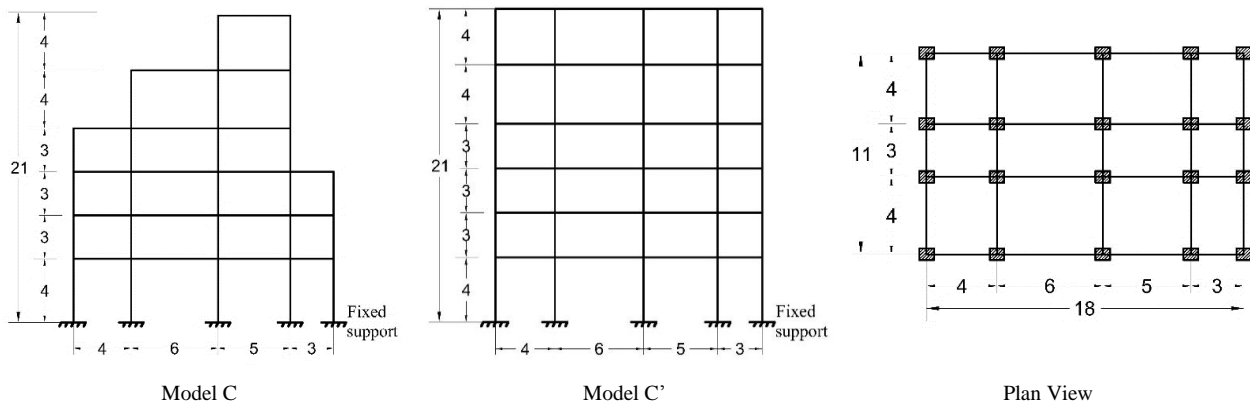
Typical Floor Elevation View - irregularity percentage (21%)

Figure 4. Description of Models

Nonlinear static analysis was conducted using SAP2000 [46]. Various parameters were taken into account during modeling, including material properties with different stress-strain relationships, expected locations and lengths of plastic hinges, and their types. The moment-curvature relationship is essential for nonlinear static analysis. Factors such as geometry, material properties, longitudinal reinforcement, shear reinforcement, and applied loads on a specific member all influence the values derived from an element's moment-curvature relationship.

A   A'   B   B'

C   C'
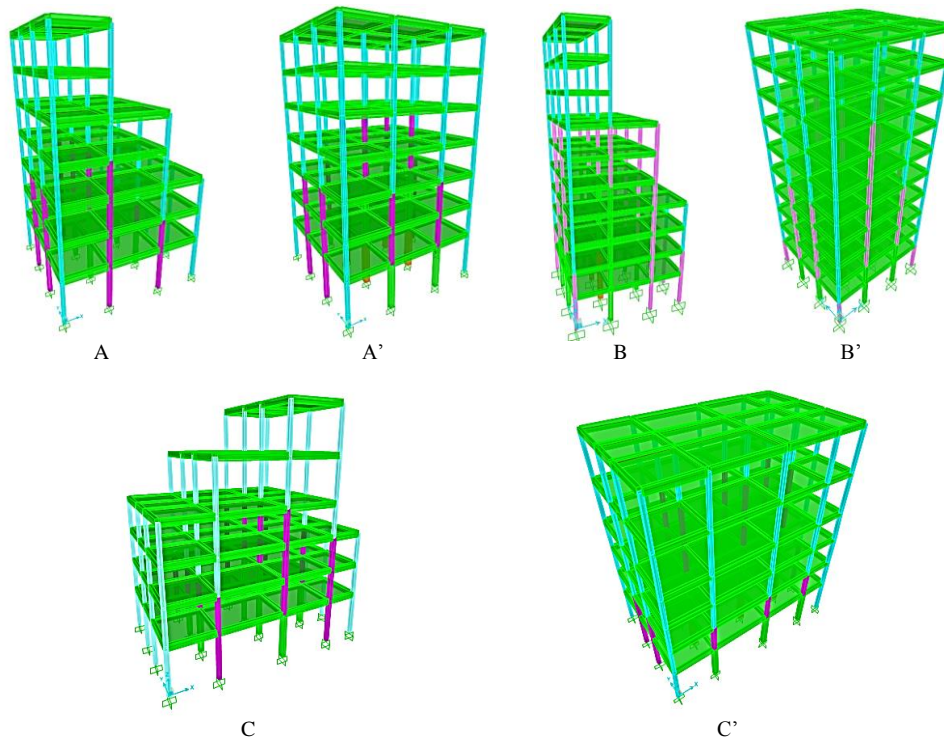
Figure 5. 3D simulation of all Multistory Buildings

Table 1. Material Properties used in simulation

Material Properties	Value
Concrete characteristic strength (F_C)	25000 kN/m^2
Rebar yield strength (F_Y)	36709780 kN/m^2
Modulus of elasticity of rebar (E_S)	360000 kN/m^2
Modulus of elasticity of concrete (E_C)	22433756 kN/m^2
Shear modulus – CONCRETE (G)	93473980 kN/m^2
Poisson's ratio for concrete (Yc)	0.2
Poisson's ratio for steel (Ys)	0.3

(a) Stress-strain curve for concrete   (b) Stress-strain curve for steel bare
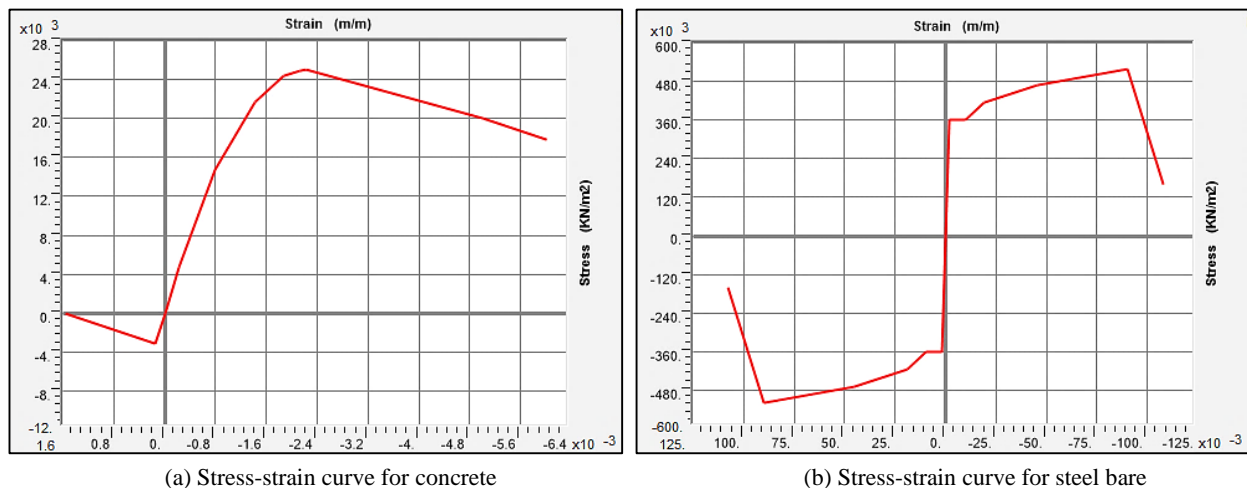
Figure 6. Stress-strain curves for used materials

RC frame structures with 6, 7, and 10 stories were designed according to ECP-203 (2020) to withstand both gravity and seismic loads (spectrum types I and II) at various seismic zones (0.15g, 0.2g, and 0.25g) as shown in Figure 7. The soil was classified as Type B and Type C according to ECP-203. For each soil type, the models were simulated using both fixed support, considering a rigid foundation, and an isolated footing system based on design outcomes. Initially, the models were simulated assuming a limited ductility moment-resisting frame with R equal to 5. Throughout the design process, the following factors were considered:

- To ensure that the standards for damage limitation are met, the inter-story drift should not be greater than 0.005 of the story height.

- Stirrups were assumed to carry shearing forces in columns as well as to enhance their ductility.
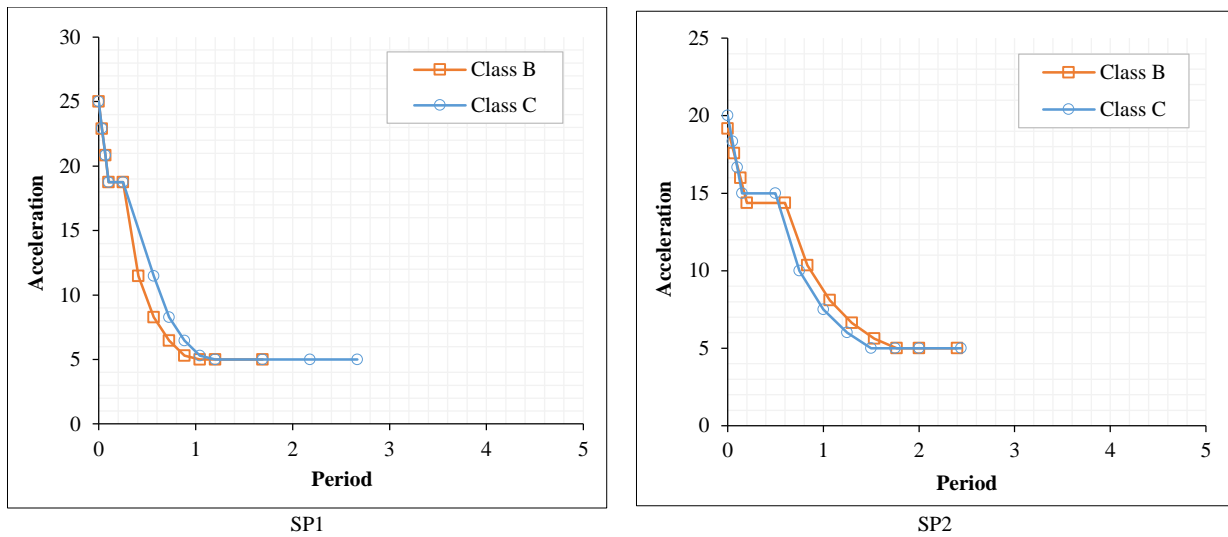
Figure 7. Applied Response Spectrum at seismic zone (0.25g)

For all models, the beams were designed with the same cross-sectional area (250 mm × 500 mm). The top and bottom reinforcement were also kept constant at (8T16) for top and bottom reinforcement.

It was noticed that the capacity/demand ratios for most columns are at lower levels in all the analyzed buildings, and within the range of 0.75 to 0.90, the reinforcement ratio of sections is shown in Table 2.

Table 2. Column sections with corresponding reinforcement ratio

Reinforcement Ratio	Column Section			
	25×25	**30×30**	**40×40**	**50×50**
μ %	1.44: 2.5	1: 1.79	1.5	1.287

6. Modelling Soil-Structure Interaction

A theory regarding the vibration of the foundation soil suggests that because buildings are more flexible than corresponding fixed-base structures, inertial interaction effects cause the natural period of the soil-structure system to lengthen. Additionally, it states that an increase in damping of the soil-structure system is caused by energy dissipation, and radiated waves from the building back into the ground. This theory distinguishes the case of flexible foundation motion used in an FB model and proposes a direct approach for SSI studies that resolves the dynamic equilibrium equation of the soil-structure assembly [46, 47].

In section 6.3 of FEMA 356, two approaches for modeling SSI are described [6]. The first approach utilizes flexible soil and a stiff foundation, with the foundation's modeling based on six formulas for each of the six degrees of freedom. The second approach involves linear flexible soil and flexible foundations, where the soil support is represented by distributed springs with homogeneous spring values dispersed throughout the footing's length. This approach is most suitable when the foundation's structural elements are flexible (refer to Figures 8 and 9).

Figure 8. Foundation modeling approaches with vertical springs presented in FEMA (2020)

Figure 9. Typical foundation modeling with vertical soil springs is based on ASCE/SEI 41-17 in SAP2000

6.1. Flexible-base Analysis

For SSI calculations, understanding the behavior of a building with a flexible base is crucial. This can be approached in two ways. Firstly, to compute radiation damping reductions, which depend on the ratio of fixe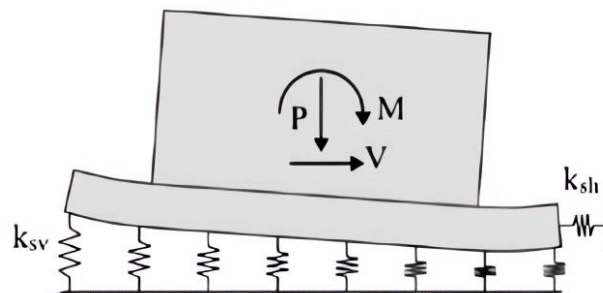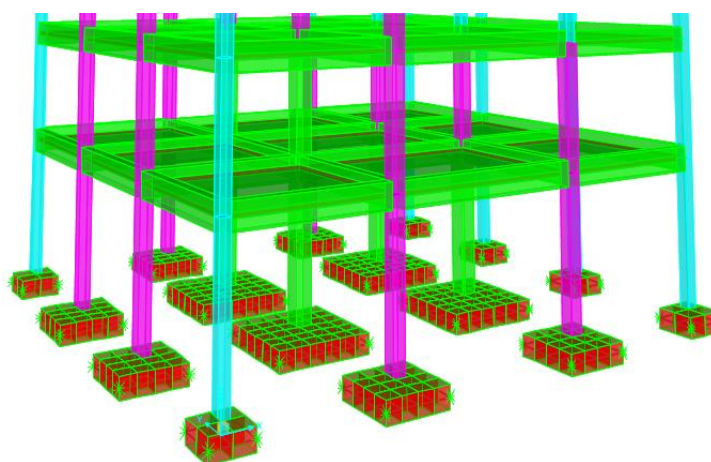d-base to flexible-base periods, it is necessary to consider the change in dynamic behavior between the fixed-base and flexible-base conditions. Secondly, to properly account for soil-structure interaction, ASCE/SEI 7-16 Section 19.1 recommends considering all aspects of foundation flexibility, including soil flexibility and the foundation's rotational, vertical, and horizontal orientations.

For analysis, ASCE/SEI 7-16 Section 12.13.3 specifies a 50% increase and decrease in soil spring values. This involves multiplying the best estimations by 1.5 and 0.5 to determine the maximum and minimum spring values.

Equation 4 for vertical soil springs is based on ASCE/SEI 41-17 Section 8.4.2.5, Technique 3, which uses a uniform spring along the footing's length (refer to Figure 9). This method leverages the relative flexibility of the concrete foundation element to the soil. Since the continuous footings extend as cantilevers beyond the frame columns, creating flexibility in the foundation structure, and because the model explicitly considers the footings' flexibility, this method appears to be suitable.

$$K_{SV} = \frac{1.3G}{B_F(1-V)} \tag{4}$$

The spring values are depending on the shear modulus of the soil, G, and Poisson's ratio, ν, B is width of footing, and the modules of subgrade reaction, (K_S) is the value in this study according to soil type shown in Table 3.

Table 3. The modules of subgrade reaction, (K_S) value

Vertical soil springs is based on ASCE/SEI 41-17 Area Spring at the bottom of footing (Stiffness/length^2)	Soil Type
K_S= 9806.6502 kN/m^2	Soil type B
K_S= 19613.3 kN/m^2	Soil type C

7. Results and Discussion

The results of the simulation, including contributing mode shapes, the effects of different soils, and seismic zones, are introduced in the next sections. The effect of different irregularities was discussed. The obtained R was compared with the corresponding value of regular buildings.

7.1. Mode Shapes

A structure's modes are its intrinsic characteristics, independent of applied loads or forces. Changes in the structure's boundary conditions (mountings) or material properties (mass, stiffness, damping) will also change the modes. Mode shapes, on the other hand, are unique. They represent the unique motion of a point to another at resonance. Therefore, the structure's irregularity percentage significantly influences the mode shape, as higher irregularity percentages result in higher torsional moments on the structure. The fundamental natural periods for all regular and non-regular buildings were determined. Figure 10 displays the first four periods for irregular structures. During analysis, these modes exhibit a modal participation factor over 95%. It was observed that the first two modes corresponded to global structural bending motions, while torsional modes appeared in the third mode. Significant bending modes for the higher floors in irregular buildings were observed in the fourth mode. The natural period is provided under each mode. Generally, a greater number of modes are required for accurate assessment of the dynamic response of irregular structures [24, 25]. Thus, it is important to consider torsion effects in the nonlinear static responses of irregular buildings.

A, T_1=1.12 Sec	B, T_1=1.43 Sec	C, T_1=1.14 Sec	A, T_2=1.12 Sec	B, T_2=1.40 Sec	C, T_2=1.14 Sec

a- First mode   **b- Second mode**

A, T=0.84	B, T=1.04	C, T=0.93	A, T=0.48	B, T=0.66	C, T=0.58

c- Third Mode   **d- Fourth mode**
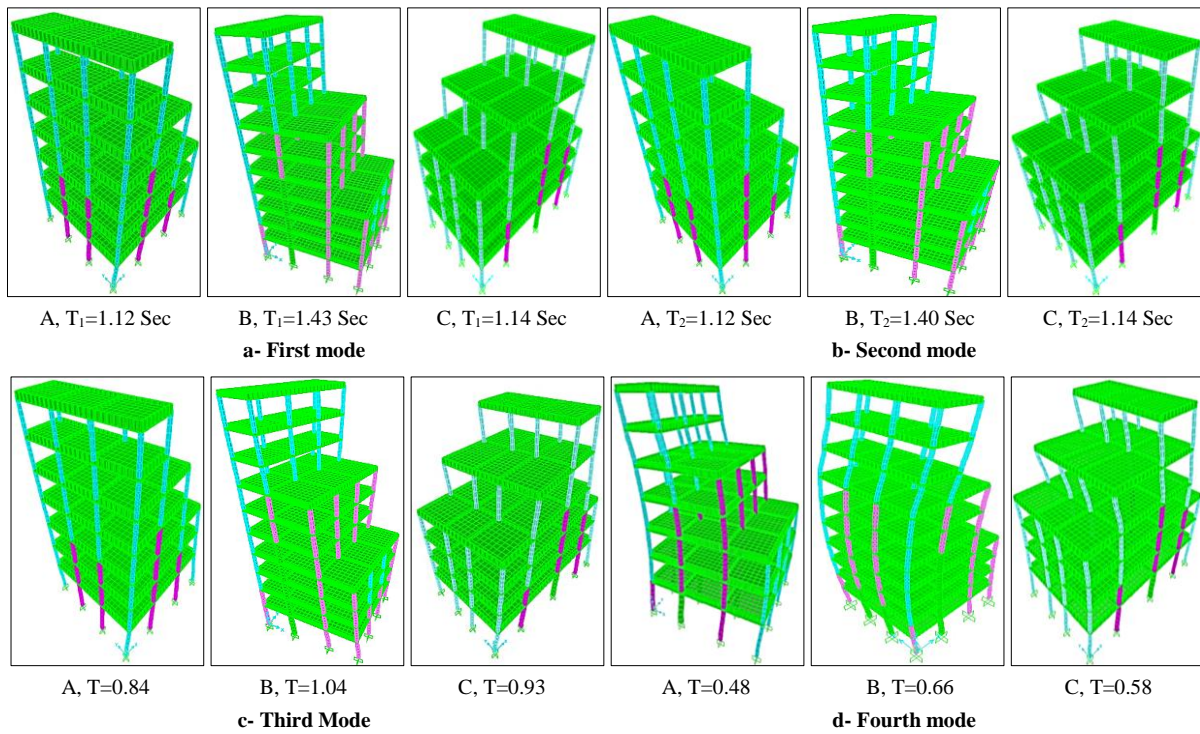
Figure 10. 3D view of vibration mode shapes of studied building models. a 1st vibration mode shape, b) 2nd vibration mode shape, c) 3rd vibration mode shape, and d) 4th vibration mode shape

The fundamental natural periods for all regular and non-regular buildings were obtained. Figure 10 shows the first four periods for irregular periods. During analysis, these modes have a modal participation factor of over 95%. It was also noted that the first two modes represented global structural bending motions. Torsional modes appeared on the third mode. Whereas significant bending modes for the higher floors in irregular buildings appeared in the fourth mode. The natural period is written under each mode. Generally, for an accurate assessment of the dynamic response of the structure, a greater number of modes are required for irregular structures [38]. So, we need to take into account the torsion effects in irregular buildings' nonlinear static responses.

7.2. Pushover Curves

The pushover curves listed in Figures 11 to 16, which draw the relationship between the top displacement and the ultimate base shear.
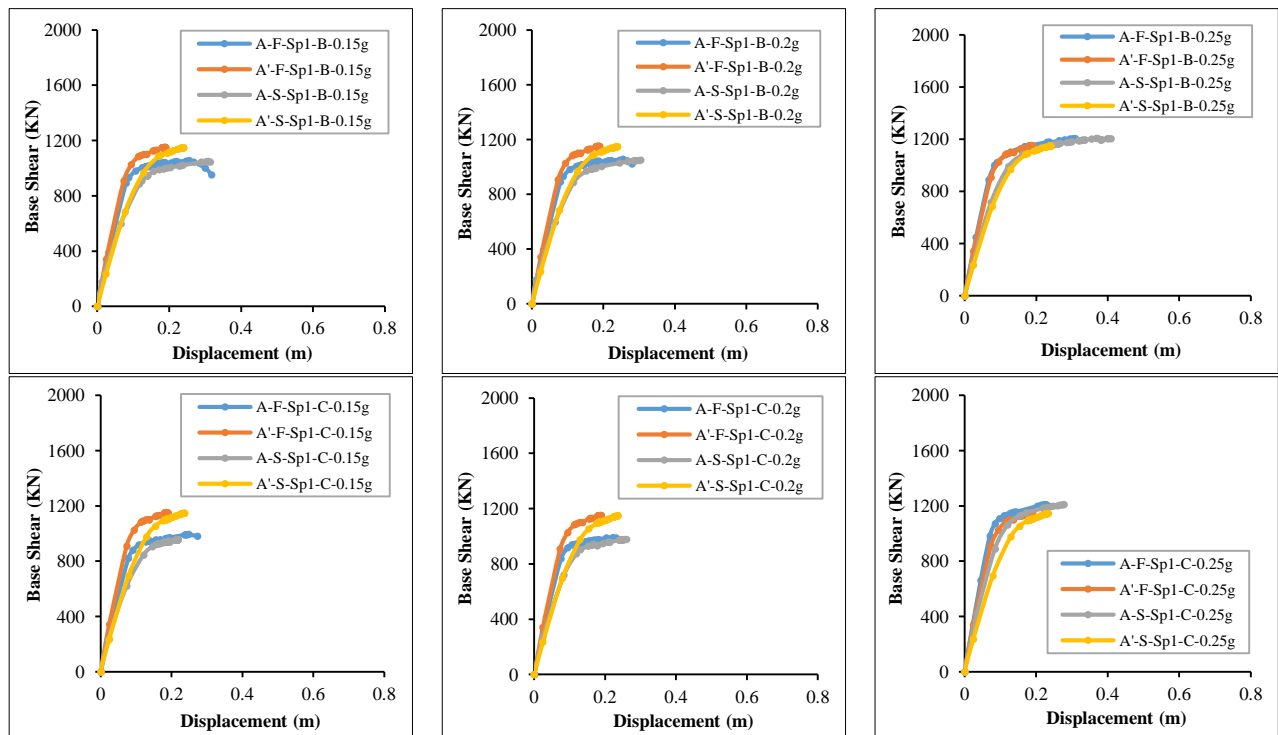
Figure 11. Pushover curves (P.O.C.) for the spectrum type I for models A, A'
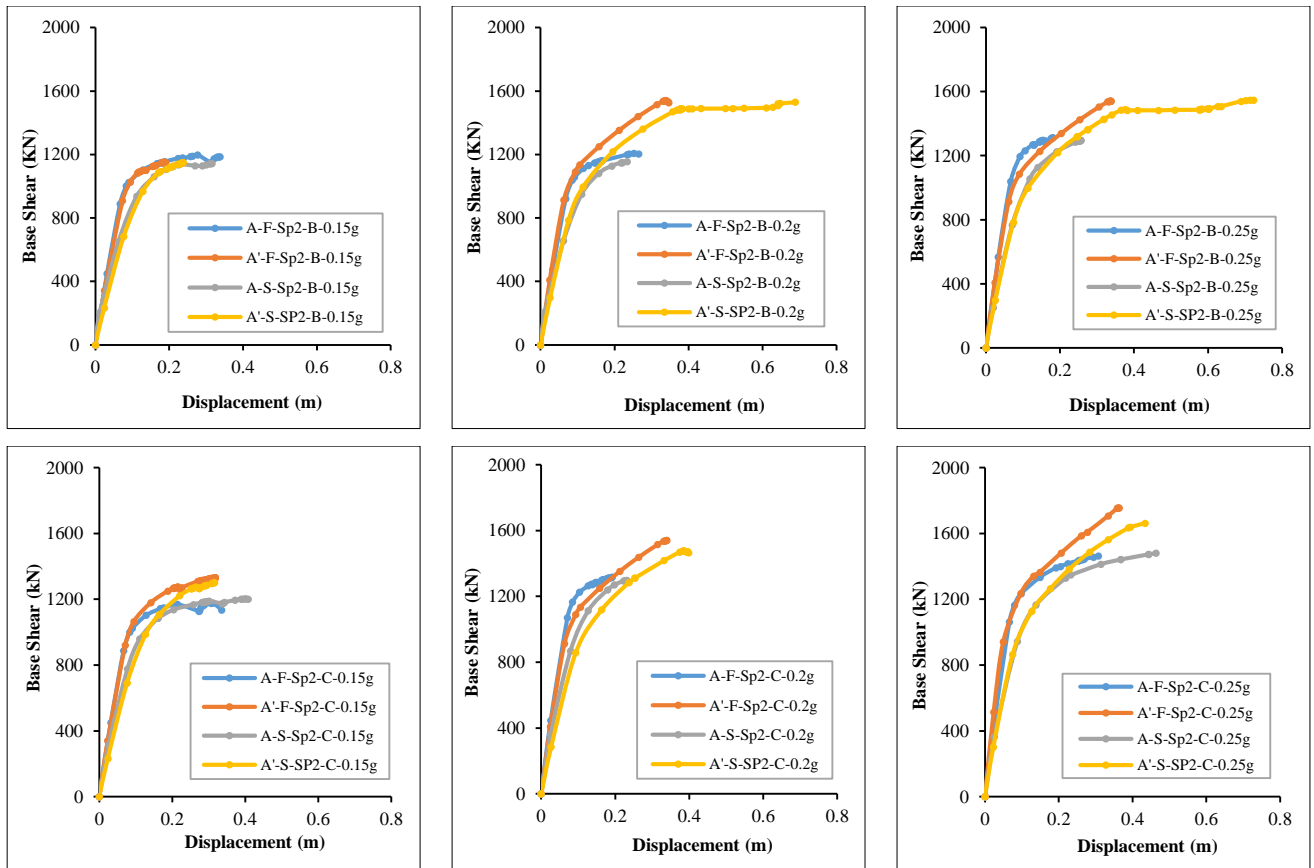
Figure 12. Pushover curves (P.O.C.) for the spectrum type II for models A, A'
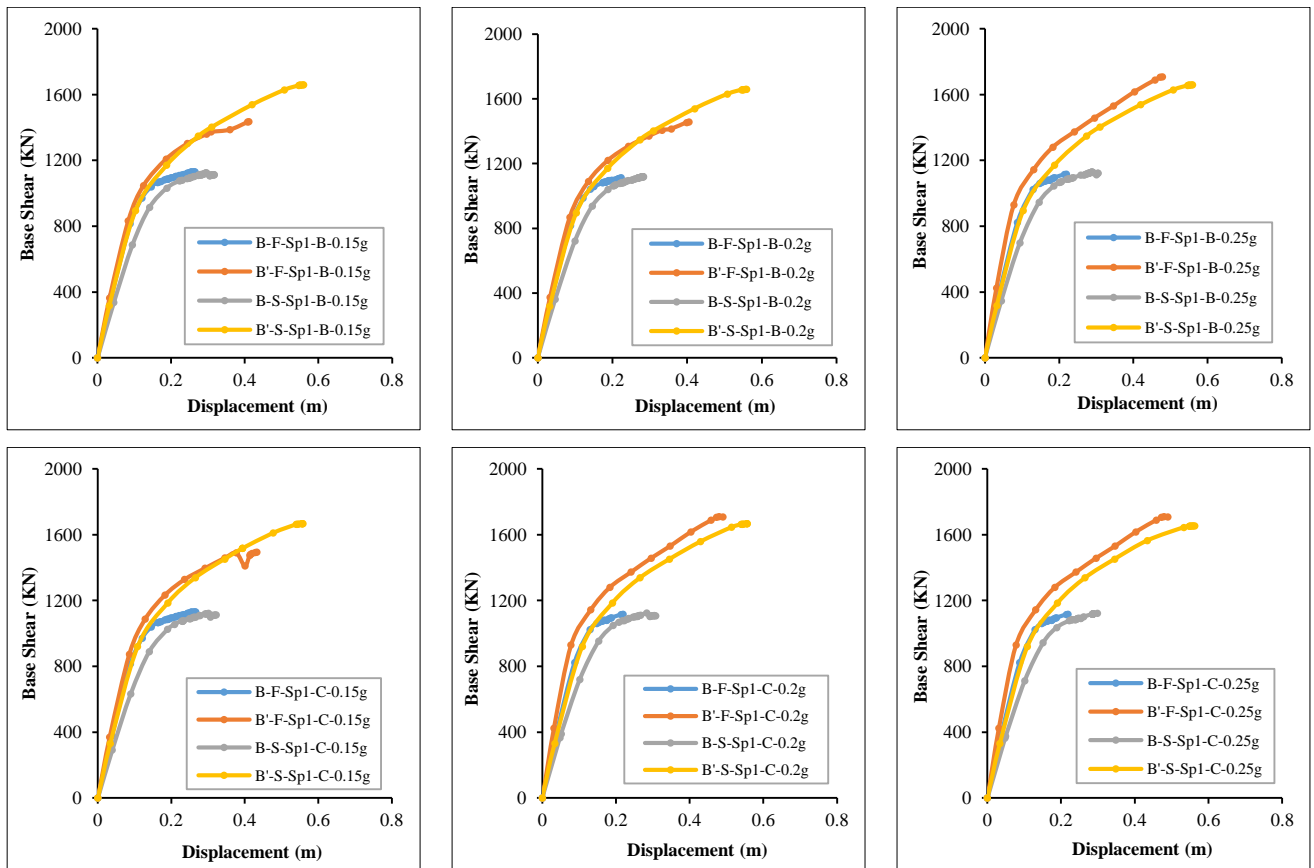
Figure 13. Pushover curves (P.O.C.) for the spectrum type I for models B, B'
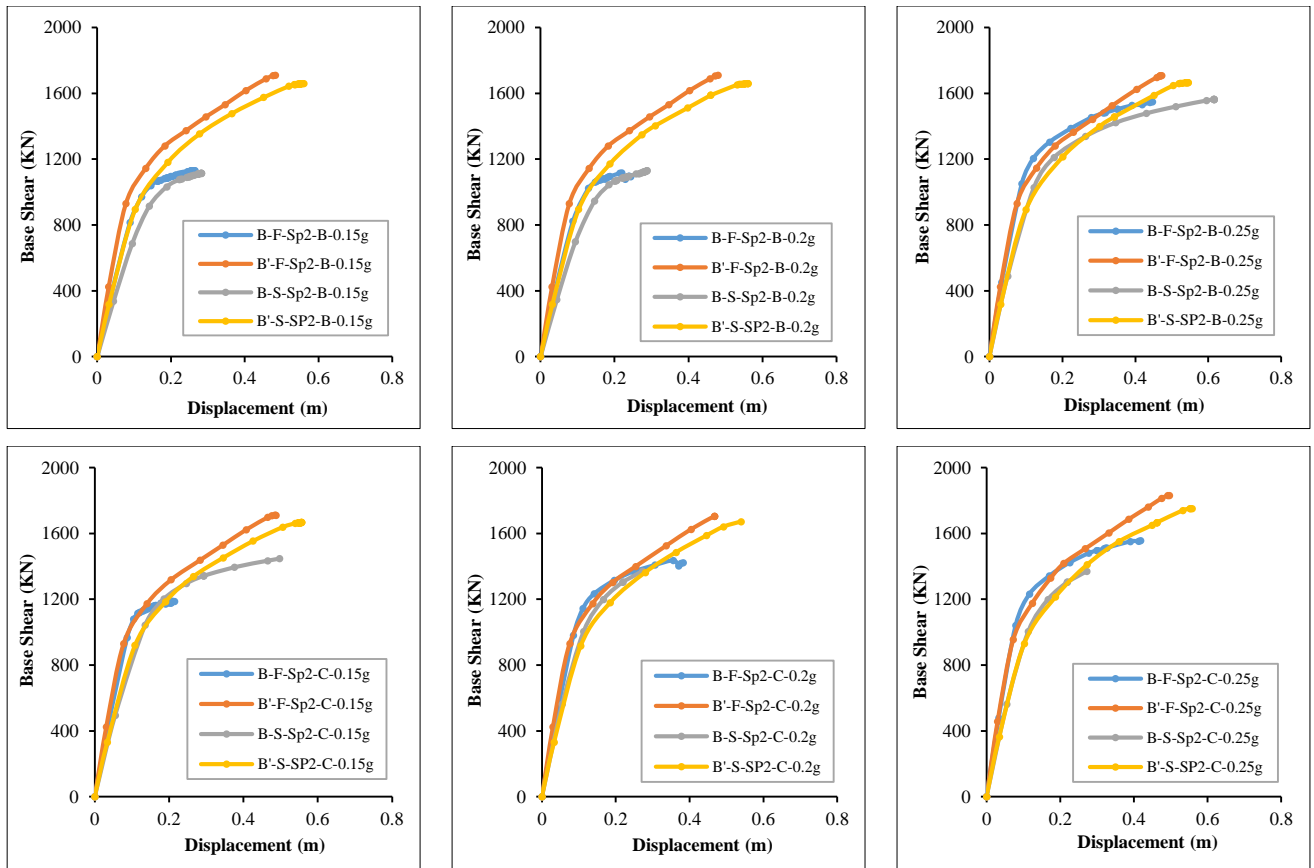
Figure 14. Pushover curves (P.O.C.) for the spectrum type II for models B, B'
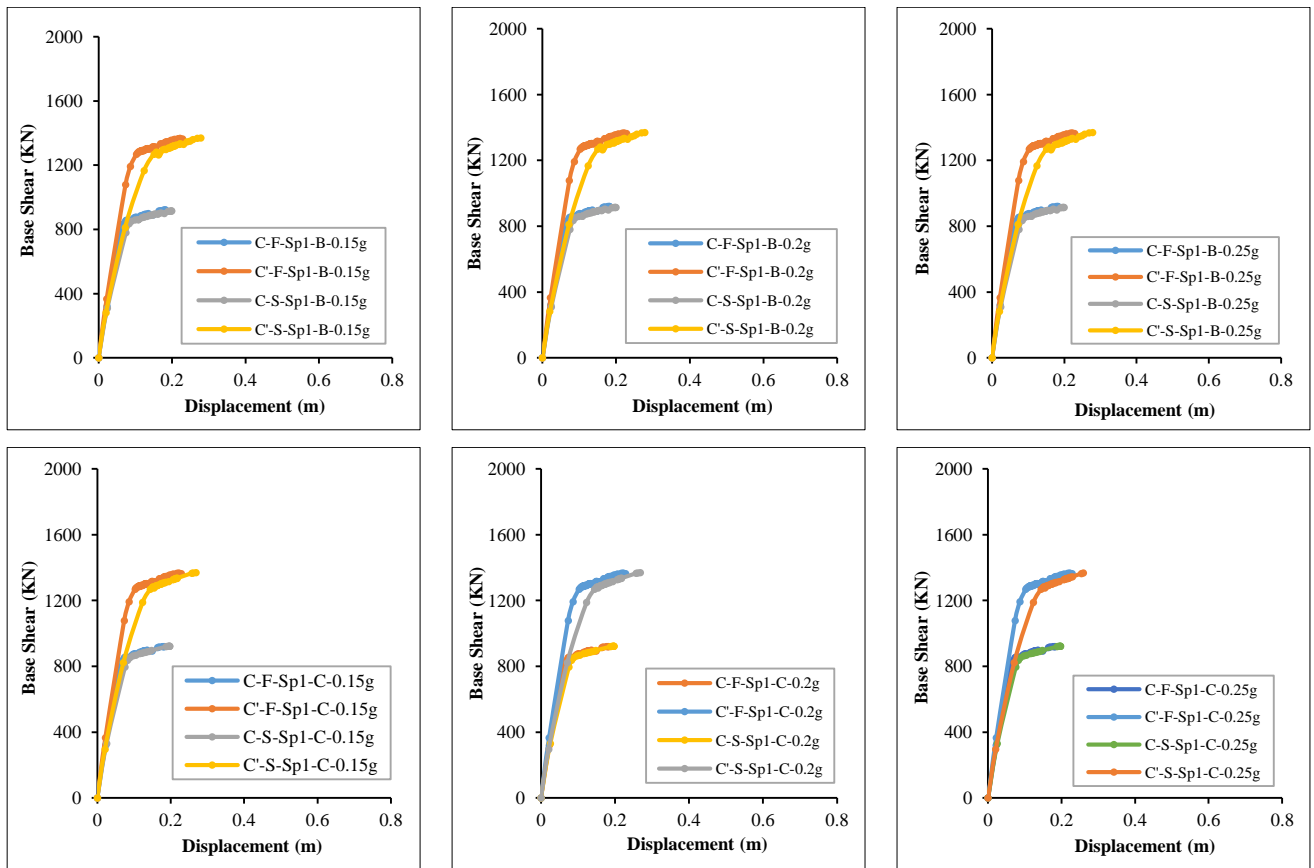
Figure 15. Pushover curves (P.O.C.) for the spectrum type I for models C, C'
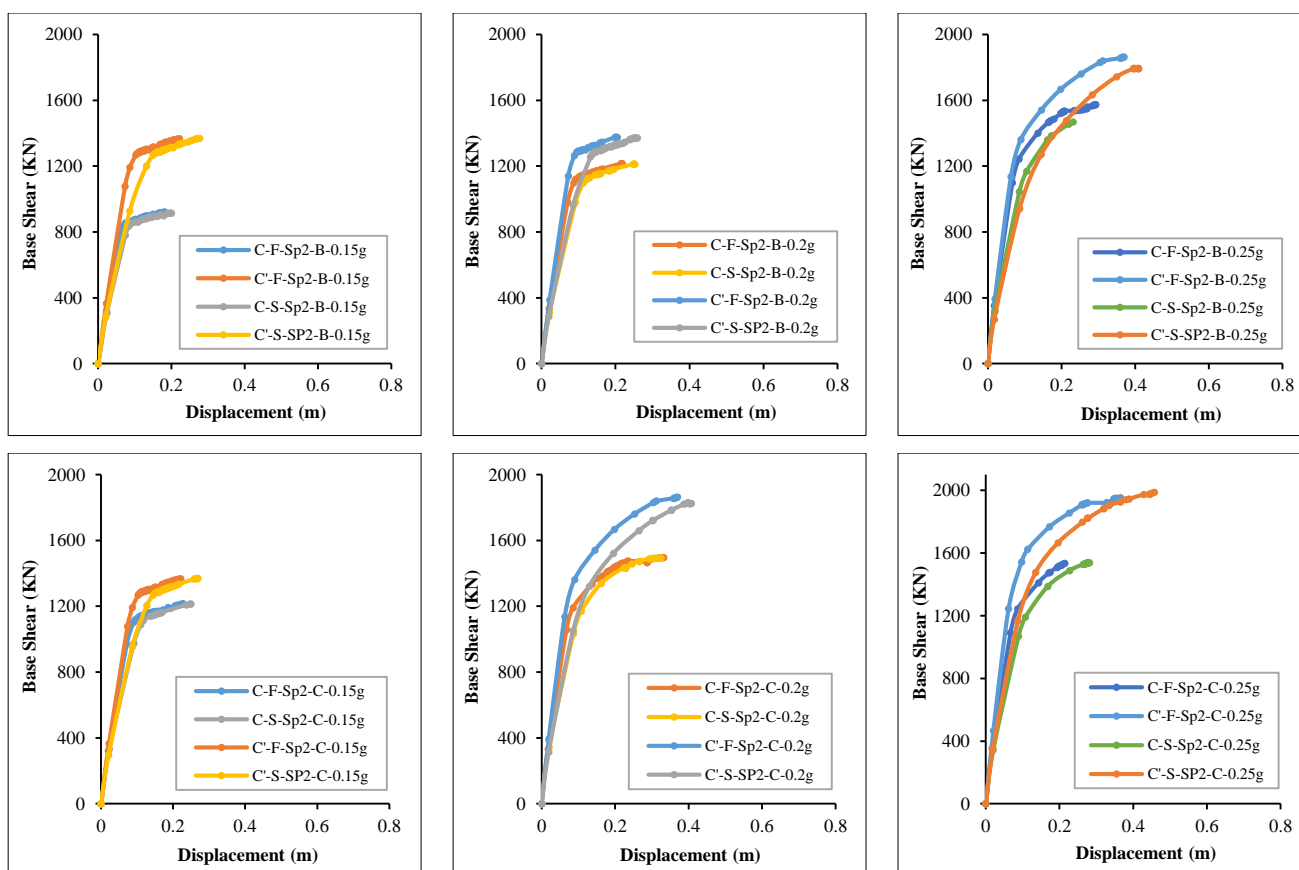
Figure 16. Pushover curves (P.O.C.) for the spectrum type II for models C, C'

Structural behavior during a weak earthquake tends to be similar across different structures, despite varying geometries and characteristics. However, at higher seismic intensities, the mass, stiffness, and geometry of a building significantly affect the shape of the pushover curve (POC). Buildings with more floors and higher irregularity percentages exhibit greater areas under the curve, resulting in higher displacement ratios, particularly when considering the effects of soil-structure interaction (SSI). This phenomenon allows all structural elements to reach their maximum deformation capacity, leading to higher displacement values.

7.3. Effect of SSI

In this section, the effect of different soil types on the structures was investigated. The obtained charts are labeled with a specific code format. For example, "A-F-Sp1-B-0.15g" represents building (A) with fixed support (F), subjected to response spectrum type I (Sp1), founded on soil type (B), in seismic zone with intensity (0.15g). In the case of isolated footing, "S" was used instead of "F". Each pair of successive rows in the upcoming graphs represents one building. Each row contains a family of curves where the seismic intensity was increased from 0.15g to 0.25g (see Table 4). The first row corresponds to spectrum type I, while the second row corresponds to spectrum type II.

The base shear value and the natural time period (NTP) were both impacted by soil-structure interaction, as illustrated in Figures 17 and 18. For the A, B, and C models, the base shear decreased by 1%, 10.5%, and 1%, respectively, when SSI was considered, especially in soft soil (type C) for SP1. Additionally, for SP2, the base shear decreased by 17%, 12%, and 1% for the A, B, and C models, respectively. Furthermore, the NTP increased by 14%, 12%, and 13% in the A, B, and C models, respectively, as seen in Figure 18. Due to the SSI effect, the structure's natural period becomes longer, with a more pronounced effect in soft soil. The natural time period is a key factor controlling the building's lateral seismic response. Therefore, evaluating this value without considering seismic design could lead to significant errors. It has been observed that the NTP increases with soil flexibility. The structure's characteristics cause the rate of increase in NTP to be higher when the soil is represented by springs, showing a higher time period than the fixed base model. This difference is less for low-rise buildings and increases with the building's height. Additionally, high-rise structures on weak soil are more affected by SSI than low-rise ones, as indicated by a parametric analysis varying the height and geometry of the building with and without SSI [45]. The influence of SSI was evident in the push-over curve, where irregular Model B (soil type C - zone 0.25g) had a maximum lateral displacement of 0.32 m, increasing by 31.5% compared to a fixed base, and 14% for regular Model B. Thus, the impact of soil representing SSI's effect on seismic design, especially for irregular structures, needs to be considered.

Table 4. Response modification factor value for fixed base (F) and isolated footing (S), for models

			A		A'		B		B'		C		C'	
Models			F	S	F	S	F	S	F	S	F	S	F	S
							Spectrum (I)							
		0.15g	6.72	7.10	7.35	7.65	5.893	6.55	6.41	6.87	7.123	7.34	7.52	7.96
	B	0.2g	6.52	7.07	6.87	7.25	5.297	6.08	5.82	6.43	6.857	7.28	7.37	7.90
		0.25g	5.42	6.14	5.87	6.32	4.060	5.18	5.00	5.92	6.126	6.60	6.65	7.32
		0.15g	5.40	6.00	5.72	6.25	4.590	5.41	4.89	5.53	5.827	6.18	6.12	6.51
	C	0.2g	4.67	5.35	4.94	5.57	3.489	4.76	4.11	5.31	5.126	5.79	5.55	6.10
		0.25g	3.79	4.56	4.18	5.13	2.523	3.48	3.29	4.20	4.495	5.30	5.14	5.83
							Spectrum (II)							
Soil Type		0.15g	5.24	5.69	5.44	5.78	4.800	5.24	4.98	5.56	5.723	6.07	5.78	6.30
	B	0.2g	4.81	5.27	5.11	5.69	4.401	4.80	4.72	5.35	5.312	5.88	5.58	6.31
		0.25g	4.64	5.12	5.05	5.70	4.139	4.37	4.45	5.12	4.895	5.49	5.27	6.03
		0.15g	4.26	4.51	4.67	5.17	3.997	4.20	4.35	4.82	4.533	5.13	4.91	5.35
	C	0.2g	3.75	4.19	4.16	5.06	3.193	3.70	3.64	4.27	4.170	4.73	4.66	5.45
		0.25g	3.26	4.01	3.72	4.79	2.597	3.39	3.46	4.70	3.816	4.47	4.39	5.28
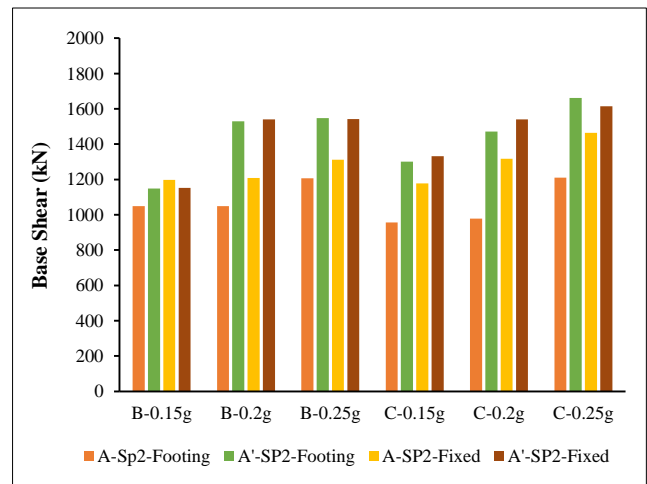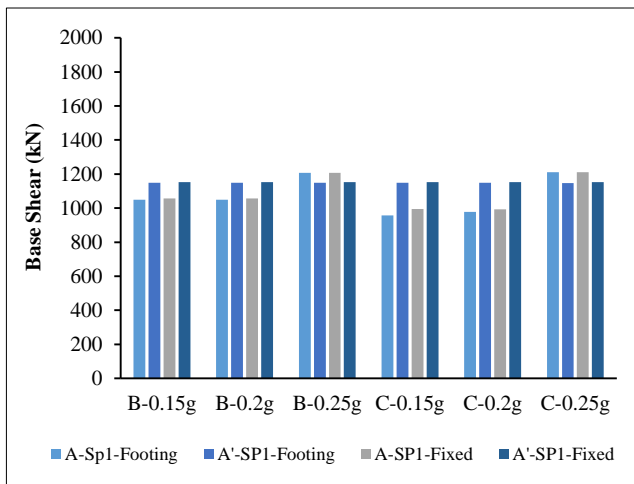
Model A,A'
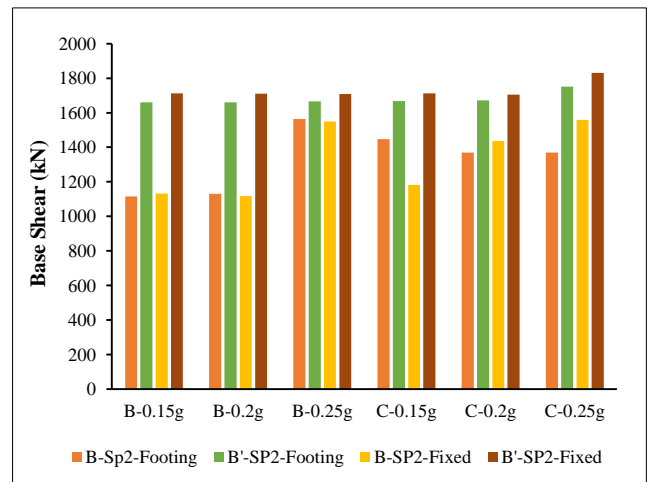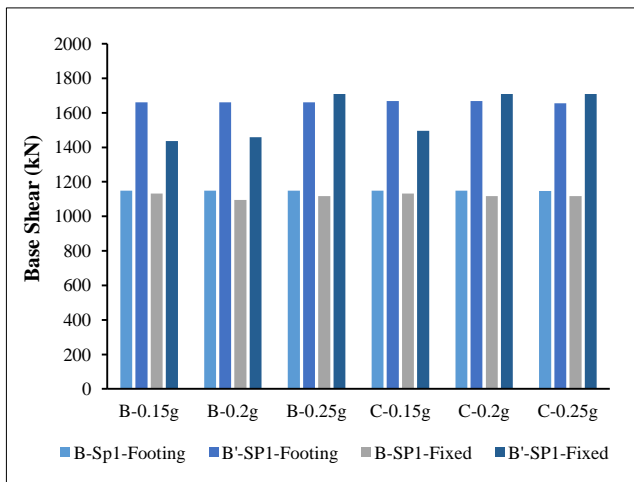
Model B,B'
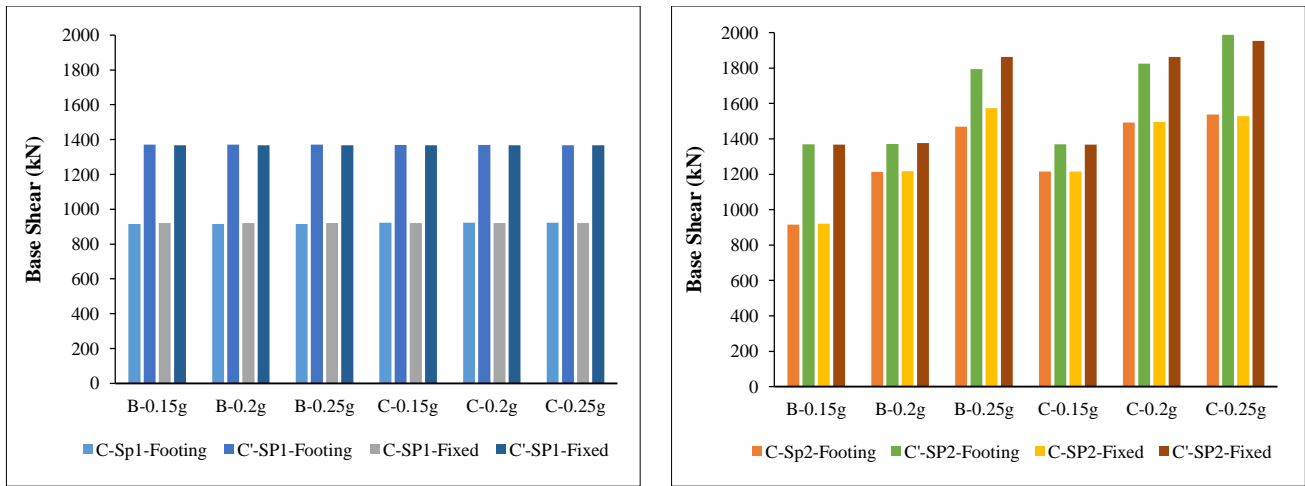
Model C,C'

Figure 17. Base shear values for models
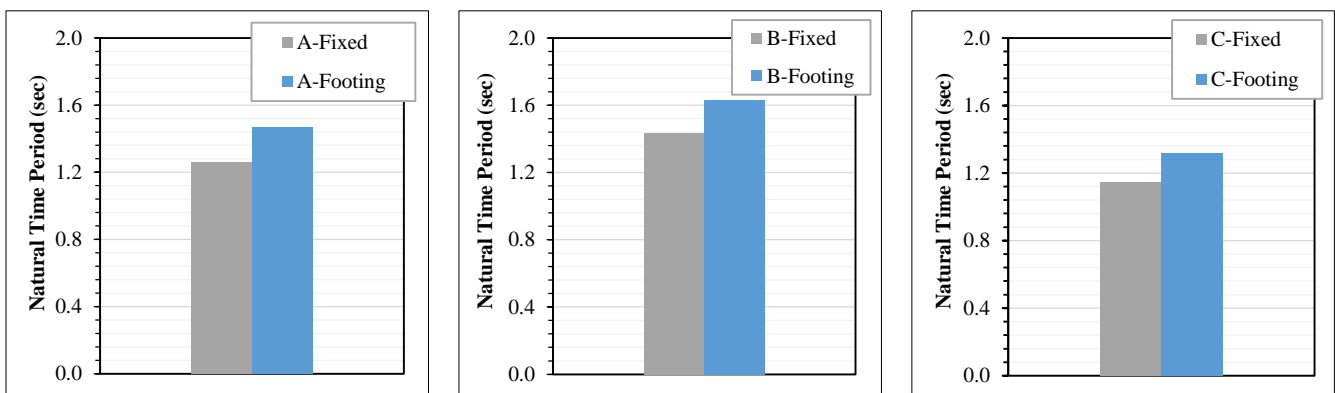
Figure 18. Natural Time Period (Sec) for models

There is an observed improvement in the natural period, roof displacement, base shear, and structure's deformation, along with an improvement in the flexibility of the soil; essentially, the conclusion will affect the response factor.

7.4. Effect of Irregularity

It was clear how the structure's irregularity on the pushover curve affected the structure's strength and how it behaved during the earthquake. The deducted area from the structure, or the degree of irregularity of the structure.

The impact of irregularity appears more pronounced in flexible structures, such as model B, highlighting that the effect is more noticeable in more flexible models. Regular and non-regular structures exhibit similar behavior in response to a weak earthquake. Figures 9 to 14 show that structures (models A, B, and C) demonstrate low ductility. However, models (A', B', and C') exhibit good ductility, with irregularity causing a decrease in maximum displacement of 0%, 54%, and 18% respectively for Sp I compared to regular models. This decreased by 22.5%, 16%, and 23% respectively for Sp II (for fixed base).

With fixed base: In both regular and irregular buildings, as the seismic zone's intensity increases, the value of R decreases, approaching the values specified in the ECP (2012) code for soil type B. For soil type C, the values were 9.3%, 23.4%, and 12.61% for models A, B, and C respectively for SP1. For SP II, the values were 12.4%, 25%, and 13.12% for models A, B, and C respectively. When representing soil with springs: Similar to the fixed base scenario, in both regular and irregular buildings, as the seismic zone's intensity increases, the value of R decreases, approaching the values specified in the ECP (2012) code for soil type B. For soil type C, the values were 11.13%, 16.5%, and 9.1% for models A, B, and C respectively for SP1. For SP II, the values were 16.2%, 28%, and 15% for models A, B, and C respectively. In tall buildings with many floors, the percentage decrease in the structure's response was higher as the seismic zone increased, particularly in weak soil (type C).

The seismic load significantly affected the structure's response, especially due to the varying percentage irregularity in the study's models. Design requirements and code standards need to consider the irregularity percentage to ensure more stable and secure seismic load designs. For instance, a 30% irregularity rate caused the reduction factor to decrease

to 23.4% for soil type C and 18% for type B (for SP1). Similarly, it decreased to 25% for soil type C and 7% for type B (for SP II).

Model C has a 21% irregularity percentage. For SP1, the reduction percentage varied from 7% to 6% in weak soil (type C) and from 5% to 4.5% in soil type B in the same seismic zone. The reduction percentage varied between 4.5% and 3.8% in soil type B. Conversely, the decrease for models B, A, and C was around 17%, 11%, and 9%, respectively, when the soil was represented by springs.

Because structures have a large reserve strength and the ability to dissipate energy—properties known as overstrength and ductility, respectively—seismic design regulations take these into account and reduce design loads using a reduction factor. This study shows that structural irregularity impacts the value of R, especially in weak soil subjected to strong seismic intensity. For instance, model B, with a 30% irregularity rate, shows a more pronounced effect. As the seismic zone becomes more intense, the decrease in the value of R is significantly less than the values listed in the ECP, approaching the values of the Euro Code. Therefore, it is necessary to review the ECP values and reduce them, especially for irregular buildings. Using the Egyptian Code values for irregular buildings, particularly after considering soil representation, is considered an unsafe design practice (see Figures 19, 20, and Table 5).

The value of R decreased as the seismic zone increased for all models. The shape or irregularity of the structure had a clear impact on the values of R with the same soil type and seismic zone, indicating that the value of R was close to the values of the Euro Code, especially in poor soil in SP2. It is indirectly impacted by the structure's shape and irregularity. The reduction in the modification factor is clearly influenced by the number of floors, and the percentage of irregularity also had an impact, with the maximum decrease in the modification factor reaching 23% in model B in loose soil (type C) for spectrum I. For springs, the maximum decrease reached 17.7% in model B for spectrum I. The decrease reached 16.2% in model A, 28% in model B, and 15.4% in model C for spectrum II in loose soil (type C).
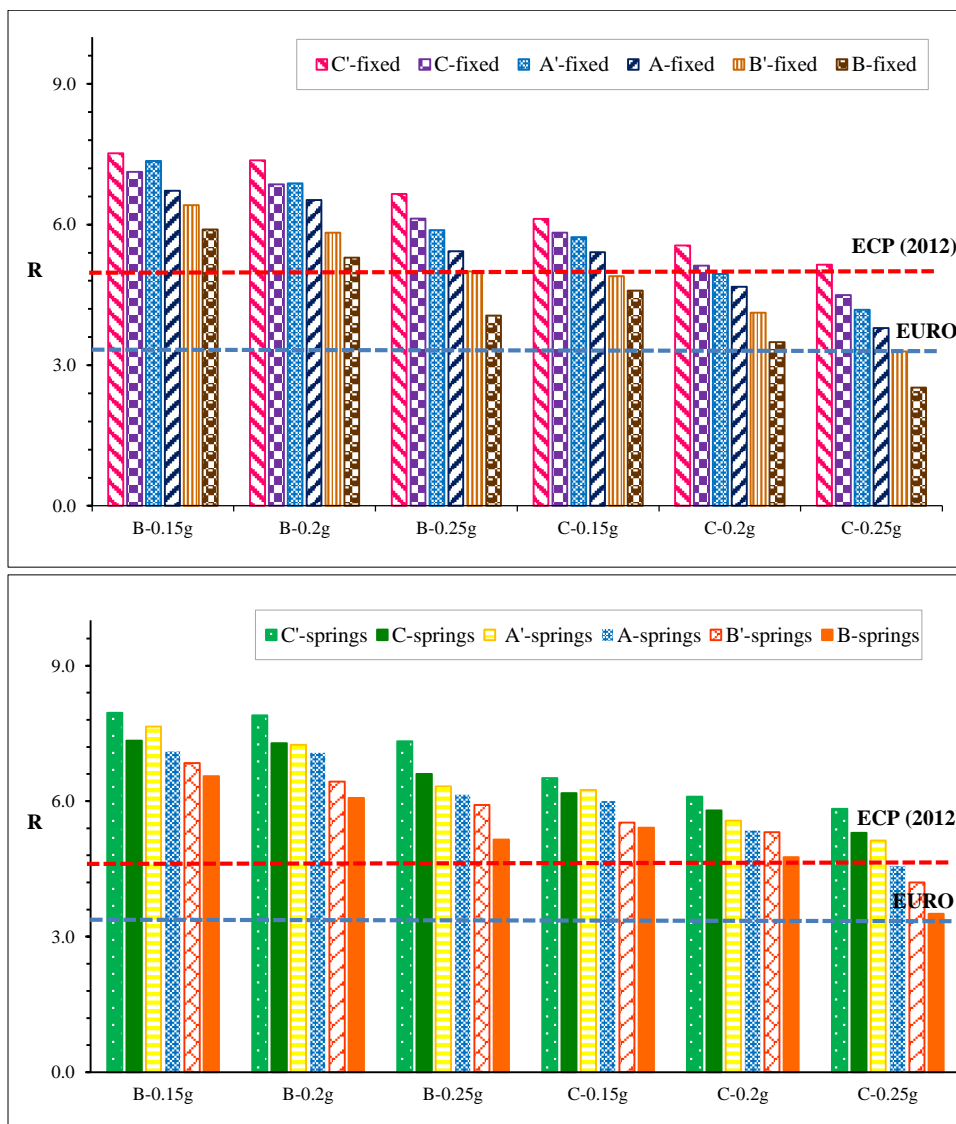
Figure 19. Response Modification factor (R) for models, (spectrum type I)
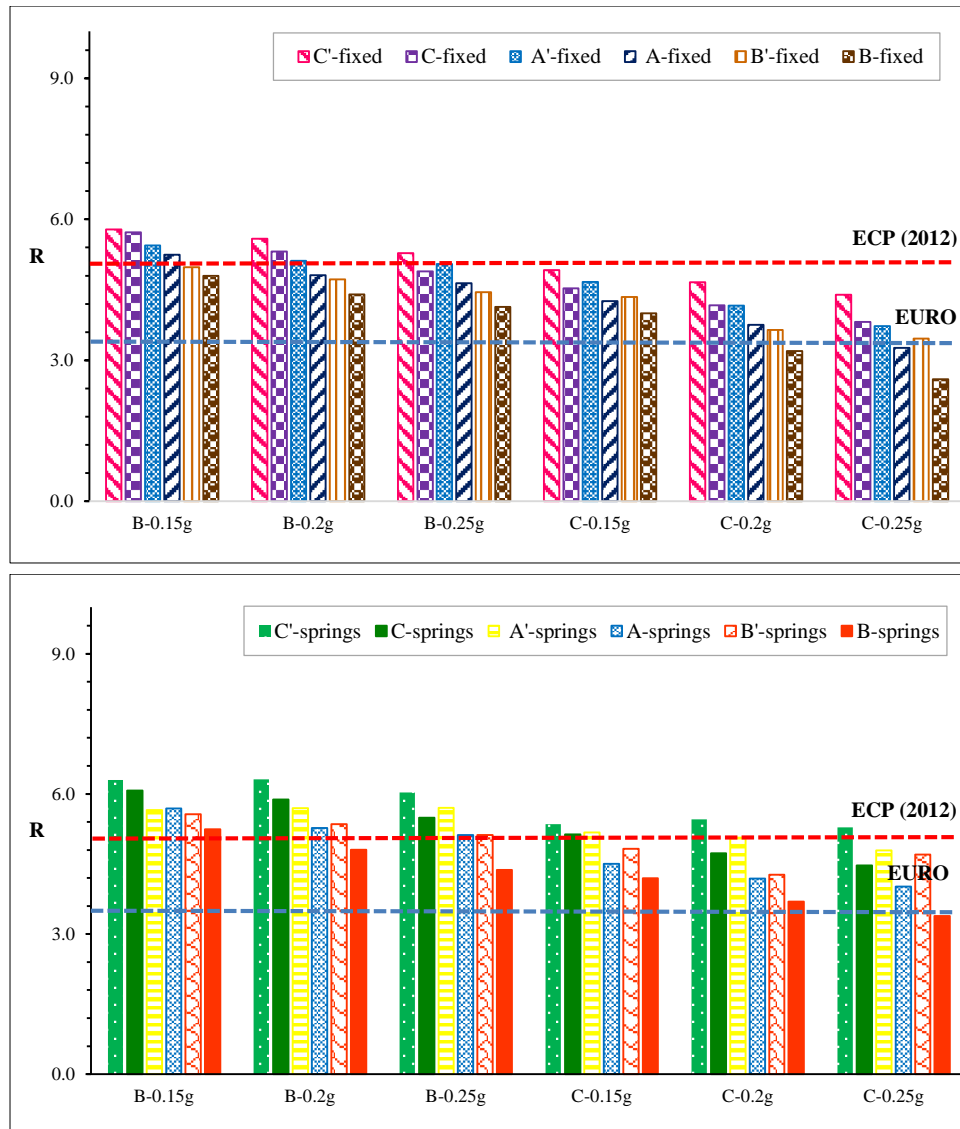
Figure 20. Response Modification factor (R) for models, (spectrum type II)

Table 5. Response factor value for fixed base (F) and isolated footing (S), for models

		A (28.6%)		B (30%)		C (21%)	
MODELS		F	S	F	S	F	S
		Spectrum I					
	0.15g	8.61	7.16	8.12	4.46	5.28	7.78
B	0.2g	5.22	2.47	9.08	5.42	6.96	7.78
	0.25g	7.67	2.91	18.83	12.42	7.92	9.83
	0.15g	5.56	3.98	6.32	2.13	4.84	5.02
C	0.2g	5.53	3.94	15.25	10.34	7.69	5.02
	0.25g	9.30	11.14	23.39	17.17	12.61	9.09
		Spectrum II					
	0.15g	3.60	1.64	3.67	5.81	1.06	3.58
B	0.2g	6.03	7.46	6.78	10.29	4.87	6.78
	0.25g	8.11	10.14	7.03	14.54	7.26	8.99
	0.15g	8.76	12.86	8.13	12.97	7.82	4.09
C	0.2g	9.79	17.31	12.49	13.50	10.56	13.32
	0.25g	12.39	16.23	24.96	28.05	13.12	15.42

(Row label "Decrease in Response Modification Factor (R) due to irregularity %" spans the table header; "Soil Type" labels the rows vertically.)

7.5. Effect of Seismic Zone

Figure 21 shows that as the zone increases Displacement also increases [40], and Base shear and lateral displacement increase with increase in the seismic intensity.
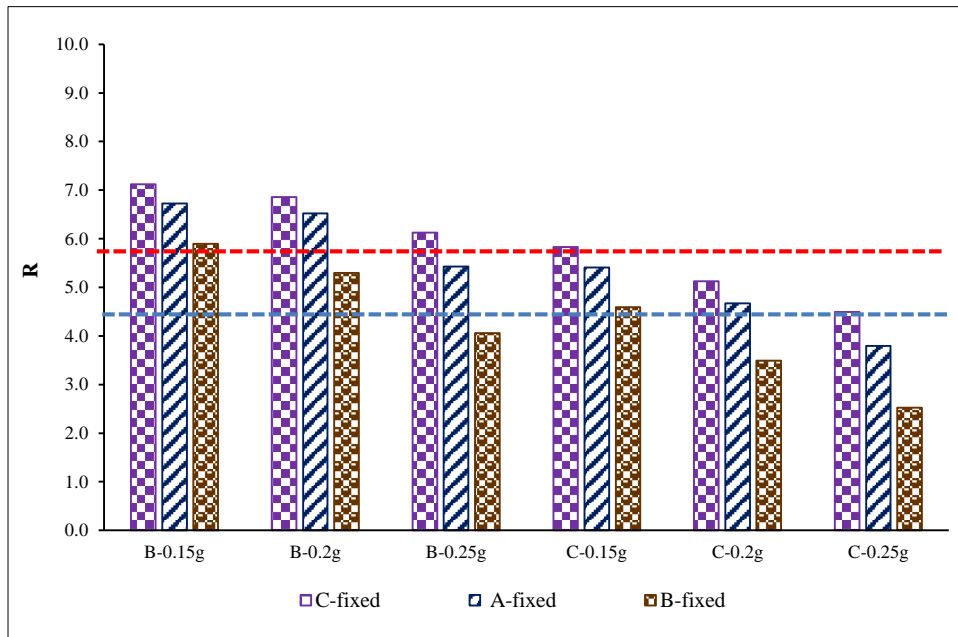
Spectrum Type II
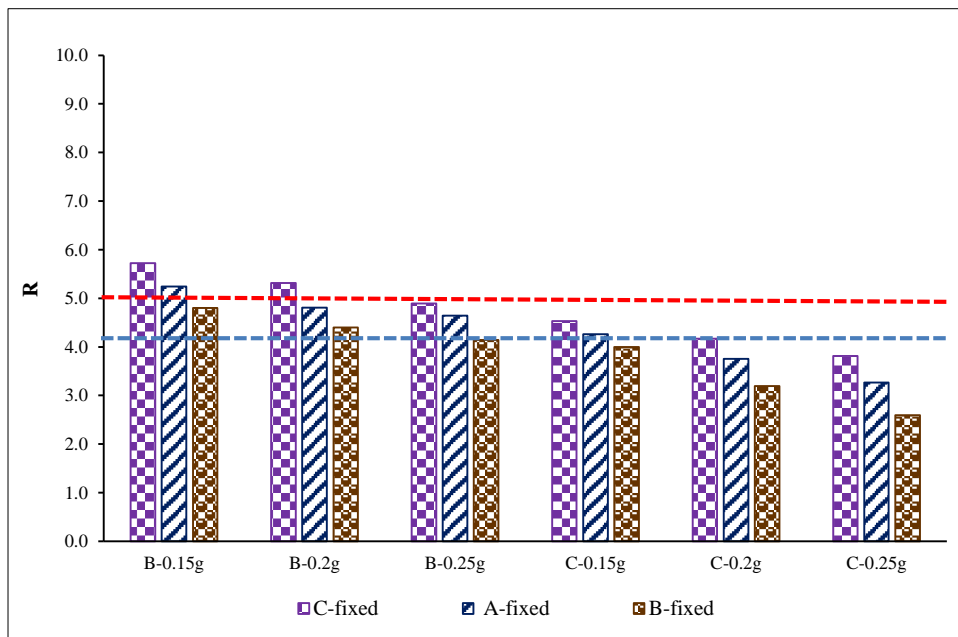
Spectrum Type II

Figure 21. Response Modification factor (R) for models

The Figure 22 illustrates how SSI affects the strength reduction factors for weak soils. Because of this, applying fixed-base strength reduction factors for interacting systems results in non-conservative design forces, hence interaction effects for weak soils cannot be ignored [39].
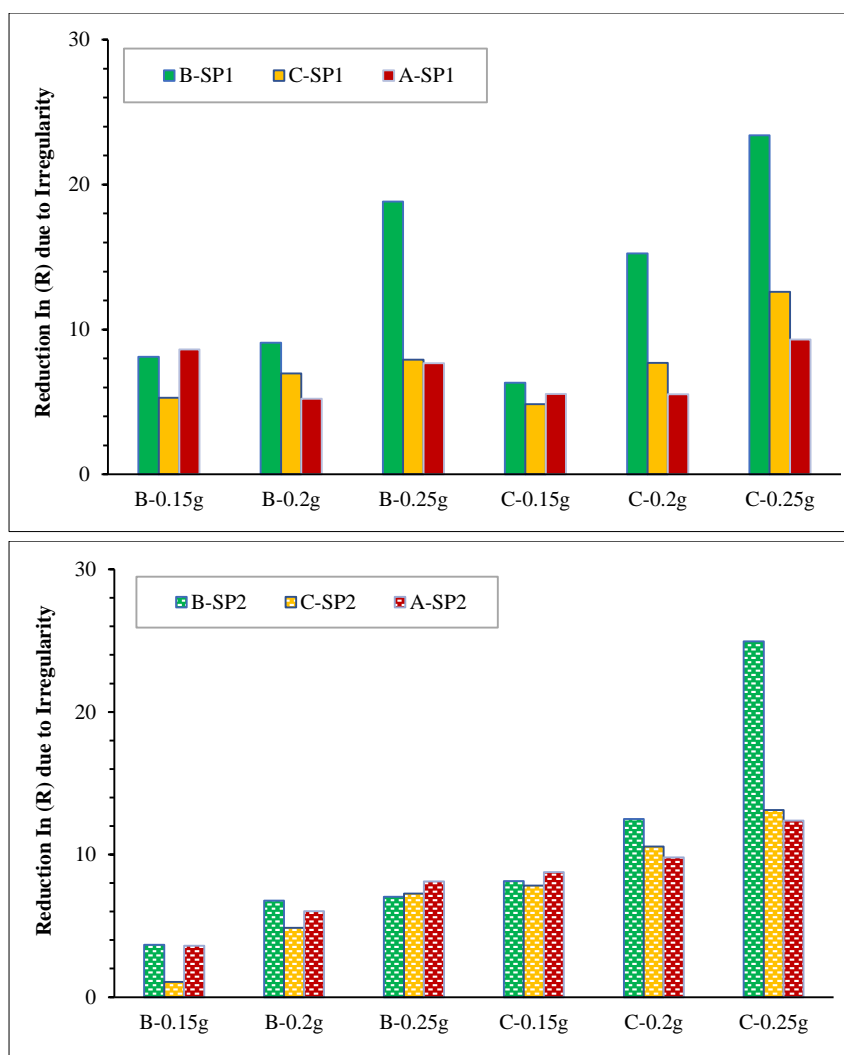
Figure 22. Reduction in Response factor due to irregularities% (R), for SP I and SP II

8. Conclusions

The present study aims to determine the effectiveness of plan and elevation irregularities in relation to seismic response within seismic zones I, II, and III, on medium and poor soil (types B & C), for both types of design response spectra given in ECP-201 (2012). The study also seeks to understand the significance of SSI or representing soil interaction with the footing (using isolated footing with springs) on R-value, base shear, lateral displacement of buildings, and the fundamental natural period of regular and irregular models. The investigation reveals the following main conclusions:

There is an observed enhancement in the natural period, roof displacement, base shear, and structure's deformation with an improvement in soil flexibility. Essentially, this conclusion will impact the response factor. If the SSI approach is not appropriately included in the investigation and design, it may be difficult to determine how safe a structure is from earthquakes accurately. When the seismic zone increases, the basic time period (TP) increases, and therefore, the response factor decreases. The natural period of the structure becomes longer due to the SSI influence, with the effect being more pronounced in soft soil. One of the main factors controlling the building's lateral seismic reaction is the NTP. Therefore, if this value is evaluated without considering seismic design, significant errors could occur. It has been demonstrated that as soil flexibility increases, so does the NTP. The irregularity resulting from increased structural rigidity seems insignificant for buildings supported by isolated footings. Regular and non-regular buildings that rely on weak soil deposits may not have sufficient structural safety guaranteed by standard design techniques if the SSI method is not used. Regular and non-regular structures behave similarly in response to weak earthquakes. The seismic zone has a significant impact on the reduction factor. As the seismic zone increases, the decrease in R's value is significantly less than the values listed in the ECP and is considered close to the Euro Code values. Therefore, it must be considered that the ECP values need to be reviewed and this percentage reduced, especially in irregular buildings. Taking the ECP Code values for irregular buildings, specifically after representing the soil and considering it, is considered an unsafe design.

9. Declarations

9.1. Author Contributions

9.2. Data Availability Statement

The data presented in this study are available in the article.

9.3. Funding

9.4. Conflicts of Interest

The authors declare no conflict of interest.

10. References

[1] Hussein, M. M., Gamal, M., & Attia, W. A. (2021). Seismic response modification factor for RC-frames with non-uniform dimensions. Cogent Engineering, 8(1), 1923363. doi:10.1080/23311916.2021.1923363.

[2] Brahmavrathan, D., & Arunkumar, C. (2016). Evaluation of Response Reduction Factor of Irregular Reinforced Concrete Framed Structures. Indian Journal of Science and Technology, 9(23), 1–8. doi:10.17485/ijst/2016/v9i23/95981.

[3] Fayed, M. N., Aboul-Nour, L. A., & El-Masry, S. S. (2018). Evaluation of seismic response modification factor of multistory buildings designed according to Egyptian code. IOSR Journal of Mechanical and Civil Engineering, 15(11), 66-68.

[4] Barakat, S. A., Husein Malkawi, A. I., & Al-Shatnawi, A. S. (1997). A Step towards Evaluation of the Seismic Response Reduction Factor in Multistorey Reinforced Concrete Frames. Natural Hazards, 16(1), 65–80. doi:10.1023/A:1007972616511.

[5] Hussain, N., Alam, S., & Mwafy, A. (2024). Developments in Quantifying the Response Factors Required for Linear Analytical and Seismic Design Procedures. Buildings, 14(1), 247. doi:10.3390/buildings14010247

[6] FEMA 356. (2000). Prestandard and commentary for the seismic rehabilitation of buildings. Federal Emergency Management Agency (FEMA), Washington, United States.

[7] ATC-40-1. (1996). Seismic Evaluation and Retrofit of Concrete Buildings; Report No. SSC 96-01, Applied Technology Council (ATC), Redwood City, United States.

[8] Fajfar, P., & Fischinger, M. (1988). N2-A Method for Non-linear Seismic Analysis of Regular Buildings. Ninth World Conference on Earthquake Engineering, 2-9 August, 1988, Tokyo, Japan.

[9] Ashwini K. C, & Dr. Y. M. Manjunath. (2017). Comparative Study of Pushover Analysis on RCC Structures. International Journal of Engineering Research & Technology, 6(6), 71–79. doi:10.17577/ijertv6is060075.

[10] Mahesh, U., Pandit, P., & Scholar, P. G. (2020). A Review on Pushover Analysis for Irregular Structures. International Journal of Engineering Science and Computing IJESC, 10(7), 26835.

[11] Elnashai, A. S., & Mwafy, A. M. (2002). Overstrength and force reduction factors of multistorey reinforced-concrete buildings. Structural Design of Tall Buildings, 11(5), 329–351. doi:10.1002/tal.204.

[12] Anagnwstopoulou, V., Zeris, C., & Karayannis, C. (2012). Evaluation of the q Factor of Irregular RC Buildings Designed According to EC8. 15th World Conference on Earthquake Engineering, 24-28 September, 2012, Lisbon, Portugal.

[13] ECP-201. (2012). ECP-201: Egyptian code for calculating loads and forces in structural work and masonry. Housing and Building National Research Center. Ministry of Housing, Utilities and Urban Planning, Cairo, Egypt.

[14] El-Mahdy, O., Hamdy, G., & YASSIN, A. (2023). Performance Based Seismic Design of Two RC High-Rise Buildings. Engineering Research Journal - Faculty of Engineering (Shoubra), 52(2), 101–113. doi:10.21608/erjsh.2023.166943.1096.

[15] Ahmed, M. M. M., Abdo, M. A. B., & Mohamed, W. A. E. W. (2023). Response modification factor evaluation for vertical irregular MRF buildings. Proceedings of the Institution of Civil Engineers: Structures and Buildings, 1–15. doi:10.1680/jstbu.22.00146.

[16] Ali, T., Eldin, M. N., & Haider, W. (2023). The Effect of Soil-Structure Interaction on the Seismic Response of Structures Using Machine Learning, Finite Element Modeling and ASCE 7-16 Methods. Sensors, 23(4), 2047. doi:10.3390/s23042047.

[17] Maharjan, S., & Bahadur, K. (2021). Study of Soil-Structure Interaction Effects on Seismic Analysis. Proceedings of 9th IOE Graduate Conference, 12 March, 2021, Lalitpur, Nepal.

[18] Abdelrhman, S. A., Naser, N. E., Sorour, T. M., & Fayed, M. N. The Effect of Soil Structural Interaction on Evaluation of Seismic Response Reduction Factor of Multi-Story Concrete Buildings. Al-Azhar University Civil Engineering Research Magazine (CERM), 43(3), 149-170.

[19] Bapir, B., Abrahamczyk, L., Wichtmann, T., & Prada-Sarmiento, L. F. (2023). Soil-structure interaction: A state-of-the-art review of modeling techniques and studies on seismic response of building structures. Frontiers in Built Environment, 9, 1120351. doi:10.3389/fbuil.2023.1120351.

[20] Janous, S. El, & Ghoulbzouri, A. El. (2024). Seismic Vulnerability of Irregular Reinforced Concrete Buildings Considering the Soil-structure Interaction. International Journal of Engineering, Transactions A: Basics, 37(1), 104–114. doi:10.5829/ije.2024.37.01a.10.

[21] Rodrigues, H., Varum, H., Arête, A., & Costa, A. (2012). Comparative efficiency analysis of different nonlinear modelling strategies to simulate the biaxial response of RC columns. Earthquake Engineering and Engineering Vibration, 11(4), 553–566. doi:10.1007/s11803-012-0141-1.

[22] Requena-Garcia-Cruz, M. V., Bento, R., Durand-Neyra, P., & Morales-Esteban, A. (2022). Analysis of the soil structure-interaction effects on the seismic vulnerability of mid-rise RC buildings in Lisbon. Structures, 38, 599–617. doi:10.1016/j.istruc.2022.02.024.

[23] Ghimire, K., & Chaulagain, H. (2021). Common irregularities and its effects on reinforced concrete building response. Structural Mechanics of Engineering Constructions and Buildings, 17(1), 63–73. doi:10.22363/1815-5235-2021-17-1-63-73.

[24] Tomer, S., & Bhandari, M. (2023). Evaluation of Seismic Response of Irregular Buildings: A Review. IOP Conference Series: Earth and Environmental Science, 1110(1), 12012. doi:10.1088/1755-1315/1110/1/012012.

[25] Allena, P., & Chowdary, T. B. (2020). Effect of Irregularities on Seismic Performance of High Rise Structures. IOP Conference Series: Materials Science and Engineering, 998(1), 12064. doi:10.1088/1757-899X/998/1/012064.

[26] ASCE/SEI 7-10. (2000). Minimum design loads for buildings and other structures. American Society of Civil Engineers (ASCE), Reston, United States.

[27] Palanci, M., Demir, A., & Kayhan, A. H. (2021). The investigation of displacement demands of single degree of freedom models using real earthquake records compatible with TBEC-2018. Pamukkale University Journal of Engineering Sciences, 27(3), 251–263. doi:10.5505/pajes.2020.47936.

[28] Chai, J. C., Miura, N., & Koga, H. (2005). Lateral displacement of ground caused by soil–cement column installation. Journal of Geotechnical and Geoenvironmental Engineering, 131(5), 623-632. doi:10.1061/(ASCE)1090-0241(2005)131:5(623).

[29] Abdel Raheem, S.E., Ahmed, M.M.M., Ahmed, M. M., & Abdel-shafy, A.G.A. (2018). Evaluation of plan configuration irregularity effects on seismic response demands of L-shaped MRF buildings. Bulletin of Earthquake Engineering, 16(9), 3845–3869. doi:10.1007/s10518-018-0319-7.

[30] Joseph, P., & Kuruvilla, R. (2021). Effects of Irregularities on the Seismic Response of a High-Rise Structure in ETABS. International Journal of Engineering Research & Technology, ICART - 2021 Conference Proceedings, Special Issue, 79-83.

[31] Freeman, S. A. (1990). On the correlation of code forces to earthquake demands. Proceedings of 4th US–Japan workshop on improvement of building structural design and construction practices, ATC-15-3 report, Redwood City, United States.

[32] Chaulagain, H., Rodrigues, H., Spacone, E., Guragain, R., Mallik, R., & Varum, H. (2014). Response reduction factor of irregular RC buildings in Kathmandu valley. Earthquake Engineering and Engineering Vibration, 13(3), 455–470. doi:10.1007/s11803-014-0255-8.

[33] HBRC. (2007). Egyptian Code of Practice for Concrete Structures, Housing and Building National Research Center (HBRC), Cairo, Egypt. (In Arabic).

[34] EN 1998-1:2004. (2004). Eurocode 8: Design of structures for earthquake resistance - Part 1: General rules, seismic actions and rules for buildings. European Committee for Standardization, Brussels, Belgium.

[35] Maheri, M. R., & Akbari, R. (2003). Seismic behaviour factor, R, for steel X-braced and knee-braced RC buildings. Engineering Structures, 25(12), 1505–1513. doi:10.1016/S0141-0296(03)00117-2.

[36] Newmark, N. M., & Hall, W. J. (1969). Seismic design criteria for nuclear reactor facilities. Proceedings of the 4th World conference on Earthquake Engineering, 13-18 January, 1969, Santiago de, Chile.

[37] Uang, C. M. (1991). Establishing R (or R w) and C d factors for building seismic provisions. Journal of structural Engineering, 117(1), 19-28.

[38] Paulay, T., & Priestley, M. N. (1992). Seismic design of reinforced concrete and masonry buildings. John Wiley & Sons, Hoboken, United States. doi:10.1002/9780470172841.

[39] Miranda, E., & Bertero, V. V. (1994). Evaluation of Strength Reduction Factors for Earthquake-Resistant Design. Earthquake Spectra, 10(2), 357–379. doi:10.1193/1.1585778.

[40] Kappos, A. J. (1997). Seismic damage indices for RC buildings: evaluation of concepts and procedures. Progress in Structural Engineering and Materials, 1(1), 78–87. doi:10.1002/pse.2260010113.

[41] Priestley, M. J. N. (2000). Performance based seismic design. Bulletin of the New Zealand Society for Earthquake Engineering, 33(3), 325–346. doi:10.5459/bnzsee.33.3.325-346.

[42] Mondal, A., Ghosh, S., & Reddy, G. R. (2013). Performance-based evaluation of the response reduction factor for ductile RC frames. Engineering Structures, 56, 1808–1819. doi:10.1016/j.engstruct.2013.07.038.

[43] IBC. (2012). International Building Code. International Code Council, Washington, United States.

[44] Lee, D. G., Cho, S. H., & Ko, H. (2005). Response Modification Factors for Seismic Design of Building Structures in Low Sesimicity Regions. Korea Earthquake Engineering Research Center, Seoul, Korea.

[45] Varum, H. S. A. (2003). Seismic assessment, strengthening and repair of existing buildings. Ph.D. Thesis, Universidade de Aveiro, Aveiro, Portugal.

[46] SAP2000 V-14. (2010). Integrated finite element analysis and design of structures basic analysis reference manual. Computers and structures INC, Berkeley, United States.

[47] Xu, C., Liu, H., Dou, P., Wang, J., Chen, S., & Du, X. (2023). Analysis on kinematic and inertial interaction in liquefiable soil-pile-structure dynamic system. Earthquake Engineering and Engineering Vibration, 22(3), 601-612. doi:10.1007/s11803-023-2190-z.

Development of a Framework for Risk-Based Integrated Safety Audit to Enhance Construction Safety Performance

Danang B. Nugroho [1, 2]*, Yusuf Latief [1], Mochamad A. Wibowo [3], Rosmariani Arifuddin [4], Fatma Lestari [5], Muhammad N. Akram [1]

[1] Department of Civil Engineering, Faculty of Engineering, University of Indonesia, Depok 16424, Indonesia.

[2] National Research and Innovation Agency, South Jakarta 12710, Indonesia

[3] Department of Civil Engineering, Faculty of Engineering, Diponegoro University, Semarang 50275, Indonesia.

[4] Department of Civil Engineering, Faculty of Engineering, Hasanuddin University, Makassar 90245, Indonesia.

[5] Occupational Health & Safety Department, Faculty of Public Health, University of Indonesia, Depok 16424, Indonesia.

Abstract

Presently, there is a notable surge in infrastructure development, leading to a heightened occurrence of accidents within the construction sector. This trend has positioned the construction industry as one of the most accident-prone areas compared to other sectors. This suggests that the current construction safety audit procedures have not proven effective in preventing accidents. Typically, audits are conducted primarily during the construction phase, with infrequent assessments during the design phase. According to the Szymberski theory, actions taken during the design phase significantly influence the occurrence of accidents more than those taken during construction. Previous research has discussed a lot about safety management systems. However, it has not discussed how to assure the quality of its implementation. Considering this, the research aims to (a) identify the processes, elements, activities, sub-elements, objectives, criteria, and risks associated with construction safety audits and (b) formulate an integrated, risk-based audit process covering both the design and construction phases. This qualitative research employed the Delphi method to gather insights from construction safety experts, and the developed audit process utilized a risk management approach. The resulting audit process integrates principles from ISO 19011:2018 and Regulation of the Minister of Public Works and Housing Number 10 of 2021. The findings revealed 34 activities in audit program management, 34 activities in audit implementation, and 32 sub-elements in audit criteria. These components are incorporated into a comprehensive construction safety audit framework, organizing audit processes, activities, and criteria. This framework underscores that improving construction safety performance is not solely confined to the construction phase but extends to the design phase as well. The audit results serve as a foundation for continuous improvement, aiding in enhancing safety performance and preventing accidents within the construction industry.

Keywords: Audit; Construction Safety; Safety Performance; Accident; Risk.

1. Introduction

In this era, Indonesia is vigorously pursuing infrastructural development, with the Ministry of Finance reporting an average annual growth of 12.7% in the infrastructure budget from 2015 to 2022 [1]. The government had officially announced the plan to relocate the Indonesian capital with the construction of Nusantara Capital City (IKN), scheduled

---

from 2022 to 2024. This initiative started with the construction of essential infrastructure, such as high-rise buildings for the Presidential Palace, the People Consultative Assembly/Parliament facility, etc. [2]. Due to the increasingly dynamic and complex lifecycle of a construction project, it is positioned as a dangerous or highly hazardous industry [3]. Statistics on occupational accidents revealed that high-rise building construction is one of the riskiest workplaces [4].

Accidents ensued as a great burden to the employee and employer in terms of absenteeism, loss of productivity, ergonomic disabilities, high costs incurred, bad company reputation, higher incidence rates of illnesses, and fatalities [5]. Managing this complexity to reduce risks could be achieved through the Construction Safety Management System (CSMS) [6]. Previous research has discussed a lot about safety management systems. However, it has not discussed how to assure the quality of its implementation. To assure the quality of the CSMS implementation, a structured and continuous audit is necessary because it provides a direct and comprehensive means to monitor the realization and effectiveness of the safety management system. Safety audit results also assist diverse companies in developing checklist standards and improved recommendations, enhancing environmental, health, and safety performance, as well as reducing the number of accidents [7, 8]. A safety audit is carried out to ensure that unsafe acts and unsafe conditions are brought to a minimum level so that there is a safe work environment. The purpose of a safety audit is to ensure that there are definitions and safe procedures for work and that the set definitions and safe procedures are practiced [9].

An audit is a systematic and, wherever possible, independent examination to determine whether activities and related results conform to planned arrangements and whether these arrangements are implemented effectively and are suitable to achieve the organization's policy and objectives [10]. Audits had been disintegrated and typically confined to a single stage of the project lifecycle, with a focus on the implementation phase, often conducted after accidents. Safety audits during the design phase are infrequent [11]. Despite Szymberski [12] stating that its activities have a more significant influence on the occurrence of accidents compared to the procurement or implementation phases, as shown in Figure 1. In his theory, Szymberski suggests that it is ideal for construction safety to be a prime consideration during the conceptual and preliminary design phases of construction projects, as there is a greater potential for accident reduction than what exists in later construction phases. This implies that efforts to control risks and prevent construction accidents cannot be assured, potentially leading to increased mishaps.
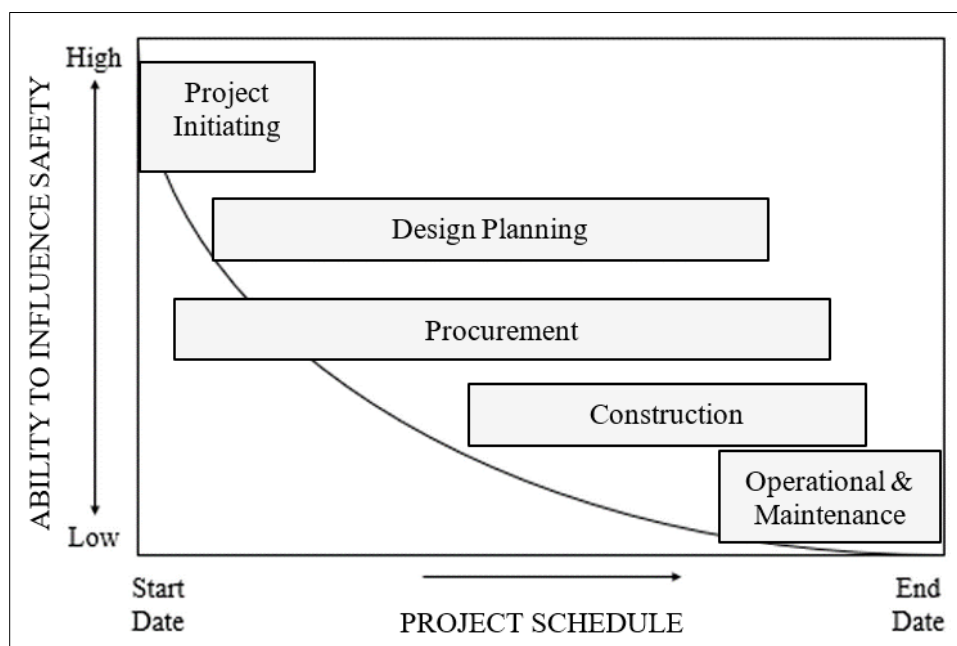
Figure 1. Time-safety influence curve [12]

The construction industry is considered high-risk as it involves dangerous and challenging work such as excavation, the erection of structural steel, and working at substantial heights [13]. Based on the International Labor Organization's (ILO) report [14], construction workers in developed countries are three to four times more likely to experience a fatal accident than workers in other industries; however, workers in less developed countries are six times more likely to suffer and experience a fatal accident than workers in other industries. Employment in the construction industry accounts for approximately 7% of global employment, and 100,000 workers die on construction sites each year, which accounts for approximately 35% of worldwide work-related deaths [15]. Indonesia experienced a significant increase in

construction accidents at work sites, as reported by Worker Insurance, with the number rising from 123,040 to 234,270 from 2017 to 2021. Workplace accidents, particularly in the construction and manufacturing sectors, account for the largest contribution at 32%. This comprises all types of projects, such as buildings, roads, bridges, tunnels, irrigation, dams, and others [11].

The most effective strategies for preventing accidents involve avoiding risks, assessing those risks that cannot be avoided, tackling the risks at source, implementing innovation, prioritizing improvement actions, replacing hazardous substances with some less dangerous ones, and implementing global policies that integrate organizational values [16]. These programs should be continuously monitored and evaluated. Based on the theory proposed by Suraji et al. [17] stated that evaluation should be conducted in the initial phases of a construction project. It was specifically proposed that audits conducted during the design phase should prioritize prevention. Therefore, auditors need to thoroughly examine the constructability of design, ensuring it prioritizes structural strength and integrates safety considerations. Globally, various accident prevention strategies have been developed, focusing on the significant influence of professional design on construction safety. Meanwhile, data obtained from Oregon, Washington, and California showed that 22% of 226 injuries were recorded between 2000 and 2002, and 42% of 224 deaths in the US between 1990 to 2003 were attributed to design [18, 19]. On average, 6.9% of serious and fatal accidents in the construction industry could be prevented through proactive measures in equipment design [20]. Contract methods, such as design-build and interaction between planners and contractors before construction, provide opportunities for these individuals to contribute to safety measures [21]. Conducting work safety audits from the planning stage to the handover stage is effective in enforcing and monitoring compliance with work safety legislation and guidelines [22]. According to Alruqi et al. [23], there is a relationship between leading indicators in construction and safety performance. Through a meta-analysis of eight studies, they found that safety auditing had a strong relationship to injuries when measured as an active indicator (when including site safety observations and inspections). Furthermore, regulatory inspections, if considered part of auditing, may contribute to improved health and safety outcomes in specific circumstances [24]. While there is a clear statistical association between audit measures and safety performance, there is no strong evidence to suggest that audits directly cause performance improvements.

Meanwhile, the Regulation of the Minister of Public Works and Housing Number 10 of 2021 addresses risk management in construction projects, covering safety aspects in four dimensions, namely human (workers), assets or technology, public, and the environment [6]. This research aims to (a) identify the processes or elements, activities or sub-elements, objectives or criteria, goals, and risks of construction safety audit, as well as (b) develop an integrated risk-based audit process covering both design and construction phases. The influence of regulation, effective application of standards, policies, and business models on auditor judgment is increasingly important in understanding and improving the quality of the resulting audit and serves as a consistent reference for continuous improvement [25]. Previous research has discussed a lot about safety management systems. However, it has not discussed how to assure the quality of its implementation. Therefore, this development of an integrated construction safety audit process will optimize the audits, enhancing their effectiveness in improving safety performance. This proactive method and principles of sustainable development lead to early identification and resolution of construction safety issues and accident prevention.

2. Research Material

2.1. Audit Process on Design and Construction Phase of High-Rise Buildings Project

An audit is an effort to examine nonconformities in the outcomes of work and confirm or compare these outcomes with predetermined criteria or plans, with the main aim of achieving continuous improvement. Its integration brings about various benefits, including optimization of business and resources, fostering organizational unity towards integrated goals, lightening workloads, and reducing certification time, costs, and documentation requirements [26]. Recognized as an important management tool and control system, auditing plays a significant role in organizational processes. As safety audits are quite costly and burdensome, an attempt should be made to achieve maximum rule compliance with the maximum level of safety audits. One starting point for optimization is the timing of audits [27]. ISO 19011:2018 provides comprehensive principles and methods for auditing management systems, specifying the competencies required by auditors. Audit operates on the fundamental principle of evidence-based assessment, perceived as a rational method to draw reliable and reproducible conclusions systematically [28]. The management of audit programs is shown in Figure 2, and ISO 19011:2018 also guides the preparation and implementation of related activities as part of these programs.
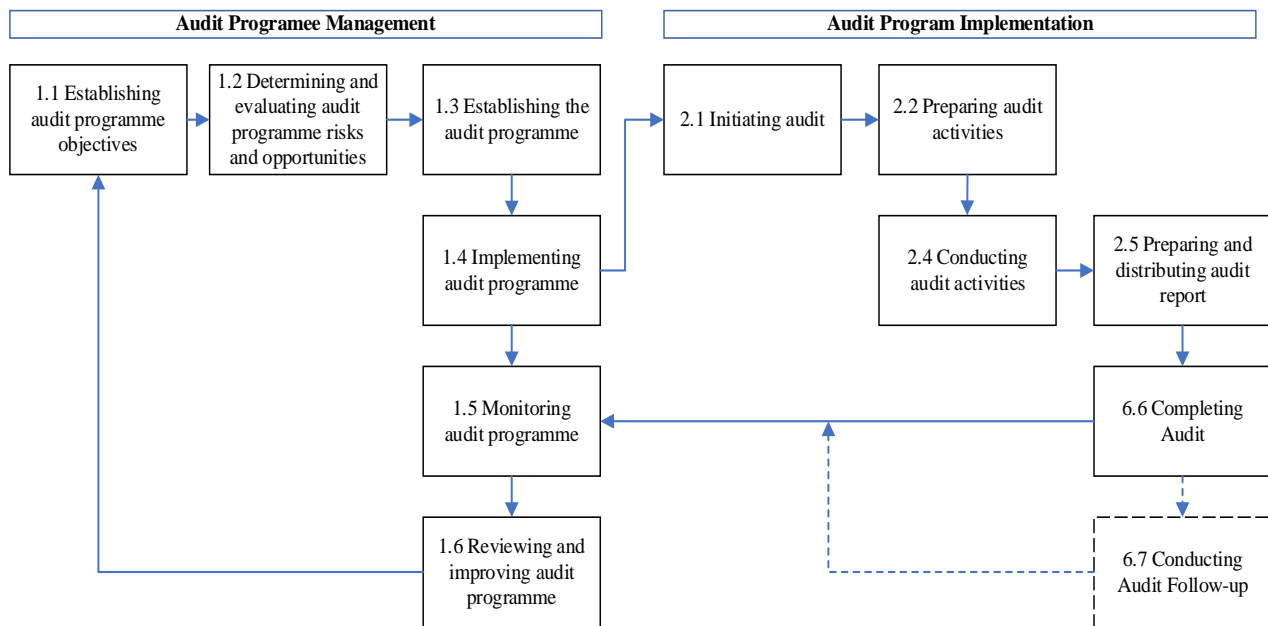
Figure 2. Process flow for managing audit programs

According to the Ministry of Public Works and Housing [6], the elements of CSMS implementation were analyzed in the audit process, namely leadership and workforce participation (sub-elements: leadership concern for external and internal issues, CSMS management organization, construction safety commitment, workforce and employee participation, as well as surveillance, learning training, responsibility, resources, and support). The audit also examines the construction safety plan, focusing on sub-elements including Hazard Identification, Risk Assessment, Determination of Risk, and Opportunity Control (HIRADC). It also assesses the engineering management and personnel action plans outlined in safety goals and programs along with ensures compliance with construction safety standards and regulations. An audit evaluates construction safety resources by considering sub-components such as resources in the form of technology, equipment, materials, costs, personnel skills, organizational awareness, management communication, and information documentation. The Construction Safety Operations focuses on addressing not only the implementation of the Construction Safety Plan (RKK) but also sub-elements such as construction accident investigation, operational management preparation, and actions in emergency situations. Lastly, audit comprised evaluation of CSMS performance implementation consists of sub-elements that include monitoring or inspection, management review, evaluations, and improvements to security measures.

High-rise buildings are defined as structures with more than eight floors [29], resulting in a comprehensive construction scope outlined by the Ministry of Public Works and Housing [30]. This scope comprised various aspects, including (a) site work preparation, (b) CSMS implementation, (c) structural, (d) architectural, (e) mechanical, (f) and electrical works, including (g) exterior building facilities, and (h) miscellaneous activities, collectively referred to as the WBS. In the context of construction methods, the design-build method is a significant method for delivering infrastructure and buildings. This method mandates the service provider to take unified responsibility for both design and construction, known for its efficiency in accelerating project timelines and reducing the general duration. Therefore, an integrated audit is needed to check deviations in design documentation and detect conscious degradation in final product quality. The audit will allow for evaluating and managing a construction firm's or their contractor's activity. All these kinds of works are made through only one procedure utilization. Moreover, audits may be used in different phases (planning, design, construction, and exploration of facilities). The engineering audit objects are constructional structures. The subjects are report information, design plans, technical and economic decisions, activity on different stages of engineering investigations, measurements of engineering defense, and risk decline [31].

2.2. Construction Safety Management System

The Ministry of Public Works and Housing [6] provides a comprehensive perspective on construction safety, defining it as all engineering activities to achieve compliance with Security, Safety, Health, and Sustainability Standards. These standards are crucial for ensuring safety in construction engineering, protecting public welfare, preserving the environment, and maintaining occupational health. Based on this, Regulation of the Minister of Public Works and Housing Number 10 of 2021 outlined specific criteria for assessing construction safety risks, including the magnitude of job risks, contract value, number of workers, types of heavy equipment used, and the level of technology application. Safety risks are assessed through a systematic calculation of their potential magnitude by determining the likelihood of events that could result in losses, pose risks to human lives, impact public safety, and harm the environment.

According to Nugroho and Latief [32], construction safety systems develop an integrated governing protocol that includes planning, engineering, controlling, organization, financing, assurance, and the investigation of narrowly avoided incidents or accident causation. This comprehensive procedure is an essential part of the general organizational process and construction project management, with the main aim of preventing deficiencies, defects, failures, and potential hazards within construction projects that could cause harm to people, the public, society, property, and the environment. It can also damage business and corporate value. CSMS needs to be implemented early, starting from the feasibility research stage of the project, ensuring adherence to Health, Safety, Security, and Environment Sustainability Standards that comprise construction engineering, public, environmental, and occupational health and safety. Suraji et al. [17] mentioned two reasons for the influence of society on construction safety. First, workers themselves can be directly influenced by external factors, e.g., pressures from the social, economic, or political climate or environmental conditions. As a result, these factors can distract them from their work, potentially leading to accidents. Second, the client is under a number of distal factors, e.g., economic, social, and political pressures, during the conceptual development of a project. This cause-and-effect process has the potential to increase workers' constraints directly or indirectly through inappropriate construction planning or inappropriate construction control procedures, leading to inappropriate site conditions, inappropriate worker actions, or inappropriate construction operations. Consequently, regular monitoring is essential to assess the extent of compliance with safety regulations as well as ensure its implementation is in accordance with the actual field conditions [33, 34]. There are two types of safety performance indicators: leading and lagging indicators (output and post-accident measurements), with lead indicators being preferred in industry and academia [35].

2.3. Enhancing Construction Safety Performance through An Integrated Risks-Based Audit

To ensure enhanced safety performance, all parties, including users and service providers, must implement a risk management process during the design and implementation phases of construction projects. The main objective is to reduce or even eliminate accidents, one of the most significant safety performance indicators. These comprehensive risk management methods include identifying and analyzing risks, hazards, controls, or responses, as well as establishing objectives and programs for each work activity, specifically those with medium- and high-risk values. The integration of risk management into construction safety planning from design to the implementation phase is crucial [6]. The systematic risk management process requires identifying, analyzing, responding to, and controlling potential risks during program implementation. Its core purpose is to enhance the likelihood and impact of positive risks while contemporarily reducing the possibility and effect of negative threats, optimizing the success of the program [36]. Risk management plays a crucial role in the decision-making process in construction project management, influencing scope, time, integration, quality, human resources, cost, communications, and project procurement. Therefore, WBS should be categorized based on work packages, methods or design, activities, material resources, equipment, labor, and the environment to identify risks. This systematic method enables the identification of risk events that might impact safety performance objectives [32].

A safety audit plays a crucial role in conducting a comprehensive safety assessment, thereby enabling contractors to reflect, strengthen, and maintain current best practices while reducing risks continually [37, 38]. According to Barretto et al. [39], the risk-based audit process aims to achieve several objectives, namely (a) verifying compliance with established requirements, (b) assessing the effectiveness of management practices, (c) identifying weaknesses in operational and management aspects to reduce accident risks, and (d) fostering a culture of continuous learning and improvement. ISO 19011:2018 introduced a risk-based method to audit principles to support these objectives. This addition enhances general competencies for auditors and adjusts terminology to reflect audit processes accurately. Furthermore, the standard extends guidelines for conducting this process, specifically focusing on the design phase [26]. For enhancing safety performance, audits should be conducted from the beginning, just after a new rule has been prescribed, and audits should be conducted continuously and should not be stopped after a certain period [40].

3. Research Method

3.1. Research Design

The method is a systematic and scientific method designed to gather data for specific purposes. In selecting this method, three influencing factors play a significant role, namely the type of questions posed, the level of control over the behavioral events under investigation, and the focus on contemporary incidents as opposed to historical activities [41]. This research adopts a qualitative method to identify the audit process, activities, objectives, goals, risk details, levels, causes, and preventive actions. Literature reviews and the Delphi method were primary data collection sources. The Delphi method, widely used as a forecasting method, provides projections for complex or uncertain future situations. It includes collecting opinions and knowledge from multiple expert panels with relevant expertise. The Delphi survey was conducted to gather information and obtain the best conclusions from experts [42, 43].

The research design structure, as shown in Figure 3, requires a two-step process. Initially, the results of the archive analysis contributed to the formulation of content and constructs for the construction safety audit procedure. These were then subjected to validation by experts using the Delphi method. In this stage, experts provided valuable feedback on the audit process, activities, objectives, goals, and risk details, specifically in the design and construction stages of high-rise buildings using the design-build method. Subsequently, the content and constructs validated by experts are further evaluated through archive analysis, focusing on identifying risk levels, causes, and preventive actions. Experts provide feedback on risk levels, causes, and preventive actions in the construction safety audit process using the Delphi method. The research was concluded with a final validation of the results obtained using the Delphi method.
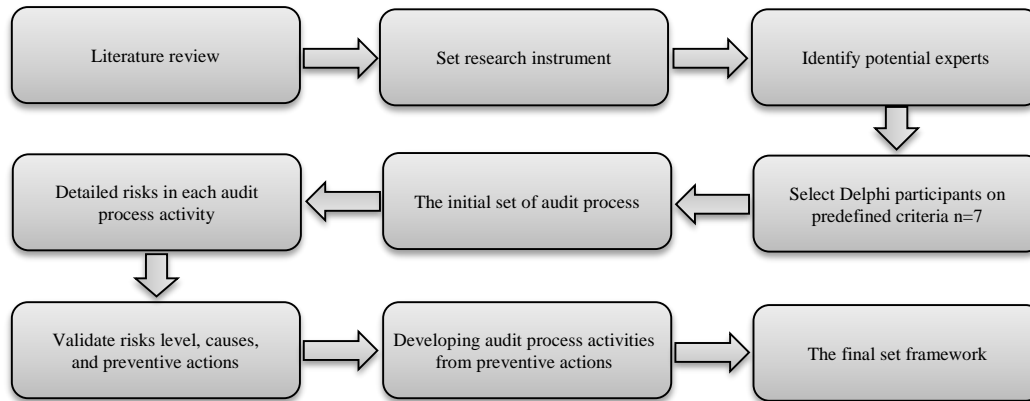
Figure 3. The research design

This research follows specific criteria for expert selection, targeting individuals who are either members of the Construction Safety Committee or possess expertise in construction with a minimum of 10 years of experience in high-rise building construction using the design-build method. Furthermore, these experts must possess a minimum educational qualification equivalent to a master's degree (S2).

3.2. The Initial Set of Construction Safety Audit Process

The instrument for the construction safety audit process was carefully designed based on archive analysis from prior research, regulations, and relevant international standards. It integrated all variables and components obtained from various literature sources, categorizing the audit process into three distinct groups, namely audit program management, implementation, and criteria, as shown in Figure 4. The instrument used secondary sources from previous research [6, 28, 44] to provide comprehensive insights into audit processes and activities. It comprises the program management phase at the organizational level, the implementation stage of a project, and criteria, risks, causes, and preventive actions. The output of this instrument included six processes in the audit and the implementation phases, as well as five elements in the criteria. An overview of audit process items used as benchmarks in developing the research instrument is shown in Table 1.
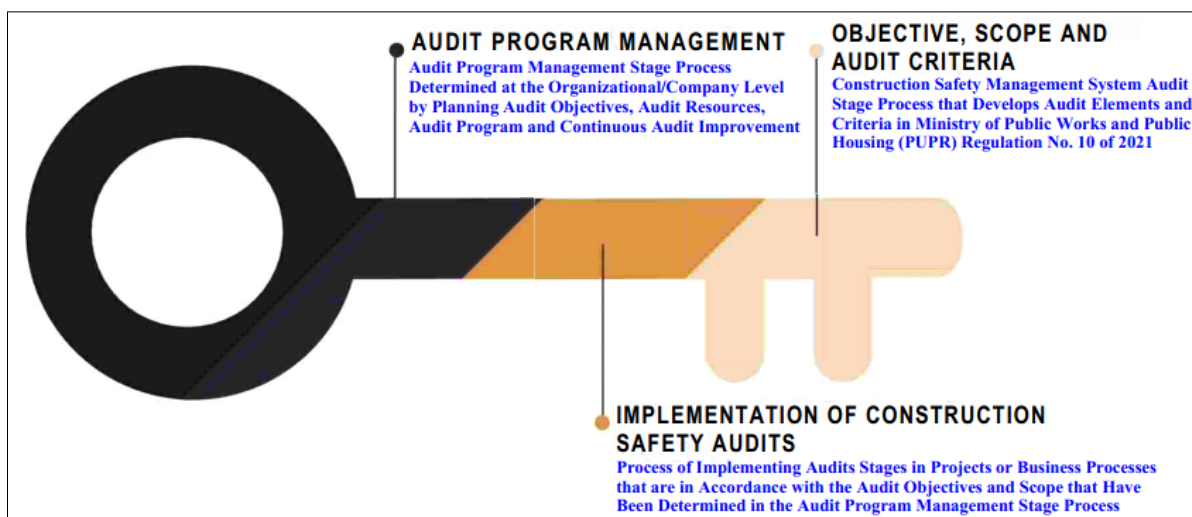
Figure 4. Construction safety audit process

Table 1. Construction Safety Performance Audit Process

Code	Audit Process/Elements
Audit Program Management	
X1.1	Establishing audit program objectives
X1.2	Determining and evaluating audit program risks and opportunities
X1.3	Establishing audit program
X1.4	Implementing audit program
X1.5	Monitoring audit program
X1.6	Reviewing and improving audit program
Audit Implementation	
X2.1	Initiating audit
X2.2	Preparing audit activities
X2.3	Conducting audit activities
X2.4	Preparing and distributing audit report
X2.5	Completing audit
X2.6	Conducting audit follow-up
Audit Criteria	
X4.1	Leadership and Worker Participation in Construction Safety
X4.2	Construction Safety Planning
X4.3	Construction Safety Support
X4.4	Construction Safety Operations
X4.5	Performance Evaluation of CSMS Implementation

3.3. The Delphi Process

The Delphi method, recognized as a standardized and interactive research method, plays a significant role in gathering perceptions or assessments from a group of experts on a specific topic. This effective method is particularly beneficial for reaching a consensus on new and complex concepts across interdisciplinary research [45]. This is likely due to variation among studies that implement Delphi and ambiguity in the literature that provides guidance for the specific parameters associated with the method. In carrying out the Delphi method, we have to: (1) understand the merits, appropriate application, and appropriate procedure of the traditional Delphi process; (2) identify and qualify potential expert panelists according to objective guidelines; (3) select the appropriate parameters of the study, such as the number of panelists, number of rounds, type of feedback, and measure of consensus; (4) identify potential biases that may negatively impact the quality of the results; and (5) appropriately structure the surveys and conduct the process in such a way that bias is minimized or eliminated [46]. The application of the Delphi method in this research is shown in Figure 5, which comprises four distinct phases, namely questionnaire design and validity examination, expert selection, survey, and data analysis.
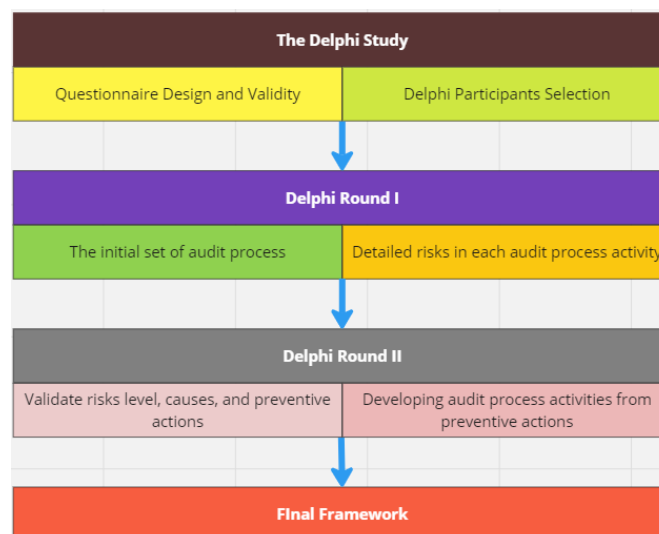
Figure 5. The Delphi process flowchart

The Delphi survey engages a total of seven experts, including members of the Construction Safety Committee and other seasoned professionals. The combined experience of these experts varies from 12 to 38 years, with three of them having over 30 years of expertise. Among the group, three experts hold a doctoral degree (S3), while the remaining four possess a master's degree (S2). Table 2 shows a comprehensive profile of these experts, who play a critical role in validating the development of the construction safety audit process.

Table 2. The Delphi Participants' Demographics

User	Position	Organization	Experience	Education
Expert 1	Committee member	Ministry of Public Works and Housing	14 years	Doctoral
Expert 2	Chairman, Committee member	Construction Safety Experts Association (PAKKI)	31 years	Master
Expert 3	Associate Professor, Committee member	Academics	38 years	Doctoral
Expert 4	Director, Committee member	Ministry of Public Works and Housing	38 years	Doctoral
Expert 5	Committee member	Ministry of Public Works and Housing	12 years	Master
Expert 6	Senior Vice President QHSE	Construction Organizations	29 years	Master
Expert 7	Vice President QHSE	Construction Organizations	20 years	Master

4. Result and Discussion

In this section, the discussion of the results is presented in two parts: (1) analyzing the initial set of processes or elements, activities or sub-elements, objectives or criteria, goals, and risks of a construction safety audit, as well as (2) a framework for an integrated risk-based audit process covering both design and construction phases.

4.1. Analyzing The Initial Set of Process/Elements, Activities/Sub-elements, Objectives/Criteria, Goals, and Risks of Construction Safety Audit

The validation outcomes obtained from expert evaluations on various facets of construction safety audits are systematically shown in Table 3. The audit program management segment includes six processes, 28 activities, 38 objectives, 65 goals, and 65 risks. Meanwhile, the audit implementation phase showed six processes, 21 activities, 54 objectives, 61 goals, and 61 risks. In audit criteria, experts identified five elements, 22 sub-elements, and a comprehensive set of 123 criteria, goals, and risks. Moreover, the validation process was extended to a thorough examination of risk details, in which experts contributed valuable insights. This collaborative effort aimed to derive cause-based preventive actions and establish distinct risk levels. Wolff et al. [47] extensively reviewed psychometric risk research and provided a general overview of perceived risk conceptualization and measurement. Specifically, subjective risks are defined as the severity level of negative outcomes measured based on their likelihood, in accordance with the widely accepted definition in psychometric and general economic literature [48, 49].

Table 3. Process/Elements, Activities/Sub-elements, Objectives/Criteria, Goals, and Risks of Construction Safety Audit

No.	Audit Process/Elements	Audit Activities /Sub-elements	Audit Objectives / Criteria	Audit Goals	Audit Risks
Audit Program Management					
X1.1	Establishing audit program objectives	2 Activities	6 Objectives	8 Goals	8 Risks
X1.2	Determining and evaluating audit program risks and opportunities	4 Activities	4 Objectives	4 Goals	4 Risks
X1.3	Establishing audit program	6 Activities	10 Objectives	27 Goals	27 Risks
X1.4	Implementing audit program	6 Activities	8 Objectives	9 Goals	9 Risks
X1.5	Monitoring audit program	5 Activities	5 Objectives	9 Goals	9 Risks
X1.6	Reviewing and improving audit program	3 Activities	5 Objectives	8 Goals	8 Risks
Audit Implementation					
X2.1	Initiating audit	2 Activities	11 Objectives	11 Goals	11 Risks
X2.2	Preparing audit activities	4 Activities	12 Objectives	18 Goals	18 Risks
X2.3	Conducting audit activities	9 Activities	22 Objectives	22 Goals	22 Risks
X2.4	Preparing and distributing audit report	2 Activities	5 Objectives	5 Goals	5 Risks
X2.5	Completing audit	2 Activities	2 Objectives	2 Goals	2 Risks
X2.6	Conducting audit follow-up	2 Activities	2 Objectives	3 Goals	3 Risks
Audit Criteria					
X3.1	Leadership and Worker Participation in Construction Safety	4 Sub-elements	16 Criteria	16 Goals	16 Risks
X3.2	Construction Safety Planning	4 Sub-elements	20 Criteria	20 Goals	20 Risks
X3.3	Construction Safety Support	5 Sub-elements	22 Criteria	22 Goals	22 Risks
X3.4	Construction Safety Operations	4 Sub-elements	49 Criteria	49 Goals	49 Risks
X3.5	Performance Evaluation of CSMS Implementation	5 Sub-elements	16 Criteria	16 Goals	16 Risks

4.2. Developing a Framework for an Integrated Risks-Based Construction Safety Audit

Conducting a relative assessment of perceived risks requires evaluating whether hazard A is deemed more or less risky compared to hazard B, even when the precise measurement of these risks is challenging. This evaluation requires a careful method, ensuring that hazards A and B are both assessed for risks in exactly the same way. Consistency is achieved by assessing them under similar conditions and at the same specificity level [50]. In the adoption of a qualitative risk assessment method that uses descriptive language, risk mapping is structured into low, medium, and high categories. The validation results obtained from experts regarding risk levels, causes, and preventive actions are systematically shown in Table 4.

Table 4. Validation Results of Risks Levels, Causes, and Preventive Actions

Code	Audit Activities / Sub-elements	Code	Risks Details	Risks Levels	Causes	Preventive Actions
X1. Audit Program Management						
X1.1. Establishing audit program objectives						
A1	The organization creates audit program objectives that consistently support audit process policies and objectives and are by its business processes	R1	Audit program objectives are not achieved and are wrong due to the many perspectives and opinions/ conflicts within an organization, as well as overlooked audit components/items.	High	Mistakenly defining audit program scope and overlooking components/items, along with numerous perspectives/opinions and conflicts within an organization.	Mistakenly defining audit program scope, overlooking components/items, and encountering numerous perspectives/ opinions as well as conflicts within an organization.
		R2	The combination of the program and audit process is not achieved according to plan due to many perspectives being combined incorrectly.	High	Mistakenly defining audit program scope and overlooking components/items, along with numerous perspectives/opinions and conflicts within an organization.	Developing detailed and straightforward policies, regulations, and procedural systems for audit program management from the initial phase to completion, including the responsible organization and adequate resources.
		R3	The unity of audit program objectives is not established, and goals are not achieved because personnel still adhere to outdated standards.	High	The competencies of the human resources managing audit program do not fulfil the organization's expectations and still adhere to outdated standards.	Implementing training programs and conducting socialization with a clear explanation of audit program implementation standards, along with creating a selection scheme for auditors through expert certification.
		R4	Audit program fails to adopt changes and lacks integration from the beginning to the end due to insufficient socialization and periodic reviews.	High	Mistakenly defining audit program scope and overlooking components/items, along with an unclear understanding of program integration by the organization.	Communicating and socializing the policy of separating audit program within audit process for each organizational level that is in accordance with the organization's goals and business.
		R5	Audit program is not properly managed because the program priority setting within the organization is inaccurate.	Medium	Mistakenly defining audit program scope and overlooking components/items, along with the program priority within the organization that is not in accordance with the objectives.	Developing detailed and straightforward policies, regulations, and procedural systems for audit program management from the initial phase to completion, including the responsible organization and adequate resources.
		R6	Audit program management is not optimal because the organization lacks interconnected process activities that function as a coherent system.	Medium	Mistakenly defining audit program scope, overlooking components/ items, and integrating process activities that are not interconnected and do not function as a coherent system.	Developing standardized business process procedures for audit program that are simple to understand yet detailed and comprehensive, accompanied by regulations supporting the program.
A69	Establishing Construction Safety Performance Improvement	R246	The CSMS audit does not depict the actual conditions in the field because the improvement in safety performance is not in accordance with the organization's business scale	Medium	Suboptimal management actions in the CSMS audit as well as the lack of capacity and capability among safety auditors and all parties that participated in the project to enhance safety performance in accordance with the organization's business scale.	Conducting analysis and re-identification of inputs, outputs, and outcomes related to CSMS implementation in accordance with procedures, policies, goals and scope, criteria, management organization, and business process along with performing evaluation for the sustainable development of CSMS.
		R247	The CSMS audit has no follow-up for improvement and enhancement because the identification of factors influencing safety and health performance improvement in the workplace are not in accordance with with the needs analysis results	Medium	The inputs, outputs, and expected outcomes related to the identification of factors influencing improvement in workplace safety and health performance is not in accordance with with the needs analysis results for CSMS implementation.	Conducting analysis and re-identification of inputs, outputs, and outcomes related to CSMS implementation in accordance with procedures, policies, goals and scope, criteria, management organization, and business process along with performing evaluation for the sustainable development of CSMS.
		R248	The CSMS audit has no follow-up for improvement and enhancement because both internal and external influences are ignored and not used as learning points to enhance safety performance	Medium	Suboptimal management actions in the CSMS audit as well as the lack of capacity and capability among safety auditors and all parties participating in the project to manage internal and external influences as learning points to improve safety performance.	Following up on the results of CSMS implementation by reporting to relevant authorities and responsible parties regarding the benefits of CSMS that generate added value along with providing rewards or penalties based on the ranking determination through the assessment of standardized parameters.

The recapitulation of risk levels shows that in the audit program management section, there are specifically 24, 36, and five high, medium, and low risks. Meanwhile, the audit implementation section has 44, nine, and seven high, medium, and low risks. In the audit criteria section, the distribution includes 85, 35, and three high, medium, and low risks. For each risk detail with identified levels, cause-based preventive actions were established. The experts also explained the causes of each risk in detail, along with their preventive actions. Additionally, a systematic pattern recognition process was conducted, grouping risks based on their underlying causes, as shown in Table 5.

Table 5. Mapping of Cause-Based Audit Activities and Risks Details

Code	Audit Activities/Sub-elements	Code	Risks Details	Code	Causes	Code	Preventive Actions
X1. Audit Program Management						
X1.1. Establishing audit program objectives						
A2	The organization ensures that audit program objectives are established for audit design and implementation. Furthermore, it ensures that the program is carried out effectively	R7	Audit program is ineffective because the expected inputs and outputs/outcomes are not in accordance with design and operational implementation	P1	The inputs, outputs, and expected outcomes of the organization is not in accordance with audit program design and operation within audit process	TP1	Conducting an analysis and re-identification of inputs, outputs, and outcomes related to the implementation of audit program in accordance with procedures, policies, goals and scope, criteria, management organization, and business process along with performing evaluation for the sustainable development of the program
A11	The organization creates and establishes procedures for audit program	R30	Audit program is ineffective because the established procedures are incorrect and are not in accordance with audit process system				
A1	The organization sets consistent audit program objectives that support the policies and goals of audit process are not in accordance with the business process of the organization	R3	The unity of audit program objectives is not established, and goals are not achieved because personnel still adhere to outdated standards	P2	The competencies of the human resources managing audit program do not fulfil the organization's expectations or requirements and still adhere to outdated standards.	TP1	Conducting an analysis and re-identification of inputs, outputs, and outcomes related to the implementation of audit program in accordance with procedures, policies, goals and scope, criteria, management organization, and business process along with performing evaluation for the sustainable development of the program
A2	The organization ensures that audit program objectives are established for audit design and implementation. Furthermore, it ensures the program is carried out effectively	R8	Communication within audit program is ineffective due to a lack of understanding related to digital technology advancements			TP2	Implementing training programs and socializing a re-explanation of audit program implementation standards, along with creating a selection scheme for auditors through expert certification
A7	The organization defines the roles and responsibilities of individuals managing audit program as well as audit team/auditors	R13	Audit program management is not in accordance with the roles and responsibilities of the selected personnel because it is not their task			TP3	Conducting specialized development and mentoring through a professional education program for engineering specialist auditors capable of managing audit program in line with objectives and standards
A8	The organization specifies the competencies of individuals managing audit program and audit team/auditors	R14	The organization struggles and makes mistakes in determining personnel who can manage audit program according to the expected competencies			TP4	Conducting a review and evaluation of audit program objectives against the expected results, with a monitoring process for program implementation
		R15	Standards and performance of audit program show no improvement because the selected personnel are not responsibly executing their tasks				
A9	The organization appoints individuals who manage and are responsible for audit program as well as audit team/auditors	R20	The quality of audit program results is poor and incorrect because the selected personnel cannot manage and are not accountable for the program				
A10	The organization establishes levels for audit program	R25	Audit program is not managed properly due to the selection of weak audit team partners who do not possess the required competencies				
		R27	The organization does not produce a high-quality audit program because performance indicators are unclear				
A11	The organization creates and establishes procedures for audit program	R31	Audit program is not managed properly because the socialization is poorly executed and cannot be measured				
A12	The organization identifies resources for audit program	R37	Audit program results are incorrect and cannot be accounted for because the allocated resources do not match the needs				

		R38	Audit program is not managed properly due to a lack of competent human resources as per requirements
		R39	Audit program objectives are not achieved because there are no financial resources according to the needs
A15	The organization appoints audit team members	R43	The quality of audit program results is poor and incorrect because the personnel assigned to audit team cannot adapt and communicate effectively with each other
A18	The organization manages and maintains records of audit program results	R48	Audit program is mismanaged due to a lack of competent resources in the field of archiving
A20	The organization monitors performance results of audit team members	R50	Audit program is not managed properly because audit team's performance does not fulfil expectations
A21	The organization monitors audit team's ability to conduct audit in accordance with the plan	R52	Audit program is not managed properly because audit team cannot resolve issues that arise during implementation
A22	The organization obtains feedback from top management, audited parties, auditors, and other relevant stakeholders	R54	The quality of audit program results is poor and incorrect because some parties do not work well or to their maximum capacity
A24	The organization reviews audit program to assess whether its objectives have been achieved	R58	Audit program objectives are not achieved and are incorrect because the results are not associated with performance, policies, and goals

After identifying cause-based preventive actions, a total of 37 such measures were classified, with 9, 13, and 15 specifically related to audit program management, implementation, and criteria. These preventive actions were then integrated into additional activities or criteria as part of the development of a risk-based construction safety audit process. The subsequent analysis of these 37 additional indicators was carried out using the Delphi method. The results showed that four indicators are considered inappropriate by experts, namely (i) re-identifying audit program implementation, followed by analysis and evaluation for the sustainable development of the program; (ii) communicating and socializing the CSMS implementation policy in the audit process for each project level in line with the goals and business process; (iii) conducting daily inspections during implementation integrated into the work; and (iv) planning a complete and orderly schedule for construction safety audit implementation with a designated responsible party for each process or activity. According to the experts, the risk response results associated with the cause-based construction safety audit process should not be eliminated because they offer additional information.

The developed framework of the construction safety audit process, as shown in Figure 6, comprised (a) 34 activities in audit program management at the organizational level, which increased goals in each process or activity from 26 to 65; (b) 34 activities in audit implementation at the project level, including the integration of ISO 19011:2018 standards, which merged with the previous process phases at the organizational level to obtain 60 goals; (c) 32 sub-elements in audit criteria were refined by adjusting the audit form in Regulation of the Minister of Public Works and Housing Number 10 of 2021 with the addition of 37 new criteria, thereby leading to a total of 123. The identification of risk factors in the audit criteria section suggested that a properly executed CSMS implementation can significantly improve construction safety performance. This observation is also consistent with preliminary research [37, 38, 50], showing that organizations with robust safety management systems and effective audits had better hazard control and safer working conditions, thereby reducing workplace accidents and improving project management.
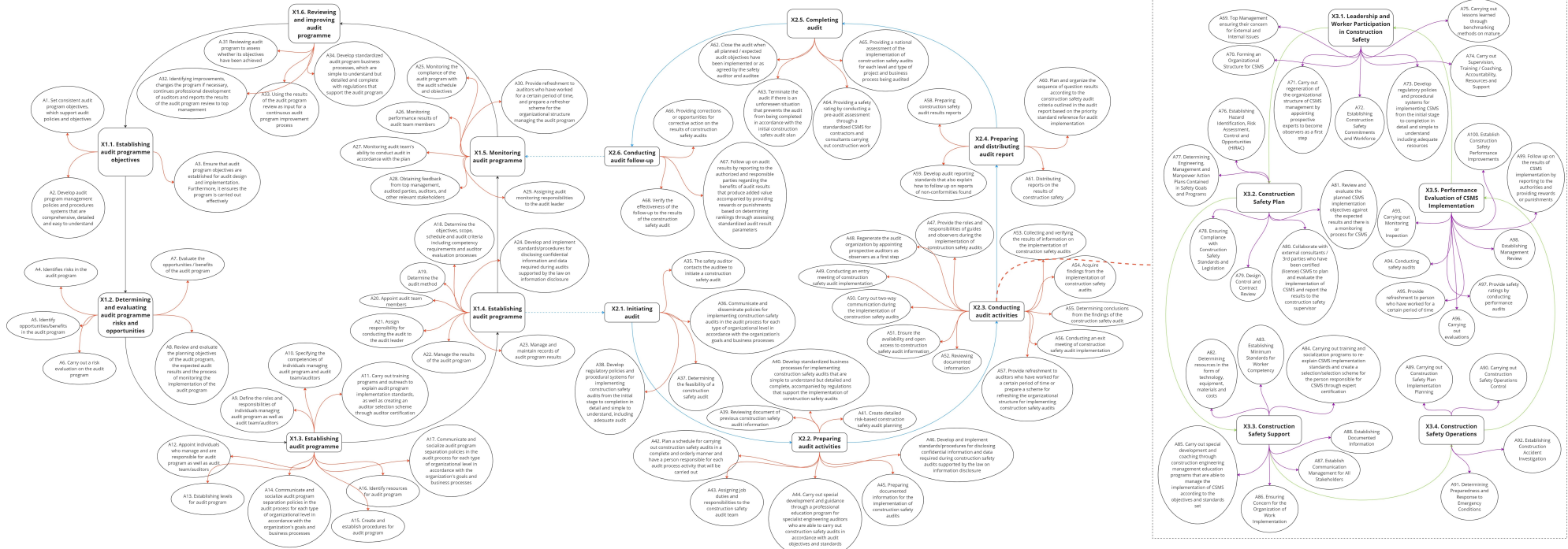
Figure 6. The framework of construction safety audit process

Construction safety audits would optimally improve construction safety performance when audits of CSMS implementation could be mitigated as well as possible. Several preventive actions or risk responses have been mapped to mitigate the detailed risks of the cause-based construction safety audit process, including conducting regular audits to evaluate the CSMS on the project and detailing a more regular audit schedule to evaluate construction safety performance. Each stage of the construction safety audit process is carried out with an assessment system so that risk prevention can be carried out as early as possible through audits that describe actual conditions in the working zone. Audit risk based along with risk control and causes, can be explained in more detail so that auditors and auditees are more aware of the potential risks that will occur in the implementation of construction safety audits. Implementing risk responses in the development of construction safety audit standards can reduce work accidents by identifying deviations earlier, thereby improving safety performance. The development of risk responses to detailed cause-based audit risks refers to the needs of each organization/company, the project's business operations, and the criteria to be audited.

Data analysis of the relationship between the development of construction safety audit process standards and construction safety performance using regression analysis. Based on the results of expert validation related to the development of construction safety audit process standards, as shown in Table 6, data was obtained which explains that the development of construction safety audit process standards, especially in the audit criteria section, has an influence and relationship with key indicators for enhancing construction safety performance, especially leading indicators such as those found in Regulation of the Minister of Public Works and Housing Number 10 of 2021, namely the implementation of Leadership and Worker Participation in Construction Safety, Implementation of Construction Safety Policy Elements, Construction Safety Programs, Construction Safety Support, and Inspections & Audits. In addition, leading indicators can also change in a short time. For example, the percentage of negative random drug results or the percentage of safety compliance based on audits. Leading indicators directly measure aspects of the CSMS, such as the frequency or timeliness of audits. The results of the construction safety audit can be further developed by the organization to become a standard inspection list, recommend improvements, improve environmental, health, and safety performance, and reduce the number of accidents.

Table 6. Influence of Construction Safety Audits on Construction Safety Performance

No.	Audit Process / Audit elements	Leading Indicators	Influence
1	Establishing audit program objectives	Application of Leadership in Construction Safety	High
		Implementation of Construction Safety Policy Elements	High
2	Determining and evaluating audit program risks and opportunities	Construction Safety Program	Medium
		Implementation of Construction Safety Policy Elements	High
3	Establishing audit program	Construction Safety Program	High
		Inspection & Audit	High
4	Implementing audit program	Construction Safety Program	Medium
		Inspection & Audit	High
5	Monitoring audit program	Inspection & Audit	High
		Construction Safety Support	Medium
6	Reviewing and improving audit program	Inspection & Audit	High
		Construction Safety Program	Medium
		Construction Safety Support	Low
7	Initiating audit	Construction Safety Program	High
8	Preparing audit activities	Construction Safety Program	High
		Inspection & Audit	Medium
9	Conducting audit activities	Inspection & Audit	High
		Construction Safety Support	Medium
10	Preparing and distributing audit report	Inspection & Audit	High
		Construction Safety Support	High
11	Completing audit	Inspection & Audit	High
		Construction Safety Support	High
12	Conducting audit follow-up	Implementation of Construction Safety Policy Elements	High
		Inspection & Audit	Medium
13	Leadership and Worker Participation in Construction Safety	Application of Leadership in Construction Safety	High
14	Construction Safety Planning	Implementation of Construction Safety Policy Elements	High
		Construction Safety Program	High
		Construction Safety Support	Medium
15	Construction Safety Support	Construction Safety Support	High
		Construction Safety Program	Medium
16	Construction Safety Operations	Construction Safety Program	High
17	Performance Evaluation of CSMS Implementation	Construction Safety Program	High
		Inspection & Audit	High

So, developing a framework for the construction safety audit process is very influential in enhancing construction safety performance. The results of the construction safety audit process can be developed as an innovative method to move away from traditional methods of records and information management to enable better management and organization of workflow processes. In practice, the current audit process is only carried out when an accident has occurred and only for certain purposes. The audit process is an important element of the CSMS because audit activities are carried out to review and evaluate the performance and effectiveness of the applicable safety management system.

5. Conclusion

In conclusion, the newly devised construction safety audit process facilitates early identification of deviations during the design phase. Given the escalating number of construction accidents, the implementation of construction safety audits has gained paramount importance. This audit process was developed by integrating principles from ISO 19011:2018 and Regulation of the Minister of Public Works and Housing Number 10 of 2021, resulting in an enhanced construction safety audit framework compared to the existing procedures. The findings revealed 34 activities in audit program management, 34 activities in audit implementation, and 32 sub-elements in audit criteria, all of which are integrated into the construction safety audit framework, systematically organizing audit processes and criteria.

This framework emphasizes that the improvement of construction safety performance extends beyond the construction phase to include the design phase. The audit results play a crucial role in continuous improvement efforts, aiming to enhance safety performance and prevent accidents in the construction industry. The analysis provided by auditors is deemed reliable when following this established audit process. The construction safety audit process framework was developed based on 21 causes of risk, leading to the identification of 37 risk responses. These responses translate into additional activities and new audit criteria, serving as a strategic approach to advancing standards in the construction safety audit process. The envisioned outcome of this construction safety audit process is an improvement in safety performance, particularly in the context of high-rise buildings using the design and build method. For future research, it is recommended to explore aspects such as the inclusion of responsible individuals and the assignment of value weights for each audit process and criterion. This suggests a shift towards a performance-based approach rather than solely adhering to conformance in construction safety audits.

6. Declarations

6.1. Author Contributions

6.2. Data Availability Statement

Data sharing is not applicable to this article.

6.3. Funding

6.4. Acknowledgements

6.5. Conflicts of Interest

The authors declare no conflict of interest.

7. References

[1] Ministry of Finance (2023). The Ministry of Finance of the Republic of Indonesia, Jakarta, Indonesia. Available online: https://www.kemenkeu.go.id/en/home (accessed on May 2023).

[2] People's Representative Council of the Republic of Indonesia. (2022). Law No. 3 of 2022 about State Capital. People's Representative Council of the Republic of Indonesia, Jakarta, Indonesia.

[3] Cheng, E. W. l., li, H., Fang, D. P., & Xie, F. (2004). Construction safety management: An exploratory study from China. Construction Innovation, 4(4), 229–241. doi:10.1108/14714170410815114.

[4] Hsu, D. J., Sun, Y. M., Chuang, K. H., Juang, Y. J., & Chang, F. L. (2008). Effect of elevation change on work fatigue and physiological symptoms for high-rise building construction workers. Safety Science, 46(5), 833–843. doi:10.1016/j.ssci.2007.01.011.

[5] Pinto, A., Nunes, I. L., & Ribeiro, R. A. (2011). Occupational risk assessment in construction industry - Overview and reflection. Safety Science, 49(5), 616–624. doi:10.1016/j.ssci.2011.01.003.

[6] JDIH. (2021). Regulation of Minister of Public Work and Housing Number 10 of 2021: Construction Safety Management System. Ministry of Public Work and Housing of the Republic of Indonesia, Jakarta, Indonesia.

[7] Robson, L. S., & Bigelow, P. L. (2010). Measurement properties of occupational health and safety management audits: a systematic literature search and traditional literature synthesis. Canadian Journal of Public Health, 101 Suppl 1, 1-7. doi:10.1007/bf03403844.

[8] Siddiquia, N. A., Madhwala, S., & Nandana, A. (2014). Assessment of Occupational Health, Safety & Environmental Problems in Chemical Industries of Uttarakhand. International Journal on OHS, Fire & Environment-Allied Science, 1(1), 020-022.

[9] Földešiová, D., Korenko, M., Ferancová, M., & Kaplík, P. (2013). Analysis of risk using FMEA. Advanced Materials Research, 801, 81–85. doi:10.4028/www.scientific.net/AMR.801.81.

[10] BS 8800. (2004). Occupational health and safety management systems - Guide. British Standard, London, United Kingdom.

[11] Nugroho, D. B., Latief, Y., Lestari, F., & Machfudiyanto, R. A. (2023). Development of the Knowledge Base Information System for Integrated Risk-Based Audit of High-Rise Buildings through Design-Build Method to Improve Construction Safety. International Journal of Safety and Security Engineering, 13(2), 267–275. doi:10.18280/ijsse.130209.

[12] Szymberski, R. T. (1997). Construction Project Safety Planning. Tappi Journal, 80(11), 69-74.

[13] Hwang, B. G., Shan, M., & Phuah, S. L. (2018). Safety in green building construction projects in Singapore: Performance, critical issues, and improvement solutions. KSCE Journal of Civil Engineering, 22(2), 447–458. doi:10.1007/s12205-017-1961-3.

[14] ILO. (2014). Safety and health in the construction sector – overcoming the challenges. International Labour Organization (ILO), Geneva, Switzerland. Available online: https://www.ilo.org/empent/Eventsandmeetings/WCMS_310993/lang--en/index.htm (accessed on February 2024).

[15] Chiang, Y.-H., Wong, F. K.-W., & Liang, S. (2018). Fatal Construction Accidents in Hong Kong. Journal of Construction Engineering and Management, 144(3), 4017121. doi:10.1061/(asce)co.1943-7862.0001433.

[16] Ivascu, L., & Cioca, L. I. (2019). Occupational accidents assessment by field of activity and investigation model for prevention and control. Safety, 5(1), 12. doi:10.3390/safety5010012.

[17] Suraji, A., Duff, A. R., & Peckitt, S. J. (2001). Development of Causal Model of Construction Accident Causation. Journal of Construction Engineering and Management, 127(4), 337–344. doi:10.1061/(asce)0733-9364(2001)127:4(337).

[18] Behm, M. (2005). Linking construction fatalities to the design for construction safety concept. Safety Science, 43(8), 589–611. doi:10.1016/j.ssci.2005.04.002.

[19] Gambatese, J. A. (2008). Research Issues in Prevention through Design. Journal of Safety Research, 39(2), 153–156. doi:10.1016/j.jsr.2008.02.012.

[20] Vasconcelos, B., & Junior, B. B. (2015). The Causes of Work Place Accidents and their Relation to Construction Equipment Design. Procedia Manufacturing, 3, 4392–4399. doi:10.1016/j.promfg.2015.07.437.

[21] Tymvios, N., & Gambatese, J. A. (2016). Perceptions about Design for Construction Worker Safety: Viewpoints from Contractors, Designers, and University Facility Owners. Journal of Construction Engineering and Management, 142(2), 4015078. doi:10.1061/(asce)co.1943-7862.0001067.

[22] Li, Z. (2010). Highway work zone safety audits for safety improvements. Engineering, Construction and Architectural Management, 17(5), 512–526. doi:10.1108/09699981011074592.

[23] Alruqi, W. M., & Hallowell, M. R. (2019). Critical Success Factors for Construction Safety: Review and Meta-Analysis of Safety Leading Indicators. Journal of Construction Engineering and Management, 145(3), 4019005. doi:10.1061/(asce)co.1943-7862.0001626.

[24] Safe Work Australia. (2013). The effectiveness of work health and safety interventions by regulators: A literature review. Safe Work Australia Website, Canberra, Australia. Available online: https://www.safeworkaustralia.gov.au/resources-and-publications/reports/effectiveness-work-health-and-safety-interventions-regulators-literature-review (accessed on May 2023).

[25] Wedemeyer, P. D. (2010). A discussion of auditor judgment as the critical component in audit quality- A practitioner's perspective. International Journal of Disclosure and Governance, 7(4), 320–333. doi:10.1057/jdg.2010.19.

[26] Mourougan, S. (2015). Planning Integrated Management System audit to ensure Conformance, Consistency and Continual Improvement. OSR Journal of Business and Management (IOSR-JBM), 17(10), 41-53.

[27] Power, M. (1997). The audit society: Rituals of verification. OUP Oxford, Oxford, United Kingdom.

[28] ISO 19011: 2018. (2018). Guidelines for Auditing Management Systems, International Organization for Standardization (ISO), Central Secretariat, Geneva, Switzerland.

[29] DPR. (2021). Implementing Regulations for Law Number 28 of 2002 concerning Buildings. Government of the Republic of Indonesia, Jakarta, Indonesia. (In Indonesian).

[30] BPIW. (2020). Regulation of Minister of Public Work and Housing Number 1 of 2020: Standards and Guidelines for Procurement of Integrated Design and Build Construction Work through Suppliers. Ministry of Public Work and Housing of the Republic of Indonesia, Jakarta, Indonesia.

[31] Nikulina, M. E., Gorobtsov, D. N., & Pendin, V. V. (2017). Engineering and Geological Audit in Design and Construction of Linear Transport Facilities. Procedia Engineering, 189, 70–74. doi:10.1016/j.proeng.2017.05.012.

[32] Nugroho, D. B., & Latief, Y. (2023). A Conceptual Framework for Knowledge Management of Integrated Design and Construction Phase Audit Process on Infrastructure Project Based on Risk, Using WBS, BIM and Web to Enhance Construction Safety Performance. Proceedings of the International Conference on Industrial Engineering and Operations Management, 1129-1139. doi:10.46254/na07.20220268.

[33] Mitropoulos, P., Abdelhamid, T. S., & Howell, G. A. (2005). Systems model of construction accident causation. Journal of construction engineering and management, 131(7), 816-825. doi:10.1061/(ASCE)0733-9364(2005)131:7(816).

[34] Dorji, K., & Hadikusumo, B. H. (2006). Safety management practices in the Bhutanese construction industry. Journal of Construction in Developing Countries, 11(2), 53-75.

[35] Jazayeri, E., & Dadi, G. B. (2017). Construction safety management systems and methods of safety performance measurement: A review. Journal of Safety Engineering, 6(2), 15-28.

[36] Sharma, S. K., & Swain, N. (2011). Risk Management in Construction Projects. Asia Pacific Business Review, 7(3), 107–120. doi:10.1177/097324701100700310.

[37] Yiu, N. S. N., Sze, N. N., & Chan, D. W. M. (2018). Implementation of safety management systems in Hong Kong construction industry – A safety practitioner's perspective. Journal of Safety Research, 64, 1–9. doi:10.1016/j.jsr.2017.12.011.

[38] Yiu, N. S. N., Chan, D. W. M., Shan, M., & Sze, N. N. (2019). Implementation of safety management system in managing construction projects: Benefits and obstacles. Safety Science, 117, 23–32. doi:10.1016/j.ssci.2019.03.027.

[39] Barretto, C. R., Drumond, G. M., & Méxas, M. P. (2022). Remote audit in the times of COVID-19: a successful process safety initiative. Brazilian Journal of Operations and Production Management, 19(3), 20221309. doi:10.14488/BJOPM.2021.048.

[40] von der Heyde, A., Brandhorst, S., & Kluge, A. (2015). The impact of safety audit timing and framing of the production outcomes on safety-related rule violations in a simulated production environment. Safety Science, 77, 205–213. doi:10.1016/j.ssci.2015.03.021.

[41] Yin, R. K. (2009). Case study research: Design and methods. SAGE, Newcastle upon Tyne, United Kingdom.

[42] Clayton, M. J. (1997). Delphi: A technique to harness expert opinion for critical decision-making tasks in education. Educational Psychology, 17(4), 373–386. doi:10.1080/0144341970170401.

[43] Ho, Y. F., & Wang, H. L. (2008). Applying fuzzy Delphi method to select the variables of a sustainable urban system dynamics model. Proceedings of the 26th international conference of system, 20-24 July, 2008, Athens, Greece.

[44] Dewi, A., Latief, Y., & Sagita, L. (2020). Activity and risk identification in audit process on integrated management system to increase performance efficiency of construction services organization in Indonesia. IOP Conference Series: Earth and Environmental Science, 426(1), 012014. doi:10.1088/1755-1315/426/1/012014.

[45] Hallowell, M. R., & Gambatese, J. A. (2010). Qualitative Research: Application of the Delphi Method to CEM Research. Journal of Construction Engineering and Management, 136(1), 99–107. doi:10.1061/(asce)co.1943-7862.0000137.

[46] Hasson, F., Keeney, S., & McKenna, H. (2000). Research guidelines for the Delphi survey technique. Journal of Advanced Nursing, 32(4), 1008–1015. doi:10.1046/j.1365-2648.2000.t01-1-01567.x.

[47] Wolff, K., Larsen, S., & Øgaard, T. (2019). How to define and measure risk perceptions. Annals of Tourism Research, 79, 102759. doi:10.1016/j.annals.2019.102759.

[48] Loewenstein, G. F., Hsee, C. K., Weber, E. U., & Welch, N. (2001). Risk as Feelings. Psychological Bulletin, 127(2), 267–286. doi:10.1037/0033-2909.127.2.267.

[49] Slovic, P. (2016). The Perception of Risk. Routledge, London, United Kingdom. doi:10.4324/9781315661773.

[50] Yiu, N. S. N., Chan, D. W. M., Sze, N. N., Shan, M., & Chan, A. P. C. (2019). Implementation of safety management system for improving construction safety performance: A Structural Equation Modelling approach. Buildings, 9(4), 89. doi:10.3390/buildings9040089.
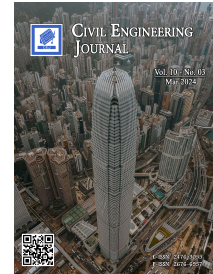
Strength and Deformability of Structural Steel for Use in Construction

Begman Kulbayev [1] , Vladimir Lapin [1*] , Alexandr Shakhnovich [1] , Yeraly Shokbarov [1] ,
Tursymbai Tuleyev [1] , Serik Aldakhov [1] , Yerken Aldakhov [1] , Alimzhan Ali [1]

[1] Kazakh Research and Design Institute of Construction and Architecture JSC, 21 Solodovnikova, Almaty, Kazakhstan.

Abstract

The purpose of the study is an experimental determination of the stress-related characteristics of the structural steel produced in the Republic of Kazakhstan for use in conventional and earthquake-resistive construction. Since 2015, the construction industry has been using European regulatory documents—Eurocodes—as a statutory framework. In particular, the Eurocode 1993 for steel structures and the Eurocode 1998 for the design of earthquake-resistant structures However, the study of stress-related properties of structural steel using experimental methods of ISO standards has not been performed. Therefore, in the construction industry of the Republic of Kazakhstan, steel-work structures have been used in fairly limited volume since 2015. The experimental studies were conducted on 7 types of structural steel with thicknesses of 8, 10, and 20 mm manufactured by Arcelor Mittal. The yield strength, ultimate tensile strength (breaking stress), and tensile strength at break were studied. The experimental studies were carried out on the basis of ISO standards. In each test run, 5 samples were used. In two series, 20 samples each were tested, which made it possible to estimate the yield strength and strength distribution functions. The correlation relationships between Brinell hardness and yield and strength limits have been studied. As a result of experimental studies, it was found that the strength and deformability parameters fully comply with the requirements of Eurocode 1993. Based on the application of the Student's test, it is revealed that the distribution functions of yield strength and resistance correspond to the normal law (Gaussian function). The calculation of a three-story, two-span residential building with box section columns for construction in an area with a seismicity of 8 points is performed by the finite element method. The work results will significantly increase the scope of Kazakhstani structural steel use in seismic and conventional areas of the Republic of Kazakhstan.

Keywords: Yield Strength; Tensile Strength; Steel Hardness; Construction Steel; Eurocode; Relative Rupture Strain.

1. Introduction

The steelwork structures meet the main requirements of construction – industriality, reduction of the volume and duration of construction works, low construction costs. Steelwork structures are widely used in construction practice, including high-rise construction. The experience in the application of steel structures in the construction industry is detailed in Vedyakov et al. [1]. The issues of the selection of steel structure materials with respect to the present-day regulatory and operational requirements and capabilities of global and domestic metallurgical production are considered in detail. Among rather actual studies, it stands to mention the theory of application of constructions from rolled steel of large thickness, the methodology of quality assessment of plates, and its work features in constructions [2]. The dependences of properties of heavy-thickness sheets and alloying, heat treatment, and peculiarities of production are analyzed. The steel performance in the fabrication and operation of structures is described. The properties of new-generation steels for large-thickness rolled products are discussed. Examples of the application of these materials in the latest unique structures are provided.

One of the latest achievements is the study of modular steel-framed high-rise buildings [3]. A module connection to the main wall to assemble modules into a main wall system plays a key role in load transfer in modular high-rise buildings. In the Republic of Kazakhstan, the application of such systems seems to be very promising. However, its mechanical mechanisms have not been systematically studied. This study proposes an innovative module connection to the main wall that can be installed and detached with good feasibility and efficiency during the construction and dismantling process.

The structural steel has the ability to resist alternating loads. The steel-framed buildings are therefore highly earthquake-resistant. In the study of Gioncu & Mazzolani [4], this is demonstrated by the example of different types of steel-frame buildings. The steel-frame buildings suffer noticeable earthquake damage, usually when there are obvious design errors. They behave well under repeated earthquake effects (aftershocks), as shown in the study [5]. Even with the most unfavorable long-period ground vibration, it is possible to develop structural solutions to ensure the seismic resistance of the building [6]. They have a plastic reserve, which allows them to successfully resist seismic impact [7]. The effect of enclosing structures on the structural steel frame response has been studied [8].

In order to use constructional steel for the design and manufacture of building structures, it is always necessary to perform a cycle of experimental studies to determine the stress-related properties of steel. Mechanical performance of structural steel, i.e., values characterizing its strength, plasticity, elasticity, and elastic constants, necessary for material selection and calculations of designed structural components, is determined by mechanical testing of standard specimens under load made of the steel types under study [9–12]. At that point, experimental studies should use the appropriate standards governing test methodologies.

Mechanical tensile testing is one of the most important types of engineering tests used for all metallic materials, which determines the material's performance. In the study of Vaz-Romero et al. [9], experiments were performed on PC52 steel samples (0.22% C) using the INSTRON 8801 universal testing machine to determine yield strength, tensile strength, strain at break, and Young's modulus. The strain rates used during the tests were within the range typical of static tensile tests as recommended in ASTM Standard E8/E8M-16a and ISO 6892-1:2016, as is typical for steel testing.

In the study of Wang & Kodur [10], the tensile tests were conducted using specimens with six different design lengths ranging from 20 mm to 140 mm, which were tested over a wide range of loading velocities from 1 m/s to 7.5 m/s. The experimental studies were also described by a mathematical model based on the finite element method. It was found that there is a strong correlation between the applied velocity and the gauge length of a specimen.

The mechanical properties of steel are important not only for evaluating the behavior of individual steel elements but also for predicting the performance of the entire structure [11]. When exposed to fire, the mechanical properties of steel deteriorate with increasing temperature. The mechanical degradation depends on the exposure temperature. In practice, degradation represents the mechanical property reduction factor recommended by specific effective design standards. The tensile properties of multilayer samples are reviewed in the study of Yang & Lin [12]. The challenging task of studying the mechanical properties of high-tensile steel samples exposed to high temperatures during welding is discussed in the study of Gardnerand & Nethrcott [13].

Therefore, mechanical tensile testing is a fairly universally applicable approach to studying the strength and deformability characteristics of structural steel. In this paper, we set the task of determining the characteristics of strength and deformability of structural steel produced by Kazakhstani plants, in particular the Arcelor-Mittal plant in Temirtau, Kazakhstan. It is necessary to determine the yield strength, tensile strength (tensile strength), and relative rupture strain. In this respect, test and sample preparation methods shall comply with the requirements of Eurocode 1993 in accordance with the relevant ISO standards: ISO 6892-1:2016 "Metallic Materials. Tensile Testing. Part 1. Method of Test at Room Temperature" and ASTM E8/E8M-16a "Standard Test Methods for Tensile Testing of Metallic Materials". These two standards specify that tensile testing for the above material characteristics shall be conducted at strain rates in the range of 10-5 s-1 to 10-3 s-1, depending on the material performance and the test method used.

It should be noted that in this statement, this task is extremely relevant. The solution to this problem will allow the steel structures to be widely used again within the Republic of Kazakhstan, the regulatory framework for construction of which, since 2015, is based on the application of Eurocodes.

Over 45% of the territory of the Republic of Kazakhstan falls within the seismically active areas, in this respect, the significant area is occupied by extremely seismically hazardous zones of 8–9 and over points on the MSK-64 scale. Therefore, solving this problem will renew the use of steel construction in seismic areas. Consequently, the cycle of studies regarding the use of Kazakhstan steel under the pressing issue of verifying the requirement of compliance with the characteristics of Kazakhstan steel Eurocode 1993 [14], started in Kazakhstan by the work of Kulbayev et al. [15, 16], will be continued. Previously, such a task was not solved in the Republic of Kazakhstan. It should be noted that the Russian Federation has also started harmonizing its regulations with foreign standards [17].

The minimum plasticity of steel shall be expressed by the ceiling limits of the following values:

- f_u/f_y – ratio of the minimum tensile strength f_u to the minimum yield strength f_y;
- Relative elongation after rupture of the sample length $5.65\sqrt{A_0}$ (where A_0 – original cross-sectional area);
- Critical strain ε_u, corresponding to the ultimate strength f_u.

The following values are recommended:

$$f_u/f_y, \geq 1.10 \qquad (1)$$

Relative elongation after rupture not less than 15%: $\qquad (2)$

$$\varepsilon_u > 15\,\varepsilon_y, \text{ where } \varepsilon_u - \text{elastic strain } (\varepsilon_y = f_y/E, \text{ Young's module}) \qquad (3)$$

The above relations should be verified by experiment.

For the case of National Annexes, condition (1) is stiffened:

$$f_u/f_y, \geq 1.30 \qquad (4)$$

Therefore, it is necessary to address the following objectives:

- The most used steel grades in the Republic of Kazakhstan need to be experimentally investigated to determine compliance with Eurocode 1993 (1)-(3) and National Annexes (4) requirements;
- To clarify requirements (4) based on the experimental studies performed;
- To establish correlations between the Brinell hardness BH and the above strength and deformability characteristics.
- To evaluate the feasibility of using Kazakhstani structural steel in earthquake-resistant construction.

Such tasks have not been investigated before.

2. Methods and Objects

The types of steel most commonly used in the Republic of Kazakhstan have been selected for experimental studies of construction steel. A batch of 8, 10, and 20 mm-thick structural steel with certificates of conformity from ARCELOR-MITTAL (Kazakhstan, Temirtau), AMET, and several metallurgical plants was obtained under the sponsorship of IMSTALCON JSC (constructional ironworks in Taraz). Table 1 shows the steel manufacturer, thickness in mm, and grade. The manufacturing and testing of samples were carried out according to GOST 6696-66, ISO 4136-89, ISO 5173-81, and ISO 5177-81. The mechanical tensile testing of structural steel specimens was carried out using a UMM-5 tensile machine with a calibration certificate dated February 24, 2023. The tensile machine is accredited for testing according to the test requirements of ST-RK ISO. In each test run, 5 specimens of 8–20 mm thickness were used (St3Sp5, 09G2S). These are the most common steel grades in the Republic of Kazakhstan. The processing of experimental data was carried out using the MATLAB mathematical package.

Table 1 shows the main stress-related properties of steel with indications of manufacturer, grade, and plate thickness taken according to the certificate information.

Table 1. Mechanical performance of structural steel

No.	Manufacture	Grade	Section, mm	Ultimate strength	Yield stress	Impact strength, J/cm²		Impact strength after aging	Elongation, %
						KCU	KCV		
1	Arcellor-Mitall	St3Sp5	8	459	316	−20°C 78	+20°C 147	KCU, +20 65	–
2	Arcellor-Mitall	St3Sp5	10	475	320	−20°C 50– 81– 69	+20°C 176– −183 −184	KCU 69– 73– 61	32
3	Arcellor-Mitall	09G2S	8	530	420	−40°C 125 120	–	+20 115 95	29
4	Arcellor-Mitall	09G2S	10	540	440	−40°C 92 92	–	+20 61 64	30
5	Amet, Ashinskiy Metallurgical Works	St3Sp5,SV	20	440–445	285–290	−20°C 49–67	+20°C 65– 85	56–76	31 31
6	Amet, Ashinskiy Metallurgical Works	09G2S	20	520–525	360–365	40 100–95	–	65–80	28 29
7	Severstal, Cherepovets	St3Sp50	10	400	245	152.7	216	187.3	32

For structural steel samples from Table 1, the value of impact strength at -20 °C is not less than 49 J/cm², which exceeds the Eurocode requirement of 34 J/cm². This is understandable; the climatic conditions in Kazakhstan and the Russian Federation are quite severe. In the production of structural steel, the factor of cold resistance (cold brittleness) of metal structures has always been taken into account.

Table 2 analyzes the ratio of tensile strength to yield strength (4). It is found that it is performed in all cases except for 09G2S-grade steel. It is known that the certificate records the minimum value of the parameter determined for the entire batch. Therefore, these 2 sheets of steel must certainly be tested.

Table 2. Strength characteristics of steel according to certificates

No.	Ultimate strength, MPa	Yield strength, MPa	Ratio (4)
1	459	316	1.45
2	475	320	1.48
3	530	420	1.26
4	540	440	1.23
5	440–445	285–290	1.54-1.53
6	520–525	360–365	1.44
7	400	245	1.63

The elongation after rupture is approximately 2 times the requirements of Eurocode 93. It should be noted that the sample of structural steel No. 7 from Table 1 is characterized by very qualitative characteristics: the highest tensile strength to yield strength ratio and the high impact strength of the new material after aging. Therefore, to verify conditions (1) and (4), experimental studies on mechanical tensile testing of Kazakhstan-made structural steel samples shall be conducted in accordance with ISO standards.

3. Results

3.1. Experimental Studies

Tensile tests of structural steel samples were carried out using the experimentation facility of SAPA INTERSYSTEM LLP. The sample size complies with the requirements of the ISO 6892-1-2010 standard. The tensile strength, yield strength, and relative elongation after rupture have been determined. The UMM-5 tensile testing machine with a calibration certificate dated February 24, 2023, was used in the tensile strength test. The organization is accredited for testing according to the test requirements under the ST-RK ISO. Figures 1 and 2 show the specimens prepared for testing and after testing.

Figure 1. Samples before testing

Figure 2. Samples after testing

Tables 3 to 5 summarize the probability characteristics of 7 series of tests with 5 samples in each of them. Table 6 summarizes the results of the calculations for testing criterion (4) in view of experimental data and using the certificate data from Table 1.

Table 3. Probabilistic characteristics of yield strength, MPa

No.	Sample average	Median value	Standard	Coefficient of variation
1	326.4	326.6	1.08	0.003
2	293.2	293.2	4.64	0.016
3	454.6	455.0	4.26	0.009
4	446.1	455.0	21.85	0.050
5	317.4	317.3	17.34	0.054
6	451.3	460.3	22.11	0.049
7	270.2	278.3	14.56	0.054

Table 4. Probabilistic values of tensile strength, MPa

No.	Sample average	Median value	Standard	Coefficient of variation
1	467.4	467.4	2.14	0.005
2	457.6	457.3	4.32	0.009
3	577.8	577.1	1.50	0.003
4	545.6	544.5	3.89	0.007
5	475.2	484.7	24.92	0.052
6	563.1	574.5	28.93	0.051
7	461.9	466.5	24.87	0.054

Table 5. Probabilistic values of relative elongation at break, %

No.	Sample average	Median value	Standard	Coefficient of variation
1	32	32	0.71	0.022
2	34	34	1.0	0.029
3	30.2	30	1.1	0.036
4	36.0	36	0.71	0.020
5	30.4	30	2.07	0.068
6	29	29	1.22	0.042
7	37	37	1.58	0.043

The analysis of Table 6 shows that for the 09G2S steel, the Eurocode requirement in terms of National Annexes is not fulfilled. This also comes out of the results of the calculation using certificate data, where for 09G2S steel, in two cases out of three, the ratio 4 is also not fulfilled. It should be noted that the estimates from experimental data and certification results are very close, except for 1 case.

Table 6. Characteristics from correlations (3) according to experimental and certificate data

No.	According to experimental data	Data from the certificates
1	1.43	1.45
2	1.36	1.48
3	1.27	1.26
4	1.22	1.23
5	1.50	1.54-1.53
6	1.25	1.44
7	1.71	1.63

In terms of relative elongation after rupture, the Eurocode 93 conditions are fulfilled for all steel grades, including 09G2S steel.

Therefore, it can be said that experimental information indicates compliance of strength and deformation characteristics of Kazakhstan steel with Eurocode requirements (1). The above results are obtained from 5 tests for each type of steel. Additional tests should be carried out (Section 3.2). Note also that condition (3) is always fulfilled due to high deformability of the Kazakhstani steel.

3.2. Testing of Two Series of Samples

Additional studies of two types of structural steel st3sp5 and 09G2S with a thickness of 10 mm were carried out under the experimentation facility of scientific centre of SAPA INTERSYSTEM LLP. In each test, 20 samples prepared according to ST RK EN standards were used. The tests were performed using ST RK ISO 0892-1-2017. This number of samples is the minimum necessary for statistical measurements.

The purpose of the study was to clarify correlation (3) and to estimate the probability distribution function of strength and deformability parameters of domestic construction steel (Section 4). This is performed as required by the Eurocode 1990, where it is proposed to determine the correspondence to one of the two distributions - normal or lognormal. Using the distribution function, it is possible to obtain the estimated values of strength and deformability characteristics with the necessary reliability.

Tables 7 and 8 set out the test results - values of relative elongation, yield strength and ultimate tensile strength.

Table 7. Values of strength and deformability parameters of St3Sp5 steel

Sample number	Elongation at break, %	Yield strength, MPa	Ultimate tensile strength (breaking stress), MPa	Ratio (3)
1	29	276.0	443.1	1.61
2	29	277.5	446.4	1.61
3	28	268.8	450.8	1.68
4	28	274.0	455.9	1.66
5	27	291.7	463.0	1.59
6	28	285.1	452.9	1.58
7	28	280.2	448.4	1.60
8	29	266.3	438.7	1.65
9	27	273.1	461.6	1.69
10	29	273.9	439.4	1.60
11	29	269.3	440.1	1.63
12	29	273.0	443.1	1.62
13	28	279.8	449.8	1.61
14	27	291.4	462.6	1.59
15	29	275.1	445.4	1.62
16	27	271.2	457.6	1.69
17	27	274.5	459.3	1.67
18	27	275.7	464.7	1,69
19	28	275.3	447.6	1.63
20	28	283.3	449.7	1,59
Average	28.05	276.8	451.0	1.63
Median value	28	275.2	449.8	1.63
Standard	0.83	6.82	8.34	
Coefficient of variation	0.03	0.03	0.02	

Pay attention to the significant adjustments to the values of the strength-to-ductility ratio. If for the 09G2S high-strength steel on a sample of 5 elements this value is 1.23, then considering the results from Table 8 this value is already 1.29. A similar change for St3Sp5 steel (Table 7) from 1.54 to 1.63. This indicates the insufficiency of 5 tests for correct determination of stress-related properties of structural steel.

The ratio (4) is practically fulfilled or will be fulfilled with further increase in the number of tests. Consequently, the requirement of the National Annexes for 09G2S steel will obviously be met if requirement (4) is slightly reduced $f_u/f_y, \geq 1.29$.

Table 8. Values of strength and deformability parameters of 09G2S steel

Sample number	Elongation at break, %	Yield strength, MPa	Ultimate strength, MPa	Ratio
1	26	449.5	581.6	1.29
2	26	461.7	585.4	1.27
3	26	454.3	588.0	1.29
4	26	465.9	585.0	1.26
5	26	457.2	585.2	1.28
6	27	440.7	576.9	1.31
7	26	460.2	585.0	1.27
8	26	450.9	582.2	1.30
9	27	458.8	579.2	1.26
10	26	453.2	587.0	1.30
11	27	442.0	579.0	1.31
12	27	460.9	577.9	1.25
13	28	441.6	574.3	1.30
14	30	440.2	564.3	1,28
15	30	428.9	561.6	1.31
16	30	429.5	563.9	1.31
17	27	458.8	578.8	1.26
18	28	439.9	573.8	1.30
19	30	430.8	564.2	1.29
20	27	445.7	576.8	1.29
Average	27	448.54	577.51	1.29
Median value	27.2	450.2	578.90	1.29
Standard	1.53	11.42	8.25	-
Coefficient of variation	0.06	0.025	0.014	-

3.3. Calculations of Building Fragment

The calculable building represents a framed metal structure with rigid disks of slabs and coverings in the form of reinforced concrete monolithic slab. The building sizes in the longitudinal direction are 24 m. The dimensions of the building transversely are 12 m. The dimensions of building between the axes are 6 m each. The building has 3 floors 3 m high. The frame stiffness in cross direction is ensured by rigid pinching of the main columns of the frame in the foundation. The spatial stability of the frame elements is ensured by a system of longitudinal and transverse metal beams and monolithic reinforced concrete slabs 200 mm thick made of B25 grade concrete.

The columns are designed from 250×8 composite boxes on the outer contour and 250×10 and 250×8 composite boxes on the inner contour. The beams are I-beams 25B1, 20B1, 18B1. Steel grade S255 STO ASCHM 20-93.

3.4. Comparative Analysis

- The calculations of a 3-storey building with metal frame work according to SNiP RK 2.03-30-2006 and NTP RK 08-01.5-2013 have been performed. The calculation was carried out on the basis of numerical method of FEA in displacements using the "LIRA-SADP 2022 R2.1" software package. The calculation was performed under the requirements of I and II limit states and accidental limit state for seismic impacts.

- The periods of the first and second forms of eigen oscillations, determined by the standards of SNiP RK 2.03-30-2006 T1=0,58s and T2=0,56s differ from those obtained according to the norms of NTP RK 08-01.5-2013, which are T1=1.01s and T2=0.94s, accordingly.

- Distortions of the 1st, 2nd and 3rd floors from seismic impact along the X Δ_κ axis varies from 0.0042m to 0.00697 m, that meets the condition (5.12) SNiP RK 2.03-30-2006, which is Δ_κ = 0.15m.

- Distortions of the 1st, 2nd and 3rd floors from seismic impact along the U Δ_κ axis varies from 0.0061m to 0.0083 m, that meets the condition NTP RK 08-01.5-2013, which is Δ_κ = 0.15m.

Therefore, transition to calculations of load-bearing metal structures of the building under SP RK EN 1998-1:2004/2012 "Design of structures for earthquake resistance - Part 1: General rules, seismic actions and rules for

buildings" and NTP RK 08-01.5-2013 results in moderate increase in consumption of materials, increases the reliability of the building as a whole.

4. Discussion

The correlation analysis of the results of experimental studies of mechanical tests was performed using the Scilab and MATLAB mathematical packages.

Linear correlation test is performed;

$$BH = A \times x + b \tag{5}$$

where x is one of the parameters - yield strength, tensile strength, relative strain at rupture. Table 9 offers three variations of the coefficients of the Equation 5. The first line of each parameter corresponds to steel St3Sp5, and the second - 09G2S. The values of correlation coefficients are also given here. Figures 3 to 5 show the correlation dependencies from Table 9.

Table 9. Parameters of linear correlation functions

Variant	Name	A	b	Correlation Coefficient	Note
1	Yield strength	0.1635	94.5384	0.61	7 points (STAT software module)
		0.1741	90.3511	0.63	
	Tensile strength	0.2720	15.9195	0.73	
		0.2945	5.5695	0.75	
	Relative rupture strain	-1.9401	213.29	-0.28	
		-0.4507	167.95	-0.07	
2	Yield strength	0.1514	101.54	0.57	5 points without special steel (STAT1 software module)
		0.1682	94.49	0.59	
	Tensile strength	0.2359	36.546	0.67	
		0.2523	29.164	0.64	
	Relative rupture strain	-3.8024	272.25	-0.32	
		-3.6448	271.97	-0.42	
3	Yield strength	0.2068	88.100	0.86	5 points without a thickness of 20 mm (STAT2 software module)
		0.2202	82.744	0,88	
	Tensile strength	0.3078	5.649	0.92	
		0.3699	-23.937	0.96	
	Relative rupture strain	-2.5725	241.116	-0.46	
		-2.2841	238,894	-0.29	
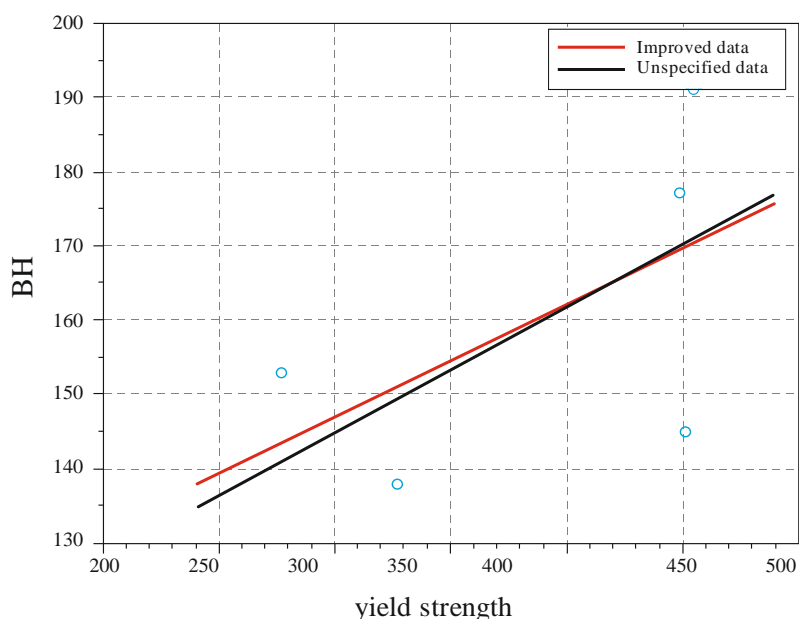
Figure 3. Correlation dependencies between yield strength and Brinell hardness (variant 3)
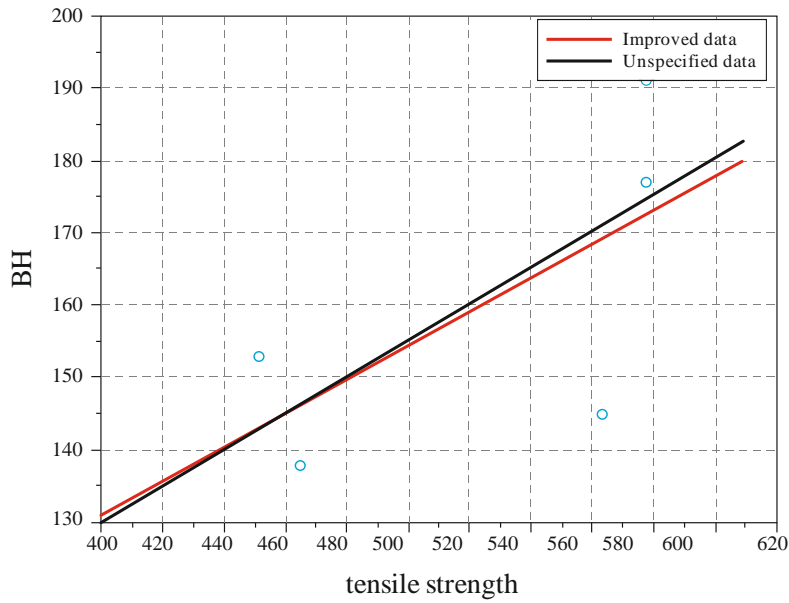
Figure 4. Correlation dependencies between tensile strength and Brinell hardness (variant 3)
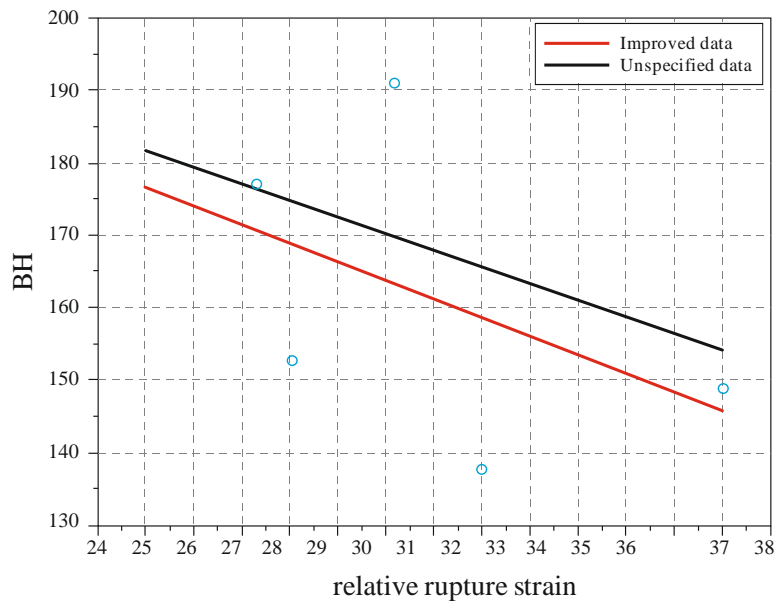
Figure 5. Correlation dependencies between relative rupture strain and Brinell hardness (variant 3)

Note that the characteristics of strength and deformability of structural steel are most accurately determined in the 3rd variant of the parameters of the linear correlation function. This is determined by the fact that the sample is the most homogeneous - 20 mm thick steel sheets are excluded. Therefore, for 8-10 mm thick steel sheets, stress-related properties should be determined according to the 3rd variant of parameters.

For example, for yield strength of steel St3Sp5

$$BH = 0.2068 * x + 88.100 \qquad (6)$$

For the tensile strength of steel St3Sp5

$$BH = 0.3078 * x + 36.546 \qquad (7)$$

For tensile strength at break of the steel St3Sp5

$$BH = 2.5725 * x + 241.116 \qquad (8)$$

By solving the above equations with respect to BH, it is possible to determine values of yield strength, tensile strength, relative strain at break by values of BH. It is possible to determine these characteristics from Figures 3 to 5 by setting the value of BH hardness.

The strongest correlation between the Brinell hardness values and tensile strength and yield strengths values (variant 3, Table 9). The correlation between the tensile strength at break and Brinell hardness values is weaker, but is available. These results are quite substantial. For simple hardness tests according to Equation 1 and coefficients from Table 9, it is possible to approximate the values of yield strength and tensile strength, as well as the values of tensile strength at break.

To estimate the distribution function of strength and deformation parameters, we will use Student's test.

For the yield strength case, the probability value p=0.845, which is close to the theoretical p =0.8156 (Figure 6). Therefore, it can be considered, a hypothesis for normality cannot be rejected. The distribution function of tensile strength corresponds to the normal distribution to a lesser extent, relative rupture strain - does not correspond to the normal distribution at all.
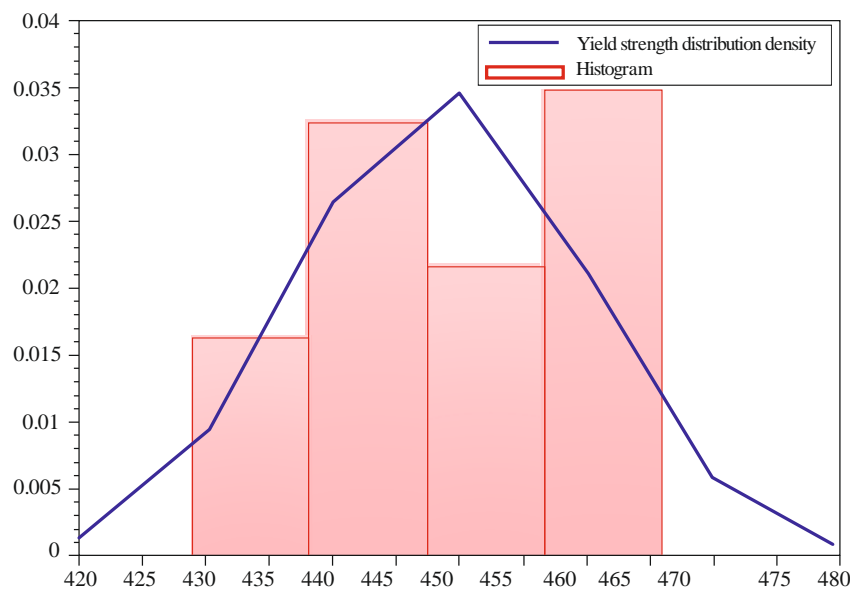

Figure 6. Yield strength distribution density

If we know the distribution function, e.g. yield strength, it is possible to determine estimated values at a given reliability.

The results of this work will contribute to the return to extensive use of steel structures in earthquake-resistant construction in the Republic of Kazakhstan. Following the introduction of a new statutory framework based on the Eurocode in 2015, the use of steel structures in seismic areas has practically stopped. It was not known whether the strength and deformation characteristics of Kazakhstani structural steel meet the requirements of the Eurocode. Whether such steel could be used in earthquake-resistive construction. At that, earthquakes with intensity up to 10 points are possible within the territory of Almaty city area [18-20], at least 40% of areas in the territory of the Republic of Kazakhstan are earthquake prone [21].

Although before 2015, steel structures have been widely used in the practice of earthquake-resistant construction even in 9-point regions. The earthquake focuses take place even within the territory of Almaty city [19]. For example, the 11-storey steel-framed building in Almaty, located at a distance of 1 km from the tectonic fault in the city, was designed in 1970 [22]. The station of engineering and seismometric service was installed on the building.

Different types of steel structures are used in seismic areas [23-26]. The use of steelwork structures is particularly attractive in high-rise construction [24]. In Gioncu & Mazzolani [4] performance f buildings with metal framing in various earthquakes is analyzed. It is noted that with the right design solution, the building successfully resists seismic impact. In this respect, attention should be paid to the rational design of butt joints [27]. It has been established that when designing steel-framed buildings, it is useful to use various damping devices [28], including the hydraulic dampers [29], as well as the brand new double dampers [30].

Therefore, the results of this work will allow designing steel structures for construction in earthquake-prone areas of the Republic of Kazakhstan, particularly, based on latest achievements in the area of optimal methods of calculation of such structures [31].

5. Conclusion

The main output of work is that structural steel produced by Arcelor-Mittal fully complies with the requirements of Eurocode 1993 and National Annexes in terms of yield strength, breaking stress (tensile strength), and relative strain at break. For National Annexes, it is proposed to correct the ratio of strength and yield strength to be equal to not less than 1.23. The tensile strength at break significantly exceeds the requirements of the Eurocode. Such results were obtained for the first time. With that, the local steel has high impact toughness characteristics, which allows structural steel to be used for construction in the northern regions of the Republic of Kazakhstan with temperatures down to -40 degrees. The calculation under Eurocode 1998 of the fragment of a frame building with closed columns at 8-point seismic impact. In this respect, the column misalignment limits are not exceeded, suggesting the design capability for steel frames of earthquake-resistant buildings in seismically active regions. The use of local structural steel will reduce the cost of earthquake engineering costs by reducing the cost of transportation costs (logistics). The wide use of steel structures in earthquake-resistant construction in areas with a seismicity of 9 points is expected in Almaty, Kazakhstan, where earthquakes with magnitudes over 8 have occurred (the Keminskoye earthquake of 1911).

The correlation dependences between the Brinell hardness of metal and values of yield strength, strength, and tensile strength at break were obtained for Kazakhstan steel for the first time. Hardness is a fundamental property of the near-surface layer of a material, which is determined experimentally quite simply. Through the hardness value, it is possible to pass to the values of impact strength. The specified empirical dependencies can be used for the operational determination of stress-related properties of structural steel, for example, when performing survey work. The estimation of the distribution function by the Student's test, which can be taken as normal, is performed for the yield strength and tensile strength.

6. Declarations

6.1. Author Contributions

Conceptualization, B.K., V.L., A.S., Y.S., T.T., S.A., Y.A., and A.A.; methodology, B.K., V.L., A.S., Y.S., T.T., S.A., Y.A., and A.A.; investigation, B.K. and V.L.; writing—original draft preparation, B.K., V.L., A.S., Y.S., T.T., S.A., Y.A., and A.A.; writing—review and editing, B.K., V.L., A.S., Y.S., T.T., S.A., Y.A., and A.A. All authors have read and agreed to the published version of the manuscript.

6.2. Data Availability Statement

The data presented in this study are contained within the article.

6.3. Funding

6.4. Acknowledgements

6.5. Conflicts of Interest

The authors declare no conflict of interest.

7. References

[1] Vedyakov, I., Odessky, P.D., Konin, D.V., Egorova, A.A. (2015). Steel for rolling I-beams with parallel faces of shelves in Industrial and civil construction (PGS), No. 6, 30-35.

[2] Odessky, P. D., & Kulik, D. V. (2005). New Generation Steel in Unique Structures. Internet Engineering, 1-176. (In Russian).

[3] Shan, S., & Mou, B. (2024). Development of an innovative module-to-core wall connection for steel-framed modular high-rise buildings. Journal of Constructional Steel Research, 214, 108494. doi:10.1016/j.jcsr.2024.108494.

[4] Gioncu, V., & Mazzolani, F. (2013). Seismic design of steel structures. CRC Press, London, United Kingdom. doi:10.1201/b16053.

[5] Jin, J., Nagae, T., & Chung, Y. L. (2023). Seismic and collapse behavior of existing high-rise steel buildings under long-period earthquakes. Journal of Constructional Steel Research, 211. doi:10.1016/j.jcsr.2023.108151.

[6] Grigorian, M., Sedighi, S., & Mohammadi, H. (2023). Plastic design of sustainable steel earthquake resistant structures. In Engineering Structures (Vol. 289). doi:10.1016/j.engstruct.2023.116178.

[7] Gryniewicz, M., Roberts, M. J., & Davies, J. M. (2021). Testing and analysis of a full-scale steel-framed building including the consideration of structure-cladding interaction. Journal of Constructional Steel Research, 181. doi:10.1016/j.jcsr.2021.106611.

[8] Baciu, F., Rusu-Casandra, A., & Pastramă, S. D. (2019). Low strain rate testing of tensile properties of steel. Materials Today: Proceedings, 32, 128–132. doi:10.1016/j.matpr.2020.03.469.

[9] Vaz-Romero, A., Rodríguez-Martínez, J. A., & Arias, A. (2015). The deterministic nature of the fracture location in the dynamic tensile testing of steel sheets. International Journal of Impact Engineering, 86, 318–335. doi:10.1016/j.ijimpeng.2015.08.005.

[10] Wang, W., & Kodur, V. (2020). Tensile test on steels at elevated temperatures. Material Properties of Steel in Fire Conditions, 3, 43–120. doi:10.1016/b978-0-12-813302-6.00003-5.

[11] Rout, M., & Murugabalaji, V. (2023). Tensile properties variation along the thickness direction of hot rolled austenitic stainless steel. Materials Science and Engineering: A, 865. doi:10.1016/j.msea.2023.144643.

[12] Yang, X. J., & Lin, F. (2023). Experimental and analytical studies on tensile behavior of kinked steel plates. Journal of Constructional Steel Research, 204. doi:10.1016/j.jcsr.2023.107874.

[13] Gardnerand, L., & Nethrcott D. (2005). Designers' Guide to Eurocode 3: Design of Steel Structures. General rules and rules for buildings. Institution of Civil Engineers (ICE), London, United Kingdom.

[14] EN 1993-1-12. (2007). Eurocode 3: Design of steel structures –Part 1-12: Additional rules for the extension of EN 1993 up to steel grades s700. European Committee for Standardization, Brussels, Belgium.

[15] Kulbayev, B., Lapin, V., Tuleyev, T., Aldakhov, S., Aldakhov, Y., & Ali, A. (2023). Hardness specification of structural steel used in the Republic of Kazakhstan. E3S Web of Conferences, 389. doi:10.1051/e3sconf/202338901002.

[16] Kulbayev, B., Lapin, V., Shakhnovich, A., Tuleyev, T., Aldakhov, S., Aldakhov, Y., & Ali, A. (2023). Experimental Research of Impact Toughness of the Kazakhstani Construction Steel— Assessment of Compliance with the Provisions of 1993 Eurocode. Open Journal of Civil Engineering, 13(04), 664–676. doi:10.4236/ojce.2023.134044.

[17] Kulbayev, B., Lapin, V., Shakhnovich, A., Tuleyev, T., Aldakhov, S., Aldakhov, Y., & Ali, A. (2023). Weld Joint Efficiency of the Kazakhstani Constructional Steel. Open Journal of Civil Engineering, 13(04), 802–813. doi:10.4236/ojce.2023.134052.

[18] Vedyakov, I. I., Odesskiy, P. D., & Gurov, S. V. (2018). About regulation of materials in the new of rules SP 16.13330. Steel structures. Actualized edition of SNIP II-23-81. Industrial and civil construction, 8, 61-69.

[19] Galperin, R. M., Nersesov, I. L., & Galperin, E. I. (1985). Seismic regime of Almaty for 1972–1982 years. Science, Moscow, Russia. (In Russian).

[20] Sadykova, A. B., Silacheva, N. V., & Stepanenko, N. P. (2021). Seismic micro zoning of the territory of Almaty on a new methodological basis. News of the National Academy of Sciences of the Republic of Kazakhstan, Series of Geology and Technical Sciences, 1(445), 127–134. doi:10.32014/2021.2518-170X.18.

[21] Kurskeev, A. K., Timush, A. V., Shatsilov, V. I., Sydykov, A., Gorbunov, P. N., & Sadykova, A. B. (2000). Seismic zoning of the Republic of Kazakhstan. Evero, Almaty, 219.

[22] Lapin, V., Makish, N., Kassenov, K., Omarov, Z., & Kassenov, D. (2021). Instrumental records received in 11 storey steel frame building during a remote earthquake. E3S Web of Conferences, 258, 9078. doi:10.1051/e3sconf/202125809078.

[23] Vedyakov, I. I., Suslov, L. S., Marisiuk, A. A., Kashin, O. V, & Novozhilov, M. V. (2023). Bearing capacity of a steel frame of a multi-storey modular building with consideration of the rigidity of quick-assembled connections. Earthquake Engineering. Constructions Safety, 6, 8–44. doi:10.37153/2618-9283-2023-6-8-44.

[24] Nemchinov, Yu. I. (2015). Seismic Resistance of High-Rise Buildings. NIISK, Kyiv, Ukraine.

[25] Fang, C., Wang, W., Qiu, C., Hu, S., MacRae, G. A., & Eatherton, M. R. (2022). Seismic resilient steel structures: A review of research, practice, challenges and opportunities. Journal of Constructional Steel Research, 191, 107172. doi:10.1016/j.jcsr.2022.107172.

[26] Wasse, A. D., Dai, K., Wang, J., & Sharbati, R. (2024). State-of-the-Art Review: Seismic Design and Performance Assessment of Special Concentrically Braced Frames Developed for Complex Industrial Building Structures. International Journal of Steel Structures, 1-16. doi:10.1007/s13296-024-00815-w.

[27] Pawar, G. D., & Dawari, V. B. (2023). Seismic design of bolted beam to column connections in tubular steel structures – A review. Materials Today: Proceedings, 1-6. doi:10.1016/j.matpr.2023.03.150.

[28] Pu, W., & He, C. (2022). Seismic design framework for steel structures with hysteretic and viscous dampers. Journal of Constructional Steel Research, 194, 107330. doi:10.1016/j.jcsr.2022.107330.

[29] Ras, A., & Boumechra, N. (2016). Seismic energy dissipation study of linear fluid viscous dampers in steel structure design. Alexandria Engineering Journal, 55(3), 2821–2832. doi:10.1016/j.aej.2016.07.012.

[30] Mahjoubi, S., & Maleki, S. (2016). Seismic performance evaluation and design of steel structures equipped with dual-pipe dampers. Journal of Constructional Steel Research, 122, 25–39. doi:10.1016/j.jcsr.2016.01.023.

[31] Gholizadeh, S., & Salajegheh, E. (2010). Optimal seismic design of steel structures by an efficient soft computing based algorithm. Journal of Constructional Steel Research, 66(1), 85–95. doi:10.1016/j.jcsr.2009.07.006.
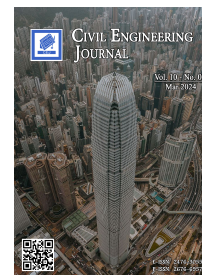
Eco-friendly 3D Printing Mortar with Low Cement Content: Investigation on Printability and Mechanical Properties

Piti Sukontasukkul [1*], Sila Komkham [1], Sittisak Jamnam [1], Hexin Zhang [2], Kazunori Fujikake [3], Avirut Puttiwongrak [4], Chayanon Hansapinyo [5]

[1] Construction and Building Materials Research Center, Department of Civil Engineering, Faculty of Engineering, King Mongkut's University of Technology North Bangkok, Bangkok 10800, Thailand.

[2] School of Computing, Engineering and the Built Environment, Edinburgh Napier University, Edinburgh EH10 5DT, Scotland, UK.

[3] Department of Civil and Environmental Engineering, National Defense Academy, Kanagawa-ken 239-8686, Japan.

[4] Geotechnical and Earth Resources Engineering, School of Engineering and Technology, Asian Institute of Technology, Khlong Nueng 12120, Thailand.

[5] Department of Civil Engineering, Faculty of Engineering, Chiang Mai University, Chiang Mai 50200, Thailand.

Abstract

The conventional approach to achieving optimal printability and buildability in 3D printing mortar relies heavily on cement, which is both costly and environmentally detrimental due to substantial carbon emissions from its production. This study aims to mitigate these issues by investigating the viability of slag as a partial substitute for cement, with the goal of developing an eco-friendly alternative. The newly formulated mortar, featuring a 30% reduction in cement content (from 830 to 581 kg/m3) and the inclusion of 0.10% micro-fibers, exhibits properties comparable to conventional 3D printing mortar. The research is structured into two parts: Part 1 focuses on determining the optimal fiber content, while Part 2 delves into the investigation of fiber-reinforced mortar with reduced cement content for 3D printing. Criteria were established to ensure mortar flow at 115%, initial printable time below 60 minutes, and 7-day compressive strength exceeding 28 MPa. Part 1 results indicate that a fiber content of 0.1% by volume meets the specified requirements. In Part 2, it was observed that increasing the slag replacement percentage extended the initial printable time and time gap. However, even at a 30% replacement rate, the initial printable time remained within the acceptable range, partially attributed to the presence of fibers in the mix. Additionally, higher slag content led to increased flow and reduced filament height in the mixes. Notably, all formulations surpassed the 7-day compressive strength threshold. These findings underscore the potential of slag as a sustainable alternative to cement in 3D printing fiber-reinforced mortar, offering promising prospects for environmentally friendly construction practices.

Keywords: 3D Printing; Eco-friendly Cement Mortar; Slag; Cement Replacement; Printable Cement Mortar; Sustainability Construction.

1. Introduction

In recent years, 3D printing has emerged as a promising technology within the construction industry, offering the potential to enhance efficiency, minimize waste, and enable the fabrication of intricate geometries. However, for widespread adoption of 3D printing, it is imperative to develop materials specifically tailored to this technology. One of the pivotal materials in this context is mortar, which is responsible for forming the structural elements of 3D-printed

buildings. The suitability of mortar for 3D printing hinges on several crucial properties [1–3]. Among these, flow is vital, denoting the material's ability to smoothly navigate through the printer nozzle. Printability, another critical attribute, refers to the material's capability to maintain its shape and adhere to the preceding layer upon extrusion. Lastly, buildability is essential, signifying the material's capacity to support subsequent layers' weight without deformation or collapse.

Traditionally, achieving satisfactory buildability and printability in 3D construction mortars involved using substantial proportions of Portland cement, often ranging from 55% to 75% by weight [4]. However, this practice can be costly and environmentally detrimental due to the high carbon emissions associated with cement production [5]. To address this, researchers have explored the use of pozzolan as a partial substitute for cement in 3D printing mortar, aiming to reduce the environmental impact and construction costs. Incorporating pozzolan in 3D printing mortars can have notable effects on both environmental considerations and construction expenses. Firstly, it can diminish the environmental impact by reducing the overall cement consumption, leading to lower carbon emissions and energy consumption during cement production. Secondly, it can lower construction costs by reducing the quantity of cement required for the mortar, presenting a dual advantage for sustainable and economical 3D printing practices.

Nevertheless, utilizing pozzolan as a substitute for cement in mortar for 3D printing yields diverse effects on printability and buildability, contingent on the type and concentration of the pozzolan employed. In the context of fly ash, Panda and Tan [6] replaced cement with fly ash in 3D printing, achieving a replacement rate of up to 80% by mass. They observed that the "ball bearing effect" of fly ash could decrease the yield stress and plastic viscosity of fresh cement composites, enhancing the pumpability of 3D printing. However, at higher replacement rates, there was a delayed initial setting and early hydration, negatively impacting buildability and printability. Rubio et al. [7] discovered that incorporating pozzolans like fly ash (24%) and silica fume (8%) into the mix, instead of replacing cement, increased yield stress, cohesiveness, and improved structure homogeneity and stability, which is advantageous for layer printing. Yet, this did not result in a reduction in cement content since both fly ash and silica fume were additional materials. In summary, while fly ash positively affected cement reduction, workability, cohesiveness, and homogeneity, its major drawback was a slower reaction rate with water, leading to prolonged setting times and lower early-age strength development, adversely affecting buildability.

Concerning ground furnace slag, its use as a substitute for cement in 3D printing mortar seemed to influence the required properties for printable mortar. For instance, Yu et al. [8] determined that slag could replace cement up to 20% by weight without compromising printability and buildability. Their study demonstrated that using up to 10% slag improved the buildability of 3D-printed concrete. However, when the slag content exceeded 20%, a significant deterioration in the rheological properties of 3D-printed concrete and an increase in initial printable time were observed. Xu et al. [9] employed a combination of fly ash/slag (FA/S) and sulfo-aluminate cement (SAC) at various proportions as a partial replacement for cement. They found that with FA content exceeding 20%, there was an increase in slump and a decrease in mechanical properties, affecting buildability. Dai et al. [10] replaced fine aggregate with slag up to 80%, noting that setting time increased gradually with rising FA content, leading to an increase in initial printable time, and both flexural and compressive strengths decreased gradually. However, their study did not result in a decrease in Portland cement content, as slag was used as a fine aggregate replacement rather than a cement replacement.

Problem Statement:

The examination of pozzolanic materials as a substitute for cement in 3D printing mortar, based on the literature review, reveals both positive and negative impacts on its properties. For fly ash, while improvements in flowability, cohesiveness, and homogeneity were noted, the sluggish chemical reaction led to significant delays in setting time and early strength gain. In the case of slag, replacing cement with slag appeared to have fewer adverse effects on initial printable time and early strength gain, but the optimal replacement rate without compromising printable mortar properties was identified at approximately 20%.

Proposed Solution:

This study proposes investigating the use of slag to replace cement in printable mortar up to approximately 30% by weight, aiming to maintain essential properties related to printability and buildability. To address concerns about delayed initial printable time and early strength gain when utilizing slag at percentages exceeding 20%, micro-fibers were introduced into the mix. The presence of micro-fibers in fresh mortar is known to enhance shape and buildability in 3D printing mortar [11–14], as well as reduce the initial printable time [14–15], mitigating the effects of slag replacement. The objective is to develop an eco-friendly mortar that meets the requirements for 3D-printed mortar while significantly reducing cement usage. The cement content in the control mix was set at 830 kg/m^3, and with a 30% replacement, the cement content can be reduced to approximately 581 kg/m^3. Various tests were conducted on the new mortar, focusing on properties such as compressive strength, flow, printability, and buildability. The study's results demonstrate the feasibility of replacing a substantial portion of cement with slag in 3D-printed mortar while still achieving properties that meet the application's requirements.

2. Research Methodology

2.1. Materials

Materials used in this study consisted of (Tables 1 and 2, Figure 1):

- Portland cement Type I with properties that follow the ASTM C150 standard.

- Silica fume with specific gravity of 2.2 and particle size between 0.03-0.30 μm. The chemical composition is given in Table 1.

- Blast furnace slag with specific gravity of 2.9 and particle size of 5.5-7.5 μm. The chemical composition is given in Table 1.

- River sand with particle size passing through sieve no. 16 and specific gravity of 2.5.

- Micro polypropylene fiber with length of 6 mm and diameter between 20-45 μm. Its properties are shown in Table 2.

- Superplasticizer type G – Polycarboxylate base with specific gravity of 1.10.

- Water retention agent – Polyethylene glycol base with specific gravity of 1.09

Table 1. Chemical composition of silica fume and slag

Mineral type (%)	SiO_2	Al_2O_3	Fe_2O_3	CaO	SO_3	MgO	Na_2O	K_2O
Silica Fume	88.3	1.2	4.8	0.5	1.1	-	-	-
Slag	32.3	15.4	0.6	39	1.2	7.2	0.7	0.4

Table 2. Properties of micro-polypropylene fiber

Property	Diameter (μm)	Length (mm)	Specific Gravity	Tensile Strength (MPa)	Modulus of Elasticity (MPa)
MFP	25 – 45	6	0.91	650	3445

Cement   Silica Fume   Slag

River Sand   Micro Fiber
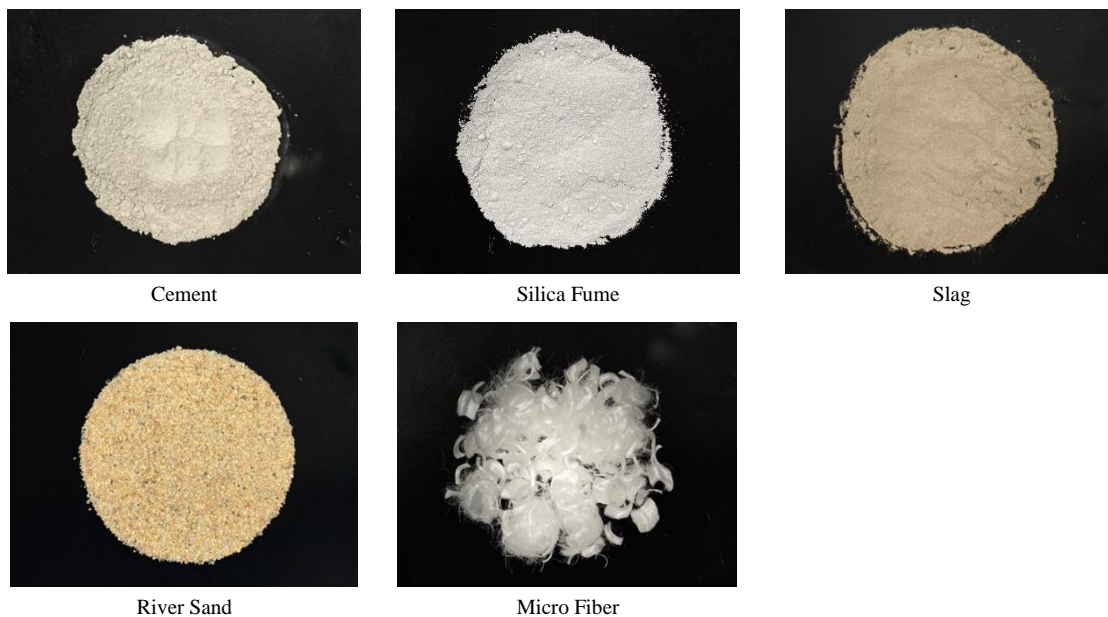
Figure 1. Granular diagram of materials

2.2. Experimental Series

The experimental series comprised two parts:

Part 1: Investigation of the optimum fiber content suitable for 3D printing mortar.

The aim of this study was to determine the optimal volume fraction of fibers that would meet the requirements of mortar for 3D printing applications. As there are currently no standard tests specific to printable cement mortar, the specifications for mortar suitable for 3D printing applications were established based on the property requirements for printable mortar [12]. For example,

- Flow > 115%

- Initial printable time < 60 minutes

- 7-day compressive strength > 28 MPa

The selection of parameters is based on the required performance of printable mortar, including factors such as flowability, printability, and buildability. Initially, cement mortar for 3D printing is in a slurry form, necessitating the ability to flow through a nozzle while maintaining its shape and withstanding pressure from subsequent layers, as well as bonding with the previous layer. Parameters were established to meet these requirements. For instance, a flow of 115% was set as the flowability requirement, while the initial printable time of 60 minutes ensures uniform extrusion without defects, aligning with printability needs. This time frame is derived from the standard concrete mixing-to-placing duration of 60 minutes to prevent stiffness. Compressive strength requirements ensure the mortar can withstand loads after 7 days. Buildability, though not initially defined, is evaluated later based on the time gap established to prevent vertical deformation during the printing of up to 10 layers. This approach ensures the stack of mortar filaments remains virtually free of vertical deformation.

The mix proportion meeting these 3D printing specifications was chosen to undergo further investigation in Part 2.

Part 2: Investigation on fiber reinforced mortar with low cement content for 3D printing.

The purpose of this test was to produce printable mortar with reduced Portland cement content while maintaining its properties and meeting the printability requirements for 3D printing mortar outlined in Part 1. The Portland cement content of the mix proportion selected from Part 1 was substituted with slag at weight percentages ranging from 0% to 30% of the cement weight. The proportions of river sand, silica fume, water, and water retention agents remained constant. However, as the addition of slag significantly impacted the workability of the mortar, the superplasticizer dosage for each mix proportion had to be predetermined to ensure sufficient flowability suitable for printing. Subsequently, the proposed mix proportions underwent printability tests to assess the initial printable time, time gap, and layer deformation (10 layers). Mechanical property was also conducted to evaluate the effect of slag replacement. The research sequence is summarized in Figure 2.
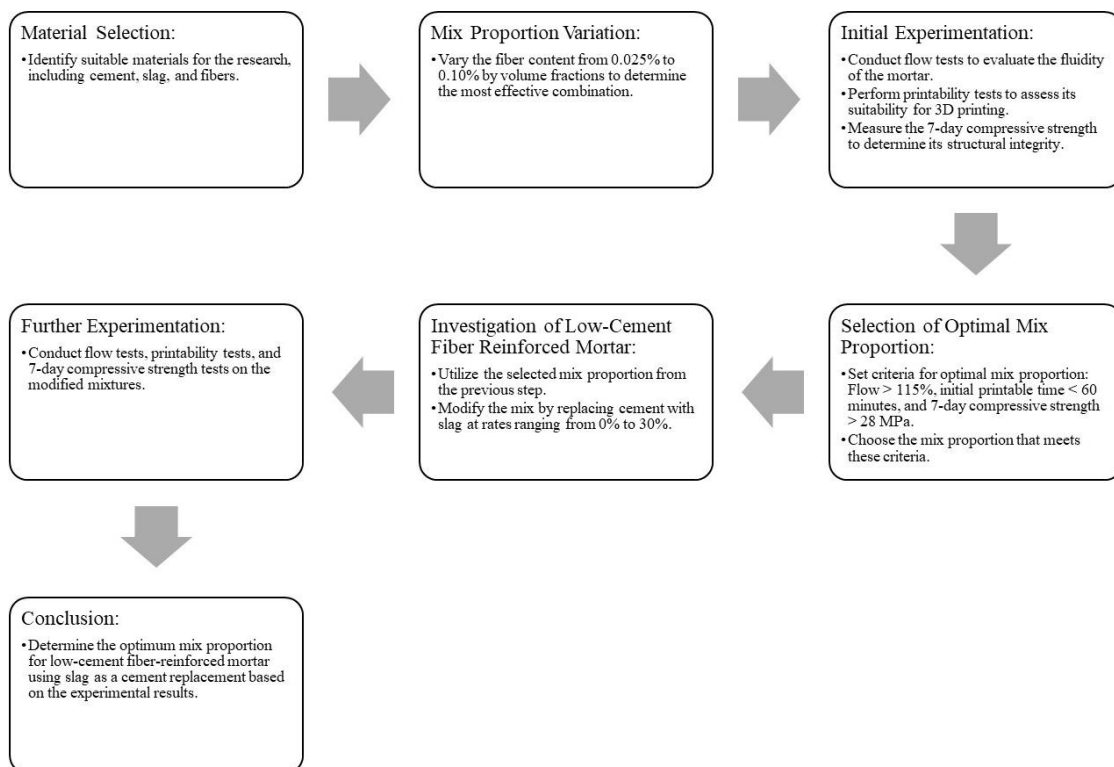
Figure 2. Schematic illustration of research sequence

2.3. Mix Proportions

For Part 1, the mix proportion primarily comprised cement, silica fume, river sand, and admixtures. The fiber content ranged from 0% to 0.1% by volume. In the control mix (plain mortar, PLN), the proportions were cement at 878 kg/m³, river sand at 1170 kg/m³, silica fume at 88 kg/m³, and water at 212 kg/m³. The superplasticizer and water retention agent were fixed at 10.0% and 2.5% by weight of the binder, respectively. In the fiber-reinforced cement mortar (FRM), the fiber content varied from 0%, 0.025%, 0.050%, 0.075%, to 0.100% by volume (PLN, FRM25, FRM50, FRM75, and PP100). Detailed mix proportions are provided in Table 3.

Table 3. Detailed mix proportion for Part 1

Specimen type	Materials (kg/m³)						
	Portland cement	Sand	Silica Fume	Water	Super plasticizer	PEG	Micro fiber
PLN							0
FRM25							0.23
FRM50	830	1170	165	212	97	24	0.45
FRM75							0.68
FRM100							0.91

For Part 2, the mix proportion selected from Part 1, which met the earlier mentioned requirements in 2.2, was utilized. The cement content was replaced with slag at rates ranging from 0% to 30% of the cement weight. Other components, including river sand, silica fume, fiber, and water content, remained constant. However, to maintain consistent workability, the optimal superplasticizer content, resulting in a flow of 115%, was determined and applied to each mix proportion. Detailed mix proportions are provided later in the experimental section after determining the optimal fiber content from Part 1.

2.4. Experimental Series

2.4.1. Flow Table Test

The test was conducted in accordance with ASTM C230 (Standard Specifications for Flow Table for Use in Tests of Hydraulic Cement). It commenced with placing an inverted cone container on the flow table and filling it with fresh cement mortar. Gradually lifting the container allowed the fresh mortar to flow and spread slightly on the flow table. Subsequently, the face of the table was raised and dropped freely 15 times, further spreading the fresh mortar. The flow diameter (D1) was determined as the average measurement of the maximum flow diameter observed at least twice. The flow percentage can then be calculated using Equation 1.

$$Flow\ (\%) = \frac{D_1 - D_0}{D_0} \times 100 \tag{1}$$

where D_0 is the original diameter (mm), D_1 is the diameter after impact (mm).

2.4.2. Printable Time

Printable time refers to the duration during which a material can be printed continuously without defects while maintaining consistent dimensional lines. It commences with the initial printable time (t_{int}) and concludes with the final printable time (t_{fin}). In the experiment, a 3D printer, designed and constructed at the Department of Civil Engineering, KMUTNB (Figure 3), was utilized to print 300 mm filaments of mortar every 5 minutes until printing was no longer feasible. The printer featured a 20 mm diameter nozzle, operated at a height of 15 mm above the floor, moved at a speed of 10 mm/s, and maintained a feed rate of 2.5 ml/s. The width of each filament was measured at 50-, 150-, and 250-mm intervals, and the average of these values represented the width (Figure 4). Results were graphed against time, illustrating changes in filament width due to the diminishing plasticity of fresh mortar over time (Figure 5). The initial printable time was recorded when the filament consistently reached its narrowest width, and the final printable time was noted when printing became inconsistent. The dimension of the filament printed at the initial printable time is referred to as the initial dimension, consisting of the initial width (w_{int}) and initial height (h_{int}).
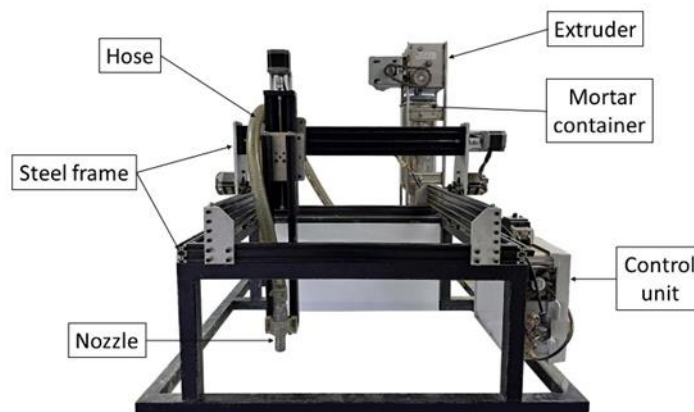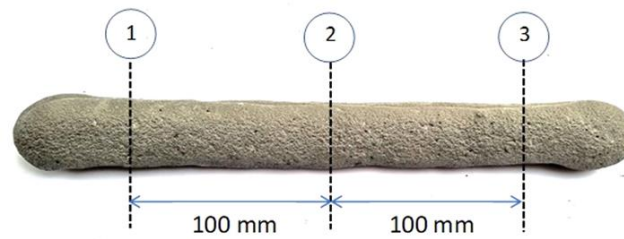

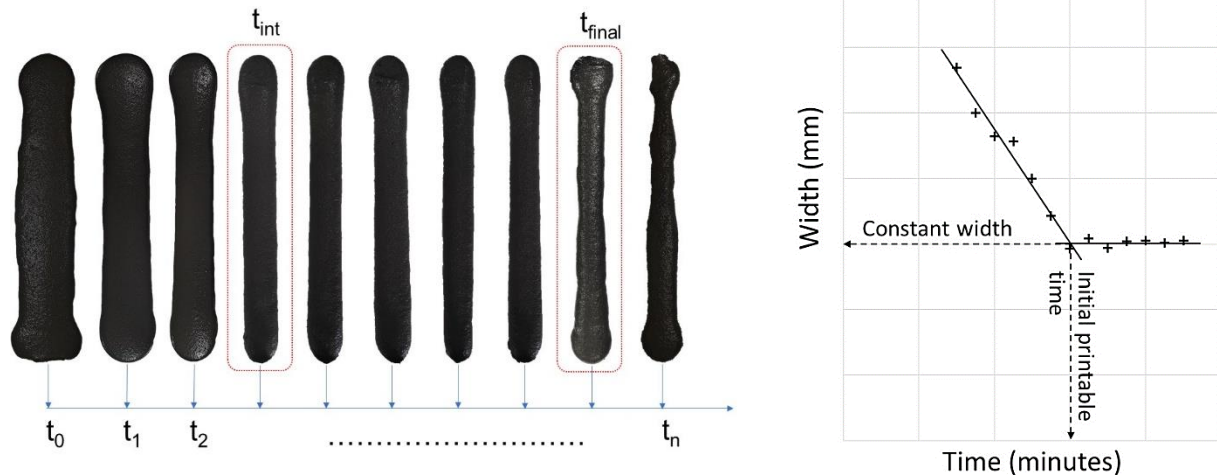**Figure 3. Small scale 3D printer**

Figure 4. Width measurement location

Figure 5. Relationship between filament width vs time

2.4.3. Time Gap without Layer Deformation

In this study, the term "time gap" denotes the duration between printing the first layer and subsequent layers without causing any deformation to the first layer. To assess this, the initial printable time obtained from section 2.4.3 was used to print the first layer. Five minutes later, a print filament was added on top of the first layer, and the deformation of the first layer was promptly measured. This process was repeated at five-minute intervals until no deformation was observed in the first layer. The earliest time at which the first layer no longer deformed is referred to as the "time gap without deformation."

The purpose of this test was to evaluate the buildability property of fresh mortar, or its ability to support weights of subsequent layers without deformation. This property can be linked to a specific time after the cement comes into contact with water. The obtained time gap was validated by printing 10 layers of each mix proportion, measuring their height, and comparing them with the expected height (which is equal to 10 times the hint). If the actual height of the 10 printed layers falls within the expected height range, it can be concluded that the obtained time gap was sufficient to prevent deformation of the previous layer during printing.

2.4.4. Mechanical Properties

Two tests were conducted, namely a compressive strength test (ASTM C109) and a flexural strength test (ASTM C348-21). As these tests are widely performed and well-established globally, detailed test procedures have been omitted from this manuscript. However, specifications regarding specimen types and test directions are provided instead.

Two types of specimens underwent both tests: cast and printed specimens. Cast specimens were cast with dimensions of $50\times50\times50$ mm for compressive strength testing and $40\times40\times160$ mm for flexural strength testing. These specimens were prepared in accordance with the corresponding standard and wrapped in plastic sheeting until the test date (7 days).

For printed specimens, they were printed in a prism shape, wrapped, and cured for 7 days. Subsequently, they were cut and polished into shapes similar to the cast specimens (Figure 6). To investigate the effect of load directions on printed specimens, the following test schemes were proposed:

- For the compression test, two load directions were proposed: perpendicular to and parallel to the print direction (Figure 7-a).

- For the flexure test, two load directions were applied: perpendicular to and transverse to the print direction (Figure 7-b).

Figure 6. Preparation of printed specimens for compression and flexure testing

(a)   (b)
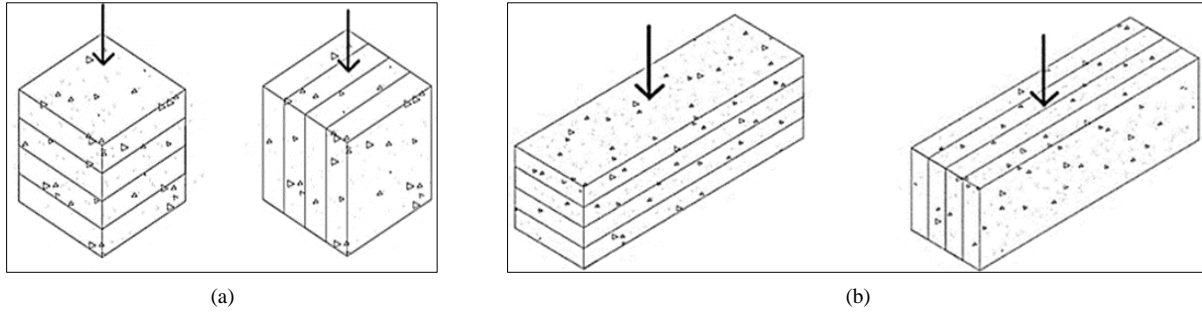
Figure 7. Load directions vs. specimen layout for (a) compression and (b) flexure testing

3. Results and Discussion

3.1. Part 1

3.1.1. Flow Test

The flow percentage of fiber-reinforced mortar for 3D printing was determined through the flow test in accordance with ASTM C230, and the results are presented in Figure 8. It was observed that the flow rate decreased as the micro polypropylene fiber content increased. This phenomenon was attributed to the increased surface area of the microfibers, which absorbed water from the mix, thereby reducing the free water content and hindering the mobility of the fresh cement mortar. Additionally, the formation of a fiber interlocking network can increase the viscosity of the mortar, making it thicker and more resistant to flow [16]. FRM100 exhibited the lowest flow rate of 129%, which was 14% lower than that of the PLN mixture. These results align with the findings of Guerini et al. [17], who reported a decrease in the workability of concrete with increasing fiber content from 0.5% to 1.0%. Similarly, Dai et al. [18] reported a decrease in flowability with an increase in waste plastic fiber content from 0.1% to 0.7%. They suspected that the dispersion of fibers prevented the contact between water and cement particles, resulting in reduced flowability.
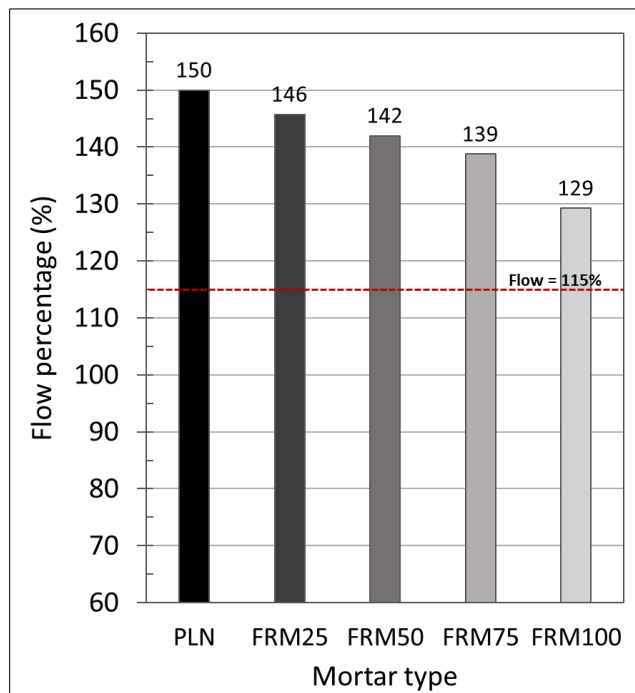
Figure 8. Flow percentage

All mix proportions tested in this study met the required flow criteria for 3D printing application, as they exhibited a flow percentage higher than 115%.

3.1.2. Initial Printable Time (T_{int})

Figures 9 depict the correlation between filament width and time. From the plotted results, the initial printable time of each mix can be calculated, as shown in Table 4. Typically, T_{int} decreases with an increase in fiber content. The highest T_{int} of 67.5 minutes was observed for plain mortar (PLN). On the other hand, the T_{int} for FRM ranged from 53-63 minutes and was lower than that of PLN. FRM100 exhibited the lowest initial printable time of 53 minutes. The addition of microfiber increased the total specific surface area of the mortar mix, necessitating more water and resulting in a lower water/cement ratio, which caused the mortar to set faster. Additionally, the addition of fibers increased the solid content of the mix, providing support to the fresh mix and allowing it to gain dimensional stability more quickly. The addition of microfiber to the mortar results in a reduction in flow, leading to increased stability of the filaments. This decrease in flow translates to a lower initial printable time, enabling FRM to commence printing more rapidly.
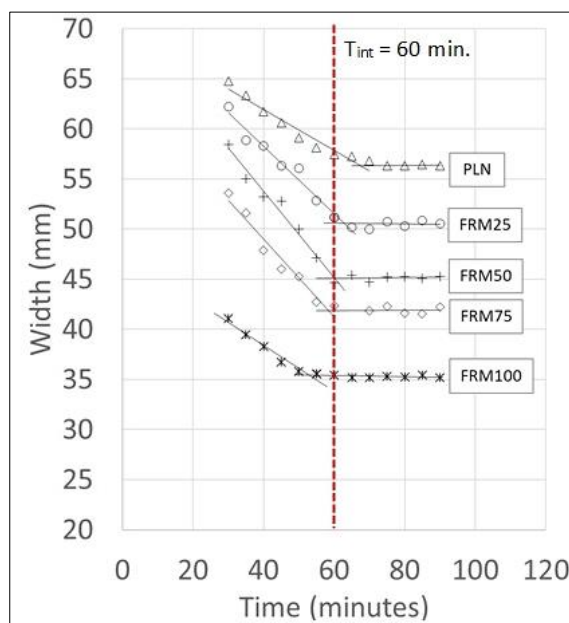
Figure 9. Filament width vs. time of plain and FRM

Table 4 illustrates the correlation between initial filament width (W_{int}) and initial printable time (T_{int}) for each mix. Wint ranges from 35 to 56 mm, with the widest width of 56 mm observed in plain mortar (PLN). The addition of fiber narrows Wint, signifying that fibers offer support to the printed filament and minimize vertical deformation. The smallest width of 35.4 mm was observed in FRM100. The initial height of the filament (H_{int}) increases with the addition of fiber, attributed to the constant volume of mortar extruded through the nozzle. Fibers reinforce the mortar matrix, providing additional structural support to the printed filaments, thus preventing deformation or sagging during printing and enhancing stability [19].

Table 4. Effect of fiber content on initial printable time and filament dimension

Concrete Type	Initial Printable time (minutes)	Width (mm)	Height (mm)
PP0	67.5	56.3	6.0
PP25	62.7	50.6	6.6
PP50	60.2	45.1	7.5
PP75	58.4	41.9	8.2
PP100	53.0	35.4	9.7

The relationship between height and time indicates that Hint increases over time, plateauing once the Tint is achieved, and height increases with fiber content. The shortest filament height of 6 mm was observed in the PLN mix, while the tallest of 9.7 mm was seen in the FRM100 mix. The enhanced stability provided by fibers enables printing of taller filaments without risk of collapse or deformation, allowing for greater height while maintaining structural integrity [20].

3.1.3. 7-day Compressive Strength

Figure 10 illustrates the compressive strength results of printed specimens tested with loads perpendicular and parallel to the print direction. The data demonstrates that the compressive strength of printed mortar increases with higher fiber content, irrespective of load direction. The addition of microfibers enhances bonding between particles and aggregates, reinforces the matrix, mitigates cracks by bridging microcracks, and increases toughness, improving load distribution and deformation resistance. This reinforcement enhances cohesion, restricts crack propagation, and enhances the mortar's capacity to withstand loads, leading to higher compressive strength [21]. The FRM100 mix exhibited the highest compressive strength values in both load directions (28.3 MPa perpendicular and 21.9 MPa parallel to print direction), while the PLN mix showed the lowest values (23.9 MPa perpendicular and 16.3 MPa parallel to print direction). Similar findings on the fiber's strengthening effect were reported by Sukontasukkul et al. [14, 15] and Panda et al. [22], where increased fiber content correlated with higher strength, potentially due to enhanced interlayer bond strength between printed layers.
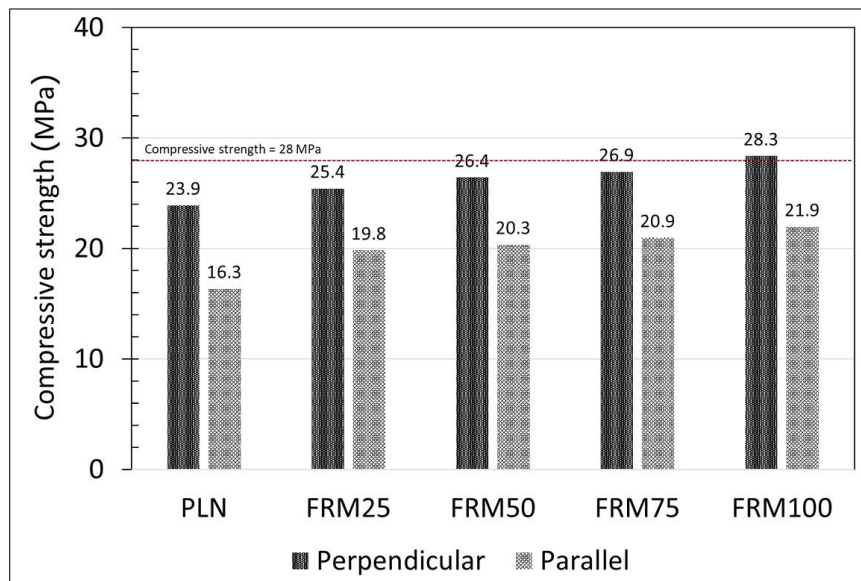
Figure 10. Compressive strength of printed specimen tested in perpendicular and parallel directions

In comparing print direction to load direction, higher compressive strength values were observed for the load direction perpendicular to the print direction compared to the load direction parallel to the print direction. This disparity in compressive strength could be attributed to the debonding between print layers and the weaker interlocking effect of fibers in the parallel load direction (Figure 11). This finding is consistent with research by Paul et al. [22] and Dai et al. [23], which suggests that layer-by-layer printing creates weaker bonds within specimens, resulting in reduced load-carrying capacity under compressive, tensile, and flexural loads, necessitating stress transfer across or along these layers. Studies by Ding et al. [24] and Ma et al. [25] further support this observation, highlighting the high anisotropic behavior of 3D printed specimens under different loading directions. Mechanical properties are significantly influenced by load and print directions. Additionally, the data indicates that fiber reinforcement can enhance the compressive strength of printed mortar, emphasizing the potential of fiber-reinforced mortar for 3D printing applications.

| (a) | (b) |
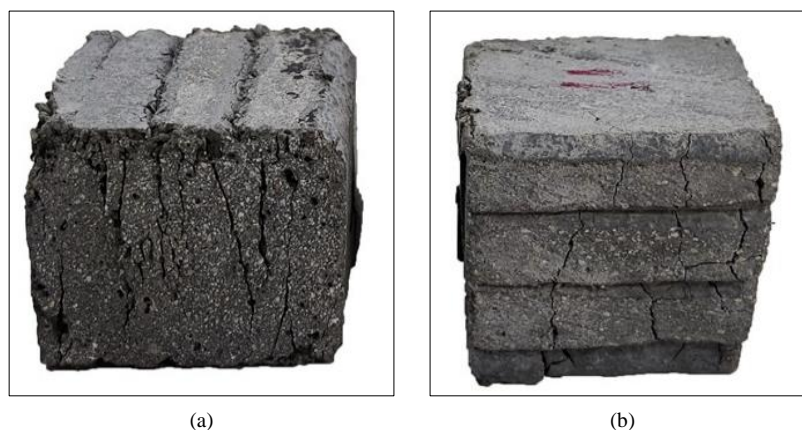
Figure 11. Failure patterns of specimens tested with load (a) parallel and (b) perpendicular to print direction

Based on the test results from flow, initial printable time, and compressive strength at 7 days, and the criteria for mix proportion selection, the FRM100 which exhibited flow of 129% (>115%), initial printable time of 53 minutes (< 60 min.), and 7-day compressive strength of 28.3 MPa (>28 MPa) was selected to continue further investigation in Part 2.

3.2. Part 2: Investigation on Fiber Reinforced Mortar with Low Cement Content for 3D Printing

3.2.1. Mix Proportions Selection based on Flow Test

In this phase of the study, as detailed in section 3.1.3, the cement content of FRM100 was substituted with slag at weight percentages of 10%, 20%, and 30%, resulting in a notable reduction in cement content from 830 to 581 kg/m^3. However, this substantial replacement of slag altered the rheological properties of the mortar, leading to a significant increase in flow (refer to Figure 10). The increased flow of concrete with the use of slag can be attributed to several factors. Firstly, slag consists of finer particles compared to cement, which enhances particle packing and lubrication within the concrete mixture, enabling improved flowability. Moreover, slag can act as a water reducer, allowing for a reduction in water content while maintaining desired workability, leading to improved flow. Lastly, the incorporation of slag can improve the rheological properties of concrete by enhancing viscosity and yield stress, promoting better flow without segregation or bleeding. These factors contribute to the enhanced flow of concrete when slag is used as a supplementary material [26, 27].

The experiment began by adjusting the superplasticizer content of each mix proportion within the range of 5% to 10%, followed by a flow test. The correlation between flow and superplasticizer content was then determined and illustrated in Figure 12. Analysis of the results revealed that, for equivalent superplasticizer content, flow increased proportionally with the amount of slag replacement. Consequently, to sustain a flow rate of 115%, adjustments were required in the superplasticizer dosage, reducing it from 7.3% to 6.3%, 5.8%, and 5.4% with slag replacement rates of 0%, 10%, 20%, and 30%, respectively. Refer to Table 5 for detailed mix proportions pertaining to Part 2.
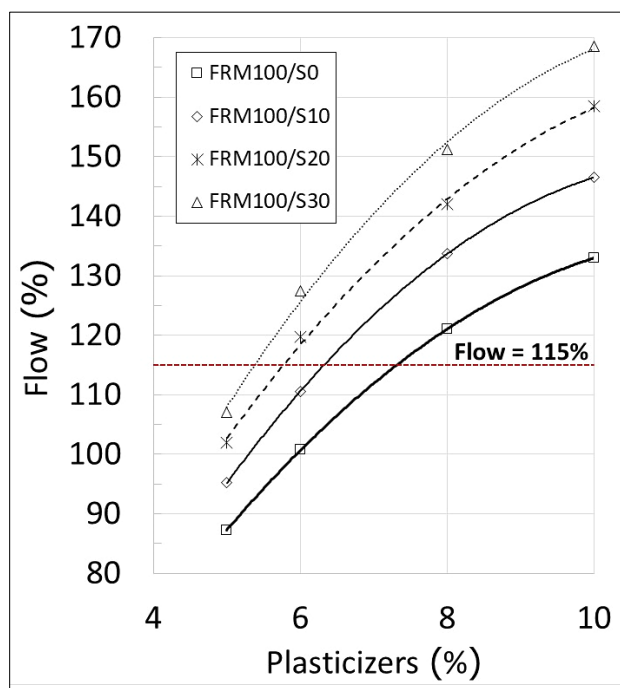
Figure 12. Relationship between flow and superplasticizer of FRM100 with slag replacement

Table 5. Detailed mix proportion for Part 2

Specimen type	Materials (kg/m^3)							Super Plasticizer (%)
	Portland cement	Sand	Silica Fume	Water	PEG	Micro fiber	Slag	
FRM100/S0	830						0	7.3
FRM100/S10	747						83	6.3
FRM100/S20	664	1170	165	٢١٢	24	0.91	166	5.8
FRM100/S30	581						249	5.4

3.2.2. Initial Printable Time

Figure 13-a illustrates the outcomes of the experiment, showcasing the correlation between filament width and time. It was observed that the filament width exhibited an increasing trend with the slag replacement rate, regardless of the printing time. This phenomenon can be attributed to the heightened flow characteristics of FRM with slag replacement (FRM/S), resulting in broader filament widths while simultaneously shortening the height, as expounded in section 3.2.1.

| (a) | (b) |
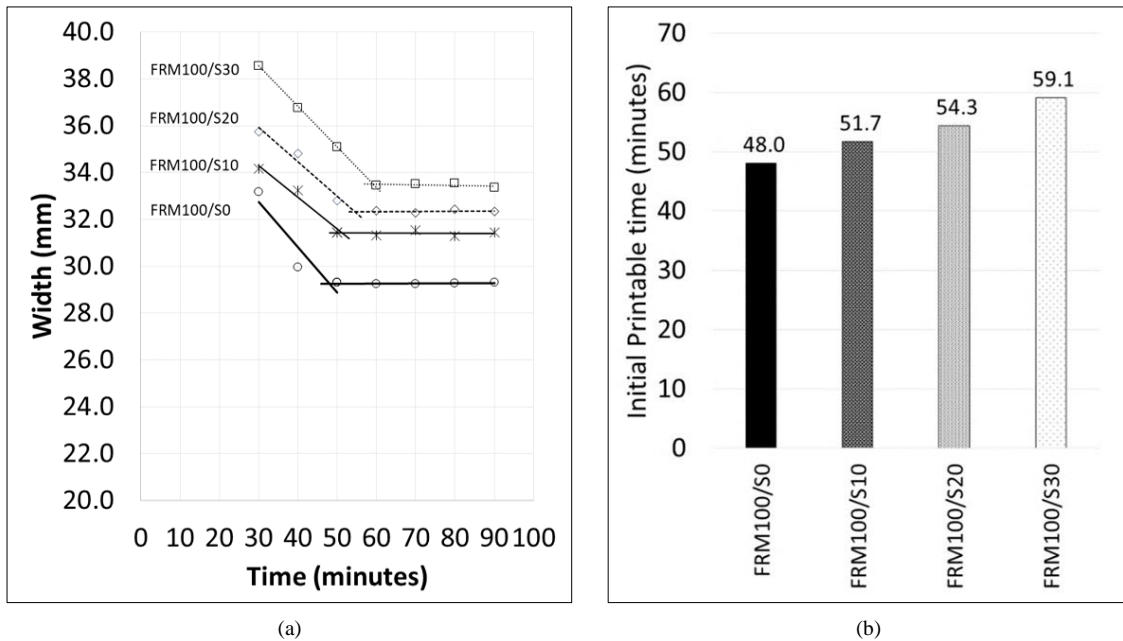
Figure 13. (a) Relationship between filament width vs. time and (b) Initial printable time

The initial printable time (t_{int}) represents the duration during which the mortar can be continuously printed at a consistently narrow width. As depicted in Figure 13-b, the tint values were determined from the filament width-time relationship. The results revealed a noticeable increase in tint from 48 to 59 minutes with the escalation of the slag replacement ratio from 0% to 30%. This decline in tint can be attributed to the reduction in cement content, which decelerates the hydration reaction rate and subsequently impacts the mortar's uniform printing ability, thereby prolonging the tint. Despite the rise in t_{int} associated with increasing slag replacement rates, all mix proportions with slag replacement up to 30% remained within the stipulated requirement of less than 60 minutes.

The increase in initial printable time related to higher slag content implies that mortar with a higher slag ratio demands a longer waiting period compared to conventional mortar, possibly causing delays in construction timelines. However, the presence of microfiber offers a mitigating factor, as it has been shown to reduce t_{int}. Consequently, the incorporation of microfiber can offset the increase in t_{int} induced by higher slag content, effectively maintaining it below the critical threshold of 60 minutes. This synergistic effect between microfiber and slag content underscores their combined potential in optimizing construction efficiency and overcoming challenges posed by extended waiting periods, thereby enhancing the feasibility of utilizing slag-based mortar in 3D printing applications.

The initial width (w_{int}) and height (h_{int}) were determined by measuring the dimensions of the printed filaments at their respective initial printable times. Three measurements were taken at different positions along each filament, with at least three filaments printed for each mortar type. The average value of these measurements was then calculated to represent each mortar type. The results are outlined in Table 6. It is evident that as the slag replacement ratio increases, the initial width (w_{int}) of the filaments also increases, ranging from 29.3 mm for FRM100/S0 to 33.5 mm for FRM100/S30. This indicates a reduction in mortar viscosity with increasing slag content. Conversely, the height decreases from 12.7 mm for FRM100/S0 to 10.8 mm for FRM100/S30. This phenomenon suggests that with a constant volume of mortar extruded from the nozzle, the broader width results in a shorter height

Table 6. Initial printable time, width, and height

| Mortar Type	t_{int}	w_{int}	h_{int}
FRM100/S0	48.0	29.3	12.7
FRM100/S10	51.7	31.4	11.7
FRM100/S20	54.3	32.3	11.2
FRM100/S30	59.1	33.5	10.8

3.2.3. Time Gap

Table 7 presents the results regarding the correlation between slag replacement rate and parameters, including time gap, expected height, and actual height attained during printing. The time gap signifies the duration between printing the initial layer and subsequent layers without inducing any deformation to the first layer. Expected height refers to the anticipated height after printing 10 layers of each mix proportion (10 x h_{int}), while actual height denotes the height obtained from printing 10 layers of each mix proportion.

Table 7. Time gap, expected height, and actual height

Mortar type	Time gap (min)	Expected height (mm)	Actual height (mm)	Difference (mm)
FRM100/S0	8	127	127.6	-0.60
FRM100/S10	8	117	117.3	-0.30
FRM100/S20	12	112	111.9	0.10
FRM100/S30	13	108	107.7	0.30

As the slag replacement ratio escalates from 0% to 30%, the time gap increases by 62.5% (from 8 minutes to 13 minutes). This implies that incorporating slag as a partial cement substitute prolongs the time gap before the first layer experiences deformation. This trend can be attributed to the slower setting of mortar with higher slag content, allowing an extended working duration before it stiffens too much for additional layering.

Moreover, the data reveals a decrease in actual height with an increasing slag replacement rate, aligning with the findings in section 3.2.2 where initial height decreases with higher slag replacement rates. Additionally, the actual height falls within a similar range to the expected height for all mix proportions, exhibiting differences ranging from 0.24% to 0.97%. This highlights the appropriateness of the attained time gap in avoiding deformation of preceding layers during printing, thereby preserving the structural integrity of the printed objects. Despite elongating the time gap, incorporating slag as a partial cement substitute up to 30%, coupled with fiber addition, maintains the required buildability characteristic of fresh mortar, with minimal deformation of the initial layer. A similar observation by Li et al. [28] highlights that fiber addition (glass) enhances dimensional stability in printed filaments, imparting practical implications for printing intricate geometries or large-scale structures.
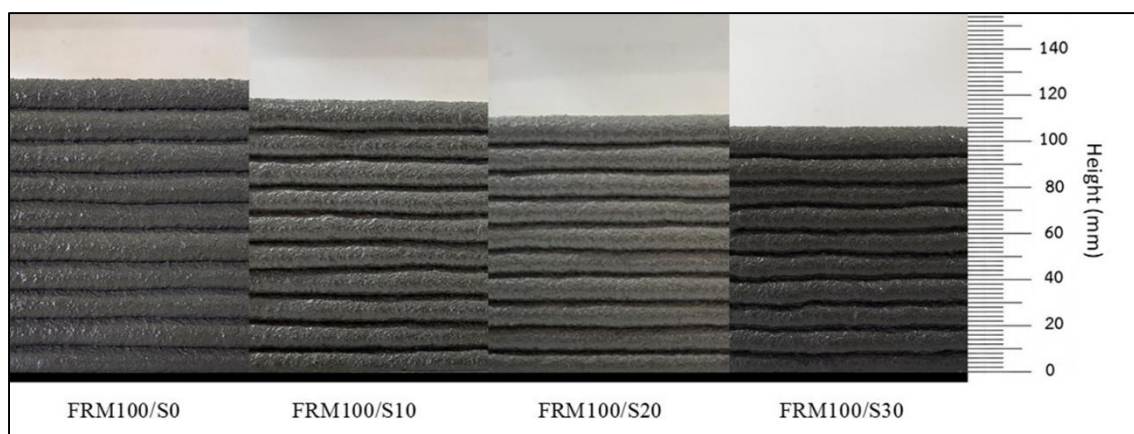
Figure 14. Actual printed height (10 layer) of FRM with slag replacement

3.2.4. Mechanical Properties

3.2.4.1. 7-day Compressive Strength

Figure 15 depicts the compressive strength of mortar with varying slag replacement ratios under two loading directions: perpendicular and parallel to the print direction. Initially, it is evident that as the slag replacement ratio increases, the compressive strength values improve in both loading directions. This enhancement can be attributed to the finer particles introduced by slag, which enhance packing and consequently bolster strength [27]. Additionally, the increased slag content fosters pozzolanic reactions, wherein it reacts with calcium hydroxide in the presence of water to form additional cementitious compounds, augmenting overall strength [29].
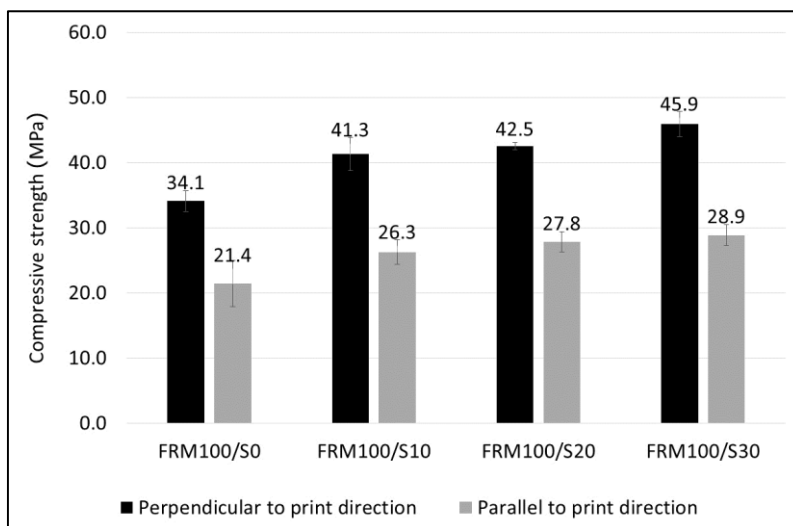
Figure 15. 7-day Compressive strength of FRM with slag replacement

Comparing the compressive strength values between perpendicular and parallel loading directions reveals a noteworthy disparity. Compressive strength in the perpendicular direction consistently surpasses that in the parallel direction for all slag replacement ratios. This discrepancy is attributed to the layer-by-layer printing process, which results in weaker bonding between adjacent layers in the parallel direction, thus yielding lower compressive strength. Conversely, the perpendicular direction benefits from interlocking between layers, bolstering compressive strength. Shakor et al. [30] underscored the significant influence of orientation angle on the mechanical properties of printed specimens, noting that optimal strength is achieved with specific printing orientations. Furthermore, within the perpendicular direction, compressive strength increases with higher slag replacement ratios, with FRM100/S30 exhibiting the highest strength. This can be attributed to the denser and more compact mortar achieved with increased slag content.

In summary, incorporating slag as a partial cement replacement enhances the compressive strength of printed mortar in both loading directions, with a more pronounced effect in the perpendicular direction. Moreover, higher slag replacement ratios correlate with greater strength gains. While most mortar types meet or exceed the 7-day compressive strength requirement (>28 MPa) in the perpendicular direction, only FRM100S30 achieves this threshold in the parallel direction.

3.2.4.2. 7-day Flexural Strength

The data provided shows the flexural strength of four different types of mortar with varying slag replacement ratios, tested with loads perpendicular and transverse to the print direction.

From the data, it can be observed that the flexural strength increases with increasing slag replacement ratio for both perpendicular and transverse loads. The flexural strength increases range from 20.5% to 25.2% for the perpendicular and transverse directions, respectively, when comparing 30% slag replacement to 0% slag replacement (Figure 16). This trend indicates that the use of slag as a partial cement replacement can improve the flexural strength of the printed objects.
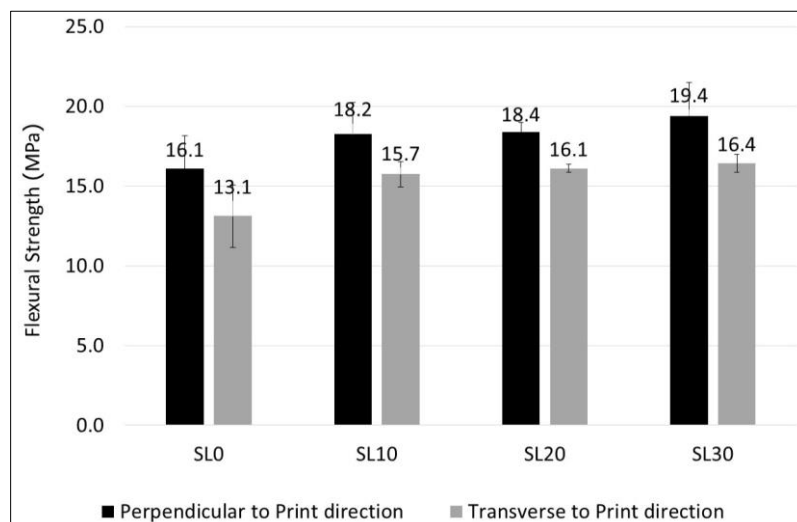

Figure 16. 7-day Flexural strength of FRM with slag replacement

Furthermore, it can be observed that the flexural strength values in the perpendicular direction consistently exceed those in the transverse direction for all mortar mixtures. This may be attributed to a combination of factors, including the layer-by-layer printing process which may result in weaker bonding between adjacent layers in the transverse direction and the expansion of the material in the transverse direction due to Poisson's effect which lead to debonding and to lower flexural strength. Shakor et al. [30] used ABAQUS to simulate the deflection of 3D printing beam subjected to load in different directions. They also found that when load was acting in perpendicular to the print direction, the beam exhibited the lowest deflection and hence, yielded the highest flexural strength.

The test results indicating higher flexural strength for specimens tested with load perpendicular to the print direction compared to those tested with load transverse to the print direction suggest important considerations for practical applications of 3D printed structures. This finding implies that the orientation of the printed structure relative to the applied load can significantly influence its strength and structural integrity. Therefore, in real-world applications, designers and engineers should carefully consider the orientation of 3D printed components to ensure optimal strength and performance.

Overall, the results suggest that the use of slag as a partial cement replacement can improve the flexural strength of 3D-printed objects and that the flexural strength is generally higher in the perpendicular direction compared to the transverse direction.

4. Conclusions

The conclusion can be divided into two parts:

Part 1: This section explores the impact of micro polypropylene fibers on the flow percentage, initial printable time, and compressive strength of fiber-reinforced mortar (FRM) for 3D printing. Results indicate that the addition of fibers decreased the flow rate due to increased surface area and water absorption. However, all mix proportions met the required flow criteria for 3D printing (115%). Moreover, the initial printable time decreased with an increase in fiber content, suggesting that fibers provide support to the fresh mix, enabling quicker dimensional stability. Among the FRM mixes, FRM75 and FRM100 met the 60-minute t_{int} requirement. Compressive strength increased with fiber content, with only FRM100 exhibiting a compressive strength higher than 28 MPa. Based on its flow, initial printable time, and compressive strength results, FRM100 was selected for further investigation on printable mortars with low cement content.

Part 2: This segment explores the effect of slag as a partial cement replacement on the rheological and mechanical properties of FRM. The replacement of cement content with slag at weight percentages of 10%, 20%, and 30% led to a significant reduction in cement content from 830 to 581 kg/m^3. However, the rheological properties of the mortar were notably affected by the slag replacement, necessitating adjustments to the superplasticizer to maintain a consistent flow of 115%. Although decreasing cement content increased the initial printable time, all mix proportions with slag replacement up to 30% remained within the required limit, partially attributed to the presence of fibers in the mix. The use of slag as a partial cement replacement influenced the initial dimensions of the printed filaments, resulting in increased filament width and shorter filament height due to higher flowability. Moreover, compressive and flexural strengths increased with slag replacement. However, both flexural strengths appeared to be dependent on the direction of load vs. the printing direction in which the perpendicular strength exceeding the parallel strength (or transverse in the case of flexural strength). Overall, this investigation suggests that using slag as a partial cement replacement up to 30% is feasible for reducing the cement content of FRM for 3D printing while maintaining workability and initial printable time and enhancing both compressive and flexural strengths.

While parameters related to printing configuration, such as nozzle shape, size, printing speed, and layer thickness, require further investigation, we recommend exploring these factors in future studies.

5. Declarations

5.1. Author Contributions

Conceptualization, P.S. and S.K.; methodology, P.S. and S.K.; validation, S.J., H.Z., K.F., A.P., and C.H.; formal analysis, S.K.; investigation, S.K.; resources, P.S.; data curation, S.K.; writing—original draft preparation, P.S., H.Z., and S.J.; writing—review and editing, P.S., H.Z., K.F., and C.H.; visualization, S.K.; supervision, P.S.; project administration, P.S.; funding acquisition, P.S. All authors have read and agreed to the published version of the manuscript.

5.2. Data Availability Statement

The data presented in this study are available on request from the corresponding author.

5.5. Conflicts of Interest

The authors declare no conflict of interest.

6. References

[1] Buswell, R. A., Leal de Silva, W. R., Jones, S. Z., & Dirrenberger, J. (2018). 3D printing using concrete extrusion: A roadmap for research. Cement and Concrete Research, 112, 37–49. doi:10.1016/j.cemconres.2018.05.006.

[2] Saruhan, V., Keskinateş, M., & Felekoğlu, B. (2022). A comprehensive review on fresh state rheological properties of extrusion mortars designed for 3D printing applications. Construction and Building Materials, 337, 127629. doi:10.1016/j.conbuildmat.2022.127629.

[3] Zhang, J., Wang, J., Dong, S., Yu, X., & Han, B. (2019). A review of the current progress and application of 3D printed concrete. Composites Part A: Applied Science and Manufacturing, 125, 105533. doi:10.1016/j.compositesa.2019.105533.

[4] Beersaerts, G., Hertel, T., Lucas, S., & Pontikes, Y. (2023). Promoting the use of Fe-rich slag in construction: Development of a hybrid binder for 3D printing. Cement and Concrete Composites, 138, 104959. doi:10.1016/j.cemconcomp.2023.104959.

[5] Dey, D., Srinivas, D., Panda, B., Suraneni, P., & Sitharam, T. G. (2022). Use of industrial waste materials for 3D printing of sustainable concrete: A review. Journal of Cleaner Production, 340, 130749. doi:10.1016/j.jclepro.2022.130749.

[6] Panda, B., & Tan, M. J. (2019). Rheological behavior of high volume fly ash mixtures containing micro silica for digital construction application. Materials Letters, 237, 348–351. doi:10.1016/j.matlet.2018.11.131.

[7] Rubio, M., Sonebi, M., & Amziane, S. (2017). 3D printing of fibre cement-based materials: fresh and rheological performances. Academic Journal of Civil Engineering, 35(2), 480-488. doi:10.26168/icbbm2017.74.

[8] Yu, Q., Zhu, B., Li, X., Meng, L., Cai, J., Zhang, Y., & Pan, J. (2023). Investigation of the rheological and mechanical properties of 3D printed eco-friendly concrete with steel slag. Journal of Building Engineering, 72, 106621. doi:10.1016/j.jobe.2023.106621.

[9] Xu, Z., Zhang, D., Li, H., Sun, X., Zhao, K., & Wang, Y. (2022). Effect of FA and GGBFS on compressive strength, rheology, and printing properties of cement-based 3D printing material. Construction and Building Materials, 339, 127685. doi:10.1016/j.conbuildmat.2022.127685.

[10] Dai, S., Zhu, H., Zhai, M., Wu, Q., Yin, Z., Qian, H., & Hua, S. (2021). Stability of steel slag as fine aggregate and its application in 3D printing materials. Construction and Building Materials, 299, 123938. doi:10.1016/j.conbuildmat.2021.123938.

[11] Liu, J., & Lv, C. (2022). Properties of 3D-Printed Polymer Fiber-Reinforced Mortars: A Review. Polymers, 14(7), 1315. doi:10.3390/polym14071315.

[12] Lesovik, V., Fediuk, R., Amran, M., Alaskhanov, A., Volodchenko, A., Murali, G., Uvarov, V., & Elistratkin, M. (2021). 3D-Printed Mortars with Combined Steel and Polypropylene Fibers. Fibers, 9(12), 79. doi:10.3390/fib9120079.

[13] Ungureanu, D., Onuțu, C., Isopescu, D. N., Țăranu, N., Zghibarcea, Ștefan V., Spiridon, I. A., & Polcovnicu, R. A. (2023). A Novel Approach for 3D Printing Fiber-Reinforced Mortars. Materials, 16(13), 4609. doi:10.3390/ma16134609.

[14] Sukontasukkul, P., Maho, B., Komkham, S., Pianfuengfoo, S., Zhang, H. (Johnson), Yoo, D. Y., Tangchirapat, W., Sae-Long, W., Limkatanyu, S., & Chindaprasirt, P. (2023). Precise determination of initial printable time for cement mortar 3D printing using a derivative method. Rapid Prototyping Journal, 29(9), 1888–1903. doi:10.1108/RPJ-03-2023-0087.

[15] Sukontasukkul, P., Panklum, K., Maho, B., Banthia, N., Jongvivatsakul, P., Imjai, T., Sata, V., Limkatanyu, S., & Chindaprasirt, P. (2022). Effect of synthetic microfiber and viscosity modifier agent on layer deformation, viscosity, and open time of cement mortar for 3D printing application. Construction and Building Materials, 319. doi:10.1016/j.conbuildmat.2021.126111.

[16] Banthia, N., & Gupta, R. (2006). Influence of polypropylene fiber geometry on plastic shrinkage cracking in concrete. Cement and Concrete Research, 36(7), 1263–1267. doi:10.1016/j.cemconres.2006.01.010.

[17] Guerini, V., Conforti, A., Plizzari, G., & Kawashima, S. (2018). Influence of steel and macro-synthetic fibers on concrete properties. Fibers, 6(3), 47. doi:10.3390/fib6030047.

[18] Dai, P., Lyu, Q., Zong, M., & Zhu, P. (2024). Effect of waste plastic fibers on the printability and mechanical properties of 3D-printed cement mortar. Journal of Building Engineering, 83, 108439. doi:10.1016/j.jobe.2024.108439.

[19] Shakor, P., Nejadi, S., & Paul, G. (2019). A study into the effect of different nozzles shapes and fibre-reinforcement in 3D printed mortar. Materials, 12(10), 1708. doi:10.3390/MA12101708.

[20] Kumar Devalla, T., Srinivas, D., Panda, B., & Sitharam, T. G. (2023). Investigation on the flexural and tensile performance of 3D printable cementitious mixtures considering the effect of fiber distribution. Materials Today: Proceedings, 1-6. doi:10.1016/j.matpr.2023.04.081.

[21] Jamnam, S., Maho, B., Techaphatthanakon, A., Ruttanapun, C., Aemlaor, P., Zhang, H., & Sukontasukkul, P. (2022). Effect of graphene oxide nanoparticles on blast load resistance of steel fiber reinforced concrete. Construction and Building Materials, 343, 128139. doi:10.1016/j.conbuildmat.2022.128139.

[22] Panda, B., Chandra Paul, S., & Jen Tan, M. (2017). Anisotropic mechanical performance of 3D printed fiber reinforced sustainable construction material. Materials Letters, 209, 146–149. doi:10.1016/j.matlet.2017.07.123.

[23] Paul, S. C., Tay, Y. W. D., Panda, B., & Tan, M. J. (2018). Fresh and hardened properties of 3D printable cementitious materials for building and construction. Archives of Civil and Mechanical Engineering, 18(1), 311–319. doi:10.1016/j.acme.2017.02.008.

[24] Ding, T., Xiao, J., Zou, S., & Zhou, X. (2020). Anisotropic behavior in bending of 3D printed concrete reinforced with fibers. Composite Structures, 254, 112808. doi:10.1016/j.compstruct.2020.112808.

[25] Ma, G., Zhang, J., Wang, L., Li, Z., & Sun, J. (2018). Mechanical characterization of 3D printed anisotropic cementitious material by the electromechanical transducer. Smart Materials and Structures, 27(7), 75036. doi:10.1088/1361-665X/aac789.

[26] Shi, C., Meyer, C., & Behnood, A. (2008). Utilization of copper slag in cement and concrete. Resources, Conservation and Recycling, 52(10), 1115–1120. doi:10.1016/j.resconrec.2008.06.008.

[27] Scrivener, K. L., & Kirkpatrick, R. J. (2008). Innovation in use and research on cementitious material. Cement and Concrete Research, 38(2), 128–136. doi:10.1016/j.cemconres.2007.09.025.

[28] Li, L. G., Xiao, B. F., Cheng, C. M., Xie, H. Z., & Kwan, A. K. H. (2023). Adding Glass Fibers to 3D Printable Mortar: Effects on Printability and Material Anisotropy. Buildings, 13(9), 2295. doi:10.3390/buildings13092295.

[29] Panda, B., & Tan, M. J. (2018). Material properties of 3D printable high-volume slag cement. Proceedings of the First International Conference on 3D Construction Printing (3DcP) in Conjunction with the 6th International Conference on Innovative Production and Construction (IPC 2018), 26-28 November, Melbourne, Australia.

[30] Shakor, P., Nejadi, S., Paul, G., & Gowripalan, N. (2023). Effects of Different Orientation Angle, Size, Surface Roughness, and Heat Curing on Mechanical Behavior of 3D Printed Cement Mortar With/Without Glass Fiber in Powder-Based 3DP. 3D Printing and Additive Manufacturing, 10(2), 330–355. doi:10.1089/3dp.2021.0067.
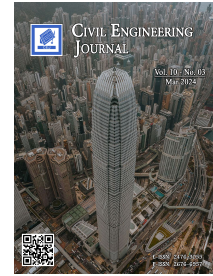
Experimental and ANN Analysis of Shearing Rate Effects on Coarse Sand Crushing

Samer R. Rabab'ah [1*], Omar H. Al Hattamleh [2], Ahmad N. Tarawneh [2], Hussien H. Aldeeky [2]

[1] Department of Civil Engineering, Jordan University of Science and Technology, P.O. Box 3030, Irbid, 22110, Jordan.

[2] Department of Civil Engineering, College of Engineering, The Hashemite University, P.O. Box 150459, Zarqa 13115, Jordan.

Abstract

The present study analyzes laboratory experiments on how shearing rate affects the shear strength and crushability of natural coarse sand, employing artificial neural network (ANN) analysis. This study tested three different coarse sands obtained from the crushing of natural rocks: Black Virgin Tuff, weathered Zeolitic Tuff, and calcareous limestone. The behavior of crushed sand specimens with consistent grading, which passed through sieve #4 and were retained on sieve #8, was analyzed using a direct shear box. The specimens were subjected to varied normal loads and shearing speeds to examine their behavior at different relative densities. The test results were analyzed using ANN to investigate the significance of shearing rates on shearing strength parameters, specifically internal mobilized peak friction, the constant volume (residual) internal friction angle, and the consequence of shearing rate on the particle's breakage index. The selected normal (Gaussian) rate significantly affected both the shear strength parameters and breakage. The loading rate increased both shear strength parameters and particle breakage. Therefore, it's highly recommended to maintain secure sets of shear strength values and comprehensive test data for assessing parameters at typical strain rates, prioritizing using slower rates whenever possible.

Keywords: Coarse Sand; Direct Shear Box; Grain Breakage; Density Index; Shearing Rate; ANN.

1. Introduction

The breakage phenomenon in granular materials has garnered significant attention from researchers within the geotechnical community. This interest stems from the widespread use of granular materials in various engineering construction projects, such as rockfill dams, railroad embankments, landslides, and driven piles. These structures encounter diverse loading scenarios, ranging from static to dynamic forces, which can lead to complex behaviors and failure mechanisms in the granular materials [1–6]. Lobo-Guerrero and Vallejo (2005, 2006) [7, 8] examined the effect of particle crushing on the capacity of driven piles. Their results indicated that the particles crushing negatively affect the capacity of piles. Okada et al. (2004) [1] reported that grain crushing was at the onset of trigging a landslide. An investigation of the excess pore water pressure generation of weathered granitic sand, taken from the source area of a typical landslide caused as a result of liquefaction, indicated that grain crushing within the failure zone is the key phenomenon of the rapid long-runout motion of landslides. Moreover, Fragaszy & Voss (1986) [9] reported that particle breakage will cause settlements and a reduction in hydraulic conductivity.

The crushing process of granular materials has the potential to alter shear strength parameters over the lifespan of construction projects, posing a threat to the integrity and safety of the project. Therefore, engineers and project managers must anticipate and mitigate the effects of crushing on shear strength parameters to ensure the long-term safety and durability of construction projects. Incorporating appropriate design considerations, monitoring techniques, and maintenance protocols can help to address the evolving properties of granular materials and mitigate potential hazards throughout the project's lifespan.

Researchers aim to investigate the factors that affect particle crushing to develop accurate predictive models and engineering strategies for mitigating risks associated with granular materials in construction and geotechnical applications. These factors include various variables such as sand grain characteristics, soil matrix properties, fabric and structure of the soil domain, loading scenarios, and type of granular materials, among many other factors [5]. Karatza et al. (2019), Xiao et al. (2019), and Varadarajan et al. (2006) studied sand grain characteristics such as angularity, morphology, and strength [10–12]. Soil matrix properties such as gradation, void distribution, and moisture content were examined by [13–16]. The fabric and structure of the soil domain, such as anisotropy [17, 18], external forces such as induced stresses [19–21], duration [20], and loading rates [22, 23], were appraised immensely. Granular materials include sands, ballast, rock fill, coral, coal, and food powder such as sugar and snow [5, 19, 24–33]. The intensity of particle breakage is appraised through the variation of the grading of granular materials using single grading, either indices or global grading indices obtained from the particle size distribution curve (PSD) [5]. Table 1 summarizes the method of various single-grading indices.

Table 1. Definition of single grading indices

Method Name	Criteria*	Remarks
Lee & Farhoomand (1967)	$B_{15} = D_{15}^i / D_{15}^f$	D_{15} = particle size corresponding to 15% finer on PSD
Marsal (1967)	$B_g = \Delta P_{max}$	ΔP_{max} = maximum difference of the PSD curves before and after the test
Nakata et al. 1999	$B_f = 1 - P_0$	P_0 = percentage of particles in current PSD smaller than the minimum particle size in the original sand
Xiao & Liu (2017)	$B_{r50} = (D_{50}^i - D_{50}^c)/(D_{50}^i - D_{50}^u)$	D_{50} = mean particle diameters

* i = initial; c = current, f = final, u = ultimate.

The global grading indices are evaluated through the changes in different areas bounded by ultimate, current, and initial PSD curves. Hardin (1985) and Einav (2007) are the most used criteria [34, 35]. Recently, Xiao et al. (2021) proposed an improved particle breakage index criterion to overcome the shortages of other criteria, such as the representation of all particle breakage in the whole domain, unique value, independent of grain side axis, and used in all types of gradation patterns [36].

Recently, there has been a noticeable shift in engineering modeling and computation toward machine learning techniques. In the last decade, machine-learning methods have been used in different fields of civil engineering [32–42] and have shown a high ability to recognize the pattern and relations between variables and the dependent. In particular, ANN mimics the interconnected nervous system of the human brain to transfer the data and recognize the pattern, as will be described in a later section.

The study is motivated by the observation that shear strength parameters, influenced by applied shear strain rate, lack relevant crushing indices when assessed across a wide range of relative initial density in crushed natural sands using conventional testing methods like triaxial compression or direct shear tests. Al-Hattamleh et al. (2023) [18] highlighted a significant gap in research concerning the examination of quasi-rates of applied shear strain on sand specimens. These quasi-rates of strain play a critical role in the development of crushing within granular materials. Yet, they are seldom explored in existing literature. Understanding the influence of these quasi-rates on the crushing behavior of granular materials is essential for accurately predicting their shear strength parameters.

This research aims to investigate the influence of normal shearing rates on breakage in various types of sands using a combination of experimental results and ANN analysis. This study will provide experimental data and analysis for these sand types to address a gap in the existing literature, particularly regarding black volcanic tuff and Zeolitic volcanic tuff and the associated shearing device methodologies. Additionally, it will outline the procedure for direct shear testing, offering valuable insights into the behavior of these sands under different shearing rates.

2. Experimental Works

2.1. Materials

Three types of sand were selected for this study: a Virgin Black Volcanic Tuff (BT), a weathered Zeolitic Volcanic Tuff (ZT), and Limestone (LT). The Al-Hala region in Al-Tafila in southern Jordan provided the BT and ZT sands. According to ASTM E1621-13 standard X-ray fluorescence spectroscopy examination, BT and ZT are both mostly constituted of SiO_2, ranging from 40% to 50%, with notable amounts of Fe_2O_3 and Al_2O_3 oxides, ranging from 12.75%

to 13.00% and from 10.67% to 12.64%, respectively. On the other hand, the Limestone (LS) was obtained from Irbid in northern Jordan. LS comprises nearly equal percentages of calcareous materials $CaCO_3$ and CaO (40-46%). The Specific gravity (Gs), Minimum Dry Density (ρ_{min}), and Maximum Dry Density (ρ_{max}) of all types of sands were conducted according to the American Society for Testing and Materials standards (ASTM) [38, 39], respectively. The Gs for BT, ZT, and LS are 2.67, 2.64, and 2.53, respectively. While the (ρ_{min} (kg/m³), ρ_{max} (kg/m³)) for BT, ZT, and LS are (1100, 1355), (900, 1030), and (1068, 1328), respectively. The grain sizes of the three varieties of sand were measured according to ASTM D6913 [40]. The grane size ranges utilized for the shear testing were specifically chosen to pass sieve #4 at 4.75mm and be retained at 2.36mm (sieve #8). Because the specimens are of the same grain size, the coefficient of uniformity and curvature are close to unity for all types of sand. As a result, the Unified Soil Classification System (USCS) classifies these sands as poorly graded sand, SP [41].

2.2. Test Setup

A direct, simple shear box (DSB) device was used to conduct the shearing of prepared specimens. The apparatus can apply vertical and horizontal forces up to 5 kN. Two linear variable differential transformers (LVDTs) measured the horizontal and vertical displacements. The device was designed to accommodate a cubical soil specimen of 6.00 cm side. The maximum grain size utilized in the test was selected to ensure that no boundary would alter the outcomes in compliance with ASTM D3080 [42] general requirements.

Dry samples of the four relative densities of the loose, medium, and very dense sand were subjected to DSB tests following ASTM D6528 [43] at three different loading rates (0.50, 1.00, and 2.00 mm/minute) under four different vertical stress conditions (136, 245, 463, and 899 kPa). Sieves analyses were performed for each test, and the results of all tests are summarized in Table 2. Data from DSB tests were analyzed to establish the shear strength parameters for each test, specifically constant volume (residual) mobilized friction angle (ϕ_r) and peak mobilized friction angle (ϕ_p). After performing the DSB test on each specimen, sieve analysis was used to determine the amount and percentage of particle breakage index (Br).

3. Results and Discussion

3.1. Experimental Results

The specimens were prepared for the DSB tests as described in Table 2. For BT sand at a shearing rate of mm/minutes, Figure 1 shows the relationship between normalized shear stresses and horizontal displacement of various relative densities. This figure shows that, as predicted, the shear stress arose as the shear displacement increased, reaching a peak value before decreasing to an asymptote value as the shear displacement increased. Sand particles moved rather easily under low normal stress conditions, and the relative displacement immediately stabilized. However, a bigger shear displacement was necessary to achieve a stable condition when the normal stress was high as it increased the contact between sand particles and made displacement more difficult.

Table 2. Summary of the conducted tests: Relative densities, applied vertical stresses, and applied shearing rates were used in tests for the sand in a direct shear test

| Relative Density (%) | Input Test Parameters | | | | | Remarks |
| | Density kg/m³ | | | Vertical Stress, σ_v: kPa | Shearing Rate (mm/minute) | |
	BT	ZT	LS			
20%	1143	996.8	1110	136	0.50, 1.00, & 2.00	
				245	0.50, 1.00, & 2.00	
				463	0.50, 1.00, & 2.00	
				899	0.50, 1.00, & 2.00	
40%	1190	1023.8	1023.8	136	0.50, 1.00, & 2.00	Sieve analyses were conducted after each test for all rates and applied vertical stresses.
				245	0.50, 1.00, & 2.00	
				463	0.50, 1.00, & 2.00	
				899	0.50, 1.00, & 2.00	
60%	1240	1051.9	105139	136	0.50, 1.00, & 2.00	
				245	0.50, 1.00, & 2.00	
				463	0.50, 1.00, & 2.00	
				899	0.50, 1.00, & 2.00	
80%	1129	1080	1270	136	0.50, 1.00, & 2.00	
				245	0.50, 1.00, & 2.00	
				463	0.50, 1.00, & 2.00	
				899	0.50, 1.00, & 2.00	

Figure 1. Normalized shear stresses vs. horizontal displacement of different relative densities for BT sand at a shearing rate of 0.50 mm/minutes

Moreover, as the relative density, Dr, increases and normal stresses decrease, a distinct peak is observed, and then, with further displacement, a softening occurs. These results are consistent with what Duncan et al. (2014) [44] assumed: the most crucial factors affecting soil strength are the effective stress applied to the soil and soil density. Thus, higher effective stress results in higher strength, and the higher the density, the higher the strength

The mobilized friction angles of the tested sands were calculated to assess the impact of using various shearing rates. The mobilized shear strength parameters ϕ_p and ϕ_r are defined as:

$$\phi_p = \tan^{-1}\frac{\tau_{peak}}{\sigma} \tag{1}$$

$$\phi_r = tan^{-1}\frac{\tau_{residual}}{\sigma} \tag{2}$$

where τ_{peak}, $\tau_{residual}$, and applying normal stresses are the peak shearing stresses.

Based on global grading indices, the particle breakage index, Br, is reported here [5]. The Einav (2007) breakage index is determined using the grain size distribution curves before and after shearing. When sheared, the gradation curves change from a wide sieve opening to a smaller one. The ZT sand specimen's grain size distribution after direct shear testing with various normal stresses and relative density of Dr=80% at a loading rate of 1mm/min is shown in Figure 2.

3.2. Artificial Neural Network Model

In this study, an ANN was selected to assess the impact of shearing load, loading rate, and the relative density of sand on the peak internal friction angles, residual internal friction angles, and breakage index. ANN has been selected for its ability to generalize and avoid overfitting [45].

ANN is a multi-layer framework; the input layer of an ANN is the first layer, representing the parameters, while the output layer is the last, containing the output. One or more hidden layers may be present between the input and output

layers, controlling the process of identifying (learning) patterns in the data. Simple processing units (PUs) comprise each layer and are completely coupled to other PUs in the layer above them (Figure 3).
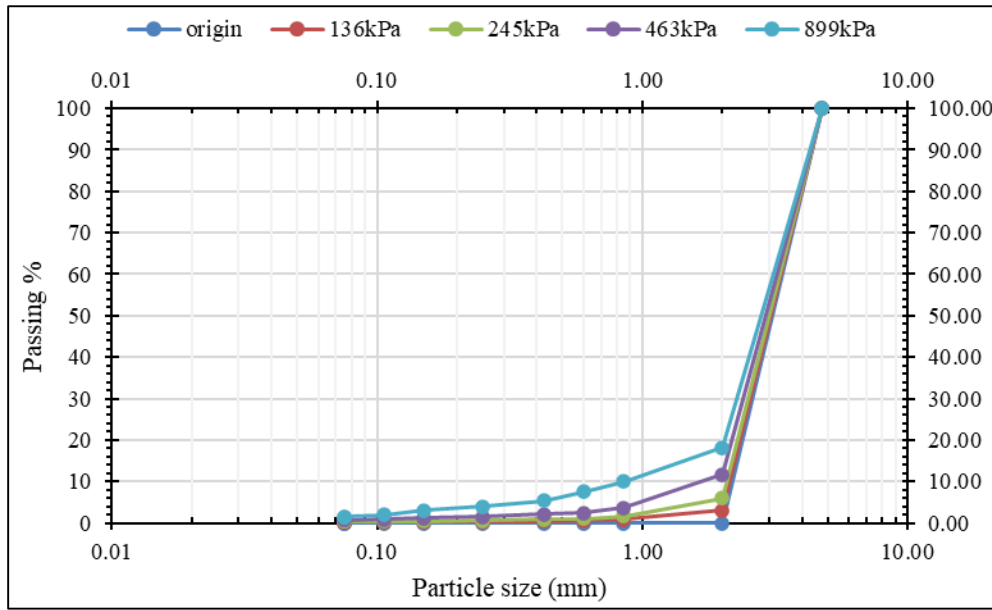
Figure 2. Sieve analysis for ZT at Dr=80%, Rate of Loading=1 mm/min, and different normal stress
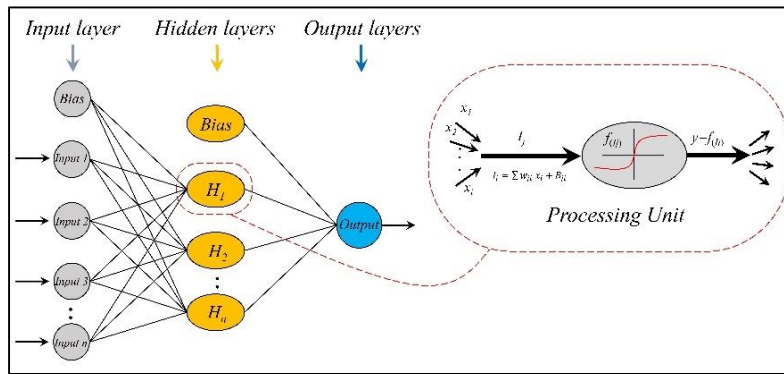
Figure 3. General structure and processing unit of ANNs

Whenever a signal or input x_i is received, the PU is multiplied by a calibrated weight w_{ji} that determines the signal's behavior and importance. Each PU adds the calibrated signals together and adds a calibrated bias value B_{ji} according to Equation 3. The output of the PU is produced by passing the combined input I_j using a nonlinear transfer function f(I_j), which will serve as the input for PUs in the following layer (Figure 3-b). This study makes use of a hyperbolic tangent sigmoid transfer function.

$$I_j = \sum w_{ji}\, x_i + B_{ji} \tag{3}$$

The training algorithm modifies the weights and bias values of Levenberg-Marquardt optimization during the training process. In order to create a network that generalizes well, it first identifies the optimal combination of squared errors and weights. It is known as Bayesian regularization. The performance function, referred to as the Mean Square error (MSE), is used to express the error (Equation 4). Training continues until MSE converges and no further advancement in the solution is achieved.

$$MSE = \frac{1}{N}\sum_{k=1}^{N}(Actual - Predicted)^2 \tag{4}$$

It should be noted that the first step required by Equation 5 is for the input variables to be normalized. The input value is shifted by the offset value of_{in} and multiplied by the gain value a_{in}. To de-normalize the signal at the output layer, remove the offset of_{on} and divide the output by the gain a_{on}.

$$x_i = X_i\, a_{in} + of_{in} \tag{5}$$

Experimentation is used to determine the number of PUs needed in the hidden layer to mimic and approximate the complex behavior (trial). In ANN modeling, the number of hidden layers should often be limited to prevent overfitting. However, overfitting was not a concern due to using Bayesian regularization in the particular instance.

3.2.1. Proposed Models

Three ANN models were developed using the ANN toolbox of MATLAB R2018b. To select the optimal PUs in the hidden layer, PUs from 1 to 10 were tested while examining the MSE, and the optimal required number of layers was found to be 2. The experimental data has been divided into a training dataset (80%) and a validation dataset (20%). In this study, the input layer includes normalized period shearing load σn, loading rate, and soil Density (Dr.), while the output layer includes peak internal friction angles ϕ_p, residual internal friction angles ϕ_r, and the breakage index Br. The three ANN models and the corresponding R^2 are shown in Figure 4.
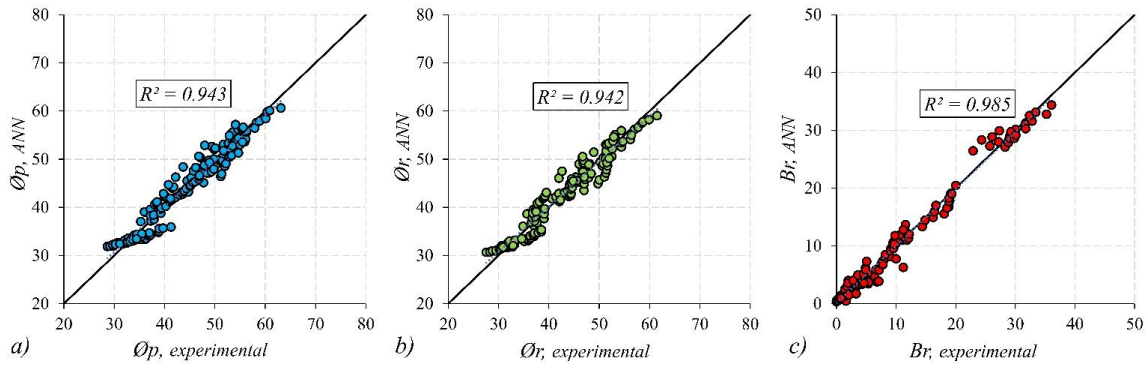
Figure 4. Developed ANN model to predict peak internal friction angles ϕp, residual internal friction angles ϕr, and the breakage index Br

In order to investigate the effect of each of the input layer variables, parametric curves were generated using the developed ANN models, as shown in Figure 5.
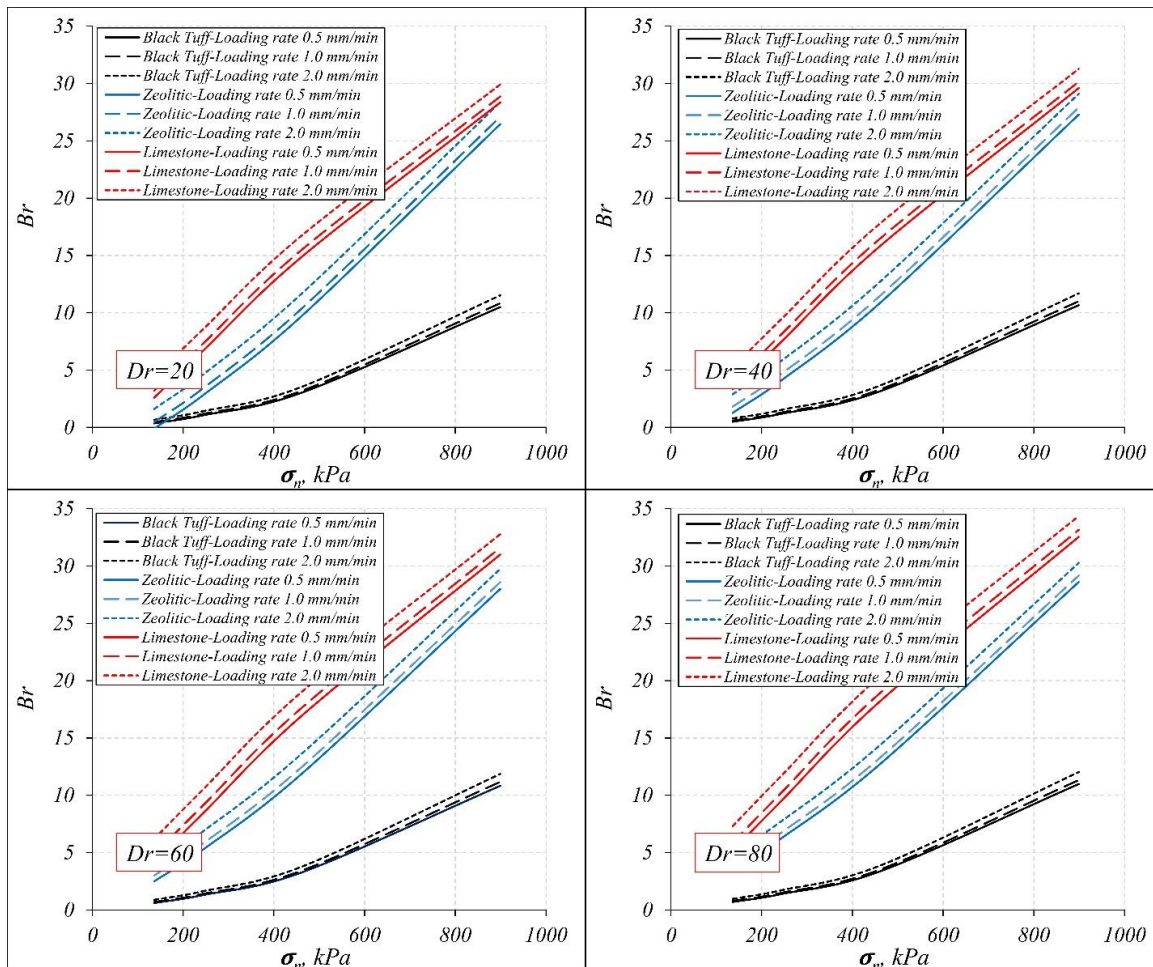
Figure 5. Particle Breakage Indices versus applied normal pressure for three types of sand at three different shearing rates for different relative densities

3.2.2. ANN Results and Discussion

Figure 5 shows the prediction of ANN models to the particle breakage indices, Br, as a function of normal applied stresses at a different shearing rate for sand specimens prepared at different relative densities. As anticipated, the amount of Br increased with the applied vertical stress and with higher relative density for all types of sands. This finding is rectified by Xiao et al. (2020) in a one-dimensional compression test for carbonate sand and by Asadzadeh and Soroush (2009) [46] for rockfill material composed of a limestone tested in direct shear such as LS here. Moreover, the particle breakage index shows a linear dependence on the applied normal stresses. regardless of the initial relative density (Figure 5) which was confirmed earlier by Asadzadeh & Soroush (2009) [46]. Conversely, for stronger materials like BT here, the particle breakage is more toward a power-like trend, as shown by Wang et al. (2021) [47].

Furthermore, the Br increases drastically with an increased rate of shearing at a given relative density despite the applied normal stress or type of sand. The reason was that the sand grains did not take enough time to rearrange or to orientate themselves, so the crushing of particles increased. Additionally, with D_r increasing, the amount of Br increased in all soil types tested. This finding was confirmed by many researchers [26, 48, 49], who showed that particle breakage is inversely proportional to the increased initial void ratio. The amount of crushing reported is higher for LS than BT and ZT sands due to weak bonds of $CaCO_3$ compared with SiO_2. This finding confirms what has been reported earlier in the literature, that crushing is directly related to particle strength [34, 50–52]. A rectification by Al-Hattamleh et al. (2023) [18], using scanning electron microscopy (SEM) supplied with energy-dispersive X-ray spectroscopy (SEM/EDX) of samples taken from the shearing zone of tested specimens, shows that the granules of original sizes which confined between 2.36 mm and 4.75 mm experience disintegration and cleavage, abrasion and grinding and surfaces' scratching.

Figure 6. Peak internal friction angles versus applied normal pressure for three types of sand at three different shearing rates for different relative densities

The prediction of ANN models for peak and residual internal friction angles is shown in Figures 6 and 7. Both figures show internal friction angles versus applied normal pressure for three types of sand at three different shearing rates for different relative densities. Both figures show that applied vertical stresses considerably lower peak and residual angles, independent of the sand samples' relative densities or the employed shear rate. The impact of exerting pressure and shearing rates, particularly at larger relative densities, are more or less reduced in residual friction angle. This result could explain the critical states line's downward migration in the compression plane [48, 49, 53, 54]. Moreover, the

effect of the shearing rate in both $\phi\tau\eta\epsilon_p$ angle (Figure 6) and ϕ_r angle (Figure 7) is pronounced. According to these findings, despite the relative density values being employed, increasing the shearing rate increased both ϕ_p and ϕ_r angles. On the other hand, a further increase in the shearing rate appeared to smooth out the growing degree of friction angles. Hence, as pointed out by Wei et al. (2021) [55], the residual shear strength decreased with increasing roundness and aspect ratio due to the effect of particle breakage. Congruently, the residual friction angles, ϕ_r, decreased with increasing applied normal stresses, as shown in Figure 7.
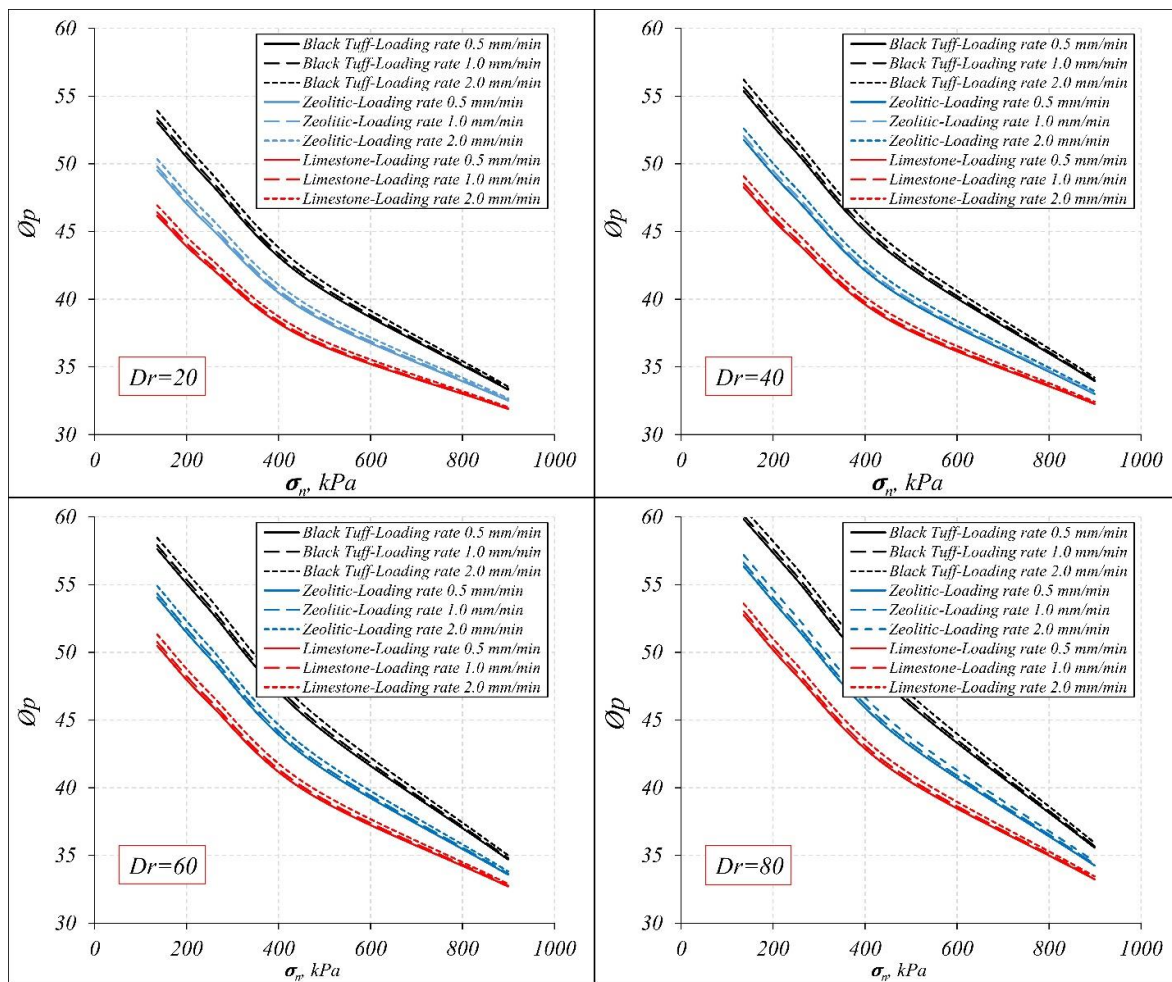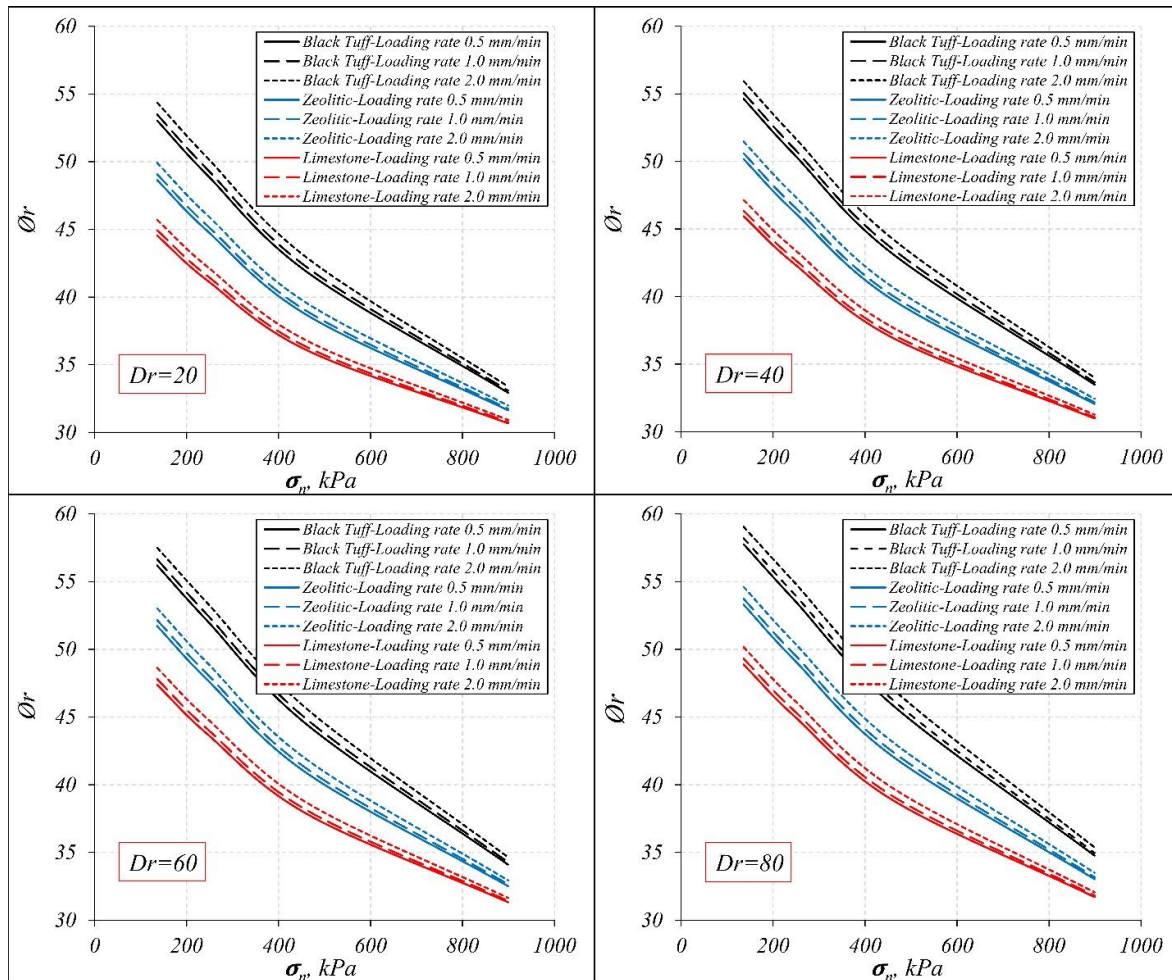

Figure 7. Residual internal friction angles versus applied normal pressure for three types of sand at three different shearing rates for different relative densities

4. Conclusions

The effect of the normal shearing rate was experimentally conducted using a direct shear device on prepared specimens of three different types of natural sand. After that, the results were analyzed using the ANN technique. The analysis includes the effect of the shearing rate on particle breakage indices and its effect on the outcome of internal peak and residual friction angles. Based on the ANN models and the parametric study, the following conclusion can be drawn:

- The interaction between relative density, normal stress, and particle crushing indices, Br, reveals insightful trends across all sand types investigated. With increasing normal stress, relative density, and shearing rate, the Br values show a noticeable increase. Additionally, as the rate of shearing increases, the peak friction angle exhibits a concurrent increase, indicative of a strengthening of interparticle contacts and resistance to shear deformation. On the other hand, results show that the residual friction angle decreases with reductions in relative density and applied normal loads, while it enhances with increasing rates of shearing. These results emphasize the sensitivity of residual friction to variations in these parameters, reflecting the evolving interparticle interactions within the sand samples.

- Moreover, the comparative analysis among sand types highlights distinctive characteristics. BT sand exhibits the highest internal peak friction angle value compared to ZT and LS sands, indicating its notable resistance to shear deformation. Conversely, the breakage index is highest for LS sand compared to BT and ZT sands, suggesting a greater tendency for particle fragmentation and degradation in LS sand. The contrasting behaviors observed highlight the varied mechanical responses of different types of sand under different loading conditions, emphasizing the importance of considering sand-specific properties in engineering and geotechnical applications.

5. Declarations

5.1. Author Contributions

Conceptualization, S.R., O.A., and H.A.; methodology, O.A. and A.T.; software, A.T.; writing—original draft preparation, S.R., O.A., and A.T; writing—review and editing, S.R. and O.A.; project administration, S.R., O.A., and H.A. All authors have read and agreed to the published version of the manuscript.

5.2. Data Availability Statement

The data presented in this study are available on request from the corresponding author.

5.3. Funding

5.4. Conflicts of Interest

The authors declare no conflict of interest.

6. References

[1] Okada, Y., Sassa, K., & Fukuoka, H. (2004). Excess pore pressure and grain crushing of sands by means of undrained and naturally drained ring-shear tests. Engineering Geology, 75(3–4), 325–343. doi:10.1016/j.enggeo.2004.07.001.

[2] Sevi, A., & Ge, L. (2012). Cyclic Behaviors of Railroad Ballast within the Parallel Gradation Scaling Framework. Journal of Materials in Civil Engineering, 24(7), 797–804. doi:10.1061/(asce)mt.1943-5533.0000460.
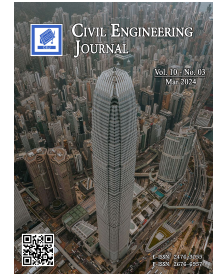
[3] Kermani, M., Konrad, J.-M., & Smith, M. (2018). In Situ Short-Term and Long-Term Rockfill Compressibility as a Function of Void Ratio and Strength of Parent Rock. Journal of Geotechnical and Geoenvironmental Engineering, 144(4), 04018009. doi:10.1061/(asce)gt.1943-5606.0001835.

[4] Altuhafi, F. N., Jardine, R. J., Georgiannou, V. N., & Moinet, W. W. (2018). Effects of particle breakage and stress reversal on the behaviour of sand around displacement piles. Geotechnique, 68(6), 546–555. doi:10.1680/jgeot.17.P.117.

[5] Xiao, Y., Desai, C. S., Daouadji, A., Stuedlein, A. W., Liu, H., & Abuel-Naga, H. (2020). Grain crushing in geoscience materials–Key issues on crushing response, measurement and modeling: Review and preface. Geoscience Frontiers, 11(2), 363–374. doi:10.1016/j.gsf.2019.11.006.

[6] Wang, Y., Cheng, Y., Yang, G., Xie, Y., Huang, H., & Liu, R. (2024). Study on the inhibitory effect of rubber on particle breakage and the impact on the volumetric deformation of calcareous sand under different loading modes. Construction and Building Materials, 414, 135014. doi:10.1016/j.conbuildmat.2024.135014.

[7] Lobo-Guerrero, S., & Vallejo, L. E. (2006). Modeling granular crushing in ring shear tests: Experimental and numerical analyses. Soils and Foundations, 46(2), 147–157. doi:10.3208/sandf.46.147.

[8] Lobo-Guerrero, S., & Vallejo, L. E. (2005). Crushing a weak granular material: Experimental numerical analyses. Geotechnique, 55(3), 245–249. doi:10.1680/geot.2005.55.3.245.

[9] Fragaszy, R. J., & Voss, M. E. (1986). Undrained compression behavior of sand. Journal of Geotechnical Engineering, 112(3), 334–347. doi:10.1061/(ASCE)0733-9410(1986)112:3(334).

[10] Karatza, Z., Andò, E., Papanicolopulos, S. A., Viggiani, G., & Ooi, J. Y. (2019). Effect of particle morphology and contacts on particle breakage in a granular assembly studied using X-ray tomography. Granular Matter, 21(3), 1-13. doi:10.1007/s10035-019-0898-2.

[11] Xiao, Y., Long, L., Matthew Evans, T., Zhou, H., Liu, H., & Stuedlein, A. W. (2019). Effect of Particle Shape on Stress-Dilatancy Responses of Medium-Dense Sands. Journal of Geotechnical and Geoenvironmental Engineering, 145(2), 04018105. doi:10.1061/(asce)gt.1943-5606.0001994.

[12] Varadarajan, A., Sharma, K. G., Abbas, S. M., & Dhawan, A. K. (2006). Constitutive Model for Rockfill Materials and Determination of Material Constants. International Journal of Geomechanics, 6(4), 226–237. doi:10.1061/(asce)1532-3641(2006)6:4(226).

[13] Hyodo, M., Wu, Y., Aramaki, N., & Nakata, Y. (2017). Undrained monotonic and cyclic shear response and particle crushing of silica sand at low and high pressures. Canadian Geotechnical Journal, 54(2), 207–218. doi:10.1139/cgj-2016-0212.

[14] Ovalle, C., & Hicher, P. Y. (2020). Modeling the effect of wetting on the mechanical behavior of crushable granular materials. Geoscience Frontiers, 11(2), 487–494. doi:10.1016/j.gsf.2019.06.009.

[15] Alonso, E. E., Romero, E. E., & Ortega, E. (2016). Yielding of rockfill in relative humidity-controlled triaxial experiments. Acta Geotechnica, 11(3), 455–477. doi:10.1007/s11440-016-0437-9.

[16] Xiao, Y., Meng, M., Wang, C., Wu, H., Fang, Q., & Liu, S. (2023). Breakage critical state of gravels with different gradings. Part I: Experimental results. Transportation Geotechnics, 42, 101087. doi:10.1016/j.trgeo.2023.101087.

[17] Al-Hattamleh, O. H., Al-Deeky, H. H., & Akhtar, M. N. (2013). The Consequence of Particle Crushing in Engineering Properties of Granular Materials. International Journal of Geosciences, 04(07), 1055–1060. doi:10.4236/ijg.2013.47099.

[18] Al-Hattamleh, O., Sharo, A., Abu Shanab, L., Aldeeky, H., & Al Dwairi, R. (2023). Effect of the quasi rate of loading in Particle Crushing and Engineering Properties of Black Tough Sand. Acta Montanistica Slovaca, 28(2), 301–313. doi:10.46544/AMS.v28i2.04.

[19] Al-Hattamleh, O., Alshalabi, F., Al Qablan, H., & Al-Rousan, T. (2010). Effect of grain crushing and bedding plane inclination on Aqaba sand behavior. Bulletin of Engineering Geology and the Environment, 69(1), 41–49. doi:10.1007/s10064-009-0238-6.

[20] Fu, Z., Chen, S., Zhong, Q., & Zhang, Y. (2019). Modeling interaction between loading-induced and creep strains of rockfill materials using a hardening elastoplastic constitutive model. Canadian Geotechnical Journal, 56(10), 1380–1394. doi:10.1139/cgj-2018-0435.

[21] Li, J., Huang, Y., Ouyang, S., Guo, Y., Gao, H., Wu, L., Shi, Y., & Zhu, L. (2022). Transparent characterization and quantitative analysis of broken gangue's 3D fabric under the bearing compression. International Journal of Mining Science and Technology, 32(2), 335–345. doi:10.1016/j.ijmst.2021.11.013.

[22] Huang, J. Y., Hu, S. S., Xu, S. L., & Luo, S. N. (2017). Fractal crushing of granular materials under confined compression at different strain rates. International Journal of Impact Engineering, 106, 259–265. doi:10.1016/j.ijimpeng.2017.04.021.

[23] Parab, N. D., Guo, Z., Hudspeth, M. C., Claus, B. J., Fezzaa, K., Sun, T., & Chen, W. W. (2017). Fracture mechanisms of glass particles under dynamic compression. International Journal of Impact Engineering, 106, 146–154. doi:10.1016/j.ijimpeng.2017.03.021.

[24] Yamamuro, J. A., Bopp, P. A., & Lade, P. V. (1996). One-Dimensional Compression of Sands at High Pressures. Journal of Geotechnical Engineering, 122(2), 147–154. doi:10.1061/(asce)0733-9410(1996)122:2(147).

[25] Miura, S., Yagi, K., & Asonuma, T. (2003). Deformation-strength evaluation of crushable volcanic soils by laboratory and in-situ testing. Soils and Foundations, 43(4), 47–57. doi:10.3208/sandf.43.4_47.

[26] Barraclough, T. W., Blackford, J. R., Liebenstein, S., Sandfeld, S., Stratford, T. J., Weinländer, G., & Zaiser, M. (2017). Propagating compaction bands in confined compression of snow. Nature Physics, 13(3), 272–275. doi:10.1038/nphys3966.

[27] Strahler, A. W., Stuedlein, A. W., & Arduino, P. (2018). Three-Dimensional Stress-Strain Response and Stress-Dilatancy of Well-Graded Gravel. International Journal of Geomechanics, 18(4), 04018014. doi:10.1061/(asce)gm.1943-5622.0001118.

[28] Yu, F. (2017). Particle Breakage and the Drained Shear Behavior of Sands. International Journal of Geomechanics, 17(8), 04017041. doi:10.1061/(asce)gm.1943-5622.0000919.

[29] Xiao, Y., Liu, H., Chen, Q., Ma, Q., Xiang, Y., & Zheng, Y. (2017). Particle breakage and deformation of carbonate sands with wide range of densities during compression loading process. Acta Geotechnica, 12(5), 1177–1184. doi:10.1007/s11440-017-0580-y.

[30] Zhang, J., Li, M., Liu, Z., & Zhou, N. (2017). Fractal characteristics of crushed particles of coal gangue under compaction. Powder Technology, 305, 12–18. doi:10.1016/j.powtec.2016.09.049.

[31] Indraratna, B., Ngo, T., & Rujikiatkamjorn, C. (2020). Performance of Ballast Influenced by Deformation and Degradation: Laboratory Testing and Numerical Modeling. International Journal of Geomechanics, 20(1), 04019138. doi:10.1061/(asce)gm.1943-5622.0001515.

[32] Yang, L., Long, Z., Kuang, D., Liu, X., & Li, Z. (2023). Influences of size, shape and strain rate on mechanical properties of single coral particle. Journal of Building Engineering, 78, 107667. doi:10.1016/j.jobe.2023.107667.

[33] Chen, J., Liu, Y., Hu, Q., & Gao, R. (2023). Effects of Particle Size and Grading on the Breakage of Railway Ballast: Laboratory Testing and Numerical Modeling. Sustainability, 15(23), 16363. doi:10.3390/su152316363.

[34] Hardin, B. O. (1985). Crushing of soil particles. Journal of Geotechnical Engineering, 111(10), 1177–1192. doi:10.1061/(ASCE)0733-9410(1985)111:10(1177).

[35] Einav, I. (2007). Breakage mechanics-Part I: Theory. Journal of the Mechanics and Physics of Solids, 55(6), 1274–1297. doi:10.1016/j.jmps.2006.11.003.

[36] Xiao, Y., Wang, C., Wu, H., & Desai, C. S. (2021). New Simple Breakage Index for Crushable Granular Soils. International Journal of Geomechanics, 21(8). doi:10.1061/(asce)gm.1943-5622.0002091.

[37] Chen, Q., Li, Z., Dai, Z., Wang, X., Zhang, C., & Zhang, X. (2023). Mechanical behavior and particle crushing of irregular granular material under high pressure using discrete element method. Scientific Reports, 13(1), 7843. doi:10.1038/s41598-023-35022-w.

[38] ASTM D854-23. (2023). Test Methods for Specific Gravity of Soil Solids by Water Displacement Method. ASTM International, Pennsylvania, United States. doi:10.1520/D0854-23.

[39] ASTM D7382-20. (2020). Standard Test Methods for Determination of Maximum Dry Unit Weight and Water Content Range for Effective Compaction of Granular Soils Using a Vibrating Hammer. ASTM International, Pennsylvania, United States. doi:10.1520/D7382-20.

[40] ASTM D6913-04(2009)E1. (2017). Standard Test Methods for Particle-Size Distribution (Gradation) of Soils Using Sieve Analysis. ASTM International, Pennsylvania, United States. doi:10.1520/D6913-04R09E01.

[41] ASTM D2487-17. (2020). Practice for Classification of Soils for Engineering Purposes (Unified Soil Classification System). ASTM International, Pennsylvania, United States. doi:10.1520/D2487-17.

[42] ASTM D3080-04. (2012). Test Method for Direct Shear Test of Soils Under Consolidated Drained Conditions. ASTM International, Pennsylvania, United States. doi:10.1520/D3080-04.

[43] ASTM D6528-17. (2017). Test Method for Consolidated Undrained Direct Simple Shear Testing of Cohesive Soils. ASTM International, Pennsylvania, United States. doi:10.1520/D6528-17.

[44] Duncan, J. M., Wright, S. G., & Brandon, T. L. (2014). Soil strength and slope stability. John Wiley & Sons, Hoboken, United States.

[45] Tarawneh, A., Almasabha, G., & Murad, Y. (2022). ColumnsNet: Neural Network Model for Constructing Interaction Diagrams and Slenderness Limit for FRP-RC Columns. Journal of Structural Engineering, 148(8), 04022089. doi:10.1061/(asce)st.1943-541x.0003389.

[46] Asadzadeh, M., & Soroush, A. (2009). Direct shear testing on a rockfill material. Arabian Journal for Science and Engineering, 34(2 B), 379–396.

[47] Wang, G., Wang, Z., Ye, Q., & Zha, J. (2021). Particle breakage evolution of coral sand using triaxial compression tests. Journal of Rock Mechanics and Geotechnical Engineering, 13(2), 321–334. doi:10.1016/j.jrmge.2020.06.010.

[48] Li, G., Liu, Y.-J., Dano, C., & Hicher, P.-Y. (2015). Grading-Dependent Behavior of Granular Materials: From Discrete to Continuous Modeling. Journal of Engineering Mechanics, 141(6), 04014172. doi:10.1061/(asce)em.1943-7889.0000866.

[49] Xiao, Y., & Liu, H. (2017). Elastoplastic Constitutive Model for Rockfill Materials Considering Particle Breakage. International Journal of Geomechanics, 17(1), 04016041. doi:10.1061/(asce)gm.1943-5622.0000681.

[50] McDowell, G. R., & Bolton, M. D. (1998). On the micromechanics of crushable aggregates. Geotechnique, 48(5), 667–679. doi:10.1680/geot.1998.48.5.667.

[51] Lade, P. V., Yamamuro, J. A., & Bopp, P. A. (1996). Significance of Particle Crushing in Granular Materials. Journal of Geotechnical Engineering, 122(4), 309–316. doi:10.1061/(asce)0733-9410(1996)122:4(309).

[52] Feda, J. (2002). Notes on the effect of grain crushing on the granular soil behaviour. Engineering Geology, 63(1–2), 93–98. doi:10.1016/S0013-7952(01)00072-2.

[53] Liu, M., Gao, Y., & Liu, H. (2014). An elastoplastic constitutive model for rockfills incorporating energy dissipation of nonlinear friction and particle breakage. International Journal for Numerical and Analytical Methods in Geomechanics, 38(9), 935–960. doi:10.1002/nag.2243.

[54] Ning, F., Liu, J., Kong, X., & Zou, D. (2020). Critical State and Grading Evolution of Rockfill Material under Different Triaxial Compression Tests. International Journal of Geomechanics, 20(2), 04019154. doi:10.1061/(asce)gm.1943-5622.0001550.

[55] Wei, H., Yin, M., Zhao, T., Yan, K., Shen, J., Meng, Q., Wang, X., & He, J. (2021). Effect of particle breakage on the shear strength of calcareous sands. Marine Geophysical Research, 42(3), 1-11. doi:10.1007/s11001-021-09440-2.

Dynamic Buckling Analysis of Ductile Damage Evolution for Thin Shell With Lemaitre's Model

Iheb Hammar [1*], Mohamed Djermane [1], Belkacem Amieur [1]

[1] FIMAS Lab, Department of Civil Engineering, Tahri Mohamed University, Bechar, 08000 Algeria.

Abstract

Thin-shell structures are used in several fields of construction and are often exposed to severe dynamic environments, making them susceptible to dynamic instabilities. These instabilities are typically preceded by varying degrees of damage to the shell, justifying the need to incorporate this behavior in the formulation of the finite elements used. The objective of this work is to evaluate the different dynamic instability criterion in the presence of damage, afterward, evaluate the influence of this behavior on the stability of shells subjected to the dynamic excitations. The methodology of this project is essentially numerical, based on the finite element method. We are asked to program the introduction of damaging behavior and Lemaitre's model criteria in the DYNCOQ program developed locally. To examine the results, two examples extracted from the literature were presented. The first model aimed to confirm the proper functioning of the program and the convergence of the plasticity criterion (Lemaitre's model). As for the second model, it allows us to test the dynamic instability. A comparison was made with experimental data from previously published literature, revealing a strong agreement between the calculated and experimental results. The obtained results prove the utility of considering this behavior in the shell analysis.

Keywords: Dynamic Buckling; Shells; Damage; Finite Element; Imperfections; Damage Measurement.

1. Introduction

The field of continuum damage mechanics was initially pioneered by McClintock (1968) [1] and has since been actively pursued by researchers, such as a ductile damage model for ductile rupture, founded on void nucleation and growth was initially offered by Gurson (1977) [2]. In this criterion, the process of creating microvoids, growth, and coalescence was taken into account by a yield surface function and an upper bound approach of a hollow sphere made of ideal plastic von Mises material. The proposed yield surface could not represent the coalescence and fracture of material due to the low growth rate of microvoids. Tvergaard and Needleman modified the original yield surface and developed a constitutive model for porous metal plasticity, named the Gurson-Tvergaard-Needleman (GTN) criterion [3]. Another well-known standard, Lemaitre's ductile damage criterion, was initially offered by Lemaitre (1985) [4]. This formulation describes the evolution of irreversible phenomena such as the growth of voids under plastic deformations by the effective stress concept. The significant advantage of this criterion is that only one material dependent damage parameter is required for each material. The damage models introduced by these researchers have gained widespread acceptance and application in the finite element method (FEM). The application of these models on the shells guided us to the work of Lee & Pourboghrat (2005) [5]. The latter has proposed a numerical simulation of the Punchless Piercing Process using Lemaitre's model. The same model was used with the tavelgard models in the work of He et al. (2020) [6].

While the plastic damaging behavior is well-documented in tensile tests, as evidenced by the research of Li et al. (2024) [7], Laboubi et al. (2023) [8], and Restrepo et al. (2018) [9], Similarly, in compression, the crack closure effect has been examined in the model proposed by De Souza Neto (2002) [10], with a concise explanation provided by Shamshiri et al. (2023) [11]. However, there is a notable scarcity of research focusing on the dynamic testing of this behavior. In this study, we employed finite element formulations, placing particular emphasis on the stress update procedure involving von Mises plasticity and the Lemaitre isotropic damage model. The primary objective was to investigate the evolution of material responses and damage progression while also predicting critical load demands. This approach enables subsequent comparisons and facilitates insights into the practical significance of this behavior.

In the literature, several researchers are studying the dynamic instabilities of thin shells [12-14], for example, treated dynamic buckling of thin shells in seismic zones, then succeed by Amieur (2019) [15] and Amieur et al. (2023) [16] with the Dynamic buckling analysis of functionally graded materials. This work essentially presents our benchmark in validating the numerical example presented in the next paper.

1.1. Theoretical Presentation of the Instability Issue

The analysis of the stability problem is primarily governed by the choice of stability criteria. In 1788, Lagrange proposed a criterion, subsequently known as the "energy criterion" for conservative discrete systems. According to this criterion, the necessary and sufficient condition for such a system to be in stable equilibrium is that its potential energy exhibits a local minimum for that state. If this energy is at a maximum, the equilibrium is unstable. Based on linearization through asymptotic developments and thus applicable to infinitely small movements, this criterion has been criticized and extended to bounded perturbations by Dirichlet (1846) [17]. This criterion does not apply to dynamic cases, non-conservative loadings, or large displacements. Even when respecting these limitations, the Lagrange-Dirichlet criterion remains subject to numerous criticisms as it is, in fact, not based on any rigorous definition of stability.

1.2. The Significance of Stability According to Lyapunov

In 1907, Lyapunov provided a precise definition of stability [18], along with the methods and fundamental results that subsequent research has referred to. Under certain conditions, according to Lyapunov's stability sense, the energy criterion constitutes a necessary but not sufficient condition for continuous static systems. According to Lyapunov, an equilibrium configuration of a system is stable if any solution to the nonlinear equations of motion, starting at time t=0 from a configuration sufficiently close to U_0 with low velocity, remains arbitrarily close to the U_0 configuration for all subsequent values of t. The term "sufficiently close configuration to U_0" is achieved through a small transient perturbation. Such a perturbation could be created by applying a small parasitic force to the system for a brief moment.

1.3. Practical Criteria for Dynamic Buckling

Researchers in the domain of dynamic instability primarily depend on three criteria to investigate critical conditions in structures subjected to dynamic loads. These criteria are: the Budiansky-Roth criterion, also known as the equation of motion resolution criterion; the phase plane criterion of total potential energy Hoff and Bruce (1953) [19], and the total potential energy criterion Simitses (1966) [20], The first two criteria are the focus of our work and will be briefly defined. It is worth noting that the use of catastrophe theory (Raftoyiannis et al. (2006) [21], and Bamberger (1981) [22]) has also been attempted in the analysis of dynamic instability. This approach has not received much attention from researchers and will not be presented in what follows. More recently, other criteria derived from the energy method with modifications have been proposed by Kounadis and Raftoyiannis (1990) [23], Koimadis (1991) [24], Koimadis (1996) [25], and Kounadis et al. (1999) [26]. These criteria are applications of the energy criterion and are still limited to simple structures (1 or 2 degrees of freedom), and do not seem to have practical significance thus far.

Budiansky and Ruth Criterion

The first and most common stability criterion is due to Budiansky (1962) [27]. It has been framed as an engineering application of Liapounov's stability criteria. In this criterion, the time displacement curve is plotted for several values of the applied load. The load value corresponding to a curve that yields a "jump" relative to its neighboring curves indicates the critical dynamic buckling value.

This criterion, originally introduced by Budiansky (1962) [27] and by Budiansky (1967) [28], which can be interpreted as an application of stability in the sense of Lyapunov, is the most commonly used in practice.

Phase Plane Criterion

The curve representing the movement is plotted in phase plan. Stable movements are characterized by limited trajectories and do not move too much away from the solution of the static equilibrium, which plays the role of a center of attraction. As the load reaches the critical value, the trajectory moves away from that pole with no oscillation around it.

1.4. Lemaitre's Model

Within this section, we present an algorithm that integrates the elasto-plastic-damage model according to Lemaitre's theory, incorporating a modified hardening law, specifically a saturation stress. This algorithm is influenced by the research of Lee & Pourboghrat (2005) [5]. The process entails determining the state variables of constitutive equations through a predictive elastic and corrective plastic step. Additionally, the J_2 plasticity theory was combined with the continuum damage mechanics (CDM) criteria. The time interval of study is denoted as [0, T], and Δ_ε represents the required strain increment to update the variables at time $t_{(i+1)}$. At $t_{(i)}$, the values of stress $\sigma_{(i)}$, plastic srain $\varepsilon_{(i)}^{pl}$, and the damage parameters $D_{(i)}$ are known. Assuming additive rule, the strain increment, Δ_ε, is defined into elastic increment $\Delta\varepsilon^{el}$ and plastic increment $\Delta\varepsilon^{pl}$ given by, $\Delta\varepsilon = \Delta\varepsilon^{el} + \Delta\varepsilon^{pl}$. For the elastic trial state $\Delta\varepsilon^{pl} = 0$, the elastic Hooke's law coupled with the damage is computed from [1].

$$\sigma^{trial} = \sigma_{(i)} + \left(1 - D_{(i)}\right)\left(\lambda \, trace(\Delta\varepsilon)I + 2\mu\Delta\varepsilon\right) \tag{1}$$

where σ^{trial} represents the elastic predictor, λ and μ are Lame's constants, and I is the identity matrix. Subsequently, the yield surface is examined using Equation 2 to determine whether the trial stress falls within the elastic domain. The trial deviatoric component of the stress tensor S^{trial}, is defined according to Equation 2.

$$\Phi^{trial} = \frac{[3J_2(S^{trial})]^{1/2}}{1 - D_{(i)}} - \sigma_y(\underline{\varepsilon}_{(i)}^{pl}) \tag{2}$$

$$S^{trial} = \sigma^{trial} - \frac{1}{3}trace(\sigma^{trial})I \tag{3}$$

If the yield condition $\Phi^{trial} \leq 0$ is satisfied, there is no plastic behavior or damage evolution, and the state variables are updated as trial values at $t_{(i+1)}$.

$$\underline{\varepsilon}_{(i+1)}^{pl} = \underline{\varepsilon}_{(i)}^{pl}, D_{(i+1)} = D_{(i)}, \sigma_{(i+1)} = \sigma_{(i)} \tag{4}$$

Alternatively, if the yield condition $\Phi^{trial} \leq 0$ is not satisfied, the process is considered to be elasto-plastic, and the plastic corrector step should be employed to calculate the plastic strain. Equation 2 must fulfill the consistency condition $\Phi = 0$ by utilizing the trial deviatoric stress in order to describe plastic flow. This condition ensures that the updated deviatoric stress $S_{(i+1)}^{trial}$ lies on the yield surface.

$$S_{(i+1)} = R_{(i+1)}q \tag{5}$$

where q represents the radial direction for the plastic correction, which needs to fulfill the hardening isotropic condition, denoted as:

$$q = \frac{S^{trial}}{|S^{trial}|} = \frac{S_{(i+1)}}{|S_{(i+1)}|} \tag{6}$$

and $R_{(i+1)}$ is the radius of the yield surface at time $t_{(i+1)}$ obtained by:

$$R_{(i+1)} = \sqrt{\frac{2}{3}}(1 - D_{(i+1)})k_{(i+1)} \tag{7}$$

$$R_{(i+1)} = \sqrt{\frac{2}{3}}R_v\left(1 - D_{(i)} - \sqrt{\frac{2}{3}}\alpha_{(i)}\Delta\gamma\right) \tag{8}$$

where;

$$R_v = \frac{2}{3}(1 + \vartheta) + 3(1 - 2\vartheta)\left(\frac{\sigma_h}{S}\right)^2 \tag{9}$$

$$\alpha_{(i)} = \frac{\sigma_{eq}^2 R_v}{2ES(1 - D)^2} \tag{10}$$

where ϑ is the Poisson ratio, σ_h is the hydrostatic stress tensor, S is the Von Mises equivalent stress.

In this research, a distinct hardening law was utilized in contrast to the original algorithm. Equation (11) incorporated the Voce-type saturation law. Consequently, the hardening modulus $h_n = d\sigma_{y,(i)}/d\underline{\varepsilon}_{(i)}^{pl}$ at the instance i is defined as follows:

$$\sigma_{y,(i)} = \sigma_{y0} + \sigma_{sat}(1 - exp\, exp\left(-w \times \underline{\varepsilon}_{(i)}^{pl}\right)) \tag{11}$$

being σ_{sat} and $S_{(i+1)}$ the material parameters, from Equation 2, can be represented by:

$$S_{(i+1)} = S^{trial} - 2\mu(1 - D_{(i)})\Delta\gamma q \tag{12}$$

Taking Equations 1, 5, and 12, we obtained the next expression that leads to a second-order equation with respect to $\Delta\gamma$.

$$A\Delta\gamma^2 + B\Delta\gamma + C = 0 \tag{13}$$

where;

$$A = \alpha_{(i)}h_{(i)} \tag{14}$$

$$B = \alpha_{(i)}\sigma_{y,(i)} - (1 - D_{(i)})(h_{(i)} + 3G) \tag{15}$$

$$C = S^{trial} - \sigma_{y,(i)}(1 - D_{(i)}) \tag{16}$$

The two roots computed of Equation 13 should satisfy the following constrains:

$$\Delta\gamma = \left(\Delta\gamma_{(j)}\right), \Delta\gamma > 0, \ j = 1,2 \tag{17}$$

Solving second-order equation, we obtained the plastic corrector ($\Delta\gamma$), which is used to update the state variables at $t_{(i+1)}$.

$$\sigma_{(i+1)} = \sigma^{trial} - 2\mu(1 - D_{(i)}\Delta\gamma q \tag{18}$$

$$\underline{\varepsilon}^{pl}_{(i+1)} = \underline{\varepsilon}^{pl}_{(i)} + \sqrt{\frac{2}{3}}\Delta\gamma \tag{19}$$

$$D_{(i+1)} = D_{(i)} + \sqrt{\frac{2}{3}}\Delta\alpha_{(i)}\Delta\gamma \tag{20}$$

Figure 1 represented the Flowchart algorithm above for the standard Lemaitre's ductile damage model of Lee & Pourboghrat (2005) [5].
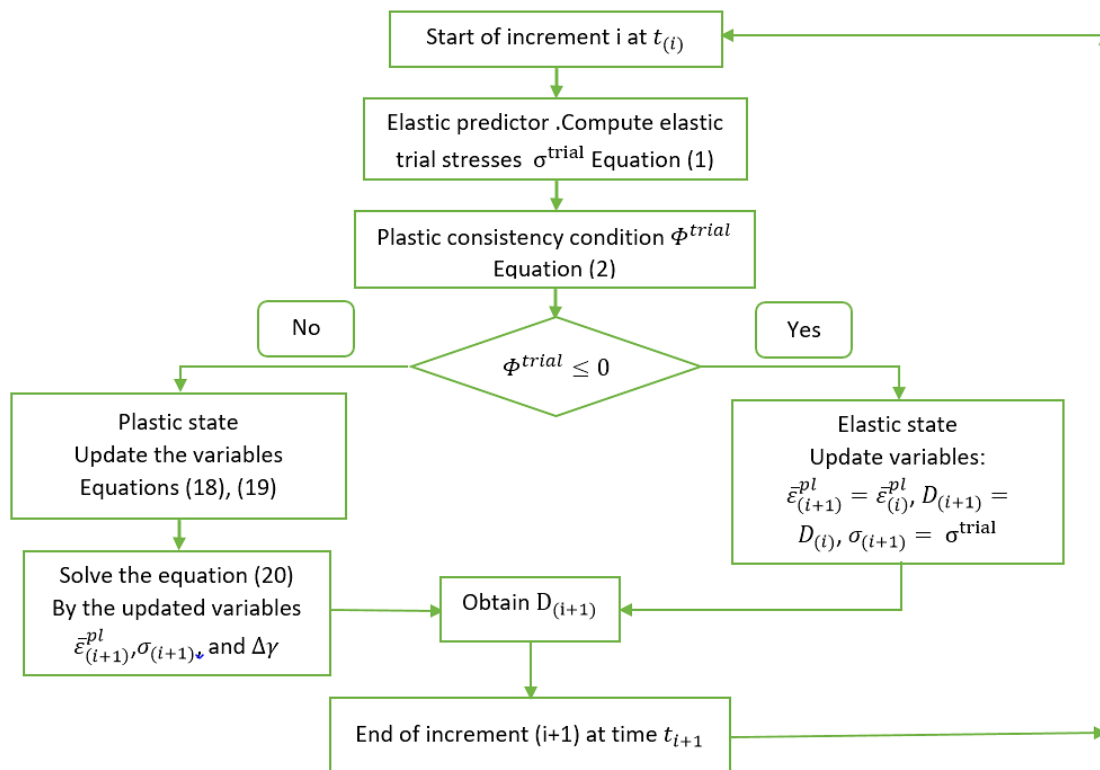
Figure 1. the Flowchart algorithm for the standard Lemaitre's damage model

The algorithm above was initially introduced by Lee & Pourboghrat (2005) [5]. It has been used repeatedly by various researchers, taking Anduquia-Restrepo et al. (2018) [9] as an example. In this work, a numerical analysis of damage evolution for a simple tensile test of Dual-Phase steel is studied. Simulations were conducted using the finite element code ABAQUS/Explicit through a VUMAT subroutine to implement Lemaitre's model. To ensure the proper functioning of the model, we simulated the example presented by Restrepo.

Figure 2 shows the comparison of the results of the curves obtained from the Restrepo simulation and load-unload tensile experiment tests with the model proposed in this work. In order to simulate exactly the same geometry and mesh, we used the geometric coordinates from an Abaqus input file similar to the Restrepo example. The obtained result confirms the good agreement between the two models and demonstrates a very close convergence to the experimental results.
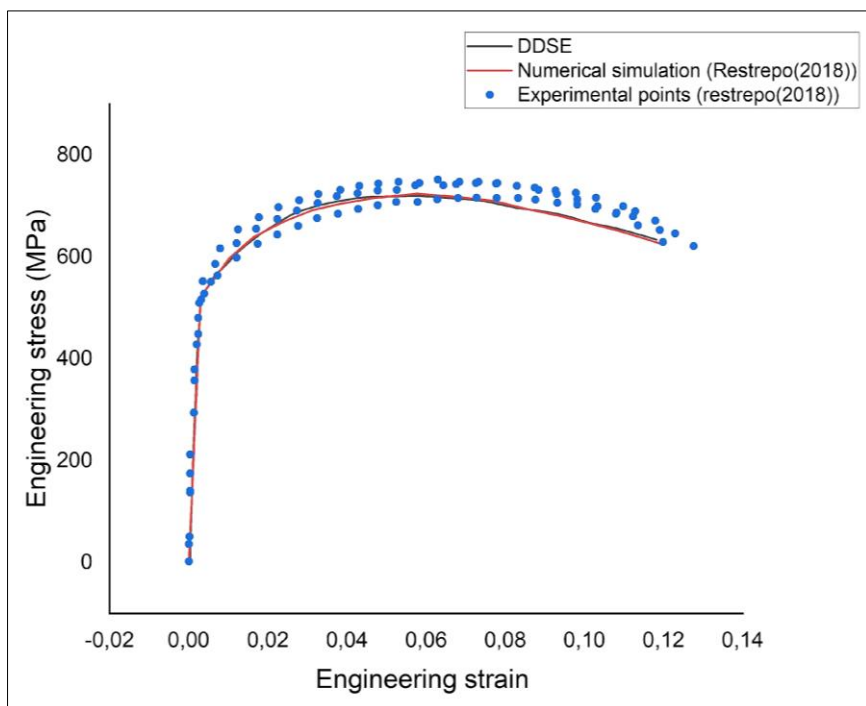
Figure 2. Comparison of engineering stress-strain tensile test

2. Numerical Application

2.1. Spherical Cap shallow Example

This widely recognized example has been examined by numerous authors employing various approaches, including Saigal and Yang (1985) [29], Nagarajan and Popov (1974) [30], and Bathe et al. (1975) [31]. In this instance, the goal is to calculate the transient response of an elastic-plastic, shallow spherical shell subjected to uniform pressure. The geometric and mechanical details of the problem are presented in Figure 3 and Table 1. It is assumed that the material follows the Von Mises criterion with isotropic hardening. A step-type pressure of 600 psi is applied to induce elastic-plastic behavior.
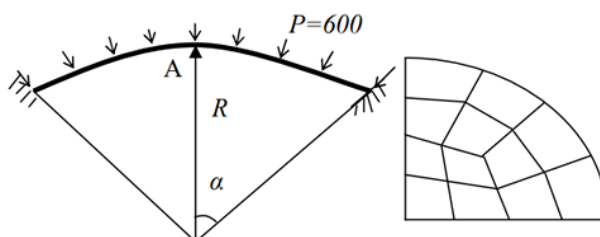
Figure 3. Spherical cap: geometry and mesh

Table 1. Geometrical and material properties

Properties	Symbol	Value
radius	R	22.7 in
thickness	e	0.41 in
Young modulus	E	10.5×10^6 psi
Poisson ratio	υ	0.3
yield	σ_0	2400 psi
Density	ρ	2.45×10^{-4} lb-sec²/in^4

The various analyses conducted are presented in Figures 4 and 5. which indicates the agreement of the results obtained with those published in previous references. Furthermore, one can conclude that:

- Damping of the peak. The differences between two successive peaks in the elastic and elastic-plastic analyses are 141.19×10^{-3} inches and 60.15×10^{-3} inches, respectively. The reason is the damping caused by the repeated process of elastic unloading and plastic loading.

- Elongation of the period due to nonlinear softening
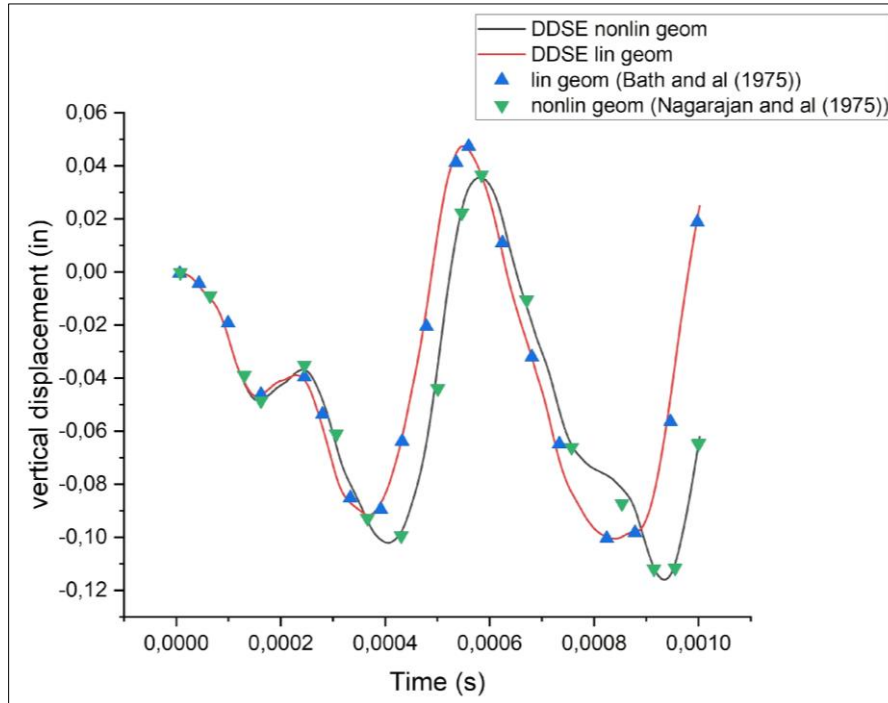
Figure 4. Elastic spherical cap displacement: comparison of results
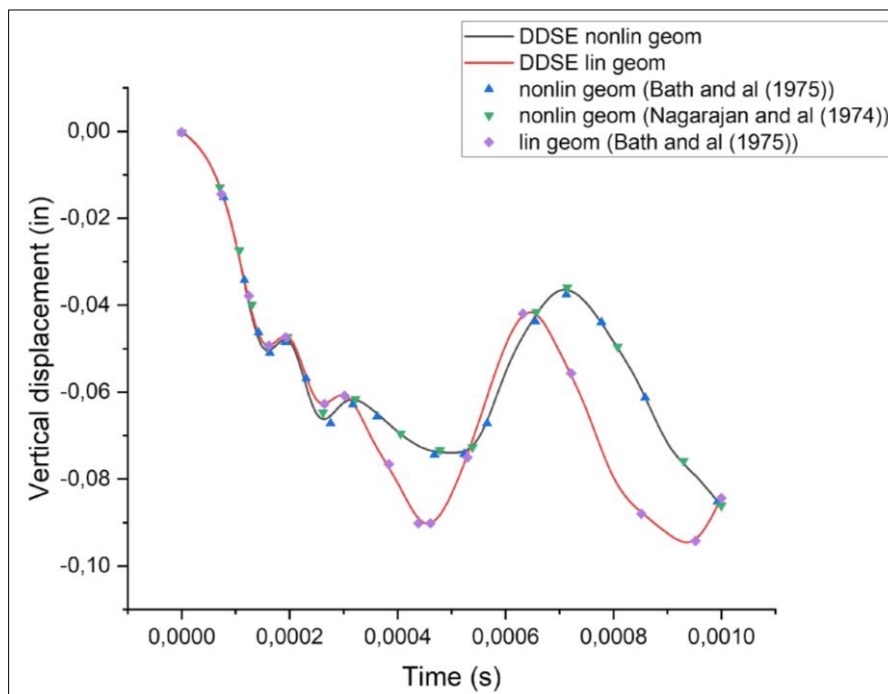
Figure 5. Elasto-plastic spherical cap displacement: comparison of results

2.2. Cylindrical Panel Example

This example is used for the first time in dynamic stability, according to Djermane (2007) [12], Djermane et al. (2007) [32], and subsequently Djermane et al. (2014) [14], Amieur et al. (2019) [15], and Amieur et al. (2023) [16] for isotropic materials.

To study this effect, we considered a mesh of (2×2) for the time increment Δt=1E-06 (s). The panel shown in Figure 6 is subjected to a distributed step pressure P, the sample geometry was modelled using 3D eight-node brick elements with an integration point. Geometrical and material properties details of the problem are presented and Table 2.
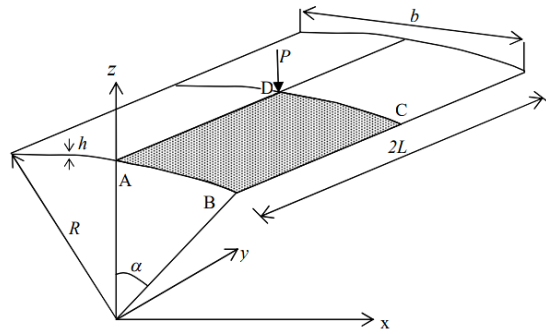
Figure 6. Example of cylindrical panel

Table 2. Geometrical and material properties

Properties	Symbol	Value
Radius	R	2.54 m
Thickness	e	6.35 mm
Height	H	25.4 m
Poisson ratio	υ	0.3
Young modulus	E	3.103 GPa
Density	ρ	7800 Kg/m³

3. Results and Discussion

In our case, we will compare between our results and the existing results, then the analysis will be extended by using an elasto-plastic damage model according to Lemaitre's theory. After collecting all the data, we obtain the results illustrated and represented in the figures below for various values of the applied load.

In Figure 7. Multiple dynamic responses for various load values are overlaid for the purpose of analysing the obtained results. An initial observation reveals that when the load is equal to or less than N = 496 N, the center displacement of the panel oscillates around the static displacement value Wc = 0.0076 m, signifying stability in this scenario. However, at time t = 0.05 s, a mere 1 N increase in the load leads to a sudden jump in the displacement, reaching nearly three and a half times the static value (Wc = 0.0270 m). In this case, the critical load is determined to be Ncr = 497 N, which agrees perfectly with the value found by Amieur et al. (2018) [16] N=498N.
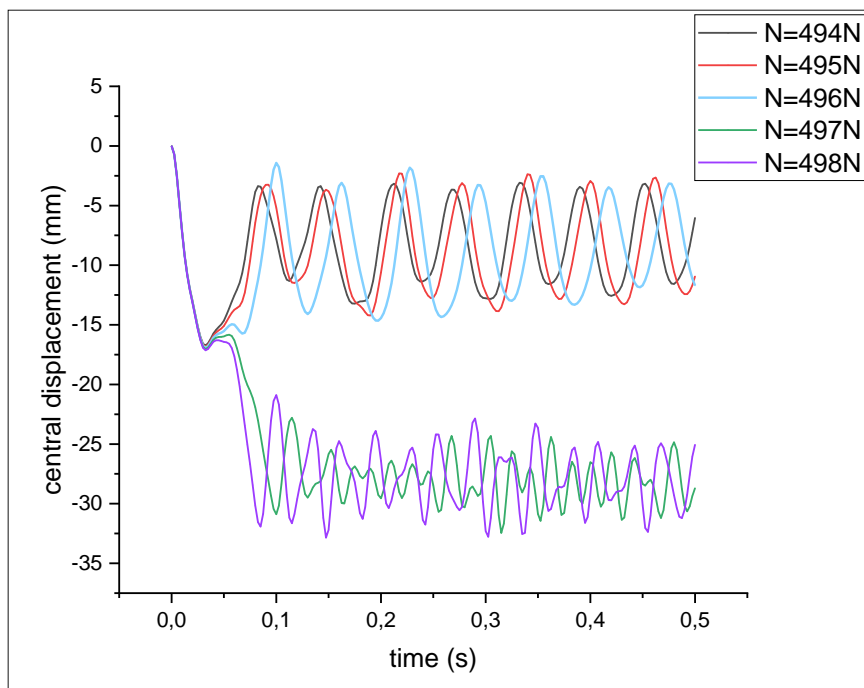
Figure 7. Determination of the critical load value (Ncr) for elastic model

Furthermore, this value can also be ascertained using the phase plane criterion illustrated in Figures 8-a and 8-b. the structure oscillates around a displacement value corresponding to velocity equal zero for load values lower than N= 496N, beyond this value and from the critical value of the load N = 497N, the trajectory makes an oscillation around this position before launching towards another equilibrium position.
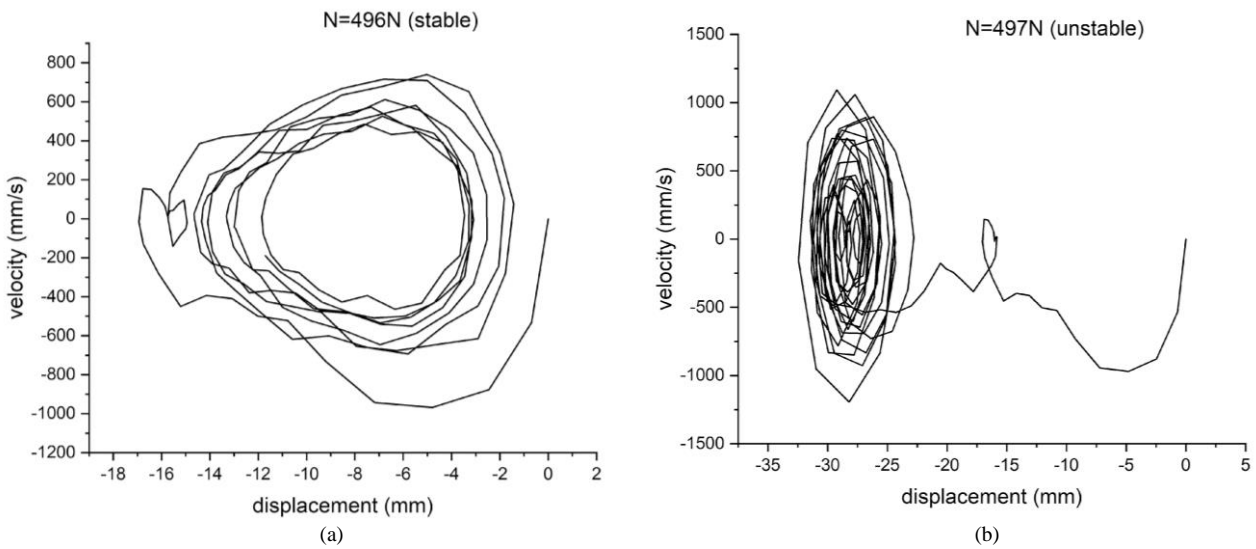
Figure 8. Phase plane diagram before and after the critical value for the elastic case

Figures 9 and 10 show the analysis as a function of the time of transverse displacement of the center of the panel, which is also the point of application of the concentrated force. Up to the value N=289N, the displacement gained is an oscillation around the position of the static balance. When the load N reaches 290N, a dynamic bifurcation to another equilibrium position is recorded. The critical value of the dynamic bifurcation is therefore equal to 290N for the von Mises criterion, while for Lemaitre's model, we notice a slight decrease of 7N between the two critical load values (Ncr). The utilization of this model revealed dynamic buckling occurring earlier when compared to the von Mises criterion. We observed a shift from N = 290N to N = 283N.
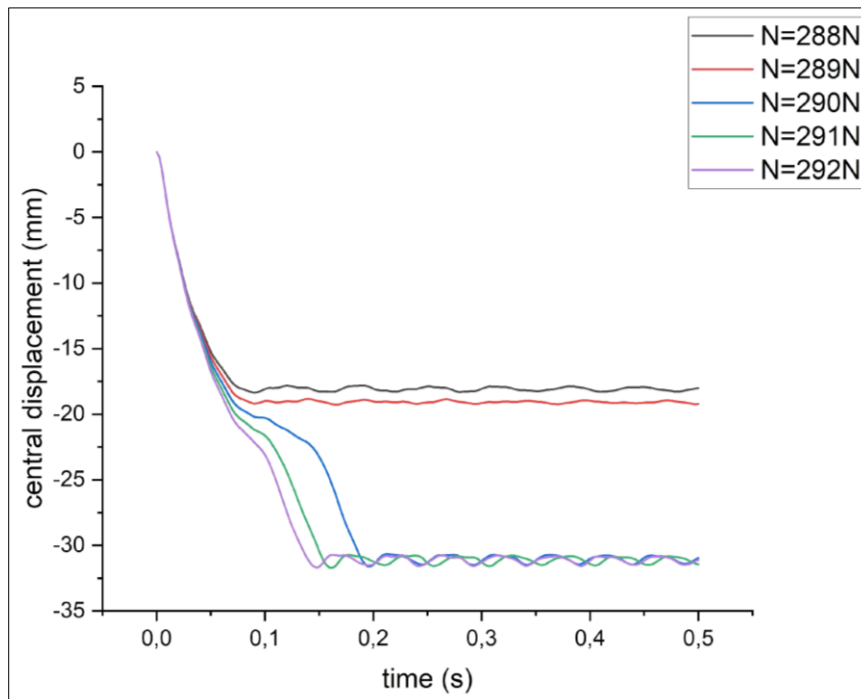
Figure 9. Determination of Ncr for von mises criterion
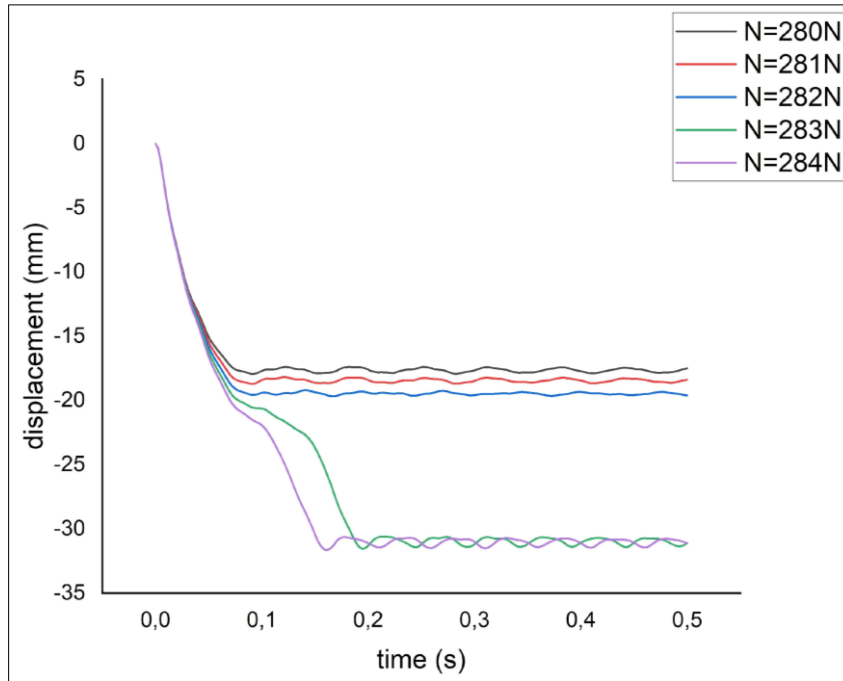
Figure 10. Determination of Ncr for Lemaitre's model

The phase plane portraits (Figure 11) for the von-mises criterion corroborate this conclusion. Indeed, for N=289N, the trajectory of the movement is stable around the static equilibrium position (Figure 11-a). When N reaches the slightly higher value of 290N, the trajectory makes some oscillations around this position before moving to another equilibrium position. The stable nature of this post-critical movement is clearly indicated in Figure 11-b, The same remarks were reported for the model of Lemaitre (Figures 12-a and 12-b) where for a value of N=282N the trajectory of the movement is stable around a value close to 18 mm. An increase of 1 N leads to a sudden jump in the displacement, reaching nearly 31 mm.
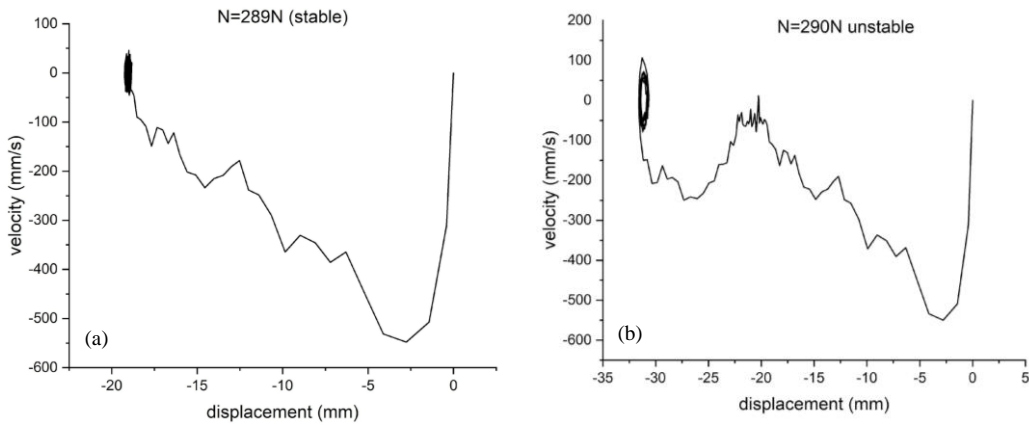
Figure 11. Phase plane diagram before and after the critical value Ncr for van mises criterion
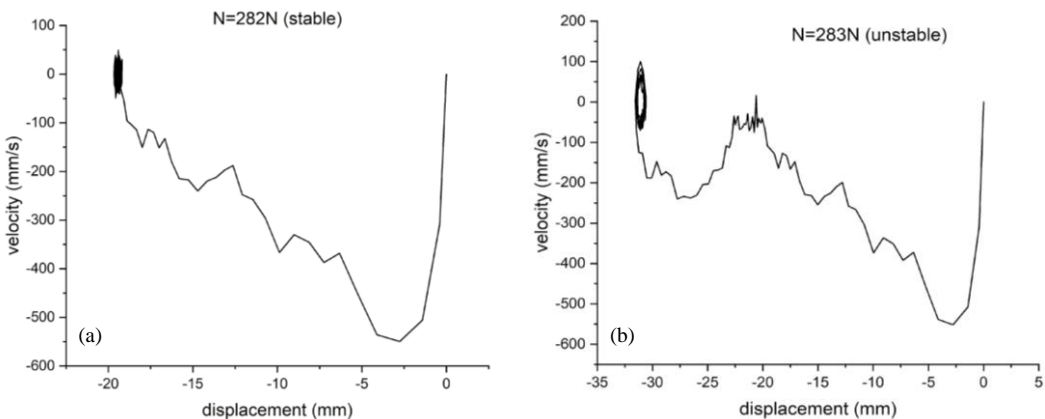
Figure 12. Phase plane diagram before and after the critical value for Lemaitre's model

Figure 13 represents the variation of the damage parameter compared to time for the critical load in the previous example. We can divide the curve into three parts: the first part, where the damage D=0 is defined for the elastic phase; the second part, where we note a considerable loss of the parameter of damage for booth value; and the last part, where all the gauss points reach the plasticity (a stabilization in the last part was noticed). We notice a considerable jump between the two values; we went from D =0.15 to D = 0.21.
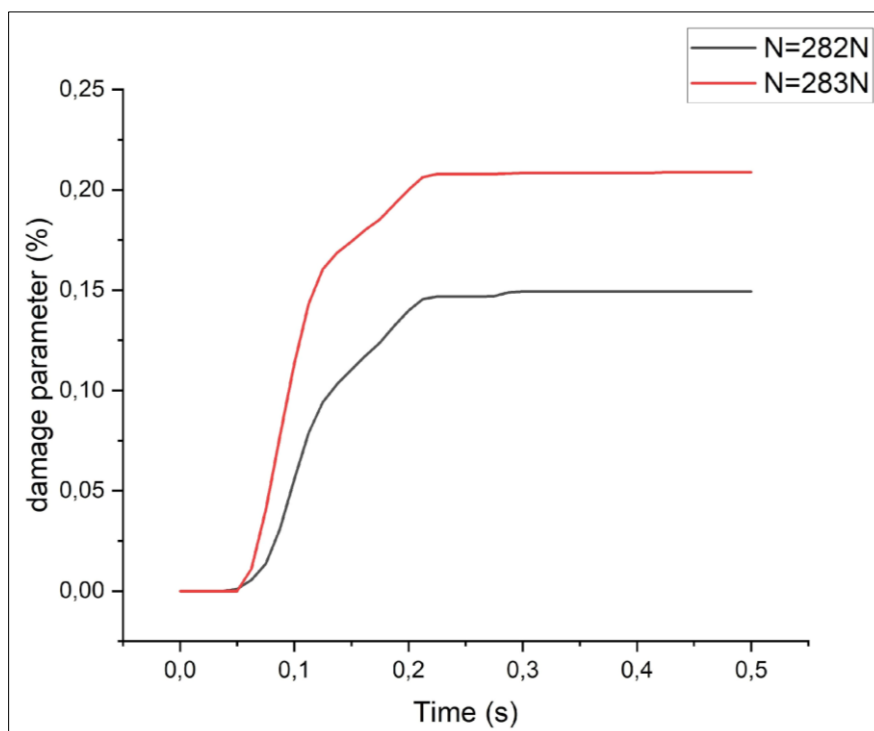
Figure 13. Damage parameter evolution of a cylindrical panel

4. Conclusion

Due to its significance in the industrial field, it has become more than necessary to discuss the stability of thin structures to optimize critical loads. In this article, an experimental methodology was used to identify the mechanical properties and damage parameters of thin shells, using the locally developed finite element program DYNCOQ to implement the Lemaitre model. The obtained results were initially compared to references in the literature cited in the first example to ensure the proper functioning of the program used and the good convergence of the damage model. Following this, the work was extended to study the dynamic buckling of thin shells using the equation of motion criterion and the phase plane criterion for determining the critical load. The experiment involved comparing both the von Mises plasticity criterion and the Lemaitre model. As a result, to conclude the research paper, first in the elastic plastic case, a noticeable decrease in the critical value compared to the elastic case is evident. There is also a slight decrease of 7N between the two plastic criteria, which is approximately a 10% loss. This value can go up to 15% if we calculate the damage parameter using the formula proposed by Lemaitre, and the final element is the minor 1 N increase in the load, which yields a substantial shift in the damage parameter values, transitioning from D = 0.15 to D = 0.21.

5. Declarations

5.1. Author Contributions

Conceptualization, I.H., M.G., and B.A.; methodology, I.H., M.G., and B.A.; formal analysis, I.H., M.G., and B.A.; data curation, I.H., M.G., and B.A.; writing—original draft preparation, I.H., M.G., and B.A.; writing—review and editing, I.H., M.G., and B.A. All authors have read and agreed to the published version of the manuscript.

5.2. Data Availability Statement

The data presented in this study are available in the article.

5.3. Funding

5.4. Conflicts of Interest

The authors declare no conflict of interest.

6. References

[1] McClintock, F. A. (1968). A criterion for ductile fracture by the growth of holes. Journal of Applied Mechanics, Transactions ASME, 35(2), 363–371. doi:10.1115/1.3601204.

[2] Gurson, A. L. (1977). Continuum theory of ductile rupture by void nucleation and growth: Part 1 - yield criteria and flow rules for porous ductile media. Journal of Engineering Materials and Technology, Transactions of the ASME, 99(1), 2–15. doi:10.1115/1.3443401.

[3] Needleman, A., & Tvergaard, V. (1984). An analysis of ductile rupture in notched bars. Journal of the Mechanics and Physics of Solids, 32(6), 461–490. doi:10.1016/0022-5096(84)90031-0.

[4] Lemaitre, J. (1985). A continuous damage mechanics model for ductile fracture. Journal of Engineering Materials and Technology, Transactions of the ASME, 107(1), 83–89. doi:10.1115/1.3225775.

[5] Lee, S. W., Pourboghrat, F. (2005). A Simulation for the Punchless Piercing Process using Lemaitre Damage Model. AIP Conference Proceedings, 778, 505–510. doi:10.1063/1.2011271.

[6] He, S., Wang, H., Bordas, S. P. A., & Yu, P. (2020). A Developed Damage Constitutive Model for Circular Steel Tubes of Reticulated Shells. International Journal of Structural Stability and Dynamics, 20(9). doi:10.1142/S0219455420501060.

[7] Li, Y., Liu, Y., Mo, X., Shen, W., Li, C., Sun, X., & Xue, F. (2024). Damage evolution and fracture of aluminum alloy based on a modified Lemaitre model. Engineering Fracture Mechanics, 295, 109778. doi:10.1016/j.engfracmech.2023.109778.

[8] Laboubi, S., Boussaid, O., Zaaf, M., & Ghennai, W. (2023). Numerical investigation and experimental validation of Lemaitre ductile damage model for DC04 steel and application to deep drawing process. International Journal of Advanced Manufacturing Technology, 126(5–6), 2283–2294. doi:10.1007/s00170-023-11244-0.

[9] Anduquia-Restrepo, J., Narváez-Tovar, C., & Rodríguez-Baracaldo, R. (2018). Computational and numerical analysis of ductile damage evolution under a load-unload tensile test in dual-phase steel. Journal of Mechanical Engineering, 64(5), 339–348. doi:10.5545/sv-jme.2017.5137.

[10] De Souza Neto, E. A. (2002). A fast, one-equation integration algorithm for the Lemaitre ductile damage model. Communications in Numerical Methods in Engineering, 18(8), 541–554. doi:10.1002/cnm.511.

[11] Shamshiri, A. R., Haji Aboutalebi, F., & Poursina, M. (2023). Presenting an explicit step-by-step algorithm for lemaitre's ductile damage model with the crack closure effect in tensile-compressive loadings. Mechanics Based Design of Structures and Machines, 51(8), 4452–4466. doi:10.1080/15397734.2021.1966309.

[12] Djermane, M. (2007). Dynamic Buckling of Thin Shells in Seismic Zones. Ph.D. Thesis, Houari-boumédièn University of Science and Technology, Bab Ezzouar, Algeria. (In French).

[13] Djermane, M., Chelghoum, A., Amieur, B., & Labbaci, B. (2007). Nonlinear dynamic analysis of thin shells using a finite element with drilling degrees of freedom. International Journal of Applied Engineering Research, 2(1), 97-108.

[14] Djermane, M., Zaoui, D., Labbaci, B., & Hammadi, F. (2014). Dynamic buckling of steel tanks under seismic excitation: Numerical evaluation of code provisions. Engineering Structures, 70, 181–196. doi:10.1016/j.engstruct.2014.03.037.

[15] Belkacem, A. (2019). Instability by dynamic buckling These Amieur 2018. Ph.D. Thesis, Université Tahri Mohammed Béchar, Béchar, Algeria. (In French).

[16] Amieur, B., Djermane, M., Zenkour, A. M., & Hammadi, F. (2023). Dynamic buckling analysis of functionally graded shells. Mechanics Based Design of Structures and Machines, 1–16. doi:10.1080/15397734.2023.2227886.

[17] Dirichlet, P.G.L. (1846). Note II: On the Stability of the Equilibrium. Works of Lagrange, 11, 457–459.

[18] Lyapunov, A. (1907). General problem of movement stability. Annals of the Faculty of Sciences of Toulouse Mathematics, 9, 203–474. doi:10.5802/afst.246.

[19] Hoff, N. J., & Bruce, V. G. (1953). Dynamic Analysis of the Buckling of Laterally Loaded Flat Arches. Journal of Mathematics and Physics, 32(1–4), 276–288. doi:10.1002/sapm1953321276.

[20] Simitses, G. (1966). Dynamic Snap-Through Buckling of Shallow Spherical Caps. 7th Structures and Materials Conference. doi:10.2514/6.1966-1712.

[21] Raftoyiannis, I. G., Constantakopoulos, T. G., Michaltsos, G. T., & Kounadis, A. N. (2006). Dynamic buckling of a simple geometrically imperfect frame using Catastrophe Theory. International Journal of Mechanical Sciences, 48(10), 1021–1030. doi:10.1016/j.ijmecsci.2006.05.010.

[22] Bamberger Y. (1981). Disaster Theory and Elastic Stability of Structures. Le Flambement des Structures L'Hermite, 323–343.

[23] Kounadis, A. N., & Raftoyiannis, J. (1990). Dynamic stability criteria of nonlinear elastic damped/undamped systems under step loading. AIAA Journal, 28(7), 1217–1223. doi:10.2514/3.25197.

[24] Koimadis, A. N. (1991). Nonlinear dynamic buckling of discrete dissipative or non-dissipative systems under step loading. AIAA Journal, 29(2), 280–289. doi:10.2514/3.10575.

[25] Kounadis, A. N. (1996). On the nonlinear dynamic buckling mechanism of autonomous dissipative/non-dissipative discrete structural systems. Archive of Applied Mechanics, 66(6), 395–408. doi:10.1007/bf00803674.

[26] Kounadis, A. N., Gantes, C. J., & Bolotin, V. V. (1999). Dynamic buckling loads of autonomous potential systems based on the geometry of the energy surface. International Journal of Engineering Science, 37(12), 1611–1628. doi:10.1016/S0020-7225(98)00136-0.

[27] Budiansky, B. (1962). Axisymmetric dynamic buckling of clamped shallow spherical shells. NASA TN, 1510, 597-606.

[28] Budiansky, B. (1967). Dynamic Buckling of Elastic Structures: Criteria and Estimates. Proceedings of an International Conference Held at Northwestern University, Evanston, Illinois, 83-106. doi:10.1016/B978-1-4831-9821-7.50010-7.

[29] Saigal, S., & Yang, T. Y. (1985). Nonlinear dynamic analysis with a 48 d.o.f. curved thin shell element. International Journal for Numerical Methods in Engineering, 21(6), 1115–1128. doi:10.1002/nme.1620210611.

[30] Nagarajan, S., & Popov, E. P. (1974). Elastic-plastic dynamic analysis of axisymmetric solids. Computers and Structures, 4(6), 1117–1134. doi:10.1016/0045-7949(74)90028-5.

[31] Bathe, K. J., Ramm, E., & Wilson, E. L. (1975). Finite element formulations for large deformation dynamic analysis. International Journal for Numerical Methods in Engineering, 9(2), 353–386. doi:10.1002/nme.1620090207.

[32] Djermane, M., Chelghoum, A., Amieur, B., & Labbaci, B. (2007). Nonlinear dynamic analysis of thin shells using a finite element with drilling degrees of freedom. International Journal of Applied Engineering Research, 2(1), 97-108.
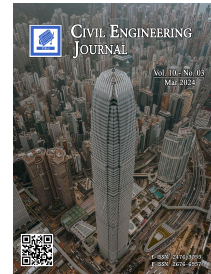
The Effectiveness of the Procurement at the Construction Services Selection Implementation Center

Sofian [1], H. Parung [1], S. Burhanuddin [1], R. Arifuddin [1*]

[1] *Department of Civil Engineering, Faculty of Engineering, Hasanuddin University, Gowa, Indonesia.*

Abstract

The construction industry still faces various challenges in some developing countries, and one of the problems is the procurement of goods and services. The allocation of public procurement funds is significant to the national GDP. It is essential to conduct comprehensive research on government procurement in the construction industry in Indonesia due to the rapid growth of the construction industry in the last decade. This research focuses on the procurement of construction goods and services in the Ministry of Public Works and Housing by looking at the perception of the government as the project owner. This research aims to identify a model of critical success factors to improve public procurement performance in the construction industry from the government's perspective. The research method includes two stages, namely, the development of critical success, which consists of crucial factors and indicators that affect the performance of public procurement in the construction industry. It is a literature study of relevant previous research results from various countries that affect these critical success factors. Then, the second stage is a survey of experts' perceptions through questionnaires. The questionnaire data analysis used SEM-PLS software to quantify the relationship model of critical success factors to improve the performance of government procurement of goods and services in the construction industry. Data processing results include: business process factors affect 97.1%, regulatory factors affect 90.1%, information system factors affect 63.1%, human resource factors affect 56.1%, organizational factors affect 46.1%, and monitoring and evaluation factors affect 38%.

Keywords: Construction Industry; Critical Succes Factors; Government; Public Procurement.

1. Introduction

Construction is one of the most significant generation divisions in the world, and its advancement impacts the business era, the dynamism of materials, and the improvement of the fundamental framework [1, 2]. All sorts of construction ventures constitute one of the fundamental civilization angles and headway in society, frequently alluded to as the civilization of numerous countries, counting the inventiveness, offices, and landmarks [3]. Unfortunately, the growth of the construction industry in some developing countries still experiences various challenges, including low productivity, low quality, unskilled labor, and project delays [4, 5]. One of the biggest challenges within the development industry is the delay in the procurement handle [6]. In comparison, the procurement process in the construction industry is one of the most significant processes influencing the growth of the industry [7]. Procurement techniques can be widely considered in developing and designing industries whose primary purpose is administration [8–10]. The procurement process in the construction sector is the process of purchasing goods, services, or works that includes two types: (i) public procurement and (ii) private procurement [11, 12].

Procurement issues in the construction industry have been investigated in several developing countries. In Niger, strategies to eliminate and reduce corrupt behavior in procuring goods and services in the construction industry have been addressed by adopting digitalization through e-procurement technology. However, the implementation of e-procurement still needs more technical experts and more investment in e-procurement technology [13]. In India, the main deviation in public procurement in the construction industry is transparency, followed by the availability of professional standards, a fair procurement process, contract monitoring, and regulatory and procedural are still challenges to create effective public construction procurement [14]. In Portugal, general construction procurement by the government has been obliged to use e-procurement, which has increased the transparency of the process, the impact on competition, and the impact on bureaucracy. Thus, they have a more straightforward decision-making structure that can reduce the difficulty of e-procurement implementation [15]. Ghana's public procurement barriers include administrative, procedural, compliance, and contract monitoring irregularities [16]. Construction material procurement contracts in Columbia's public procurement still predominantly use traditional construction methods that require standardization in procurement management to ensure adequate supply chain processes and best prices with high-quality requirements in line with stakeholder needs [1].

Similarly, over the past five years, Indonesia's construction sector has become a driver of economic growth due to significant government spending on infrastructure development. Infrastructure development is increasing evenly throughout Indonesia. Increased and massive infrastructure development certainly requires a procurement process in the construction sector with improved performance. The procurement development of construction project units in Indonesia is still generally moo, at level two out of five, requiring assistance capacity-building programs for obtainment units in Indonesia and progressed obtainment arranging as the primary and most critical portion of the acquirement preparation [5]. Open development acquirement in Indonesia stipulates seven standards for acquirement execution, to be specific: (i) proficient, (ii) commonsense, (iii) straightforward, (iv) open & competitive, (v) reasonable, and (vi) responsible. This paper is an early-stage inquiry to assess the use of open acquirement principles within the construction division [17].

Research related to the existence of government procurement units in public procurement in the construction sector has developed models and measured maturity indices on the capabilities of procurement units as implementers. However, increasing the capacity of the procurement unit must be accompanied by an increase in the performance of the procurement process itself. Further research is needed to look at more comprehensively the behavior and correlation of supporting factors or critical success factors that affect the performance of the public procurement process in Indonesia. This study follows up on the research gap on critical success factors that influence the improvement of public procurement in the Indonesian construction sector. The study's results aim to provide information to the Indonesian government about mitigating the risks associated with implementing procurement in demanding infrastructure projects throughout Indonesia.

2. Literature Review

2.1. Public Procurement

Public procurement is self-explanatory because the definition is clear: public means government, and procurement means purchase or purchase. Besides, the reason for public procurement is the method of acquiring products, administrations, and works by the government and state-owned companies [18]. Hence, open procurement may be a handle in which public organizations obtain or buy items within the frame of products, services, or sometimes a combination of merchandise and administrations [19]. Common procurement standards oversee open obtainment administration, counting setting up a system for executing a code of conduct for all parties explicitly included or in a roundabout way in actualizing open procurement. The beneficiaries of a public procurement system are the entire population of a country through the public goods and services provided, including transport systems, public utilities, education systems, and health and other public services and facilities [20]. State-funded public sector procurement, its principles, implementation mechanisms, and methods are regulated by each country [21, 22]. The legal regulation for public sector procurement in Indonesia is through the Presidential Regulation of the Republic of Indonesia Number 12 of 2018 on Government Procurement of Goods or Services.

2.2. Public Procurement in Construction Industry in Indonesia

The construction industry is a fundamental portion of the acquirement framework, with the standard definition of acquirement as securing products, administrations, or development components from third parties at the leading price, and within the adjusted amount, with the proper rights, time, and put [23]. The construction industry with infrastructure building products for the public has been regulated through the Minister of Public Works and Public Housing Regulation No. 12 of 2021.

2.3. Construction Service Selection Center (CSSC)

Construction Services Selection Implementation Centre has been established in 34 provinces in Indonesia to replace the Procurement Service Unit. With work units, independent human resources, and better business processes, the process

and results of public procurement are expected to be more effective, efficient, transparent, quality, and accountable. The establishment of CSSC is a step by the Ministry of Publics Work and Housing to implement nine strategies to prevent irregularities in the procurement of goods and services, namely (1) reorganizing the organizational structure of the PSU and PGS working group; (2) strengthening human resources; (3) improving the mechanism for preparing the Own Estimate Price; (4) fostering the provision of services both contractors and consultants; (5) inspection of work results involving the Development Finance Supervisory Agency; (6) reducing risks in organizational units, centers, and work units; (7) establishment of an internal compliance unit; (8) establishment of an inspectorate for investigation and strengthening the capacity of auditors; and (9) continuous monitoring of fraud prevention tools with information technology. To improve the standards and professionalism of goods and services procurement to encourage the acceleration of reliable infrastructure development, CSSC has enormous tasks and responsibilities. Priorities and strategies are used to optimize the performance of the procurement process, including planning and development of procurement human resources, integration of the planning process with procurement implementation, availability of SOPs in implementing the strategy, having measurable performance targets, having a map of potential risks, developing information systems, and independence and freedom from corruption, collusion, and nepotism.

2.4. Critical Success Factors for Public Construction Procurement

The definition of critical success factors is an essential component for proper project execution that must be done because, without this component, the project will not be successful or will not succeed in achieving specific targets or goals in a project or work. Before starting a project, it is imperative to identify these CSFs. According to Mojumder et al. [24], "*The importance of identifying those relatively few variables that are crucial to the attainment of strategy, goals, objectives then is ultimately derived from limited information processing ability of the manager. We call these crucial variables, critical variables, or critical success factors*".

The results of the literature review obtained critical success factors of public procurement in the construction industry from several countries found that regulatory factors (XR) affecting the implementation of public procurement in construction projects include: (XR1) Availability of Procurement Regulations; (XR2) Compliance with Procurement Regulations; and (XR3) Understanding of Procurement Regulations [14, 16]. Furthermore, Organisational Factors (XO) are concluded to affect the procurement of goods and services in the construction industry consisting of (XO1) Availability of organizational culture with anti-corruption integrity in the procurement unit; XO2) Availability of Key Performance Indicators (KPIs) for the procurement unit; (XO3) Developing an adaptive and responsive organizational attitude; and (XO4) Support for the procurement team from top management [25].

3. Method

3.1. First Stage

The first stage is the development of critical success factors consisting of factors and indicators that improve public construction procurement performance. The development of critical success factors was carried out with a literature study on relevant previous research. The review results of critical success factors are then grouped based on factors and indicators. Furthermore, grouping is done based on substance. Furthermore, indicators that affect each of these factors are developed.

3.2. Second Stage

The second stage: A perception survey of critical success factors was conducted based on the results of the first stage, namely the development of critical success factors that affect the improvement of public construction procurement performance. Perception survey via questionnaire involving 263 public construction procurement experts. The experts selected as respondents are personnel of the procurement unit or Construction Service Selection Centre (CSSC) Ministry of Public Works and Housing in 34 provinces. Expert selection is based on > 5 years of experience in public construction procurement. The scale for measuring the significance of the influence of each critical success factor in the questionnaire using a Likert scale includes: (i) score 5: very significant, (ii) Score 4: Significant, (iii) Score 3: Neutral, (iv) Score 2: Not significant, (v) Score 1: Very insignificant. SEM-PLS was used to analyze the quantifiable relationship of critical success factors consisting of factors and indicators (X) on the improvement of public construction procurement performance carried out by the procurement unit or Construction Service Selection Center of the Ministry of Public Works and Housing (Y).

The overall conceptual framework of the research is depicted in Figure 1.
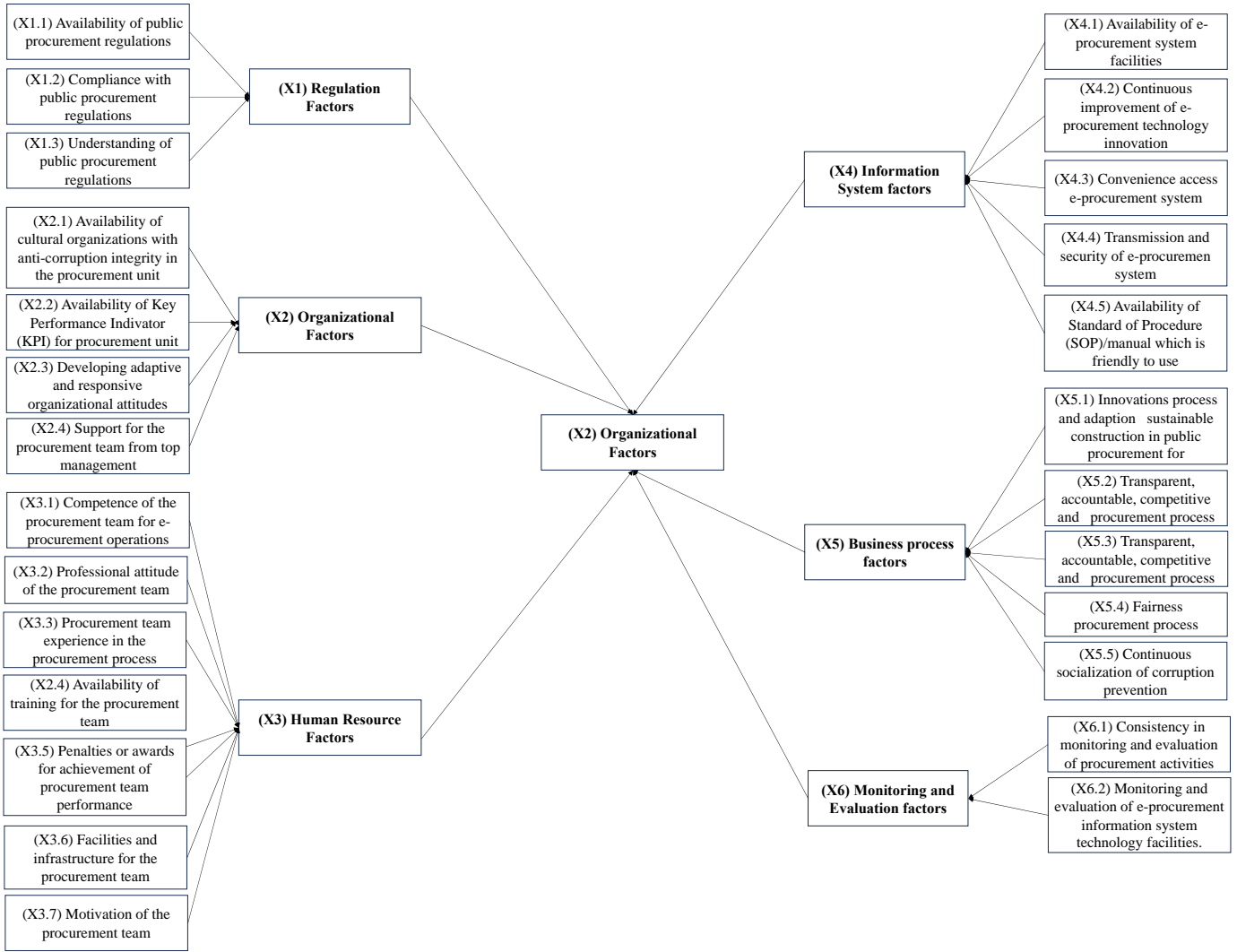
Figure 1. Research Conceptual Framework

Furthermore, the operational framework of the study is shown in Figure 2.
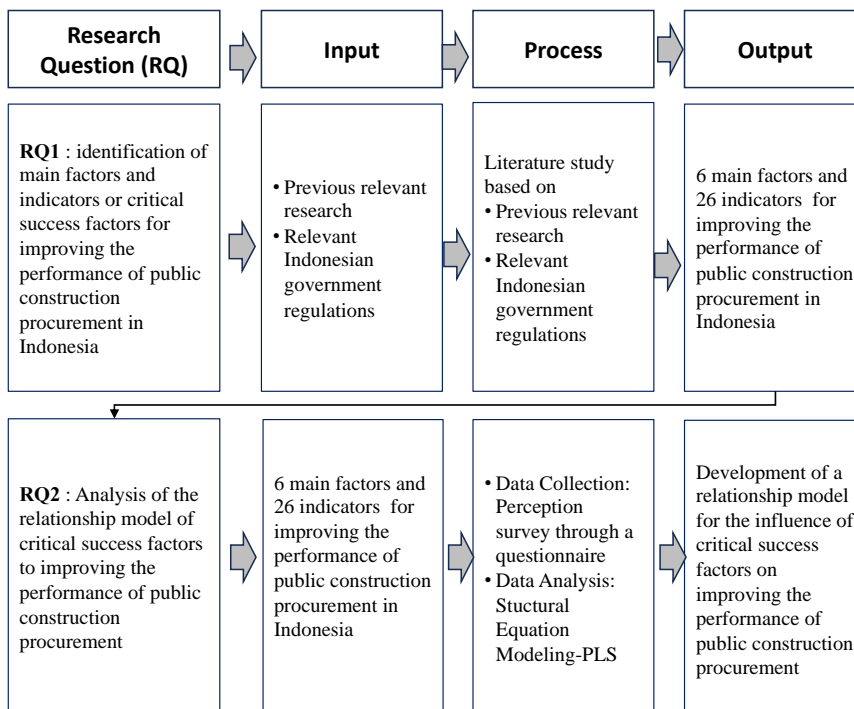
Figure 2. Research Operational Framework

4. Results and Discussion

4.1. Profile of Respondent

Furthermore, an analysis is carried out regarding the profile of respondents, which includes: (i) the total amount of respondent data collected, (ii) the amount of respondent data based on regional division, (iii) the amount of data based on age grouping, (iii) the amount of respondent data based on position. The results of the respondent's data profile are outlined in Table 1.

Table 1. Profile of Respondent

No	Location	Amount of Data		Experience			Education		
		SUM	%	< 5 years	>5 years	>15 years	S1	S2	S3
1	Western Indonesia	121	46,01%	64	46	11	60	59	2
2	Central Indonesia	102	38,78%	45	45	12	68	32	2
3	Eastern Indonesia	40	15,21%	11	23	6	33	7	0
	Total	263	100%	120	114	29	161	98	4

Based on the data profile analysis, the data is almost evenly distributed throughout Indonesia, so it can be concluded that the data already represent Indonesia as a whole. Based on experience in the public construction procurement process, 54.4% were obtained above five years. It shows that experience.

4.2. Structural Equation Modelling (SEM) Analysis

4.2.1. Validity and Reliability Test

Discriminant Validity is calculated to decide the esteem of Discriminant Valitidy (Fornell Lacker Basis), which is the esteem of the relationship between the variable itself and the variable with other factors, should not be littler than other factors. The substantial respect must be more prominent than the esteem of the variable, and the other factors appear in Table 2.

Table 2. Determinant Validity Count Value (Fornell Lacker Criterion)

Variable	XR	XO	X3	X4	X5	X6	Y
X1	**0.850**						
X2	0.737	**0.816**					
X3	0.719	0.753	**0.820**				
X4	0.655	0.680	0.774	**0.830**			
X5	0.683	0.800	0.778	0.705	**0.751**		
X6	0.405	0.461	0.578	0.644	0.579	**0.952**	
Y	0.630	0.672	0.705	0.662	0.745	0.503	**1,000**

Reliability Number Comes about the comes about of Reliability Checks (Composite Unwavering quality and Cronbach's Alpha), characterized as the instrument's viability in measuring the esteem of its pointers. The reliability test is carried out by looking at the Composite Reliability esteem of the build marker. The Reliability Tally Esteem (Composite Reliability and Cronbach's Alpha) will be palatable in case ≥ 0.7.

Based on the calculated results, it has shown that the computed value of Reliability (Cronbach's Alpha and Composite Reliability) for all constructs is more significant than 0.7, which indicates that the instrument has met the reliability criteria so that it can be said to be reliable and powerful to use in research.

This Reliability Test measures the consistency of the questionnaire, namely the indicators of each variable or construct. In this study, variable Y only has one needle, so there is no value for the reliability calculation results. Meanwhile, Discriminant validity is the measurement of indicators with the indicators themselves, which is carried out to ensure that each concept of each latent variable is different from other variables. For variable Y, this study only consists of 1 indicator, so there is no value for the validity calculation results (Table 3).

The results of the validity calculation were carried out utilizing the Concurrent Legitimacy test (Normal Fluctuation Extricated). This method is to degree the Average Variance Extricated esteem with the estimation esteem (Average Variance Extricated) must meet each variable has affection, to be specific ≥ 0.5. Based on the calculated results in Table 4, the Merged Validity test (Average Variance Extricated) for all develops is more noteworthy than 0.5, so the assessed demonstration meets the discriminant validity criteria.

Table 3. Value of Discriminant Validity (Cross Loading)

	X1	X2	X3	X4	X5	X6	Y
X1.1	0.856	0.597	0.57	0.526	0.544	0.323	0.488
X1.2	0.898	0.645	0.615	0.596	0.619	0.357	0.587
X1.3	0.793	0.628	0.647	0.545	0.571	0.351	0.523
X2.1	0.706	0.793	0.664	0.595	0.641	0.416	0.592
X2.2	0.506	0.746	0.563	0.425	0.581	0.217	0.49
X2.3	0.57	0.806	0.628	0.442	0.638	0.323	0.511
X2.4	0.565	0.793	0.692	0.575	0.6	0.352	0.485
X2.5	0.514	0.761	0.609	0.515	0.608	0.354	0.498
X2.6	0.575	0.811	0.651	0.562	0.624	0.436	0.539
X3.1	0.598	0.699	0.798	0.596	0.606	0.394	0.56
X3.2	0.63	0.749	0.802	0.603	0.718	0.365	0.603
X3.3	0.562	0.598	0.799	0.591	0.62	0.417	0.542
X3.4	0.489	0.504	0.736	0.636	0.577	0.479	0.492
X3.5	0.564	0.67	0.76	0.603	0.661	0.436	0.559
X3.6	0.527	0.566	0.744	0.64	0.573	0.558	0.501
X3.7	0.529	0.593	0.803	0.558	0.658	0.524	0.567
X4.1	0.515	0.554	0.641	0.857	0.52	0.495	0.494
X4.2	0.472	0.501	0.621	0.84	0.494	0.516	0.473
X4.3	0.549	0.551	0.627	0.818	0.572	0.427	0.554
X4.4	0.649	0.648	0.692	0.837	0.628	0.479	0.618
X4.5	0.523	0.485	0.581	0.83	0.506	0.55	0.503
X4.6	0.53	0.549	0.633	0.857	0.582	0.586	0.59
X4.7	0.495	0.475	0.62	0.787	0.551	0.568	0.508
X4.8	0.586	0.608	0.701	0.815	0.645	0.643	0.613
X5.1	0.498	0.57	0.613	0.622	0.769	0.494	0.594
X5.2	0.634	0.722	0.724	0.578	0.894	0.434	0.649
X5.3	0.679	0.777	0.777	0.624	0.914	0.475	0.697
X5.5	0.403	0.483	0.545	0.411	0.707	0.418	0.485
X6.1	0.386	0.4	0.551	0.588	0.522	0.954	0.487
X6.2	0.384	0.456	0.551	0.64	0.525	0.95	0.47
Y	0.63	0.664	0.705	0.662	0.741	0.503	1

Table 4. Value of Discriminant Validity (Cross Loading)

Variable	Cronbach's alpha	rho_A	Composite Reliability	AVE
X1	0.807	0.815	0.886	0.723
X2	0.876	0.878	0.888	0.572
X3	0.891	0.893	0.892	0.674
X4	0.936	0.939	0.947	0.69
X5	0.841	0.861	0.857	0.563
X6	0.897	0.898	0.951	0.907

4.2.2. Model Evaluation Results

The results of processing questionnaire data with SEM-PLS software obtained inner model test with R-Square shown in Table 5.

Table 5. Inner Model Test (R-Square)

Y	R-square	Adjusted R-square
	0.609	0.600

Based on the table above, it can be seen that the R-Square for improving the performance of public construction procurement at the Construction Service Selection Center (CSSC) is 0.609 or 60.9%. Based on the table above, the R-Square value is in the range of 50-75 (substantial), which means it has good goodness of fit.

The results of processing questionnaire data with SEM-PLS software obtained inner model tests with Path Coefficients are shown in Table 6.

Table 6. Inner Model Test (Path Coefficients)

	X1	X2	X3	X4	X5	X6	Y
X1							0.126
X2							0.053
X3							0.089
X4							0.166
X5							0.407
X6							0.034
Y							-

The direction of variable influence can be derived from the results of this study as follows.

- X1 (Regulation) has a POSITIVE effect on Y (Procurement Performance)

- X2 (Organization) has a POSITIVE effect on Y (Procurement Performance)

- X3 (Human Resources) has a POSITIVE effect on Y (Procurement Performance)

- X4 (Information Systems) has a POSITIVE effect on Y (Procurement Performance)

- X5 (Business Process) has a POSITIVE effect on Y (Procurement Performance)

- X6 (Monitoring & Evaluation) has a POSITIVE effect on Y (Procurement Performance)

These results show that variables X1 (regulation), X2 (organization), X3 (human resources), X4 (information systems), X5 (business processes), and X6 (monitoring & evaluation) show a positive influence on Y (performance of goods and services procurement). These results indicate that these six variables are Critical Success Factors for Goods and Services Procurement in Indonesia.

4.2.3. Model Results: Inner Model Test (Significance T-Statistic)

The results of processing questionnaire data with SEM-PLS software obtained inner model test with Significance T-Statistic shown in Table 7.

Table 7. Inner Model Test (Significance T-Statistic)

	Real Sample (O)	Sample Average (M)	Standard Deviation (STDEV)	T-Statistic (/STDEV|)	P-values	
X1 → Y	0.901	0.891	0.07	2.713	0.003	Positive
X2 → Y	0.461	0.471	0.072	2.027	0.021	Positive
X3 → Y	0.561	0.611	0.082	2.894	0.029	Positive
X4 → Y	0.631	0.671	0.092	2.775	0.038	Positive
X5 → Y	0.971	0.941	0.063	3.118	0.001	Positive
X6 → Y	0.380	0.310	0.075	2.039	0.049	Positive

Testing the primary speculation appears that the relationship between administrative factors and the execution of the Construction Project leads to a way coefficient esteem of 0.901 with a t-value of 2.713. The t-value is more prominent than the t table (1.960), and the P-esteem is less than 0.005. This result means that control includes a positive and noteworthy relationship with progressing Construction Services Selection Implementation Centre's capacity to become a solid acquirement specialist in Indonesia.

Testing the second hypothesis revealed that the relationship between organizational variables and construction project performance yielded a path coefficient value of 0.461 and a t-value of 2.027. The obtained t-value is greater than

the t-table (1.960), and the p-value is less than 0.005. This result means the organization is building positive and meaningful relationships to improve Construction Services Selection Implementation Centre's ability to become a trusted sourcing agent in Indonesia.

The results of testing the third hypothesis show that the relationship between the Human Resources variable and the performance of the Construction Project Procurement leads to a path coefficient value of 0.561 with a t value of 2.894. The t value obtained is greater than the t table (1.960), and the P value is less than 0.005. This result means that Human Resources (HR) has a positive and significant relationship with improving Construction Services Selection Implementation Centre's ability to become a reliable procurement agent in Indonesia.

The results of testing the fourth hypothesis show that the relationship between the Information System variable and the performance of the Construction Project Procurement leads to a path coefficient value of 0.631 with a t value of 2.775. The t value obtained is greater than the t table (1.960), and the P value is smaller than 0.005. This result means that the Information System has a positive and significant relationship with improving Construction Services Selection Implementation Centre's ability to become a reliable procurement agent in Indonesia.

The results of testing the fifth hypothesis show that the relationship between the Business Process variable and the performance of the Construction Project Procurement leads to a path coefficient value of 0.971 with a t value of 3.118. The t value obtained is greater than the t table (1.960), and the P value is smaller than 0.005. This result means that the Business Process has a positive and significant relationship with improving Construction Services Selection Implementation Centre's ability to become a reliable procurement agent in Indonesia.

The results of testing the sixth hypothesis show that the relationship between the Monitoring & Evaluation variable and the performance of the Construction Project Procurement leads to a path coefficient value of 0.380 with a t value of 2.039. The t value obtained is greater than the t table (1.960), and the P value is less than 0.005. This result means that Monitoring & Evaluation has a positive and significant relationship with improving Construction Services Selection Implementation Centre's ability to become a reliable procurement agent in Indonesia.

4.2.4. Inner Model Test Result (Model Fit)

As a result of this research, we created a model and tested whether the model we created was good. To calibrate the model, the researchers used an internal model test (model fit) (see Figures 3 to 5). The internal model test (model goodness of fit) is a value that indicates how good the investigated model is. Tolerances are measured against the values displayed on NFI in PLS (See Table 8).
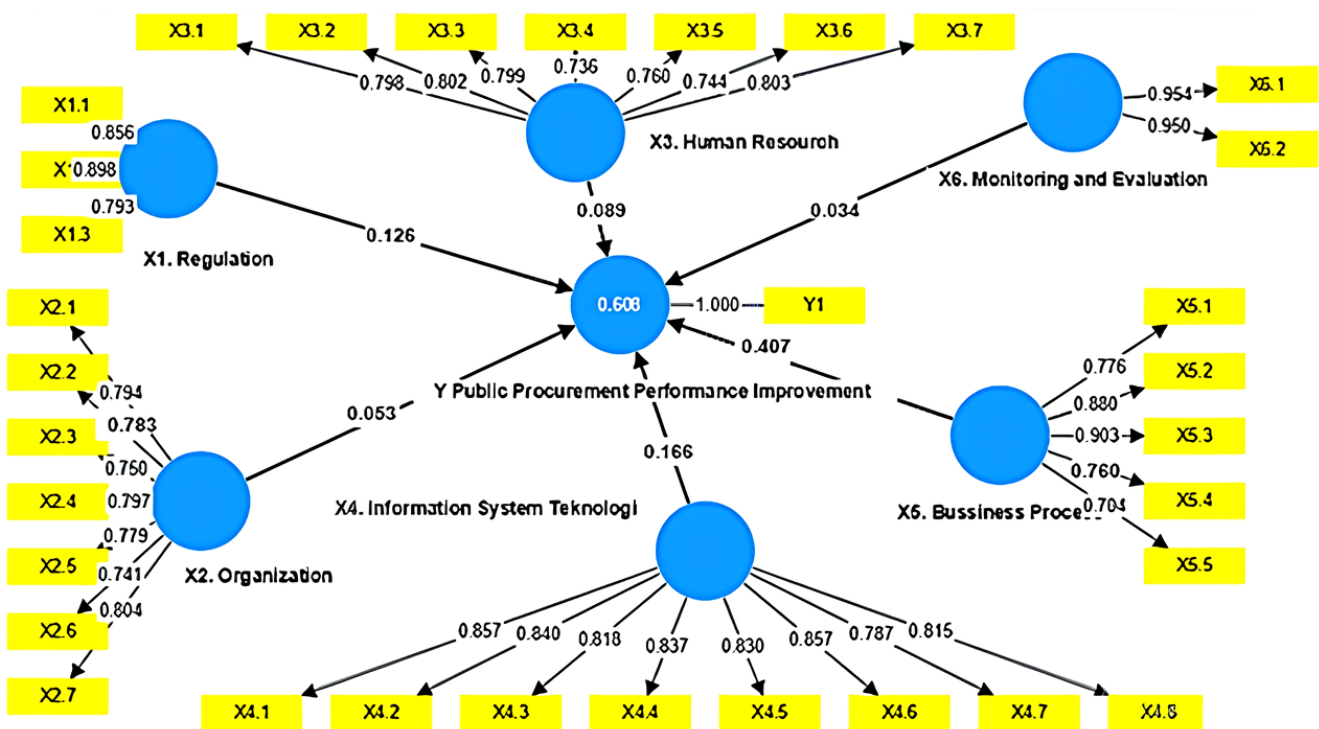

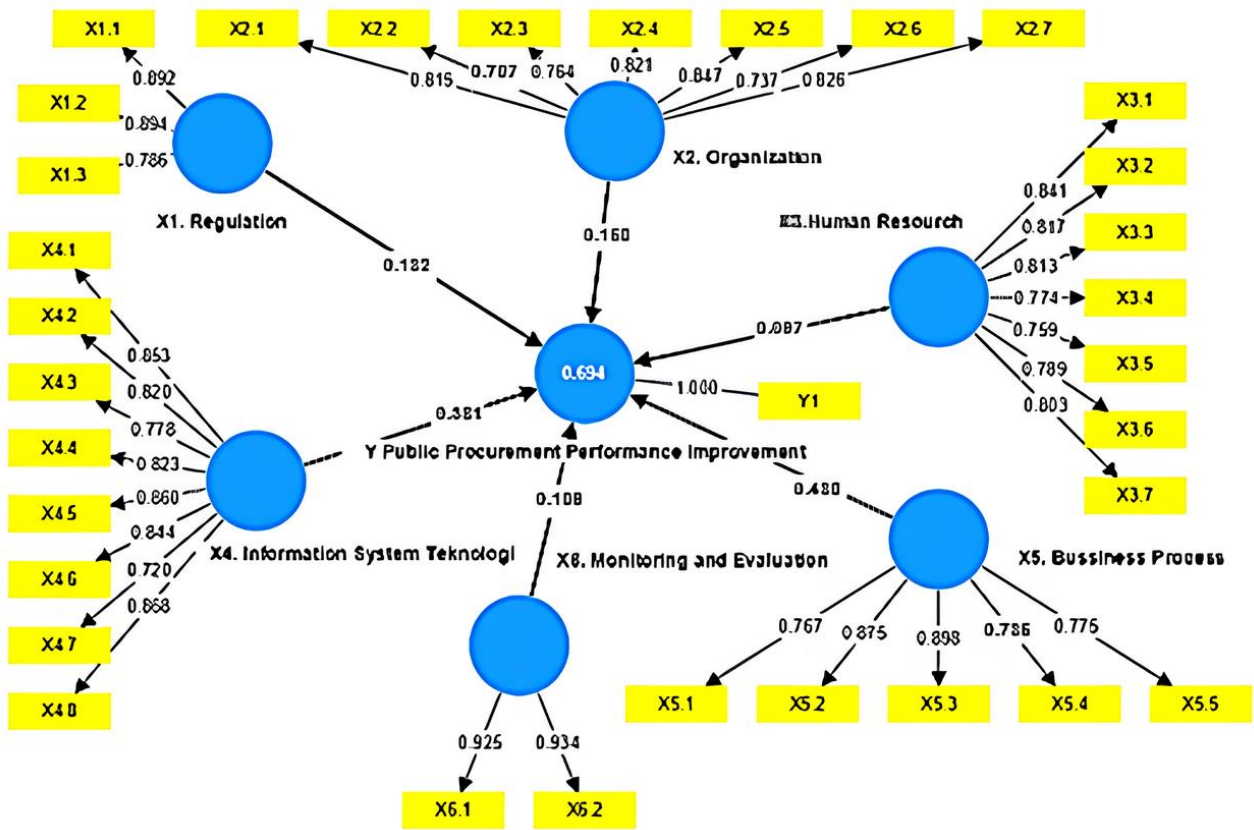**Figure 3. Inner Model Test (Model Fit) for All of Indonesia**

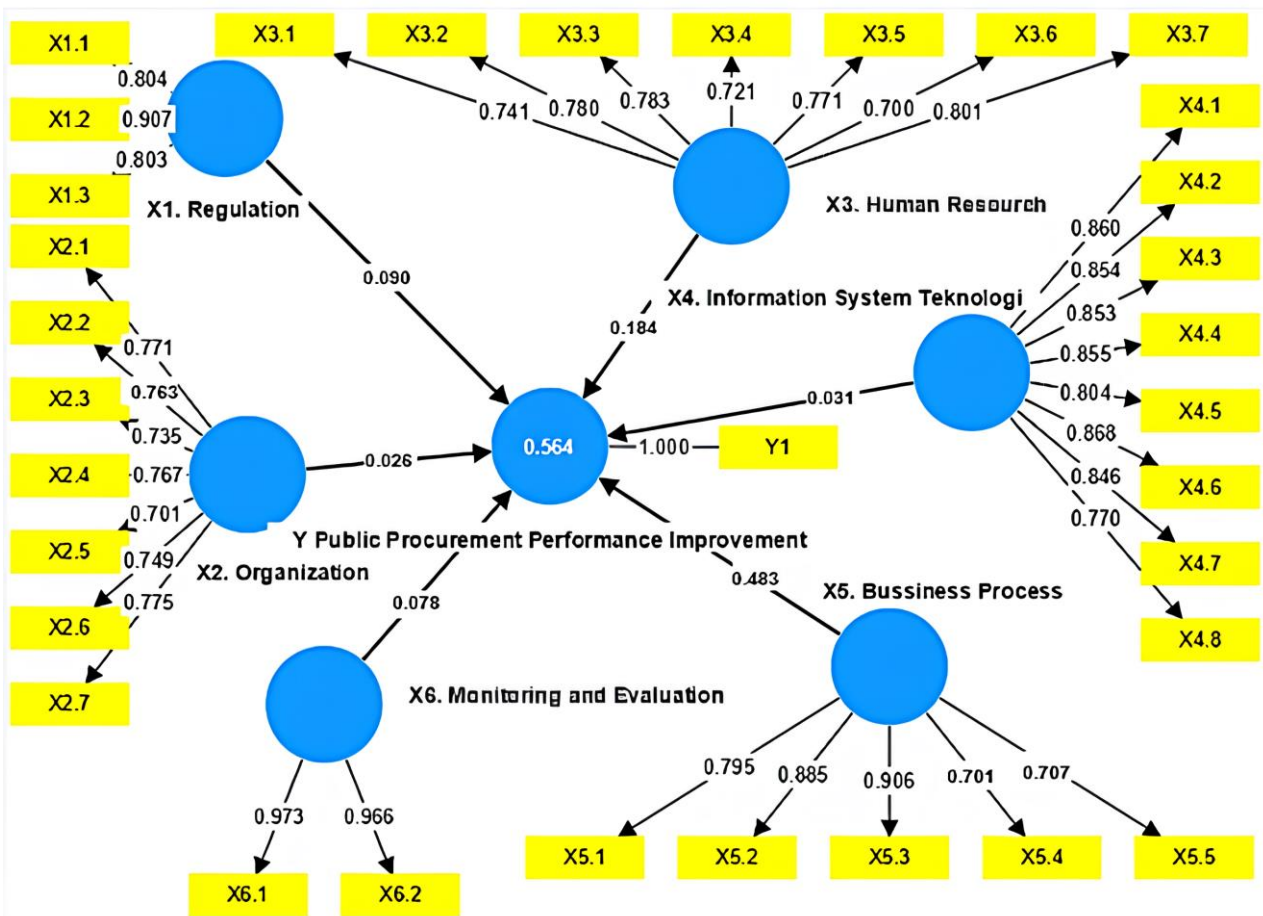**Figure 4. Inner Model Test (Model Fit) for Respondents Data With < 5 Years of experience**

Figure 5. Inner Model Test (Model Fit) for Respondent Data > 5 Years

Table 8. Inner Model Test Value (Model Fit)

	Saturated model	**Estimated model**
SRMR	0.067	0.067
d_ULS	2,536	2,536
d_G	1,116	1,116
Chi-square	1,606,184	1,606,184
NFI	0.770	0.770

The calculated results show that the Model Fit value is the NFI value = 0.770. It means that the NFI value has shown that the model built is good. The percentage of the model produced is obtained by NFI x 100%, so the ratio of the model built is obtained by NFI = 0.770×100% = 77.0% Fit model. It means that the sustainable construction model built has 77.0% declared fit and can be implemented in the goods and services procurement unit.

4.3. Hypothesis Testing

Hypothesis testing is utilized to test whether there is an impact of exogenous factors on endogenous factors. The test criteria state that if T-Statistic ≥ T-table (1.96), it is famous that exogenous factors have a positive and noteworthy impact on endogenous factors. The results of significance testing are shown in Table 9.

Table 9. Inner Model Test (Significance T-Statistic)

Hypothesis	**Factors**	**Result**
1	Regulation	Accepted
2	Organizational	Accepted
3	Human Resource	Accepted
4	Information System	Accepted
5	Business Process	Accepted
6	Monitoring & Evaluation	Accepted

5. Conclusions

The equation obtained from the results of this data analysis is:

$$Y1 = 0.901X1 + 0.461X2 + 0.561X3 + 0.631X4 + 0.971X5 + 0.380X6$$

(1)

The magnitude of the regulatory variable value of 90.1% means that the regulatory variable in this study influences the ability of the Construction Services Selection Implementation Centre to become a reliable procurement agent in Indonesia by 90.1%.

The magnitude of the organizational variable value of 46.1% means that the organizational variables in this study influence the ability of the Construction Services Selection Implementation Centre to become a reliable procurement agent in Indonesia by 46.1%.

The value of the Human Resources variable, namely 56.1%, means that the Human Resources (HR) variable in this study influences increasing the Construction Services Selection Implementation Centre's ability to become a reliable procurement agent in Indonesia by 56.1%. The magnitude of the value of the Information System variable, namely 63.1%, means that the Information System variable in this study influences the ability of the Construction Services Selection Implementation Centre to become a reliable procurement agent in Indonesia by 63.1%.

The magnitude of the Business Process variable value of 97.1% means that the Business Process variable in this study influences increasing the Construction Services Selection Implementation Centre's ability to become a reliable procurement agent in Indonesia by 97.1%.

The value of the Monitoring & Evaluation variable, namely 38%, means that the Monitoring & Evaluation variable in this study influences the ability of the Construction Services Selection Implementation Centre to become a reliable procurement agent in Indonesia by 38%.

The value of the Monitoring & Evaluation variable, namely 38%, means that the Monitoring & Evaluation variable in this study influences the ability of the Construction Services Selection Implementation Centre to become a reliable procurement agent in Indonesia by 38%.

6. Declarations

6.1. Author Contributions

6.2. Data Availability Statement

6.3. Funding

6.4. Conflicts of Interest

7. References

[1] Hernandez-Carrillo, C. G., Sarmiento Rojas, J. A., Rueda Varon, M. J., Göiza-Pinzón, F. D., & Toloza-Gordillo, L. M. (2023). Evaluation of preferences for concrete admixtures using statistical perception techniques in the procurement management for the Colombian construction market. Procedia Computer Science, 219, 1977–1984. doi:10.1016/j.procs.2023.01.498.

[2] Alvanchi, A., Shiri, N., & Alikhani, H. (2020). In-depth investigation of project planning and control software package application in the construction industry of Iran. International Journal of Engineering, 33(10), 1817-1825. doi:10.5829/ije.2020.33.10a.01.

[3] Langevin, J., Wen, J., & Gurian, P. L. (2015). Simulating the human-building interaction: Development and validation of an agent-based model of office occupant behaviors. Building and Environment, 88, 27-45. doi:10.1016/j.buildenv.2014.11.037.

[4] Mohd Fateh, M. A., Mohamed, M. R., & Omar, S. A. (2022). The Involvement of Local Skilled Labour in Malaysia's Construction Industry. Frontiers in Built Environment, 8, 1–19. doi:10.3389/fbuil.2022.861018.

[5] Nurhendi, R. N., Khoiry, M. A., & Hamzah, N. (2019). Review on factors influencing labour productivity in construction project. International Journal of Recent Technology and Engineering, 7(6), 837–844.

[6] He, C., Milne, A., & Ataullah, A. (2023). What explains delays in public procurement decisions? Economic Modelling, 121, 106201. doi:10.1016/j.econmod.2023.106201.

[7] Abduh, M., Sukardi, S. N., Wirahadikusumah, R. D., Oktaviani, C. Z., & Bahagia, S. N. (2023). Maturity of procurement units for public construction projects in Indonesia. International Journal of Construction Management, 23(13), 2171–2184. doi:10.1080/15623599.2022.2046941.

[8] Arts, J., Hanekamp, T., Linssen, R., & Snippe, J. (2016). Benchmarking integrated infrastructure planning across Europe–Moving forward to vital infrastructure networks and urban regions. Transportation Research Procedia, 14, 303-312. doi:10.1016/j.trpro.2016.05.024.

[9] Lăzăroiu, G., Ionescu, L., Uţă, C., Hurloiu, I., Andronie, M., & Dijmarescu, I. (2020). Environmentally responsible behavior and sustainability policy adoption in green public procurement. Sustainability (Switzerland), 12(5), 2110. doi:10.3390/su12052110.

[10] Nurmandi, A., & Kim, S. (2015). Making e-procurement work in a decentralized procurement system: A comparison of three Indonesian cities. International Journal of Public Sector Management, 28(3), 198–220. doi:10.1108/IJPSM-03-2015-0035.

[11] Sandi, P. V., Rohman, M. A., & Utomo, C. (2020). A concept to evaluate procurement principles implementation of public construction project in Surabaya. IOP Conference Series: Materials Science and Engineering, 930(1), 012005. doi:10.1088/1757-899X/930/1/012005.

[12] Masudin, I., Aprilia, G. D., Nugraha, A., & Restuputri, D. P. (2021). Impact of E-Procurement Adoption on Company Performance: Evidence from Indonesian Manufacturing Industry. Logistics, 5(1), 16. doi:10.3390/logistics5010016.

[13] Afolabi, A., Ibem, E., Aduwo, E., & Tunji-Olayeni, P. (2022). Digitizing the grey areas in the Nigerian public procurement system using e-Procurement technologies. International Journal of Construction Management, 22(12), 2215–2224. doi:10.1080/15623599.2020.1774836.

[14] Tabish, S. Z. S., & Jha, K. N. (2011). Analyses and evaluation of irregularities in public procurement in India. Construction Management and Economics, 29(3), 261–274. doi:10.1080/01446193.2010.549138.

[15] Costa, A. A., Arantes, A., & Valadares Tavares, L. (2013). Evidence of the impacts of public e-procurement: The Portuguese experience. Journal of Purchasing and Supply Management, 19(4), 238–246. doi:10.1016/j.pursup.2013.07.004.

[16] Owusu, E. K., Chan, A. P. C., Hosseini, M. R., & Nikmehr, B. (2020). Assessing procurement irregularities in the supply-chain of ghanaian construction projects: A soft-computing approach. Journal of Civil Engineering and Management, 26(1), 66–82. doi:10.3846/jcem.2020.11659.

[17] Montalbán-Domingo, L., García-Segura, T., Amalia Sanz, M., & Pellicer, E. (2019). Social Sustainability in Delivery and Procurement of Public Construction Contracts. Journal of Management in Engineering, 35(2), 4018065. doi:10.1061/(asce)me.1943-5479.0000674.

[18] Siyal, S., & Xin, C. (2020). Public Procurement. Global Encyclopedia of Public Administration, Public Policy, and Governance. Springer, Cham, Switzerland. doi:10.1007/978-3-319-31816-5_344-1.

[19] Thai, K. V. (2001). Public procurement re-examined. Journal of Public Procurement, 1(1), 9–50. doi:10.1108/jopp-01-01-2001-b001.

[20] Fourie, D., & Malan, C. (2020). Public procurement in the South African economy: Addressing the systemic issues. Sustainability (Switzerland), 12(20), 1–23. doi:10.3390/su12208692.

[21] Lynch, J., & Angel, J. (2013). Public procurement: Principles, categories and methods. Procurement Classroom Series, 2, Victoria, Canada.

[22] Komakech, R. A. (2016). Public procurement in developing countries: Objectives, principles and required professional skills. Public Policy and Administration Research, 6(8), 20-29.

[23] Ruparathna, R., & Hewage, K. (2015). Review of Contemporary Construction Procurement Practices. Journal of Management in Engineering, 31(3). doi:10.1061/(asce)me.1943-5479.0000279.

[24] Mojumder, A., Singh, A., Kumar, A., & Liu, Y. (2022). Mitigating the barriers to green procurement adoption: An exploratory study of the Indian construction industry. Journal of Cleaner Production, 372. doi:10.1016/j.jclepro.2022.133505.

[25] Sabarish P, Dinesh, S., & Preetha, R. (2016). Literature Study on Socio-Economic Factors of Construction Industry in Developing Countries. International Journal of Science, Engineering and Technology Research, 5(11), 2278–7798.

Experimental Study on Hollow Steel Sections Under Elevated Temperature

Prakash Murugan [1], Alireza Bahrami [2]*, Vishal Murugan [1], Ajish Kumaran [1]

[1] *Department of Civil Engineering, College of Engineering and Technology, SRM Institute of Science and Technology, SRM Nagar, Kattankulathur – 603 203, Tamil Nadu, India.*

[2] *Department of Building Engineering, Energy Systems and Sustainability Science, Faculty of Engineering and Sustainable Development, University of Gävle, 801 76 Gävle, Sweden.*

Abstract

Structures known as modular buildings are made in factories and then moved to construction sites, where they are assembled. The efficacy of modular structures under many uncertainties has to be thoroughly investigated as demand rises; fire is one such uncertainty. The purpose of this study is to ascertain how high temperature affects the components of modular constructions. In the current study, hollow steel columns and beams were taken into account as components of a modular construction. Using ABAQUS, several situations were examined depending on the span length to determine the important locations of the members. Experimental research was conducted on the critical regions identified by the analysis, and the results were contrasted with those of the analysis. A high-temperature localized heating furnace was used for the experimental testing. The findings demonstrated that for spans of 250 mm and 500 mm, the central area of the beams was essential, and the load-carrying capacity was six times less than that of heating at the extremities of the beams. Similar to the beams, columns exhibited less fluctuation than the beams and were weaker in the bottom area when exposed to high temperature. When compared to other places, the capacity was reduced by 1.1 times, and in Case 1, the capacity reduction with regard to loading was 1.68 times greater.

Keywords: Modular Building; Elevated Temperature; Hollow Steel Section; Critical Fire Region; Finite Element Analysis.

1. Introduction

Buildings undergo many natural and man-made disasters during their lifetime. One such type that has been given attention is the effect of seismicity. Many analytical and experimental research works have been conducted in this area. However, facts tell us that the number of people who lose their lives is not due to the direct effect of the earthquake but to indirect effects such as fire, among many other things [1]. Hence, it is crucial that the materials used in building construction can withstand a fire for a certain period of time. In this regard, it is important to keep in mind that at the temperatures that may be anticipated under fire conditions, the strength and deformation capabilities of regularly utilized building materials dramatically deteriorate [2]. The kind and quantity of combustible elements present affect this temperature development, among other factors. The term "fire resistance" refers to how long a building component can tolerate the heat exposure in accordance with the standard fire curve [3, 4]. The right performance criteria must be established before it is possible to assess a building component's fire resistance [5]. There are essentially two approaches that can be employed to determine fire resistance: an experimental approach and an analytical or fire engineering technique.

The modular building technique is a rapidly expanding methodology that may be used instead of conventional on-site construction. A modular structure comprises several premade sections known as "modules" [6]. Modules are manufactured in a faraway place to create permanent residential or commercial structures and fabricated on-site. Apartments, schools, offices, and any other facility in which repeated units are desirable are all examples of modular construction [7]. Modular construction is utilized mainly for low-rise dwellings in America, Japan, and some areas of Europe. At the same time, the growing urban population necessitates the construction of additional high-rise structures [8].

Cast-in-place and prefabrication technologies were compared together with two common housing projects by Cao et al. [9]. Several methods, including on-site measurements and interviews, were used to acquire the data. The research was divided into several areas, including resource depletion, energy use, and construction waste discharge. The building health effect assessment system and the construction environmental performance evaluation system were utilized to compute the two construction technologies. With a total consumption drop of 20.49%, the outcome indicated that prefabricated houses were more energy efficient than traditional residential construction. Simplicity, homogeneity, repetition, and economies of scale are ideal design practices for high-rise structures. This building method's appeal stems from its inherent benefits over traditional construction methods. Excellent productivity, good quality, shorter timelines, less waste creation, efficiency of cost, and less generation of noise are just a few benefits.

A thorough conceptual framework was offered by Gunawardena et al. [10], which may be used to choose the ideal structural system depending on the circumstances. In order to optimize the building, a multidisciplinary approach will assess the structural systems, construction materials, constructability, cost of construction, and speed. They have discussed many optimization algorithm types that are employed in building design, how they may be modified to assess a prefabricated structure, and which elements would prevail as crucial performance indicators in the search for the best prefabricated modular building solution. Using a dynamic case study-based assessment, Boafo et al. [11] characterized prefabricated levels and analyze the performance of prefabricated modules while considering acoustic constraints, resistance to seismic forces, thermal properties, energy demand, and life cycle analysis of current prefabricated examples. The modules can be categorized into two groups based on the method of load transfer: self-supporting load-bearing modules and frame-supported modules [12]. The loads are distributed through the walls of the modules. Because of this point, the building heights are normally restricted to four to eight stories, and the compressive resistance of the walls is essential. On the other hand, for frame-supported modules, loads are distributed by edge beams attached to corner posts, and the posts need to have high compression resistance. Figure 1 shows a typical steel frame module.

Figure 1. Steel frame module

Modules are made to be lifted, and each module has specific lift points. Forklifts may be utilized in the manufacturer's yard, although cranes are typically employed to lift them [13]. Deflection parameters selected to safeguard delicate components are frequently used to define the quantity and placement of lift points. Existing standards, such as American Standard and DNV Offshore Standard, provide general guidance on the design of lifters. Developing countries need high-rise buildings for accommodation. Only the application of contemporary construction techniques built on standardization, unification, and typification can justify it economically.

The focus of experts' efforts is finding ways to lower construction costs. It should be highlighted that one of the most advanced and promising current trends in architectural and construction development worldwide is the use of off-site manufactured modules, or modular construction. Modular buildings are more durable than traditional buildings because of the independent engineering done in a factory [14]. The seismic performance of a frame structure was measured utilizing energy dissipation characteristics taking into consideration the seismic forces, thermal properties, and energy demand, revealing that the frame was stable and ductile up to high drift levels; there was no significant stiffness degradation with cyclic loading, and the structure had good energy dissipation per cycle in every loading step, demonstrating a higher seismic capacity for modular buildings [15]. Wu et al. [16] investigated how the mechanical

characteristics of a modular prefabricated steel-concrete composite internal joint (MPCIJ) were affected by the key parameters. MPCIJ was subjected to cyclic stress using the finite element analysis (FEA) software ABAQUS. Comparisons were made between the experimental and FEA results' hysteresis curves and mechanisms of failure. Various parameters' effects on structural performance were examined once the dependability of the numerical model was confirmed. The shear mechanism and bearing capacity calculation techniques were provided based on test and FEA findings. Kumar et al. [17] compared the structural and mechanical performances of the low-alloy cold-formed steel sections at different temperatures for developing high-fire performance steel structures. Precast structural systems are more economical than steel structures, according to Kim et al. [18], but their slower construction speed prohibits them from being widely used. This is because installing lateral bracing beams during erection is challenging. By swiftly and easily joining column-beam sections to beam sections, a structural approach is offered for lateral bracing during construction.

The lean tool kaizen was suggested by Nahmens et al. [19] as a practical and effective methodology for sustainability that concentrated on enhancing the environmental and socioeconomic performances of modular building processes. Numerous case examples are provided in this study to display how lean has an influence on the sustainability of modular housing. Ramaji & Memari [20] discussed multi-story modular building methods. They mentioned the challenges faced by structural designers when attempting to eliminate horizontal load transfer, gravity, and load path discontinuity. In addition to applicable building code requirements, the approaches for the modular system and modeling needed for assessing the buildings are given. The challenges of developing and detailing different structural sections and systems were also assessed. Additionally, any special structural safety factors that must be taken into account during design and construction were listed. Blast-resistant portable buildings are generally 40 feet long, 10–15 feet wide, and approximately 10 feet tall, and are subjected to blast impulses. It was found that during the blast reaction, there were a lot of sliding and flipping and requirements of positive pressure, and the traditional loading standards were the criteria for an appropriate degree of significance and building protection. Fireproofing measures with three layers of gypsum boards can safeguard the columns and ensure a 3-hour fire-resistance rating. The fireproofing measure with a layer of gypsum board and mineral wool experienced early gypsum board failure and a smaller rating [21].

A recent study by academicians from the University of Cambridge and Edinburgh Napier University found that modular buildings were able to save almost 28000 metric tons of carbon (i.e., approximately 45% less carbon) compared to traditional methods, as illustrated in Figure 2 [22]. Embodied carbon, which is released during the production and transportation of materials, accounts for 11% of global emissions, which is more than that of the carbon produced by the aviation and shipping industries combined and can also be reduced.

Figure 2. Modular building in Cambridge center for housing and planning research

The significance of the research is that modular systems can be utilized in explosively hazardous areas, such as petroleum areas and chemical processing industries [23]. It will also help us determine the areas of failure and what can be done to reduce the failure of the modules. With increasing attention given to high-density urban areas and limited working spaces, modular prefabrication can act as an excellent replacement for conventional buildings [21].

However, previous research failed to identify the influence of elevated temperatures and identify the critical region in a hollow steel section. The critical region under high temperatures is the portion where heating the small part of the member gives a similar reaction to heating the entire member. A small-intensity fire in the critical region could trigger the global collapse of the structure. This article will also act as a research foundation for future temperature studies of modular elements. The aim of the current study is to determine the behavior of beams and columns of a modular system (sub-assemblage element) analytically and experimentally under elevated temperature to find the critical region. Observing the critical region under fire would help engineers strengthen the structural members to perform well under fire scenario. This article includes an analytical study of the elements of modular buildings, such as beams and columns, under different load cases at different locations, and the performance of the critical section is obtained using an experimental study.

2. Material and Methods

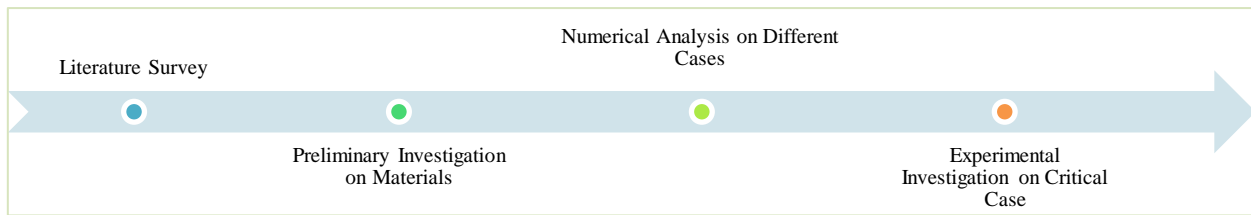The methodology of this research is represented in Figure 3.

Figure 3. Methodology of current research work

2.1. Hot-Rolled Sections

Hot-rolled mild steel sections were taken for analysis and experimental purposes because it is simpler to produce, shape, and form hot-rolled steel [24]. Starting with a billet of still steel that has been heated to 1700 °F, the steel is rolled through the mill into the desired shape and is then cooled [25]. It has the properties of increased toughness and ductility and can be made into any shape. Hot-rolled steel angles or hollow sections are frequently used as corner posts. Moreover, the modular industry employs a variety of module shapes, including slope-end, stepped, faceted, and tapered modules [26]. The rectangular-shaped module, however, continues to be popular in buildings. Note that while corner-supported modules are unlikely to be utilized, wall-supported modules are compatible with any shape. Modular buildings are usually constructed in steel sections, and mostly either channel sections or hollow sections are used [27]. Due to their high strength, excellent ductility, light weight, and other advantages, square hollow steel tubular sections are frequently employed in the construction of steel [28, 29]. Steel has poor fire resistance, and hence, it is important to study fire in steels, as they form the primary component of modular buildings [30]. In this article, hollow sections are taken into consideration, as the number of studies on these sections is very low.

3. Analytical Study of Beams and Columns at Elevated Temperature

3.1. Analysis of Beams

The models were created, and the necessary studies were carried out using the FEA software ABAQUS. A total of 60 beams were modeled because of the variation in loading and temperature applications at different locations of the beams. Finite element models with a constant height of 1.5 m, outside dimensions of 100 mm × 100 mm, and a thickness of 5 mm were created to do the numerical analyses. The predefined temperature was set to 29 °C. To conduct the necessary FEA, thermal characteristics such as density, thermal conductivity, and specific heat were needed. A coupon test was performed, and the corresponding results are listed in Table 1. Table 2 presents these temperature-dependent variations in value along with the respective temperatures.

Table 1. Coupon test results

Specimen No.	Average thickness (mm)	Yield stress (N/mm²)	Ultimate stress (N/mm²)	Percentage of elongation
1	4.8	300.06	480.86	23.33
2	4.7	317.72	491.88	21.67

Table 2. Properties of hollow steel section for finite element modeling [31]

Temperature (°C)	Young's modulus (N/mm²)	Thermal conductivity (W/m K)	Linear expansion	Specific heat (J/kg K)
29	200000	53.33	0	439.8
100	200000	50.67	0.00001248	487.6
200	180000	47.34	0.00001288	529.8
300	160000	44.01	0.00001328	564.7
400	140000	40.68	0.00001368	605.9
500	120000	37.35	0.00001408	666.5
600	62000	34.02	0.00001448	759.9
700	26000	30.69	0.00001488	1008.2
800	18000	27.3	0.0000141	803.3

Other properties include a Poisson ratio of 0.3 and a steel density of 7850 kg/m^3. To obtain the plasticity values, a coupon test was done for the steel material [32].

The type of analysis performed was transient because of the involvement of the temperature and time. Analysis was performed on various segments, such as 250 mm, 500 mm, 750 mm, and 1500 mm, under different loading cases, including 10%, 20%, 30%, 40%, and 50%. A temperature of 800 °C was taken since the hot-rolled sections are subjected to rolling at temperatures varying from 850–1200 °C so that the critical temperature can be achieved. Figure 4 depicts the cases taken for the application of the temperature to various regions of the beams.

Case 1	Case 2	Case 3	Case 4	Case 5	Case 6

250 mm

Case 1	Case 2	Case 3

500 mm   **500 mm**   **500 mm**

Case 1	Case 2

750 mm   **750 mm**

Case 1

1500 mm
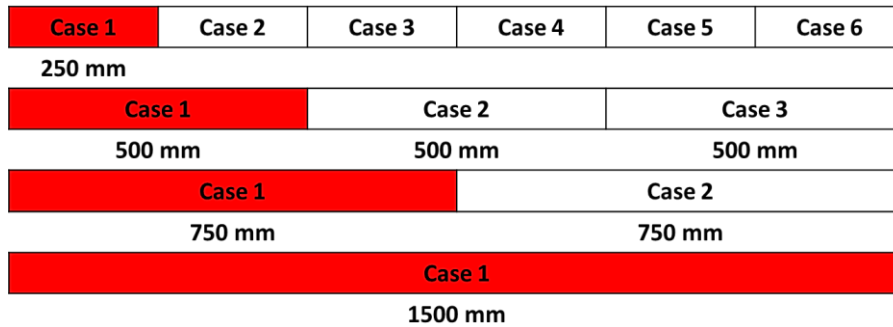
Figure 4. Different cases taken for analysis of beams

3.2. Analysis of Columns

A total of 60 columns were modeled owing to the variation in loading and temperature applications at different locations of the columns. Finite element models with a constant height of 1.5 m with outside dimensions of 100 mm × 100 mm and a thickness of 5 mm were created to conduct the numerical analyses. The predefined temperature was set to 29 °C. Analysis was performed on various segments, such as 250 mm, 500 mm, 750 mm, and 1500 mm, under different loading cases, including 50%, 60%, 70%, 80%, and 90%, with the view that the column can take a large amount of load. A base plate with dimensions of 200 mm × 200 mm was given with a thickness of 20 mm to apply the load. Surface-to-surface connections were provided. The type of support given was pinned support, which was provided at the bottom of the column. Figure 5 shows the cases taken for the application of the temperature to various regions of the columns. Figure 6 indicates a typical model and mesh of the column.

Case 1	Case 2	Case 3	Case 4	Case 5	Case 6

250 mm

Case 1	Case 2	Case 3

500 mm   **500 mm**   **500 mm**

Case 1	Case 2

750 mm   **750 mm**

Case 1

1500 mm

Figure 5. Different cases taken for analysis of columns

Figure 6. Typical model and mesh of column

4. Experimental Study of Beam and Column at Elevated Temperature

4.1. Testing Materials

Two specimens of hollow square steel sections were taken with dimensions of 100 mm × 100 mm × 5 mm, which were 1500 mm long, of which one was a beam, and another was taken as a column. The type of material used was hot-rolled steel [33]. The steel was painted, and then markings were placed on the beam and column. Figure 7 displays the specimens before and after painting.

Figure 7. Specimens before and after painting

4.2. Temperature Test on Beam

Beam was placed with a boundary condition of 100 mm from either side of the beam, and the type of loading given was four-point loading, and loading was given at l/3 distance from either side of the boundary conditions. The type of support provided was pinned support. Based on the ana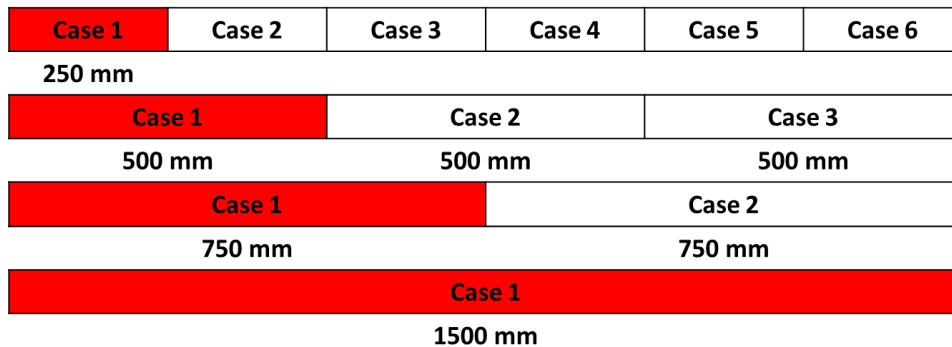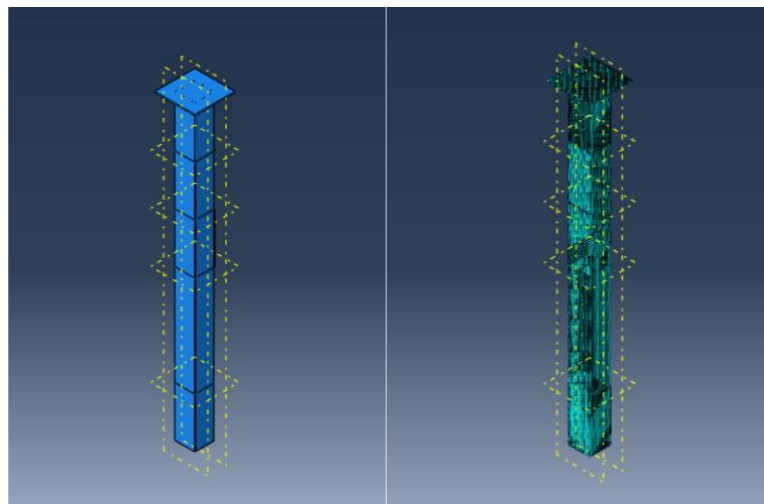lytical results, the middle section of the beam (i.e., the middle 500 mm of the beam) was found to be critical, and hence, the oven was placed at the center. A girder was prepared to apply the load with a gap in the middle so that the oven could be fitted in the place. An in-house fabricated localized heating furnace was utilized to apply the temperature. The oven could reach temperatures up to 1000 °C. It could fit a member of a cross section of 125 mm × 125 mm and a span of 600 mm. Loading was applied to the beam with the help of a manual-type loader using a hydraulic jack. A test load of 25 kN at a rate of 5 kN and the deflection of the beam were taken employing the two dial gauges located at the point of loading, which can be seen in Figures 8 and 9. The test load was given based on a certain percentage based on the ultimate load found through the analytical study. After the application of the test load, the loading was locked, and the temperature was set to 200 °C according to the result obtained from the analysis. The time taken to reach 200 °C was noted for a regular interval of one minute. Once the oven reached the temperature mentioned, the temperature was measured utilizing an infrared gun at the midpoints marked at 100 mm intervals from the center of the beam (a total of 9 points were marked on the beam) at regular intervals, and the deflection at both dial gauges was noted regularly at intervals of 10 minutes. After 4 hours, the furnace was switched off, cooling was performed for 90 minutes, and the deflection and temperature values were again taken similarly at regular intervals for 10 minutes.

Figure 8. Experimental test setup for beam at elevated temperature
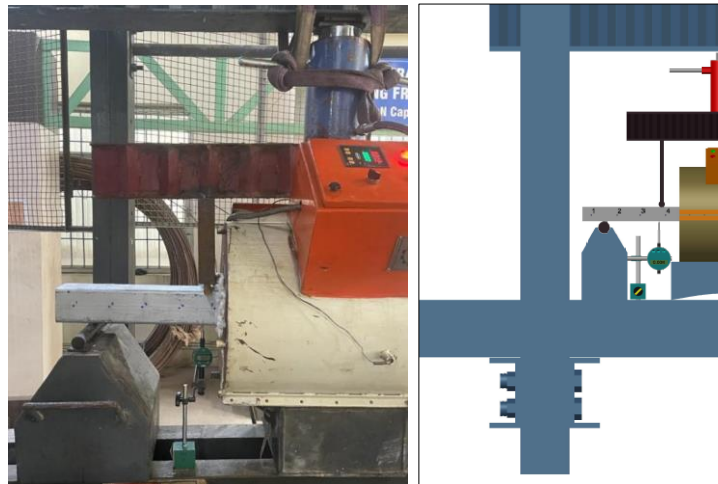
Figure 9. Dial gauge at point of loading

4.3. Temperature Test on Column

As the bottom of the columns was found to be critical, with the knowledge that usually the fire starts from the bottom of the column, the oven was placed 10 cm from the bottom of the column. Six points were marked on the column above at 10 cm to measure the temperature. Similarly, a point was marked 10 cm from the bottom of the column to take the readings. The test load of 250 kN was given initially, and then the temperature was provided. A dial gauge was placed to take the deflection values regularly, similar to those of the beam. Initially, it was provided up to a temperature of 600 °C, and then it was kept constant for 4 hours, and temperatures were taken from center points through infrared thermometers at regular intervals of 10 minutes. After that, the temperature input was stopped, cooling was done for 4 hours, and readings were taken similarly every 10 minutes. Figure 10 illustrates the experimental test setup for the column at the elevated temperature.
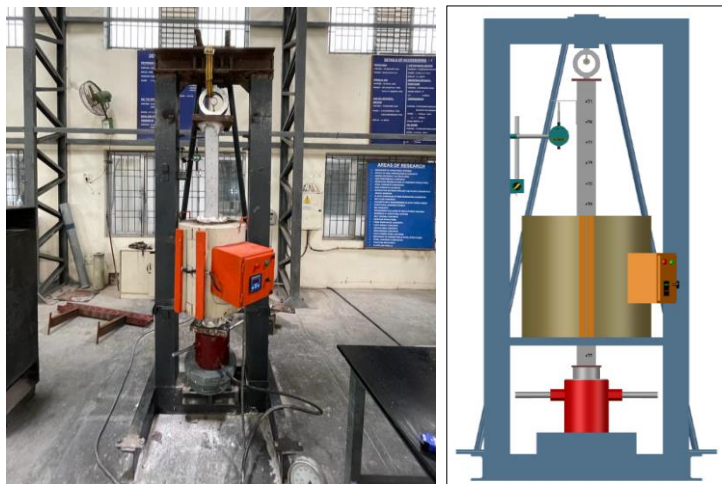
Figure 10. Experimental test setup for column at elevated temperature

5. Results and Discussion

5.1. Analytical Results of Beams

The time taken for the specimen to fail, the temperature the specimen was able to handle before failing, and the deflection values obtained during the time of failure taken from the analysis of the beams for different loadings at various locations were tabulated and compared to obtain the cooling behavior of the beams.

5.1.1. Effect of Temperature on 250 mm of Beams

The effect of the temperature on a region of 250 mm of the beams is demonstrated in Figure 11. A minimal effect can be observed as the temperature covers only 250 mm of the whole span. Case 3 with 50% loading was critical in terms of the temperature, and it was able to take 5 times less temperature when compared to 50% loading of Case 1. The time taken for Case 3 under 50% loading is 6.25 times less than that of Case 1 under 50% loading. From the analysis, it was found that the maximum deflection was found at 10% loading under Case 2. This must be because, with less loading, the effect of expansion on the beams with respect to the temperature might have been high. Table 3 summarizes the analytical results for 250 mm of the beams.
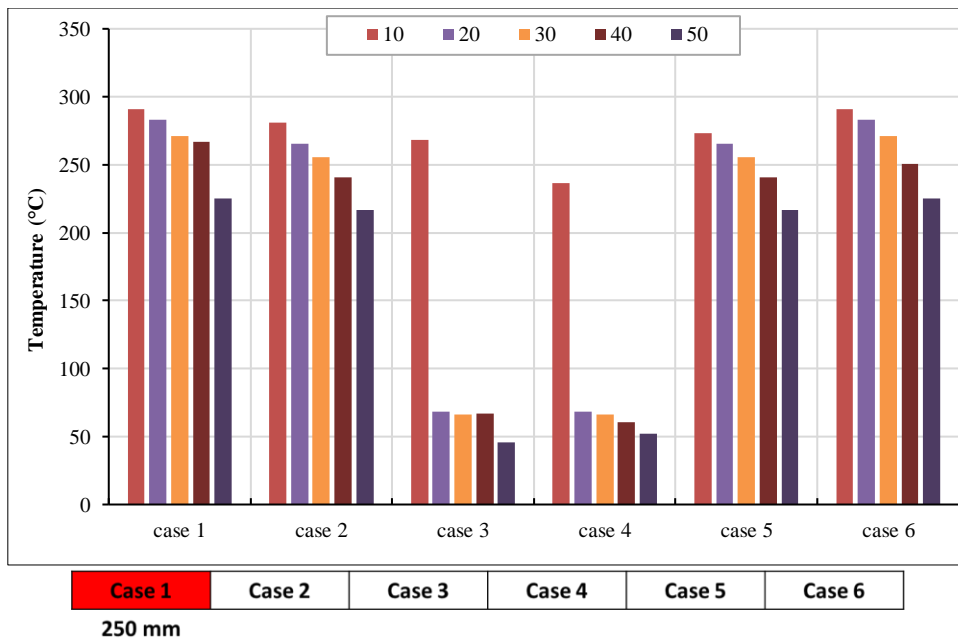
(a)
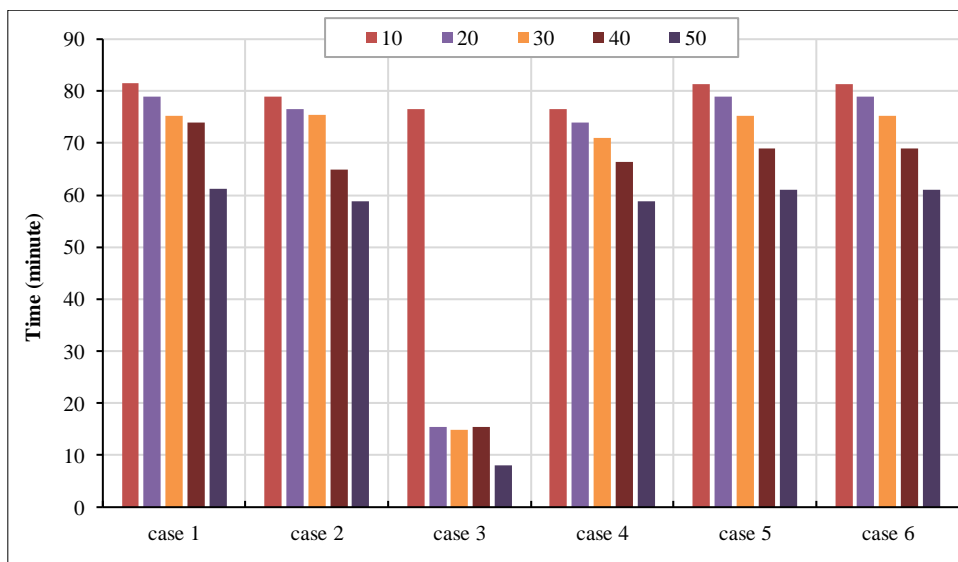
(b)
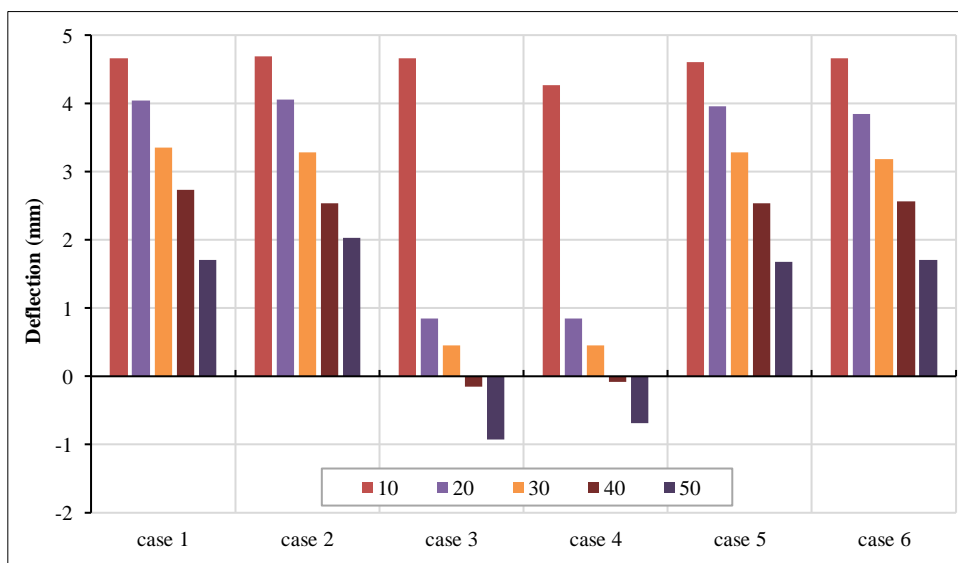
(c)

Figure 11. (a) Temperature for 250 mm of beams, (b) Time for 250 mm of beams, (c) Deflection for 250 mm of beams

Table 3. Analytical results for 250 mm of beams

Length	Type of cases	Load percentage (%)	Corresponding applied load (kN)	Temperature resisted (°C)	Time of resistance (minute)	Deflection (mm)
250 mm	Case 1	10	13.6	290.7	81.4	4.6
		20	27.2	282.7	79	4
		30	40.8	270.7	75.2	3.3
		40	54.4	266.5	73.9	2.7
		50	68	225	61.1	1.7
	Case 2	10	13.6	281	79	4.6
		20	27.2	265.3	76.5	4
		30	40.8	255.5	75.4	3.2
		40	54.4	240.8	64.8	2.2
		50	68	216.6	58.8	2
	Case 3	10	13.6	268	76.5	4.6
		20	27.2	68	15.5	0.8
		30	40.8	66	14.9	0.4
		40	54.4	64.5	14.7	-0.1
		50	68	45.7	8	-0.9
	Case 4	10	13.6	236.6	76.5	4.2
		20	27.2	68	74	0.8
		30	40.8	66	70.9	0.4
		40	54.4	60.5	66.3	-0.08
		50	68	52	58.8	-0.7
	Case 5	10	13.6	273.3	81.4	4.6
		20	27.2	265.3	79	3.9
		30	40.8	255.5	75.2	3.2
		40	54.4	240.8	68.9	2.5
		50	68	216.6	61.1	1.6
	Case 6	10	13.6	290.7	81.4	4.6
		20	27.2	282.7	79	3.8
		30	40.8	270.7	75.2	3.1
		40	54.4	250.5	68.9	2.5
		50	68	225.3	61.1	1.7

5.1.2. Effect of Temperature on 500 mm of Beams

Figure 12 depicts the effect of the temperature on a region of 500 mm of the beams. The effect can be seen clearly as 1/3 of the span is getting heated. Case 2 with 50% loading was critical in terms of the temperature, and it was able to take 3.45 times less temperature when compared to 50% loading of Case 1. It can also be found that Case 1 and Case 3 had similar effects on the temperature of the beams. The time taken for Case 2 under 50% loading is 4.9 times less than that of Case 1 under 50% loading. The maximum deflection was found at 10% loading under Case 2. Table 4 provides the analytical results for 500 mm of the beams.

(a)

867
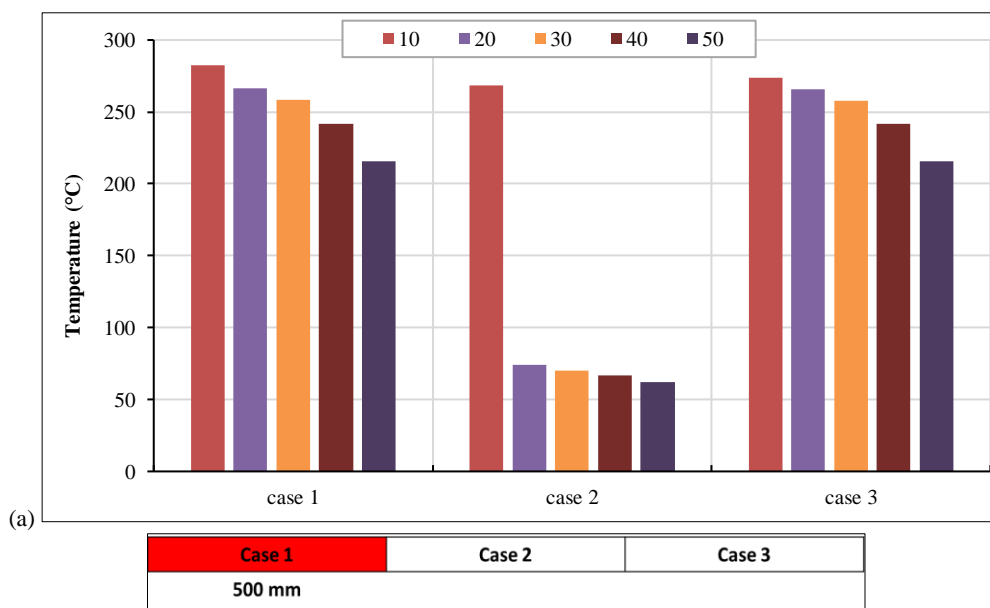
Figure 12. (a) Temperature for 500 mm of beams, (b) Time for 500 mm of beams, (c) Deflection for 500 mm of beams

Table 4. Analytical results for 500 mm of beams

Length	Type of cases	Load percentage (%)	Corresponding applied load (kN)	Temperature resisted (°C)	Time of resistance (minute)	Deflection (mm)
		10	13.6	282.76	79	4.69
		20	27.2	266.7	74	3.962
	Case 1	30	40.8	158.7	71.54	3.3
		40	54.4	241.5	66.16	2.53
		50	68	215.4	58.05	1.659
		10	13.6	268.45	76.5	4.69
		20	27.2	74	15.76	0.947
500 mm	Case 2	30	40.8	70.13	14.26	0.46
		40	54.4	67	13.3	0.019
		50	68	62	11.77	-0.49
		10	13.6	274	76.5	4.6
		20	27.2	266	74	3.8
	Case 3	30	40.8	258	71.53	3.3
		40	54.4	241.5	66.1	2.53
		50	68	215.4	58.05	1.659

5.1.3. Effect of Temperature on 750 mm of Beams

The effect of the temperature on a region of 750 mm of the beams is shown in Figure 13. The effect is obvious, as 1/2 of the span is subjected to high temperatures. Case 1 and Case 2 had similar kinds of responses in terms of the temperature resisted when half of the beams was subjected to heating. It was found that the maximum deflection was at 10% loading in Case 1 and Case 2, both indicating similar values. Table 5 displays the analytical results for 750 mm of the beams.

Figure 13. (a) Temperature for 750 mm of beams, (b) Time for 750 mm of beams, (c) Deflection for 750 mm of beams

Table 5. Analytical results for 750 mm of beams

Length	Type of cases	Load percentage (%)	Corresponding applied load (kN)	Temperature resisted (°C)	Time of resistance (minute)	Deflection (mm)
750 mm	Case 1	10	13.6	274	76.5	4.67
		20	27.2	264.6	73.36	3.99
		30	40.8	250.76	69	3.268
		40	54.4	232.5	63.36	2.48
		50	68	210.76	56.59	2.48
	Case 2	10	13.6	274	76.5	4.67
		20	27.2	264.6	73.36	3.99
		30	40.8	250.76	69	3.268
		40	54.4	232.5	63.36	2.48
		50	68	210.76	56.59	1.64

5.1.4. Effect of Temperature on 1500 mm of Beams

Figure 14 represents the effect of the temperature for a region of 1500 mm of the beams. The overall span is subjected to high temperature and becomes less effective (Table 6).
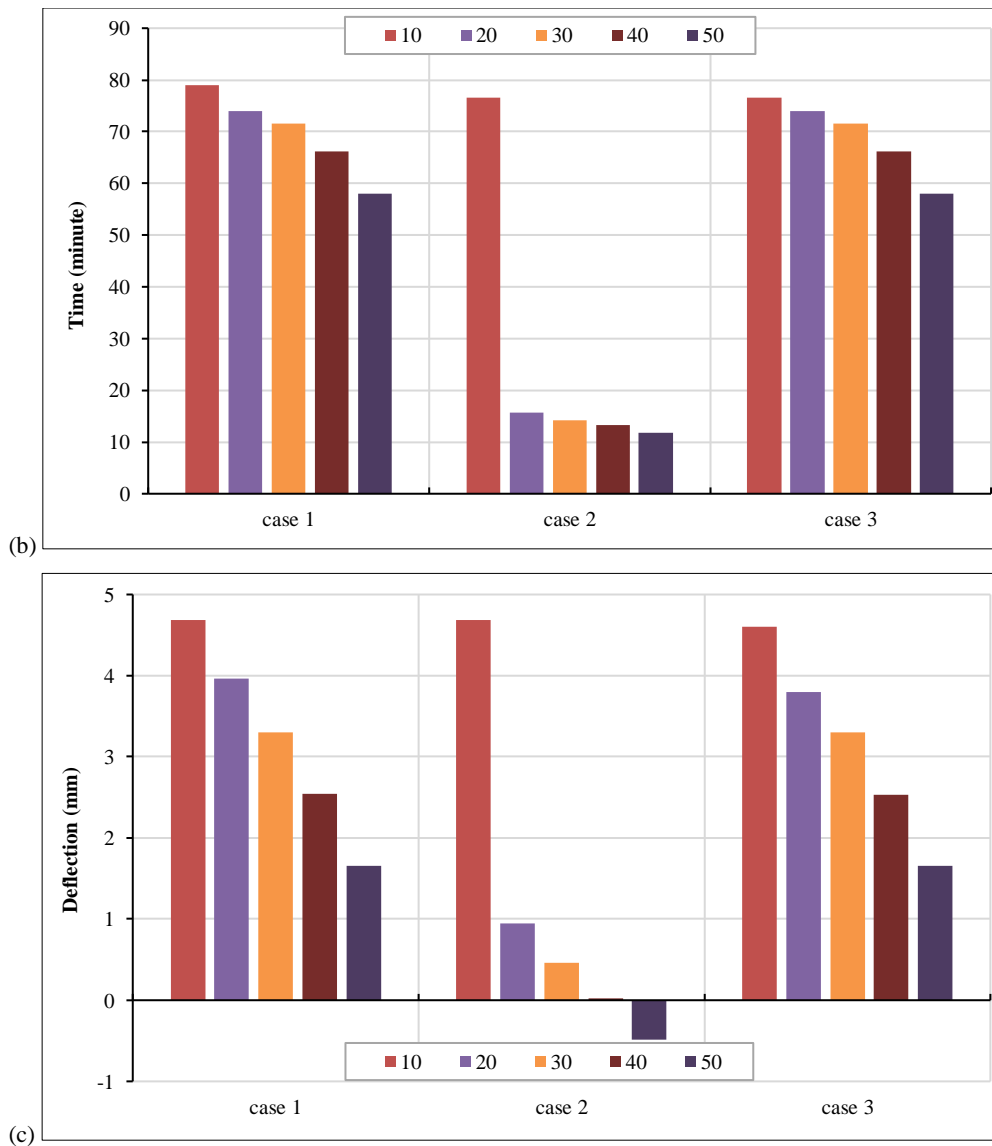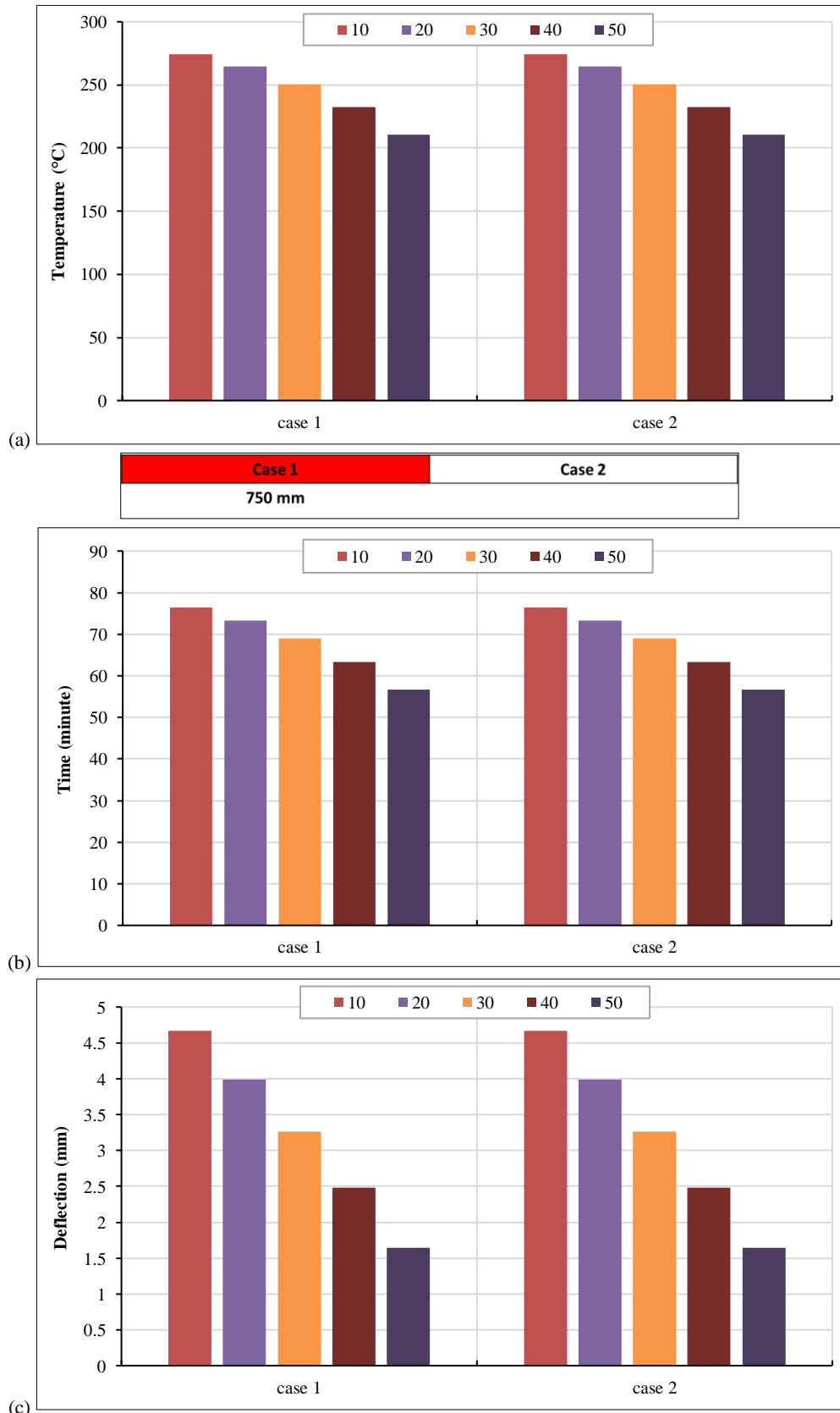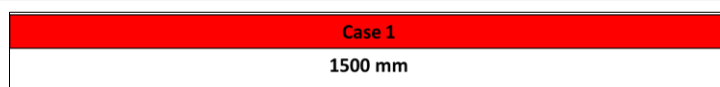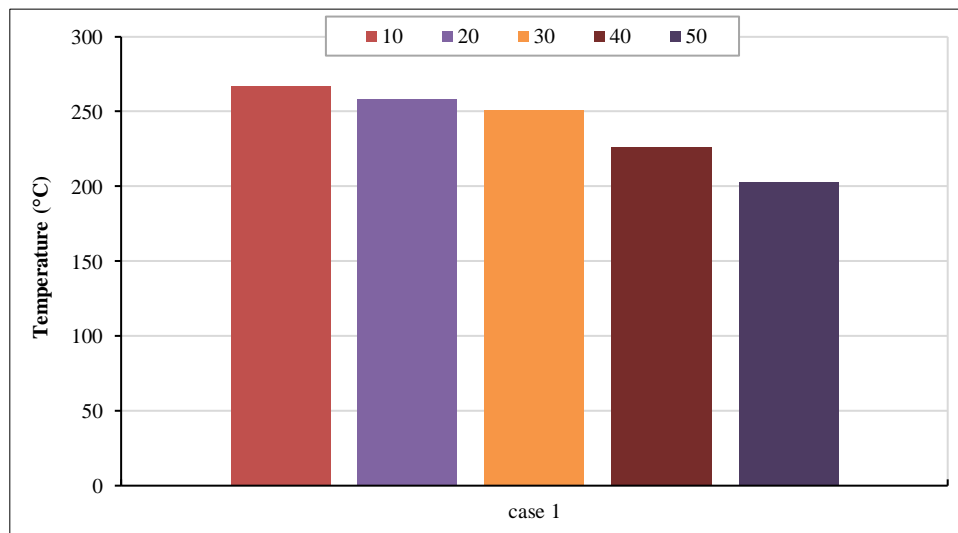

(a)

(b)
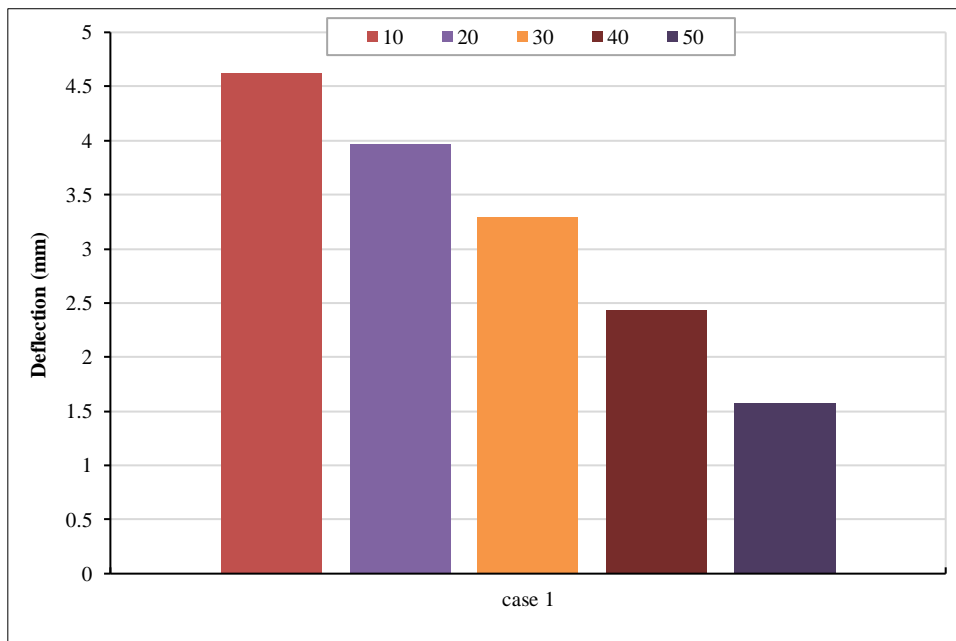
(c)

Figure 14. (a) Temperature for 1500 mm of beams, (b) Time for 1500 mm of beams, (c) Deflection for 1500 mm of beams

Table 6. Analytical results for 1500 mm of beams

Length	Type of cases	Load percentage (%)	Corresponding applied load (kN)	Temperature resisted (°C)	Time of resistance (minute)	Deflection (mm)
		10	13.6	266.7	74	4.62
		20	27.2	258.76	71.53	3.97
1500 mm	Case 1	30	40.8	250.76	69	3.3
		40	54.4	226.76	61.56	2.44
		50	68	202.76	54.1	1.58

Hence, it was finally concluded that the critical case of the beams was Case 2 in the 500 mm case and Cases 3 and 4 in the 250 mm case, demonstrating that the critical region was in the middle portion of the beams.

5.2. Analytical Results of Columns

The temperature, time, and deflection variations for the columns are presented in this section for different types of loadings at various locations. There were no significant changes with respect to the temperature at various locations, and the change was minimal. In addition, it was found that there was a symmetry in values on the ends of the columns.

5.2.1. Effect of Temperature on 250 mm of Columns

The effect of the temperature for a region of 250 mm of the columns is illustrated in Figure 15. Minimal effect can be observed as the temperature covers only 250 mm of the whole span. Table 7 displays the temperature at which the columns exceed the ultimate stress found using the coupon test. It can be seen from the table that Case 6 with 90% loading was critical in terms of the temperature, but the difference in the temperature was not as significant as in the columns. Case 3 was critical with 90% loading. The maximum deflection was witnessed in Case 5 with 90% loading.
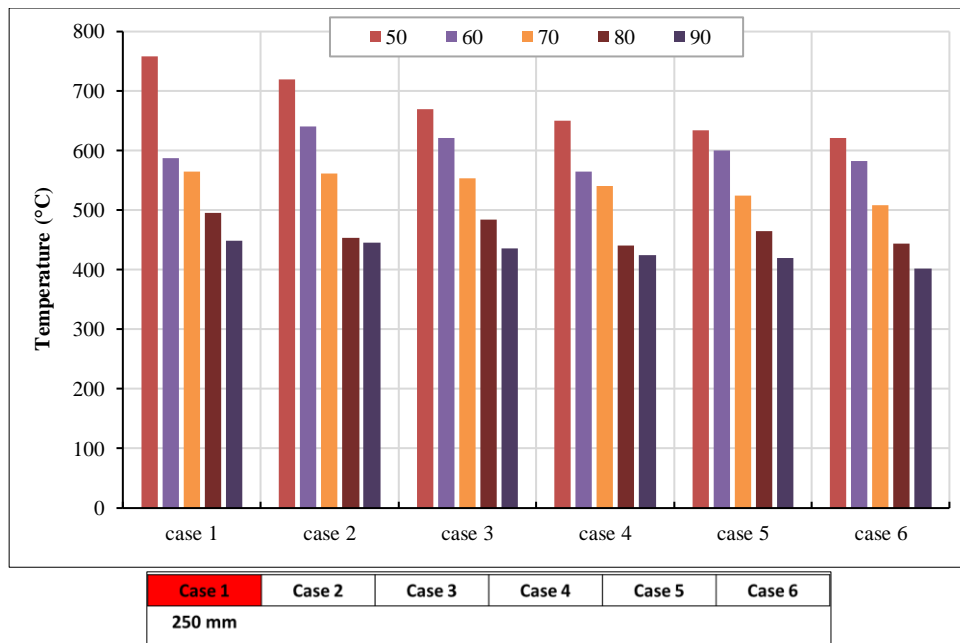
(a)
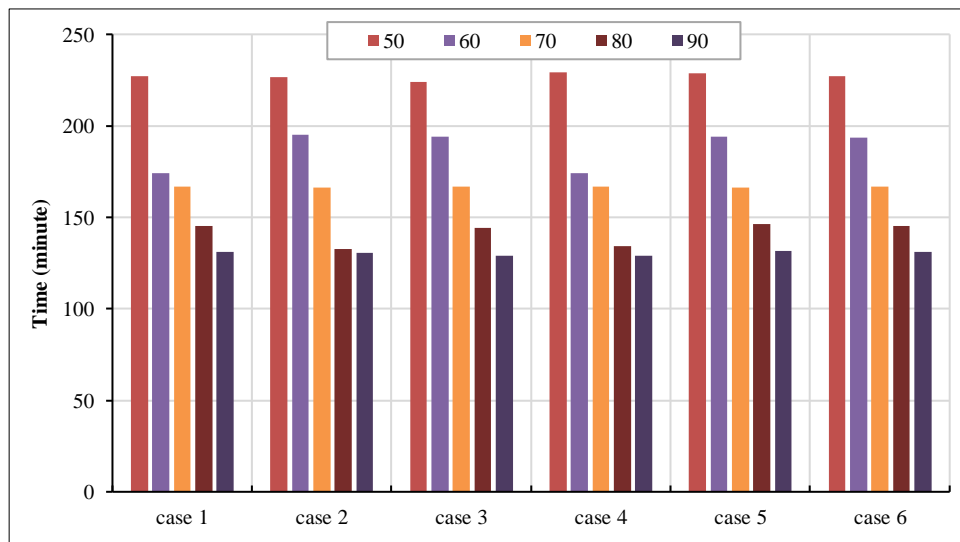
(b)
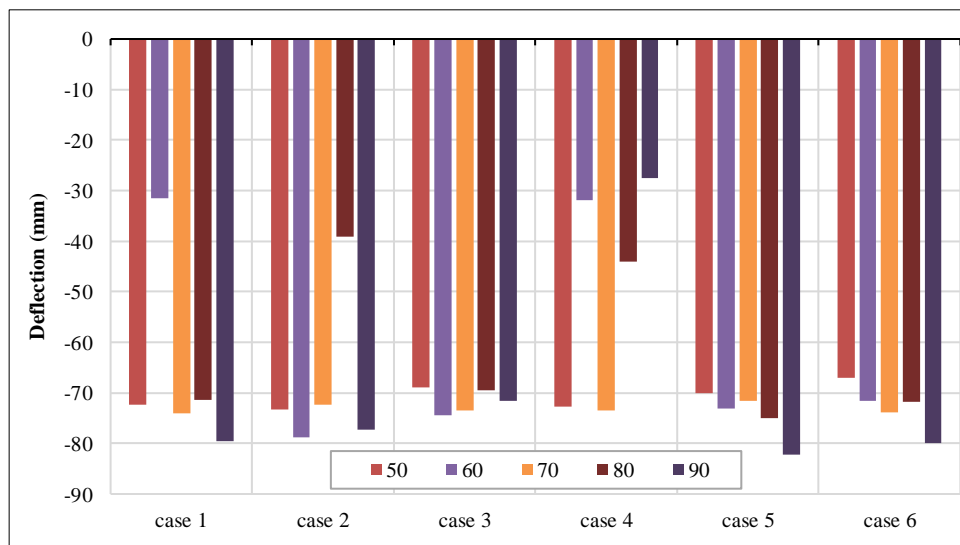
(c)

Figure 15. (a) Temperature for 250 mm of columns, (b) Time for 250 mm of columns, (c) Deflection for 250 mm of columns

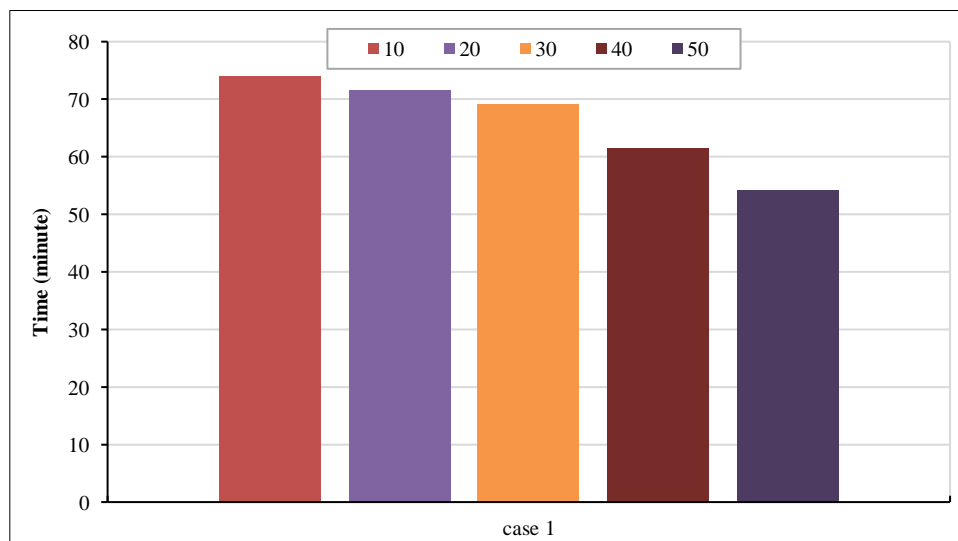**Table 7. Analytical results for 250 mm of columns**

Length	Type of cases	Load percentage (%)	Corresponding applied load (kN)	Temperature resisted (°C)	Time of resistance (minute)	Deflection (mm)
250 mm	Case 1	50	463.5	758	226.95	-72.25
		60	556.2	588	174.15	-31.5
		70	648.9	565	166.95	-74.09
		80	741.6	495.9	145.35	-71.45
		90	834.3	449.6	130.95	-79.6
	Case 2	50	463.5	720.4	226.38	-73.3
		60	556.2	641.1	195.35	-78.7
		70	648.9	561.1	166.48	-72.4
		80	741.6	453.7	132.8	-39.14
		90	834.3	446	130.4	-77.29
	Case 3	50	463.5	669.37	224.02	-68.9
		60	556.2	622.1	194.14	-74.5
		70	648.9	554.1	166.75	-73.4
		80	741.6	483.6	144.33	-69.5
		90	834.3	435.2	129	-71.5
	Case 4	50	463.5	650.8	229	-72.7
		60	556.2	564.8	174.2	-31.8
		70	648.9	541.5	166.6	-73.4
		80	741.6	440.8	134	-44.1
		90	834.3	425.4	129.05	-27.43
	Case 5	50	463.5	634.12	228.8	-70.14
		60	556.2	600	193.9	-73.07
		70	648.9	524.7	166.25	-71.67
		80	741.6	464.78	146.3	-75.08
		90	834.3	419.66	131.4	-82.3
	Case 6	50	463.5	621	226.95	-67.02
		60	556.2	581.9	193.35	-71.65
		70	648.9	508.2	166.95	-73.8
		80	741.6	444.8	145.35	-71.7
		90	834.3	401.9	130.95	-79.86

5.2.2. Effect of Temperature on 500 mm of Columns

The effect of the temperature for a region of 500 mm of the columns is depicted in Figure 16. Here, all the cases showed similar trends, but Case 1 with 90% loading indicated faster failure than the other cases. In accordance with the time variations of the columns subjected to heating, it was found that Case 1 and Case 3 displayed similar trends. Case 2 with 90% loading failed faster than the other cases. Case 1 with 90% loading exhibited higher deflection than the other cases. Table 8 demonstrates the analytical results for 500 mm of the columns.

(a)

(b)

(c)

Figure 16. (a) Temperature for 500 mm of columns, (b) Time for 500 mm of columns, (c) Deflection for 500 mm of columns

Table 8. Analytical results for 500 mm of columns

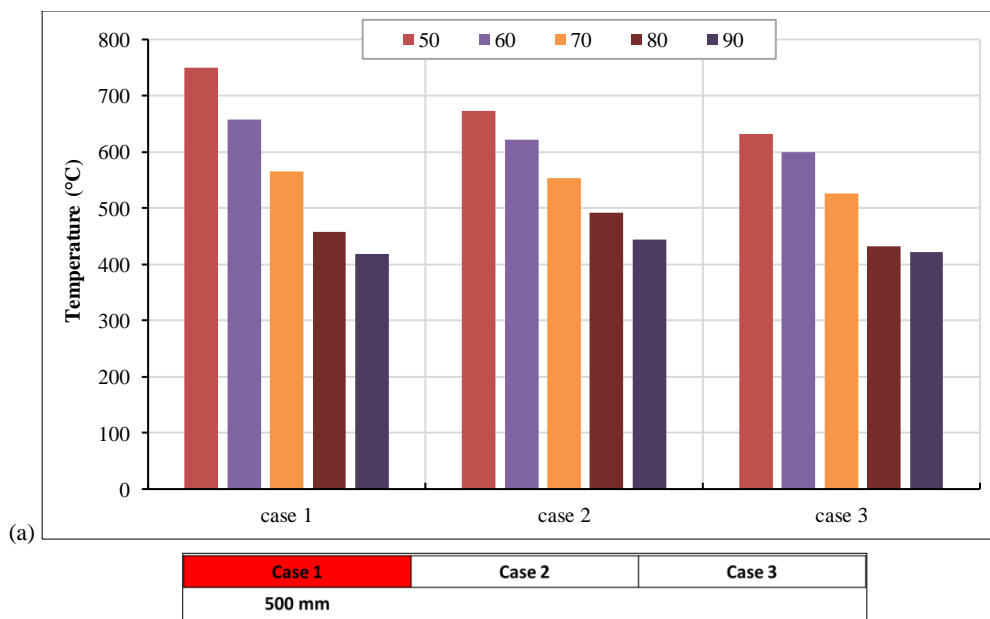| Length	Type of cases	Load percentage (%)	Corresponding applied load (kN)	Temperature resisted (°C)	Time of resistance (minute)	Deflection (mm)
		50	463.5	750.3	224.55	-71.2
		60	556.2	657.8	195.75	-78
	Case 1	70	648.9	565	166.9	-73.8
		80	741.6	457.3	133.35	-40.9
		90	834.3	418	130.95	-79.8
		50	463.5	673	226.5	-72.25
		60	556.2	322	194.13	-74.5
500 mm	Case 2	70	648.9	554	166.75	-73.4
		80	741.6	491	146.8	-77
		90	834.3	444	130.28	-76.3
		50	463.5	632	226.95	-72.1
		60	556.2	599.9	193.35	-67.88
		70	648.9	526	166.95	-72.9
	Case 3	80	741.6	432	135.75	-48.9
		90	834.3	422	130.95	-79.7

5.2.3. Effect of Temperature on 750 mm of Columns

Figure 17 illustrates the effect of the temperature for a region of 750 mm of the columns. Table 9 summarizes the effect of the temperature on the columns when subjected to heating for 750 mm. Case 1 and Case 2 displayed similar trends, where there was a decrease in the capacity with an increase in the temperature, but Case 2 exhibited slightly less capacity than Case 1. Case 1 with 90% loading took less time to fail, making it critical. Case 2 with 90% loading depicted higher deflection.
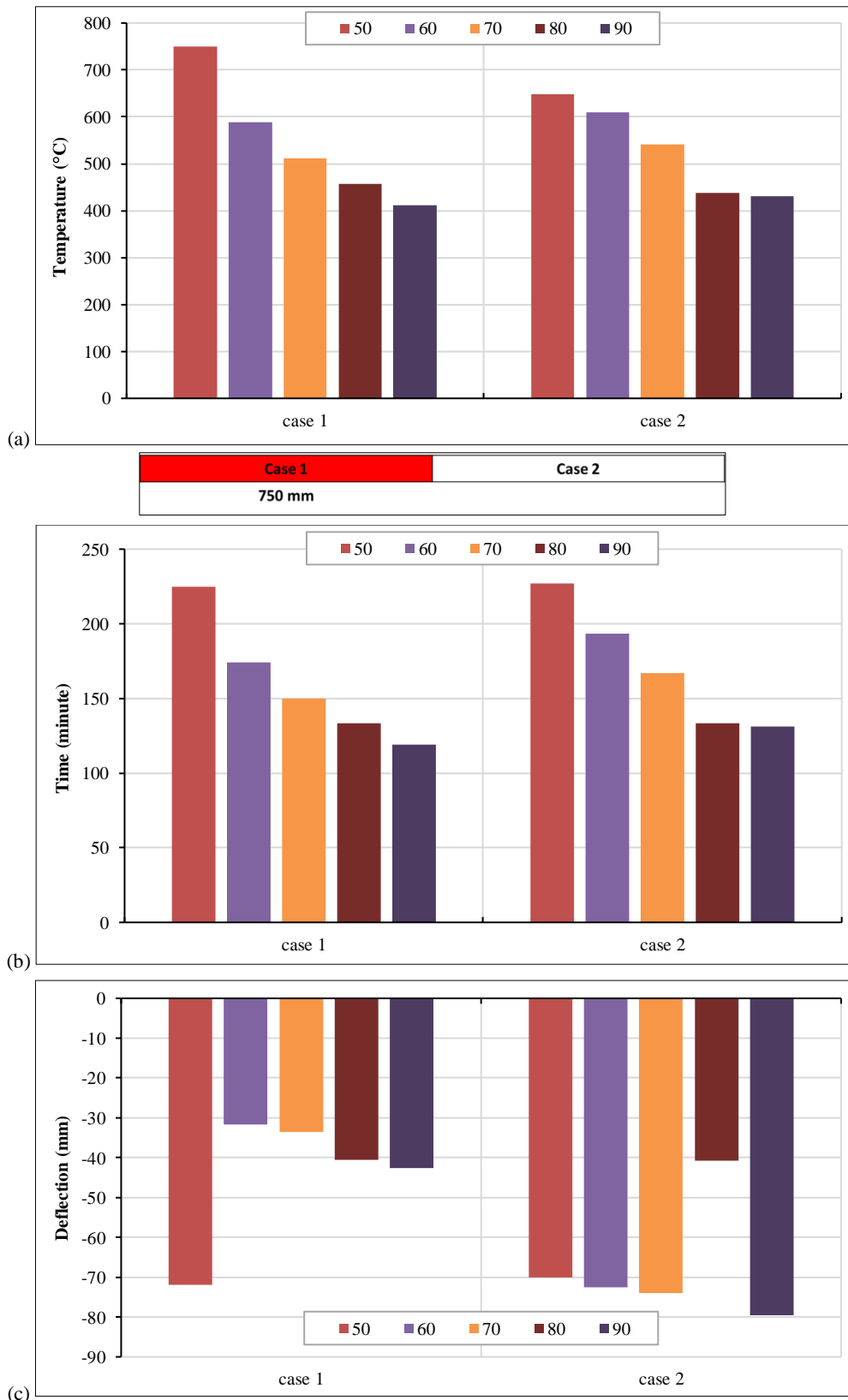
Figure 17. (a) Temperature for 750 mm of columns, (b) Time for 750 mm of columns, (c) Deflection for 750 mm of columns

Table 9. Analytical results for 750 mm of columns

Length	Type of Cases	Load percentage (%)	Corresponding applied load (kN)	Temperature resisted (°C)	Time of resistance (minute)	Deflection (mm)
750 mm	Case 1	50	463.5	750.3	224.55	-71.9
		60	556.2	588.4	174.15	-31.7
		70	648.9	511.35	150.15	-33.58
		80	741.6	457.3	133.35	-40.59
		90	834.3	411.1	118.95	-42.59
	Case 2	50	463.5	648	226.95	-70.08
		60	556.2	610.2	193.35	-72.6
		70	648.9	542	166.95	-74.06
		80	741.6	438.7	133.35	-40.7
		90	834.3	431.2	130.995	-79.6

5.2.4. Effect of Temperature on 1500 mm of Columns

The effect of the temperature for a region of 1500 mm of the columns is shown in Figure 18. Table 10 presents the effect of the temperature on the columns when subjected to heating for 1500 mm. There was a decrease in the capacity with an increase in loading, revealing faster failure when there was 90% loading compared to 50% loading. With the increase in load, there was a decrease in time for the columns to fail. The columns with 50% loading failed faster than the others. There was no uniformity in the trend, and the 60% loading case had a higher deflection than the other cases.
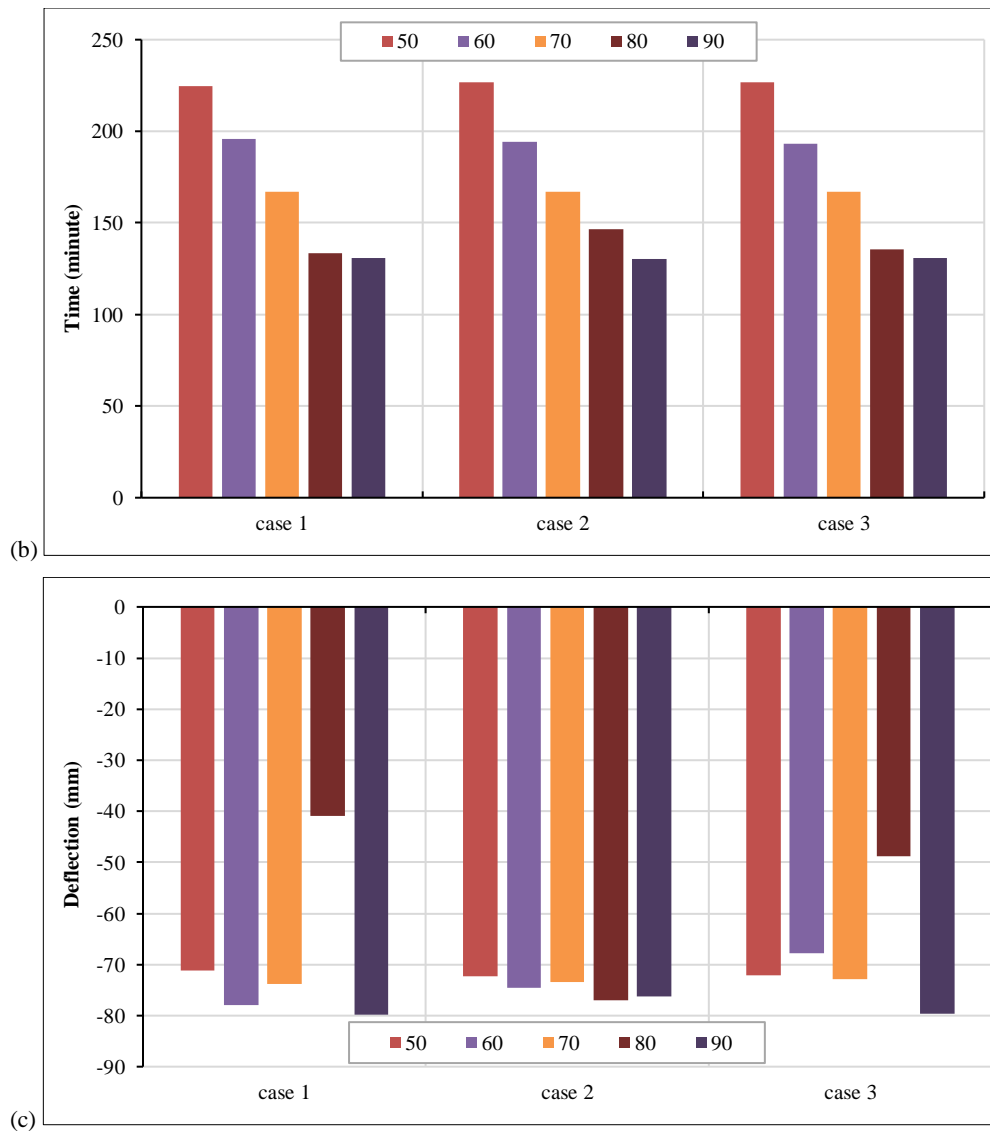
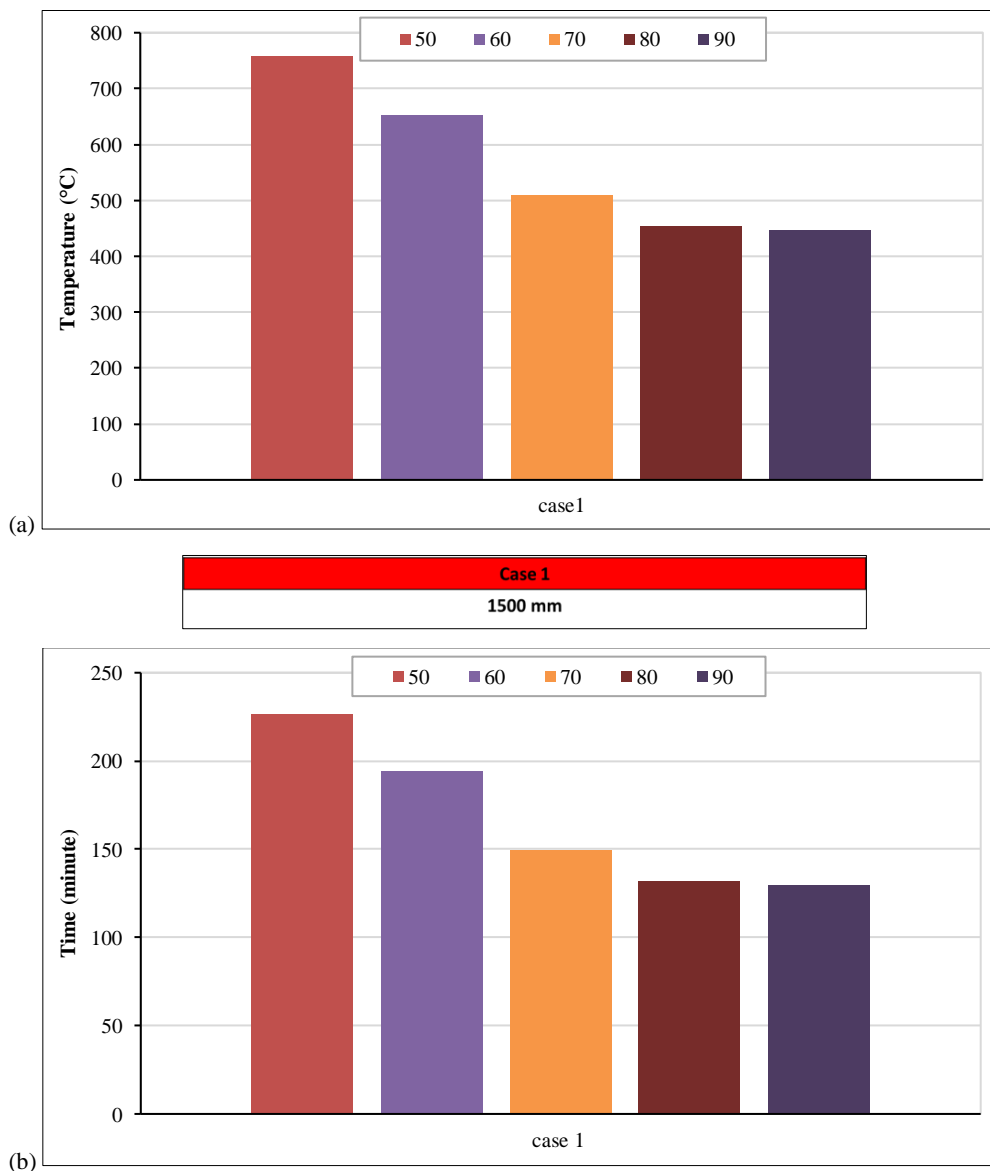

(a)

Case 1

1500 mm

(b)

(c)
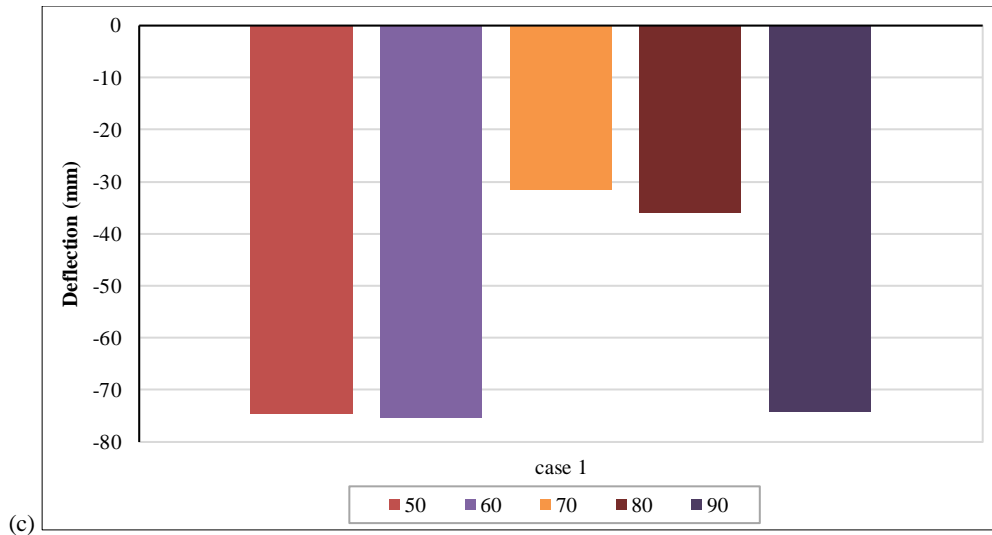
Figure 18. (a) Temperature for 1500 mm of columns, (b) Time for 1500 mm of columns, (c) Deflection for 1500 mm of columns

Table 10. Analytical results for 1500 mm of columns

Length	Type of cases	Load percentage (%)	Corresponding applied load (kN)	Temperature resisted (°C)	Time of resistance (minute)	Deflection (mm)
		50	463.5	757	226.6	-74.6
		60	556.2	653	194.2	-75.48
1500 mm	Case 1	70	648.9	509	149.4	-31.46
		80	741.6	453	131.9	-36
		90	834.3	446	129.8	-74.2

It was found that there was no uniformity in the behavior like the beams but there were several Cases where Case 1 indicated decreased strength and with the fact that the fire started from the bottom of the columns, it was critical and was taken for the Case to experiment.

6. Experimental Test Results of Beam and Column

6.1. Experimental Test Results of Beam

The beam was subjected to bending at the points of loading, and when the temperature was applied, there was a slow reduction in the deflection, illustrating the expansion of the beam, which again increased when the beam was left to unseat after 4 hours. The time versus temperature plots for various points on the beam are plotted in Figure 19, where a vertical line at 240 minutes demonstrates the heating line that separates the heating phase and cooling phase.
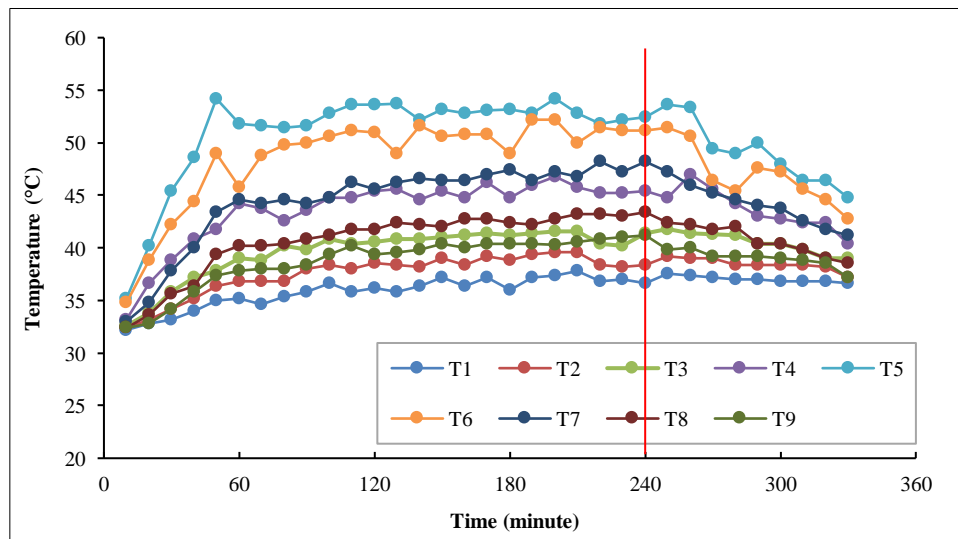
Figure 19. Temperature versus time for beam

Figure 20 provides the deflection profile at the point of loading on the left side of the beam when it was subjected to combined loading and temperature. It was found that with an increase in the temperature, the deflection decreased. The maximum deflection of 2.41 mm occurred at 10 minutes from the time of heating.
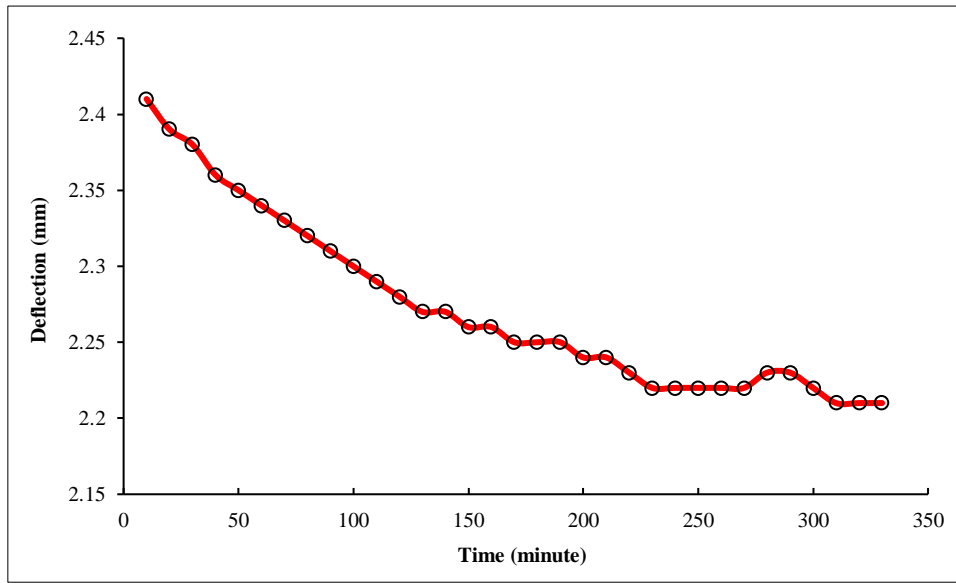
Figure 20. Deflection, left dial gauge

Figure 21 depicts the deflection profile at the point of loading on the right side of the beam when it was subjected to combined loading and temperature. The maximum deflection of 2.36 mm occurred at 10 minutes from the time of heating.
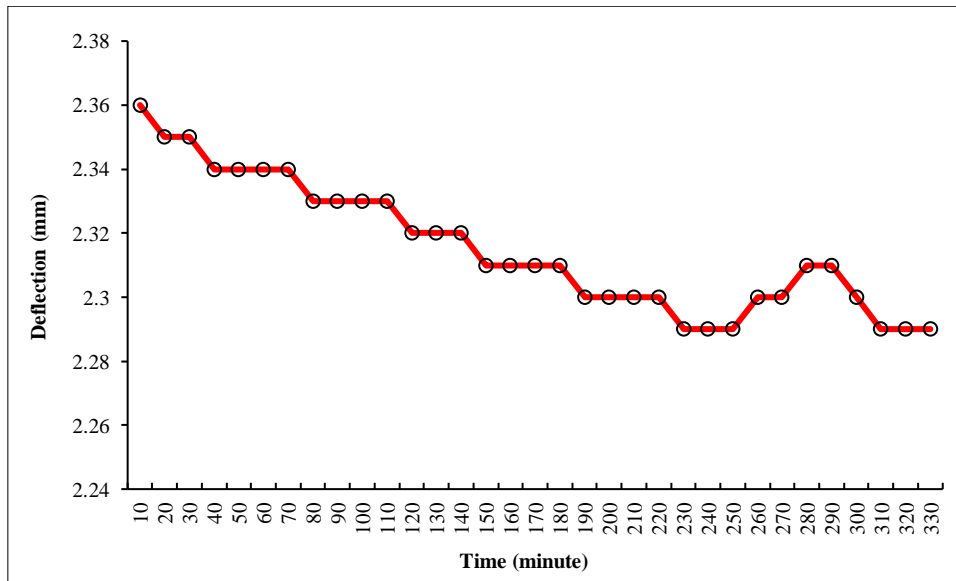
Figure 21. Deflection, right dial gauge

Deflection Check of Beam

The observed experimental and numerical deflections can be verified using the theoretical approach. From this approach, the reliability of the analysis can be verified. The deflection during loading obtained from the beam was consistent with the numerical calculations given below.

$$\text{Deflection} = \frac{Fx}{6EI}(3al - 3a^2 - x^2) = \frac{12.5 \times 1000 \times 1500}{3 \times 6 \times 2 \times 100000 \times 271.1 \times 10000}(3(500)(1500) - 3(500)^2 - 500^2) = 2.4 \text{ mm} \tag{1}$$

6.2. Experimental Test Results of Column

The column experienced buckling at the point where the temperature was applied, but the deflection was well within the maximum value. The buckling of the column can be seen in Figure 22. Also, Figure 23 shows the time versus temperature graph for the initial application of the temperature on the column up to 600 °C.

Figure 22. Buckling of column after effect of temperature
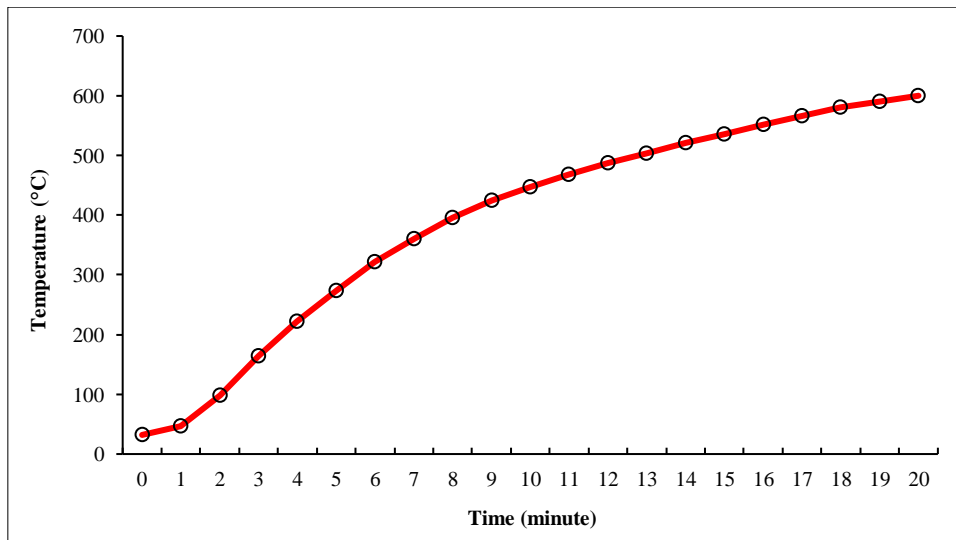
Figure 23. Initial temperature graph

There was a sudden increase in the deflection when the temperature was applied, and the deflection increased after a certain period. This was due to the expansion of steel because of the increase in the temperature. Figure 24 displays heating and cooling of the column conducted for a total of 5 hours with 4 hours of heating excluding the initial heating. There was a significant decrease in the temperature and deflection when compared to those of the beam revealing a sensitive profile even though the ability to take the temperature was higher when compared to that of the beam. Figure 25 represents the deflection profile of the column.
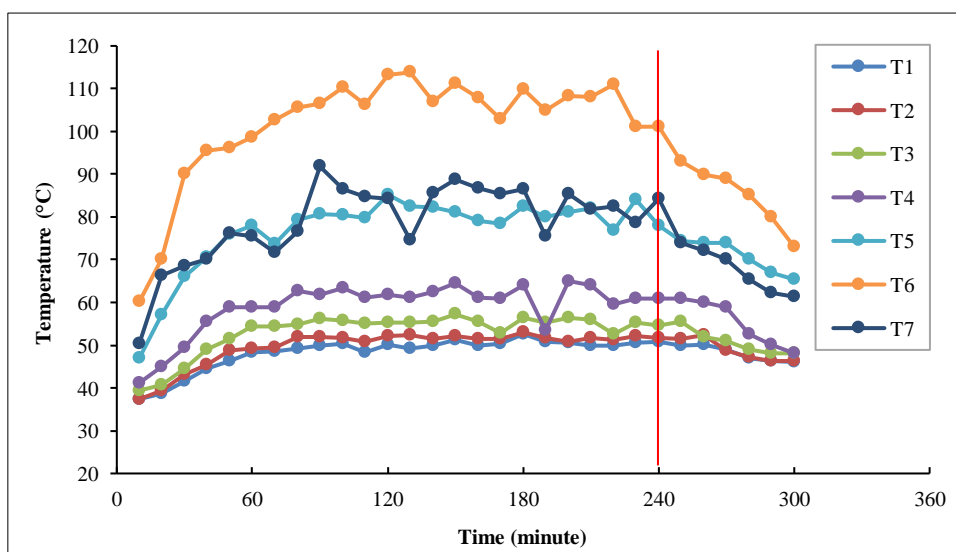
Figure 24. Temperature versus time for column
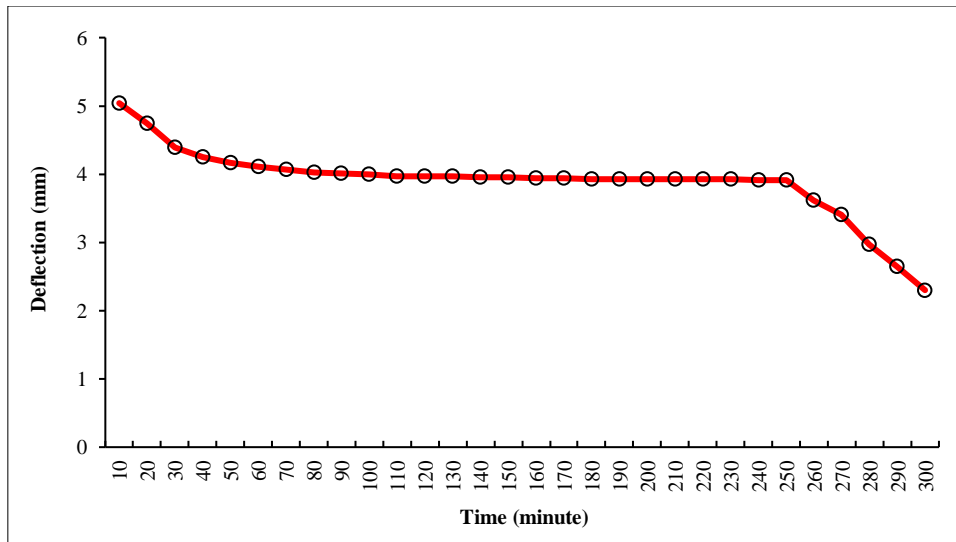
Figure 25. Deflection of column

Deflection Check of Column

The observed experimental and numerical deflections can be verified using the theoretical approach. From this approach, the reliability of the analysis can be verified. The maximum allowable deflection of the column as per IS:800-2007 [34] is:

$$\text{Deflection} = \frac{H}{150} = \frac{1500}{150} = 10 \text{ mm} \tag{2}$$

6.3. Comparison of Experimental Study and Finite Element Models

The results obtained from the experimental study of the critical beam and column were analyzed using ABAQUS, and the results of the analysis are discussed below.

### 6.3.1. Beam

When compared to the experimental results of the beam, the temperature in the analysis varies uniformly in time, and there are also symmetrical values on either side of the beam, which is not the case in real life. This can be observed in Figure 26, where the temperature curves of T1 and T9 overlap, which is similar in Cases T3, T4, T7, and T8. This may be due to the variation in room temperature with respect to time, the cooling effect owing to the heat loss and the capacity of the oven to maintain the temperature, and the variation in the temperature within the oven since the heat starts from the middle point of the oven and there is some difference in the heat within the oven, which is not the case in the analysis. The failure pattern of the beam is indicated in Figure 27, which is similar to that of the experimental study, which can be witnessed in Figure 28.
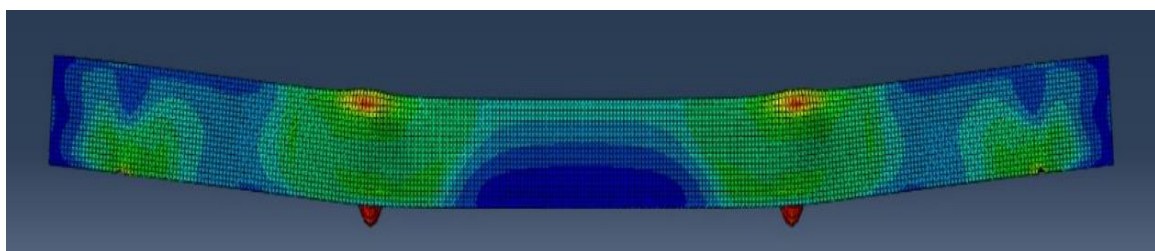
Figure 26. Failure pattern of beam in analytical study

Figure 27. Failure pattern of beam in experimental study
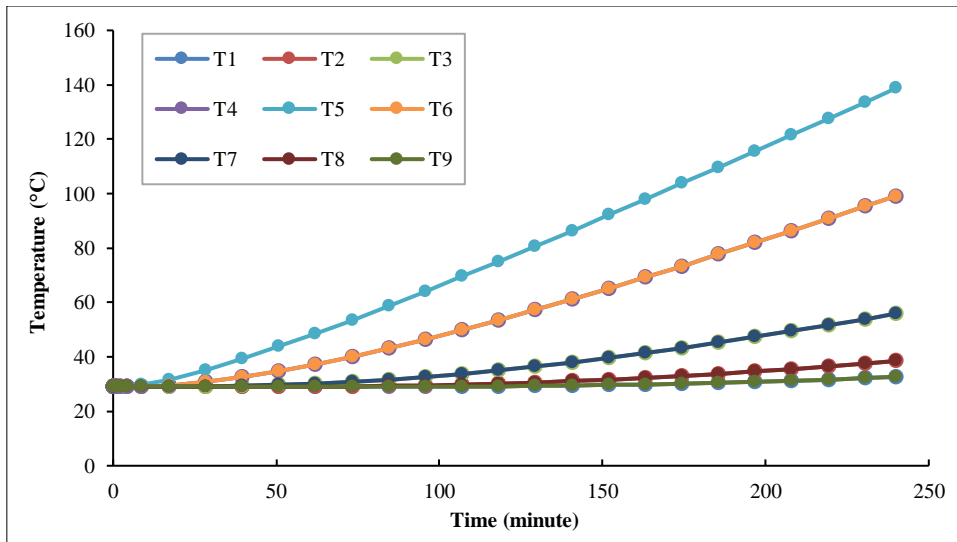
Figure 28. Temperature versus time for beam using analysis

6.3.2. Column

When compared to the experimental results of the column, the temperature in the analysis varies uniformly in time, and there are also symmetrical values on either side of the column in Cases T6 and T7, which is not the case in real life. Figure 29 illustrates the temperature variation of the points marked on the column using analysis. Figure 30 depicts the failure pattern of the column using the experimental and analytical studies.
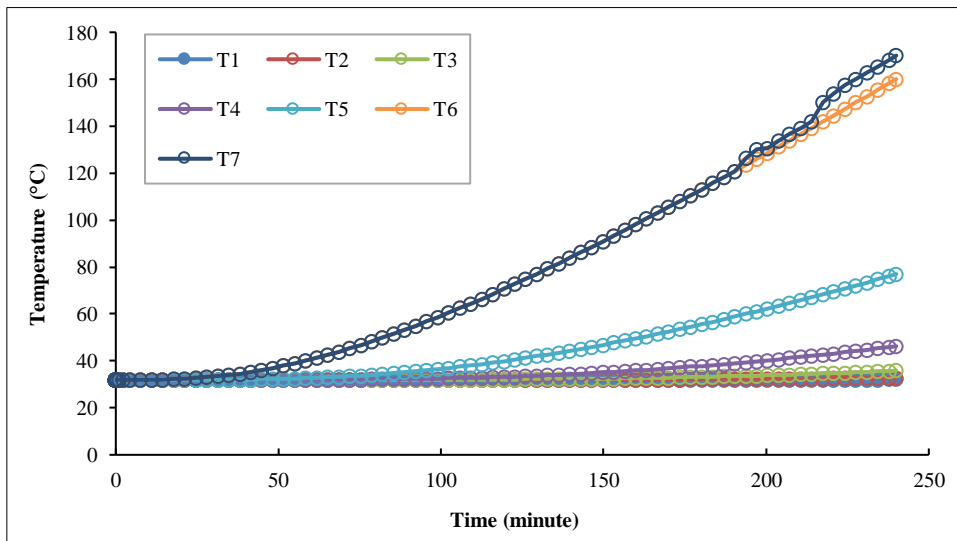
Figure 29. Temperature versus time for column using analysis
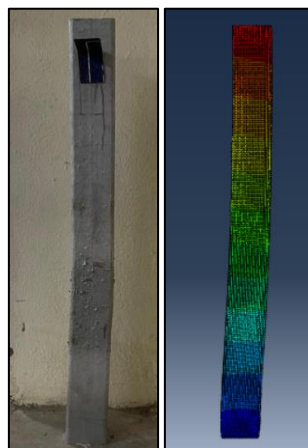
Figure 30. Failure pattern of column in experimental and analytical studies

7. Conclusions

The hollow steel section was considered for beams and columns and investigated under the elevated temperature. Different cases were considered in terms of region and load percentages. In terms of region, cases such as 250 mm, 500 mm, 750 mm, and 1500 mm were taken into account. For the load percentages, the load cases were 10%, 20%, 30%, 40%, and 50% of the ultimate load for the beams and 50%, 60%, 70%, 80%, and 90% of the ultimate load for the columns. The following conclusions were drawn from the study:

Beams

- The critical region in the beams was found to be in the middle portions, specifically in Case 3 and Case 4 for 250 mm of the beams and Case 2 for 500 mm of the beam. This may be because of the conductance of the heat on either side of the beams, which is not the case if the beams are heated from one end of the beams. Hence, it can be concluded that the middle portions of the beams are weak in terms of the elevated temperature.

- The resistance time decreased with increasing loading in all cases.

- There was a decrease in the deflection concerning the temperature and time because of the combined action of loading and expansion created due to the temperature rise, and a maximum deflection of 4.6 mm occurred in all cases with 10% loading.

Columns

- It was also found that the trend was quite similar for all the cases of the columns, where with an increase in the load, the temperature needed to reach the ultimate stress was reduced. In other words, the temperature was inversely proportional to the load. The decrease in the capacity concerning loading was 1.68 times higher in Case 1 than in the other cases; hence, it was taken to be critical.

- The resistance time also decreased with increasing loading, and there was a decrease in the resistance time of approximately 1.7 times for 90% loading when compared to 50% loading.

- There was an irregularity in the deflection concerning the temperature and time because of the combined action of loading and temperature, and a maximum deflection of 79 mm occurred when the ends of the column were subjected to the elevated temperature.

- The behavioral study of the beams and columns was conducted, and it was found that the change in the deflection concerning the temperature and time is significant for the column when compared to that of the beams based on the temperature and deflection variations obtained from the experimental study.

- The effect of the temperature on the analysis was uniform when compared to the experimental results, and the results were slightly higher compared to the experimental study.

The investigation helps the designers understand the principles while designing members to withstand fire scenarios. Furthermore, the research can be extended toward the influence of fire on beam-column sub-assemblage sections, which are meant to be more critical.

8. Declarations

8.1. Author Contributions

Conceptualization, P.M. and A.B.; methodology, P.M. and A.B.; validation, P.M., A.B., and V.M.; formal analysis, A.B. and V.M.; investigation, A.B., V.M., and A.K.; resources, A.B.; writing—original draft preparation, A.B. and A.K.; writing—review and editing, A.B. All authors have read and agreed to the published version of the manuscript.

8.2. Data Availability Statement

The data presented in this study are available in the article.

8.3. Funding

The authors received no financial support for the research, authorship, and/or publication of this article.

8.4. Conflicts of Interest

The authors declare no conflict of interest.

9. References

[1] Vishal, M., & Satyanarayanan, K. S. (2021). A review on research of fire-induced progressive collapse on structures. Journal of Structural Fire Engineering, 12(3), 410–425. doi:10.1108/JSFE-07-2020-0023.

[2] Zhong, Y., Su, A., & Zhao, O. (2023). Post-fire local buckling behaviour of cold-formed S700 high strength steel circular hollow sections under axial compression: Experiments, modelling and design. Thin-Walled Structures, 184, 110511. doi:10.1016/j.tws.2022.110511.

[3] Khoury, G. A. (2000). Effect of fire on concrete and concrete structures. Progress in Structural Engineering and Materials, 2(4), 429–447. doi:10.1002/pse.51.

[4] Vishal, M., & Satyanarayanan, K. S. (2022). Experimental investigation on the heat dissipation and postfire structural performance of a reinforced concrete column with biomimicked geometry. Fire, 5(6), 205. doi:10.3390/fire5060205.

[5] Huang, B., Qiu, X., Zhu, J., Song, H., & Zhang, Z. (2023). Residual performance of compression stiffened welded hollow spherical joints after exposure to elevated temperatures. Journal of Constructional Steel Research, 208, 108001. doi:10.1016/j.jcsr.2023.108001.

[6] Agha, A., Shibani, A., Hassan, D., & Zalans, B. (2021). Modular construction in the United Kingdom housing sector: barriers and implications. Journal of Architectural Engineering Technology, 10(2), 236.

[7] Vishal, M., & Satyanarayanan, K. S. (2023). Study on optimum concrete cover thickness in RC beam and columns under high temperature. Journal of Structural Fire Engineering, 14(4), 461–480. doi:10.1108/JSFE-11-2022-0035.

[8] Ferdous, W., Bai, Y., Ngo, T. D., Manalo, A., & Mendis, P. (2019). New advancements, challenges and opportunities of multi-storey modular buildings – A state-of-the-art review. Engineering Structures, 183, 883–893. doi:10.1016/j.engstruct.2019.01.061.

[9] Cao, X., Li, X., Zhu, Y., & Zhang, Z. (2015). A comparative study of environmental performance between prefabricated and traditional residential buildings in China. Journal of Cleaner Production, 109, 131–143. doi:10.1016/j.jclepro.2015.04.120.

[10] Weerasinghe, P., Samarasinghe, T., Gunawardena, T., Nguyen, K., Mendis, P., Ngo, T., & Aye, L. (2018). An optimum construction strategy for multi-story residential prefabricated modular buildings. ZEMCH 2018 International Conference, 29-1 January, 2018, Melbourne, Australia.

[11] Boafo, F. E., Kim, J. H., & Kim, J. T. (2016). Performance of modular prefabricated architecture: Case study-based review and future pathways. Sustainability, 8(6), 558. doi:10.3390/su8060558.

[12] Bertram, N., Fuchs, S., Mischke, J., Palter, R., Strube, G., & Woetzel, J. (2019). Modular construction: From projects to products. McKinsey & Company, New York, United States.

[13] Kalam, L. (2021). Finite Element Analysis of Complex Vectorbloc Beam-Column Connections. Ph.D. Thesis, University of Windsor, Windsor, Canada.

[14] Lee, J., & Kim, J. (2017). BIM-Based 4d simulation to improve module manufacturing productivity for sustainable building projects. Sustainability (Switzerland), 9(3), 426. doi:10.3390/su9030426.

[15] Kamali, M., & Hewage, K. (2016). Life cycle performance of modular buildings: A critical review. Renewable and Sustainable Energy Reviews, 62, 1171–1183. doi:10.1016/j.rser.2016.05.031.

[16] Wu, C., Zhou, Y., Liu, J., Mou, B., & Shi, J. (2021). Experimental and finite element analysis of modular prefabricated composite beam-column interior joints. Journal of Building Engineering, 43(May), 102853. doi:10.1016/j.jobe.2021.102853.

[17] Kumar, W., Sharma, U. K., & Pathak, P. (2023). Comparison of mechanical and structural performance of fire-resistant steels at elevated temperatures. Structures, 48, 478–491. doi:10.1016/j.istruc.2022.12.103.

[18] Kim, S., Hong, W. K., Kim, J. H., & Kim, J. T. (2013). The development of modularized construction of enhanced precast composite structural systems (Smart Green frame) and its embedded energy efficiency. Energy and Buildings, 66, 16–21. doi:10.1016/j.enbuild.2013.07.023.

[19] Nahmens, I., & Ikuma, L. H. (2012). Effects of lean construction on sustainability of modular homebuilding. Journal of architectural engineering, 18(2), 155–163. doi:10.1061/(asce)ae.1943-5568.0000054.

[20] Ramaji, I. J., & Memari, A. M. (2013). Identification of structural issues in design and construction of multi-story modular buildings. Proceedings of the 1st residential building design and construction conference, 20-21 February, 2013, Bethlehem, United States.

[21] Harrison, B. F. (2003). Blast resistant modular buildings for the petroleum and chemical processing industries. In Journal of Hazardous Materials, 104(1–3), 31–38. doi:10.1016/S0304-3894(03)00232-2.

[22] CCHPR (2023). CCHPR Launches New Report on Modular Homes. Department of Land Economy, University of Cambridge, Cambridge, United Kingdom. Available online: https://www.landecon.cam.ac.uk/news/cchpr-launches-new-report-modular-homes (accessed in October 2023).

[23] Yu, Y., Tian, P., Man, M., Chen, Z., Jiang, L., & Wei, B. (2021). Experimental and numerical studies on the fire-resistance behaviors of critical walls and columns in modular steel buildings. Journal of Building Engineering, 44(July), 102964. doi:10.1016/j.jobe.2021.102964.

[24] Arrais, F., Lopes, N., & Vila Real, P. (2023). Fire design of stainless steel columns with hollow circular and elliptical sections. Journal of Constructional Steel Research, 210, 108085. doi:10.1016/j.jcsr.2023.108085.

[25] Chen, Z., Liu, J., & Yu, Y. (2017). Experimental study on interior connections in modular steel buildings. Engineering Structures, 147, 625–638. doi:10.1016/j.engstruct.2017.06.002.

[26] Gardner, L., Saari, N., & Wang, F. (2010). Comparative experimental study of hot-rolled and cold-formed rectangular hollow sections. Thin-Walled Structures, 48(7), 495–507. doi:10.1016/j.tws.2010.02.003.

[27] Mohammed, A., & Afshan, S. (2023). Modelling and design of stainless steel hollow section beam-column members in fire. International Journal of Steel Structures, 23(1), 120–138. doi:10.1007/s13296-022-00683-2.

[28] Yan, J. B., Cao, J., Xie, P., Li, N., & Xie, J. (2023). Circular hollow stainless-steel tubes subjected to low-temperature eccentric compression loads. Structures, 54, 1164–1178. doi:10.1016/j.istruc.2023.05.092.

[29] Gatheeshgar, P., Poologanathan, K., Gunalan, S., Shyha, I., Sherlock, P., Rajanayagam, H., & Nagaratnam, B. (2021). Development of affordable steel-framed modular buildings for emergency situations (Covid-19). Structures, 31(2121), 862–875. doi:10.1016/j.istruc.2021.02.004.

[30] AISI S100-16. (2016). North American Specification Steel Structural Members. American Iron and Steel Institute, Washington, United States.

[31] EN 1991-1-7. (2006). Eurocode 1: Action on structures - Part 1-7: General actions - Accidental actions. European Committee for standardization, Brussels, Belgium.

[32] Kesawan, S., & Mahendran, M. (2018). Post-fire mechanical properties of cold-formed steel hollow sections. Construction and Building Materials, 161, 26–36. doi:10.1016/j.conbuildmat.2017.11.077.

[33] Luo, F. J., Ding, C., Styles, A., & Bai, Y. (2019). End plate–stiffener connection for SHS column and RHS beam in steel-framed building modules. International Journal of Steel Structures, 19(4), 1353–1365. doi:10.1007/s13296-019-00214-6.

[34] IS:800-2007. (2007). Indian Standard Code of Practice for General Construction in Steel. Bureau of Indian Standards, New Delhi, India.
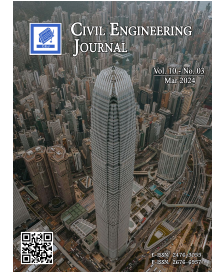
Application of the Arrhenius Equation in Predicting the Temperature Susceptibility of Unmodified and Modified Bituminous Binder

Tangudu Srikanth [1], Ajithkumar Padmarekha [1*]

[1] Department of Civil Engineering, SRM Institute of Science and Technology, Kattankulathur– 603203, Tamil Nadu, India.

Abstract

Bitumen is a temperature-susceptible material. The performance of the bitumen largely depends on the sensitivity of its characteristic properties to the variation in temperature. This paper uses the Arrhenius equation to predict the temperature-sensitive properties of various bitumens. Three modified and unmodified binders of various grades were tested under study shear, frequency mode (oscillatory shearing), and time mode (multiple stress creep and recovery) at different temperatures from 10 to 70ºC. This paper focuses on the activation energy to understand the temperature-susceptible behavior of the bitumen and the influence of aging on the bitumen. To analyze the temperature susceptibility of the bitumen, Steady shear, MSCR, and LAOS tests were performed. From these tests, parameters such as viscosity, dynamic modulus, energy dissipation, and creep compliance at different temperatures were observed to follow the Arrhenius equation. The activation energy constant of the Arrhenius equation is found to vary with the characteristic function used. It is also statistically proven that the activation energy depends on the shear rate or shear stress, indicating that the temperature-susceptible properties of the bitumen are shear rate-dependent. Also, as the bitumen ages, its temperature-susceptible properties improve.

Keywords: Activation Energy; Aging of Bitumen; Arrhenius Equation; Creep Compliance; Energy Dissipation; F Test; Temperature Susceptibility.

1. Introduction

Bitumen is extensively used as a binder in the paving of roads. Bitumen is a viscoelastic material, and its characteristic properties largely depend on temperature. The temperature of bitumen in the pavement may vary from -10 °C to 70°C [1]. This range of temperature depends on the geographical location. At higher temperatures, bitumen exhibits viscoelastic fluid-like behavior and as the temperature reduces, the behavior changes to viscoelastic solid-like and further to elastic [2, 3]. The performance of bitumen largely depends on its temperature-sensitive nature. For instance, if one considers pavement deformation in the pavement, bitumen plays a key role in controlling the deformation. One may demand 'high' viscosity bitumen to control pavement deformation. It is understood that the viscosity of the bitumen depends on the temperature and hence the accumulation of permanent deformation depends on the sensitivity of the viscosity variation with the temperature. The material that exhibits the least variation in its characteristic properties over a range of temperatures is said to be more temperature-susceptible. The temperature-susceptible nature of the binder plays a key role in the selection of the binder. However, the existing methods of grading (viscosity grade and performance grade) do not consider the temperature-susceptible properties of bitumen [4, 5].

---

* Corresponding author: padmarea@srmist.edu.in

doi http://dx.doi.org/10.28991/CEJ-2024-010-03-015

Heukelom [6] made a first attempt to understand the temperature susceptibility of bitumen. The temperature susceptibility chart for bitumen was plotted using penetration, softening temperature, Flash point, and viscosity. The temperature-sensitive characteristics of the bitumen can be understood better using shear viscosity and oscillatory shear tests [2, 7]. Padmarekha and Krishnan [2] captured the viscoelastic solid-fluid transition in the temperature range of 20 to 70 ^{0} C using linear viscoelastic parameters. Nivitha et al. [8] studied the temperature sensitivity of the bitumen using Fourier transform infrared (FTIR) spectroscopy and observed viscoelastic solid-fluid transformation in the temperature range of 35 to 65 ^0C. The time-temperature superposition principle (TTSP) has been widely applied to predict the response of bitumen at any temperature if the response of the bitumen at a reference temperature is known. For this purpose, it is assumed that the temperature sensitivity characteristics of the bitumen follow the William-Landel-Ferry equation (WLF) [9] or the Arrhenius equation [10].

WLF equation was introduced for the polymers, and it is derived based on the free volume theory. A shift factor is introduced to shift the characteristic properties measured at any temperature to the reference temperature. The shift factor (a_T) is given in Equation 1.

$$\log a_T = \frac{-C_1(T - T_{ref})}{C_2 + (T - T_{ref})},$$ (1)

where, T_{ref} is the reference temperature, C_1 and C_2 are constants. Williams et al. [9], proposed C_1 as 8.86 and C_2 as 101.6 K and these constants are considered universal constants. WLF equation is applicable above the glass transition temperature. Literature on bitumen proposed different combinations of WLF constants for bitumen [11, 12]. There is a complexity in applying the WLF equation is the transitory regime of bitumen [13].

Arrhenius's equation describes the effect of temperature on the viscosity of the material and it is given in Equation 2.

$$\ln \lambda = \ln K + \left[\frac{E}{RT}\right],$$ (2)

where λ is the relaxation time, T is the temperature, E is an activation energy constant, K and R are other constants. Cheung & Cebon [14] proposed that the temperature sensitivity of the bitumen below its glass transition temperature follows the Arrhenius relationship, and at higher temperatures, the WLF relationship was found to be valid. Atul Narayan et al. [15] quantified the temperature-susceptible property of modified and unmodified bitumen at the high-temperature region using the Arrhenius equation and suggested a methodology for high-temperature bitumen grading activation energy constant. In the current investigation activation energy is used to understand the temperature-susceptible properties of the bitumen.

Viscoelastic characteristic parameters such as viscosity, dynamic modulus, and creep compliances were used to determine the activation energy of the binder. Maze [16] applied this activation energy concept to the EVA-modified binder, and the typical activation energy was observed to be 67 kJ/mol. Salomon & Zhai [17] observed the activation energy of the bitumen to vary from 44 kJ/mol to 90 kJ/mol for neat and modified binders. These activation energy values were obtained from the viscosity of the binders measured at 110 and 160 ℃. It was also observed that the same grade (PG) of binders exhibited significantly different activation energy. Dongre et al. [18] reported activation energy between 192 to 243 kJ/mol for six different bitumen's. Salomon & Zhai [19] used the activation energy obtained from the viscosity measured between 80 and 200 °C to rank the temperature susceptibility of different asphalt binders. Saboo et al. [20] reported the activation energy values calculated from the creep compliance, and a new ranking parameter was defined.

The activation energy of bitumen was found to vary with factors such as binder type, aging condition, modifier type, and viscoelastic characteristic parameters used. Literature shows inconsistencies in the trend in the variation of activation energy with the above-mentioned parameters. For instance, Garcia-Morales et al. [21] found that polymer addition leads to a reduction in activation energy, while Ait-Kadi et al. [22] found that the presence of polymer in asphalt results in an activation energy increase. Wang et al. [23] observed that chemical-based additives had insignificant effects on the activation energies while wax-based additives significantly decreased the activation energies. Various hypotheses based on the trend in the variation of activation energy have also been proposed. For Instance, Jamshidi et al. [24] related the trend in variation of activation energy with the phase angle and it was observed that the binder with a higher phase angle has higher activation energy. The activation energy was observed to increase on aging [25, 26]. Haider et al. [27] correlated activation energy and performance grading parameters and showed that high viscous binders have higher activation energy. Notani et al. [28] observed that the increase in the percentage of crumb rubber increases the activation energy. Wang et al. [23] established the relation between molecular weight and activation energy. The activation energy decreases as the molecular weight increases.

In addition to the temperature-susceptible characteristic behavior, the response of the bitumen is also shear-susceptible. Raouf and Williams [29], have studied the shear rate susceptibilities of bio-oils, it was observed that the

relationship between the viscosity of bio-oils and temperature and shear rates are log-linear–like bitumen binders. Ingram et al. [30], stated that reduction in the viscosity due to temperature is more significant as compared with shear rate. One can expect that the temperature behavior of the bitumen may depend on its shear susceptibility.

One can see many complexities related to the activation energy, and irrespective of the extent of complexity evolved, AE can be viewed as a tool to predict the temperature-susceptible behavior of bitumen. For this purpose, one needs a clear understanding of how the activation energy of bitumen differs with test protocol, binder type, and aging of bitumen. The steady shear test (for determining mixing and compaction temperature), oscillatory shear test (for performing grading and fatigue damage-related studies), and multiple stress creep and recovery (rutting-related studies) are the widely used test protocols in bitumen characterization. In this experimental investigation, various grades of unmodified bitumen and modified bitumen with different additives (crumb rubber, elastomer, and plastomer) were subjected to steady shear, oscillatory shear, and multiple stress creep and recovery, and the viscosity, dynamic modulus, energy dissipation, and creep compliance were measured at different temperatures. The application of the Arrhenius equation to these parameters was studied and AE's were determined. The significance of the variation in the AE among these characteristic functions was statistically verified. This paper focuses on the activation energy as a tool to understand the temperature susceptible behavior of the bitumen. To understand the influence of aging, the AE was determined for three different aging conditions includes unaged, short-term aged, and long-term aged bitumen. The details of the material used, and the experimental protocol are given in the following section.

2. Research Methodology

Figure 1 shows the flowchart of the research methodology through which the objectives of this study were achieved.
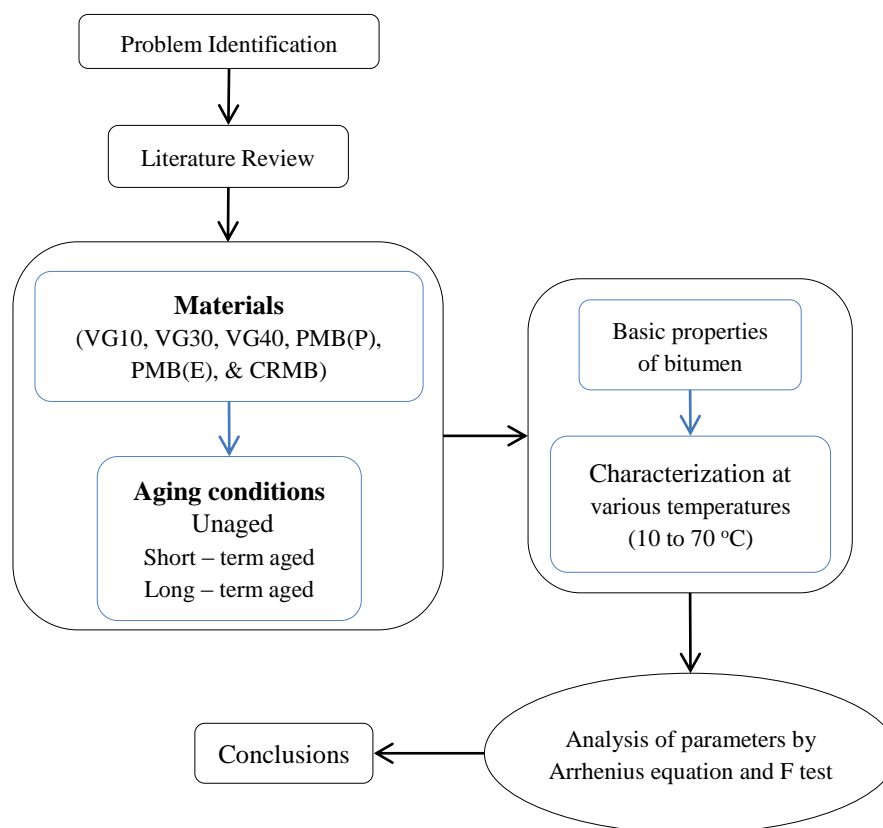
Figure 1. Research methodology flowchart

3. Experimental Investigation

3.1. Materials

This experimental investigation is conducted using six types of bitumen out of which three are unmodified bitumen and others are modified bitumen. The unmodified bitumen of grade VG10, VG30 and VG40 as per IS73, 2018 [4] is used in this experimental investigation. Table 1 lists the basic properties of the unmodified bitumen. From the three modified bitumen used, one is the plastomer-modified bitumen (PMB(P)), the second is elastomer-modified bitumen (PMB(E)), and the third one is the crumb-rubber-modified bitumen(CRMB). The basic properties of modified binders

used in this investigation are given in Table 2. All six binders were tested at unaged (UA), short-term aged (STA) and long-term aged (LTA) conditions. The short-term aging is carried out using a rolling thin film oven following ASTM D2872, 2022 [31]. The short-term aged sample is then subjected to long-term aging in pressure aging vessel following ASTM D6521, 2022 [32].

Table 1. Basic properties of unmodified bitumen

Characteristic properties	VG10	VG30	VG40
Penetration at 25˚C, 0.1 mm, 100 g, 5 s, 0.1 mm	99	61	40
Softening Point, (R&B), ºC	42	48	53
Absolute viscosity at 60˚C, Poises	1143	2677	3640
Kinematic viscosity at 135˚C, cSt	365	510	652
Tests on residue from rolling thin film oven test:			
a) Viscosity ratio at 60˚C	2.29	2.54	3.8
b) Ductility at 25˚C, cm	>100	>100	28
Temperature corresponding to the $|G^*|/\sin \delta$ of 2.1 kPa of short-term aged binder (25 mm plate, 1 mm gap at 10 rad/s), in °C	66.3	71.4	76.1
Temperature corresponding to $|G^*|\sin \delta$ of 5000 kPa of long-term aged binder (8 mm plate, 2 mm gap at 10 rad/s), in °C	15.2	22.9	19.7

Table 2. Basic properties of modified bitumen

Characteristic properties	PMB(P)	PMB(E)	CRMB60
Penetration at 25˚C, 0.1 mm, 100 g, 5 s, 0.1 mm	31	34	25
Softening Point, (R&B), ºC	76	57	66
The elastic recovery of half thread in ductilometer at 15°C, percent	25	64	69
Separation, the difference in softening point (R&B), °C	3.4	3	11
Viscosity at 150°C, Poise	2.6	5	-
Temperature corresponding to the $|G^*|/\sin \delta$ of 2.1 kPa of short-term aged binder (25 mm plate, 1 mm gap at 10 rad/s), in °C	77.9	84.0	93.7
Temperature corresponding to $|G^*|\sin \delta$ of 5000 kPa of long-term aged binder (8 mm plate, 2 mm gap at 10 rad/s), in °C	25.0	17.0	14.7

4. Experimental Methods

Three different sets of experiments were conducted using a dynamic shear rheometer (DSR) of the MCR102 model (Anton Paar make). The first set of experimental investigations is a steady shear test, the second is the large amplitude oscillatory shear testing (LAOS) and the third one is the multiple stress creep and recovery (MSCR) test. All these tests were conducted using parallel plate geometry of 25 mm diameter with a sample height of 2 mm. In the steady shear test, all the materials were sheared at a constant shear rate of 0.5 s^{-1} as shown in Figure 2-a. The temperature of the sample during the test was maintained constant and the material was sheared for 10 minutes. The test was conducted for every 10^0 C temperature increment in the range of 40 to 80^0 C.

In the second set of experimental investigations, the bitumen was subjected to repeated oscillatory shearing in strain-controlled mode using LAOS protocol and the material was continuously sheared for 10 minutes. The strain amplitude, frequency and temperature during shearing were maintained constant during testing as shown in Figure 2-b. The test was conducted for three different strain amplitudes of 1, 5 and 10% and three different frequencies of 1, 5 and 10 Hz. The test was conducted for every 5^0 C temperature increment up to 70^0 C. The lowest temperature for testing each sample is fixed based on the maximum torque of 200 mNm. Also, sufficient care was taken while testing the material at a lower temperature with a 25 mm diameter plate. Table 3 shows the details of LAOS tests conducted for the VG30 grade of bitumen. A total of 224 numbers of LAOS tests were conducted using VG30 bitumen grade. Likewise, the total number of LAOS test conducted on VG10, VG40, PMB(E), PMB(P) and CRMB bitumen were 252, 211, 217, 220 and 217 respectively. During testing, the complete torque and stress waveform data were collected for every 10 cycles of shearing and each waveform data consisted of 512 data points.

(a) Steady shear test protocol   (b) LAOS test protocol – 1% strain and 5 Hz frequency

(c) MSCR test protocol
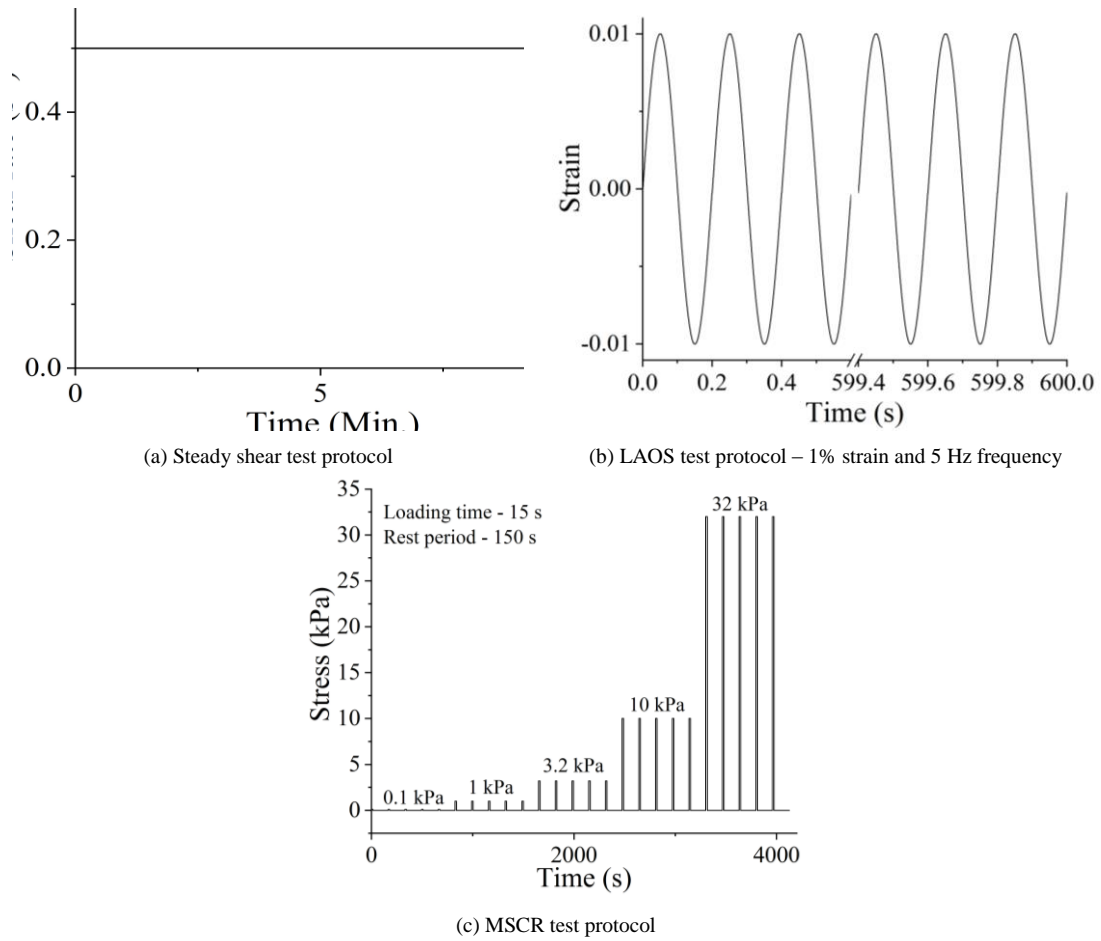
Figure 2. Experimental test protocols

Table 3. LAOS test details of VG30 bitumen

Material aging condition	LAOS			
	Temperature interval (°C)	Strain (%)	Frequency (Hz)	Number of tests
	20 – 70	1		11
	25 – 70	5	1	10
	30 – 70	10		9
UA	25 – 70	1		10
	35 – 70	5	5	8
	35 – 70	10		8
	25 – 70	1		10
	35 – 70	5	10	8
	40 – 70	10		7
	20 – 70	1		11
	30 – 70	5	1	9
	30 – 70	10		9
STA	25 – 70	1		10
	35 – 70	5	5	8
	40 – 70	10		7
	30 – 70	1		9
	40 – 70	5	10	7
	45 – 70	10		6
	25 – 70	1		10
	35 – 70	5	1	8
	35 – 70	10		8
	30 – 70	1		9
LTA	40 – 70	5	5	7
	45 – 70	10		6
	35 – 70	1		8
	45 – 70	5	10	6
	50 – 70	10		5
Total				**224**

The third set of experimental investigations is the repeated creep and recovery test with each cycle of shearing consisting of the application of constant shear stress for 15 seconds followed by a recovery time of 150 seconds. The test was conducted for five different stress magnitudes of 0.1, 1, 3.2, 10 and 32 kPa. Five cycles of loading and unloading were applied at each stress level and the schematic of the MSCR test is shown in Figure 2-c. The temperature during testing was maintained constant and the experiment was conducted for every 5^0 C increment in the temperature range of 20 to 70^0 C. Figure 3 shows the images of the equipment, sample preparations, sample testing.

(a) Equipment

(b) Sample Preparation

(c) Placing of sample in the equipment

(d) Testing of sample

Figure 3. Images of the equipment, sample preparations, sample testing

5. Results and Discussion

5.1. Steady Shear Test

Figure 4 shows the apparent viscosity of selected samples (VG30-UA and PMB(P)-UA) measured at different temperatures. As expected, the apparent viscosity reduced with an increase in temperature. The viscosity reached a steady state after a few seconds of shearing and a steady viscosity value at 200th seconds was selected for further analysis. Figure 5 compares the viscosity of different binders at different aging conditions. At any given temperature, the addition of a modifier increased the viscosity of the binder. As expected, the viscosity increased with aging and the percentage increase with aging varied with binder and temperature of interest. PMB(E) binder at 30°C exhibited a maximum percentage increase of 92% from UA to LTA condition and CRMB binder at 80°C exhibited a minimum percentage increase of 53%.

(a) VG30-UA   (b) PMB(E)-UA
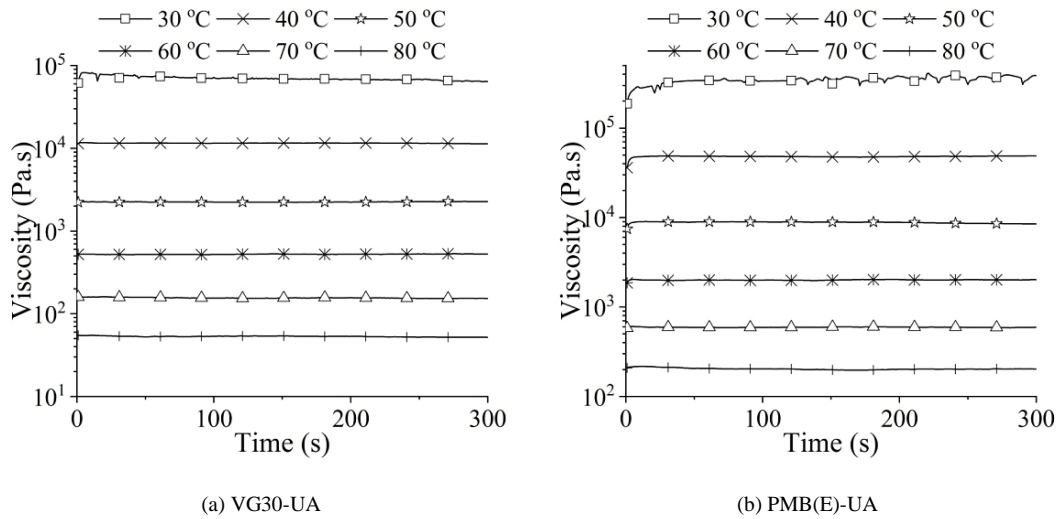
Figure 4. Steady shear viscosity at different temperatures

(a) $30^0 C$ (b) $80^0 C$
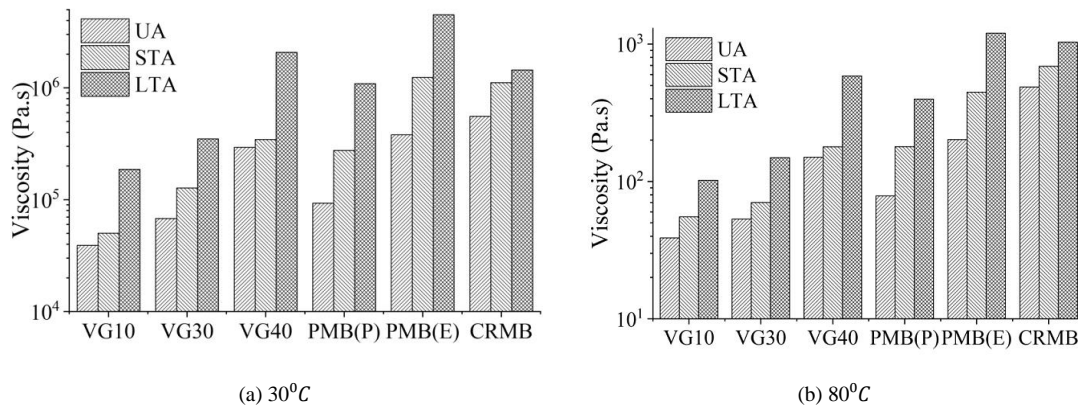
Figure 5. Comparison of viscosity of different binders at different aging conditions

Among six binders tested, the viscosity of CRMB binder is found to be less prone to aging change. The variation of viscosity with temperature of all binders tested and for all aging conditions is shown in Figure 6. The logarithm of viscosity exhibited a linear relation with the inverse of temperature measured in K^{-1}. The Arrhenius equation (discussed in equation 1) is fitted to the viscosity-temperature experimental data and the slope of the linear line is considered as the Activation Energy (AE). The AE of all the samples tested are tabulated in Table 4. All the values tabulated here correspond to R^2 of 0.99 or more. The AE constant represents the temperature-susceptible nature of the binder. The material with high value of AE indicates high sensitivity to changes in temperature. AE determined based on viscosity was observed to increase with aging. In the unmodified binder, VG10 is observed to be least susceptible to change in temperature when compared to VG30 and VG40. In a modified binder CRMB is least susceptible to change in temperature. From Table 4 one can state that the AE of all STA binders except VG30 increases to about 2 %, whereas the VG30 STA binder increases to about 7 % when compared with the UA binder. Similarly, the AE of all LTA binders except CRMB increases to about 10 %, whereas CRMB LTA binder increases to about 4 % when compared with the UA binder.

a) Unaged binders   b) Short-term aged binders
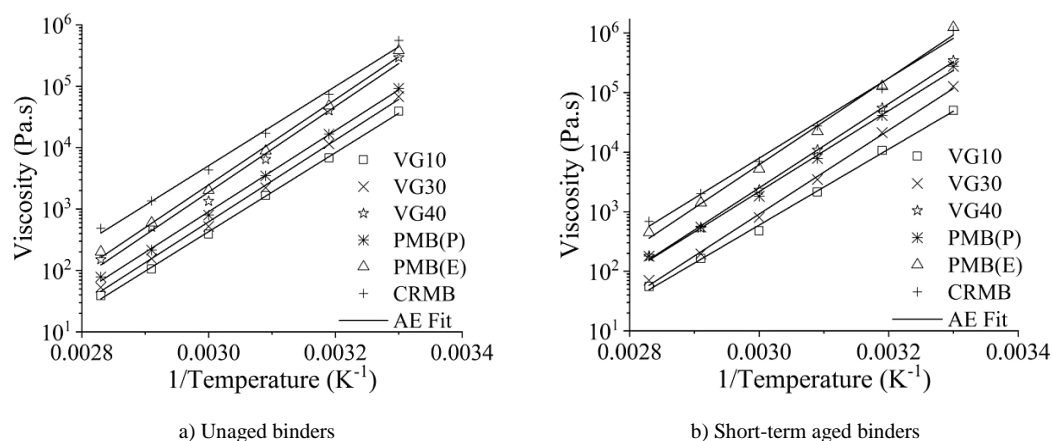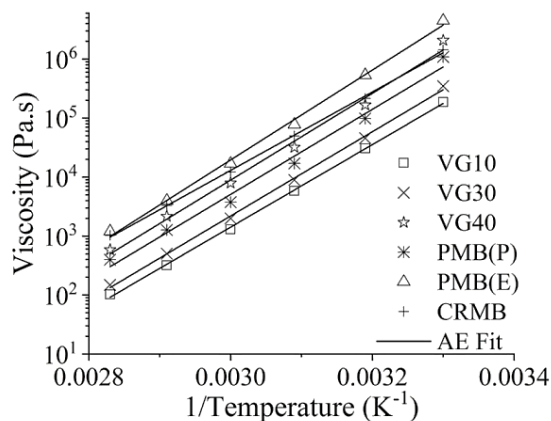
c) Long-term aged binders

Figure 6. Viscosity – temperature relation of various binders and the corresponding AE fit

Table 4. Activation energy for different bitumen based on the viscosity

Binder	Activation Energy (kJ/mol)		
	UA	STA	LTA
VG10	123	122	134
VG30	127	135	137
VG40	134	135	141
PMB(P)	127	130	138
PMB(E)	133	139	146
CRMB	124	129	127

The AE of the binders was compared with Salomon and Zhai [17, 19] and was observed to follow the trend.

5.2. Oscillatory Shear Testing

5.2.1. Activation Energy form Dynamic Modulus

In the experimental investigation, the oscillatory shear test was conducted by selecting the strain amplitude in the linear and nonlinear regime, and the complete stress, strain, and strain rate waveform was recorded using the LAOS protocol. The sample stress, strain, and strain rate waveform data recorded for CRMB-LTA binder at 10% strain amplitude, 10 Hz frequency, and 50°C is shown in Figure 7-a. The dynamic modulus is computed as the ratio of first harmonic stress to strain amplitude. The harmonic stress intensity is computed using the Fast Fourier Transform (FFT) algorithm. The FFT of the sample stress waveform is shown in Figure 7-b. From the FFT results, first-order harmonic is used in the computation of dynamic modulus.
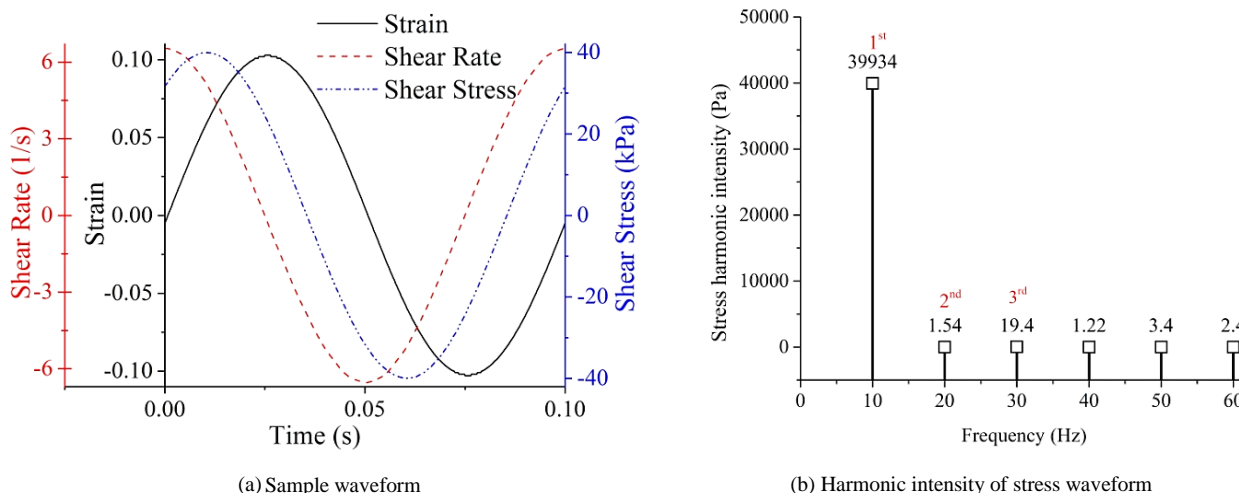
(a) Sample waveform

(b) Harmonic intensity of stress waveform

Figure 7. Shear stress waveform and the corresponding harmonic intensity

Figure 8 shows the dynamic modulus of long-term aged CRMB binder when tested at 1 and 10 Hz frequency. The variation in dynamic modulus with the inverse of temperature follows the Arrhenius equation and the slope (AE) is observed to be independent of frequency and the strain amplitude. The dynamic modulus of various binders measured at 5% strain amplitude, 5 Hz frequency at different temperatures and the corresponding AE fit for each binder is shown in Figure 9. The corresponding AE is tabulated in Table 5. The AE based on dynamic modulus decreased on aging unlike AE obtained based on the steady shear viscosity value. From Table 5 one can state that the AE of all STA binders decreased to about 1 % when compared with the UA binder. Similarly, the AE of all LTA binders except CRMB decreased to about 3 %, whereas the CRMB LTA binder decreased to about 9 % when compared with the UA binder.

(a) 1 Hz   (b) 10 Hz
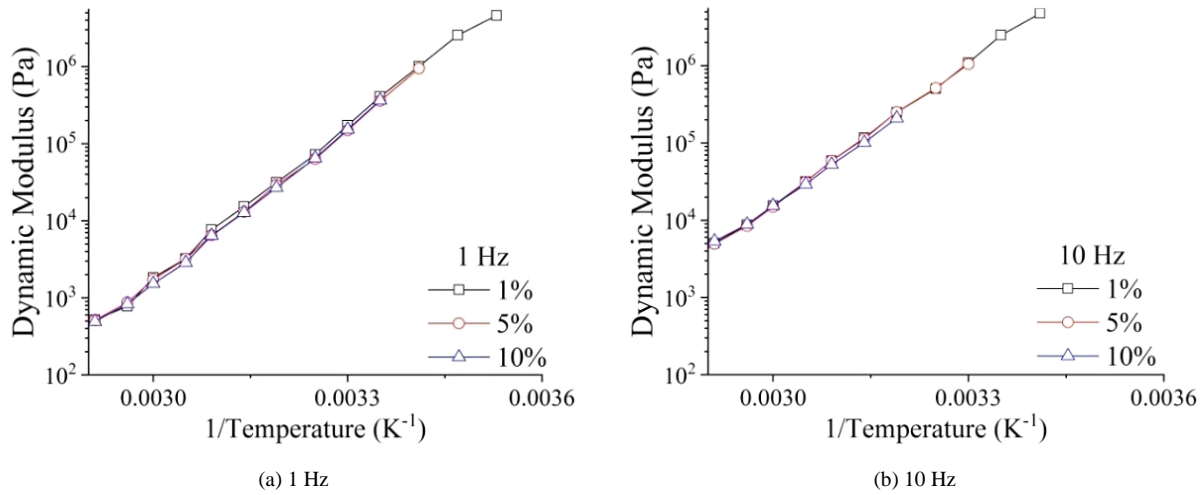
Figure 8. Variation of dynamic modulus with temperature inverse – CRMB-LTA binder

(a) Unaged   (b) Short-term aged

(c) Long-term aged
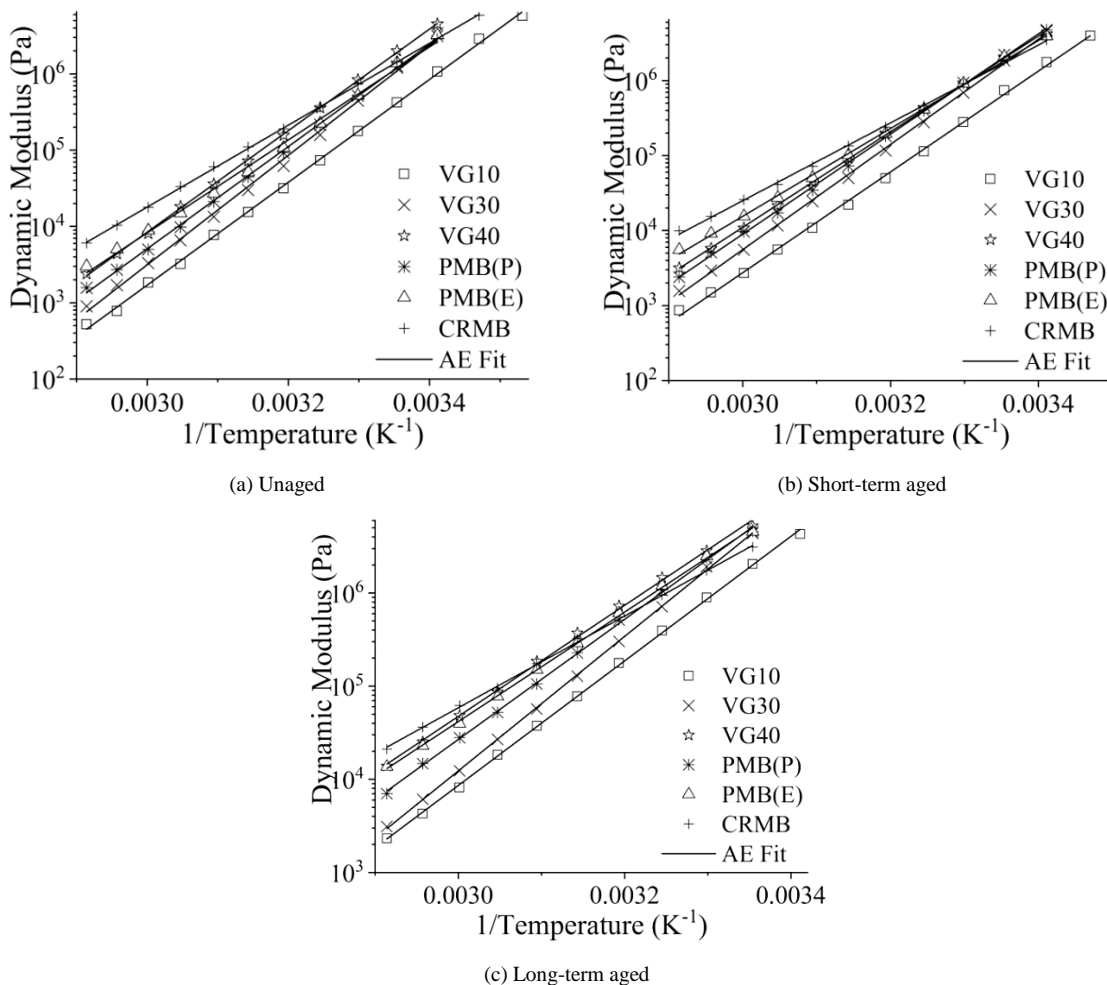
Figure 9. Dynamic modulus – temperature relation of binders and the corresponding AE fit

Table 5. Activation energy for different bitumen based on Dynamic modulus

| Binder	Activation Energy (kJ/mol)		
	UA	STA	LTA
VG10	129	129	128
VG30	138	137	134
VG40	127	122	114
PMB(P)	128	128	123
PMB(E)	117	113	113
CRMB	103	99	94

5.2.2. Activation Energy form Energy Dissipation (ED)

The viscoelastic material dissipates energy and the extent of dissipation depends on the temperature of interest. When the material is subjected to sinusoidal strain, the resultant stress waveform may contain higher-order harmonic contribution. It is understood that the energy dissipation due to sinusoidal strain is purely due do the first-order harmonic stress [33]. Hence, the energy dissipation is computed using Equation 3, where ϵ_1 represents first-order harmonic strain, σ_1 is the first-order harmonic stress and δ_1 is the corresponding lag. Here, in the strain-controlled test, the material is subjected to sinusoidal strain and hence ϵ_1 is the same as the strain amplitude.

$$ED = \pi \epsilon_1 \, \sigma_1 \sin \delta_1. \tag{3}$$

Figure 10 shows the comparison ED of different binders at UA, STA, and LTA conditions. In the strain-controlled test, ED decreases with temperature and it exhibited exponential decrease with temperature. The ED at any given temperature increases with aging. The ED is also expected to be dependent on frequency and strain amplitude. The variation of ED with temperature and shear rate is shown in Figure 11. At any given ED increased with an increase in shear rate. Further, the temperature dependency of ED is captured using the Arrhenius equation. The shear rate dependency of ED is captured from the variation of AE with the shear rate.

(a) Unaged condition

(b) Short-term aged

(c) Long-term aged
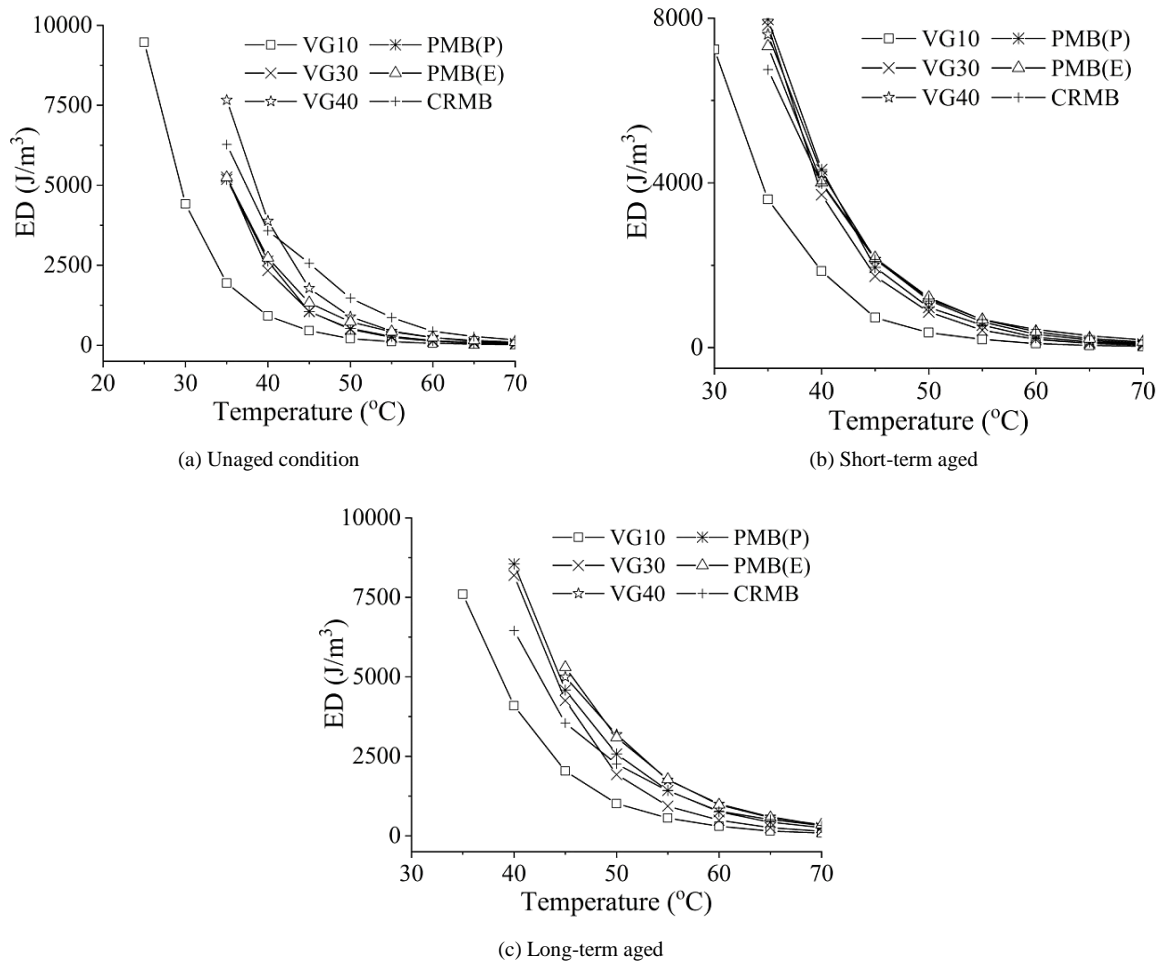
Figure 10. ED of unmodified and modified binders at different aging conditions at 5% strain amplitude and 5 Hz frequency

(a) VG30-UA   (b) PMB(E)-UA
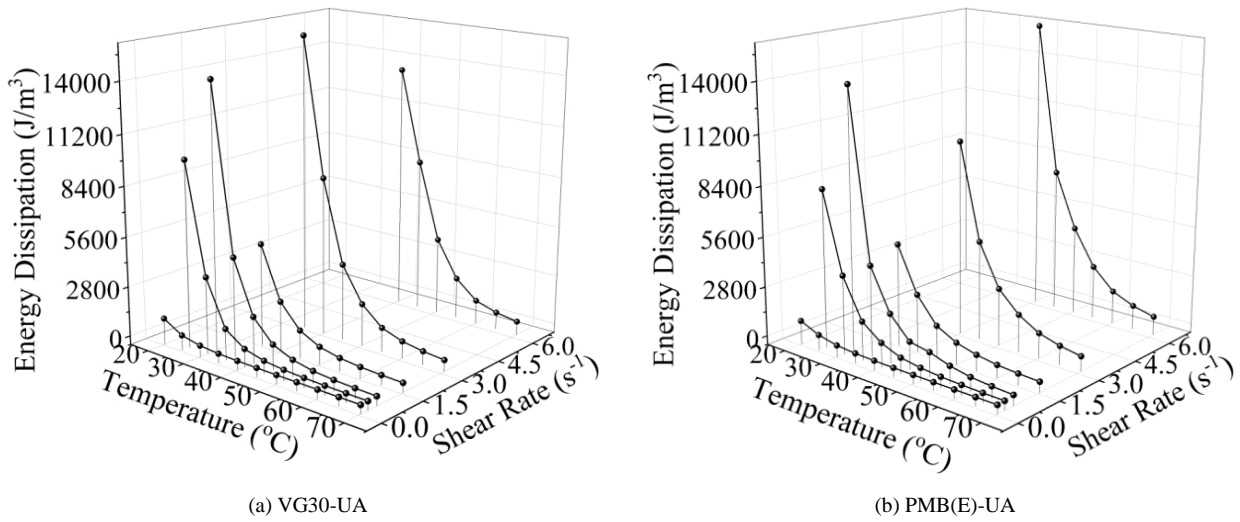
Figure 11. Variation of ED with shear rate and temperature

Figure 12 shows the logarithm variation of ED of selected samples with the inverse of temperature. The logarithm of ED with the inverse of temperature at all frequencies and strain amplitude tested exhibited a linear relation. The Arrhenius equation is fitted to an ED function and the corresponding slope value (AE) for the R^2 of 0.99 for CRMB binder at UA, STA, and LTA condition is tabulated in Table 6. AE decreased with aging. Also, AE is found to depend on the shear rate. From Table 6 one can state that AE is a dependent of shear rate. It was also observed that the AE of all the STA binders decreased to about 2 % at the low shear rate and 18 % at the high shear rate. A similar, trend was observed in the other bonders also.

(a) VG10-UA   (b) PMB(P)-UA

(c) CRMB-UA
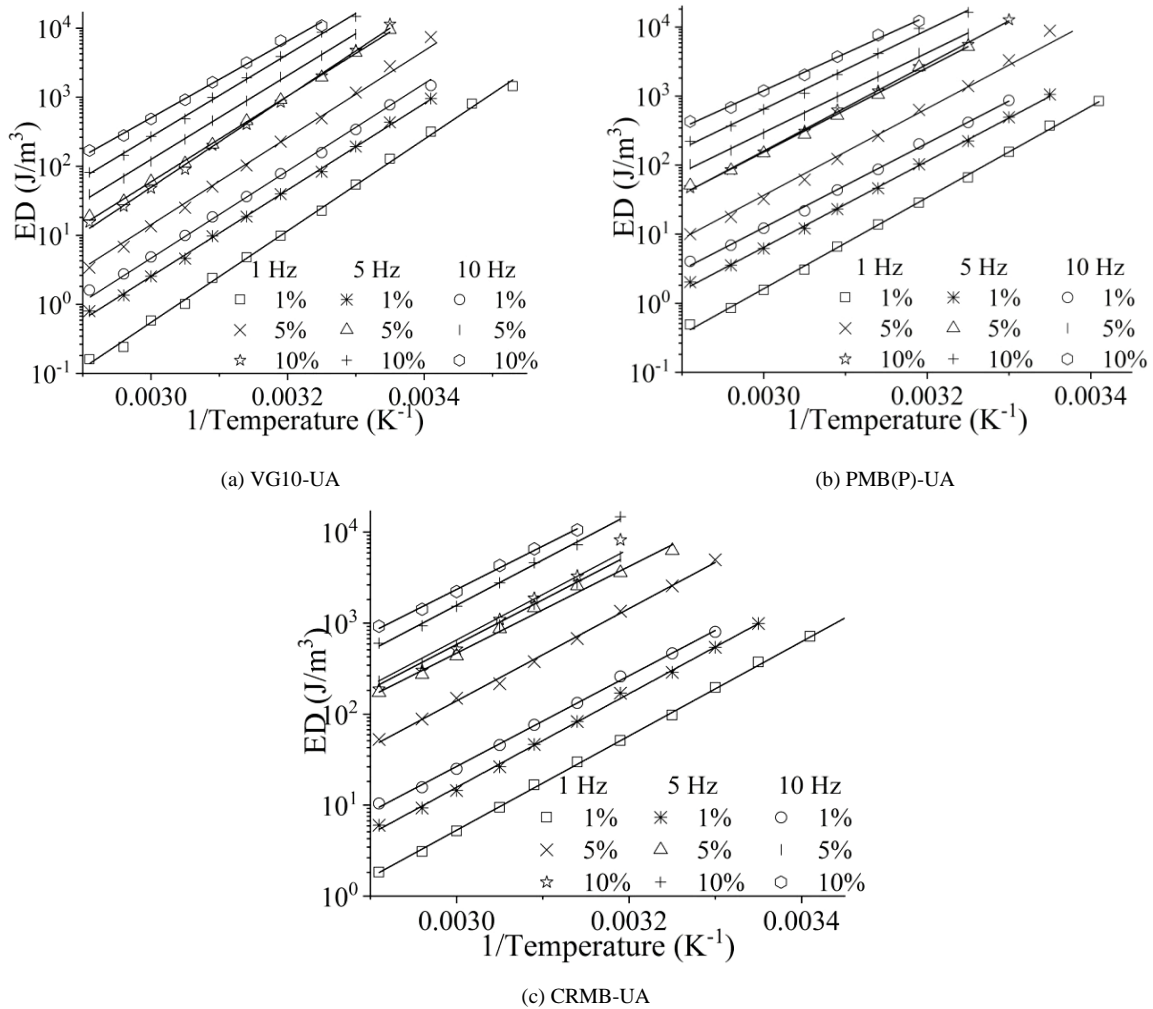
Figure 12. Variation of ED with temperature inverse for different UA binders

Table 6. Activation Energy of CRMB binder computed from Energy dissipation

Frequency (Hz)	Strain (%)	Shear rate (s⁻¹)	AE (kJ/mol)		
			UA	RTFO	PAV
	1	0.0625	99	97	90
1	5	0.312	97	92	92
	10	0.623	112	91	81
	1	0.312	98	92	91
5	5	1.57	91	91	90
	10	3.12	95	87	79
	1	0.623	110	90	81
10	5	3.12	94	88	79
	10	6.23	91	85	77

Figure 13 shows the variation of AE with shear rate. With the increase in shear rate, the activation energy constant decreased for all the binders. The shear rate dependency is more prominently observed at the lower shear rate.

(a) UA

(b) STA

(c) LTA
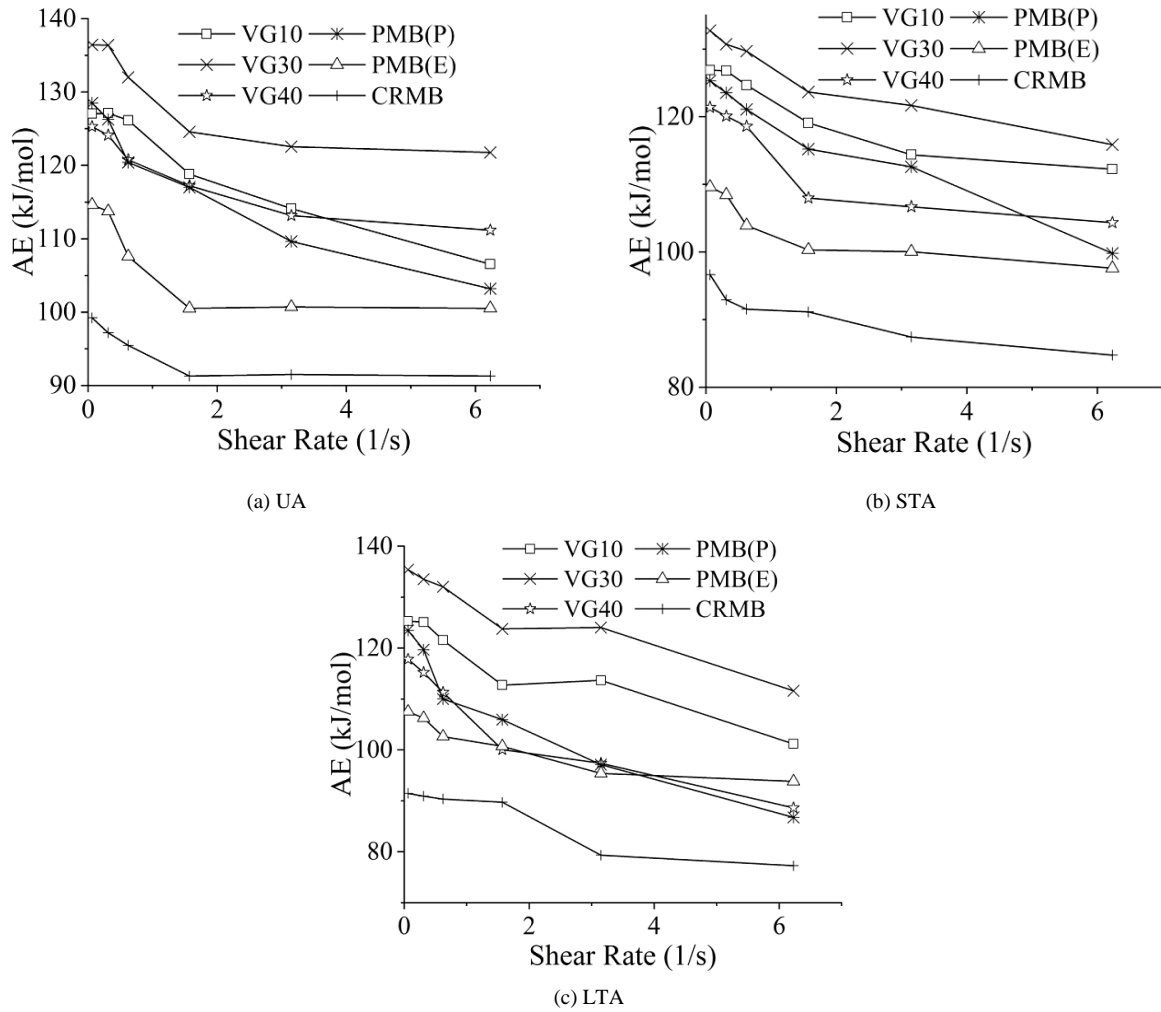
Figure 13. Variation of AE as a function of shear rate for all binders of different aging conditions

To check whether the influence of shear rate on AE is significant, ANOVA analysis (F test) is carried out. For this purpose, AE is separated into three groups based on the shear rate (SR). AE corresponding to SR ≤ 0.315 are grouped under one, AE corresponding to SR between 0.315 and 1.570 are considered under the second group and AE corresponding to SR greater than 1.570 under the third group. Table 7 shows the grouped data of the VG30-UA binder

for ANOVA analysis. It is hypothesized that the mean activation energy of the binder is the same for each of the three levels of shear rate and the F value was determined using Equation 4.

$$F = \frac{SS_{Tr}/Dof}{SS_E/error} \tag{4}$$

Here, $\frac{SS_{Tr}}{Dof}$ represents the mean sum of squares of AE between the groups and $\frac{SS_E}{error}$ represents the mean sum of squares of AE within the groups. SS_{Tr} and SS_E are computed using Equations 5 to 7.

$$SS_T = \sum_{i=1}^{k}\sum_{j=1}^{n} x_{ij}^2 - \frac{1}{kn}T^2 \tag{5}$$

$$SS_{Tr} = \frac{1}{n}\sum_{i=1}^{k} T_i^2 - \frac{1}{kn}T^2 \tag{6}$$

$$SS_E = SS_T - SS_{Tr} \tag{7}$$

Here, x_{ij} represents activation energy, T represents the group total, k is the number of groups, and, n is the number of observations in a group. Dof represents the degree of freedom which is $n - 1$ and, $error$ is given by $n(n-1)$. The F value of all the samples were documented in Table 8. The F value corresponding 5% level of significance was found to be 5.143. From Table 8, it is clear that F values of energy dissipation-based AE for most of the binders are shear rate dependent. Hence, the AE obtained from the energy dissipation was found to depend on the strain amplitude and the frequency of shearing. Here, it has to be highlighted that AE obtained from the dynamic modulus is independent of strain amplitude and frequency.

Table 7. Grouping of ED-based AE of VG30-UA binder for ANOVA

Sl. No.	SR - Shear Rate, AE - Activation Energy	Observations			Total (T)	Mean (s)
1	SR ≤ 0.3150	0.0625	0.3120	0.3150	-	-
	AE	136	136	128	401	134
2	0.3150 < SR ≤ 1.5700	0.6230	0.6250	1.5700	-	-
	AE	132	123	125	379	126
3	SR > 1.5700	3.1200	3.1500	6.2300	-	-
	AE	123	119	122	363	121
					1143	127

Table 8. F value for Energy dissipation and Jnr

Binder	UA		STA		LTA	
	ED	J_{nr}	ED	J_{nr}	ED	J_{nr}
VG10	5.2	74.7	5.4	64.4	1.7	70.7
VG30	6.7	39.1	1.9	298.6	1.1	260.5
VG40	5.6	40.8	5.3	208.6	5.2	94.1
PMB(P)	16.5	125.5	1.6	193.1	5.2	96.7
PMB(E)	9.7	39.1	10.2	30.3	5.4	34.1
CRMB	6.4	43.3	8.7	22.5	9.0	31.6

5.3. Multiple Stress Creep and Recovery Test

Figure 14 shows the sample creep and recovery cycle of CRMB-STA at 1 kPa measured at 30°C. The non-recoverable creep compliance (J_{nr}) is computed from ε_0, the strain at the beginning of any creep cycle and ε_r, the strain measured at the end of the recovery cycle. J_{nr} is computed following Equation 8 stated in ASTM D7405 [34].

$$J_{nr} = \frac{\varepsilon_r - \varepsilon_0}{\sigma} \qquad\qquad\qquad (8)$$

where, σ represents the stress magnitude. Here, it has to be highlighted that the test procedure adopted in this paper differs from the standard ASTM D7405 [34] in two ways. The first difference is the magnitude of stress used for testing. To check the influence of stress on the activation energy, the test was conducted at five different shear stresses 0.1, 1, 3.2, 10, and 32 kPa. This test protocol also differs from the standard MSCR test in terms of creep and recovery time used for testing. An extended creep time of 15 seconds and a recovery time of 150 seconds were chosen to give sufficient time for the material to reach a steady state while shearing. Jnr for each cycle is computed and the average of 5 cycles is used in the computation of activation energy.
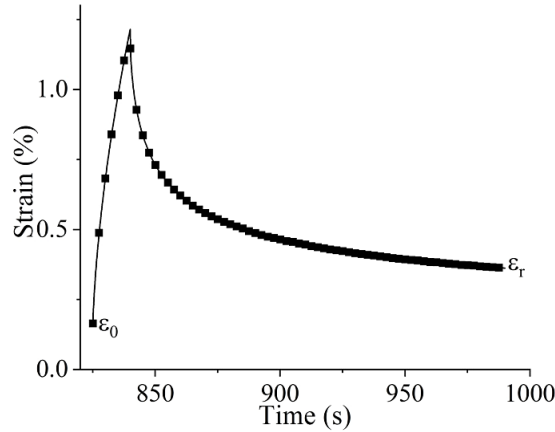
Figure 14. Sample creep and recovery cycle corresponding to CRMB-STA at 1 kPa and 30 ^{0} C

Figure 15 shows the logarithm variation of J_{nr} of selected samples with the inverse of temperature. The logarithm of J_{nr} with the inverse of temperature at all stress levels exhibited a linear relation. The Arrhenius equation is fitted to a J_{nr} function and the corresponding slope value (AE) for the R^2 of 0.99 for PMB(E) binder at UA, STA, and LTA condition is tabulated in Table 9. AE increase on aging. Also, AE is found to depend on the stress. The consolidated AE of the binders was tabulated in Table 10.
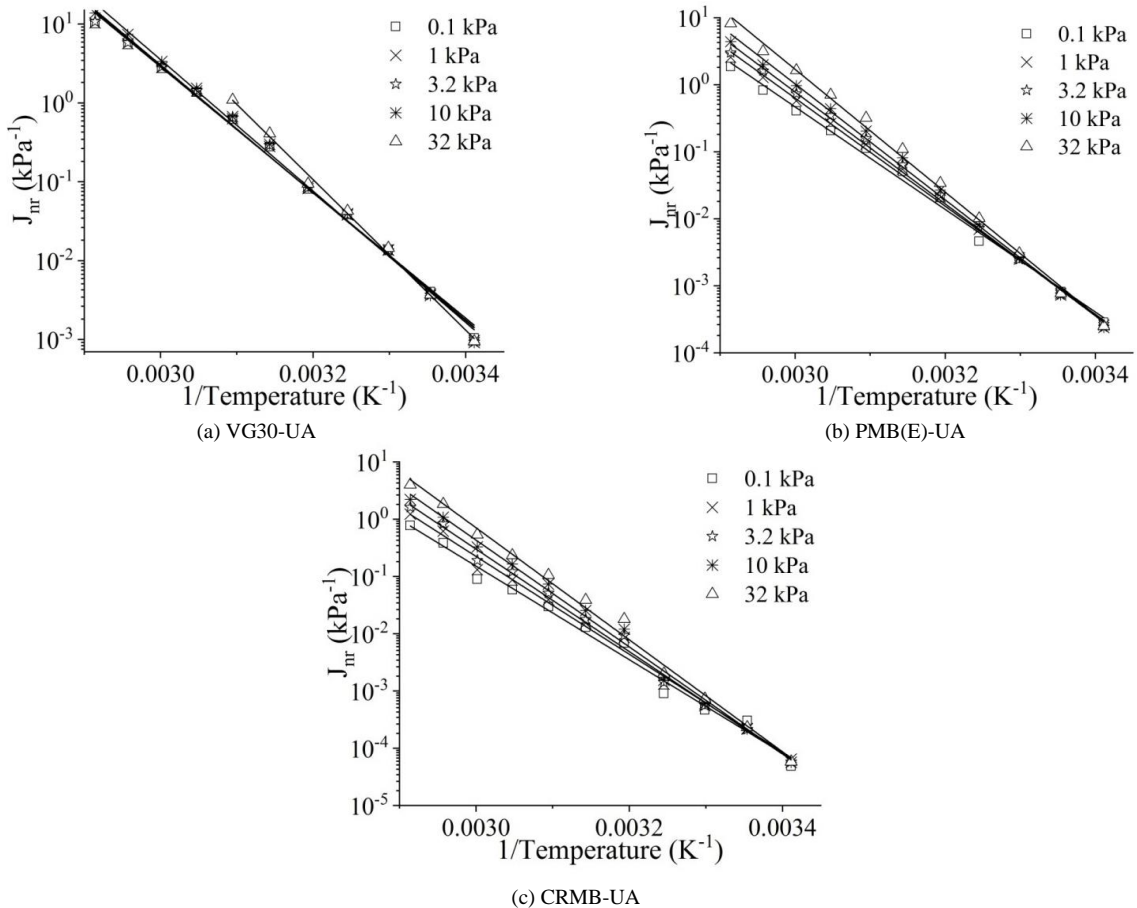
Figure 15. Variation of creep compliance with temperature inverse for different unaged binders

Table 9. Activation Energy of PMB(E) binder from Jnr

Stress	AE (kJ/mol)		
	UA	RTFO	PAV
0.1 kPa	147	134	150
1 kPa	154	149	158
3.2 kPa	160	158	165
10 kPa	166	166	175
32 kPa	176	179	184

Table 10. Consolidate values of AE from Jnr

Binder	Activation Energy (kJ/mol)		
	UA	STA	LTA
VG10	143 – 194	151 – 188	166 – 179
VG30	152 – 183	156 – 190	165 - 197
VG40	163 – 179	165 -204	171 - 210
PMB(P)	148 – 176	155 – 194	173 - 202
PMB(E)	146 – 176	134 – 179	149 - 184
CRMB	156 – 187	139 – 195	140 - 194

To check the influence of stress in the Jnr-based activation energy, ANOVA analysis is carried out. For this purpose, AE is separated into three groups based on stress levels (σ). AE corresponding to $\sigma \leq 0.1$ kPais considered under Group 1, σ between 0.1 and 10 kPa is considered under Group 2, and $\sigma > 10\ kPa$ is considered under Group 3. The sample grouped data corresponding to VG30-UA is shown in Table 11. The F values for all the samples are determined using Equation 4 and the values are tabulated in Table 8. For the 5% level of significance, the F value in the table indicates that AE depends on the stress level.

Table 11. Grouping of Jnr-based AE of VG30-UA binder for ANOVA

Sl. No.	σ– Stress (kPa), AE - Activation Energy (kJ/mol)	Observations		Total (T)	Mean (s)
1	$\sigma \leq 0.1$	0.1	1.0000	-	-
	AE	153	154	307	153
2	$0.1 < \sigma \leq 10$	3.2000	10.0000	-	-
	AE	155	160	315	157
3	$\sigma > 10$	10.0000	10.0000	-	-
	AE	183	183	365	183
	T - Total and s – mean			**987**	**165**

6. Conclusions

The viscoelastic function of bitumen such as viscosity, dynamic modulus, energy dissipation and non-recoverable creep compliance follows the Arrhenius equation. The activation energy of the Arrhenius equation is viewed as a tool for predicting the temperature susceptibility of bitumen. The following conclusions were made from the detailed experimental investigation:

- The activation energy of any bitumen varied with the choice of viscoelastic parameters.

- The activation energy of bitumen was found to be sensitive to the shear rate/stress variation. This indicates that the temperature susceptibility of the bitumen is shear rate/stress-dependent. The variation is more dominant when the test is conducted at a lower shear rate/stress.

- While comparing the activation energy of PMB(E), and PMB(P) with an unmodified binder, the variation in AE of these binders does not follow any trend. This can be due to differences in shear rate/stress exhibiting low-temperature susceptibility character when compared to unmodified bitumen.

Likewise, the variation in activation energy of bitumen on aging does not follow any trend. For instance, the activation energy based on viscosity and Jnr increases on aging and the activation energy based on dynamic modulus and energy dissipation decreases on aging. This non-trend can be attributed to the difference in the shear-susceptibility of the binder.

7. Declarations

7.1. Author Contributions

Conceptualization, T.S. and A.P.; methodology, T.S. and P.A.; validation, T.S. and P.A.; formal analysis, T.S. and P.A.; investigation, T.S.; resources, T.S. and P.A.; data curation, T.S. and P.A.; writing—original draft preparation, T.S. and P.A.; writing—review and editing, T.S. and P.A.; supervision, P.A.; project administration, P.A. All authors have read and agreed to the published version of the manuscript.

7.2. Data Availability Statement

The data presented in this study are available in the article.

7.3. Funding

7.4. Conflicts of Interest

The authors declare no conflict of interest.

8. References

[1] Nivitha, M. R., & Krishnan, J. M. (2014). Development of Pavement Temperature Contours for India. Journal of The Institution of Engineers (India): Series A, 95(2), 83–90. doi:10.1007/s40030-014-0074-y.

[2] Padmarekha, A., & Krishnan, J. M. (2013). Viscoelastic Transition of Unaged and Aged Asphalt. Journal of Materials in Civil Engineering, 25(12), 1852–1863. doi:10.1061/(asce)mt.1943-5533.0000734.

[3] Nivitha, M. R., & Murali Krishnan, J. (2016). What is Transition Temperature for Bitumen and How to Measure It? Transportation in Developing Economies, 2(1), 1–8. doi:10.1007/s40890-015-0009-y.

[4] IS73. (2013). Paving Bitumen-Specification (4th REVISION). Bureau of Indian Standards, New Delhi, India.

[5] ASTM, D6373-21a. (2023). Standard Specification for Performance-Graded Asphalt Binder. ASTM International, Pennsylvania, United States. doi:10.1520/D6373-21A.

[6] Heukelom, W. (1969). A bitumen test data chart for showing the effect of temperature on the mechanical behavior of asphaltic bitumens. Institute of Petroleum, 55(5460), 404-417.

[7] Storm, D. A., Barresi, R. J., & Sheu, E. Y. (1996). Development of solid properties and thermochemistry of asphalt binders in the 25-65°C temperature range. Energy & Fuels, 10(3), 855–864. doi:10.1021/ef9502564.

[8] Nivitha, M. R., Prasad, E., & Krishnan, J. M. (2019). Transitions in unmodified and modified bitumen using FTIR spectroscopy. Materials and Structures/Materiaux et Constructions, 52(1), 1–11. doi:10.1617/s11527-018-1308-7.

[9] Williams, M. L., Landel, R. F., & Ferry, J. D. (1955). The Temperature Dependence of Relaxation Mechanisms in Amorphous Polymers and Other Glass-forming Liquids. Journal of the American Chemical Society, 77(14), 3701–3707. doi:10.1021/ja01619a008.

[10] Ferry, J. D. (1980). Viscoelastic properties of polymers. John Wiley & Sons, Hoboken, United States.

[11] Rajan, S., Sutton, M. A., Oseli, A., Emri, I., & Matta, F. (2017). Linear viscoelastic creep compliance and retardation spectra of bitumen impregnated fiberglass mat and polymer modified bitumen. Construction and Building Materials, 155, 664–679. doi:10.1016/j.conbuildmat.2017.08.030.

[12] Zoorob, S. E., Mturi, G. A., Sangiorgi, C., Dinis-Almeida, M., & Habib, N. Z. (2018). Fluxing as a new tool for bitumen rheological characterization and the use of time-concentration shift factor (AC). Construction and Building Materials, 158, 691–699. doi:10.1016/j.conbuildmat.2017.10.020.

[13] Lesueur, D. (2009). The colloidal structure of bitumen: Consequences on the rheology and on the mechanisms of bitumen modification. Advances in Colloid and Interface Science, 145(1–2), 42–82. doi:10.1016/j.cis.2008.08.011.

[14] Cheung, C. Y., &Cebon, D. (1997). Experimental study of pure bitumens in tension, compression, and shear. Journal of Rheology, 41(1), 45–74. doi:10.1122/1.550858.

[15] Atul Narayan, S. P., Murali Krishnan, J., Little, D. N., & Rajagopal, K. R. (2016). Mechanical behaviour of asphalt binders at high temperatures and specification for rutting. International Journal of Pavement Engineering, 18(10), 916–927. doi:10.1080/10298436.2015.1126272.

[16] Maze, M. (1996). Viscosity of EVA Polymer-Modified Bitumens: Modelling. No. 5170 Section 5. Euraspahlt&Eurobitume Congress, 7-10 May, 1996, Strasbourg, France.

[17] Salomon, D., & Zhai, H. (2002). Ranking asphalt binders by activation energy for flow. Journal of Applied Asphalt Binder Technology, 2(2), 52-60.

[18] Dongre, R., Myers, L., D'Angelo, J., Paugh, C., & Gudimettla, J. (2005). Field evaluation of Witczak and Hirsch models for predicting dynamic modulus of hot-mix asphalt (with discussion). Journal of the Association of Asphalt Paving Technologists, 74.

[19] Salomon, D., & Zhai, H. (2004). Asphalt binder flow activation energy and its significance for compaction effort. Proceedings of 3rdEuroasphalt&Eurobitume congress, 12-14 May 2004, Vienna, Austria.

[20] Saboo, N., Singh, B., & Kumar, P. (2019). Development of High-Temperature Ranking Parameter for Asphalt Binders Using Arrhenius Model. Journal of Materials in Civil Engineering, 31(12), 4019297. doi:10.1061/(asce)mt.1943-5533.0002965.

[21] Garća-Morales, M., Partal, P., Navarro, F. J., Marı́nez-Boza, F., Gallegos, C., González, N., González, O., & Muñoz, M. E. (2004). Viscous properties and microstructure of recycled EVA modified bitumen. Fuel, 83(1), 31–38. doi:10.1016/S0016-2361(03)00217-5.

[22] Ait-Kadi, A., Brahimi, B., &Bousmina, M. (1996). Polymer blends for enhanced asphalt binders. Polymer Engineering & Science, 36(12), 1724–1733. doi:10.1002/pen.10568.

[23] Wang, H., Liu, X., Apostolidis, P., & Scarpas, T. (2018). Rheological behavior and its chemical interpretation of crumb rubber modified asphalt containing warm-mix additives. Transportation Research Record, 2672(28), 337–348. doi:10.1177/0361198118781376.

[24] Jamshidi, A., Hamzah, M. O., Shahadan, Z., & Yahaya, A. S. (2015). Evaluation of the Rheological Properties and Activation Energy of Virgin and Recovered Asphalt Binder Blends. Journal of Materials in Civil Engineering, 27(3), 4014135. doi:10.1061/(asce)mt.1943-5533.0001024.

[25] Luo, X., Gu, F., & Lytton, R. L. (2019). Kinetics-based aging prediction of asphalt mixtures using field deflection data. International Journal of Pavement Engineering, 20(3), 287–297. doi:10.1080/10298436.2017.1293262.

[26] Luo, X., Gu, F., & Lytton, R. L. (2015). Prediction of field aging gradient in asphalt pavements. Transportation Research Record, 2507(1), 19–28. doi:10.3141/2507-03.

[27] Haider, S. W., Mirza, M. W., Thottempudi, A. K., Bari, J., &Baladi, G. Y. (2011). Characterizing Temperature Susceptibility of Asphalt Binders Using Activation Energy for Flow. Transportation and Development Institute Congress 2011. doi:10.1061/41167(398)48.

[28] Notani, M. A., Arabzadeh, A., Satvati, S., TarighatiTabesh, M., GhafariHashjin, N., Estakhri, S., & Alizadeh, M. (2020). Investigating the high-temperature performance and activation energy of carbon black-modified asphalt binder. SN Applied Sciences, 2(2), 1–12. doi:10.1007/s42452-020-2102-z.

[29] Raouf, M. A., & Williams, R. C. (2010). Temperature and shear susceptibility of a nonpetroleum binder as a pavement material. Transportation Research Record, 2180(2180), 9–18. doi:10.3141/2180-02.

[30] Ingram, L., Mohan, D., Bricka, M., Steele, P., Strobel, D., Crocker, D., Mitchell, B., Mohammad, J., Cantrell, K., & Pittman, C. U. (2008). Pyrolysis of wood and bark in an auger reactor: Physical properties and chemical analysis of the produced bio-oils. Energy and Fuels, 22(1), 614–625. doi:10.1021/ef700335k.

[31] ASTM D2872-22. (2022). Standard Test Method for Effect of Heat and Air on a Moving Film of Asphalt (Rolling Thin-Film Oven Test). ASTM International, Pennsylvania, United States. doi:10.1520/D2872-22.

[32] ASTM D6521-22. (2022). Standard Practice for Accelerated Aging of Asphalt Binder Using a Pressurized Aging Vessel (PAV). ASTM International, Pennsylvania, United States. doi:10.1520/D6521-22.

[33] Kalelkar, C., Lele, A., & Kamble, S. (2010). Strain-rate frequency superposition in large-amplitude oscillatory shear. Physical Review E - Statistical, Nonlinear, and Soft Matter Physics, 81(3), 31401. doi:10.1103/PhysRevE.81.031401.

[34] ASTM D7405. (2015). Standard Test Method for Multiple Stress Creep and Recovery (MSCR) of Asphalt Binder Using a Dynamic Shear Rheometer. ASTM International, Pennsylvania, United States.
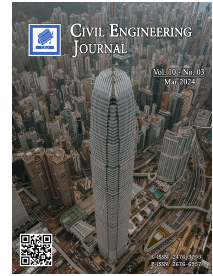
Evaluation of Alkali-Activated Mortar Incorporating Combined and Uncombined Fly Ash and GGBS Enhanced with Nano Alumina

Barham Ali [1]*

[1] Department of Civil Engineering, Tishk International University, Erbil, Iraq.

Abstract

The present research focuses on assessing the fresh and hardened properties as well as the durability performance of alkali-activated mortar in an ambient environment and the impact of integrating nano-alumina (NA) at a 2% ratio as a substitute for binder materials in alkali-activated mortar (AAM). Additionally, it assesses the effectiveness of alkali-activated mortar employing different blends of ground granulated blast furnace slag (GGBS) and fly ash as environmentally friendly substitute building materials. Fly ash (FA), ground granulated blast slag (GGBS), and an equal mixture of GGBS and FA make up these binder ingredients. As a result, the main binders contain GGBS, FA, or a 50/50 mixture of GGBS and FA. The sodium hydroxide (NaOH) concentration is fixed at a 12-molarity level, and the alkali activator solution to binder ratio is kept at 0.5. In the alkali solution, the ratio of sodium silicate to sodium hydroxide is always 2.5. The study evaluates various properties of AAM, such as compressive strength, flowability, unit weight, flexural tensile strength, and durability, under ambient conditions at a steady room temperature of 23±3°C. Results indicate that AAM mixtures devoid of NA exhibit a higher flow rate compared to those containing NA. Nonetheless, the flowability of AAM mixtures aligns well with standard requirements, being modest yet adequate. Significantly, the inclusion of NA enhances the mechanical properties and durability of AAM, demonstrating its beneficial effects.

Keywords: Alkali Activated Mortar; Nano Alumina; Mechanical Properties; Durability; Fresh Properties.

1. Introduction

Concrete is recognized as the world's most extensively utilized cementitious material. Anticipated growth in building material demand is significant in many countries in the near future. Despite the widespread availability and ease of supply of ordinary Portland cement (OPC), it remains the predominant concrete binder, leading to an annual increase in OPC production by approximately 3% [1]. This prominence of OPC, a major contributor to greenhouse gas emissions, places the concrete industry at the forefront of releasing unfavorable greenhouse gases [2]. Technological advancements have spurred the development of building materials that are not only more energy-efficient and environmentally friendly but also less expensive than traditional materials. Among these innovations, the production of cementitious materials stands out. Consequently, comprehensive research has been conducted to enhance their properties. In 1970, Davidovits [3] introduced a novel inorganic polymer known as alkali-activated concrete (AAC), which boasts superior mechanical properties compared to ordinary Portland cement [4].

The geopolymerization process, a form of green technology, plays a pivotal role in reducing global CO_2 emissions. Studies reveal that producing one ton of AAC results in approximately 164 kg of CO_2 emissions, significantly less than the emissions from OPC concrete, thereby contributing to the mitigation of global warming [5–9]. AAC, an inorganic

alumino-silicate polymer, is synthesized from various alumino-silicate sources, such as metakaolin and red mud, and activated by highly alkaline chemical solutions. These sources also include industrial by-products like fly ash (FA), slag, and others from steel production [5, 7]. Replacing cement-based concrete with AAC can significantly reduce CO_2 emissions. Furthermore, this replacement involves using industrial by-products such as fly ash, ground granulated blast furnace slag (GGBS), metakaolin, and rice husk ash as primary ingredients [8, 10]. Alkali-activated composites, engineered as novel binders rich in aluminosilicate materials, are derived from these raw materials. These composites, capable of synthesizing pozzolan with high alkali-activated solutions, have demonstrated promising results in sustainable development, exhibiting enhanced strength and porosity [11].

Recent studies have explored the partial or complete substitution of cement-based concrete with various nanomaterials. Despite the superior mechanical properties, workability, and durability of conventional concrete, alkali-activated composites integrated with nanomaterials offer greater strength and durability. Most research indicates that the optimal content of binder materials in alkali-activated concrete paste and mortar is around 1-2 percent by weight, with a particle size of 10 nm [12]. Recent studies underscore the significant impact of nanomaterials in enhancing concrete properties, a development attributed to advancements in nanotechnology [13–17]. The quality of concrete is greatly affected by the characteristics of the transition zone (TZ) between the cement paste and aggregate. Incorporating nano-silica (NS) has been shown to densify the microstructure and enhance hydrated phases (C–S–H), counteracting $Ca(OH)_2$ leaching, and serve as an effective nano-filler due to NS's high pozzolanic characteristics [13, 14]. Additionally, the use of nano-silica has been proven to decrease overall permeability in hardened concrete, thereby improving its mechanical and durability characteristics [15, 18–21]. Phoo-ngernkham et al. [22] reported that the inclusion of 3% nano-$SiO2$ and nano-Al_2O_3 resulted in compressive strengths of 48.1 and 46.1 MPa and flexural strengths of 5.23 and 5.26 MPa, respectively, after 90 days.

Xavier et al. [23] found that the addition of nano-alumina to an AAC mix enhances the geopolymerization process, thereby improving mechanical performance due to the effective participation of nano-alumina in chemical activation. This performance, however, begins to decline with increased alumina content due to a weakened bond effect. The production of C-S-H/C-A-S-H in a fly ash/slag alkali-activated concrete using potassium silicate and potassium hydroxide initiates hardening. The hardening process depends on the availability of calcium ions and the system's pH, with the rapid formation of C-A-S-H, K-A-S-H, and (Ca, K)-A-S-H. Slower calcium ion dissolution rates have been shown to enhance the compressive strength of alkali-activated concrete, as prolonged geopolymerization yields better results [24]. As reported, one billion tons of fly ash are produced annually worldwide as a byproduct of burning coal for electricity [25]. According to previous studies, fly ash is a crucial raw material, often serving as a partial replacement for Portland cement in concrete technology production [26, 27]. Researchers commonly agree that fly ash is rich in aluminosilicate, with sodium hydroxide and sodium silicate being the predominant alkali binder solutions [28–30].

The GGBS slag activity index recorded was 62% after seven days and 108% after twenty-eight days. The slag composition must include at least two-thirds of the total mass of CaO, MgO, and SiO_2, with the remainder primarily comprising Al_2O_3 and a few other oxides [31, 32]. The mass ratio of (CaO + MgO) to SiO_2 should exceed 1.0 [33, 34]. Mallikarjuna & Gunneswara Rao [35] stated that using GGBS and fly ash as source materials enables alkali-activated concrete to achieve significant strength, even when cured outdoors. The higher calcium content in GGBS is believed to enhance compressive strength. Notably, particle size, alkali concentration, shape, calcium content, and the origins of fly ash and slag influence the properties of alkali-activated concrete. Furthermore, calcium content dramatically affects strength and the development of compressive strength, with higher slag content leading to quicker strength development and greater compressive strength at an early stage [36]. Therefore, this study investigates the impact of NA presence on the fresh and hardened properties, as well as the durability performance of alkali-activated mortar in an ambient environment. It also evaluates the performance of alkali-activated mortar using various combinations of fly ash and ground granulated blast furnace slag (GGBS) as sustainable alternative building materials.

2. Sustainable Building Practices: Why Fly Ash and GGBS Outperform PC

Sustainable building practices have gained increasing importance recently as the construction industry strives to diminish its environmental impact and enhance energy efficiency. In this vein, the utilization of sustainable materials is pivotal, as they can help in reducing greenhouse gas emissions, conserving natural resources, and minimizing waste. Fly ash and ground granulated blast-furnace slag (GGBS) are two such materials that have proven to surpass OPC in sustainability aspects [37].

Fly ash, a by-product of coal-fired power plants, consists of finely ground coal particles captured by pollution control equipment. When incorporated into concrete, fly ash enhances the material's strength and durability, decreases its permeability, and augments its resistance to sulfates and acids. Additionally, fly ash has a lower carbon footprint than PC, as it repurposes a waste product and reduces the demand for virgin materials [38-41]. Similarly, GGBS, a byproduct of iron and steel production, when used in concrete, improves material durability and chemical attack resistance. It also boasts a lower carbon footprint than PC, thanks to its origin from industrial waste, thereby reducing the need for virgin

materials. Moreover, GGBS has been found to diminish the heat generated during curing, making it ideal for large concrete structures [42-44]. While Portland cement is a fundamental component in concrete and widely used in construction, its production is energy-intensive and generates substantial greenhouse gases, including carbon dioxide. Additionally, the extraction of raw materials for OPC production, such as limestone, clay, and sand, can lead to significant environmental damage, including habitat destruction and soil erosion. OPC is also susceptible to chemical attacks, potentially causing concrete structures to deteriorate over time [44, 45]. Comparing the sustainability of fly ash, GGBS, and OPC involves considering embodied energy, carbon footprint, and resource depletion. In all these categories, fly ash and GGBS outperform PC, being produced from waste products and reducing the need for virgin materials. Furthermore, their application in concrete has demonstrated improvements in material durability and chemical attack resistance, thereby decreasing maintenance and repair needs over time [36, 46, 47].

In summary, the incorporation of fly ash and GGBS in construction presents numerous advantages over using Portland cement. These materials, derived from waste products, diminish the need for virgin materials and decrease the construction industry's carbon footprint. Moreover, they have shown to enhance the durability and resistance of concrete, reducing maintenance and repair needs over time. As the construction industry continues to emphasize sustainability, the adoption of fly ash and GGBS is likely to increase, presenting a sustainable alternative to traditional building materials [48].

3. Research Significance

The significance of this research lies in its exploration of sustainable building materials, specifically the use of fly ash and GGBS as alternatives to OPC in concrete. As the construction industry increasingly focuses on reducing its environmental footprint, the shift towards more eco-friendly materials becomes imperative. This study not only highlights the environmental benefits of using fly ash and GGBS but also sheds light on their practical advantages in terms of enhancing concrete's durability and strength. Firstly, the environmental impact of traditional construction practices, particularly the extensive use of PC, is a growing concern.

The production of OPC is energy-intensive, contributing significantly to greenhouse gas emissions. Additionally, the extraction of raw materials required for OPC causes considerable environmental degradation. In contrast, fly ash and GGBS, being by-products of industrial processes, offer a way to repurpose waste materials, thereby reducing landfill use and the need for virgin material extraction. Their lower carbon footprint is a vital factor in the pursuit of sustainable construction practices. Secondly, the enhanced performance characteristics of concrete made with fly ash and GGBS cannot be overlooked. This research underlines how these materials improve the strength, durability, and chemical resistance of concrete. These properties are particularly important for structures exposed to harsh environmental conditions or heavy usage. The use of these alternative materials can lead to longer-lasting buildings and infrastructure, reducing the need for frequent repairs and replacements. This not only has cost-saving implications but also minimizes the construction-related disruptions and environmental impacts over the lifespan of a structure.

Finally, this study has the potential to influence policy and practice in the construction industry. By providing empirical evidence of the benefits of using fly ash and GGBS, it could encourage policymakers and industry leaders to adopt more sustainable practices. The findings could guide regulations and standards, promoting the use of environmentally friendly materials. Moreover, this research contributes to the broader discourse on sustainable development, demonstrating practical ways the construction industry can adapt to meet global sustainability goals.

4. Material and Methods

4.1. Materials Characteristics

In the current study, nano-alumina (NA) with a ratio of 2% was utilized, characterized by particle sizes ranging from 20−30 nm in gamma shape. Three distinct types of binders were evaluated: high-calcium fly ash (FA) conforming to ASTM C 618 [49] standards, GGBS, and a combination of FA and GGBS used collectively as binding agents. Tables 1 and 2 detail the chemical compositions of these materials, as analyzed by X-ray fluorescence (XRF), and the physical properties of the binders. Furthermore, Figure 1 presents the physical appearance of FA and GGBS as observed under SEM analysis. Table 3 provides a comprehensive overview of the properties of nano-alumina. In this investigation, silica sand, with particles ≥ 500 μm, was employed as the fine aggregate.

The study also utilized a solution of sodium silicate (Na_2SiO_3) and sodium hydroxide (NaOH) as an alkali activator, maintaining a ratio of 2.5. A local supplier provided sodium silicate with a composition of Na_2O at 17.98%, SiO_2 at 28.1%, and H_2O at 53.92% by mass. This study discovered that the sodium hydroxide was 98% pure, flaky in shape, and had a molarity of 12 M, which was identified as the optimal ratio [26, 50]. Additionally, the superplasticizer Glenium 51 was obtained from the BASF Company.

Table 1. Chemical composition and physical properties of fly ash and ground granulated blast slag

Component	CaO	SiO$_2$	Al$_2$O$_3$	Fe$_2$O$_3$	MgO	TiO$_2$	SO$_3$	K$_2$O	P$_2$O$_3$	Mn$_2$O$_3$	Na$_2$O	SrO	LOI
FA (%)	15.48	48.43	17.15	11.96	1.35	2.68	0.82	0.41	0.4	0.17	0.0019	0.2	1.47
S (%)	47.75	28.17	8.6	0.42	3.89	0.94	1.45	0.29	0.06	0.47	0.02	0.076	0.2
NA (%)	-	-	99.9	-	-	-	-	-	-	-	-	-	
NS (%)		99.8											

Table 2. Physical properties of fly ash, ground granulate blast slag

Physical Properties	Specific surface area (m^2/kg)	Size (μm)	Density (kN/m^3)	Moisture content (%)	Color	Length (mm)
S	418	-	2.9	0.1	Light grey	-
FA	360	<45	<2.6	<1.0	gray	-

Table 3. Properties of nano alumina

Additives	Particle size (mm)	Purity	Color	Shape
NA	20–30	99.9%	White	Gama

Fly Ash   GGBS
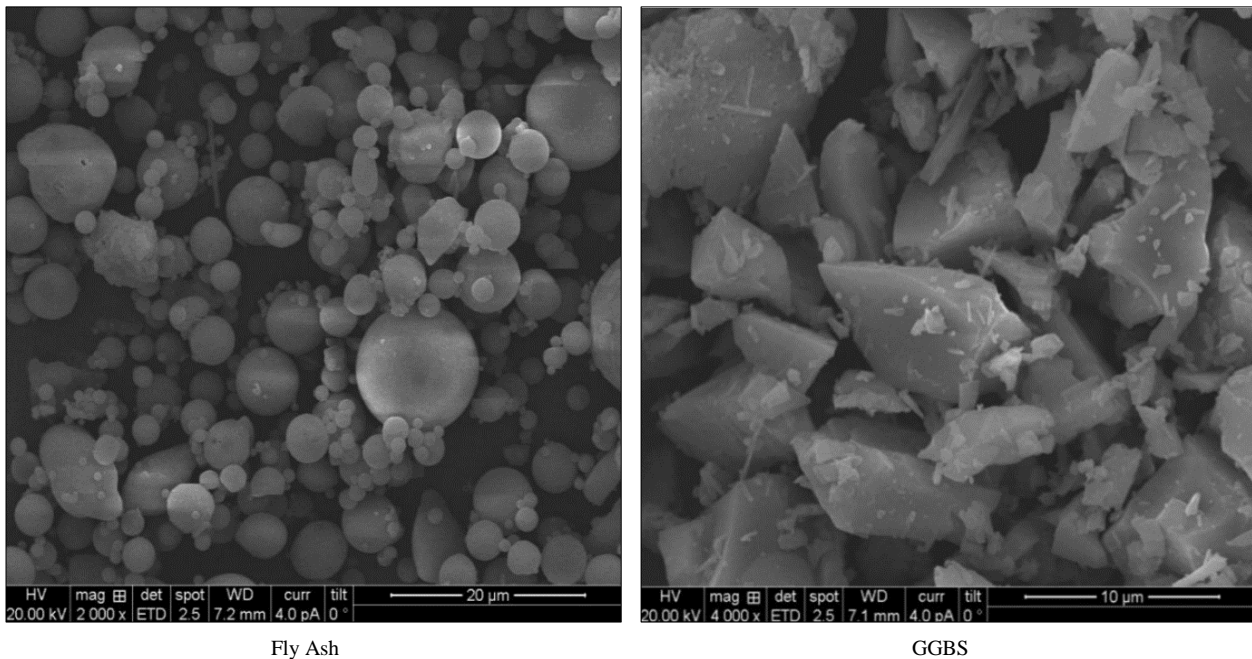
Figure 1. SEM analysis of FA and GGBS [51]

4.2. Mix Design

The mixtures incorporated 100% FA, 100% GGBS, and a 50% FA and 50% GGBS blend, each constituting a consistent total binder content of 650 kg/m^3. Drawing from prior research [50, 52-54], the study affirmed the Na2SiO3/NaOH ratio of 2.5 with 12 molarity of sodium hydroxide as the optimal proportion [55-57], hence adopting this value. The mixing process involved blending the dry materials, silica sand, FA, and GGBS, for 2.5 minutes. The nano-alumina was incrementally added to the mix and stirred for an additional 2 minutes. Subsequently, the alkaline solution and the superplasticizer were gradually introduced over a period of 1 minute to the dry mixture. Finally, the concoction was thoroughly mixed for two more minutes [14, 58]. In this experiment, nano-alumina constituted 2% of the binder's weight. Three identical specimens for each test were meticulously cast. For a visual representation of the sample preparation and testing sequence, please refer to Figure 2, which shows the flow diagram of the study's methodical approach, including how samples were prepared and tests were administered.

Table 4. Quantity of materials of alkali-activated concrete mortar (kg/m^3)

Mix. No	FA	GGBS	NA	Sodium Silicate	Sodium Hydroxide	Fine Aggregate	Superplasticizer
M1	650	-	-	92.9	232.1	1040	13
M2	-	650	-	92.9	232.1	1040	13
M3	325	325	-	92.9	232.1	1040	13
M4	637	-	13	92.9	232.1	1040	13
M5	-	637	13	92.9	232.1	1040	13
M6	318.5	318.5	13	92.9	232.1	1040	13
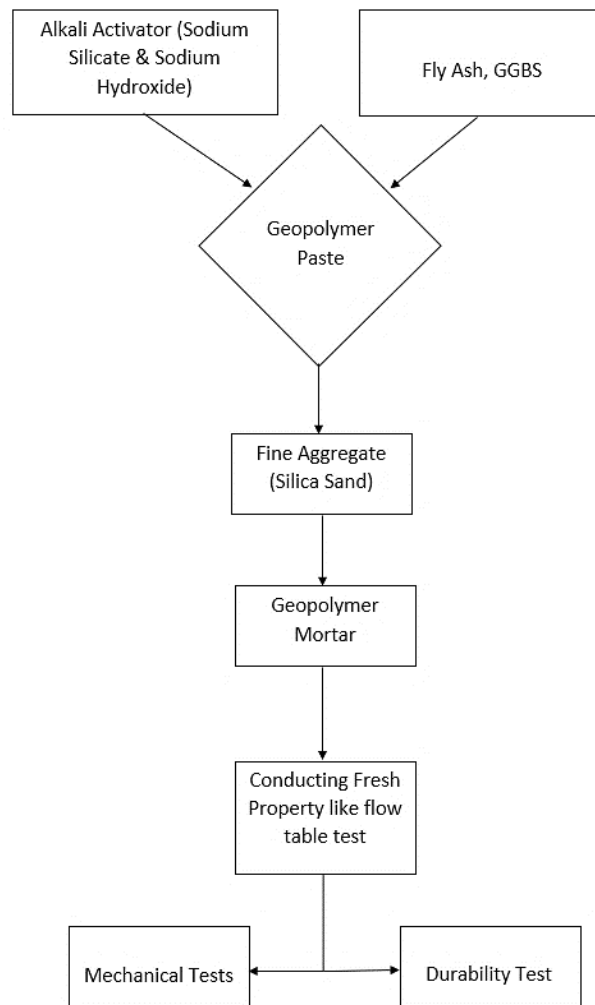
Figure 2. Experimental Workflow: A detailed flowchart that outlines the systematic methods for sample preparation and alkali-activated mortar (AAM) mix testing

4.3. Curing Condition

After casting, the specimens were shielded with plastic sheets to prevent the evaporation of the alkaline solution for 24 hours following the formation of alkali-activated concrete mortar. Post 24 hours, the specimens were carefully demolded and stored in a controlled laboratory environment at 23±3°C and 60% relative humidity for 28 days after casting.

4.4. Hardened Properties Test

The compressive strength of the AAM was evaluated in accordance with ASTM C109 [58, 59]. For each mixture, three identical specimens were tested [59]. The flexural strength was determined following ASTM C348 [60]. Specimens manifestly flawed or exhibiting strengths deviating by more than 10% from the average value of all specimens prepared from the same mix and tested concurrently were deemed non-representative and thus excluded from consideration.

5. Results and Discussion

5.1. Fresh Properties

5.1.1. Flowability

Figure 3 and 4 show the results of the laboratory test that evaluated the flowability of mixes of alkali-activated mortar (AAM). Mixtures that include fly ash (FA) and those that include ground granulated blast furnace slag have quite different flow properties (GGBS). Remarkably, AAM mixes including FA showed more flowability than those containing GGBS. Previous research has set expectations that are contradicted by this flowability discrepancy [61, 62]. The use of high-calcium fly ash as the FA in this investigation may explain why the perceived discrepancy was not as strong.
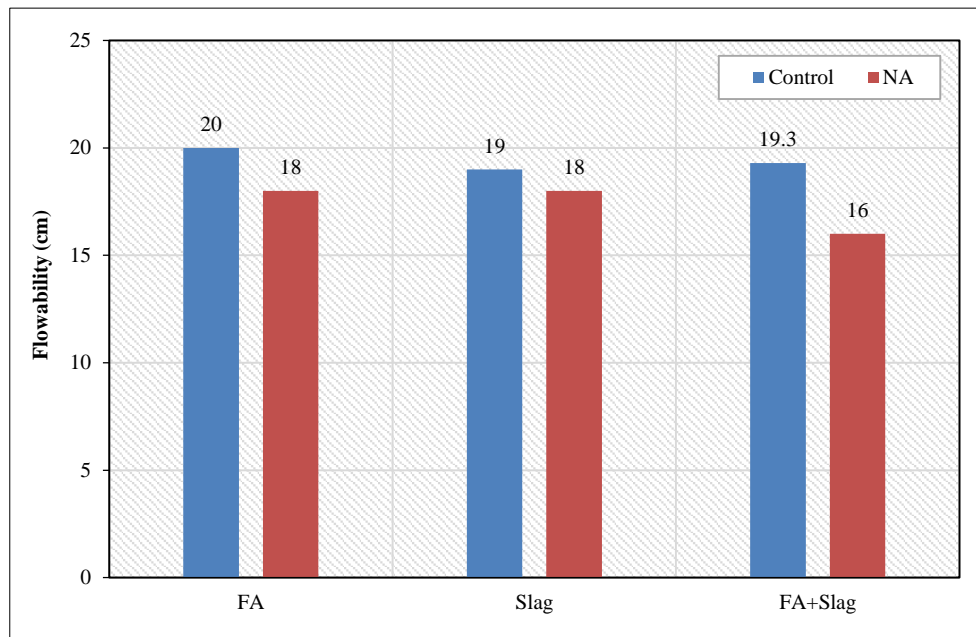
Figure 3. Flowability of AAM mixtures

Figure 4. Execution of Flow Table Test

5.1.2. Unit Weight

Figure 5 illustrates the unit weight results. Consistent with previous findings, AAM mixes with FA had a lower unit weight than those with GGBS, owing to GGBS's higher specific gravity. The addition of NA increased the unit weight of AAM mixes, regardless of the binder type, indicating that NA enhances the mixes' density and concrete microstructure [56, 57]. Research has shown that concrete's unit weight increases with the addition of nano-materials, while its permeability decreases [63].
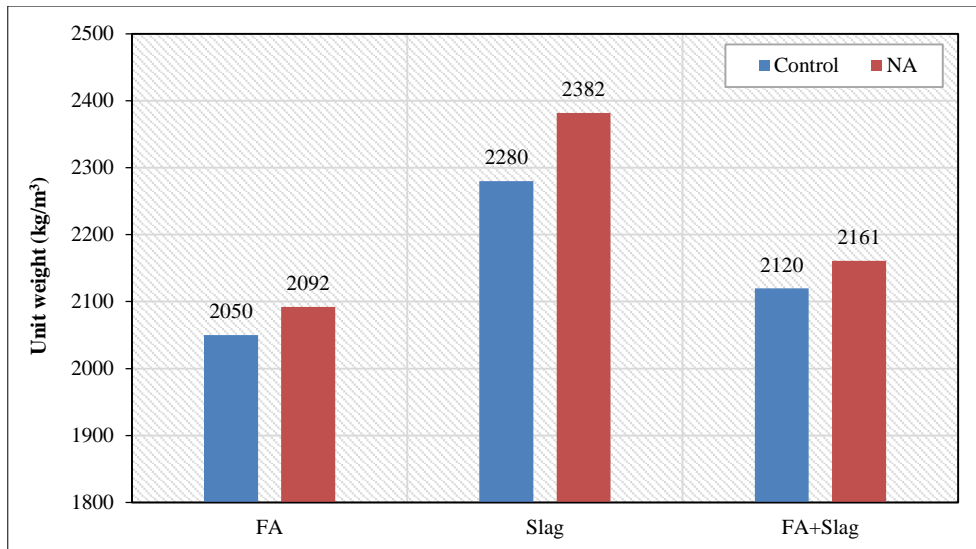
Figure 5. Unit weight of AAM mixtures

5.2. Mechanical Properties

5.2.1. Compressive Strength

Figure 6 shows the compressive strength values of AAM specimens, which show interesting trends in the effect of various binders. Incorporating ground granulated blast furnace slag (GGBS) into AAM mixtures clearly results in higher compressive strength than using fly ash alone (FA). This finding is in line with predictions, considering GGBS's pozzolanic reactivity and additional cementitious characteristics. Figure 7 depicts the sample's compressive test and can be used as an example.
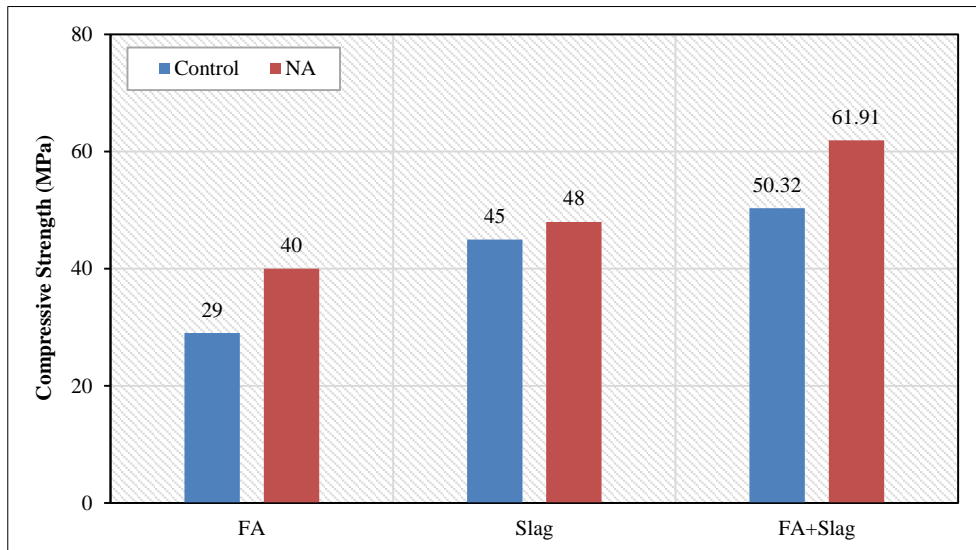
Figure 6. Compressive strength of AAM mixtures

Figure 7. Compressive Testing of AAM Sample

Using a synergistic combination of the two binders, with half FA and half GGBS, produces mixes with the highest compressive strength. All the materials' reactions and activations contributed to this outstanding performance, which is a result of a synergistic impact that improves the AAM's mechanical properties in general.

Furthermore, one of the most important factors in increasing compressive strength is the incorporation of nano-silica (NA) into the AAM matrix. Consistent with other results in concrete investigations [56, 57], this discovery reiterates the positive effect of nano-silica on the mechanical properties of materials activated by alkalis. It should be noted that mixes including FA and the combined binder ingredients exhibit a more pronounced enhancement ratio compared to blends having only GGBS. The significance of taking binder combinations into account when optimizing AAM characteristics is highlighted by this discrepancy, which implies a distinct interaction between nano-silica and the individual binders. Mixes including FA and the combined binder ingredients had a more noticeable enhancement ratio compared to mixes containing only GGBS.

5.2.2. Flexural Strength

The flexural tensile strength of AAM (see Figure 9), shown in Figure 8, also varied with the binder type. Consistent with prior research, AAM specimens with FA had lower flexural tensile strength compared to those with GGBS, attributed to GGBS's higher reactivity [62]. The addition of NA increased the flexural tensile strength of FA-inclusive mixes, but had a detrimental effect on mixes with GGBS. This indicates that NA enhances the bond strength and microstructure of concrete in FA-inclusive mixes [58]. Studies have found that incorporating 2% nano-materials increases concrete's flexural tensile strength and decreases its permeability [14]. Specimens with 2% nano-alumina acted as fillers, occupying pore spaces and enhancing the interaction between binder phases (FA and GGBFS). The AAM matrix's role is significant in enhancing the material's overall strength, as observed in SEM captures where the cohesion between reactive materials and pore spaces is strengthened with the addition of nano-alumina [57].

Figure 8. Flexural tensile strength of AAM mixtures

Figure 9. The apparatus used for conducting flexural strength tests, featuring the test devices and samples of alkali-activated mortar (AAM)

5.3. Durability Properties

Indeed, studying the water absorption characteristics in AAM mixtures plays a crucial role in understanding their durability properties. This section discusses the water absorption percentages of various AAM specimens, as shown in Figure 10. In general, the water absorption percentages observed range from 10.04% to 11.66%, indicating a moderat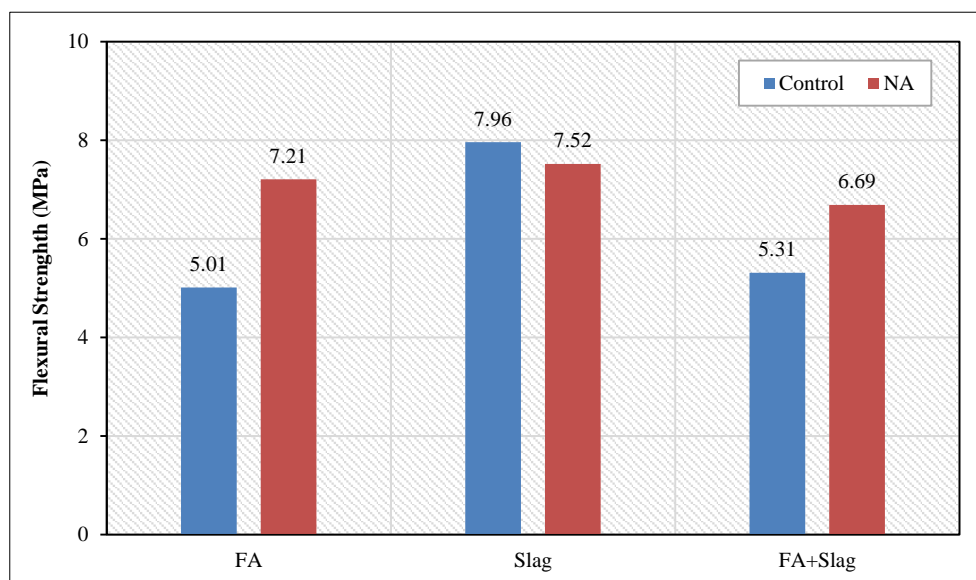e variance influenced by the constituent materials. Specimens with FA show a water absorption of 10.06%, which is relatively lower compared to GGBS at 11.02%. This suggests that FA may impart a denser microstructure to the AAM, consequently reducing the porosity and absorption capacity. In specimens where FA and GGBS are combined, the water absorption percentage is 10.26%, illustrating a slight effect where the combination of both materials does not significantly deviate from the individual values. This indicates that the complementary properties of FA and GGBS in AAM might contribute to an optimized pore structure, balancing the material's overall porosity and density. The addition of NA, particularly in combinations with FA (11.66%) and GGBS (11.15%), results in higher water absorption rates. This increase can be attributed to the high surface area of NA, which potentially increases the porosity within the AAM matrix. The lowest water absorption rate is observed in the FA+GGBS+NA combination at 10.04%, which is intriguing as it suggests that the trio-combination effectively counterbalances the individual effects of each constituent. The enhanced packing density and improved microstructural integrity achieved through this combination could be responsible for this reduced absorption rate.
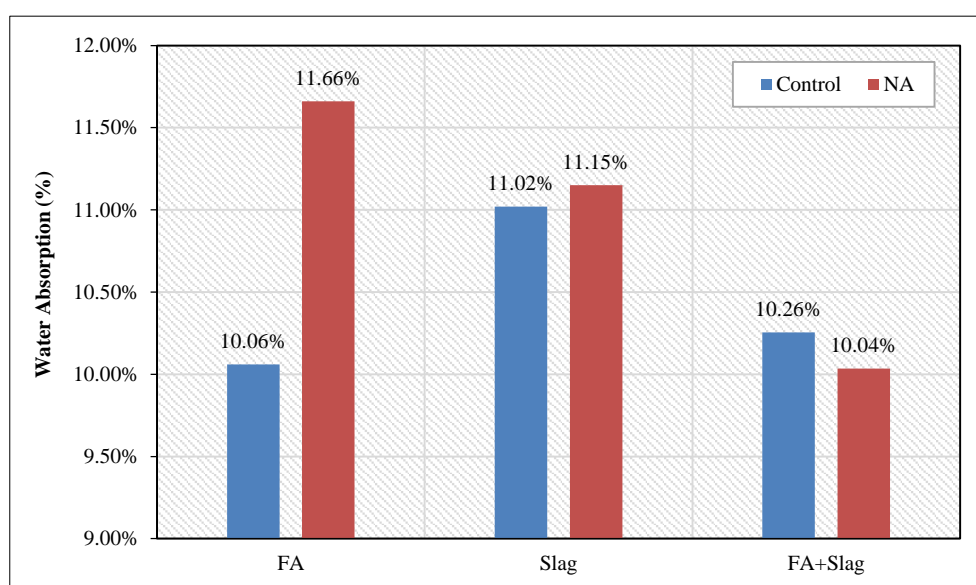
Figure 10. Water absorption of AAM mixtures

6. Conclusions

This study explored the fresh and hardened properties of AAM with an emphasis on the role of NA as a substitute for binder materials. The major findings and implications from this research are as follows, along with identified limitations and directions for future research:

- The incorporation of NA was found to negatively affect the flowability of AAM mixtures. This effect was more pronounced in mixtures that included FA compared to those with GGBS. This suggests a nuanced interaction between NA and different binder types that requires further exploration.

- All AAM mixes, regardless of the binder type, experienced an increase in unit weight with the addition of NA. This finding indicates that NA contributes to a denser mix and potentially enhances the microstructure of the concrete.

- The study confirmed that NA significantly improves the compressive strength of AAM, in line with previous research. Mixtures incorporating FA and combined binders exhibited greater strength improvements compared to those with GGBS alone.

- The flexural tensile strength of AAM specimens increased with the addition of NA in FA mixes, while a decrease was observed in GGBS mixes. This suggests that the pore-filling mechanisms of NA vary depending on the binder type, impacting the overall strength differently.

While this research offers an extensive evaluation of the mechanical and durability aspects of AAM with NA, it is limited by its focus on static conditions and a singular NA concentration of 2%. The absence of dynamic testing leaves a gap in understanding AAM's response to varied loads and environmental stresses, crucial for applications in seismic

zones or fluctuating climates. Moreover, the controlled room temperature of the experiments does not reflect the range of climatic conditions AAM might face in real-world scenarios. Future research should, therefore, prioritize dynamic testing, explore the effects of diverse environmental conditions, investigate a broader spectrum of NA concentrations, and delve into the microstructural analysis of AAM with NA to offer a more comprehensive understanding of its properties and applicability.

7. Declarations

7.1. Data Availability Statement

The data presented in this study are available in the article.

7.2. Funding

The author received no financial support for the research, authorship, and/or publication of this article.

7.3. Conflicts of Interest

The author declares no conflict of interest.

8. References

[1] McCaffrey, R. (2002). Climate change and the cement industry. Global cement and lime magazine (Environmental Special Issue), 15–19.

[2] Malhotra, V. M., & Mehta, P. K. (2008). High performance, high-volume fly ash concrete for building sustainable and durable structure (3rd Ed.). American Coal Ash Association (ACAA) Publication, Denver, United Sattes.

[3] Davidovits, J. (1991). Geopolymers - Inorganic polymeric new materials. Journal of Thermal Analysis, 37(8), 1633–1656. doi:10.1007/BF01912193.
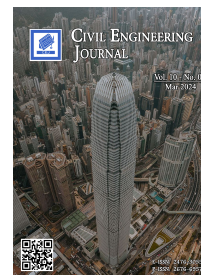
[4] Gharzouni, A., Samet, B., Baklouti, S., Joussein, E., & Rossignol, S. (2016). Addition of low reactive clay into metakaolin-based geopolymer formulation: Synthesis, existence domains and properties. Powder Technology, 288, 212–220. doi:10.1016/j.powtec.2015.11.012.

[5] Davidovit, J. (2008). Geopolymer Chemistry and Applications (5th Ed.). Geopolymer Institute, Saint-Quentin, France.

[6] Singh, B., Ishwarya, G., Gupta, M., & Bhattacharyya, S. K. (2015). Geopolymer concrete: A review of some recent developments. Construction and Building Materials, 85, 78–90. doi:10.1016/j.conbuildmat.2015.03.036.

[7] Khale, D., & Chaudhary, R. (2007). Mechanism of geopolymerization and factors influencing its development: A review. Journal of Materials Science, 42(3), 729–746. doi:10.1007/s10853-006-0401-4.

[8] Hardjito, D., Wallah, S. E., Sumajouw, D. M. J., & Rangan, B. V. (2004). On the development of fly ash-based geopolymer concrete. ACI Materials Journal, 101(6), 467–472. doi:10.14359/13485.

[9] Reddy, M. S., Dinakar, P., & Rao, B. H. (2016). A review of the influence of source material's oxide composition on the compressive strength of geopolymer concrete. Microporous and Mesoporous Materials, 234, 12–23. doi:10.1016/j.micromeso.2016.07.005.

[10] Naik, T. R. (2007). Sustainability of the cement and concrete industries. Proceedings of the International Conference on Achieving Sustainability in Construction, 19–25, doi:10.1680/asic.34044.0017.

[11] Kubba, Z., Fahim Huseien, G., Sam, A. R. M., Shah, K. W., Asaad, M. A., Ismail, M., Tahir, M. M., & Mirza, J. (2018). Impact of curing temperatures and alkaline activators on compressive strength and porosity of ternary blended geopolymer mortars. Case Studies in Construction Materials, 9, 205. doi:10.1016/j.cscm.2018.e00205.

[12] Sumesh, M., Alengaram, U. J., Jumaat, M. Z., Mo, K. H., & Alnahhal, M. F. (2017). Incorporation of nano-materials in cement composite and geopolymer based paste and mortar – A review. Construction and Building Materials, 148, 62–84. doi:10.1016/j.conbuildmat.2017.04.206.

[13] Görhan, G., Aslaner, R., & Şinik, O. (2016). The effect of curing on the properties of metakaolin and fly ash-based geopolymer paste. Composites Part B: Engineering, 97, 329–335. doi:10.1016/j.compositesb.2016.05.019.

[14] Çevik, A., Alzeebaree, R., Humur, G., Niş, A., & Gülşan, M. E. (2018). Effect of nano-silica on the chemical durability and mechanical performance of fly ash based geopolymer concrete. Ceramics International, 44(11), 12253–12264. doi:10.1016/j.ceramint.2018.04.009.

[15] Qing, Y., Zenan, Z., Deyu, K., & Rongshen, C. (2007). Influence of nano-SiO_2 addition on properties of hardened cement paste as compared with silica fume. Construction and Building Materials, 21(3), 539–545. doi:10.1016/j.conbuildmat.2005.09.001.

[16] Li, H., Xiao, H. G., Yuan, J., & Ou, J. (2004). Microstructure of cement mortar with nano-particles. Composites Part B: Engineering, 35(2), 185–189. doi:10.1016/S1359-8368(03)00052-0.

[17] Sobolev, K., Flores, I., Hermosillo, R., & Torres-Martínez, L. M. (2006). Nanomaterials and nanotechnology for high-performance cement composites. Proceedings of ACI session on nanotechnology of concrete: recent developments and future perspectives, 7 November, 2006, United States.

[18] Quercia, G., & Brouwers, H. J. H. (2010). Application of nano-silica (nS) in concrete mixtures. 8th fib Ph.D. Symposium in KGS, 20-23 June, 2010, Lyngby, Denmark.

[19] Belkowitz, J., & Armentrout, D. L. (2009). The investigation of nano silica in the cement hydration process. Master Thesis, University of Denver, Colorado, United States.

[20] Alzeebaree, R., Çevik, A., Mohammedameen, A., Niş, A., & Gülşan, M. E. (2020). Mechanical performance of FRP-confined geopolymer concrete under seawater attack. Advances in Structural Engineering, 23(6), 1055–1073. doi:10.1177/1369433219886964.

[21] Alzeebaree, R., Gülsan, M. E., Nis, A., Mohammedameen, A., & Cevik, A. (2018). Performance of FRP confined and unconfined geopolymer concrete exposed to sulfate attacks. Steel and Composite Structures, 29(2), 201–218. doi:10.12989/scs.2018.29.2.201.

[22] Phoo-ngernkham, T., Chindaprasirt, P., Sata, V., Hanjitsuwan, S., & Hatanaka, S. (2014). The effect of adding nano-SiO2 and nano-Al2O3 on properties of high calcium fly ash geopolymer cured at ambient temperature. Materials and Design, 55, 58–65. doi:10.1016/j.matdes.2013.09.049.

[23] Xavier, C. S. B., & Rahim, A. (2022). Nano aluminium oxide geopolymer concrete: An experimental study. Materials Today: Proceedings, 56, 1643–1647. doi:10.1016/j.matpr.2021.10.070.

[24] Puligilla, S., & Mondal, P. (2013). Role of slag in microstructural development and hardening of fly ash-slag geopolymer. Cement and Concrete Research, 43(1), 70–80. doi:10.1016/j.cemconres.2012.10.004.

[25] Central Electrical Authority (CEA). (2015). Report on fly ash generation at coal/lignite based thermal power stations and its utilization in the country for the year 2014-2015. Central Electricity Authority (CEA), New Delhi, India.

[26] Adak, D., Sarkar, M., & Mandal, S. (2014). Effect of nano-silica on strength and durability of fly ash based geopolymer mortar. Construction and Building Materials, 70, 453–459. doi:10.1016/j.conbuildmat.2014.07.093.

[27] Okoye, F. N., Durgaprasad, J., & Singh, N. B. (2016). Effect of silica fume on the mechanical properties of fly ash based-geopolymer concrete. Ceramics International, 42(2), 3000-3006. doi:10.1016/j.ceramint.2015.10.084.

[28] Duxson, P., Fernández-Jiménez, A., Provis, J. L., Lukey, G. C., Palomo, A., & van Deventer, J. S. (2007). Geopolymer technology: the current state of the art. Journal of materials science, 42, 2917-2933. doi:10.1007/s10853-006-0637-z.

[29] Ning, Y., Fielding, L. A., Nutter, J., Kulak, A. N., Meldrum, F. C., & Armes, S. P. (2019). Spatially Controlled Occlusion of Polymer-Stabilized Gold Nanoparticles within ZnO. Angewandte Chemie - International Edition, 58(13), 4302–4307. doi:10.1002/anie.201814492.

[30] Lee, W. H., Wang, J. H., Ding, Y. C., & Cheng, T. W. (2019). A study on the characteristics and microstructures of GGBS/FA based geopolymer paste and concrete. Construction and Building Materials, 211, 807–813. doi:10.1016/j.conbuildmat.2019.03.291.

[31] Chishi, A. K., & Gautam, L. (2023). Sustainable use of silica fume in green cement concrete production: a review. Innovative Infrastructure Solutions, 8(7), 195. doi:10.1007/s41062-023-01164-z.

[32] Khanday, S. A., Hussain, M., & Das, A. K. (2023). Durability of peat stabilized by RHA based geopolymer formed by adding pure alumina and bauxite powder. European Journal of Environmental and Civil Engineering, 27(13), 3812–3833. doi:10.1080/19648189.2022.2154851.

[33] Jethwani, R., Thakur, M. S., & Das Adhikary, S. (2020). Development of Geopolymer Concrete for Sustainable Infrastructures. Advances in Sustainable Construction Materials and Geotechnical Engineering. Lecture Notes in Civil Engineering, 35, Springer, Singapore. doi:10.1007/978-981-13-7480-7_1.

[34] Hassan, A., Arif, M., & Shariq, M. (2019). Use of geopolymer concrete for a cleaner and sustainable environment – A review of mechanical properties and microstructure. Journal of Cleaner Production, 223, 704–728. doi:10.1016/j.jclepro.2019.03.051.

[35] Mallikarjuna Rao, G., & Gunneswara Rao, T. D. (2015). Final Setting Time and Compressive Strength of Fly Ash and GGBS-Based Geopolymer Paste and Mortar. Arabian Journal for Science and Engineering, 40(11), 3067–3074. doi:10.1007/s13369-015-1757-z.

[36] Hua, X., Provis, J. L., Van Deventer, J. S. J., & Krivenko, P. V. (2008). Characterization of Aged Slag Concretes. ACI Materials Journal, 105(2), 131–139. doi:10.14359/19753.

[37] Liu, Z., Takasu, K., Koyamada, H., & Suyama, H. (2022). A study on engineering properties and environmental impact of sustainable concrete with fly ash or GGBS. Construction and Building Materials, 316, 125776. doi:10.1016/j.conbuildmat.2021.125776.

[38] Bilodeau, A., & Mohan Malhotra, V. (2000). High-volume fly ash system: Concrete solution for sustainable development. ACI Structural Journal, 97(1), 41–48. doi:10.14359/804.

[39] Gupta, S., & Chaudhary, S. (2020). Use of fly ash for the development of sustainable construction materials. New Materials in Civil Engineering, 677–689, Butterworth-Heinemann, Oxford, United Kingdom. doi:10.1016/b978-0-12-818961-0.00021-1.

[40] Nayak, D. K., Abhilash, P. P., Singh, R., Kumar, R., & Kumar, V. (2022). Fly ash for sustainable construction: A review of fly ash concrete and its beneficial use case studies. Cleaner Materials, 6, 100143. doi:10.1016/j.clema.2022.100143.

[41] Xu, G., & Shi, X. (2018). Characteristics and applications of fly ash as a sustainable construction material: A state-of-the-art review. Resources, Conservation and Recycling, 136, 95–109. doi:10.1016/j.resconrec.2018.04.010.

[42] Arivalagan, S. (2014). Sustainable studies on concrete with GGBS as a replacement material in cement. Jordan Journal of Civil Engineering, 8(3), 263–270.

[43] Higgins, D. (2007). Briefing: GGBS and sustainability. Proceedings of the Institution of Civil Engineers - Construction Materials, 160(3), 99–101. doi:10.1680/coma.2007.160.3.99.

[44] Saeed, N. M., Omer, B., Jamal, A. S., & Dheyaaldin, M. H. (2023). Performance of cement mortar modified with GGBFS at elevated temperatures with various w/b ratios and superplasticizer dosages. Construction and Building Materials, 368, 130493. doi:10.1016/j.conbuildmat.2023.130493.

[45] Pacheco-Torgal, F., & Jalali, S. (2011). Nanotechnology: Advantages and drawbacks in the field of construction and building materials. Construction and Building Materials, 25(2), 582–590. doi:10.1016/j.conbuildmat.2010.07.009.

[46] Ahmad, J., Kontoleon, K. J., Majdi, A., Naqash, M. T., Deifalla, A. F., Ben Kahla, N., Isleem, H. F., & Qaidi, S. M. A. (2022). A Comprehensive Review on the Ground Granulated Blast Furnace Slag (GGBS) in Concrete Production. Sustainability (Switzerland), 14(14), 8783. doi:10.3390/su14148783.

[47] Yilmazoglu, A., Yildirim, S. T., Behçet, Ö. F., & Yıldız, S. (2022). Performance evaluation of fly ash and ground granulated blast furnace slag-based geopolymer concrete: A comparative study. Structural Concrete, 23(6), 3898–3915. doi:10.1002/suco.202100835.

[48] Mohammed, M., Shafiq, N., Abdallah, N. A. W., Ayoub, M., & Haruna, A. (2020). A review on achieving sustainable construction waste management through application of 3R (reduction, reuse, recycling): A lifecycle approach. IOP Conference Series: Earth and Environmental Science, 476(1). doi:10.1088/1755-1315/476/1/012010.

[49] ASTM C618-22. (2002). Standard Specification for Coal Fly Ash and Raw or Calcined Natural Pozzolan for Use in Concrete. ASTM International, Pennsylvania, United States. doi:10.1520/C0618-22.

[50] Riahi, S., & Nazari, A. (2012). RETRACTED: The effects of nanoparticles on early age compressive strength of ash-based geopolymers. Ceramics International, 38(6), 4467–4476. doi:10.1016/j.ceramint.2012.02.021.

[51] T. O. (2014). Experimental Investigations on Strength, Durability, Sustainability and Economic Characteristics of Geo-Polymer Concrete Blocks. International Journal of Research in Engineering and Technology, 3(6), 115–122. doi:10.15623/ijret.2014.0306021.

[52] Assaedi, H., Shaikh, F. U. A., & Low, I. M. (2017). Effect of nanoclay on durability and mechanical properties of flax fabric reinforced geopolymer composites. Journal of Asian Ceramic Societies, 5(1), 62–70. doi:10.1016/j.jascer.2017.01.003.

[53] Saini, G., & Vattipalli, U. (2020). Assessing properties of alkali activated GGBS based self-compacting geopolymer concrete using nano-silica. Case Studies in Construction Materials, 12, 352. doi:10.1016/j.cscm.2020.e00352.

[54] Singh, B., Rahman, M. R., Paswan, R., & Bhattacharyya, S. K. (2016). Effect of activator concentration on the strength, ITZ and drying shrinkage of fly ash/slag geopolymer concrete. Construction and Building Materials, 118, 171–179. doi:10.1016/j.conbuildmat.2016.05.008.

[55] Alzeebaree, R., Çevik, A., Nematollahi, B., Sanjayan, J., Mohammedameen, A., & Gülşan, M. E. (2019). Mechanical properties and durability of unconfined and confined geopolymer concrete with fiber reinforced polymers exposed to sulfuric acid. Construction and Building Materials, 215, 1015–1032. doi:10.1016/j.conbuildmat.2019.04.165.

[56] Dheyaaldin, M. H., Mosaberpanah, M. A., & Alzeebaree, R. (2022). Performance of Fiber- Reinforced Alkali- Activated Mortar with/without Nano Silica and Nano Alumina. Sustainability (Switzerland), 14(5), 2527. doi:10.3390/su14052527.

[57] Dheyaaldin, M. H., Mosaberpanah, M. A., & Alzeebaree, R. (2022). Shrinkage behavior and mechanical properties of alkali activated mortar incorporating nanomaterials and polypropylene fiber. Ceramics International, 48(16), 23159–23171. doi:10.1016/j.ceramint.2022.04.297.

[58] Gülşan, M. E., Alzeebaree, R., Rasheed, A. A., Niş, A., & Kurtoğlu, A. E. (2019). Development of fly ash/slag based self-compacting geopolymer concrete using nano-silica and steel fiber. Construction and Building Materials, 211, 271–283. doi:10.1016/j.conbuildmat.2019.03.228.

[59] ASTM C109/C109M-20. (2020). Standard Test Method for Compressive Strength of Hydraulic Cement Mortars. ASTM International, Pennsylvania. United States. doi:10.1520/C0109_C0109M-20.

[60] ASTM C348-21. (2021). Flexural strength of hydraulic-cement mortars. ASTM International, Pennsylvanian United States. doi:10.1520/C0348-21.

[61] Mohammedameen, A., Younis, K. H., Alzeebaree, R., Arbili, M. M., & Ibrahim, T. K. (2022). Performance of Self-compacting Geopolymer Concrete with and Without Portland Cement at Ambient Temperature. Geotechnical Engineering and Sustainable Construction. Springer, Singapore. doi:10.1007/978-981-16-6277-5_52.

[62] Kurtoglu, A. E., Cevik, A., Farhan, O. H., Alzeebaree, R., Gülşan, E., & Kurtoglu, A. E.; Cevik, A.; Farhan, O. H..; Alzeebaree, R.; Gülşan, M. E. (2017). Sea Water Resistance of Fly Ash- and Slag-Based Geopolymer. 2nd International Energy & Engineering Conference, 12-13 October, 2017, Gaziantep, Turkey.

[63] Mohammedameen, A., Gülşan, M. E., Alzeebaree, R., Çevik, A., & Niş, A. (2019). Mechanical and durability performance of FRP confined and unconfined strain hardening cementitious composites exposed to sulfate attack. Construction and Building Materials, 207, 158–173. doi:10.1016/j.conbuildmat.2019.02.108.

Influence of Gypsum on the Residual Properties of Fly Ash-Slag-Based Alkali-Activated Concrete

Sandeep G. S. [1], Poornachandra Pandit [1*], Shreelaxmi Prashanth [1*], Jagadisha H. M. [1]

[1] Department of Civil Engineering, Manipal Institute of Technology, Manipal Academy of Higher Education, Manipal, Karnataka 576104, India.

Abstract

High-temperature exposures of concrete lead to serious damage in concrete structures, resulting in the significant decay of mechanical properties and spalling of concrete. Alkali-activated concretes (AAC) of blended aluminosilicate precursors and activators have been proven to have higher thermal endurance than conventional portland cement concrete. Incorporation of gypsum (GY) in alkali-activated systems has proven to positively impact the mechanical properties when adopted in controlled amounts. GY releases SO_4^{2-} to the binder system, which helps in the formation of ettringites, along with Ca^{2+}, which leads to the formation of hydrates. This causes a reduction in porosity and improves strength gain. Incorporation of GY into the fly ash-slag-based alkali-activated system further improves thermal endurance by retaining considerable residual strengths even after 800°C exposure. In the present study, the influence of GY on the residual mechanical properties of fly ash-slag-based AAC is investigated to explore the thermal endurance of the ternary mix at elevated temperatures. The mechanical properties of fly ash (FA), Ground Granulated Blast Furnace Slag (GGBS), and gypsum (GY) ternary blended AAC subjected to elevated temperatures are studied in comparison with conventional portland cement concrete (control mix). AAC design mixes with varying proportions of GY as a replacement to FA-GGBS precursor are tested for mechanical properties to obtain the optimum mix. The residual mechanical properties of the FA-GGBS-GY optimum ternary AAC mix are obtained after exposure to elevated temperatures up to 800°C. The morphology and microstructural characteristics of AAC are studied by Scanning Electron Microscopy (SEM) and Energy-Dispersive X-ray Spectroscopy (EDS) analyses to investigate the influence of gypsum on the thermal endurance of concrete when exposed to elevated temperatures. Improved thermal endurance is observed for AAC when FA-GGBS precursors are replaced with 5% of GY as compared to the thermal endurance of conventional portland cement concrete (PCC) of the same compressive strength.

Keywords: Alkali Activated Concrete (AAC); Fly Ash (FA); Ground Granulated Blast Furnace Slag (GGBS); Gypsum (GY); Elevated Temperature; Microstructure Analysis.

1. Introduction

There is a continuously increasing global demand for cement to meet the necessities and requirements of rapid infrastructure growth. This has necessitated the large-scale usage of cement in recent years. Global production of cement reached 4.1 Gt in 2019 and is expected to grow up to 12–23% by 2050 [1]. It is estimated that approximately 1 ton of CO_2 is released during the production of 1 ton of cement, accounting for about 5% of total global CO_2 emissions [2]. At present, studies are being focused on the 100% replacement of portland cement (PC) with an alternative binder to achieve sustainability in concrete production. Research on the utilization of aluminosilicate-based industrial wastes in concrete production has been trending in recent years. Alkali-activated concrete (AAC) is one of the efficient alternatives that

has the potential to replace conventional portland cement concrete (PCC). In AAC, portland cement is entirely replaced by aluminosilicates or calcium aluminosilicates like coal fly ash, blast furnace slag, metakaolin, silica fume, steel slag, zeolite, etc., and activated using an alkaline activator/s.

Fly ash (FA) is being used as a primary alternative cementitious material all over the world because of its abundance and easy availability [3–6]. More than 196 million tons of FA is being generated in India, which requires considerably large area of land for disposal. Coal-based thermal power plants are the major source of power generation in India to meet the energy demands of the large population. Coal reserves in India are expected to last for more than 100 years [5]. The utilization of FA in sustainable construction is being considered as a primary and effective means of reducing the quantity of FA that is being disposed of on the land as a landfill. AAC with FA as a primary precursor offers similar to superior mechanical and durability characteristics as compared to conventional concrete [7, 8]. The extent of these characteristics largely depends on the source and type of FA as well as the proportions of other blending ingredients used. The usage of FA as a sole precursor in AAC requires heat curing for better and faster polymerization. Also, the mechanical strength attained is moderate. Hence, the addition of calcium aluminosilicates like GGBS to FA in the production of concrete eliminates the demand for heat curing and yields moderately higher strength.

Gypsum (GY) is commonly used in the production of portland cement as a retarding agent. Most of the researchers have studied fly ash, blast furnace slag, steel slag, red mud, metakaolin, and other alumina and/or silica precursor-based binders or mortars to investigate the influence of synthetic gypsums like phosphogypsum (PG) or desulfurized/flue gas desulfurized gypsum (DG). PG is a synthetic gypsum, which is a byproduct of the fertilizer industry produced from phosphate rock, whereas DG is an industrial by-product obtained by desulfurization and purification of flue gas generated after combustion of sulfur-containing fuels (coal, oil, etc.). The phosphorus and fluorine impurities in PG demand careful reuse in concrete production. DG can be used as a substitute for natural gypsum in concrete production. However, there are certain issues and considerations associated with its use in concrete. As DG contains higher levels of sulfates compared to natural gypsum, there is a risk of sulfate attack, compromising its durability and long-term performance. Variations in the chemical composition depending on the source and the specific desulfurization process may cause inconsistencies in the quality of the concrete. Natural gypsum is obtained by mining or quarrying. The total global production of gypsum from mines in 2022 amounted to an estimated 150 million metric tons. The United States is the world's largest producer of crude gypsum and has the world's largest reserves. The abundant gypsum reserves can be utilized in the production of AAC.

In recent years, studies on blended alkali-activated binder systems have gained momentum as they offer improved properties because of the formation of silicate hydrates like calcium aluminosilicate hydrate (C-A-S-H) and sodium aluminosilicate hydrate (N-A-S-H), making the matrix of an alkali-activated system more compact and denser with a refined crack pattern than conventional concrete with a compact pore system [9, 10]. In AAC, hydroxides and silicates of sodium and potassium are commonly used as alkali activators. The gel system formed due to alkali activation in AAC depends on the properties and proportion of precursors along with the activators used. The reaction products from blended systems are complicated and different from those produced when precursors are used in isolation [11, 12]. If the precursor has a low calcium content, like FA (class F), metakaolin, etc., the major chemical reaction products formed are (N-A-S-H). While the high calcium precursors like GGBS, etc. generate (C-A-S-H) as the major reaction product. In the case of blended systems, the predominant chemical reaction products formed are the combination of (C-S-H), (C-A-S-H), and (N-A-S-H) in varying proportions. The proportions of the aforesaid reaction products depend on the proportions of CaO, SiO_2, and Al_2O_3 content in the binders [13–15].

Incorporation of GY into aluminosilicate precursors in alkali-activated materials reduces drying shrinkage and hence enhances dimensional stability [16–18]. The addition of GY has been observed to increase the compressive strength of alkali-activated materials [16, 19, 20]. GY ionizes and releases Ca^{2+} and SO_4^{2-} to a reaction system and is hence expected to improve the performance of the FA-GGBS-based alkali-activated system. However, few studies have shown detrimental effects on compressive strength depending on the proportion of the GY in the binders and the characteristics of the activators used [21–24]. Gypsum has been used as a sulfate activator in FA/slag-based geopolymer pastes, which created favorable conditions for the diffusion and penetration of ions for the activation of FA/slag precursors and led to the formation of ettringite [25]. PG promoted the alkali-activation reaction and reduced setting times when FA/GGBS was partially substituted with phosphogypsum in PG-based alkali-activated binders [26]. A 10% substitution of GGBS with PG in a 50:50 FA/GGBS blend was found to be beneficial. The increased amount of gypsum (up to 15%) in the FA/slag blended pastes was observed to increase pore distribution, which reduced capillary tension and subsequently led to drying shrinkage. Incomplete dissolution of gypsum and a reduction in the formation of ettringites and hydrates were also observed [17]. Optimal strength was obtained with the incorporation of 6% GY of precursor mass content in the FA-slag-based geopolymer cement when a large amount of slag and a small amount of FA were used [27].

The strength properties of FA-GGBS-based alkali-activated materials with DG were optimized by varying curing times and alkali activator modulus. The formation of ettringites due to the incorporation of DG was observed to fill the

tiny micro-cracks, thus forming a denser matrix [28]. DG promoted additional polymerization, ultimately resulting in increased strength in the low-alkaline reaction system. Controlling DG content is recommended to prevent volume filling effect of unreacted DG, which makes the system porous. Modification of the AAC binder matrix for a higher Si/Al ratio offers better residual mechanical strengths after elevated thermal exposures by inhibiting damage due to pore-pressure build-up [29]. When alkali-activated FA and GGBS-based geopolymers are exposed to high temperatures, the sintering reaction heals the micro/meso pores/cracks partially and reduces the adverse impact of re-crystallization on the gel skeleton, leading to the retention of mechanical strength after 600 °C exposure [30]. Higher slag content in the binder induces better mechanical properties to the FA-GGBS-based AAC, but increased brittleness is detrimental to the residual strengths of concrete. FA-based geopolymers offer moderate mechanical properties as compared to FA-GGBS binary systems. Hence, FA and GGBS ratios need to be carefully adopted in the concrete mix to get the advantage of both mechanical properties and better thermal endurance.

Studies on gypsum-based blended concretes are relatively scarce. In general terms, expansion of aggregates and shrinkage of the binder, when the concrete is exposed to elevated temperatures, result in the debonding of aggregates and binder, thus reducing the mechanical and durability properties of concrete. Studies on concrete that mimics real-world applications are needed for societal acceptance.

Concrete is exposed to high temperatures as a building material in various applications like chimneys, metallurgical industries, in case of fire accidents, etc. High-temperature exposures lead to serious damage to concrete structures, resulting in the significant mechanical decay and spalling of concrete. It is essential to adopt high-temperature-resistant concrete for the intended serviceability and to ensure the safety of life. In the present study, FA-GGBS-GY-based ternary blend AAC has been adopted, and residual mechanical properties are investigated at elevated temperatures in comparison with conventional PCC. The study focuses on the use of GY as one of the binders in the FA-GGBS-based ternary system while limiting it to 10% of the total precursor content.

This article presents an investigation on the influence of Gypsum incorporated as a partial substitution for FA-GGBS-based alkali-activated binder systems on the residual properties of FA-GGBS-based AAC. The concrete mix proportions with an alkali-activated FA-GGBS-GY binder system along with the methodology adopted to ascertain the worth of the developed concrete against thermal endurance are presented. The phases developed at each of the elevated temperature levels are presented through micro-analysis. Residual mechanical properties are also tested.

2. Materials

In the present study, FA and GGBS are used as major alkali-activated binder precursors, and the influence of the incorporation of GY as a partial replacement (up to 10%) for FA and GGBS is investigated. The chemical composition of AAC precursors is given in Table 1. SEM images and the elemental composition of AAC precursors and PC are shown in Figure 1. SEM images indicate particles of FA as spherical, GGBS as angular, GY as flaky, and PC as irregularly shaped. A combination of sodium silicate (Na_2SiO_3) and 12M sodium hydroxide (NaOH) alkaline solutions is used as an alkaline activator. M-Sand, used in the present study, conforms to Zone 1 as per IS:383 (1970), with particle sizes ranging between 4.75 mm and 150 μm. The size of coarse aggregates and their proportions in the mix are fixed to match the DIN B grading curve to achieve dense packing [31]. The combined grading of coarse aggregates adopted in the concrete mixes consists of 19% of 20 mm passing, 20% of 12.5 mm passing, 22% of 6.3 mm passing, and 39% of 4.75 mm passing. PC of grade 43 has been used in the control mix. Preliminary tests on PC, precursors, alkaline activator solutions, and aggregates are conducted and reported in Table 2.

Table 1. Chemical composition of AAC precursor materials

Component	FA (%)	GGBS (%)	GY (%)
SiO_2	61.8	40	19.83
Al_2O_3	24.98	4.1	11.63
Fe_2O_3	4.47	2.0	6.20
CaO	3.08	42.0	18.86
MgO	1.77	6.20	5.75
K_2O	0.94	-	1.47
Na_2O	0.28	-	0.05
SO_3	0.31	0.10	43.99
Loss of ignition	1-1.5	0.25	20.36
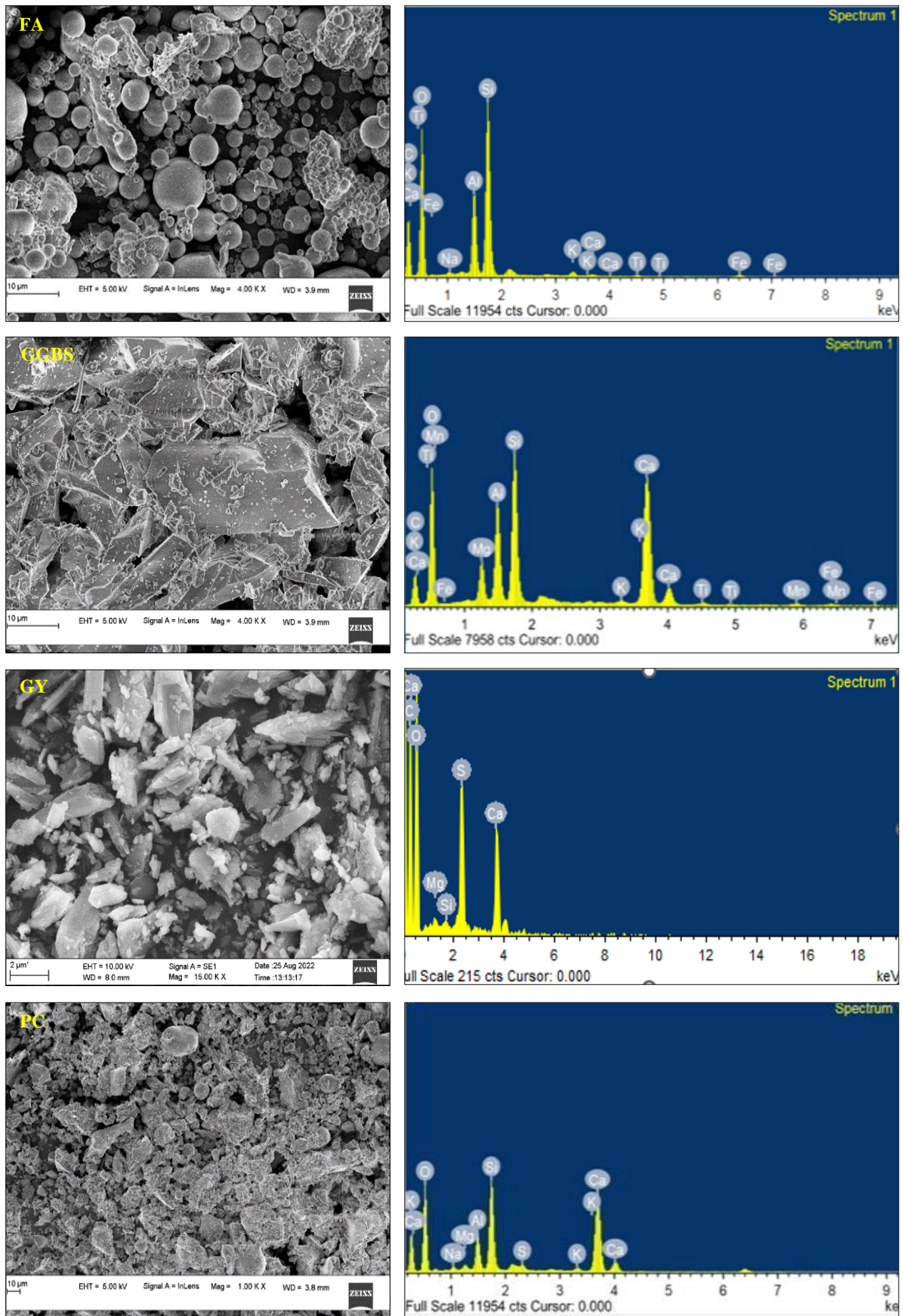
Figure 1. SEM and EDS images of AAC precursors and PC

Table 2. Properties of AAC materials

Physical Property	Raw material	
	FA (Class F)	2.12
	GGBS	2.80
	GY	2.64
Specific gravity	Sodium silicate (Na_2SiO_3) - 46.0% w/w	1.57
	Sodium hydroxide (NaOH) solution – 12M 40.4% w/w	1.46
	Coarse aggregates	2.60
	Fine aggregates	2.60
Fineness modulus	Coarse aggregates	7.76
	Fine aggregates	3.54

3. Research Methodology

The methodology adopted to investigate the influence of GY on the residual properties of FA-GGBS-based AAC in comparison with conventional PCC (control mix) is represented in Figure 2. Alkaline solution content, precursor ratio, activator (Na_2SiO_3 to NaOH) ratio, and NaOH molarity are fixed by conducting trials for designing an AAC mix of required compressive strength and workability [31]. Design mix proportions adopted in casting AAC specimens are given in Table 3. For the preparation of AAC, aggregates and precursors are dry mixed initially in the concrete mixer followed by the addition of activators. Na_2SiO_3 to NaOH activators are prepared at least 24 hours before the mixing time and mixed at least 3 hours before the concrete preparation. Mixing of concrete is continued for 3-5min to get a uniform and workable mix by adding the required amount of water. Alkali-activated ternary mixes are prepared by replacing FA-GGBS precursors with varying percentages of GY in the increments of 2.5% designated as GY0, GY2.5, GY5, GY7.5 and GY10 representing 0%, 2.5%, 5%, 7.5% and 10% replacement respectively. For PCC, 43-grade cement is used, and the concrete mix is designed as per IS:10262 (2019).
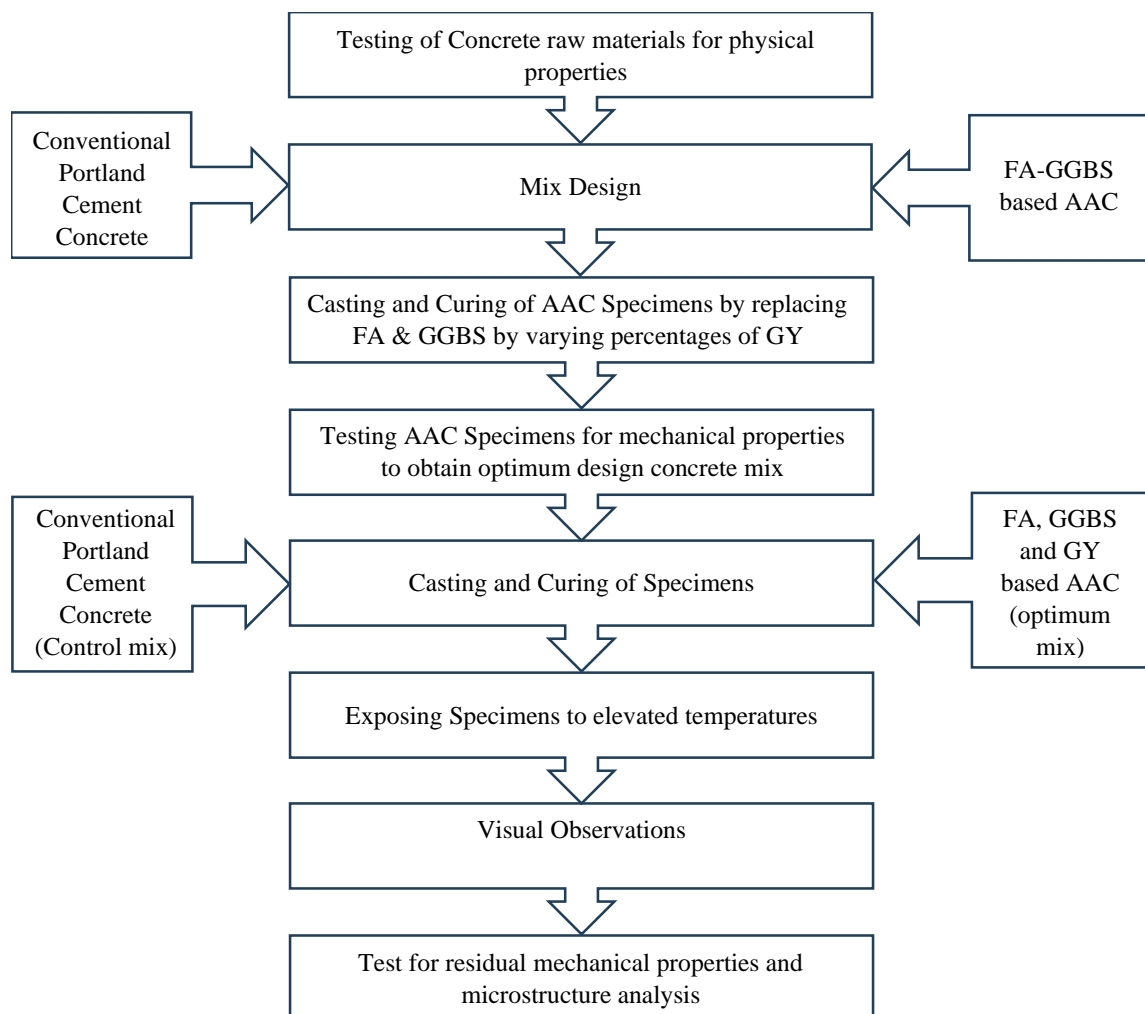
Figure 2. Methodology flow chart of the study

Table 3. Mix Proportions of AAC

Component	GY0	GY2.5	GY5	GY7.5	GY10
FA (class F) in kg/m^3	350	341.25	332.50	323.75	315
GGBS in kg/m^3	150	146.25	142.50	138.75	135
GY in kg/m^3	0	12.50	25	37.50	50
Sodium Hydroxide (NaOH) solution – 12M 40.4% w/w		57 kg/m^3			
Sodium silicate (Na2SiO3) - 46.0% w/w		143 kg/m^3			
Fine aggregates – M sand		667 kg/m^3			
Coarse aggregates		1041 kg/m^3			
(Alkali activator solution / Binder content) ratio		0.4			
Workability		50 mm slump, medium workable concrete			

Cube specimens of size 100 mm, cylinder specimens of 100 mm diameter and 150 mm height, and beam specimens of 150 mm × 100 mm × 100 mm are cast for all AAC mixes and air-cured at room temperature. Specimens are tested for mechanical properties after 7 and 28 days. The optimum AAC mix is obtained by comparing the mechanical strengths of specimens of all AAC mixes. Using optimum AAC mix; cube, beam, and cylinder specimens are cast along with PCC specimens. After 28 days of curing, one set of PCC (water curing) and AAC (air curing) specimens are tested for mechanical strengths. Another set of specimens is exposed to elevated temperatures of up to 800°C in an electric furnace. The temperature in the furnace is raised at a constant rate of 5.5°C/min. After reaching the designated temperature (200°C, 400°C, 600°C and 800°C), specimens are retained for 2 hours in the furnace [29]. After 2 hours of retention time, the furnace is switched off and allowed to cool down until room temperature is reached. The Specimens are taken out of the furnace and tested for residual strengths. Binder samples extracted from the AAC and PCC specimens after elevated temperature exposures are subjected to Scanning Electron Microscopy (SEM) and Energy-Dispersive X-ray Spectroscopy (EDS) analyses.

4. Results and Discussions

AAC specimens with varying percentages of GY are tested for compressive, tensile, and flexure strengths to obtain an AAC mix with the optimum percentage of GY. Concrete specimens with the optimum percentage of GY are then exposed to elevated temperatures to obtain the residual strengths to investigate the influence of GY on AAC. Chemical reactions between FA, GGBS, and GY led to the formation of new complex crystalline products. A few unreacted compounds of precursors are also found throughout the process of alkali activation.

4.1. The Optimum Percentage of GY as a Replacement for FA-GGBS in AAC

AAC mixes are prepared by replacing FA and GGBS with GY at varying percentages (0%, 2.5%, 5%, 7.5%, and 10%). Figure 3 shows the influence of GY on the compressive, split tensile, and flexure strengths of AAC at 7 and 28 days. Positive impact up to 5% replacement and negative impact with the increase in the percentage of replacement from 5% to 10% is observed.
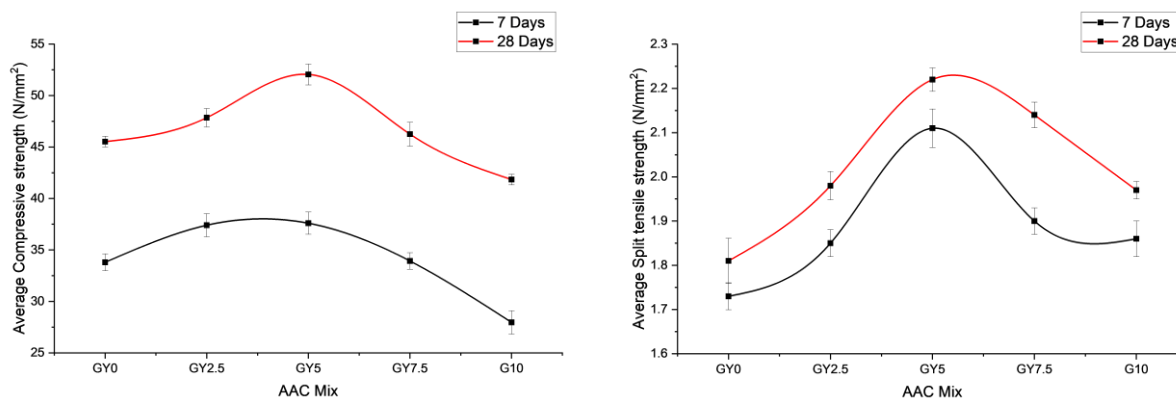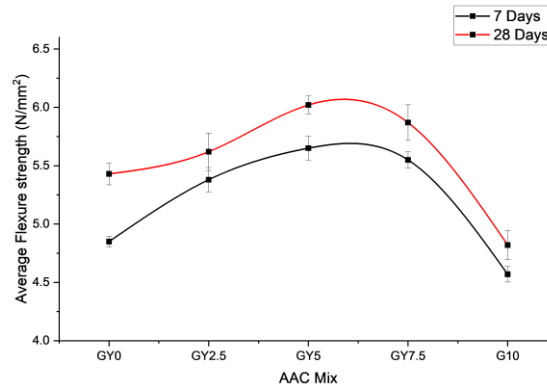
Figure 3. Variation in mechanical strengths of AAC with varying GY content at 7 and 28 days

The mechanical strengths of all AAC mixes considered for the study are tabulated in Table 4. GY5 attained 14.34%, 12.27%, and 11.07% higher compressive, split tensile, and flexure strengths respectively at 28 days than GY0. As compared to GY5, compressive, split tensile, and flexure strengths of GY7.5 are reduced by 11.14%, 3.6%, and 2.49% respectively, and 19.62%, 11.26%, and 19.93% respectively for GY10 AAC mix. According to strength tests, the AAC mix with 5% GY possessed higher mechanical strengths than the control AAC mix, GY0. However, the addition of GY beyond 5% decreased the strength of AAC. Similar results were reported in earlier studies with FA and PG [32]. Based on this observation, GY5 is considered as the optimum mix for elevated temperature exposures.

Table 4. Mechanical strengths of AAC with varying GY content at 7 and 28 days

AAC Mix	Average Compressive strength in N/mm²		Average Split tensile strength in N/mm²		Average flexure strength in N/mm²	
	7 days	28 days	7 days	28 days	7 days	28 days
GY0	33.8	45.52	1.73	1.81	4.85	5.43
GY2.5	37.4	47.85	1.85	1.98	5.38	5.62
GY5	37.6	52.05	2.11	2.22	5.65	6.02
GY7.5	33.93	46.25	1.90	2.14	5.55	5.87
GY10	27.96	41.84	1.86	1.97	4.57	4.82

Binders extracted from GY0, GY2.5, GY5, GY7.5, and GY10 AAC specimens are subjected to microstructure analysis and surface morphology is observed. SEM images of all samples considered for the study are shown in Figure 4. The chemical reactions of the ternary blend alkali activation process are complex. They involve dissolution, polymerization, and subsequent reformation of various silicate, aluminate, and calcium-based compounds. These reactions resulted in new phases, which helped to develop the strength, durability, and overall performance of AAC. The alkalis in the activator solution (NaOH and Na_2SiO_3) led to the dissolution and release of (Si^{2+}) and (Al^{3+}) from the FA. Similarly, under the action of alkalis, (Ca^{2+}) and (SiO_4^{4+}) ions were released from GGBS. Released ions combined with alkali metal ions and generated gel-like crystalline structures, primarily composed of calcium silicate hydrate (C-S-H), calcium aluminosilicate hydrate (C-A-S-H), Sodium aluminosilicate hydrate (N-A-S-H) and other compounds by polymerization in FA-GGBS-based AAC which contributed to the binding properties and strength gain in AAC [33]. GY, predominantly composed of calcium sulfate dihydrate, contributes calcium (Ca^{2+}) ions to the system in the presence of alkalis.
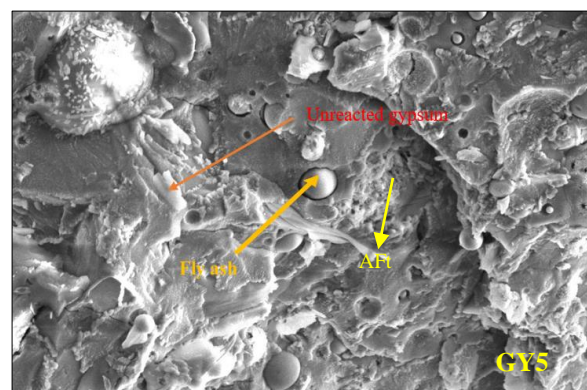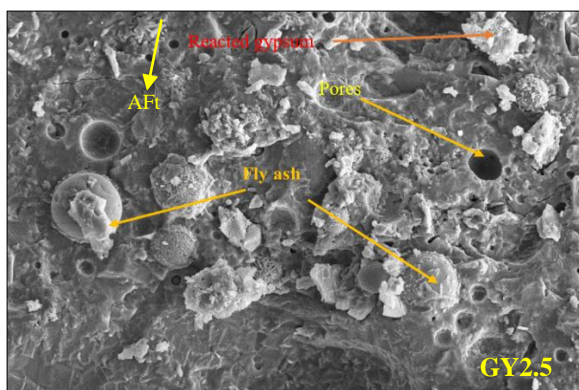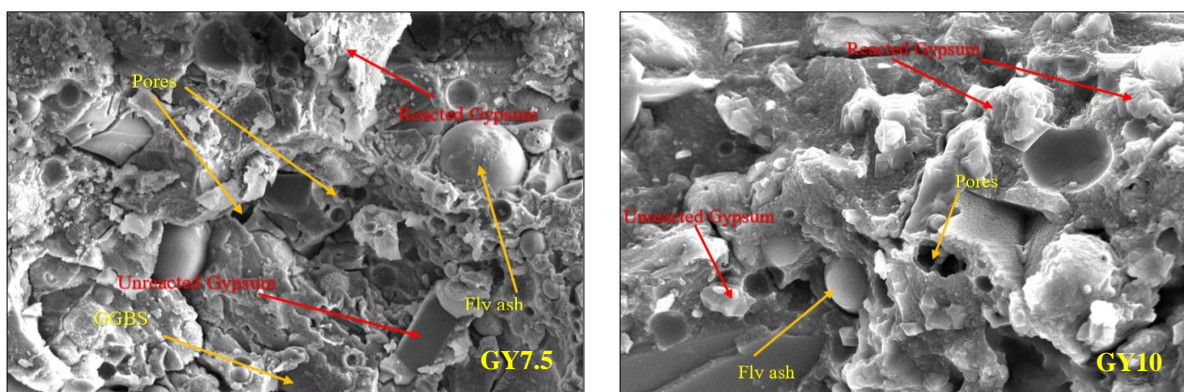
Figure 4. SEM images of AAC with varying GY content

GY in AAC ternary binder released (SO_4^{2-}) ions into the binder paste. Dissolved (Ca^{2+}) and (SO_4^{2-}) ions in the FA-GGBS-GY blend, combined with transformed aluminium hydroxide $[Al(OH)_6]^{3-}$ to form ettringite (AFt). These needle-shaped AFt crystals reduced the porosity by filling the pores, thus improving the strength [34]. Thus (C-S-H), (C-A-S-H), (N-A-S-H), and AFt are responsible for dense microstructure leading to the strength gain when GY content was ≤5%. With the increase in GY content to 7.5% and 10%, the formation of excessive AFt led to the destruction of the gel structure of AAC binders due to the volume expansion leading to increased porosity. This increased porosity subsequently led to the deterioration of the strength. Similar results were obtained in an earlier study with Desulfurization gypsum [33]. Additionally, since a certain percentage of FA-GGBS is replaced with GY, the formation of reaction products is reduced due to the lower dissolution rate of (Ca^{2+}), (Si^{2+}), and (Al^{3+}) ions. Higher $CaSO_4$ content has been proven to cause adverse effects on the formation of the (C-S-H), (C-A-S-H), and (N-A-S-H) gel [17]. SEM images of GY7.5 and GY10 AAC shown in Figure 4 indicate the existence of a considerable number of pores and unreacted precursors than GY5 AAC indicating the adverse effect of AFt and incomplete dissolution of precursors in the activator solution respectively. These are responsible for the reduction in strengths because of an increase in porosity and lesser gel formation. A larger amount of GY acts as a barrier for the formation of reaction products which reduces the cohesion in the microstructure resulting in the reduction of mechanical strengths.

Elements and elemental ratios of different AAC mixes considered for the study are listed in Table 5. An increase in the ratios of (Ca/Si), (Si/Al), (Na/Al), (Ca/(Si+Al)), and (Na/(Si+Al)) is observed with the increase in the replacement of GY with FA-GGBS up to 5% and decrease is observed with further increase in the GY replacement. Increase in the ratios of (Ca/Si), (Si/Al), (Na/Al), (Ca/(Si+Al)), and (Na/(Si+Al)) is observed from 0.769, 2.252, 0.83, 0.533, and 0.255 to 1.204, 2.990, 0.908, 0.902, and 0.228 respectively for G5 AAC mix w.r.t GY0. Higher (Ca/Si), Ca/(Si+Al), and (Na/(Si+Al)) ratios of a mix indicate a higher rate of polymerization due to enhanced dissolution of precursors leading to the formation of denser reaction products. (Ca/Si) and (Ca/(Si+Al)) ratios dominate over (Na/(Si+Al)) ratio for G5 AAC which indicate (C-S-H) and (C-A-S-H) as major crystalline reaction products formed. (Si/Al) ratio is the most critical factor for residual properties in the AAC system at elevated temperatures and the mix with a higher (Si/Al) ratio offers better resistance to elevated temperature exposures [35–37]. G5 AAC with high elemental ratios, high (Si/Al) ratio, and relatively better mechanical properties as compared to other mixes considered for the study is adopted as the optimum mix for elevated temperature exposures.

Table 5. EDS analysis of AAC samples at ambient temperature

AAC Mix	Elements (% by wt.) and their ratio								
	Na	Ca	Si	Al	Ca/Si	Si/Al	Na/Al	Ca/(Si+Al)	Na/(Si+Al)
GY0	5.33	11.13	14.46	6.42	0.769	2.252	0.830	0.533	0.255
GY2.5	2.01	8.93	10.50	3.83	0.850	2.741	0.525	0.624	0.140
GY5	3.65	14.48	12.02	4.02	1.204	2.990	0.908	0.902	0.288
GY7.5	2.72	10.50	12.96	4.90	0.810	2.644	0.555	0.587	0.152

4.2. Residual Mechanical Strengths of PCC and G5 AAC

Specimens are exposed to elevated temperatures after 28 days of ambient temperature curing for G5 AAC and water curing for PCC specimens. Electric furnace temperature is gradually increased at a constant rate of 5.5°C/min till the designated temperature i.e., 200°C, 400°C, 600°C, and 800°C is reached. Specimens are retained for 2 hours at the

designated temperature. After retention time, the furnace is switched off and allowed to cool until room temperature is reached. The specimens are taken out of the furnace and tested for mechanical strengths to investigate the influence of GY on the residual properties of FA-GGBS-GY-based AAC as compared to PCC.

The visual appearances of G5 AAC and PCC specimens after exposure to elevated temperatures are shown in Figures 5 and 6. Surface layers of PCC specimens are seen to be disintegrated and spalled off on 800^0C exposures. PCC specimens suffered a higher level of disintegration at elevated temperatures as compared to AAC specimens due to the early loss of bond between binder and aggregates because of considerable dehydration; and because of early gel structure disintegration. The binder matrix in AAC appeared to be more stable and denser than PCC binder offering better resistance to exposed elevated temperatures.

Figure 5. Concrete specimens after exposure to 800℃

Figure 6. The visual appearance of G5 AAC and PCC beam specimens after exposure to 400℃

Variations in the mechanical strengths of PCC and G5 AAC specimens at elevated temperature exposures from 200℃ to 800℃ are shown in Figure 7. Residual mechanical strengths of PCC and G5 AAC specimens after exposure to elevated temperatures relative to their mechanical strengths at ambient temperature are tabulated in Table 6. AAC specimens showed higher residual mechanical properties than PCC specimens at every exposure temperature considered. Maximum reduction in compressive strength is observed between 600℃-800℃ for PCC specimens and between 400℃-600℃ for G5 AAC specimens. Similarly, PCC and G5 AAC specimens lost maximum split tensile and flexure strengths between 200℃-400℃. After exposure to 800℃ exposure, G5 AAC specimens retained considerable mechanical properties to an extent of 25% to 47%, whereas PCC specimens lost almost 85% to 100% w.r.t ambient strengths. At 800℃, the relative residual compressive, split tensile, and flexure strengths of PCC specimens w.r.t mechanical strengths at ambient temperature are observed to be 0.15, 0.01, and 0 as compared to 0.53, 0.2, and 0.25 respectively for G5 AAC specimens. Lower cracking and spalling, and higher residual mechanical strengths of G5 AAC at higher temperature exposures indicate their better performance and hence are considered to offer excellent endurance at elevated temperature exposures as compared to PCC.
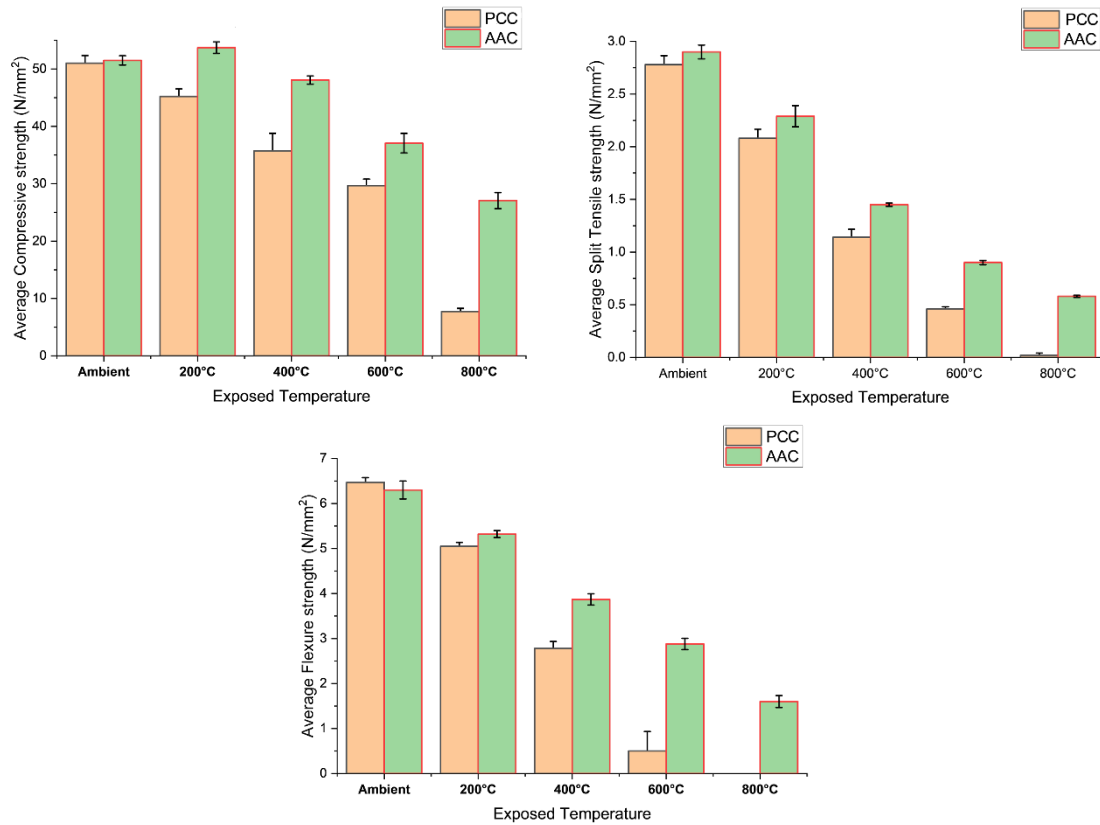
Figure 7. Residual mechanical strengths of PCC and G5 AAC specimens at different elevated temperature exposures

Table 6. Residual mechanical strengths of specimens after exposure to elevated temperatures relative to mechanical strengths at ambient temperature

	Specimens	Exposure temperature			
	Al	200 ºC	400 ºC	600 ºC	800 ºC
Relative residual compressive strengths	PCC	0.89	0.70	0.58	0.15
	G5 AAC	1.04	0.94	0.72	0.53
Relative residual split tensile strengths	PCC	0.75	0.41	0.17	0.01
	G5 AAC	0.79	0.50	0.31	0.20
Relative residual flexure strengths	PCC	0.78	0.43	0.08	0
	G5 AAC	0.85	0.61	0.46	0.25

From the SEM images of G5 AAC in Figure 8, no cracks are visible at 800°C, and minor cracks are visible at 600°C exposure. This is due to the sintering of hydrates and unreacted precursor particles which resulted in the greater inter-particle connectivity between 600°C-800°C [29]. Sintering of hydrates in G5 AAC filled up micro to macro cracks formed on exposure to elevated temperatures up to around 800°C. This in turn helped in the retention of residual mechanical strengths at elevated temperature exposures.
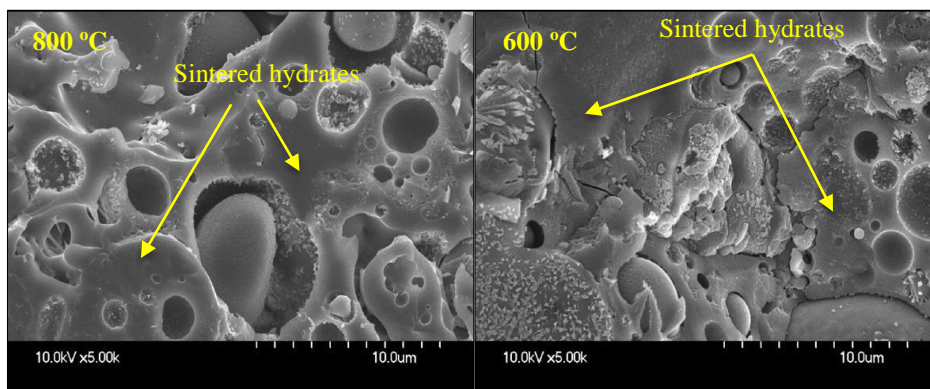
Figure 8. SEM images of G5 AAC specimens after exposure to 600°C and 800°C

EDS analysis results of PCC and G5 AAC samples are shown in Tables 7 and 8 respectively. Reduction in (Ca/Si) and (Si/Al) ratios of PCC with the increase in exposure temperature from 200°C to 800°C is observed due to the decomposition and disintegration of (C-S-H) gel which resulted in the loss of mechanical strengths. An increase in the elemental ratios of G5 AAC with the increase in exposure temperature up to 200°C is observed due to the enhanced polymerization which resulted in the increased mechanical strengths as per Table 6. At different elevated temperatures the specimens are exposed to, in the present study, the elemental ratios of G5 AAC are higher than those of PCC. This indicates a higher amount of thermal degradation of PCC gel structure than G5 AAC and thus justifies higher thermal endurance of G5 AAC than PCC with considerable residual strengths at elevated temperatures. This behavior proves G5 AAC mix is a better alternative to PCC for elevated temperature exposure applications up to 800°C.

Table 7. EDS analysis of PCC samples after exposure to elevated temperatures

Exposure Temperature	Elements (% by wt.) and their ratio				
	Ca	Si	Al	Ca/Si	Ca/(Si+Al)
Ambient	12.57	9.67	12.08	1.30	0.80
200ºC	6.15	7.88	11.76	0.78	0.67
400ºC	2.99	5.45	9.40	0.55	0.58
800ºC	2.46	5.12	11.63	0.48	0.44

Table 8. EDS analysis of G5 AAC samples after exposure to elevated temperatures

| Exposure Temperature	Elements (% by wt.) and their ratio								
	Na	Ca	Si	Al	Ca/Si	Si/Al	Na/Al	Ca/(Si+Al)	Na/(Si+Al)
Ambient	13.41	17.55	9.00	9.38	1.95	0.96	1.43	0.96	0.73
200ºC	16.74	25.97	12.92	11.24	2.01	1.15	1.49	1.08	0.69
400ºC	9.34	11.29	6.45	7.59	1.75	0.85	1.23	0.80	0.67
800ºC	5.82	5.34	3.40	6.54	1.57	0.52	0.89	0.54	0.59

5. Conclusions

- Partial replacement of FA-GGBS precursors with 5% GY in an alkali activation system is found to be beneficial in improving the mechanical properties of AAC. The microstructures of the FA-GGBS-GY ternary blended concrete showed better thermal endurance as compared to PCC and hence is a potential alternative for elevated temperature applications.

- The optimum mix design of FA-GGBS-GY-based AAC is obtained by replacing FA-GGBS (70:30) with 5% GY. The formation of ettringite (AFt) crystals filled up the initial pores and improved mechanical strength. With the increase in GY content to 7.5% and 10%, excessive ettringite (AFt) formed led to the destruction of the gel structure due to the volume expansion. This increased the porosity and deteriorated the strength.

- GY5 AAC specimens showed higher residual mechanical properties than PCC specimens at every elevated exposure temperature considered. GY5 AAC specimens offered higher resistance to spalling and cracking than PCC specimens and retained better residual mechanical properties on elevated temperature exposures up to 800℃.

- At every elevated temperature exposure considered in the present study, between 200℃ to 800℃, the elemental ratios of GY5 AAC are higher than those of PCC. This indicates a higher amount of thermal degradation of PCC gel structure than GY5 AAC. Strong gel structure, sintering of unreacted precursor particles and binder matrix at higher temperatures in AAC helped in retaining considerable residual mechanical strengths than PCC even after exposure to elevated temperatures up to 800℃. This justifies better-elevated temperature endurance of Fly ash-slag-gypsum-based AAC than PCC.

6. Declarations

6.1. Author Contributions

Conceptualization, S.G., P.P., and S.P.; methodology, S.G. and J.H.; formal analysis, S.G. and J.H.; investigation, S.G.; resources, S.G.; data curation, S.G.; writing—original draft preparation, S.G.; writing—review and editing, S.G., S.P., P.P., and J.H.; visualization, S.G. and J.H.; supervision, S.G. and J.H.; project administration, S.G.; funding acquisition, S.G. All authors have read and agreed to the published version of the manuscript.

6.2. Data Availability Statement

The data presented in the study are available in the article.

6.3. Funding

The article publishing charges was provided by Manipal Academy of Higher Education, Manipal, Karnataka, India.

6.4. Conflicts of Interest

The authors declare no conflict of interest.

7. References

[1] Guo, Y., Luo, L., Liu, T., Hao, L., Li, Y., Liu, P., & Zhu, T. (2024). A review of low-carbon technologies and projects for the global cement industry. Journal of Environmental Sciences (China), 136, 682–697. doi:10.1016/j.jes.2023.01.021.

[2] Plaza, M. G., Martínez, S., & Rubiera, F. (2020). Co2 capture, use, and storage in the cement industry: State of the art and expectations. Energies, 13(21). doi:10.3390/en13215692.

[3] Farooq, F., Jin, X., Faisal Javed, M., Akbar, A., Izhar Shah, M., Aslam, F., & Alyousef, R. (2021). Geopolymer concrete as sustainable material: A state of the art review. Construction and Building Materials, 306. doi:10.1016/j.conbuildmat.2021.124762.

[4] Provis, J. L., Palomo, A., & Shi, C. (2015). Advances in understanding alkali-activated materials. Cement and Concrete Research, 78, 110–125. doi:10.1016/j.cemconres.2015.04.013.

[5] Rastogi, A., & Paul, V. K. (2020). A critical review of the potential for fly ash utilisation in construction-specific applications in India. Environmental Research, Engineering and Management, 76(2), 65–75. doi:10.5755/J01.EREM.76.2.25166.

[6] Zhuang, X. Y., Chen, L., Komarneni, S., Zhou, C. H., Tong, D. S., Yang, H. M., Yu, W. H., & Wang, H. (2016). Fly ash-based geopolymer: Clean production, properties and applications. Journal of Cleaner Production, 125, 253–267. doi:10.1016/j.jclepro.2016.03.019.

[7] Pradhan, P., Dwibedy, S., Pradhan, M., Panda, S., & Panigrahi, S. K. (2022). Durability characteristics of geopolymer concrete - Progress and perspectives. Journal of Building Engineering, 59. doi:10.1016/j.jobe.2022.105100.

[8] Singh, B., Ishwarya, G., Gupta, M., & Bhattacharyya, S. K. (2015). Geopolymer concrete: A review of some recent developments. Construction and Building Materials, 85, 78–90. doi:10.1016/j.conbuildmat.2015.03.036.

[9] Mehta, A., Siddique, R., Ozbakkaloglu, T., Uddin Ahmed Shaikh, F., & Belarbi, R. (2020). Fly ash and ground granulated blast furnace slag-based alkali-activated concrete: Mechanical, transport and microstructural properties. Construction and Building Materials, 257. doi:10.1016/j.conbuildmat.2020.119548.

[10] Kamath, M., Prashant, S., & Kumar, M. (2021). Micro-characterisation of alkali activated paste with fly ash-GGBS-metakaolin binder system with ambient setting characteristics. Construction and Building Materials, 277. doi:10.1016/j.conbuildmat.2021.122323.

[11] Lecomte, I., Henrist, C., Liégeois, M., Maseri, F., Rulmont, A., & Cloots, R. (2006). (Micro)-structural comparison between geopolymers, alkali-activated slag cement and Portland cement. Journal of the European Ceramic Society, 26(16), 3789–3797. doi:10.1016/j.jeurceramsoc.2005.12.021.

[12] Wang, X. Y., & Lee, H. S. (2010). Modeling the hydration of concrete incorporating fly ash or slag. Cement and Concrete Research, 40(7), 984–996. doi:10.1016/j.cemconres.2010.03.001.

[13] Castellote, M., Alonso, C., Andrade, C., Castro, P., & Echeverría, M. (2001). Calorimetric study of alkaline activation of calcium hydroxide-metakaolin solid mixtures. Cement and Concrete Research, 31(2), 25–30. doi:10.1016/S0008-8846(00)00435-X.

[14] Ruiz-Santaquiteria, C., Fernández-Jiménez, A., & Palomo, A. (2016). Alternative prime materials for developing new cements: Alkaline activation of alkali aluminosilicate glasses. Ceramics International, 42(8), 9333–9340. doi:10.1016/j.ceramint.2016.03.111.

[15] Garcia-Lodeiro, I., Palomo, A., Fernández-Jiménez, A., & MacPhee, D. E. (2011). Compatibility studies between N-A-S-H and C-A-S-H gels. Study in the ternary diagram Na2O-CaO-Al2O3-SiO 2-H2O. Cement and Concrete Research, 41(9), 923–931. doi:10.1016/j.cemconres.2011.05.006.

[16] Chang, J. J., Yeih, W., & Hung, C. C. (2005). Effects of gypsum and phosphoric acid on the properties of sodium silicate-based alkali-activated slag pastes. Cement and Concrete Composites, 27(1), 85–91. doi:10.1016/j.cemconcomp.2003.12.001.

[17] Son, H., Park, S. M., Seo, J. H., & Lee, H. K. (2019). Effect of CaSO4 incorporation on pore structure and drying shrinkage of alkali-activated binders. Materials, 12(10). doi:10.3390/MA12101673.

[18] Hanjitsuwan, S., Injorhor, B., Phoo-ngernkham, T., Damrongwiriyanupap, N., Li, L. Y., Sukontasukkul, P., & Chindaprasirt, P. (2020). Drying shrinkage, strength and microstructure of alkali-activated high-calcium fly ash using FGD-gypsum and dolomite as expansive additive. Cement and Concrete Composites, 114. doi:10.1016/j.cemconcomp.2020.103760.

[19] Ghosh, A., & Subbarao, C. (2001). Microstructural Development in Fly Ash Modified with Lime and Gypsum. Journal of Materials in Civil Engineering, 13(1), 65–70. doi:10.1061/(asce)0899-1561(2001)13:1(65).

[20] Jeong, Y., Park, H., Jun, Y., Jeong, J. H., & Oh, J. E. (2016). Influence of slag characteristics on strength development and reaction products in a CaO-activated slag system. Cement and Concrete Composites, 72, 155–167. doi:10.1016/j.cemconcomp.2016.06.005.

[21] Yoon, S., Park, H., Yum, W. S., Suh, J. Il, & Oh, J. E. (2018). Influence of calcium sulfate type on evolution of reaction products and strength in NaOH- and CaO-activated ground granulated blast-furnace slag. Applied Sciences, 8(12), 2500. doi:10.3390/app8122500.

[22] Wang, D., Wang, Q., & Huang, Z. (2020). New insights into the early reaction of NaOH-activated slag in the presence of CaSO4. Composites Part B: Engineering, 198. doi:10.1016/j.compositesb.2020.108207.

[23] An, Q., Pan, H., Zhao, Q., Du, S., & Wang, D. (2022). Strength development and microstructure of recycled gypsum-soda residue-GGBS based geopolymer. Construction and Building Materials, 331. doi:10.1016/j.conbuildmat.2022.127312.

[24] Hamdan, A., Song, H., Yao, Z., Alnahhal, M. F., Kim, T., & Hajimohammadi, A. (2023). Modifications to reaction mechanisms, phase assemblages and mechanical properties of alkali-activated slags induced by gypsum addition. Cement and Concrete Research, 174. doi:10.1016/j.cemconres.2023.107311.

[25] Cong, P., & Mei, L. (2021). Using silica fume for improvement of fly ash/slag based geopolymer activated with calcium carbide residue and gypsum. Construction and Building Materials, 275. doi:10.1016/j.conbuildmat.2020.122171.

[26] Feng, Y., Xue, Z., Zhang, B., Xie, J., Chen, C., Tan, J., & Zhao, C. (2023). Effects of phosphogypsum substitution on the performance of ground granulated blast furnace slag/fly ash-based alkali-activated binders. Journal of Building Engineering, 70. doi:10.1016/j.jobe.2023.106387.

[27] Wang, Y., Huo, H., Chen, B., & Cui, Q. (2023). Development and optimization of phosphogypsum-based geopolymer cement. Construction and Building Materials, 369. doi:10.1016/j.conbuildmat.2023.130577.

[28] Luan, Y., Wang, J., Ma, T., Wang, S., & Li, C. (2023). Modification mechanism of flue gas desulfurization gypsum on fly ash and ground granulated blast-furnace slag alkali-activated materials: Promoting green cementitious material. Construction and Building Materials, 396. doi:10.1016/j.conbuildmat.2023.132400.

[29] Tu, W., & Zhang, M. (2023). Behaviour of alkali-activated concrete at elevated temperatures: A critical review. Cement and Concrete Composites, 138. doi:10.1016/j.cemconcomp.2023.104961.

[30] Luo, Y., Li, S. H., Klima, K. M., Brouwers, H. J. H., & Yu, Q. (2022). Degradation mechanism of hybrid fly ash/slag based geopolymers exposed to elevated temperatures. Cement and Concrete Research, 151. doi:10.1016/j.cemconres.2021.106649.

[31] Reddy, M. S., Dinakar, P., & Rao, B. H. (2018). Mix design development of fly ash and ground granulated blast furnace slag based geopolymer concrete. Journal of Building Engineering, 20, 712–722. doi:10.1016/j.jobe.2018.09.010.

[32] Rashad, A. M. (2015). Potential use of phosphogypsum in alkali-activated fly ash under the effects of elevated temperatures and thermal shock cycles. Journal of Cleaner Production, 87(1), 717–725. doi:10.1016/j.jclepro.2014.09.080.

[33] Wang, J., Ma, T., Luan, Y., Wang, S., & Zhang, Y. (2023). Investigation on the effects of desulfurization gypsum on the engineering properties of ternary geopolymers: Improving the utilization of industrial wastes. Journal of Cleaner Production, 414. doi:10.1016/j.jclepro.2023.137638.

[34] Li, Y., Liu, X., Li, Z., Ren, Y., Wang, Y., & Zhang, W. (2021). Preparation, characterization and application of red mud, fly ash and desulfurized gypsum based eco-friendly road base materials. Journal of Cleaner Production, 284. doi:10.1016/j.jclepro.2020.124777.

[35] Thokchom, S., Mandal, K. K., & Ghosh, S. (2012). Effect of Si/Al Ratio on Performance of Fly Ash Geopolymers at Elevated Temperature. Arabian Journal for Science and Engineering, 37(4), 977–989. doi:10.1007/s13369-012-0230-5.

[36] Lahoti, M., Wong, K. K., Yang, E. H., & Tan, K. H. (2018). Effects of Si/Al molar ratio on strength endurance and volume stability of metakaolin geopolymers subject to elevated temperature. Ceramics International, 44(5), 5726–5734. doi:10.1016/j.ceramint.2017.12.226.

[37] He, R., Dai, N., & Wang, Z. (2020). Thermal and Mechanical Properties of Geopolymers Exposed to High Temperature: A Literature Review. Advances in Civil Engineering, 2020. doi:10.1155/2020/7532703.
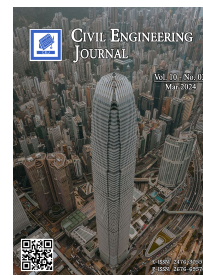
Integrating Technology and Heritage Design for Climate Resilient Courtyard House in Arid Region

Afaq H. Chohan [1*] , Jihad Awad [1] , Muhammad A. Ismail [1, 2] , Mohammad S. Arar [1]

[1] Department of Architecture, College of Architecture, Art and Design, Ajman University, Ajman, UAE.

[2] Department of Architecture, Faculty of Built Environment, University of Malaya, 50603 Kuala Lumpur, Malaysia.

Abstract

This research has investigated the sustainability and climate resilience of courtyard houses of adobe architecture in the UAE. It analyzed design effectiveness in terms of power consumption, CO_2 emissions, thermal comfort, and daylight use, employing simulations to assess building structures and construction systems. Adopting a three-phase mixed-methods approach, the study began with a literature review on courtyard house design, construction, and environmental performance, emphasizing sustainable design and passive ventilation. The second phase involved a case study of a UAE courtyard house (Al Midfa), including site visits, interviews, and energy consumption and CO_2 emission data collection. The final phase used building energy simulation software to model energy performance and evaluate passive ventilation's role in reducing energy consumption and CO_2 emissions, with simulation results validated against real-world data. Advanced Sefaira simulations with the Energy Plus Engine identified one out of seven modified models (M5) as exceptionally thermally efficient, influencing the architectural design of the Al Midfa house. To transform the Al Midfa house into a sustainable climate-resistant structure, the research suggested retrofitting with new glazing and insulation on the inside of external walls and on the roof surface at a combined U-value of 0.4 W/m^2 to enhance energy efficiency without altering the exterior. A notable innovation was the use of injected cellulose insulation in wall systems, combining efficient insulation with architectural aesthetics, signifying a shift towards energy-efficient interior modifications. The study's findings contribute to the evolution of traditional house designs toward climate change resilience and a sustainable future.

Keywords: Adobe Architecture; CO_2 Emission; Energy Consumption; Thermal Condition; Traditional Construction; Courtyard House in Hot & Dry Climate.

1. Introduction

This study emerges as a scholarly response to the escalating concerns over climate change and the resultant impact of constructed environments on greenhouse gas emissions, precipitating a heightened emphasis on environmentally sustainable design and energy preservation approaches. The principle of climate resilience underpins the development of architectural structures and infrastructural systems robust enough to endure climate change impacts [1]. While traditional courtyard dwellings are architecturally tailored to the specific climatic challenges of their locations, the integration of climate resilience with these vernacular structures has become a focal area within architectural and environmental design scholarship. Recent trends indicate an increasing inclination to merge these two domains, aiming to establish structures that are both environmentally sustainable and resilient, aligning seamlessly with local ecological contexts.

---

* Corresponding author: a.chohan@ajman.ac.ae

The standard traditional courtyard house, especially when constructed using Adobe technology, is characterized by the employment of earthen materials and has historically represented a paradigm of sustainable architecture. In the contemporary context of climate change, such courtyard architectures have been recognized for their inherent sustainability and passive design principles. The thermal mass attributes of adobe materials in these structures significantly contribute to their energy efficiency. Adobe walls, with their capacity to absorb, retain, and subsequently dissipate heat, play a pivotal role in stabilizing indoor temperatures, thereby diminishing the dependence on mechanized temperature regulation systems. This contributes to a reduction in energy consumption while simultaneously elevating the thermal comfort of the inhabitants [2].

Adobe technology not only lends a contextually harmonious and aesthetically pleasing aspect to courtyard houses but also amplifies their eco-friendly characteristics. Utilizing local natural resources like clay, sand, and straw, adobe construction minimizes the environmental impact and carbon emissions associated with building processes [3]. In traditional courtyard houses, the fusion of natural adobe materials is always linked with aesthetic considerations. The case study of Al Midfa House demonstrated how the use of earthen materials fosters a seamless blend between the built environment and its natural surroundings, preserving the cultural and architectural essence of traditional courtyard houses in the UAE and similar arid regions. However, integrating such traditional structures into contemporary urban settings presents considerable challenges.

In the context of the urban setting of courtyard houses, Baiz & Fathulla [4] delved into the incorporation of courtyard housing in Baghdad's urban areas, underscoring the climatic advantages of courtyards, such as enhanced natural ventilation and thermal comfort, and proposing them as sustainable urban housing solutions. Considering the courtyard as a vital outer space in traditional houses of the hot and arid climate of Amiriparyan & Kiani [5], they examined the central courtyard's pivotal role in traditional Iranian houses, particularly in historic cities like Isfahan, Shiraz, and Yazd. The study emphasized the courtyard's importance in both urban planning and intra-house spatial organization, highlighting its contribution to creating cohesive and continuous living spaces, thereby shaping the architectural narrative of 17th- to 19th-century Iranian homes. Regarding the interrelation between design and orientation of courtyards, additional studies have scrutinized the impact of courtyard spatial patterns on microclimate conditions in regions experiencing hot summers and cold winters. These investigations have illuminated the pivotal role of courtyard design and orientation in fostering sustainable and energy-efficient environments [6–8].

Subsequently, continuing on the influence of shape geometry and spatial arrangement over courtyard efficiency, Soflaei et al. [9] have explored how courtyard design and layout impact the microclimate and sustainability of traditional houses in Iran's hot-arid region. The study assessed courtyards' physical and environmental characteristics that enhance energy efficiency, examining six houses in Kerman and Isfahan. The study, using the Koppen climate classification, developed design guidelines and formulas based on courtyard dimensions and proportions, offering a blueprint for sustainable building designs applicable in similar climates. Similarly, another study by Sun et al. [10] investigated the role of enclosed patios in climate adaptation and microclimate regulation in buildings. Their research developed design guidelines to improve thermal comfort, utilizing both qualitative and quantitative methods. The study identified crucial design aspects, such as maintaining proportional dimensions, increasing window numbers, and adding semi-open spaces. Notably, optimal designs for four-sided and three-sided patios were determined, enhancing both the thermal efficiency and aesthetic appeal of these spaces.

In addition, Soflaei et al. [11] and Benoudjafer [12] explored the synergy between natural energy, vernacular architecture, and adobe technology, elucidating the thermal comfort and energy efficiency afforded by adobe in hot arid climates' courtyard houses. Concurrently, Nguyen & Reiter [13] examined passive and low-energy cooling strategies suitable for hot, humid regions, emphasizing Adobe technology's contribution to enhancing thermal performance in courtyard houses. Kamal & Rahman [14] conducted a comprehensive study on the historical, current, and future roles of earth architecture, particularly adobe technology, in courtyard houses. They emphasized the sustainability and energy efficiency prospects of these materials. Investigations into the influence of courtyard geometry on summer microclimate in traditional buildings underscored the imperative of optimizing courtyard dimensions to enhance thermal mitigation capabilities [15, 16]. Additionally, Vellinga [17] offered a historical perspective on courtyard housing, discussing the potential limitations of passive thermal comfort and ventilation in these traditional structures.

The discussion above can be summarized as that the use of adobe technology, along with the implementation of passive ventilation techniques, courtyard spatial morphology, and microclimate considerations, can greatly improve thermal comfort in hot and arid climates. Studies of traditional adobe houses demonstrate the effectiveness of these traditional methods in achieving energy-efficient and sustainable house design. By reviving and incorporating these techniques into modern architecture, we can create comfortable living spaces that minimize the use of energy and promote sustainable living.

In addition to the above research, many simulation experiments and studies have been conducted to measure the design of traditional adobe courtyards towards sustainability, thermal effectiveness, and hybrid living space. Al-Hafith et al. [18] evaluated DesignBuilder's ability to simulate courtyard thermal behavior, uncovering significant discrepancies

between its simulations and real-world measurements. The study found DesignBuilder's modeling often inaccurately predicts heat gain and air temperature due to challenges in replicating the effects of heat radiation, natural ventilation, and shading. This highlights the complexity of accurately simulating courtyard thermal dynamics in software like DesignBuilder. Besides, Abdulkareem [19] investigated the high energy consumption of mechanical air-cooling in the Middle East and proposed the use of traditional architecture for energy efficiency. The study emphasized optimizing courtyard microclimates to enhance thermal comfort and advocated integrating traditional methods with renewable energy strategies for sustainable architecture, moving beyond superficial revivals to a holistic approach combining historical and modern practices.

Saadatjoo et al. [20] have analyzed the microclimatic effects and ventilation in semi-outdoor spaces using computational fluid dynamics (CFD). Their study of various apartment buildings with differing terrace widths and porosity levels showed that porosity increased internal air velocity, although not significantly. Double-sided models were found to be more effective than single-sided or lateral ones in air regulation, with a unique correlation observed between terrace and courtyard air velocities. This suggests double-sided models as balanced designs for optimal airflow. Continuing with experimentation through simulation modeling, Han et al. [21] have explored how different spatial layouts affect courtyard microclimates using field measurements and ENVI-met simulations. Key factors like air temperature, solar radiation, airflow, and humidity were examined. The study found that ground coverings greatly influence temperature and humidity, recommending a specific mix of lawn, marble, water, and trees to optimize courtyard conditions, especially in library courtyards. The study recommends a combination of lawn, marble, water surfaces, and landscape tree coverage in proportions of 25%, 25%, 50%, and 75%, respectively, as optimal design elements for improving the microclimate conditions in the inner courtyards of libraries.

In the context of the courtyard's thermal comfort, Ibrahim et al. [22] have studied optimizing courtyard blocks for thermal moderation in various climates, particularly focusing on Cairo's hot-arid environment. The study used Grasshopper and Ladybug tools in Rhino 3D to analyze design parameters like cooling loads and the Universal Thermal Climate Index. It found that minimizing interspaces in courtyard blocks across three different extension types was most effective for thermal efficiency, offering crucial insights for urban design in hot-arid climates. Similarly, another study through simulation has also explored the issues of thermal comfort and daylight provision and suggested moderation in courtyard design. Besides, Guedouh et al. [23] have investigated the balance between thermal and luminous environments in courtyard buildings in hot, arid regions. Through on-site measurements and DesignBuilder simulations, they analyzed different building morphologies. The study found that while courtyards excel at daylighting, their thermal regulation is less effective. This research helps identify optimal designs for enhancing both daylight and thermal efficiency in challenging hot and arid climates. Continuing with the assessment of thermal comfort of courtyards, another study has presented the concept of ATC (adaptive thermal comfort) in courtyard houses. The study investigated the effect of seasonal occupant movement on thermal comfort in courtyard houses. Their study highlighted that traditional behaviors significantly boost Adaptive Thermal Comfort (ATC), especially during winter in northern courtyard zones, where ATC can increase by 10.1 to 23.7%. This research emphasizes the value of vernacular strategies in enhancing indoor thermal comfort [24]. Furthermore, the Courtyard Thermal Usability Index (CTUI) was developed to improve the thermal efficiency of courtyards in hot climates, focusing on Baghdad. This index calculates the percentage of comfortable hours relative to total use. Analyzing 360 courtyards with Envi-met 4.2, the study found that courtyards in Iraq offer only 38% comfortable hours annually. Key factors affecting thermal comfort include the courtyard's width-to-height ratio and the Mean Radiant Temperature (MRT), providing insights for designing efficient courtyards in hot climates [25].

Regarding the interrelationship between the thermal comfort of a courtyard and its design in an urban context, Taleb & Abumoeilak [26] have conducted a study to optimize courtyard designs for thermal performance in urban communities in hot arid regions, focusing on Dubai's sustainable city residential cluster. Utilizing ENVI-met software, they simulated and compared four courtyard layouts: U-shaped, linear, central buildings with square courtyards, and U-shaped buildings with square courtyards. The simulations evaluated outdoor thermal behavior, wind speed, and humidity distribution. Their findings showed that the fourth scenario, U-shaped buildings with square courtyards, significantly improved microclimatic conditions, reducing relative humidity from 56.27 to 48% and temperature from 43.03 to 41.03°C. Whereas, Sahebzadeh et al. [27] explored 11 strategies and tools used traditionally in Iran to establish sustainable, comfortable homes in its extreme climates. These strategies include optimizing density, orientation, introversion, seasonal design, local materials, ground thermal capacity, natural ventilation, wall properties, insulation, native elements, and integrating water and plants. Tools like courtyards, Showãdãn, and Bahãr-khãb were discussed. The research provides a comprehensive guideline for sustainable building practices in Iran and the Middle East's harsh climates.

The discussion above asserts that a courtyard in a hot and arid region acts as an ecological battery, severing its occupants both in summer and winter. However, its importance cannot be ignored in humid climates as well. It has been explored that, despite courtyards' declining use in new housing in tropical regions, their potential for promoting passive ventilation and daylight is significant. The study from a humid region found that in courtyards, polycarbonate shading

elements hinder ventilation while increasing shade. Utilizing simulations, the research examined the configurations of various courtyard terrace houses in Penang, Malaysia. Results indicated that a semi-enclosed courtyard with shading devices optimizes environmental conditions, contributing to the design of modern terrace houses in hot-humid climates [28].

The review above about courtyard houses has been conducted in the context of their thermal comfort, shape, orientation, material application, and adaptive applications. This review suggests that a low-energy consumption strategy in courtyard houses has the potential to significantly reduce energy consumption and improve sustainability. Passive solar design, natural ventilation and cooling, and the use of renewable energy sources can all contribute to achieving low energy consumption. However, careful consideration of various factors such as climate, site location, thermal mass, and occupant behavior is necessary to maximize the effectiveness of these strategies. Overall, the design of low-energy-consumption courtyard houses is a promising approach to sustainable housing design. To summarize the review above, Table 1 has been assembled to extract the key findings of previous studies.

Table 1. Literature Review Key Findings

No	Study	Key Findings
1.	[18]	DesignBuilder struggles with accurate simulation of courtyard thermal behavior, especially in replicating heat radiation, natural ventilation, and shading.
2.	[19]	Investigated high energy use of mechanical air-cooling in the Middle East and advocated for traditional architecture for better energy efficiency.
3.	[20]	Studied microclimatic effects in semi-outdoor spaces, finding porosity slightly increases air velocity; double-sided models are more effective.
4.	[9]	Explored courtyards' impact on microclimate in Iran's BWks region, providing sustainable building design guidelines based on courtyard properties.
5.	[21]	Examined how various ground coverings in courtyards affect microclimates, suggesting specific material combinations for optimal conditions.
6.	[22]	Focused on optimizing thermal efficiency of courtyard blocks in Cairo's hot-arid climate using Grasshopper and Ladybug-tools.
7.	[23]	Investigated the balance between thermal and luminous environments in hot, arid courtyard buildings, finding courtyards excel in daylighting but not in thermal regulation.
8.	[10]	Developed design guidelines for enclosed patios to enhance thermal comfort, identifying key design elements for optimal thermal efficiency.
9.	[5]	Highlighted the central courtyard's role in traditional Iranian houses, emphasizing its importance in urban planning and intra-house spatial organization.
10.	[24]	Investigated how seasonal occupant movement affects thermal comfort in courtyards, finding it significantly enhances Adaptive Thermal Comfort (ATC).
11.	[25]	Developed Courtyard Thermal Usability Index (CTUI) for Baghdad courtyards, showing courtyards in Iraq offer 38% comfortable hours annually.
12.	[28]	Explored ways to enhance environmental conditions in terrace house courtyards in hot-humid climates, finding semi-enclosed courtyards with shading devices most effective.
13.	[27]	Provided a comprehensive guideline of 11 strategies and tools for sustainable, comfortable homes in Iran's extreme climates.
14.	[26]	Studied courtyard design optimization for thermal performance in hot arid regions, identifying U-shaped buildings with square courtyards as best for microclimatic conditions.

In the context of climate resilience in traditional courtyard houses, Table 2 highlights specific research gaps that have been instrumental in shaping the direction of this study. While existing research provides a substantial foundation on the role and design of traditional courtyard houses in mitigating climate impacts, there remain unexplored areas that hold significant potential for enhancing our understanding of climate resilience in these structures. Recognizing these gaps, this study aims to delve deeper into aspects that have been overlooked or insufficiently addressed in previous research.

Table 2. Research Focus and Gaps in Comparative Studies

Research focus	Comparative studies addressing the focus	Identified gaps in research
Design and Adobe Construction Courtyard House	[5, 9]	Limited exploration of adobe construction techniques in courtyard houses.
Courtyard House as Low Energy Model	[19, 26, 28]	Need for more studies on the adaptation of courtyard designs in modern low-energy models.
Inner Thermal Comfort of Courtyard House	[10, 18, 20, 24]	More research on specific strategies to enhance inner thermal comfort in different climatic conditions is required.
Adaptation to Climate Resilient Design Techniques	[10, 19, 27]	Further exploration of adapting traditional design techniques for modern climate resilience is needed.
Transforming Existing Courtyard House in UAE as Low Energy Climate Resilient Living.	[26]	A gap exists in comprehensive studies specifically focused on transforming existing courtyard houses in the UAE for energy efficiency and climate resilience.

2. Research Validation

This research comprehensively addresses the identified gaps in Table 2 by integrating traditional and contemporary design philosophies. It aims to expand the exploration of adobe construction techniques in courtyard houses, considering their natural insulation properties and suitability for hot climates. The study focuses on courtyard houses as low-energy models, investigating how their traditional design can be adapted to modern sustainable practices. This includes enhancing inner thermal comfort through innovative, climate-responsive strategies, particularly in diverse climatic conditions.

Moreover, the research delves into adapting traditional design techniques for modern climate resilience. This involves exploring how these age-old methods can be synergized with advanced technologies to create sustainable, climate-resilient living spaces. A significant part of the study is dedicated to transforming existing courtyard houses in the UAE into models of low-energy, climate-resilient living. This includes detailed case studies and practical implementations, considering the unique environmental and cultural context of the UAE. The findings contribute to sustainable urban development, offering insights into preserving architectural heritage while meeting contemporary environmental challenges.

3. Factors Contributing to Climate Change in Gulf Countries

Climate change is a global issue that affects every nation, and Gulf countries are no exception. The Gulf region is home to several countries, including the UAE, that are highly vulnerable to climate change due to their geographic location, extreme weather conditions, and dependence on fossil fuels [29]. This section aims to assess the factors contributing to climate change in Gulf countries and provide an understanding of their impact on the environment.

The Gulf region is known for its high temperature and humidity levels, which can contribute to the increased use of air conditioning and, thus, higher energy consumption. The energy sector in Gulf countries is heavily reliant on fossil fuels, leading to high levels of greenhouse gas emissions [30]. Additionally, rapid urbanization and industrialization have increased the demand for energy and transportation, further exacerbating the environmental impact of these activities [31]. Some other studies outline the other factors contributing to climate change in Gulf countries, including desertification, soil degradation, and water scarcity. The lack of sustainable farming practices, coupled with excessive use of water resources, has resulted in a decline in soil fertility and productivity. The Gulf region is also one of the most water-scarce areas in the world, with high levels of water consumption and low levels of renewable water resources [32, 33].

To address these environmental challenges in GCC countries, various potential solutions have been proposed. One solution is to diversify the energy mix by promoting renewable energy sources such as solar and wind power [34]. The implementation of sustainable farming practices, such as drip irrigation and the use of drought-resistant crops, can help reduce water consumption and improve soil fertility [35]. Additionally, the promotion of public transportation and the use of electric vehicles and hydrogen fuel cells can help reduce the environmental impact of transportation [36–38].

The above studies can be summarized as, the Gulf countries face significant challenges regarding climate change, including high levels of greenhouse gas emissions, energy consumption, and water scarcity. These challenges require a comprehensive and coordinated approach involving the government, private sector, and civil society. Solutions such as the promotion of renewable energy, sustainable housing, farming practices, and public transportation can help address these challenges and ensure a sustainable future for the Gulf region.

4. Research Aims and Objectives

The concept of low energy consumption in courtyard houses has gained popularity in recent years due to its potential for reducing energy usage and improving sustainability in housing design. This study aims to explore the effectiveness of courtyard house design in climate resilience and change scenarios. By evaluating energy consumption, CO_2e emission materials, their thermal performance, daylighting usability, and resilience factors, the research seeks to provide valuable insights into designing environmentally friendly and energy-efficient buildings.

The primary objectives of this research are to:

- Investigate the Emirati courtyard house in the context of adobe architecture design and construction.
- Analyze the challenges of courtyard house design and its effectiveness as a sustainable model and climate resilience.

Evaluate the effectiveness of power consumption and CO_2e, thermal comfort, daylight utility, and climate resilience of building structures and construction systems through simulation.

5. Methodology

The research employs a mixed-methods approach, combining both quantitative and qualitative data collection and analysis. This research is conducted in three phases. In the first phase, a comprehensive literature review is conducted to gather information on the design and construction of courtyard houses, their historical and cultural contexts, and their environmental performance. The review focuses on the principles of sustainable design, passive ventilation, and wind catcher effectiveness. In the second phase, a case study was conducted in a selected courtyard house in the UAE, and its architectural design and construction were analyzed to identify key design elements that contribute to low energy consumption. Besides this qualitative case study, analysis involved site visits, interviews with architects, engineers, and building occupants, and the collection of data on energy consumption and CO_2 emissions.

The data collected through the literature review and case study analysis was filtered to identify trends and relationships between the variables of interest. The third phase involves the creation of a simulation model to evaluate the energy consumption and CO_2 reduction potential of courtyard houses. This involves the use of building energy simulation software, such as Sefaira, to model the energy performance of a typical courtyard house. A building performance simulation is carried out to assess the effectiveness of passive ventilation in reducing energy consumption and CO_2 emissions in courtyard houses. The simulation is based on energy usage and CO_2 emissions, thermal comfort, and daylighting Plus software and considers various scenarios for ventilation and insulation. In the final phase, the simulation results are analyzed and compared to real-world data to determine the accuracy and validity of the simulation model. Figure 1 shows the flow diagram of the research methodology.
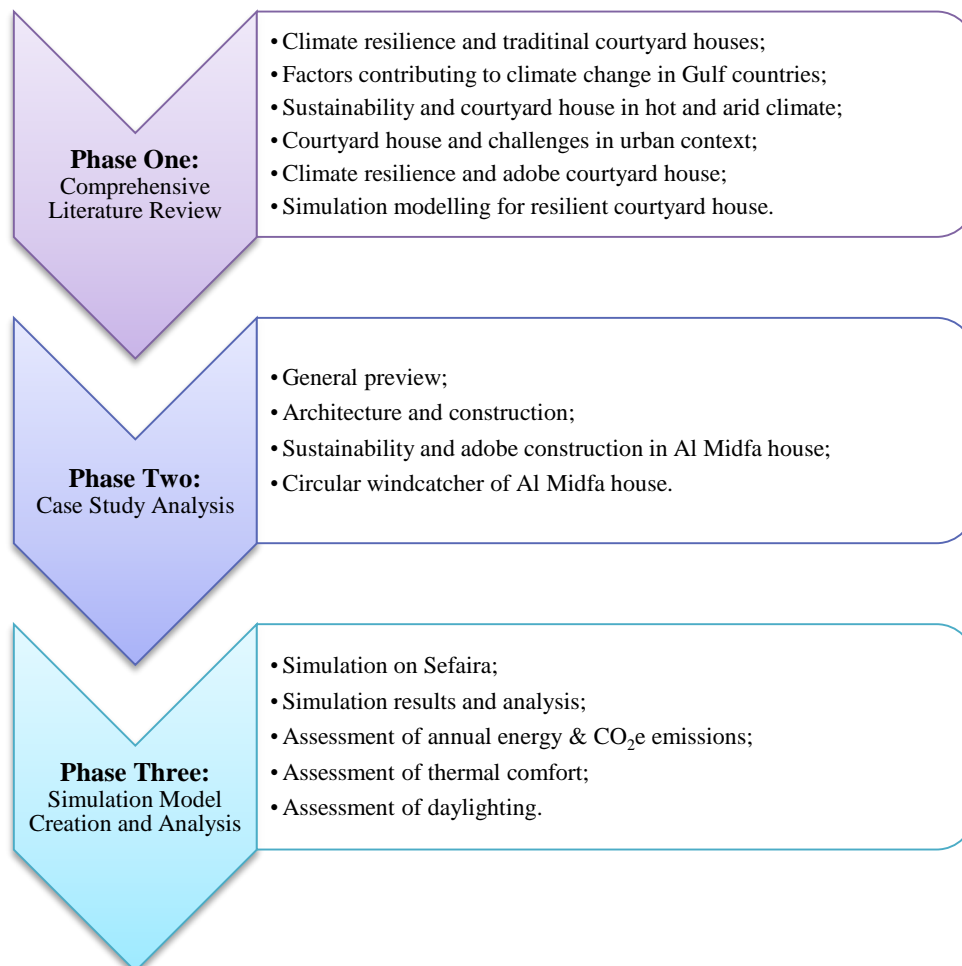
Phase One:
Comprehensive
Literature Review

- Climate resilience and traditinal courtyard houses;
- Factors contributing to climate change in Gulf countries;
- Sustainability and courtyard house in hot and arid climate;
- Courtyard house and challenges in urban context;
- Climate resilience and adobe courtyard house;
- Simulation modelling for resilient courtyard house.

Phase Two:
Case Study Analysis

- General preview;
- Architecture and construction;
- Sustainability and adobe construction in Al Midfa house;
- Circular windcatcher of Al Midfa house.

Phase Three:
Simulation Model
Creation and Analysis

- Simulation on Sefaira;
- Simulation results and analysis;
- Assessment of annual energy & CO_2e emissions;
- Assessment of thermal comfort;
- Assessment of daylighting.

Figure 1. Research Flow Diagram

5.1. Phase One: Comprehensive Literature Review

At the very outset, the research emphasizes the importance of laying a strong foundational understanding of the subject matter. Therefore, the first phase involves an exhaustive literature review. This review intends to mine relevant information on the design and construction methodologies of courtyard houses, considering their deeply rooted historical and cultural contexts. Moreover, the environmental performance of these structures is of utmost importance to this research. Special attention is given to the principles of sustainable design, understanding the nuances of passive ventilation, and gauging the effectiveness of wind catchers. This phase offers insights into existing academic knowledge and presents a coherent framework for the subsequent phases of the study.

5.2. Phase Two: Case Study Analysis

In the succeeding phase, the spotlight shifts to an empirical exploration of a selected courtyard house located in the UAE. The choice of this region is significant, given its historical ties and architectural relevance to courtyard houses [39]. This case study, through a qualitative lens, delves deep into understanding the architectural design and construction practices employed. The primary aim is to ascertain the key design elements pivotal to ensuring low energy consumption. However, this investigation is not limited to merely analyzing architectural blueprints. A more holistic approach has been adopted, which encompasses site visits, stakeholder interviews including architects, engineers, and the very occupants of the building, and rigorous data collection focusing on metrics like energy consumption and CO_2 emissions. This comprehensive approach ensures that the research captures the full essence and complexities of the subject.

Following the collection of data, meticulous efforts were directed towards its analysis. The objective was to discern patterns, trends, and any significant relationship between the variables of interest that emerged from both the literature review and the empirical case study.

5.3. Phase Three: Simulation Model Creation and Analysis

With the foundation laid and empirical data at hand, the third phase transitions to a more technical realm. Here, the research introduces the concept of a simulation model. This model's central goal is to evaluate the potential of courtyard houses in terms of energy consumption reduction and CO_2 mitigation. To achieve this, the study harnesses the capabilities of advanced building energy simulation software like Sefaira. This software recreates the energy performance dynamics of a quintessential courtyard house. Key aspects of this simulation include assessing the role of passive ventilation in energy and CO_2 emission reduction. The process incorporates other software tools, focusing on parameters like energy utilization, CO_2 emissions, thermal comfort, and daylighting. The simulation, while rigorous, is also versatile, considering multiple scenarios encompassing different ventilation and insulation strategies.

Concluding this phase, the resultant simulation data undergoes a thorough analysis. The essence of this analysis is not just understanding the simulation's results but comparing them against real-world data. This juxtaposition aims to determine the simulation model's accuracy, ensuring its validity and applicability in real-world contexts. In summation, this research, through its phased approach, endeavors to provide a holistic understanding of courtyard houses, from historical relevance to future sustainability potential, as shown in Figure 2.
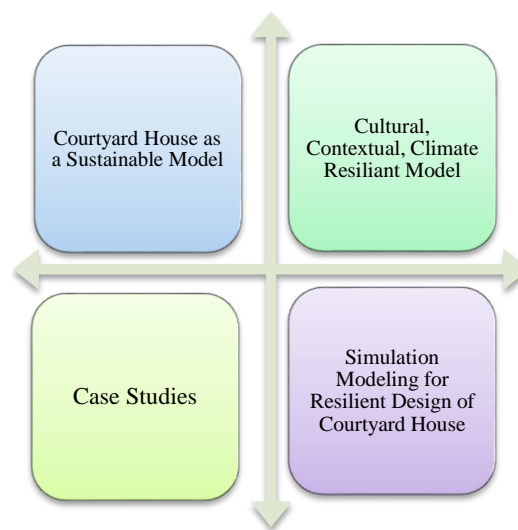
Courtyard House as a Sustainable Model

Cultural, Contextual, Climate Resiliant Model

Case Studies

Simulation Modeling for Resilient Design of Courtyard House

Figure 2. Research Matrix

6. Sustainability and Courtyard House in Hot and Arid Climate

This study considers that the integration of traditional Adobe technology and passive ventilation techniques in courtyard house design is exciting. The central courtyard is not only aesthetically pleasing but also contributes to the building's sustainability by enhancing ventilation and cooling. The consideration of microclimate factors and the use of natural materials further promote sustainable living. The traditional courtyard house is an architectural typology that has been prevalent in various cultures and geographical locations for centuries [40, 41]. By examining the literature on this topic, this review highlights the inherent characteristics of traditional courtyard houses, which provide an embedded sustainable approach and foster the potential for adaptation to future climatic changes. In addition, its design presents an accurate blend of passive design, cultural adaptability, and urban context. Many studies have examined the correlation between a courtyard with sustainability and investigated various parameters defining the role of a courtyard in promoting sustainability in a courtyard house.

The courtyard house design showcases the importance of sustainable architecture. The incorporation of natural adobe materials and passive ventilation techniques, such as wind catchers and courtyard spatial morphology, contributes to energy efficiency and sustainable living. The central courtyard also enhances the aesthetics of the building while providing functional benefits [42]. The integration of traditional adobe technology and passive ventilation techniques, along with the consideration of microclimate factors, promotes energy-efficient and sustainable living. The central courtyard provides a functional and sustainable design solution [43]. According to Fernandes et al. [44], courtyard houses are a great example of how sustainable architecture can be achieved using traditional techniques. The use of natural adobe materials and passive ventilation techniques, such as wind catchers and courtyard spatial morphology, contributes to energy efficiency and sustainable living. The central courtyard provides an aesthetically pleasing and sustainable design feature [45].

The sustainable features of the courtyard house design are noteworthy because of the incorporation of natural adobe materials and passive ventilation techniques, along with the consideration of microclimate factors, which promote energy-efficient and sustainable living; moreover, the central courtyard also provides functional and sustainable design solutions [46]. House design became admirable because of the courtyard and its sustainable features. The integration of traditional adobe technology and passive ventilation techniques, along with the consideration of microclimate factors, contributes to energy efficiency and sustainable living. The central courtyard also enhances the aesthetics of the building while providing sustainable design solutions [47]. Whereas the study of Friess & Rakhshan [48] emphasized that courtyard houses in the Middle East use local materials, architectural elements such as wind towers, and cultural context are important in achieving sustainability and energy efficiency. In addition, the courtyard shapes and designs play a crucial role in achieving sustainable thermal comfort and energy efficiency by employing, as mentioned, the shading performance of various polygonal courtyard forms [49].

Discussion under this section can be précised as that the sustainability features of courtyard houses are outstanding. The incorporation of natural adobe materials and traditional passive ventilation techniques, including wind catchers and courtyard spatial morphology, creates a comfortable and energy-efficient living space. The central courtyard not only adds to the visual appeal of the building but also provides functional benefits, such as improved air quality and cooling. The combination of these sustainable features showcases the potential of traditional design techniques in modern architecture. In terms of passive design strategies, traditional courtyard houses consistently emphasize the significance of their design principles in providing climate resilience. A key element is the central courtyard, which acts as a microclimate regulator, improving thermal comfort and allowing for natural ventilation. Furthermore, the compact layout, combined with thick walls and small openings, minimizes heat gain during hot periods and retains warmth during cold periods, enhancing energy efficiency. Additionally, the use of local materials with high thermal mass and insulation properties contributes to the overall climate adaptability of the courtyard house.

Thus, it could be concluded that the design principles and passive strategies employed in traditional courtyard houses offer a sustainable and contextually adaptable approach to addressing current and future climatic challenges. As such, the traditional courtyard house can serve as an inspiration for contemporary urban design, promoting climate resilience and fostering a more sustainable built environment.

6.1. Courtyard House and Challenges of Urban Context

While traditional courtyard houses exhibit various sustainable characteristics, they also face certain challenges that warrant further examination. This section of the study explores literature sources that critically discuss the problems associated with traditional courtyard houses, focusing on aspects such as privacy, maintenance, and adaptation to contemporary needs. According to Al Kodmany [50] and Bekleyen & Dalkiliç [51], the level of privacy is a major concern in traditional courtyard houses. The study highlights issues related to visual and acoustic privacy, which arise due to the shared nature of courtyards and the proximity of living spaces. The study of Wang et al. [52] has discussed the challenges of urbanization and its impact on building energy consumption and efficiency, emphasizing the difficulties of integrating traditional courtyard houses into rapidly growing modern cities while maintaining their sustainable features.

Maintenance and tidiness are major challenges in traditional Iranian courtyard houses of Iran. The authors emphasize the complexity of preserving and restoring historical structures while addressing the evolving needs of contemporary occupants [53]. However, various other studies have investigated factors influencing occupants' window opening behavior in a naturally ventilated building. The authors highlight that the reliance on natural ventilation in traditional courtyard houses may not always result in optimal indoor air quality, as occupant behavior and preferences can be unpredictable [54, 55]. Moreover, studies by Al Surf et al. [56] and Ghaffarianhoseini et al. [57] have discussed the challenges of integrating traditional courtyard houses with modern green building concepts. The authors emphasize the need for balancing the preservation of cultural heritage with the adoption of contemporary sustainable and smart building technologies.

Whereas cultural and contextual adaptability is profoundly present, traditional courtyard houses are not a one-size-fits-all solution. Various literature points out their adaptability to different cultural and climatic contexts. In regions with

hot arid climates, such as the Middle East, the courtyard houses often feature wind towers and water elements to increase the cooling effect of air movement [58, 59]. In contrast, in regions with cold climates, such as Northern China, the courtyard houses employ a south-facing orientation to maximize solar gain and heat retention [60, 61] These examples showcase the adaptability and versatility of courtyard houses in addressing specific climatic challenges.

While the courtyard house is also being presented as an example of urban context and contemporary relevance. Some studies emphasized courtyard geometry and layout; the traditional courtyard house is increasingly recognized for its relevance in urban contexts and contemporary living. Research underscores the capacity of these structures to significantly contribute to sustainable urban development. The unique design of courtyard houses, characterized by their high-density living spaces intertwined with communal green areas, cultivates a robust sense of community. Such architectural arrangements not only promote social interaction among residents but also play a crucial role in mitigating the urban heat island effect. This blend of traditional design and communal living space offers a model for modern urban development that harmoniously balances private living with communal engagement [62, 63]. Furthermore, the courtyard house model's inherent flexibility allows for the integration of modern technologies, such as photovoltaic panels and rainwater harvesting systems, to further enhance its environmental performance [64, 65].

The discussion above has revealed several challenges associated with traditional courtyard houses, such as privacy concerns, maintenance issues, and adaptation to contemporary needs. These critical perspectives highlight the importance of considering both the advantages and disadvantages of courtyard houses when assessing their suitability for modern urban environments. Further research and innovative approaches are necessary to address these challenges and maximize the potential of traditional courtyard houses as sustainable architectural models.

6.2. Climate Resilience and Adobe Courtyard House

Climate change has become a significant concern globally, with the increase in the frequency and severity of natural disasters such as rising temperatures, storms, floods, and wildfires. Traditional courtyard houses have been recognized for their ability to provide climate resilience and offer a sustainable solution to climate change. The traditional courtyard house has been found to offer several benefits, including natural ventilation, shading, and thermal comfort. Studies have shown that traditional courtyard houses can reduce energy consumption by up to 50% compared to modern buildings [66, 67]. The use of traditional building materials such as adobe and mud bricks has also been found to have a positive impact on the environment, with a low carbon footprint but Adobe construction is vulnerable to climate change and poses a threat to the cycle of life [68].

However, there are also several challenges associated with traditional courtyard houses. For instance, some studies have noted the susceptibility of these houses to earthquakes and the precedent rate of rainfall [69] and the difficulty in adapting them to changing social needs and lifestyles [70]. Additionally, the use of traditional building materials may lead to maintenance and durability issues in extreme weather and seismic conditions [71, 72]. To address these challenges, various potential solutions have been proposed, one solution is to integrate modern building technologies with traditional building methods, such as using lightweight and earthquake-resistant materials. Another proposed solution is to introduce green roofs and walls to improve insulation and reduce heat absorption [73, 74]. Additionally, the integration of renewable energy systems, such as solar panels and wind turbines, can enhance the climate resilience of traditional courtyard houses [75].

One of the key benefits of traditional courtyard houses is that they provide natural ventilation and cooling, which can help to reduce energy consumption and greenhouse gas emissions. For example, in studies conducted by Du et al. [76] and Subramanian et al. [77] it was found that traditional houses with courtyards have significantly lower indoor temperatures than modern houses without courtyards. This is because the courtyard provides a shaded outdoor space that allows for natural air circulation and reduces heat gain.

However, while traditional courtyard houses can be effective in reducing energy consumption and increasing resilience to climate change, there are also challenges associated with their design and construction. For example, traditional materials and building techniques may not meet modern safety standards, and the cultural significance of these structures may make it difficult to implement changes that are necessary for climate resilience. One approach to addressing these challenges is to incorporate modern materials and technologies into the design of traditional courtyard houses. In the studies conducted by Manioğlu & Yılmaz [78] and Cabeza et al. [79], it was found that the use of modern materials and technologies such as insulation and double-glazed windows can improve the energy efficiency of traditional courtyard houses without compromising their cultural significance.

Another challenge associated with traditional courtyard houses is the need to adapt them to changing environmental conditions. For example, in areas that are prone to flooding or sea level rise, it may be necessary to raise the elevation of the house or modify the design of the courtyard to accommodate rising water levels. The studies suggest that the use of adaptive design strategies such as elevated ground, amphibian construction, and building water barriers can help to increase the resilience of traditional courtyard houses to climate change [80, 81].

Discussion under this section can be resolved as the combination of traditional courtyard houses and climate resilience has the potential to create sustainable and resilient buildings that are adapted to local environmental conditions. However, it is important to address the challenges associated with their design and construction and to incorporate modern materials and technologies to improve their energy efficiency and resilience. However potential solutions such as integrating modern building technologies, introducing green roofs and walls, and integrating renewable energy systems can address these challenges.

7. Case Study of Al Midfa House Sharjah

In this section of the case study, an examination of numerous factors was conducted in the research, along with obtaining crucial information. Aspects such as tangible dimensions, design aspects, materials properties, techniques for building with adobe, and weather-related data were meticulously scrutinized. To collect vital details, an exhaustive examination of the location was carried out, followed by sifting and handling the data to develop a three-dimensional representation needed for the climate resilience simulation process.

Al Midfa House, also known as Majlis Al Midfa, stands as a testament to traditional Emirati architecture in the heart of the Sharjah heritage district, near Souk Al Arsa (Al Arsa bazaar) and a short walk from Sharjah Corniche, in the United Arab Emirates, as shown in Figure 3. This historic building, over a century old, is constructed using adobe, comprising clay, sand, and date palm fonds and barks, a material prevalent in the Middle East. It claims the UAE's only circular wind tower, "barjeel" differing from the common square designs of most wind towers, adding a unique architectural feature to the site. The house, named after Ibrahim Bin Mohammed Al Midfa who established the nation's first newspaper in 1927, has been a significant cultural hub for scholars and traders. Serving as a meeting point for discussions on poetry, literature, and politics, the Majlis Al Midfa has played an integral role in the UAE's cultural and historical narrative [81-83].
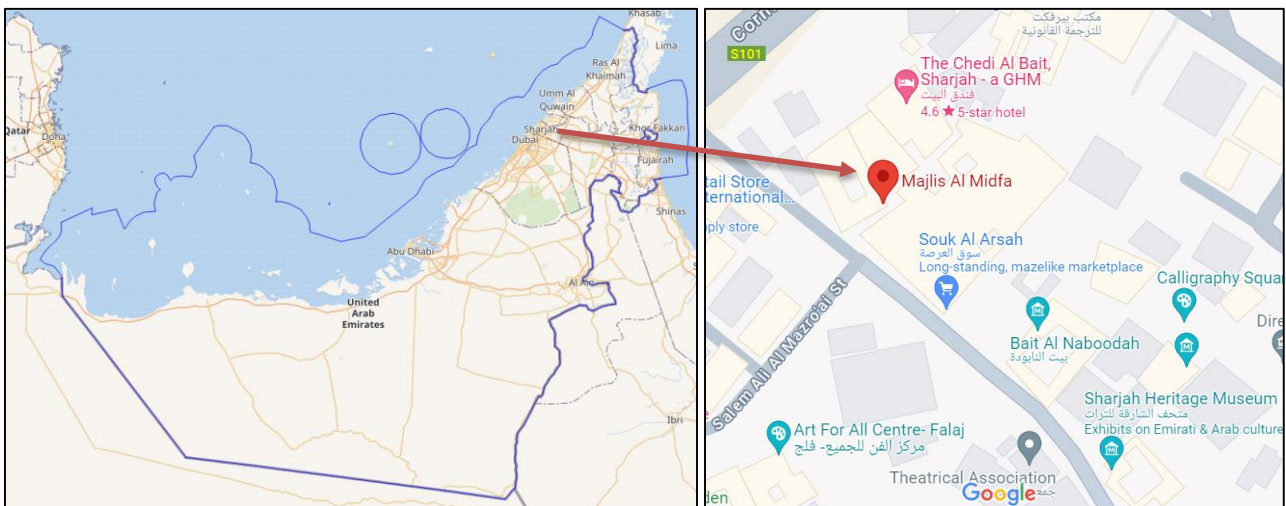

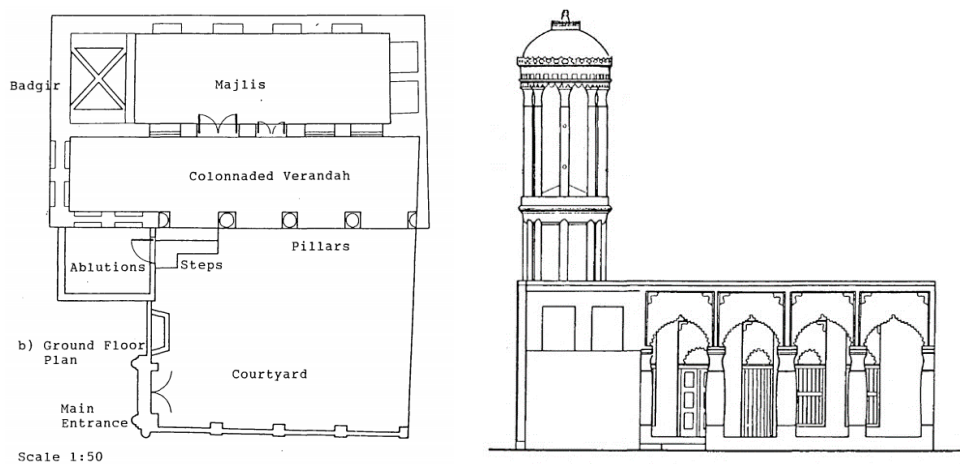**Figure 3. Location Al Midfa House [83]**

Figure 4. The Al Midfa House plan (left) and elevation from the courtyard (right) [84]

7.1. Architectural Planning

As depicted in Figures 4 and 5, Al Midfa House is situated on a 10 x 13-meter land parcel in Sharjah's heritage district. Originally, the ground floor was designed as a male guest house or "Majlis" for the Al Midfa family. The house's facade faces west and is bordered by narrow passages on the west, south, and north sides. Differing from typical traditional designs, Al Midfa House features only one entrance, which is positioned on the northern side. The house's design incorporates a straightforward geometric configuration consisting of one square and two rectangles: the courtyard, the veranda, and the Majlis or guest room respectively.

The primary offset entrance opens into a courtyard, which connects to a colonnaded veranda that leads to the Majlis hall. The house is arranged with the ground floor courtyard as the foremost space, the veranda as an intermediate area, and the Majlis guest room, equipped with a wind catcher, situated at the rear. The only wet space in the house, the ablution and toilet room for guests, is located along the western external wall adjacent to the entrance. An elegantly circular wind catcher, or "brajeel," is vertically extended over the first-floor roof. However, no physical access has been designed to reach the rooftop.

The ground floor house of Al Midfa features an intelligent design with a wind catcher positioned in the guest room, facing a west-north orientation. Entry to the guest room is through Mughal Arch colonnaded verandas, which run along the guest room's length and effectively block direct heat and light from entering the rooms from the south. Additionally, the ablution and toilet facilities are conveniently located in the courtyard, ensuring easy access and privacy.

Overall, Al Midfa House exemplifies a well-designed traditional UAE residence that embodies cultural sensitivity in its entrance and gathering spaces. The courtyard, positioned in front of the colonnaded veranda, serves as the home's focal point, providing a sense of openness and connection to the outdoors. The guest room is strategically located to optimize functionality. Overall, the Al Midfa guest house is thoughtfully designed to offer comfort, privacy, and convenience, with the verandas, courtyard, and toilets placed in strategic locations to ensure the guest room remains well-ventilated and protected from direct heat and light.

7.2. Sustainability and Adobe Construction

Adobe architecture provides a distinctive visual and cultural appeal, contributing to a sense of belonging and community cohesion in hot, arid environments. Nevertheless, it is vital to strike a balance between preserving cultural heritage and adhering to contemporary building codes and safety standards [85]. While adobe structures may exhibit a degree of resilience to extreme weather occurrences, it is essential to examine the possibilities for reinforcement and retrofitting to bolster their capacity to cope with evolving climatic conditions [86, 87]. Exploring the materials and construction methods employed in traditional UAE houses yields significant insights into eco-friendly design principles and the conservation of architectural cultural heritage. The construction techniques used in traditional UAE houses, which incorporate adobe and coral stone masonry, exhibit durability and resistance, having been honed over centuries to withstand severe environmental challenges.

Examining the materials and construction techniques applied in Al Midfa houses reveals considerable knowledge about environmentally conscious design strategies and the preservation of architectural cultural heritage. Al Midfa houses utilize building methods such as adobe and coral stone masonry, which have been developed and refined over generations to withstand harsh environmental conditions. The construction process involves using sun-dried mud bricks and coral stones bonded with mud mortar, which are then reinforced by palm fronds. These locally sourced materials not only symbolize the region's cultural identity but also promote ecological sustainability. Conversely, the use of gypsum plaster and decorative wood carvings in Al Midfa house interiors highlights the area's rich artistic and cultural traditions.

The inclusion of load bearing, thick walls, and small windows in Al Midfa house designs helps to minimize heat absorption and maximize natural airflow, resulting in comfortable living spaces well-adapted to the region's hot and arid climate. Roof construction studies have indicated that traditional house roof designs in hot, arid climates often feature elements such as high-pitched roofs made of palm barks tied together, covered with palm thatches, and sealed with mortar surfaces. Overhangs and shading devices are also incorporated to shield interiors from direct sunlight and decrease heat gain [88, 89]. Additionally, the use of reflective roofing materials, like white or light-colored paints or limestone mortar coverings, can help diminish heat absorption and enhance energy efficiency in hot, arid climates [90, 91].

Al Midfa house's roof design and construction embody several features suited to Sharjah's hot and arid climate. High-pitched roofs are built using palm barks fastened together and covered with palm thatches, then reinforced with mortar surfaces to ensure water resistance. Overhangs, verandahs, and shading devices are incorporated into the design to safeguard interiors from direct sunlight and reduce heat gain. Furthermore, reflective roofing materials, such as white or light-colored paints or limestone mortar coverings, are employed to minimize heat absorption. These elements guarantee that Al Midfa House maintains a comfortable living environment even in Sharjah's hot and humid climate.

7.3. Circular Windcatcher of Al-Midfa House

Wind towers serve as a distinctive cultural and architectural feature in the Gulf region, signifying the interconnection between time-honored construction methods and modern urban settings. Researchers advocate for the ongoing

importance of wind towers in preserving the architectural heritage of the region while fostering environmentally sustainable urban design. Integrating wind tower design concepts into contemporary architecture is vital for promoting eco-friendly living in hot, arid climates [92-94].

The Al Midfa house showcases a distinct circular, multi-faceted wind tower with an innovative 'X' blade configuration. Positioned on a circular plan over a square base, the wind tower is situated on the eastern side of the dwelling to capture winds from the southwest and northwest. This strategic placement enables the wind tower to make the most of prevailing breezes, offering a natural ventilation solution for the guest room.

The 'X' blade structure of the wind tower excels in capturing air currents from various directions, channeling them into the home, and delivering a consistent flow of cool air. By placing the wind tower on the eastern side of the property, it can effectively utilize wind from the most advantageous directions, maximizing its ability to provide natural ventilation [95]. The inclusion of a cylindrical, multi-faceted wind tower with an 'X' blade design in the Al Midfa house presents an efficient strategy for establishing a natural ventilation system. The wind tower's well-considered placement and design ensure that it can optimally harness prevailing winds, creating a comfortable and refreshing living environment for the inhabitants.

7.4. Research Challenges

This study on design, adobe construction, and climate resilience in courtyard houses faced various challenges. Accessing case studies and analyzing traditional Adobe structures was difficult due to their private ownership or heritage status. Additionally, replicating traditional construction methods required specialized knowledge of historical architecture, which varied regionally and lacked comprehensive documentation. Proving courtyard houses as low-energy models were complicated by diverse architectural styles and climatic adaptations, requiring an extensive review and comparison of scattered data. Simulating indoor thermal comfort and climate resilient design adaptations in UAE encountered limitations in capturing complex dynamics of traditional buildings and uncertainty in future climate scenarios. Moreover, developing guidelines for transforming existing Emirati courtyard houses into energy-efficient, climate-resilient structures involved balancing cultural heritage with modern sustainability requirements, posing challenges in retrofitting while maintaining architectural integrity.

8. Simulation Modelling for Climate Resilient House

Simulation modelling is an essential tool for architects and engineers to design climate-resilient houses that can withstand the impacts of climate change. Climate-resilient houses are designed to reduce energy consumption and minimize the environmental impact of buildings while providing comfortable living conditions for occupants. This critical review aims to assess the effectiveness of simulation modelling for designing climate-resilient houses and provide examples of its successful application.

Simulation modeling is a crucial tool in designing climate-resilient houses, allowing for the evaluation of building performance under different climatic conditions. Simulation modeling enables architects and designers to optimize the building design, leading to energy efficiency and reduced environmental impact [96]. Simulation modeling can aid in the selection of appropriate materials, systems, and technologies, ensuring that the house is resilient and sustainable [97]. Various case studies have demonstrated the effectiveness of simulation modeling in designing climate-resilient houses. For example, in Australia, the use of simulation modeling was instrumental in the design of a sustainable house that can withstand bushfires and extreme weather events [98]. Similarly, in the United States, simulation modeling was used to optimize the design of a net-zero energy house that can generate electricity and minimize its carbon footprint [99, 100]. To address the challenges of climate change, various potential solutions have been proposed. One solution is to promote the use of renewable energy systems such as solar panels, wind turbines, and geothermal systems [101]. The implementation of green roofs and walls can enhance the thermal performance of the building and mitigate the urban heat island effect. Furthermore, the use of natural ventilation, shading devices, and daylighting can improve indoor air quality and reduce energy consumption [102, 103].

Successful application of simulation modelling for climate-resilient houses can be seen in various case studies. For example, in the United Kingdom, simulation modelling was used to design a passive solar house that achieved a 60% reduction in energy consumption compared to conventional houses [104]. In India, simulation modelling was used to design a low-cost, energy-efficient house for low-income families that reduced energy consumption by 50% [105]. Similarly, in Japan, simulation modelling was used to design a sustainable house that reduced energy consumption by 80% [106].

This section can be précised as, that simulation modelling plays a critical role in designing houses that are resilient to climate change, as it allows architects and designers to optimize building performance across various climatic conditions. By integrating renewable energy systems, green roofs and walls, and natural ventilation, the sustainability and resilience of the house can be improved. As a result, simulation modelling offers an effective approach to designing climate-resilient houses and mitigating the impacts of climate change.
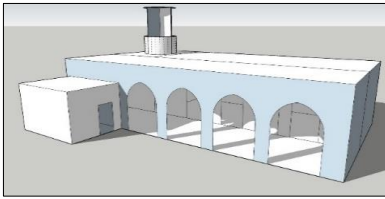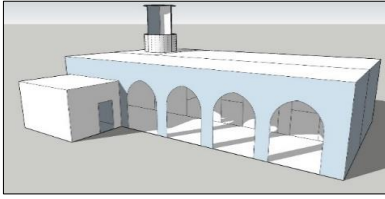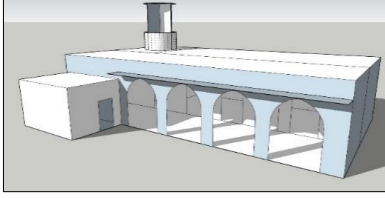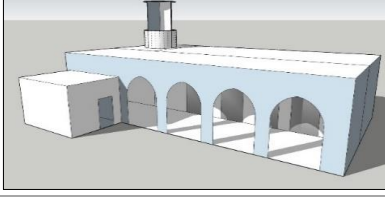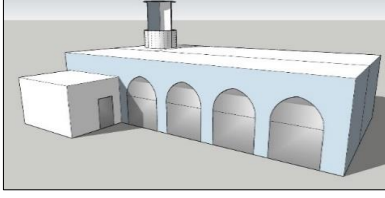
8.1. Simulation on Sefaira

A simplified Sketchup model was created according to Sefaira's requirements. External and internal walls, roof, operable glass, and shading were assigned to each surface. Sefaira was then launched to perform daylighting and energy

studies. The building specifications were based on U-values for uninsulated walls and roofs [107, 108]. Standard values were used as the authors lacked access to laboratory equipment to calculate the actual combined U-value of the mud wall and roof constructions. Sefaira is used to analyse the daylighting performance, energy consumption and thermal comfort based on ASHRAE 55 predicted mean vote (PMV) standard.

The baseline Sefaira model was then uploaded to the Sefaira System for additional analysis and specification changes. The baseline model was initially configured to use natural ventilation (free running) instead of air conditioning. Except for the M7, air conditioning was chosen to run with a 20°C to 25°C setpoint indoor temperature and full occupancy throughout the year. To adapt to the severe desert climate, air conditioning integration is critical in the UAE. The Sefaira simulation was run for each of the seven alterations listed in Table 3. The changes are modest in nature, intending to increase the basic model's resilience to climate change. Sefaira's energy analysis is powered by the dependable Energy Plus engine and displays all energy expenditure components. Renewable energy generation via PV can also be factored into the study to further minimize energy consumption. A thermal comfort study based on the ASHRAE 55 PMV standard is included in the same simulation to determine whether internal zones (rooms) are thermally comfortable.

Table 3. Simulated models, designs and specification

Simulation model	Model design	Specifications/modifications
Base model (BM)		▪ Mud walls throughout at 1.2 W/m² U-value ▪ Mud roof with timber rafters at 1.2 W/m² U-value ▪ No glazing and naturally ventilated
Modification 1 (M1)		▪ 0.6 m deep shading device and air-conditioned
Modification 2 (M2)		▪ 0.9 m deep shading device and air-conditioned
Modification 3 (M3)		▪ Operable glazing to enclose the *Majlis* (main room) and air-conditioned
Modification 4 (M4)	 Same exterior design for M4, M5, M6 and M7	▪ 2 m high operable glazing to enclose the colonnade with shading at a high level ▪ Operable glazing to enclose the Majlis (main room) and air-conditioned
Modification 5 (M5)		▪ Insulation on the inside surface of external walls surface at a combined U-value of 0.4 W/m² ▪ Insulation on the roof surface at combined U-value of 0.4 W/m² ▪ 2 m high operable glazing to enclose the colonnade with shading at a high level ▪ Operable glazing to enclose the *Majlis* (main room) and air-conditioned
Modification 6 (M6)		▪ All M5 modifications ▪ 90 m² roof mounted PV solar system
Modification 7 (M7)		▪ The same as M6 but naturally ventilated

The simulation parameters (design loads, design temperatures, annual diversity factors, ventilation and outside air, HVAC and day schedules) for the baseline model are set to closely resemble the actual case study. Similar parameters are used for the modified models to isolate the effects of physical design and specification changes, renewable energy generation addition and natural ventilation. The HVAC system specified for the simulation is fan coil unit with central plant for all models. The authors did not consider any overhead or underfloor systems as these would greatly alter the case study interior architecture. Further, the use of variable refrigerant flow (VRF) fan coils and packaged terminal heat pump (PTHP) split system are not considered as they would result in 20% and 27% increase respectively in baseline model annual net electricity use, despite their perceived savings in electricity.

To complete the analysis, all seven alterations are compared to the base model in Sefaira and carefully assessed for a more precise comparison. Finally, the authors suggest the best chance for implementation.

8.2. Simulation Results and Analysis

Figure 5 demonstrates that the suggested modern improvements to the traditional UAE house resulted in improved energy results. The EUI decreases from 90 kWh/m^2/yr for the base model (BM) to -77 kWh/m^2/yr for the Modification 6 (M6) model, which includes operable windows, better insulated walls and roof (0.4W/m^2), and a 90m^2 solar PV system. This solar PV system was sized depending on available roof space for the installation of 45 units of 2.0m^2 solar PV modules. Its installation not only offsets the whole energy consumption for the house, but it also generates 15,688 kWh of surplus electricity (nearly 100% extra) that can be profitably exported into the national power grid. Minimally, to counteract the M5 76 kWh/m^2/yr EUI and 15,569 kWh annual electricity usage, just 23 units of identically sized solar PV modules are required. Interestingly, the MI, M2 and M3 with shading devices and internal glass between the Majlis and veranda had a somewhat reduced EUI than the base model at 88 kWh/m^2/yr, indicating that they were ineffective in lowering annual energy use.

8.3. Annual Energy Use and CO₂e Emissions

The energy demand for M1-M6 is computed using a fan coil unit with a central plant air-conditioning system, which is the worldwide default cooling system for a Sefaira residential building. On the contrary, VAV with central plant is the default for healthcare and laboratories, while packaged rooftop VAV with reheat is the default for offices, schools, retail, and anything else [109]. The fan coil with a central plant system was kept for the energy use simulation since it is equivalent to systems utilized in UAE residential structures. Lighting and plug load defaults were also preserved. All simulated models' design loads (50 m^2/person occupant density, 5 W/m^2 equipment power density, and 10 W/m^2 lighting power density) are based on Sefaira's default values for residential buildings [110]. For both the base model and the M7, the air conditioning is programmed to always be turned off.

The annual energy use comparison in Table 4 shows that as additional modifications are made to the base model, the energy demand rises from 18,004 kWh (base model) to 18,330 kWh (M4). This is primarily due to the advent of operable windows, which separates rooms into different zones that require their air-conditioning, resulting in reduced efficiency. When insulation is added, however, the total annual energy demand drops to 15,569kWh, which is approximately 13.5% less than the base model.

Table 4. Overall simulation results showing the peak cooling load, energy usage intensity (EUI), annual net electricity use, annual net CO₂e emissions and the annual energy cost for all eight simulated models

Model	EUI (kWh/m²/yr)	Annual net electricity use (kWh)	Annual net CO₂e emission	DEWA Electricity Tariff				Annual energy cost (AED)
				1 to 2000 kWh	2001 to 4000 kWh	4001 to 6000 kWh	6000+ kWh	
BM	90	18,004	9,060	150.00	179.91	209.90	1500.50	2040.31
M1	88	17,606	8,857	150.00	179.91	209.90	1450.75	1990.56
M2	88	17,583	8,846	150.00	179.91	209.90	1447.88	1987.68
M3	88	17,664	8,887	150.00	179.91	209.90	1458.00	1997.81
M4	91	18,330	9,228	150.00	179.91	209.90	1541.25	2081.06
M5	76	15,569	7,785	150.00	179.91	209.90	1196.13	1735.93
M6	-77	-15,688	-7,844	150.00	179.91	209.90	1211.00	1750.81
M7	40	8,162	4,081	150.00	179.91	209.90	270.25	810.06

Annual energy cost is calculated based on Dubai Electricity & Water Authority (DEWA) 2019 residential sector electricity tariff for UAE nationals [111].

This annual energy demand is greatly reduced when the house is naturally ventilated (M7), as shown in Table 4. The total energy cost for this form of ventilation is also significantly cheaper, at AED810.06 (USD220.55) per year,

compared to AED1,735.93 (USD472.63) for the M5, and AED2,040.31 (USD555.50) for the base model. M5 and M7 lead to 14.9% and 60.3% cost savings per year compared to the base model. Operating the Al Midfa house on natural ventilation mode translates to significant electricity cost savings but at the expense of thermal comfort. In addition, the yearly CO_2e emission for M7 that runs on natural ventilation is the lowest at 4,081 $kgCO_2e$/year, compared to 9,228 $kgCO_2e$/year for M4 and 7,785 $kgCO_2e$/year for M5.

Referring to Table 5, the cooling energy use for the M4 is 9,081 kWh per year, compared to 9,130 kWh for the standard model and 7,045 kWh for the M5 with insulation. These correspond to approximately 48.8% (M4), 50.0% (base model), and 45.3% (M5) of total yearly energy consumption. The remaining annual energy use is accounted for by lighting, equipment use, and pumps. With the addition of insulation, the total peak cooling coil load is reduced from 18.1 kW (M4) to 10.8 kW (M5).

Table 5. Cooling energy analysis in comparison to the total electricity use for all simulated models

Model	Annual net electricity use (kWh)	Yearly cooling energy (kWh)	Percentage of the annual electricity use	Total peak cooling coil load (kW)
BM	18,004	9130	50.71%	15.8
M1	17,606	8498	48.27%	16.9
M2	17,583	8483	48.25%	16.9
M3	17,664	8540	48.35%	17.1
M4	18,330	9081	49.54%	18.1
M5	15,569	7045	45.25%	10.8
M6	-15,688	7045	44.96%	10.8
M7	8,162	838	10.27%	0.9

As previously stated, M6, with similar modifications to M5 but a 90 m^2 solar PV system, can generate 31,257 kWh of electricity per year and fully offset M5's 15,569 kWh per year energy demand, while potentially producing approximately 100% excess electricity that can be fed into the power grid for profit at AED1,750.81. This aligns with the UAE's goal of generating up to 75% of its energy from renewable sources by 2050 [112]. However, this 90 m^2 PV system may be too heavy for the roof. To counteract the overall energy consumption for M5, a smaller system with only 23 modules (46 m^2) at 21 kg per module [113], equivalent to 483 kg (10.5 kg per square meter or nearly 1 pound per square foot) can be used instead. This smaller system would be lighter on the vernacular structure and would cause no structural harm.

Overall, both the installation of insulation that reduces the building envelope U-value (resulting in significant annual energy use reduction) and the installation of a solar PV system are in line with Sharjah's declaration as a conservation city, to reduce energy use and use cutting-edge power conservation technologies [114].

8.4. Thermal Comfort

Sefaira evaluates predicted mean vote (PMV) based on ASHRAE 55. All simulated models were created with four zones based on existent rooms. If the PMV is between a -0.5 and 0.5 range for more than 98% of the occupied hours, the zone is considered passed. The PMV results for all models are summarized in Table 6.

Table 6. PMV results summary from Sefaira based on ASHRAE 55

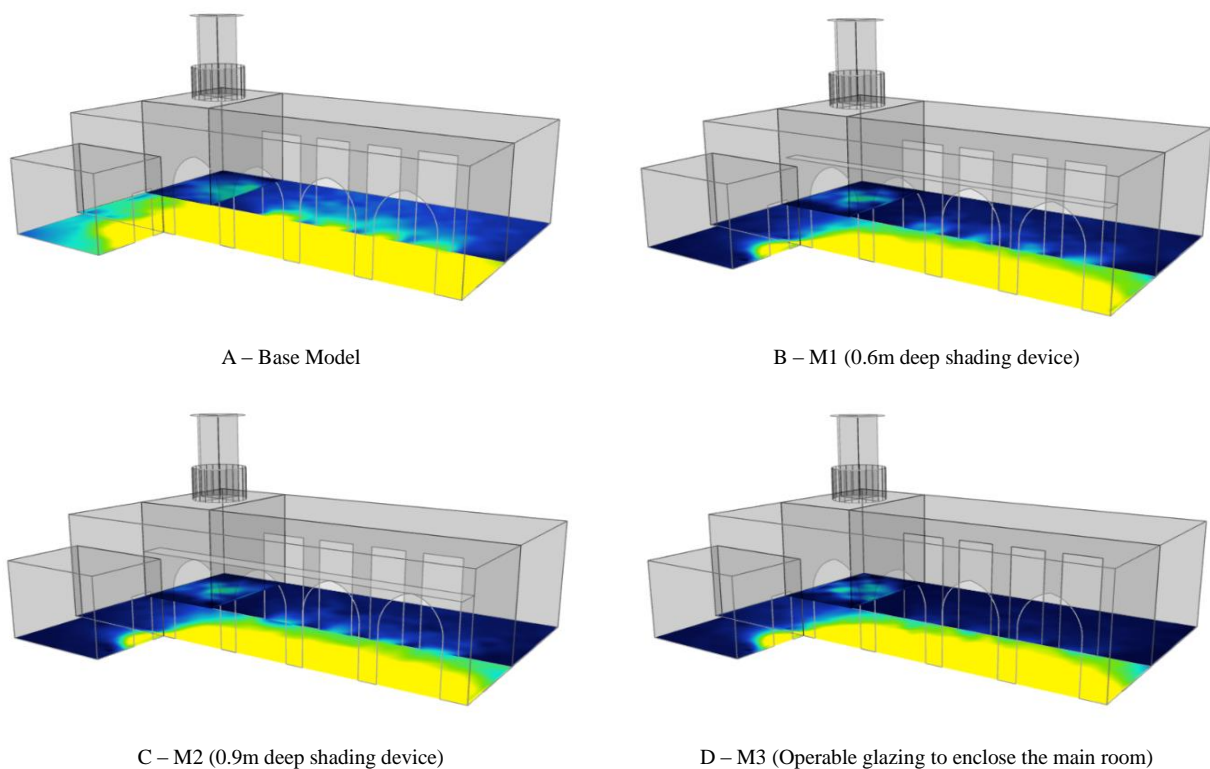| Model	# of pass zone	# of failed zone	Worst zone	Remark
BM	0	4	PO3 (ablution)	59.1% under target
M1	0	4	PO3 (ablution)	42.8% under target
M2	0	4	PO3 (ablution)	42.5% under target
M3	0	4	PO3 (ablution)	42.9% under target
M4	0	4	PO2 (verandah)	51.8% under target
M5	0	4	PO2 (verandah)	33.2% under target
M6	0	4	PO2 (verandah)	33.2% under target
M7	0	3	PO2 (verandah)	78.3% under target

Clearly, the M5 and M6 outperformed all other models, with more than 75% of hours being thermally comfortable at PO1, PO3, and PO4 (see Table 6). Ultimately, all zones failed because they were outside of the -0.5 and 0.5 range for more than 98% of the occupied hours (see Table 7). PO4 or the guest room below the wind catcher is the best zone since it gets plenty of fresh air. Nonetheless, this situation is undesirable because the majority of people will be in zones PO1 (*Majlis*), PO2 (veranda), and PO3 (ablution), necessitating constant air-conditioning. PMV results for M7 are worse, since zones PO1-PO3 are only comfortable for about 25% of the time (see Table 7). Only the guest room passed this test with a score of 99.4%. This problem may be improved if big openings were provided between each zone to allow air brought down through the wind catcher to circulate freely. M7 simulation was rerun with only one zone per floor (no sub-divisions) and the results were a failure (74.5% under target) since this zone is only thermally pleasant for 23.5% of the time, too hot for 67.5% of the time, and too cold for 9.1% of the time. As a result, air conditioning is essential to maintain thermal comfort.
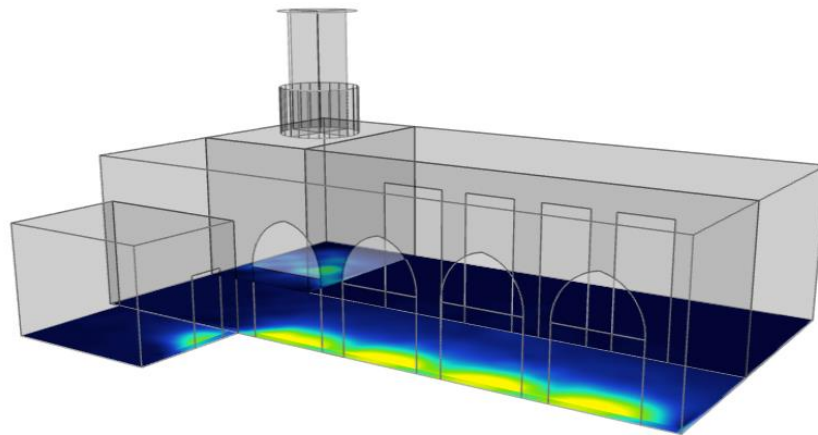
Table 7. ASHRAE 55 PMV evaluation failure results for M5, M6 and M7

Zones	M5 and M6				M7			
	Comfortable (% of hours)	Too hot (% of hours)	Too cold (% of hours)	Under target (%)	Comfortable (% of hours)	Too hot (% of hours)	Too cold (% of hours)	Under target (%)
PO1 (*Majlis*)	84.9	8.5	6.6	13.1	20.1	79.4	0.5	77.9
PO2 (verandah)	64.8	33.1	2.1	33.2	19.7	70.6	9.7	78.3
PO3 (ablution)	76.4	17.4	6.2	21.6	23.6	65.2	11.3	74.4
PO4 (guest room)	89.9	16.0	8.5	8.1	99.4	0.0	0.6	1.4 (over target)

8.5. Daylighting

Daylighting in the UAE's hot and arid climate is always a challenge for any style of structure. This issue is caused by excessive heat input through windows or openings in the building envelope that allow natural light to enter. As a result, shading mechanisms are required to prevent direct sunlight from entering through openings, while internal surface colours and reflecting materials can diffuse sunshine over a larger area and deeper into the building. This paper's case study house, Al Midfa, includes large openings along the front length of the veranda (PO2) and comparable openings into the *Majlis* (PO1). Furthermore, the wind catcher tower features small openings to allow air to move while yet allowing some natural lighting into zone PO4. The same Sefaira models (base model, M1, M2, M3, and M4) were utilized to analyse the inside daylighting conditions. Figure 5 depicts the Sefaira simulation results, which make use of the Radiance and DAYSIM engines [115].
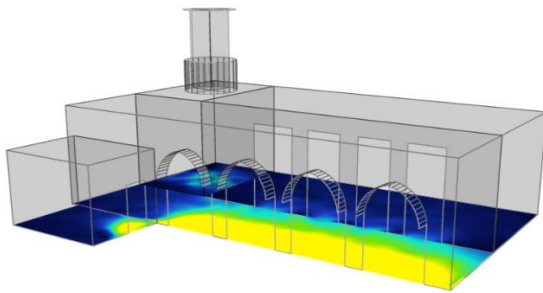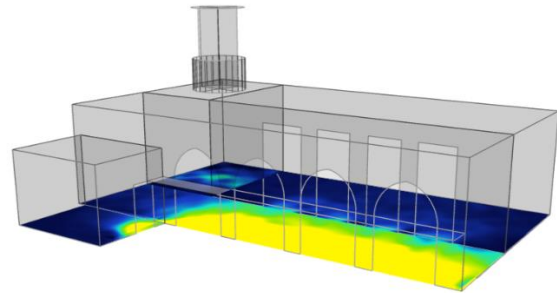
A – Base Model

B – M1 (0.6m deep shading device)

C – M2 (0.9m deep shading device)

D – M3 (Operable glazing to enclose the main room)

Lux levels on March 21 at 9AM measured at 0.85 meters above the floor plate. Time does not take into account daylight savings time.

| ■ 0 | ■ 200 | ■ 400 | ■ 600 | ■ 800+ |

E – M4 (Operable glazing to enclose the main room and 2m high operable glazing to enclose the colonnade with shading at a high level. M4 is similar in design to M5, M6 and M7)

F - M8 (with a 0.6m deep shading device that follow the profile of the arched entry)

G - M9 (with a 0.9m deep shading device at 2m above the veranda entry)

Figure 5. Lux levels for A – Base Model, B – M1, C – M2, D – M3, E – M4, F – M8, and G – M9

According to the simulation, the base model has the best natural daylight penetration, with the veranda (PO2) being primarily over lit at 7.91% average sunshine factor. Meanwhile, the Majlis is generally dark, with an average daylight factor of 0.77%. The majority of the daylight enters through the veranda. The remaining zones are generally dark as well. This daylighting pattern is shared by M1 (which has a 0.6 m deep shading device above the veranda entrance) and M2 (which has a deeper 0.9 m shading device in the same area). The shading mechanisms had little effect on the amount of daylight that entered the veranda and ablution. On the contrary, the addition of glazing along the aperture into the *Majlis* in M3 successfully reduced daylight penetration into the Majlis, which was already mostly dark. Furthermore, new external glazing along the veranda obstructed more sun penetration, resulting in an underlit veranda (PO2) with a 1.28% average daylight factor (see Table 8).

Table 8. Daylighting Radiance simulation results from Sefaira

Model	Zones	Daylight Factor		
		Average	Minimum point	Uniformity ratio
BM	PO1	0.77%	0.10%	0.13
	PO2	7.91%	0.40%	0.05
	PO3	0.97%	0.20%	0.21
	PO4	1.36%	0.20%	0.15
M1	PO1	0.72%	0.1%	0.14
	PO2	6.96%	0.4%	0.06
	PO3	0.94%	0.2%	0.21
	PO4	1.34%	0.20%	0.15
M2	PO1	0.69%	0.10%	0.14
	PO2	6.17%	0.30%	0.05
	PO3	0.85%	0.20%	0.24
	PO4	1.35%	0.20%	0.15

	PO1	0.30%	0.00%	0.00
M3	PO2	7.89%	0.40%	0.05
	PO3	1.01%	0.20%	0.20
	PO4	1.36%	0.20%	0.15
	PO1	0.01%	0.00%	0.00
M4 (the same as M5, M6 and M7)	PO2	1.28%	0.10%	0.08
	PO3	0.43%	0.10%	0.23
	PO4	1.32%	0.20%	0.15
	PO1	0.58%	0.10%	0.17
M8	PO2	5.23%	0.36%	0.06
	PO3	0.95%	0.20%	0.21
	PO4	1.43%	0.20%	0.14
	PO1	0.68%	0.10%	0.15
M9	PO2	6.00%	0.30%	0.05
	PO3	0.88%	0.20%	0.23
	PO4	1.20%	0.20%	0.17

Two more models were also simulated. M8 has a 0.6m deep shading device that follows the profile of the arched entry, while M9 has a 0.9 m horizontal shading device that is situated 2 m above the veranda entry. Similar to the base model, these new improvements enabled great sunshine penetration onto the veranda. Overall, the Majlis (PO1) is mostly dark, the veranda (PO2) is mostly bright, and the guest room (PO3) and ablution (PO4) are mostly dark. This summarized finding is consistent across all models studied. Furthermore, for all examined models, the spatial daylight autonomy (sDA) and annual sunlight exposure (ASE) are both 0.00%.

9. Discussion

In the realm of sustainable architecture and energy-efficient design, the utilization of cutting-edge simulation tools, such as the Sefaira simulations, offers crucial insights into the thermal performance of different building models. Among the investigated models, the M5 version emerged as a leading contender, exhibiting impressive thermal efficiency characteristics that surpassed its counterparts. This article provides an in-depth analysis of the M5 model, focusing on its key attributes and potential implications for the architectural design of the Al Midfa house.

The triumph of the M5 model in the context of thermal performance primarily hinges on its strategic implementation of additional insulation within the building envelope. This enhancement has led to a commendable 13.5% decrease in annual energy consumption in comparison to the original prototype. Moreover, the M5 design requires a reduced amount of energy for cooling purposes, a crucial factor in optimizing energy efficiency. However, the advantages of M5 are not devoid of complications. A significant challenge emerged from the ASHRAE 55 PMV examination, where all the rooms within the M5 model were found to fail the test. In particular, an alarming 33.2% of the 203 m^2 dwellings were found to fall short of the expected standard. Despite this drawback, the dry bulb temperature measurements demonstrated a reassuring consistency, with all four designated zones adhering to the setpoint range 100% of the time.

The intricacies of M5's design further extend to its daylighting characteristics. Comparable in its design approach to M4, the M5 model necessitates a substantial utilization of artificial illumination to maintain adequate visibility. Energy simulations accurately mirror this necessity, revealing an energy expenditure of 4,811.37 kWh/year, accounting for 30.9% of the total annual energy demand for artificial lighting alone. While this figure might appear significant, it is important to acknowledge that M5's energy consumption for cooling and artificial lighting can be effectively neutralized by employing a solar photovoltaic (PV) system. The solar solution proposed involves the mounting of 23 solar panels, each measuring 2.0m^2, effortlessly accommodated on the flat roof. This strategic initiative not only enhances energy self-sufficiency but also harmonizes with the architectural aesthetics of the Al Midfa house.

However, the introduction of M5's recommended changes will inevitably influence the architectural identity of the Al Midfa house. Such alterations necessitate careful selection of building materials, emphasizing the choice between framed or frameless windows, and insulation panels mounted on the interior surfaces of the walls and roof. The desired method aims to minimize alterations to the exterior architecture, thus preserving the building's visual integrity.

Injectable cellulose insulation represents an innovative solution to diminish the impact on interior architecture, but its compatibility with Adobe wall and roof constructions remains an area of uncertainty. The integration of the solar PV system on the roof presents no challenge concerning the weight-bearing capacity of the existing roof structure. Additionally, the concealed positioning of the panels ensures that they remain invisible from an eye-level external view.

The M5 model, as revealed through Sefaira simulations, offers a compelling solution in terms of thermal performance. Although accompanied by some challenges, the model proposes a visionary approach to energy efficiency and architectural integration. Its reliance on enhanced insulation, balanced artificial lighting, and the strategic incorporation of a solar PV system provides a resilient pathway towards future-proofing the Al Midfa house. The careful consideration of material selection and aesthetic coherence further underscores the holistic nature of the M5 design, promising a sustainable and harmonious coalescence of form and function.

10. Conclusions

Al Midfa House exemplifies the creativity and expertise of traditional Emirati builders and architects. The house exemplifies the use of sustainable and eco-friendly materials, as well as the use of traditional design aspects that take into account the climate and cultural setting of the region. Today, many architects and builders in the UAE draw inspiration from Emirati architecture's rich legacy. They are aiming to conserve and promote this distinctive architectural style. Therefore, this house must be resistant to climate change to last for many more generations. The conclusion of the study on the M5 model's implementation in the Al Midfa house presents a synthesis of various elements that reflect the complex balance between architectural integrity, sustainability, and resilience towards climate change. The success of such an approach lies in its ability to respond adeptly to the multifaceted challenges of contemporary living while prioritizing the environment.

The findings of the ASHRAE 55 PMV examination were not favorable for the M5 model, with all rooms failing to meet the required standards. Despite this drawback, the implications of the M5 model go far beyond this singular aspect. The changes recommended by M5 extend to the very core of the Al Midfa house's architecture, shaping its character and enhancing its resilience against climate change. More importantly, these modifications are aligned with the global movement towards sustainable living, positioning the Al Midfa house on a trajectory toward becoming a zero-carbon residence.

The transformation of the Al Midfa house into a model of sustainability is not a simplistic endeavor but a process replete with challenges and opportunities. It demands a meticulous exploration of new building materials and retrofits, focusing on windows (both framed and frameless) and insulation panels to be mounted on the interior surfaces of the walls and roof. These specific changes were identified as the most effective means of improving energy efficiency without altering the exterior architecture. The aim here is not just to make superficial adjustments but to infuse the building with features that enhance its performance and aesthetics.

The idea of utilizing injected cellulose insulation in the wall system represents a significant innovation in this direction. The potential benefits of this material are considerable, offering efficient insulation without compromising the architectural aesthetics of the building. It exemplifies a new way of thinking about insulation, one that acknowledges the importance of interior alterations in achieving energy efficiency.

Yet, the journey towards a zero-carbon Al Midfa house and its climate resilience does not stop with insulation and window modifications. The integration of a solar photovoltaic (PV) system within the existing roof structure is a key aspect of this transformation. What is remarkable about this initiative is that it transcends mere technical feasibility. By confirming that adding solar panels to the roof will not pose any weight-related problems to the existing structure, it reassures stakeholders that this ambitious goal is within reach. The introduction of solar energy not only symbolizes the house's commitment to renewable energy but also establishes it as a frontrunner in the transition towards a sustainable future. The Al Midfa House's transformation through the M5 model's recommendations is not an isolated case but rather a reflection of a broader societal shift towards sustainability. It showcases a pathway to resilience and adaptability that is cognizant of the imperatives of climate change and a world where energy efficiency is no longer a choice but a necessity.

In conclusion, the complex yet harmonious interplay of the M5 model's recommendations for the Al Midfa house presents a roadmap towards a future where architecture is not merely a static entity but a dynamic force in the fight against climate change. It transcends conventional boundaries, integrating innovation in materials, design, and technology to create a living space that is both practical and sustainable. The lessons learned from this study are not confined to a single dwelling but extend to the broader architectural community, providing insights and inspiration for a new generation of buildings that embody the principles of sustainability, resilience, and beauty. The Al Midfa house stands as a testament to what is achievable when creativity and responsibility converge, creating a home that is not just a shelter but a beacon of sustainable living in a rapidly changing world.

11. Declarations

11.1. Author Contributions

Conceptualization, A.H.C., J.A., M.A.I., and M.S.A.; methodology, A.H.C.; formal analysis, M.A.; investigation, M.A.; resources, M.S.A.; data curation, A.H.C. and J.A.; writing—original draft preparation, A.H.C.; writing—review and editing, J.A. and M.S.A. All authors have read and agreed to the published version of the manuscript.

11.2. Data Availability Statement

The data presented in this study are available on request from the corresponding author.

11.3. Funding

11.4. Acknowledgements

11.5. Conflicts of Interest

The authors declare no conflict of interest.

12. References

[1] Chohan, A. H., Awad, J., Ani, A. I. C. H. E., & Sher, B. K. (2023). Challenges of climate change & resilient housing design solution. Sustainable Energy Technologies: Proceedings of the 20th International Conference on Sustainable Energy Technologies, 15–17 August, 2023, Nottingham, United Kingdom.

[2] Azarbayjani, M., & Thaddeus, D. J. (2022). High Comfort – Low Impact: Integration of Thermal Mass in Pursuit of Designing Sustainable Buildings. Achieving Building Comfort by Natural Means, Springer, Chem, Switzerland. doi:10.1007/978-3-031-04714-5_3.

[3] Sharaf, F. (2020). The impact of thermal mass on building energy consumption: A case study in Al Mafraq city in Jordan. Cogent Engineering, 7(1), 1804092. doi:10.1080/23311916.2020.1804092.

[4] Baiz, W. H., & Fathulla, S. J. (2017). Urban Courtyard Housing Form as a Response to Human Need, Culture and Environment in Hot Climate Regions: Baghdad as a Case Study. International Journal of Engineering Research and Applications, 6(9), 10–19. doi:10.9790/9622-0609011019.

[5] Amiriparyan, P., & Kiani, Z. (2016). Analyzing the homogenous nature of central courtyard structure in formation of Iranian traditional houses. Procedia-social and behavioral sciences, 216, 905-915. doi:10.1016/j.sbspro.2015.12.087.

[6] Cantón, M. A., Ganem, C., Barea, G., & Llano, J. F. (2014). Courtyards as a passive strategy in semi dry areas. Assessment of summer energy and thermal conditions in a refurbished school building. Renewable Energy, 69, 437–446. doi:10.1016/j.renene.2014.03.065.

[7] Yang, L., Fu, R., He, W., He, Q., & Liu, Y. (2020). Adaptive thermal comfort and climate responsive building design strategies in dry–hot and dry–cold areas: Case study in Turpan, China. Energy and Buildings, 209, 109678. doi:10.1016/j.enbuild.2019.109678.

[8] Xu, C., Li, S., Zhang, X., & Shao, S. (2018). Thermal comfort and thermal adaptive behaviours in traditional dwellings: A case study in Nanjing, China. Building and Environment, 142, 153–170. doi:10.1016/j.buildenv.2018.06.006.

[9] Soflaei, F., Shokouhian, M., & Mofidi Shemirani, S. M. (2016). Traditional Iranian courtyards as microclimate modifiers by considering orientation, dimensions, and proportions. Frontiers of Architectural Research, 5(2), 225–238. doi:10.1016/j.foar.2016.02.002.

[10] Sun, Q., Fan, Z., & Bai, L. (2024). Influence of space properties of enclosed patio on thermal performance in hot-humid areas of China. Ain Shams Engineering Journal, 15(2), 102370. doi:10.1016/j.asej.2023.102370.

[11] Soflaei, F., Shokouhian, M., Abraveshdar, H., & Alipour, A. (2017). The impact of courtyard design variants on shading performance in hot- arid climates of Iran. Energy and Buildings, 143, 71–83. doi:10.1016/j.enbuild.2017.03.027.

[12] Benoudjafer, I. (2022). When social practices produce space and create passive cooling systems in hot arid region. Technium Social Sciences Journal, 27, 932–944. doi:10.47577/tssj.v27i1.5316.

[13] Nguyen, A. T., & Reiter, S. (2014). A climate analysis tool for passive heating and cooling strategies in hot humid climate based on Typical Meteorological Year data sets. Energy and Buildings, 68, 756–763. doi:10.1016/j.enbuild.2012.08.050.

[14] Kamal, R., & Rahman, M. S. (2018). A study on feasibility of super adobe technology -an energy efficient building system using natural resources in Bangladesh. IOP Conference Series: Earth and Environmental Science, 143, 12043. doi:10.1088/1755-1315/143/1/012043.

[15] Dabaieh, M., & Eybye, B. T. (2016). A comparative study of human aspects in acclimatization of adobe vernacular architecture: A case from Denmark and Egypt. A/Z ITU Journal of the Faculty of Architecture, 13(1), 29–41. doi:10.5505/itujfa.2016.09709.

[16] Taleghani, M., Tenpierik, M., & van den Dobbelsteen, A. (2014). Introduction into courtyard buildings in different climates. A+ BE| Architecture and the Built Environment, 4(18), 53-86.

[17] Vellinga, M. (2014). Vernacular architecture and sustainability: Two or three lessons. Vernacular Architecture: Towards a Sustainable Future, CRC Press, Boca Raton, United States.

[18] Al-Hafith, O., Satish, B. K., Bradbury, S., & Wilde, P. De. (2017). Simulation of courtyard spaces in a desert climate. Energy Procedia, 142, 1997–2002. doi:10.1016/j.egypro.2017.12.401.

[19] Abdulkareem, H. A. (2016). Thermal Comfort through the Microclimates of the Courtyard. A Critical Review of the Middle-eastern Courtyard House as a Climatic Response. Procedia-Social and Behavioral Sciences, 216, 662–674. doi:10.1016/j.sbspro.2015.12.054.

[20] Saadatjoo, P., Badamchizadeh, P., & Mahdavinejad, M. (2023). Towards the new generation of courtyard buildings as a healthy living concept for post-pandemic era. Sustainable Cities and Society, 97, 104726. doi:10.1016/j.scs.2023.104726.

[21] Han, J., Li, X., Li, B., Yang, W., Yin, W., Peng, Y., & Feng, T. (2023). Research on the influence of courtyard space layout on building microclimate and its optimal design. Energy and Buildings, 289, 113035. doi:10.1016/j.enbuild.2023.113035.

[22] Ibrahim, Y., Kershaw, T., Shepherd, P., & Elkady, H. (2022). Multi-objective optimisation of urban courtyard blocks in hot arid zones. Solar Energy, 240, 104–120. doi:10.1016/j.solener.2022.05.024.

[23] Guedouh, M. S., Zemmouri, N., Hanafi, A., & Qaoud, R. (2019). Passive strategy based on courtyard building morphology impact on thermal and luminous environments in hot and arid region. Energy Procedia, 157, 435–442. doi:10.1016/j.egypro.2018.11.208.

[24] Pilechiha, P., Norouziasas, A., Ghorbani Naeini, H., & Jolma, K. (2022). Evaluation of occupant's adaptive thermal comfort behaviour in naturally ventilated courtyard houses. Smart and Sustainable Built Environment, 11(4), 793–811. doi:10.1108/SASBE-02-2021-0020.

[25] Al-Hafith, O., BK, S., & de Wilde, P. (2023). Assessing annual thermal comfort extent in central courtyards: Baghdad as a case study. Smart and Sustainable Built Environment, 12(3), 660–681. doi:10.1108/SASBE-09-2021-0154.

[26] Taleb, H. M., & Abumoeilak, L. (2021). An assessment of different courtyard configurations in urban communities in the United Arab Emirates (UAE). Smart and Sustainable Built Environment, 10(1), 67–89. doi:10.1108/SASBE-08-2019-0116.

[27] Sahebzadeh, S., Dalvand, Z., Sadeghfar, M., & Heidari, A. (2020). Vernacular architecture of Iran's hot regions; elements and strategies for a comfortable living environment. Smart and Sustainable Built Environment, 9(4), 573–593. doi:10.1108/SASBE-11-2017-0065.

[28] Gunasagaran, S., Saw, E. S., Mari, T. S., Srirangam, S., & Ng, V. (2023). Courtyard configuration to optimize shading, daylight and ventilation in a tropical terrace house using simulation. International Journal of Architectural Research: Archnet-IJAR, 17(1), 109–123. doi:10.1108/ARCH-12-2021-0354.

[29] Alharbi, F. R., & Csala, D. (2021). Gulf cooperation council countries' climate change mitigation challenges and exploration of solar and wind energy resource potential. Applied Sciences, 11(6), 2648. doi:10.3390/app11062648.

[30] Mahmood, H., & Furqan, M. (2021). Oil rents and greenhouse gas emissions: spatial analysis of Gulf Cooperation Council countries. Environment, Development and Sustainability, 23(4), 6215–6233. doi:10.1007/s10668-020-00869-w.

[31] Mahmood, H., Asadov, A., Tanveer, M., Furqan, M., & Yu, Z. (2022). Impact of Oil Price, Economic Growth and Urbanization on CO2 Emissions in GCC Countries: Asymmetry Analysis. Sustainability, 14(8), 4562. doi:10.3390/su14084562.

[32] Abumoghli, I., & Goncalves, A. (2020). Environmental challenges in the MENA region. UN Environmental Program, United Nations, Nairobi, Kenya.

[33] Abulibdeh, A., Zaidan, E., & Al-Saidi, M. (2019). Development drivers of the water-energy-food nexus in the Gulf Cooperation Council region. Development in Practice, 29(5), 582–593. doi:10.1080/09614524.2019.1602109.

[34] Abdmouleh, Z., Alammari, R. A. M., & Gastli, A. (2015). Recommendations on renewable energy policies for the GCC countries. Renewable and Sustainable Energy Reviews, 50, 1181–1191. doi:10.1016/j.rser.2015.05.057.

[35] Romero, P., Navarro, J. M., & Ordaz, P. B. (2022). Towards a sustainable viticulture: The combination of deficit irrigation strategies and agroecological practices in Mediterranean vineyards. A review and update. Agricultural Water Management, 259, 107216. doi:10.1016/j.agwat.2021.107216.

[36] Elrahmani, A., Hannun, J., Eljack, F., & Kazi, M. K. (2021). Status of renewable energy in the GCC region and future opportunities. Current Opinion in Chemical Engineering, 31, 100664. doi:10.1016/j.coche.2020.100664.

[37] Mendez, C., Contestabile, M., & Bicer, Y. (2023). Hydrogen fuel cell vehicles as a sustainable transportation solution in Qatar and the Gulf cooperation council: a review. International Journal of Hydrogen Energy, 48(99), 38953–38975. doi:10.1016/j.ijhydene.2023.04.194.

[38] Abubakar, I. R., & Alshammari, M. S. (2023). Urban planning schemes for developing low-carbon cities in the Gulf Cooperation Council region. Habitat International, 138, 102881. doi:10.1016/j.habitatint.2023.102881.

[39] Ibrahim, I. (2019). Eco-traditional courtyard houses in UAE: A case study of the Sharjah museums. WIT Transactions on the Built Environment, 183, 15–24. doi:10.2495/ARC180021.

[40] Zamani, Z., Heidari, S., & Hanachi, P. (2018). Reviewing the thermal and microclimatic function of courtyards. Renewable and Sustainable Energy Reviews, 93, 580–595. doi:10.1016/j.rser.2018.05.055.

[41] He, B. J. (2019). Towards the next generation of green building for urban heat island mitigation: Zero UHI impact building. Sustainable Cities and Society, 50, 101647. doi:10.1016/j.scs.2019.101647.

[42] Mohora, I., & Anghel, A. A. (2019). Revitalization Proposals for Green Interior Courtyards in the Historical Centre of Timisoara. IOP Conference Series: Materials Science and Engineering, 471, 82027. doi:10.1088/1757-899X/471/8/082027.

[43] Gupta, R., & Joshi, M. (2021). Courtyard: A look at the relevance of courtyard space in contemporary houses. Civil Engineering and Architecture, 9(7), 2261–2272. doi:10.13189/cea.2021.090713.

[44] Fernandes, J., Mateus, R., Bragança, L., & Correia Da Silva, J. J. (2015). Portuguese vernacular architecture: The contribution of vernacular materials and design approaches for sustainable construction. Architectural Science Review, 58(4), 324–336. doi:10.1080/00038628.2014.974019.

[45] El-Shorbagy, A. (2010). Traditional Islamic-Arab House: Vocabulary and Syntax. International Journal of Civil & Environmental Engineering, 10(4), 15–20.

[46] Alabid, J., & Taki, A. (2017). Optimising residential courtyard in terms of social and environmental performance for Ghadames Housing, Libya. Proceedings of 33rd PLEA International Conference: Design to Thrive, PLEA 2017, 2-5 July, 2017, Edinburgh, Scotland.

[47] Liu, Y. Q., Wang, A. L., Hou, J., Chen, X. Y., & Xia, J. S. (2020). Comprehensive evaluation of rural courtyard utilization efficiency: A case study in Shandong Province, Eastern China. Journal of Mountain Science, 17(9), 2280-2295. doi:10.1007/s11629-019-5824-x.

[48] Friess, W. A., & Rakhshan, K. (2017). A review of passive envelope measures for improved building energy efficiency in the UAE. Renewable and Sustainable Energy Reviews, 72, 485–496. doi:10.1016/j.rser.2017.01.026.

[49] Ozarisoy, B., & Altan, H. (2021). Systematic literature review of bioclimatic design elements: Theories, methodologies and cases in the South-eastern Mediterranean climate. Energy and Buildings, 250, 111281. doi:10.1016/j.enbuild.2021.111281.

[50] Al-Kodmany, K. (1999). Residential visual privacy: Traditional and modern architecture and urban design. Journal of Urban Design, 4(3), 283–311. doi:10.1080/13574809908724452.

[51] Bekleyen, A., & Dalkiliç, N. (2011). The influence of climate and privacy on indigenous courtyard houses in Diyarbakır, Turkey. Scientific Research and Essays, 6(4), 908–922.

[52] Wang, Y. P., Wang, Y., & Wu, J. (2009). Urbanization and informal development in China: Urban villages in Shenzhen. International Journal of Urban and Regional Research, 33(4), 957–973. doi:10.1111/j.1468-2427.2009.00891.x.

[53] Foruzanmehr, A., & Vellinga, M. (2011). Vernacular architecture: Questions of comfort and practicability. Building Research and Information, 39(3), 274–285. doi:10.1080/09613218.2011.562368.

[54] Zhang, Y., & Barrett, P. (2012). Factors influencing occupants' blind-control behaviour in a naturally ventilated office building. Building and Environment, 54, 137–147. doi:10.1016/j.buildenv.2012.02.016.

[55] Shi, Z., Qian, H., Zheng, X., Lv, Z., Li, Y., Liu, L., & Nielsen, P. V. (2018). Seasonal variation of window opening behaviors in two naturally ventilated hospital wards. Building and Environment, 130, 85–93. doi:10.1016/j.buildenv.2017.12.019.

[56] Al Surf, M., Susilawati, C., & Trigunarsyah, B. (2012). Analyzing the literature for the link between the conservative Islamic culture of Saudi Arabia and the design of sustainable housing. Proceedings of 2nd International Conference Socio-Political and Technological Dimensions of Climate Change, 19-21 November, 2012, Selangor, Malaysia.

[57] Ghaffarianhoseini, A., Berardi, U., & Ghaffarianhoseini, A. (2015). Thermal performance characteristics of unshaded courtyards in hot and humid climates. Building and Environment, 87, 154–168. doi:10.1016/j.buildenv.2015.02.001.

[58] Markus, B. (2016). A review on courtyard design criteria in different climatic zones. African Research Review, 10(5), 181. doi:10.4314/afrrev.v10i5.13.

[59] Nasrollahi, N., Hatami, M., Khastar, S. R., & Taleghani, M. (2017). Numerical evaluation of thermal comfort in traditional courtyards to develop new microclimate design in a hot and dry climate. Sustainable Cities and Society, 35, 449–467. doi:10.1016/j.scs.2017.08.017.

[60] Wang, F., & Liu, Y. (2002). Thermal environment of the courtyard style cave dwelling in winter. Energy and Buildings, 34(10), 985–1001. doi:10.1016/S0378-7788(01)00145-1.

[61] Soflaei, F., Shokouhian, M., & Zhu, W. (2017). Socio-environmental sustainability in traditional courtyard houses of Iran and China. Renewable and Sustainable Energy Reviews, 69, 1147–1169. doi:10.1016/j.rser.2016.09.130.

[62] Zhu, J., Feng, J., Lu, J., Chen, Y., Li, W., Lian, P., & Zhao, X. (2023). A review of the influence of courtyard geometry and orientation on microclimate. Building and Environment, 236. doi:10.1016/j.buildenv.2023.110269.

[63] Abu-Ghazzeh, T. M. (1999). Housing layout, social interaction, and the place of contact in Abu-Nuseir, Jordan. Journal of Environmental Psychology, 19(1), 41–73. doi:10.1006/jevp.1998.0106.

[64] Luo, X., & Huang, J. (2022). The Exploration of New Courtyard Architecture Based on the Guidance of Architectural Culture and Technology. Advances in Civil Engineering, 2022, 1-12. doi:10.1155/2022/5029647.

[65] Hyde, R. (Ed.). (2012). Bioclimatic Housing. Routledge, London, United Kingdom. doi:10.4324/9781849770569.

[66] Al-Sallal, K. A., Al-Rais, L., & Dalmouk, M. Bin. (2013). Designing a sustainable house in the desert of Abu Dhabi. Renewable Energy, 49, 80–84. doi:10.1016/j.renene.2012.01.061.

[67] Zhao, M., Mehra, S. R., & Künzel, H. M. (2022). Energy-saving potential of deeply retrofitting building enclosures of traditional courtyard houses − A case study in the Chinese Hot-Summer-Cold-Winter zone. Building and Environment, 217, 109106. doi:10.1016/j.buildenv.2022.109106.

[68] Alrashed, F., Asif, M., & Burek, S. (2017). The role of vernacular construction techniques and materials for developing zero-energy homes in various desert climates. Buildings, 7(1), 17. doi:10.3390/buildings7010017.

[69] Konya, A. (2013). Design primer for hot climates. Elsevier, Amsterdam, Netherlands.

[70] Agha, R. H. M. (2022). The possible application of intelligent systems in traditional courtyard houses in Iraq. Applied Engineering and Technology, 1(1), 11–23. doi:10.31763/aet.v1i1.666.

[71] Chandel, S. S., Sharma, V., & Marwah, B. M. (2016). Review of energy efficient features in vernacular architecture for improving indoor thermal comfort conditions. Renewable and Sustainable Energy Reviews, 65, 459–477. doi:10.1016/j.rser.2016.07.038.

[72] Pardo, J. M. F. (2023). Challenges and Current Research Trends for Vernacular Architecture in a Global World: A Literature Review. Buildings, 13(1), 162. doi:10.3390/buildings13010162.

[73] Saadatian, O., Sopian, K., Salleh, E., Lim, C. H., Riffat, S., Saadatian, E., Toudeshki, A., & Sulaiman, M. Y. (2013). A review of energy aspects of green roofs. Renewable and Sustainable Energy Reviews, 23, 155–168. doi:10.1016/j.rser.2013.02.022.

[74] Ragheb, A., El-Shimy, H., & Ragheb, G. (2016). Green Architecture: A Concept of Sustainability. Procedia - Social and Behavioral Sciences, 216, 778–787. doi:10.1016/j.sbspro.2015.12.075.

[75] Perera, A. T. D., Javanroodi, K., & Nik, V. M. (2021). Climate resilient interconnected infrastructure: Co-optimization of energy systems and urban morphology. Applied Energy, 285, 116430. doi:10.1016/j.apenergy.2020.116430.

[76] Du, X., Bokel, R., & van den Dobbelsteen, A. (2014). Building microclimate and summer thermal comfort in free-running buildings with diverse spaces: A Chinese vernacular house case. Building and Environment, 82, 215–227. doi:10.1016/j.buildenv.2014.08.022.

[77] Subramanian, C., Ramachandran, N., & Kumar, S. S. (2016). Comparative Investigation of Traditional, Modern and designed Solar Passive Building for thermal comfort in Thanjavur region. International Journal of Innovations in Engineering and Technology, 7(2), 283–291.

[78] Manioğlu, G., & Yilmaz, Z. (2008). Energy efficient design strategies in the hot dry area of Turkey. Building and Environment, 43(7), 1301–1309. doi:10.1016/j.buildenv.2007.03.014.

[79] Cabeza, L. F., de Gracia, A., & Pisello, A. L. (2018). Integration of renewable technologies in historical and heritage buildings: A review. Energy and Buildings, 177, 96–111. doi:10.1016/j.enbuild.2018.07.058.

[80] Molua, E. L. (2009). Accommodation of climate change in coastal areas of Cameroon: Selection of household-level protection options. Mitigation and Adaptation Strategies for Global Change, 14(8), 721–735. doi:10.1007/s11027-009-9194-5.

[81] Prosun, P. (2011). The LIFT House: An amphibious strategy for sustainable and affordable housing for the urban poor in flood-prone Bangladesh. Master Thesis, University of Waterloo, Waterloo, Canada.

[82] SCTDA. (2024). Majlis Al Midfa. A square with a one-of-a-kind wind tower in the whole of UAE, Relive past gatherings in a historic square with a unique landmark. Sharjah Commerce & Tourism Development Authority (SCTDA), Sharjah, United Arab Emirates. Available online: https://www.visitsharjah.com/activities/heritage/majlis-al-midfa/ (accessed on February 2024).

[83] Google Map. (2023). Location of Majlis Al Midfa Building, Sharjah, United Arab Emirates. Available online: https://maps.app.goo.gl/CxFa2BoNMgjoV2KN9 (accessed on February 2024).

[84] Anderson, G. (1991). Sharjah, UAE: the urban conservative dilemma. Master Thesis, Durham University, Durham, United Kingdom.

[85] Kazimee, B. A. (2012). Heritage and sustainability in the Islamic built environment. Wit Press, Billerica, United States.

[86] Golubchikov, O., & Badyina, a. (2012). Sustainable housing for sustainable cities: a policy framework for developing countries, UN-HABITAT, Nairobi, Kenya.

[87] Correia, M., Dipasquale, L., & Mecca, S. (2010). Versus: heritage for tomorrow. Vernacular knowledge for sustainable architecture. Firenze University Press, Firenze, Italy. doi:10.36253/978-88-6655-742-5.

[88] Ly, P., Birkeland, J., & Demirbilek, N. (2010). Applying environmentally responsive characteristics of vernacular architecture to sustainable housing in Vietnam. Sustainable Architecture & Urban Development, 4, 287-306.

[89] Aldersoni, A., Albaker, A., Alturki, M., & Said, M. A. (2022). The Impact of Passive Strategies on the Overall Energy Performance of Traditional Houses in the Kingdom of Saudi Arabia. Buildings, 12(11). doi:10.3390/buildings12111837.

[90] Guedes, M. C. (2013). Sustainable Architecture in Africa. Sustainability, Energy and Architecture, Academic Press, Cambridge, United States. doi:10.1016/b978-0-12-397269-9.00016-5.

[91] Pisello, A. L., Paolini, R., Diamanti, M. V., Fortunati, E., Castaldo, V. L., & Torre, L. (2016). Nanotech-based cool materials for building energy efficiency. Nano and Biotech Based Materials for Energy Building Efficiency, Springer, Cham, Switzerland. doi:10.1007/978-3-319-27505-5_9.

[92] Gharahshir, M. (2019). Implementation of sustainable architecture patterns in hot and dry regions of Iran by investigating on vernacular sustainable architecture patterns. Master Thesis, University of Applied Sciences, Erfurt, Germany.

[93] Badr, S. (2014). Towards Low Energy Buildings through Vernacular Architecture of Arab Cities. Alexandria University, Alexandria, Egypt.

[94] Chohan, A. H., & Awad, J. (2022). Wind Catchers: An Element of Passive Ventilation in Hot, Arid and Humid Regions, a Comparative Analysis of Their Design and Function. Sustainability, 14(17), 11088. doi:10.3390/su141711088.

[95] Varela-Boydo, C. A., Moya, S. L., & Watkins, R. (2021). Analysis of traditional windcatchers and the effects produced by changing the size, shape, and position of the outlet opening. Journal of Building Engineering, 33, 101828. doi:10.1016/j.jobe.2020.101828.

[96] Mauree, D., Naboni, E., Coccolo, S., Perera, A. T. D., Nik, V. M., & Scartezzini, J. L. (2019). A review of assessment methods for the urban environment and its energy sustainability to guarantee climate adaptation of future cities. Renewable and Sustainable Energy Reviews, 112, 733–746. doi:10.1016/j.rser.2019.06.005.

[97] Jalaei, F., & Jrade, A. (2015). Integrating building information modeling (BIM) and LEED system at the conceptual design stage of sustainable buildings. Sustainable Cities and Society, 18, 95–107. doi:10.1016/j.scs.2015.06.007.

[98] He, Y., Kwok, K., Mason, M., & Douglas, G. (2013). How should future building structure and emergency response cope with bushfire attacks? Australasia Fire Authority Council. Conference, 2–5 September, 2013, Melbourne, Australia.

[99] Charron, R., & Athienitis, A. (2006). Design and optimization of net zero energy solar homes. ASHRAE Transactions, 112(2), 285–295.

[100] Athienitis, A. K., & O'Brien, W. (2015). Modeling, design, and optimization of net-zero energy buildings. Ernst & Sohn, Berlin, Germany. doi:10.1002/9783433604625.

[101] Owusu, P. A., & Asumadu-Sarkodie, S. (2016). A review of renewable energy sources, sustainability issues and climate change mitigation. Cogent Engineering, 3(1), 1167990. doi:10.1080/23311916.2016.1167990.

[102] Heidari, A., Taghipour, M., & Yarmahmoodi, Z. (2021). The effect of fixed external shading devices on daylighting and thermal comfort in residential building. Journal of Daylighting, 8(2), 165–180. doi:10.15627/JD.2021.15.

[103] Roetzel, A., & Tsangrassoulis, A. (2012). Impact of climate change on comfort and energy performance in offices. Building and environment, 57, 349-361. doi:10.1016/j.buildenv.2012.06.002.

[104] Lomas, K. J. (1996). The U.K. Applicability Study: An Evaluation of Thermal Simulation Programs for Passive Solar House Design. Building and Environment, 31(3), 197–206. doi:10.1016/0360-1323(95)00050-X.

[105] Nutkiewicz, A., Jain, R. K., & Bardhan, R. (2018). Energy modeling of urban informal settlement redevelopment: Exploring design parameters for optimal thermal comfort in Dharavi, Mumbai, India. Applied Energy, 231, 433–445. doi:10.1016/j.apenergy.2018.09.002.

[106] Shimoda, Y., Sugiyama, M., Nishimoto, R., & Momonoki, T. (2021). Evaluating decarbonization scenarios and energy management requirement for the residential sector in Japan through bottom-up simulations of energy end-use demand in 2050. Applied Energy, 303, 117510. doi:10.1016/j.apenergy.2021.117510.

[107] Bajic, V. (2022). Typical wall construction thermal properties. Sefaira, London, United Kingdom. Available online: https://support.sefaira.com/hc/en-us/articles/4416428261649 (accessed on February 2024).

[108] Bajic, V. (2022). Typical roof construction thermal properties. Sefaira, London, United Kingdom. Available online: https://support.sefaira.com/hc/en-us/articles/4416435350417 (accessed on February 2024).

[109] Lutheran, A. (2022). Default HVAC Systems for new projects. Sefaira, London, United Kingdom. Available online: https://support.sefaira.com/hc/en-us/articles/206249303-Default-HVAC-Systems-for-new-projects (accessed on June 2023).

[110] Corney, A. (2015). Design Loads & Outside Air in the Space Use Tab Explained. Sefaira, London, United Kingdom. Available online: https://support.sefaira.com/hc/en-us/articles/204380595-Design-Loads-Outside-Air-in-the-Space-Use-Tab-Explained (accessed on February 2024).

[111] Federal Competitiveness and Statistics Centre. (2019). Electricity 2019. Federal Competitiveness and Statistics Centre, Dubai, UAE. Available online: https://datasource.kapsarc.org/explore/dataset/electricity-tariff-by-authority-slab-consumption-and-sector/table/?disjunctive.authority&disjunctive.sector&disjunctive.consumption_slab&disjunctive.nationality&sort=authority (accessed on February 2024).

[112] SolarFeeds. (2023). Solar Power Statistics in United Arab Emirates 2021. SolarFeeds, Ontario, United States. Available online: https://www.solarfeeds.com/mag/solar-power-statistics-in-uae-2021/ (accessed on February 2024).

[113] Photovoltaic Solar Energy. (2023). Dimensions of photovoltaic panels: how to choose them correctly? Available online: https://photovoltaicsolarenergy.org/dimensions-of-photovoltaic-panels-how-to-choose-them-correctly/ (accessed on May 2023).

[114] SEWA. (2023). The Declaration of Sharjah City of Conservation. Sharjah Electricity and Water Authority (SEWA), Sharjah, UAE. Available online: https://www.sewa.gov.ae/en/content.aspx?P=4JVpzOgumWxxDeo5mu1mhQ%3D%3D (accessed on February 2024).

[115] Poudel, N. (2022). Section 4: An Introduction to Sefaira Daylighting Visualization. Sefaira, London, UK. Available online: https://support.sefaira.com/hc/en-us/articles/360001328352-Section-4-An-Introduction-to-Sefaira-Daylighting-Visualization (accessed on February 2024).
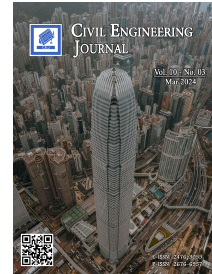
Bond Strength of Rectangular CFSST Columns after Exposed to Elevated Temperature

Anandapadmanaban K. [1], A. S. Santhi [1*]

[1] School of Civil Engineering, Vellore Institute of Technology Vellore-632014, India.

Abstract

This article investigates the bond- behavior of Rectangular Concrete-filled stainless-steel tubular (RCFSST) columns under post-fire conditions. The main objective of this research was to obtain τ-s relationship of RCFSST columns under the combined effects of high temperature and concrete age. A total of sixteen specimens, including four reference specimens, were tested with different parameters, namely: i) temperature (600 °C, 800 °C & 1000 °C) ii) different concrete ages (30 days, 60 days, 90 days & 180 days). Analyzing the τ-s curves of the test specimens, chemical adhesion and micro-locking were the principal forces contributing to bond strength at lower concrete ages under post-fire conditions. At a higher concrete age, RCFSST specimens displayed a longer curve after the inflection point, indicating the contribution of macro-locking forces in amplifying the bond-strength. Five distinct curve types were found from the experiments. Type 1 curves with three stages, i) initial linear, ii) non-linear, and ii) final linear stage, had a higher frequency among the other types. For 90-day cured specimens, a decline in bond strength was observed at higher temperatures, but for 180 days cured specimens, a significant rise was seen under post-fire conditions. A new set of τ-s relations for RCFSST columns with different concrete ages under post-fire was established.

Keywords: Bond-Behaviour; Rectangle Stainless-Steel; Concrete Age; Concrete-Filled Stainless-Steel Tubular Columns; Push-Out Test.

1. Introduction

In the context of innovative composite structures, concrete-filled stainless-steel tubular (CFSST) columns contribute more beneficial features in the construction field. The merits of encasing concrete with steel tubes perform better in most of the complex loading conditions. Higher ductility and energy dissipation characteristics [1], competence in seismic zones [1], higher static load resisting capacity, and transverse impact resistance capabilities [2] make these structures an inevitable choice among engineers. Currently, there is a demand for the performance of these structures under various fire scenarios. With these rises in demand, research on exploring new probabilities for enhancing the fire performance of these structures is being carried out.

One of the most crucial features that needs to be optimized in these situations is the bond between steel and concrete. The bond between the inner side of the steel tube and the core concrete plays a vital role in developing a composite action. Without sufficient bond development, the concrete core and stainless-steel act as individual elements, supporting the load disjointedly. Generally, the bond between the inner part of the steel tube and the outer surface of the core concrete takes place through interface frictional forces between the steel and concrete surface, chemical adhesive forces, and mechanical interlock forces [3], as shown in Figure 1. The interface friction force between stainless steel and concrete provides a major contribution to the shear resistance, whereas significant contributions were also noted from

the chemical adhesive force and the mechanical interlock forces [3]. Figure 2 shows the ideal response of the CFST column under the push-out test [4]. Various factors influence the bond between the inner tube and concrete infill in CFSST columns. The factors include steel tube thickness, concrete shrinkage, type of aggregates, temperature in core concrete, shape of the sections [5], and surface roughness.
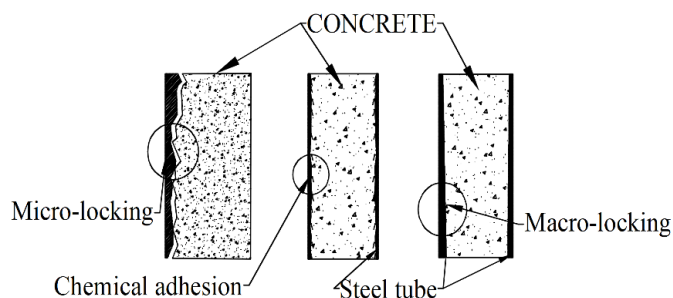

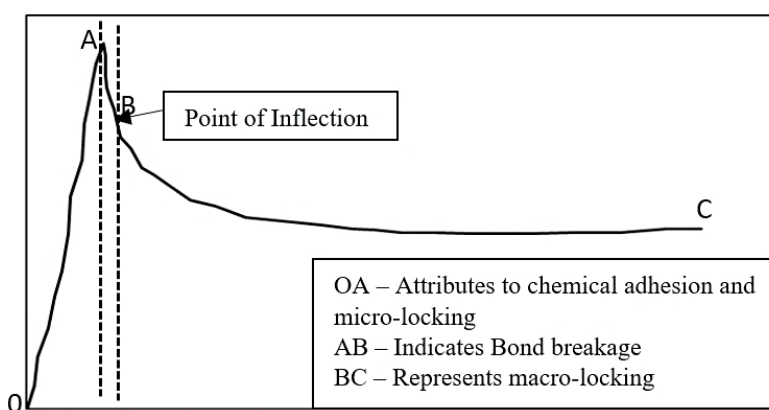**Figure 1. Illustration of various bond mechanism in CFST columns**

Figure 2. Ideal τ-s curve of CFST columns

Circular CFST sections have more advanced bond strength than other sections. Hoop stresses developed in circular sections increase the confinement of concrete, resulting in higher bond strength. Rectangular and square sections have lower bond strengths. This is due to the fact that the corner regions of rectangular and square sections are ineffective in bonding and reduce bonding capacity. In rectangular CFST columns, the major contribution to the bond strength was governed by the macro-locking mechanism. The influence of friction and chemical adhesion was less significant [6].

Steel tubes with smooth inner surfaces reduce friction between the inner surface and concrete, resulting in a reduction in bond strength [5]. Concrete with light-weight aggregate demonstrates higher bond strength when compared to normal aggregates [7]. A series of tests on the bond strength of steel-encased concrete and concrete-encased steel composite columns were conducted with normal and ultra-high-performance concrete (UHPC) [8]. Concrete-encased steel columns with both normal and UHPC concrete displayed a significant increase in bond strength compared to steel-encased concrete columns. A series of tests were conducted by embedding reinforcing bars in UHPC concrete in CFST columns, and a simplified local bond-slip model was proposed [9]. Test variables include anchorage length (2d, 5d, 7d), where d is the diameter of the embedded bar. For anchorage lengths less than twice the diameter of the bar, a uniform bond-stress distribution was observed during pull-out tests. Whereas, for anchorage length less than 7d, a linear distribution of bond stress was observed.

Concrete shrinkage is also an important factor that affects the bond strength, and measures have been taken to reduce shrinkage by replacing normal concrete with expansive concrete, which exhibited better results [5]. The age of concrete increases the shrinkage effects. For longer-lasting concrete, the steel type had a lesser influence on bond strength [5]. Special provisions such as welding internal rings and shear studs were employed to increase the bond capacity of composite sections, and welding internal rings showed enhanced bond strength [10]. Post-fire test results show a clear contribution of shape effects and temperature effects on the bond strength of CFST columns [11]. However, in square columns, an increase in bond strength was absorbed after exposing the specimens for up to 180 minutes after initial decrement. This was explained by the thermal expansion of the concrete core, resulting in an increase in frictional resistance between steel and concrete surfaces. Four different types of curves were categorized [5] for carbon steel,

stainless steel, circular, and square cross-sections, namely Type A, Type B, Type-C, and Type-D curves, as shown in Figure 3. Type A curve has an early linear segment, following a non-linear curve before reaching the peak point, beyond which bond stress reduces gradually. Carbon steel specimens exhibited a Type A response. Type B exhibited a similar trend as in Type A, but in the post-peak stage, a significant drop in bond stress was observed, followed by a recovery in bond stress. Stainless steel exhibited a Type B response. Types C and D had an initial linear portion as well, but their curves tend to have an upper trail during the entire loading stage. Type C and Type D responses were observed in the post-fire push-out test.
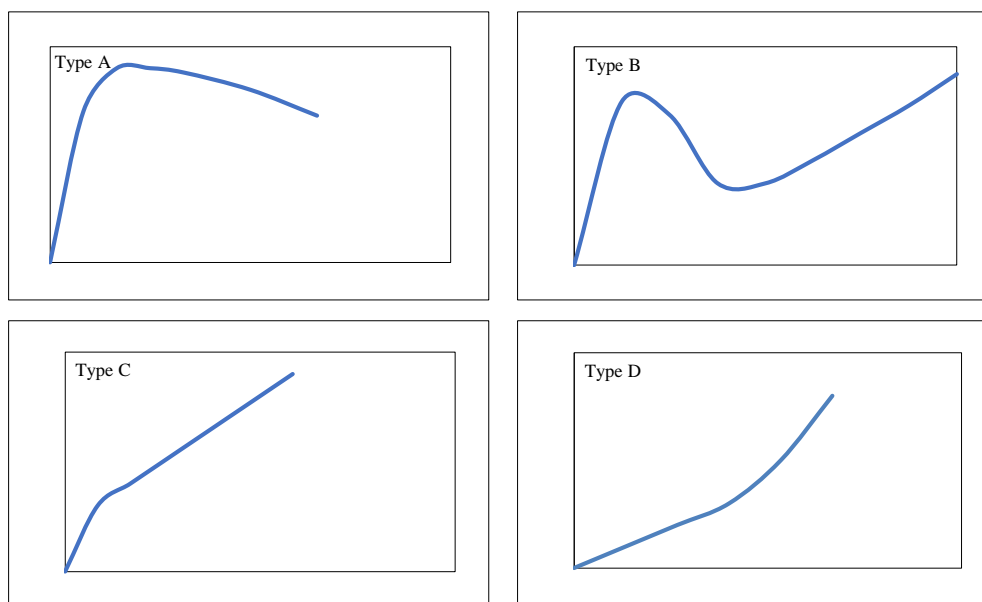
Figure 3. Typical Bond-slip curve for push-out tests on CFST columns

A series of push-out tests with CFST columns with different concrete infills were reported in the literature [3, 5, 7, 11–16]. Prediction models for the bond capacity of circular and square CFST columns were developed using Artificial Neural Networks (ANN) [17]. Thickness of steel tube, compression strength of concrete, and concrete age was fed as input parameters, and using experimental data from the literature, a prediction model was generated that showed better accuracy. To investigate the effects of shrinkage and creep, CFST columns were subjected to a 490-day shrinkage test [18]. Analysis of test results showed that concrete shrinkage and creep had a higher influence on the development of confining effects. It was also observed that the outer tube had no appreciable influence on initial stiffness under service loading conditions. The bond strength of square CFST columns with an H-shaped outer steel casing was also investigated at ambient temperatures [19]. It is reported that chemical adhesion mechanisms predominated at the initial stages of loading. Around 39% of micro-locking mechanisms had a higher influence on the bond capacity of square H-shaped CFST columns.

Investigations on post-fire push-out tests on square and circular CFST were conducted with different temperatures and mass replacement percentages of recycled coarse aggregate (RCA) [20]. It was observed that circular CFST specimens displayed better bond behavior and higher interfacial damage resistance characteristics than square CFST columns. The temperature and RCA had different influences on the test specimens, as the replacement of RCA decreased the bond strength in CFST columns. The bond behavior of CFST with light-weight concrete containing rock-wool waste was investigated under post-fire conditions [21]. The presence of rock wool enhanced the bond strength of CFST columns under post-fire conditions. The provision of internal rings inside steel tubes enhanced the bond strength to an appreciable extent, even at high temperatures [5]. Increasing the axial load ratio also contributes to the development of higher bond strength in CFST columns under post-fire conditions. A series of tests on post-fire push-out tests on elliptical, circular, and square cross-sectional shapes were conducted [22]. Circular CFST columns had higher bond strength among the three shapes, with elliptical CFST columns displaying the lowest bond strength values.

The test results of ambient and post-fire bond strength of CFST columns [21–26] from the literature are shown in Figure 4 for comparison with Japanese, Chinese, and Eurocode values. It can be seen that bond strength in CFST columns has enhanced over the past decade.
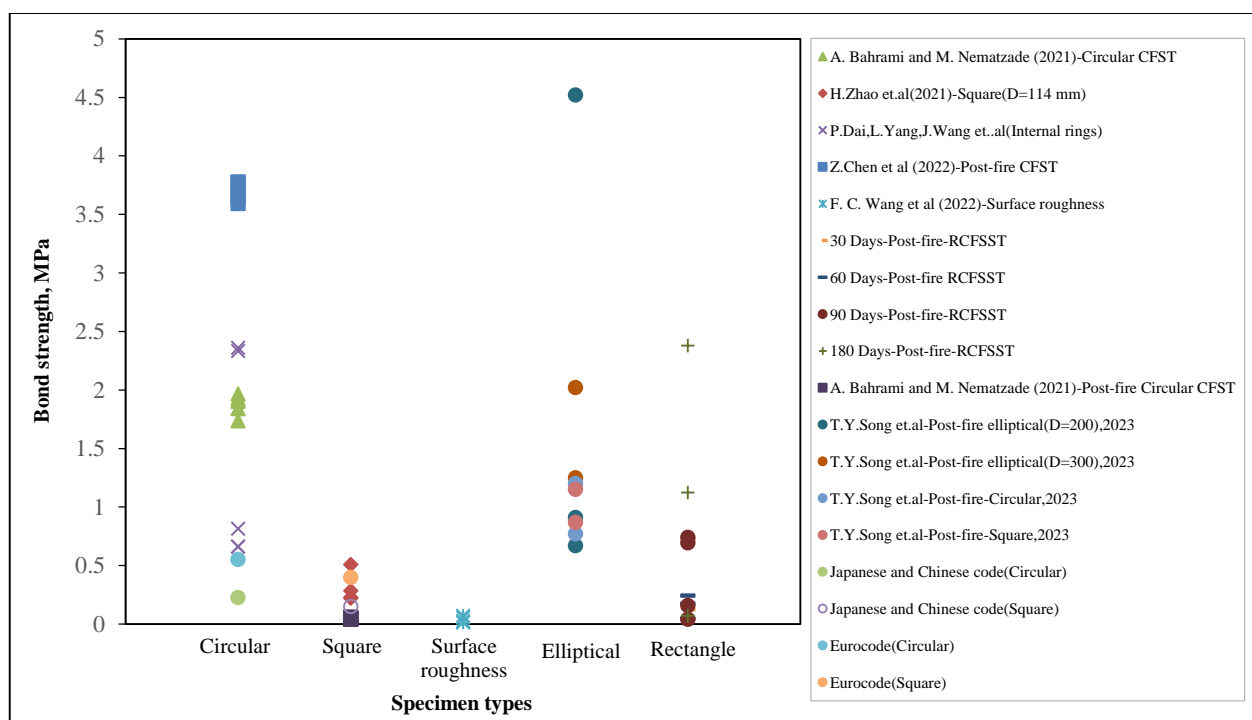
Figure 4. Bond strength of ambient and post-fire CFST columns from test results and literature

The post-fire bond strength of rectangular CFSST columns is little known. Literature studies have always been limited to circular and square CFSST columns. Investigation of other shapes will help the research community gain a better understanding of the behavior of composite columns. Lower bond strengths in rectangular sections make them less demanding. On the other hand, rectangular sections are more feasible during connections, precisely in beam-column connections [4]. They show appreciable resistance to global buckling. Sections other than circular ones would exhibit an uneven temperature distribution [27]. Critical examination of the performance of such sections creates new research interests. This investigation is carried out to provide sufficient research background on the post-fire bond strength of rectangle-shaped CFSST columns.

RCFSST columns with varied concrete ages were examined under post-fire conditions in this investigation, and the combined effects of high temperature and concrete age on the bond strength of RCFSST columns have been explored. A new set of experimental data on the post-fire bond strength of rectangular concrete-filled stainless steel tubular columns for different concrete ages was recorded for the first time. New τ-s curves were observed from the results. Precise post-fire bond-slip models should be established to perform numerical simulations in the future. The recorded data will assist such research.

2. Experiments

2.1. General

A total of 16 RCFSST columns were cast and tested after subjecting the specimens to specific temperature ranges and cooling them to ambient room temperature.

The parameters considered in the test include

- Temperature (T): 600 °C, 800 °C, 1000 °C

- Concrete age: 30 days, 60 days, 90 days, and 180 days

The dimensions of the rectangular columns were 100 mm (depth) × 50 mm (width) × 2 mm (thickness). The specimen details are shown in Table 1. The temperature of the specimens was denoted by the letter "T" preceded by the respective numerical, whereas the age of the concrete was denoted by the letter "D" preceded by the numerical denoted in days. For example, in the specimen label "30D600T", "D30" represents the concrete age of 30 days. "600T" represents the temperature of 600 °C. Reference specimens are indicated with the letter "R" followed by their respective concrete ages. For example, in the reference specimen label "R60D", the letter "R" represents the reference specimen, and "60D" represents the concrete age of 60 days.

Table 1. Details of test specimen

S. No.	Specimen ID	Length, L (mm)	Depth, D (mm)	Height, h(mm)	t (mm)	T° C	Nu	τu	Su	Curve type
1	R30D	100	50	500	2	20	5.11	0.04	15.28	-
2	30D600T	100	50	500	2	600	16.36	0.127	17.69	1
3	30D800T	100	50	500	2	800	93	0.727	26.29	3
4	30D1000T	100	50	500	2	1000	-	-	-	-
5	R60D	100	50	500	2	20	8.13	0.05	24.92	2
6	60D600T	100	50	500	2	600	90.41	0.244	35.79	5
7	60D800T	100	50	500	2	800	-	-	-	-
8	60D1000T	100	50	500	2	1000	64.56	0.175	28.91	5
9	R90D	100	50	500	2	20	7.43	0.04	37.90	2
10	90D600T	100	50	500	2	600	20.88	0.158	3.01	1
11	90D800T	100	50	500	2	800	94.93	0.742	35.70	1
12	90D1000T	100	50	500	2	1000	88.83	0.695	35.52	4
13	R180D	100	50	500	2	20	37.77	0.275	20.75	5
14	180D600T	100	50	500	2	600	-	-	-	-
15	180D800T	100	50	500	2	800	143.9	1.125	25.21	1
16	180D1000T	100	50	500	2	1000	306.07	2.394	22.06	4

2.2. Material Properties

2.2.1. Stainless Steel

Tensile tests were carried out to determine the material properties of stainless steel using tensile coupons cut from the specimens. The test was conducted using an INSTRON tensile testing machine in accordance with ASTM E8. In order to measure the longitudinal strains, strain gauges were positioned along the longitudinal region of the coupons, and readings were recorded using data acquisition systems. An extensometer is fixed to the coupon up to the elastic limit to determine the modulus of elasticity of the material. The material properties obtained from the test are tabulated in Table 2, where E_0 is the elastic modulus, 0.2 is 0.2% proof strength, u is the ultimate stress, and μ is the Poisson ratio of the material.

Table 2. Properties of stainless-steel

Section	$\sigma_{0.2}$ (MPa)	σ_u (MPa)	E_o (MPa)	μ_s
SS304	346	715	190,000	0.3

2.2.2. Concrete

Concrete of grade M40 was filled inside the rectangular hollow stainless-steel tubes. Standard concrete cubes of nominal dimension (150 mm × 150 mm × 150 mm) were cast along the test specimens and tested for their compressive strength. The measured average compressive strength of concrete is listed in Table 3. At high temperatures, concrete with a higher paste-aggregate ratio had a severe strength reduction compared to normal-strength concrete (NSC) mixes. Hence, for the experiments involving high temperature exposure, a moderate grade of M40 was adopted.

Table 3. Compressive strength of concrete cube specimens

Specimen	Compressive cube strength, f_c' (MPa)	Mean value
C600	50.75	51.55
	49.46	
	54.44	
C800	55.95	54.42
	52.88	
	54.44	
C1000	55.24	55.27
	55.11	
	55.46	

2.3. Selection of Parameters

The temperature range of 600 to 1000 °C was chosen as the desired target temperature for this investigation. The reduction rate of concrete's compressive strength increases between 400–800 °C [28, 29]. In the case of steel, stainless steel exhibits higher mechanical strength due to the effect of cold working [30]. However, after 700 °C, the effect of cold working becomes less influential as stainless steel attains recrystallization temperature [31]. Since a critical point is attained for both concrete and stainless steel between 400–800 °C, it is essential to investigate the adequacy of bond-strength in these temperature ranges. Another parameter investigated in this study is the age of concrete. As the age of concrete increases, shrinkage effects take place. After 180 days of curing, the influence of the steel type (carbon or stainless steel) on the bond strength of CFST columns is minimized. Hence, CFST specimens were cured for 28 days, 60 days, 90 days, and 180 days in this experiment to examine the effects of high temperatures on different concrete ages. Establishing the bond stress-slip relationship for CFST columns with older concrete assists in numerical simulations. The sensitivity of other values of the selected parameters is beyond the scope of this experiment and will be addressed through numerical simulations in the future.

2.4. Preparation of the Test Specimens

Rectangular tubular columns of SS304 stainless-steel material were bought from the vendor and cut into desired lengths of 500 mm for the tests. Stainless-steel tubes had 2B surface finishes and were in polished condition. The chemical composition of the stainless steel adopted in the tests is tabulated in Table 4. Hollow tubes were then filled with concrete. As this study was carried out by a push-out testing procedure, the top and bottom parts of the stainless steel were filled with foam material up to 15 mm, such that the concrete was filled up to a certain limit inside the hollow tube, leaving a gap of 15 mm on either side of the hollow tube. After casting, the specimens were cured inside a curing tank for 30 days, 60 days, 90 days, and 180 days, respectively. Casting and curing conditions were maintained evenly to ensure homogeneous conditions. After curing, both ends of the rectangular CFSST columns were closed with mild steel plates to prevent direct exposure of fire to concrete and placed inside an electric furnace. The electric furnace has the capability of supplying a maximum temperature of 1000 °C.

Table 4. Chemical composition of Austenitic stainless steel (SS304)

ASTM Designation	% by Mass				
	Carbon (C)	Silica (Si)	Manganese (Mn)	Chromium (Cr)	Nickel (N)
314	0.20	1.5-2.5	2.00	24.00-26.00	19.00-22.00

2.5. Fire Test Procedure

In order to expose the test specimens to high temperatures, 12 specimens, excluding the reference specimens, were placed inside an electric furnace, as shown in Figure 5. A heating rate of 10 °C/min was maintained. The adopted heating rate was kept constant for all the test specimens. The temperature-time curve adopted in this study consists of four parts: first, the specimens were heated to the desired temperature range (600, 800, or 1000 °C) and next, the temperature was maintained for a desired duration to ensure uniform temperature distribution across the specimen; furthermore, the specimens were subjected to cooling without the influence of an external environment; and lastly, the specimens were allowed to cool down to room temperature inside the furnace. It is to be noted that the air-cooled specimens had fewer effects on post-fire strength deterioration, and hence the specimens were naturally allowed to cool to ambient temperatures. After reaching a target temperature of 30 °C, the specimens were taken out of the furnace. A sudden drop in temperature can be observed from the temperature-time curve, as shown in Figure 6. The electric furnace took about 10–13 hours to reach ambient temperature. The temperature-time curve was observed to be uniform for all the specimens.
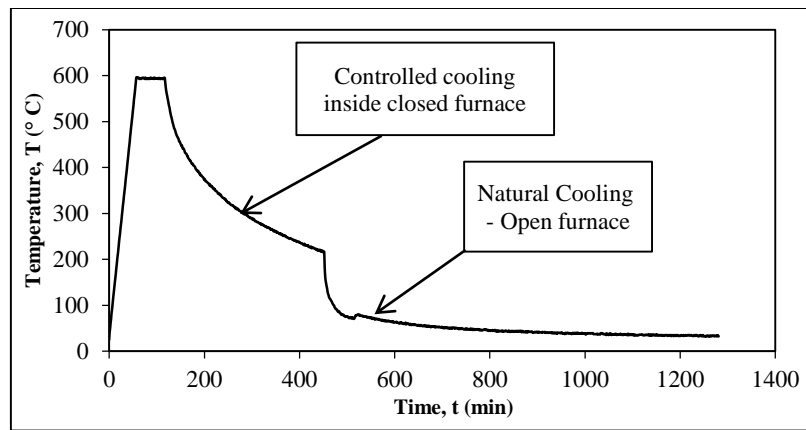

Figure 5. Electrical furnace for post-fire tests

Figure 6. Heating and cooling curve adopted in the study

2.6. Loading Procedure

A detailed flowchart of the methodology adopted in this study is shown in Figure 7. In order to find the bond strength of RCFSST columns, the concrete inside the steel tube has to be pushed out, and the load required to push out or cause slippage of the concrete from the hollow tube was taken as the bond strength of the specimen. Hence, after cooling the specimens to room temperature, the specimens were then loaded on the Universal Testing Machine (UTM) at the Strength of Materials Laboratory, Vellore Institute of Technology, Vellore, India. A steel block of size (95 mm x 45 mm x 50 mm) was placed over the top layer of the specimens such that the steel block bears the applied load and transfers it to the concrete present inside the hollow tube.
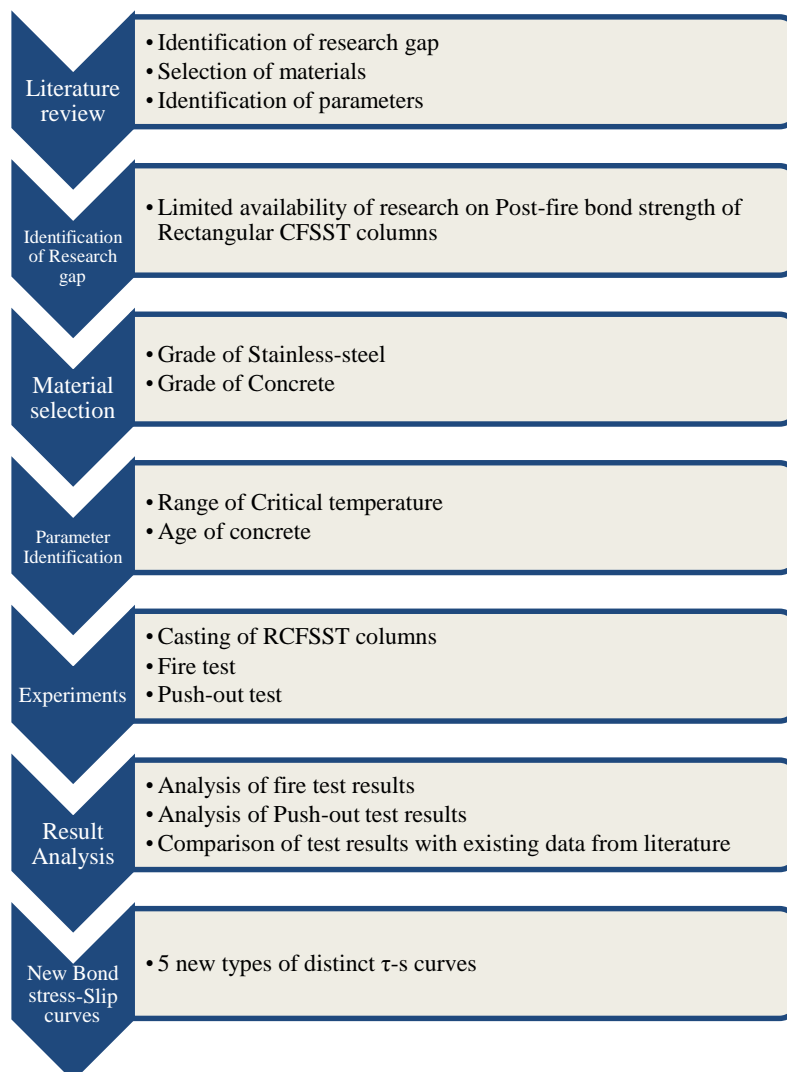

Figure 7. Flow chart for methodology adopted in the study

When a load was applied using UTM, the steel block placed above the concrete layer pushed the concrete down, causing slippage of the concrete. The loading setup is shown in Figure 8. An LVDT was placed at the bottom of the specimen to measure the displacement of the concrete from the outer steel tube. Axial displacements were also observed by recording the movement of the cross-head travel of the UTM. The maximum load obtained during the test is considered the load required to cause slippage, and bond stress is calculated using the obtained load from the experiments. The experiment was carried out without any discrepancies.
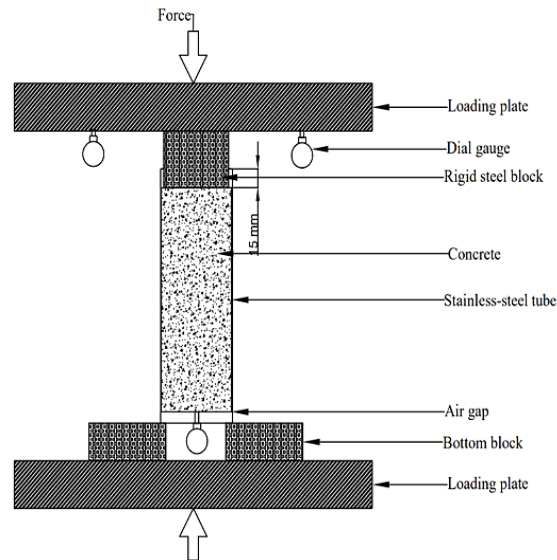
Figure 8. Push-out test setup for post-fire RCFSST columns

## 3. Test Results and Discussion

3.1. Fire Test Results

Generally, stainless steel exhibits a silvery-white color. When the specimens were taken out of the furnace after attaining an ambient temperature, appreciable color changes were noted on the outer surface of the stainless-steel material, as shown in Figure 9. The color of the outer tube gradually became darker, from silvery white at room temperature to grayish black at 1000 °C. Small flakes of the stainless-steel material were ruptured from the surface of the steel tube at 1000 °C. Higher integrity of the concrete was observed at lower temperatures and prevailed to a certain extent during the loading conditions. Around 800 °C, minute cracks were observed on the concrete surface, and minute parts of the concrete disintegrated at 1000 °C.
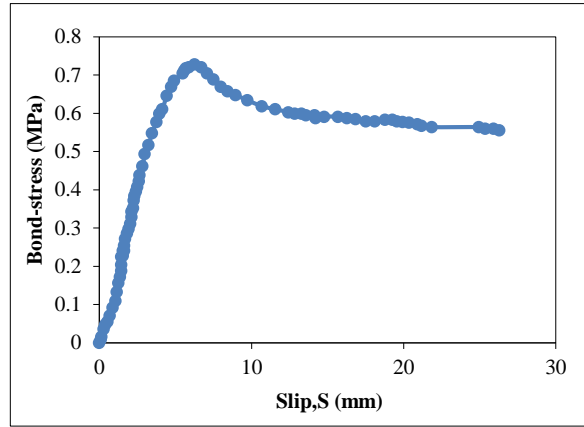

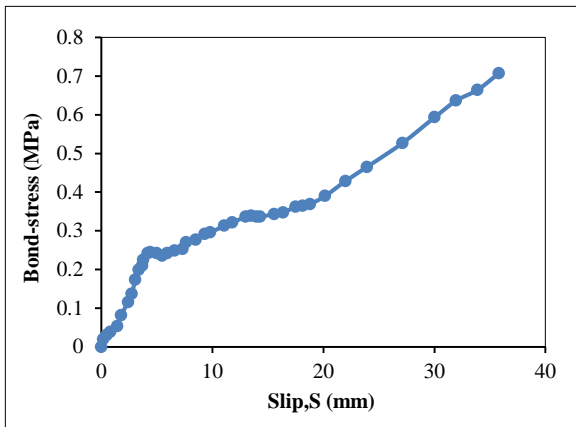**Figure 9. Post-fire test on RCFSST columns**

3.2. Push-out Test Results

Figure 10 shows the bond(τ)-slip(s) curves of the test specimens. The following characteristics were observed from the bond stress-slip curve:
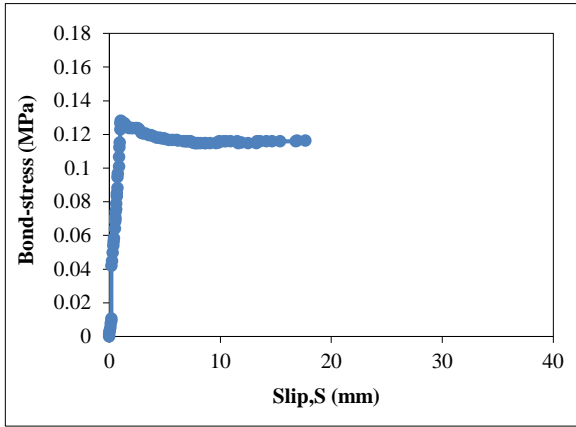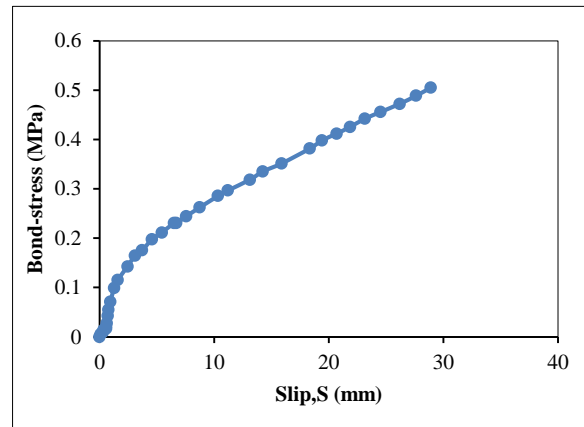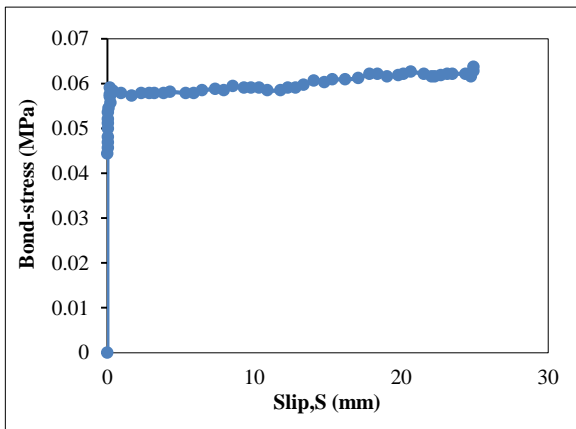
i) τ-s curve of specimen 30D600T

ii) τ-s curve of specimen 30D800T

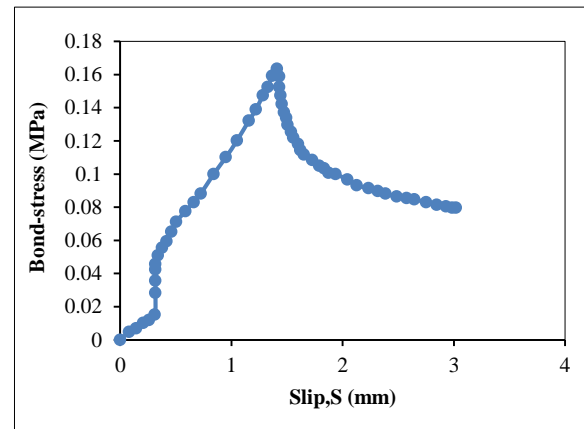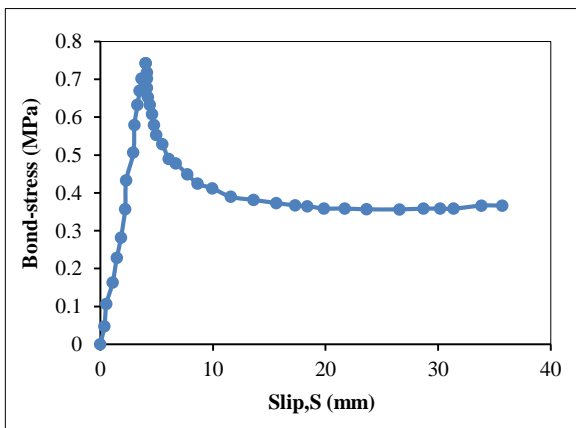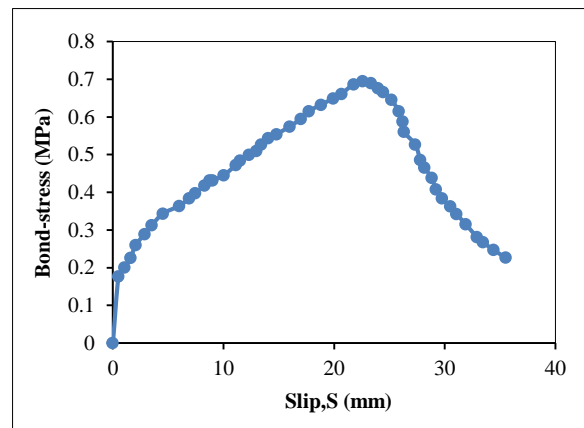iii) τ-s curve of specimen 60D600T

iv) τ-s curve of specimen 60D1000T

v) τ-s curve of specimen R60D

vi) τ-s curve of specimen 30D600T

vii) τ-s curve of specimen 90D800T

viii) τ-s curve of specimen 90D1000T
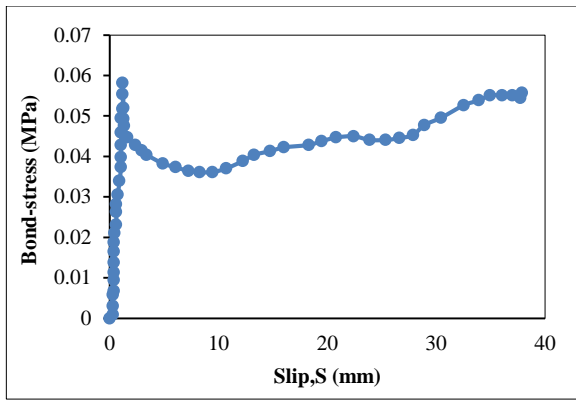
vix) τ-s curve of specimen R90D
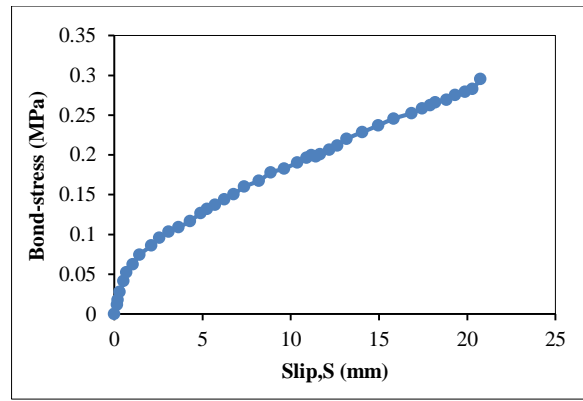
x) τ-s curve of specimen 180D600T
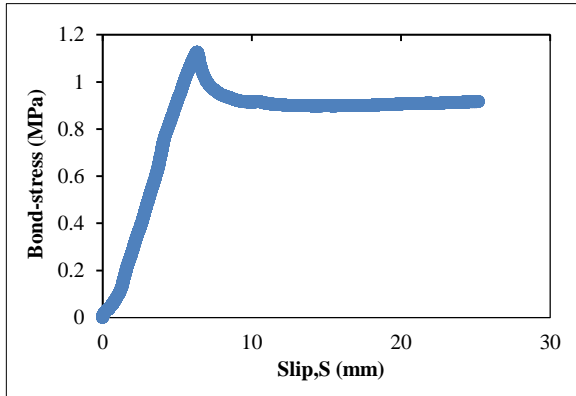
xi) τ-s curve of specimen 180D800T
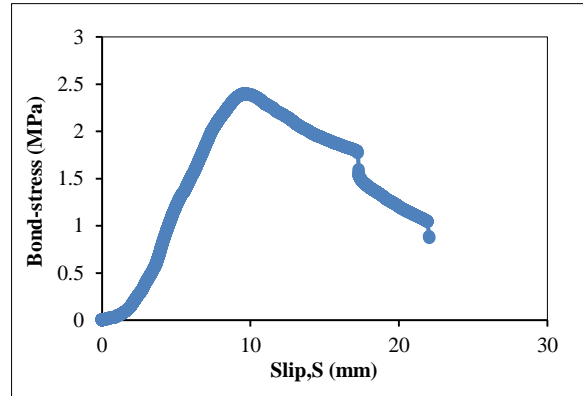
xii) τ-s curve of specimen 180D1000T

Figure 10. Bond-stress(τ)-Slip(s) curves obtained from push-out test of RCFSST specimens

- The bond stress-slip curves can be categorized into five different types of curves, namely Type 1, Type 2, Type 3, Type 4, and Type 5, respectively, as shown in Figure 11. However, the effect of temperature and concrete age was found to be random.
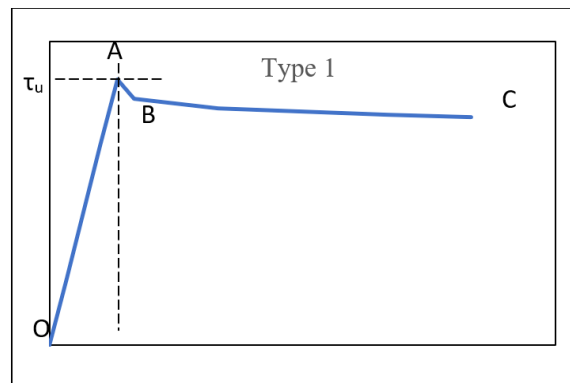
i) Type 1 τ-s curve
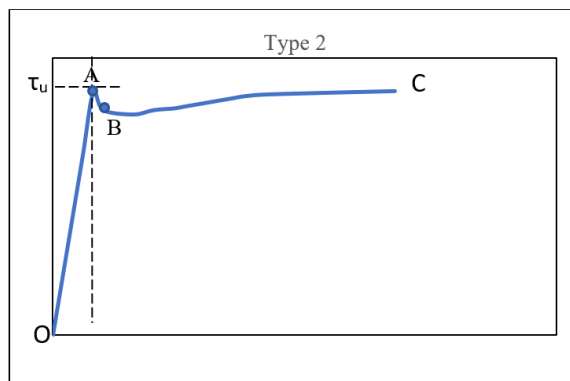
ii) Type 2 τ-s curve
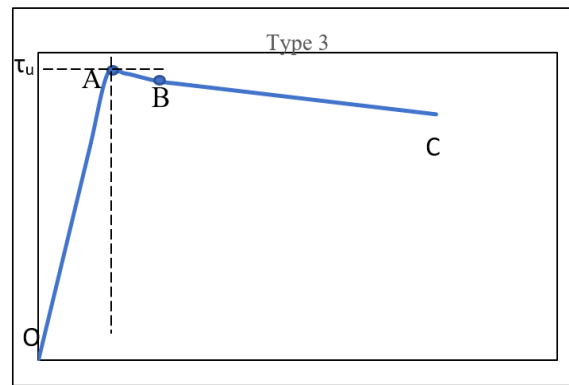
iii) Type 3 τ-s curve
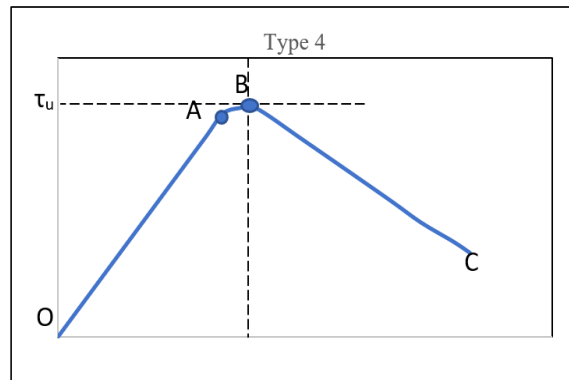
iv) Type 4 τ-s curve
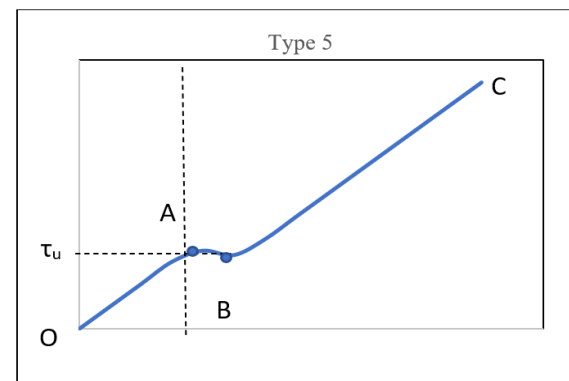
v) Type 5 τ-s curve

Figure 11. Classification of τ-s curves obtained from the test results

- The Type 1 curve had three stages: i) the initial linear stage (OA), where the bond stress gradually increases linearly; ii) the non-linear stage (AB), where the bond stress drops with a gradual slope; and iii) the linear stage (BC), where the bond stress has a further decrease. The Type 2 curve also displayed three stages: i) the initial linear stage (OA), where the bond stress had a linear increase; and ii) & iii) two non-linear stages, Curves AB and BC. Unlike the Type 1 curve, the bond stress had a gradual increase in the later stage (BC);

- The Type 3 curve is also similar to the Type 1 and Type 2 curves. The only difference is that the Type 3 curve exhibited a gradual slope (BC) after achieving the non-linear stage (AB), whereas in the Type 1 and Type 2 curves, a steep slope was observed in later stages. The Type 4 curve is a two-stage curve with an initial linear stage (OA) and a non-linear stage (AB). The Type 5 curve displayed a similar trend as the Type 2 curve, but at the third stage (BC), the rate of increase in bond stress was so high;

- Based on the occurrence of the curve shapes observed from the test results, four specimens (33%), namely 30D600T, 90D600T, 90D800T, and 180D800T, exhibited Type 1, three specimens, namely 60D600T, 60D1000T, and R180D, presented a Type 5 curve (25%), two specimens, R90D and R60D, showed a Type 2 curve (16%), and two specimens, 90D1000T and 180D1000T, displayed a Type 4 curve (16%). The specimen labeled 30D800T exhibited a Type 3 curve (8.3%);

- The bond strength of the specimens can be determined from the bond stress-slip curve obtained from the test results. For specimens presented on the on the Type 1, Type 3, and Type 4 curves, the maximum point on the τ-s curve was

taken as the ultimate bond strength (τ_u) of the specimens. For specimens that exhibited Type 2 and Type 5 curves, prediction of ultimate bond strength becomes challenging since the τ-s curve kept increasing through the test, and hence no definite point can be taken as τ_u. However, a change of slope at BC was noted in Type 2 and Type 5 curves. The ascending stage BC of both the Type 2 and Type 5 curves had a lower slope than the initial linear stage (OA), and hence point A is taken as τ_u in both cases.

3.3. Influence of parameters on bond strength of RCFSST columns

3.3.1. High Temperature

The influence of high temperatures on the bond strength of RCFSST column specimens with different concrete ages is shown in Figure 12. From the test results, it is noted that at initial ages of concrete, the impact of increasing the temperature was much higher. The bond strength of the test specimens showed a substantial increase up to 800 °C for all concrete ages considered in this study. The bond strength test specimens can be categorized into two distinct types based on their test results: i) Type A – Specimens with a concrete age of 30 days, 60 days, and 90 days; and ii) Type B – Specimens with a concrete age of 180 days.

i) Effect of temperature on bond strength (30-day strength)

ii) Effect of temperature on bond strength (60-day strength)

iii) Effect of temperature on bond strength (90-day strength)

iv) Effect of temperature on bond strength of RCFSST (180-day strength)
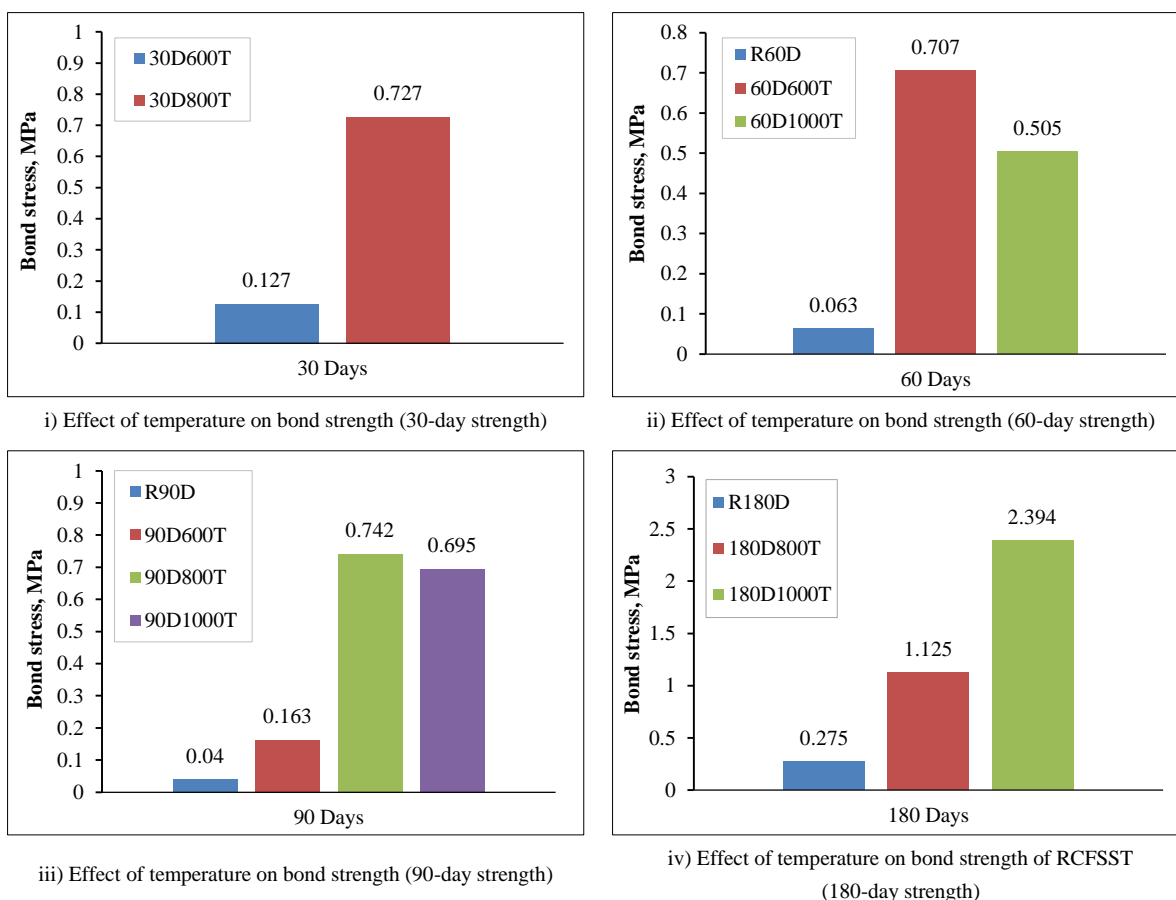
Figure 12. Effect of high temperature on bond-strength of RCFSST columns for various concrete ages

Type A – Specimens in this category exhibited an increase in bond strength up to 800 °C. The influence of temperature was higher for the initial age of concrete. In other words, the rate of increase in bond strength of the test specimens was influenced by concrete age, as the rate deteriorates when concrete ages more. However, beyond 800 °C, the increase in temperature had a detrimental effect on the post-fire bond strength of RCFSST columns. In comparison with reference specimens that were tested without any fire exposure, a significant increase in bond strength was observed when the temperature was raised to 600 °C, as shown in Figures 12(i)–12(iv). The % increase in bond strength was much higher when the temperature was increased to 600 °C than the % increase in bond strength when the temperature was elevated from 600 °C to 800 °C. All the specimens in Type A displayed a similar trend. The rate of decrease in bond strength beyond 800 °C was also influenced by concrete age, as the rate was reduced with an increase in concrete age. In other words, the rate of decrease in bond strength had an inversely proportional relationship with concrete age.

Type B – Specimens in this category displayed a significant increase in bond strength for all temperature ranges. The influence of temperature was much higher for specimens of this type than for Type A specimens. Unlike Type A specimens, which had a decrease in bond strength beyond 800 °C, Type B specimens exhibited superior bond strength

when the temperature was increased to 1000 °C. However, the rate of increase in bond strength decreases with an increase in temperature. Below 800 °C, the rate of increase in bond strength was much higher than the increase rate from 800 °C to 1000 °C. The rate of increase in bond strength of Type B specimens displayed a higher percentage than the rate of increase in bond strength of Type A specimens within identical temperature ranges. Type B specimens displayed much higher bond strengths than type A specimens. The maximum bond strength observed in Type A specimens was 0.727 MPa, whereas in Type B specimens, the maximum bond strength was 2.394 MPa. Type B specimens presented τ-s curves of Type 1, Type 4, and Type 5, whereas Type A specimens demonstrated all five curve types.

3.3.2. Concrete Age

Specimens under the same temperature range for different concrete ages were compared to investigate the influence of concrete age on the post-fire bond strength of RCFSST columns, as shown in Figure 13. It was very clear that the increase in concrete age maximizes the bond strength of post-fire RCFSST columns. At 600°C, the specimens with a 90-day concrete age demonstrated an increase in bond strength when compared to specimens with a concrete age of 30 days. However, at 800 °C, the increase in bond strength was not much appreciable for specimens with concrete ages of 30 days, 60 days, and 90 days. At 1000 °C, the influence of concrete age was much higher. The post-fire bond strength of RCFSST column specimens exhibited a higher rate of increase as the concrete became older. At all three temperatures considered in this study, an increase in concrete age resulted in an increase in the post-fire bond strength of the RCFSST column specimens. A higher rate of increase in bond strength was observed for specimens with a concrete age of 180 days. Specimens with a concrete age of 180 days exhibited better performance under all the temperature ranges adopted in this study. The maximum post-fire bond strength achieved by the specimen 180D1000T, which was cured for 180 days and exposed to a temperature of 1000 °C. Comparing the influence of temperature and concrete age parameters, concrete age provided a significant contribution to maximizing the post-fire bond strength of RCFSST columns.
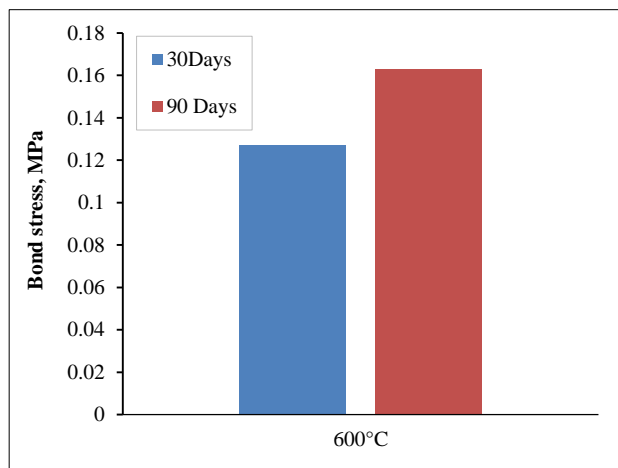
i) Effect of concrete age on bond strength (600°C)
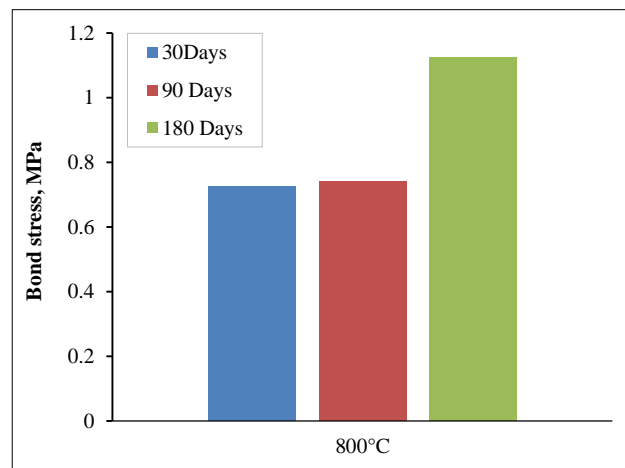
ii) Effect of concrete age on bond strength(800°C)
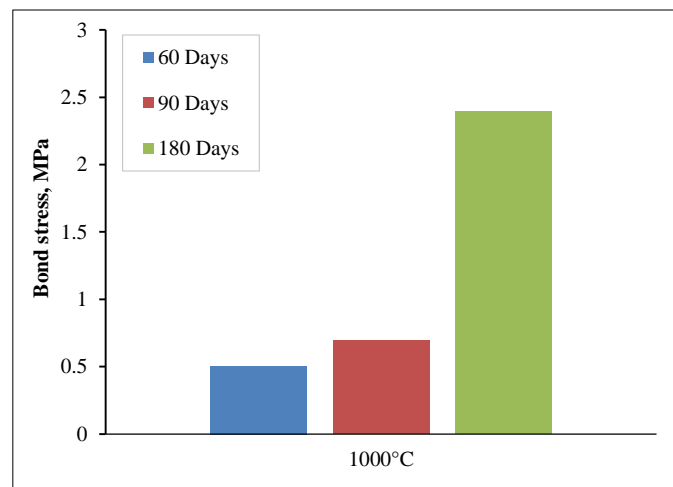
iii) Effect of concrete age on bond strength (1000°C)

Figure 13. Effect of concrete age on post-fire bond strength of RCFSST columns

4. Bond Strength of Concrete Filled Stainless-Steel Tubular Columns

4.1. Bond Strength at Ambient Temperature

Analyzing the τ-s curves of RCFSST columns at ambient temperatures, the 60-day specimen and the 90-day specimen exhibited Type-2 curves, which had a three-stage τ-s curve, namely one linear and two non-linear curves, as mentioned in the previous sections. The slope of the curve OA decreases with an increase in concrete age. The test specimen R60D displayed a steeper slope than the specimen R90D, as shown in Figure 14. Generally, the linear region (OA) is associated with chemical adhesion and micro-locking mechanisms. As concrete ages, the adhesive mechanism and micro-locking mechanism degrade, causing the resulting curve. Comparing the point of inflection B of the τ-s curves of ambient temperature test specimens, specimens with higher concrete age had a sharp inflection point B. From the test results, it was very clear that the specimen with a 90-day concrete age displayed higher non-linearity in the later stage (BC) of the τ-s curve. Macro-locking attributes to the "BC" region of the curve. As the concrete ages, shrinkage increases, resulting in a reduced macro-locking mechanism.
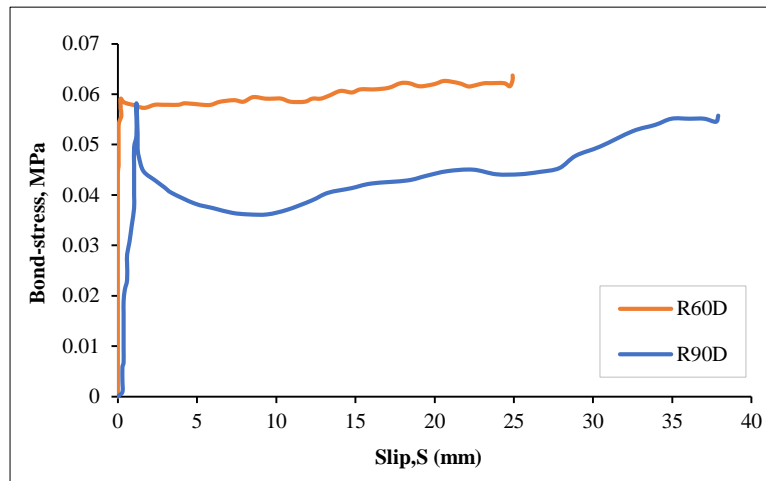
Figure 14. τ-s curve for ambient temperature RCFSST columns with different concrete ages

Meanwhile, the specimens displayed a very minor change in $τ_u$, for different concrete ages. The reduction factors obtained from the test results for ambient-temperature RCFSST specimens and the reduction factors reported in the literature [21, 23, 32, 33] for various parameters are shown in Figure 15. It was clear from Figure 15 that the bond strength can be enhanced by providing internal rings, but on the other hand, the change in surface roughness of the internal steel tube also contributed to a greater extent. An increase in CRA content also contributed to enhancing bond strength. Light-weight concrete-filled steel tubes incorporating rook wool waste had a declining strength compared to normal CFST specimens.
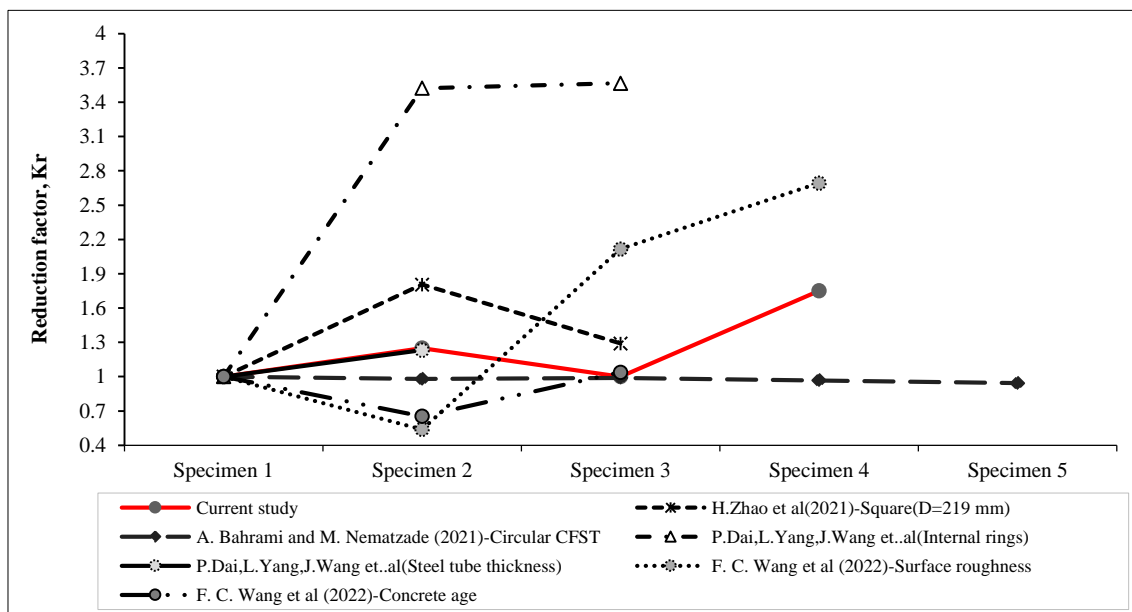
Figure 15. Reduction factors of ambient temperature bond strength of CFST columns from test results and literature

4.2. Bond Strength of CFSST and CFST Columns Under Post-Fire Condition

The characteristics of the τ-s curve of RCFSST specimens were examined in each temperature range, as shown in Figures 16-a to 16-c. Around 600°C, the RCFSST specimens displayed Type 1 and Type 5 τ-s curve characteristics. Type 1 curve was associated with 30 and 90-day specimens, while 60-day specimens displayed type 5 curve features at 600 °C. The linear region OA of the τ-s curve for 30 and 90-day specimens demonstrated similar slopes, whereas higher slope values were noted in 60-day specimens. The τ-s curve of 30 days and 90 days displayed a variation after the inflection point B of the τ-s curve, whereas both specimens exhibited a declining trend in their later stages (BC). In the case of the 60-day specimen, the curve BC had a positive slope.

a) τ-s curves for 600 °C

b) τ-s curves for 800 °C

c) τ-s curves for 1000 °C
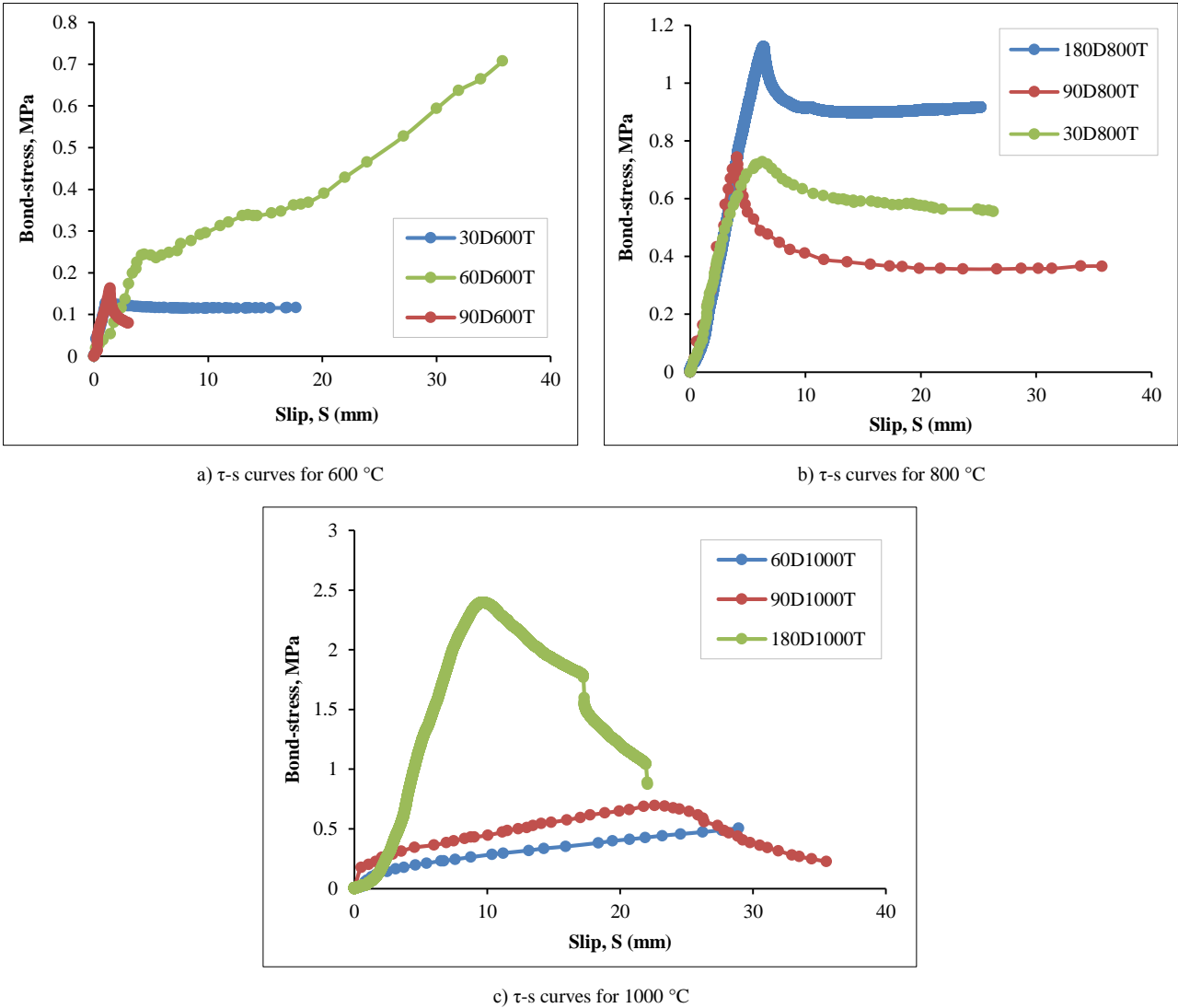
Figure 16. Comparison of τ-s curves for different temperature ranges

At 800 °C, the slope of the linear curve OA for all the specimens, irrespective of their concrete age, displayed similar trends. Except for the 30-day specimen, all the other specimens had a Type 1 classification with three-stage curve characteristics. At 1000 °C, the linear region OA of the τ-s curve for the specimens with lower concrete ages (Type A) was short in comparison with specimens with a concrete age of 180 days (Type B). It is evident that at 180 days, chemical adhesion and micro-locking were ineffective, resulting in shorter linear branch OA. The linear region OA was followed by a short AB region, which indicates the loss of bond was sudden. The specimens exhibited a larger BC region of the τ-s curve than Type A specimens. Comparisons of bond strength for different concrete ages are shown in Figures 17 (a) to (d). As bond strength in rectangular columns is mostly governed by the macro-locking mechanism, an increase in the non-linear portion BC verifies the intactness of macro-locking. Type B specimens at this temperature zone were associated with the Type 4 category of the τ-s curve. The post-fire bond-strength reduction factor (k_r) obtained from the test results was compared with the reduction factors (k_r) reported in the literature [20–22], as shown in Figure 18.

a) Comparison of τ-s curves for concrete age=30 days

b) Comparison of τ-s curves for concrete age=60 days

c). Comparison of τ-s curves for concrete age=90 days

d) Comparison of τ-s curves for concrete age=180 days
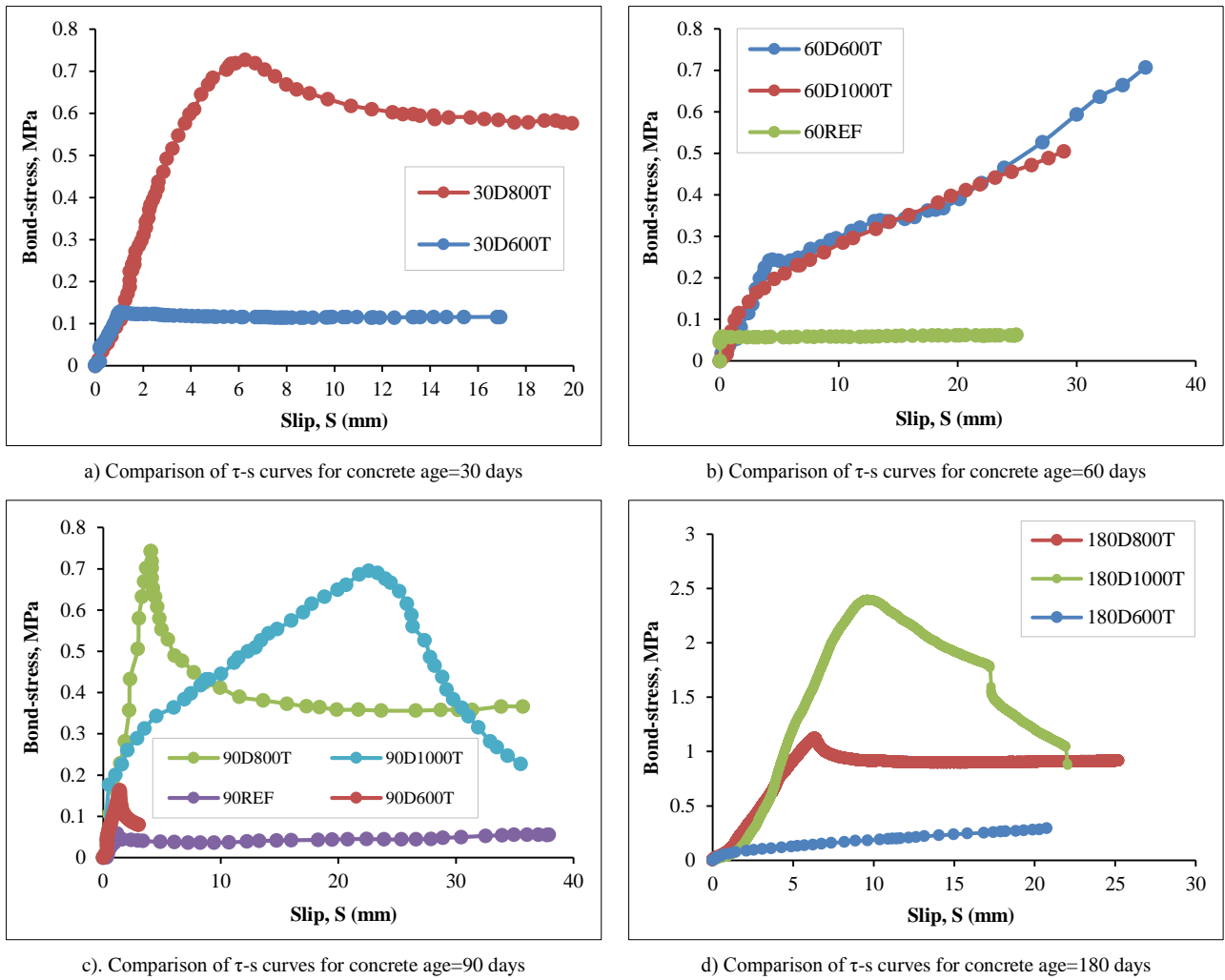
Figure 17. Comparison of τ-s curves for different concrete ages
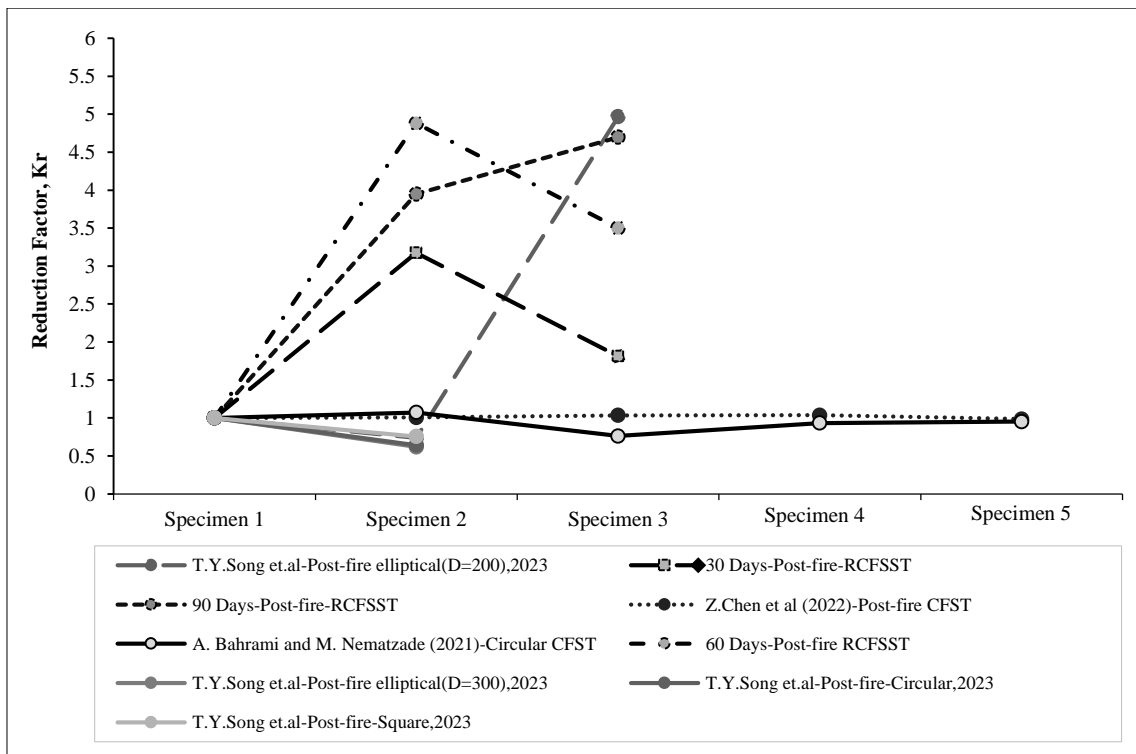
Figure 18. Comparison of reduction factors of post-fire bond strength of CFST columns from test results and literature

4.3. Comparison of Experimental Data with Existing Literature

A comparison of the relative increase in bond strength of CFST columns is shown in Figure 19. At ambient temperatures, rectangular CFSST columns displayed lower bond strength in comparison with other shapes of CFST columns [22]. Circular CFST columns exhibited higher bond strength, followed by square and rectangular specimens, with elliptical CFST having the least bond strength at earlier ages of concrete. It is obvious that hoop stress developed in circular CFST columns enhances bond capacity [5]. But as the age of concrete increased, the relative increase in bond strength of rectangular CFSST columns had substantial growth. In other words, the rate of increase in bond strength from the 30-day curing period to 180 days was noted to be significantly higher in rectangular CFSST columns. Around a 68% increase in bond strength was observed in rectangular CFSST columns with 180-day curing. In the case of circular columns, no appreciable increase in bond capacity was observed, as reported in the literature [22].
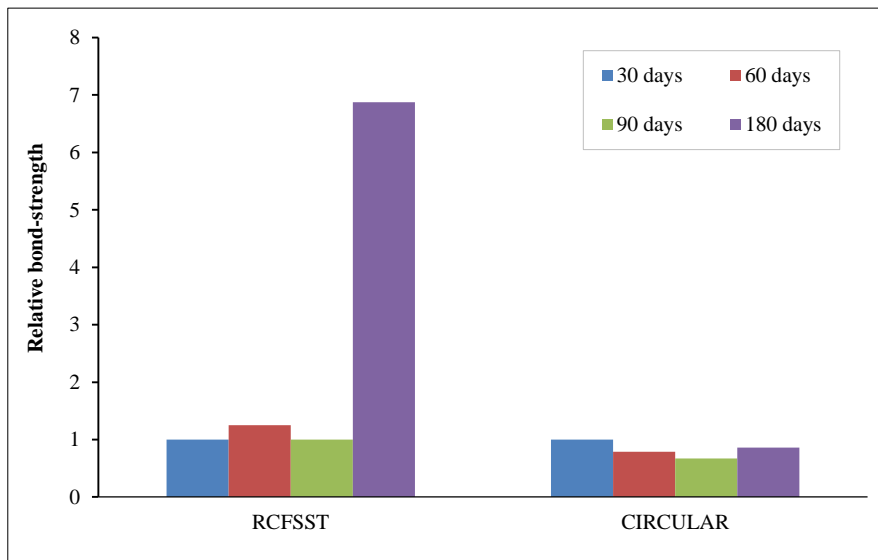
Figure 19. Comparison of relative bond-strength for different concrete ages from the literature [22] at room temperature

A comparison of the relative increase in bond strength for different shapes of CFST columns at 600 °C and ambient temperatures, as reported in the literature, is shown in Figure 20. At earlier concrete ages, around 600 °C, the post-fire bond strength of square-shaped specimens exhibited an appreciable increase in bond capacity in comparison with ambient-temperature square specimens. The rate of increase was highest in square specimens, followed by circular and rectangular specimens. However, higher bond strength capacity was displayed by circular CFST columns. A comparison of different shapes and their relative increase in bond strength in comparison with room-temperature specimens is shown in Figure 21.
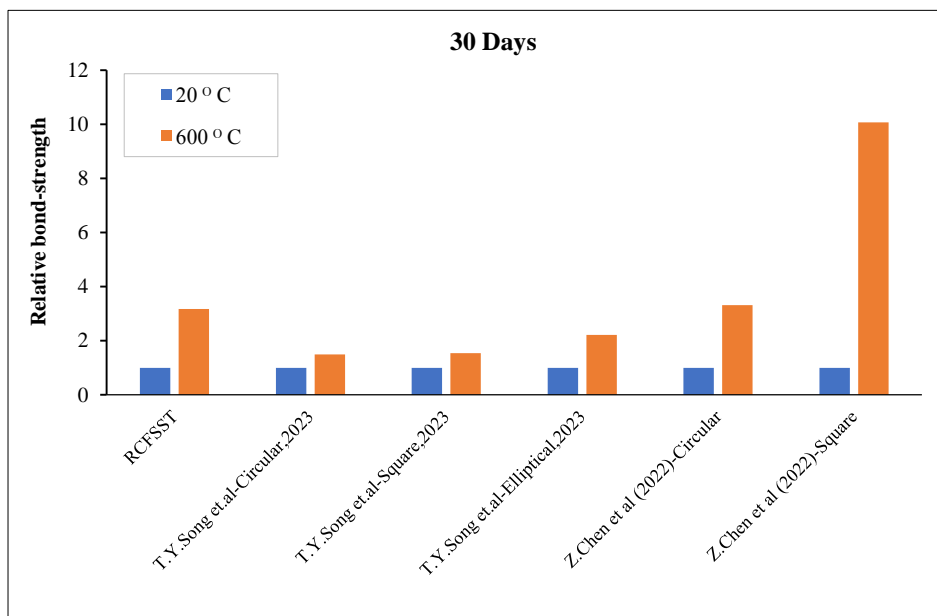
Figure 20. Comparison of post-fire bond-strength for different shapes of CFST from the literature [20, 22]
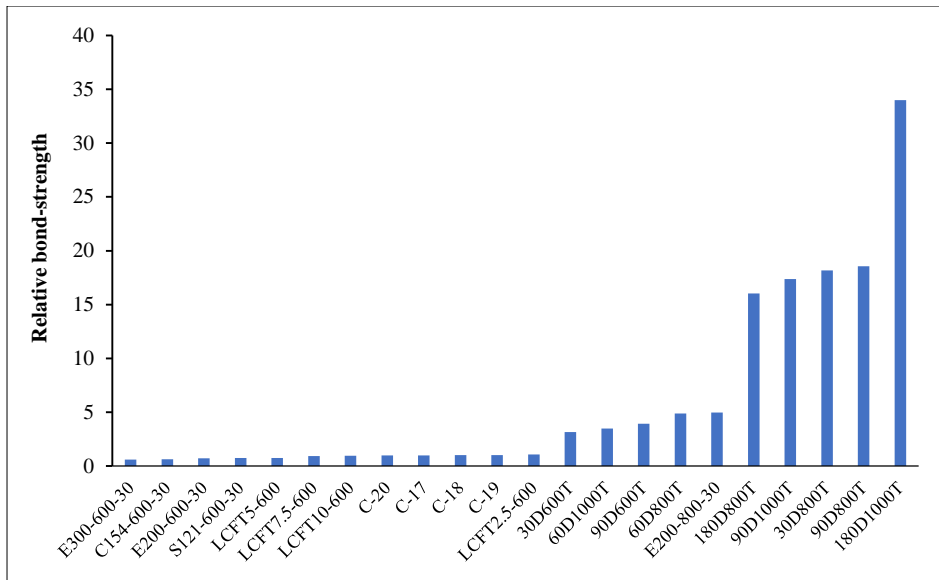
Figure 21. Comparison of relative post-fire bond strength of CFST columns [21, 22] with room temperature specimens

It can be seen that for higher temperatures and older ages of concrete, rectangular specimens exhibited a relatively higher rate of increase in bond strength in comparison with room temperature. Around a 35% increase was observed for rectangular specimens in relation to room-temperature RCFSST columns. The combined effect of concrete age and high temperature had a positive influence on the relative increase in bond capacity of RCFSST columns. In addition to hoop stresses in circular CFST columns, micro-locking and chemical adhesion mechanisms govern the bond capacity in circular and square CFST columns [3]. As the temperature increases, the chemical bond between stainless steel and concrete breaks. Hence, the influence of these parameters deteriorates. However, in rectangular CFSST columns, bond capacity is mostly governed by macro-locking mechanisms [5], and hence lower temperatures have little influence on the bond capacity of RCFSST columns. A summary of the experimental results is shown in Figure 22.
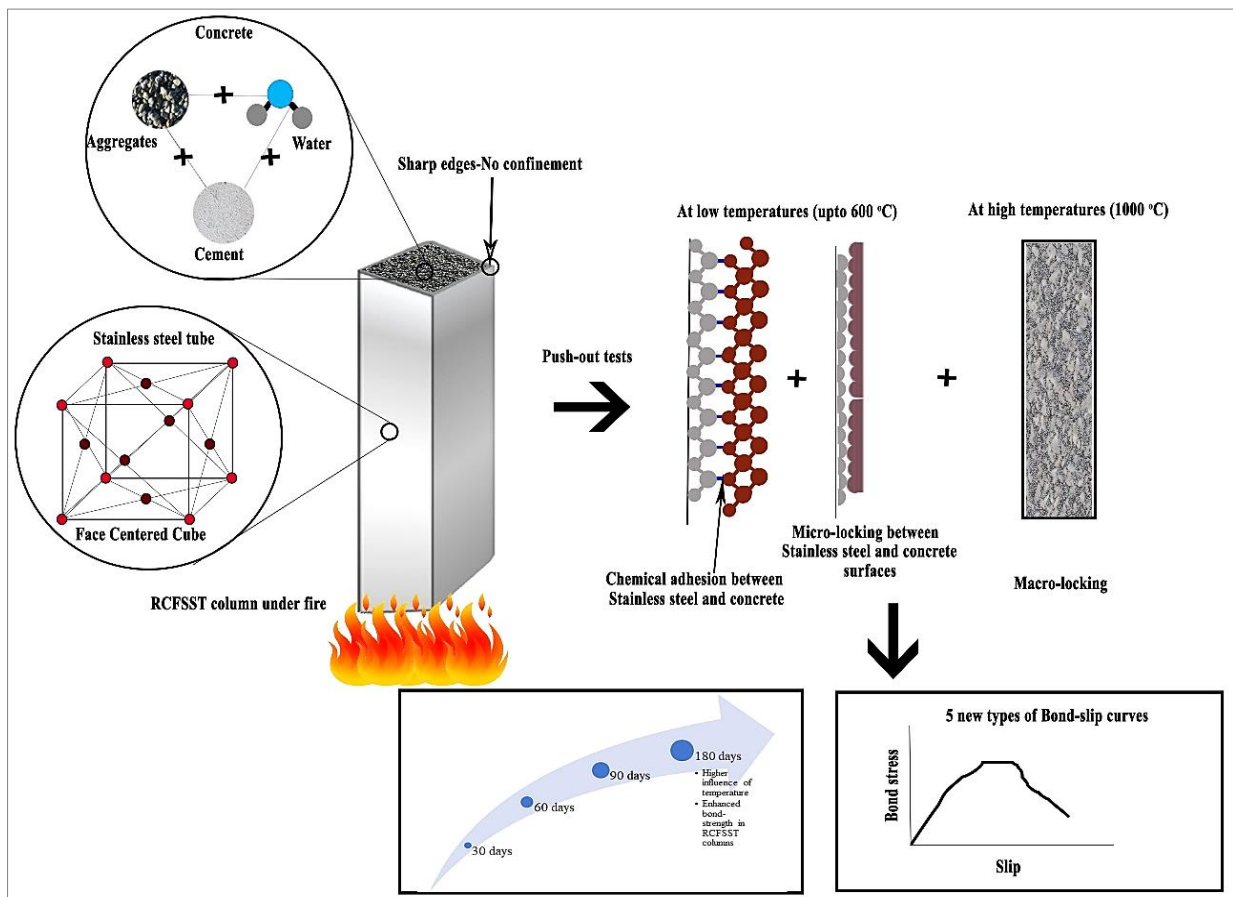
Figure 22. Summary of the experimental results

5. Conclusions

An experimental investigation on the bond strength of rectangular concrete-filled steel tubular columns after fire exposure has been carried out, and the following conclusions were observed:

- Post-fire push-out tests on rectangular CFSST columns were carried out, and the results were compared with existing literature. Push-out tests on ambient temperature test specimens indicate that the rectangular stainless steel tubular columns exhibited lower bond strength than other shapes reported in the literature. Despite this, the bond between rectangular stainless steel and the core concrete significantly increases as the concrete ages.

- It is noted that after exposure to heating and cooling, the bond between the rectangular stainless-steel tube and the core concrete was intact even at earlier concrete ages, and as the concrete aged, the bond strength had substantial growth even under higher temperatures. It is also worth noting that the post-fire test specimens displayed higher resistance against slip during the loading stage of the test. As the concrete ages, this resistance increases to an appreciable extent.

- The test results indicate that high temperatures had a lesser influence on bond strength when compared to the influence of concrete age. For the same concrete age, a rise in temperature resulted in a minor increase in bond strength. However, beyond the recrystallization temperature, the bond strength gradually declined for Type A specimens. When the specimens were cured for around 180 days., i.e., for Type B specimens, elevated temperature had a substantial influence on the bond strength of rectangular CFSST specimens.

- Based on the obtained τ-s results, five types of τ-s curves were observed, each with distinct curve characteristics. Most of the test specimens fall under the type 1 curve, which displayed a three-stage τ-s curve, followed by the type 5 curve with an increase in bond stress beyond the inflection point. It can be concluded that the post-fire bond between the rectangular stainless-steel tube and concrete core displayed appreciable strength at later stages of curing. Other shapes, such as circular or elliptical CFST columns, displayed similar strength at a much earlier concrete age.

It is evident from the τ-s curve that macro-locking was the principal contributing factor for the development of bond strength in RCFSST columns under the post-fire scenario at older ages of concrete infill. At lower concrete ages, chemical adhesion and micro-locking played a pivotal role in governing the bond strength of RCFSST columns under post-fire.

6. Declarations

6.1. Author Contributions

Conceptualization, A.K. and A.S.S.; methodology, A.K.; formal analysis, A.K.; investigation, A.K.; resources, A.S.S.; data curation, A.K.; writing—original draft preparation, A.K.; writing—review and editing, A.S.S.; supervision, A.S.S.; project administration, A.S.S. All authors have read and agreed to the published version of the manuscript.

6.2. Data Availability Statement

The data presented in this study are available in the article.

6.3. Funding

The authors received no financial support for the research, authorship, and/or publication of this article.

6.4. Conflicts of Interest

The authors declare no conflict of interest.

7. References

[1] Liao, F.-Y., Han, L.-H., Tao, Z., & Rasmussen, K. J. R. (2017). Experimental Behavior of Concrete-Filled Stainless Steel Tubular Columns under Cyclic Lateral Loading. Journal of Structural Engineering, 143(4), 1–15. doi:10.1061/(asce)st.1943-541x.0001705.

[2] Yousuf, M., Uy, B., Tao, Z., Remennikov, A., & Liew, J. Y. R. (2013). Transverse impact resistance of hollow and concrete filled stainless steel columns. Journal of Constructional Steel Research, 82, 177–189. doi:10.1016/j.jcsr.2013.01.005.

[3] Chen, Y., Feng, R., Shao, Y., & Zhang, X. (2017). Bond-slip behaviour of concrete-filled stainless steel circular hollow section tubes. Journal of Constructional Steel Research, 130, 248–263. doi:10.1016/j.jcsr.2016.12.012.

[4] Qu, X., Chen, Z., Nethercot, D. A., Gardner, L., & Theofanous, M. (2015). Push-out tests and bond strength of rectangular CFST columns. Steel and Composite Structures, 19(1), 21–41. doi:10.12989/scs.2015.19.1.021.

[5] Song, T.-Y., Tao, Z., Han, L.-H., & Uy, B. (2017). Bond Behavior of Concrete-Filled Steel Tubes at Elevated Temperatures. Journal of Structural Engineering, 143(11), 1–12. doi:10.1061/(asce)st.1943-541x.0001890.

[6] Lakshmanan, S., & Subramanian, N. (2005). Development length of reinforcing bars - Need to revise Indian Codai Provisions. Indian Concrete Journal, 79(10), 22.

[7] Mouli, M., & Khelafi, H. (2007). Strength of short composite rectangular hollow section columns filled with lightweight aggregate concrete. Engineering Structures, 29(8), 1791–1797. doi:10.1016/j.engstruct.2006.10.003.

[8] Xie, K., Huang, K., Huang, L., & Zhu, T. (2023). Experimental study of bond behavior between concrete-filled steel tube and UHPC-encased. Construction and Building Materials, 409, 134016. doi:10.1016/j.conbuildmat.2023.134016.

[9] Xu, T., Bian, X., Liu, Z., Yang, J., & Zhang, Z. (2023). Local bond stress–slip relationship of ribbed reinforcing bars embedded in UHPC: Experiment, modeling, and verification. Journal of Building Engineering, 68, 106122. doi:10.1016/j.jobe.2023.106122.

[10] Tao, Z., Song, T.-Y., Uy, B., & Han, L.-H. (2016). Bond behavior in concrete-filled steel tubes. Journal of Constructional Steel Research, 120, 81–93. doi:10.1016/j.jcsr.2015.12.030.

[11] Tao, Z., Han, L. H., Uy, B., & Chen, X. (2011). Post-fire bond between the steel tube and concrete in concrete-filled steel tubular columns. Journal of Constructional Steel Research, 67(3), 484–496. doi:10.1016/j.jcsr.2010.09.006.

[12] Feng, R., Chen, Y., He, K., Wei, J., Chen, B., & Zhang, X. (2018). Push-out tests of concrete-filled stainless steel SHS tubes. Journal of Constructional Steel Research, 145, 58–69. doi:10.1016/j.jcsr.2018.02.016.

[13] Guan, M., Lai, Z., Xiao, Q., Du, H., & Zhang, K. (2019). Bond behavior of concrete-filled steel tube columns using manufactured sand (MS-CFT). Engineering Structures, 187, 199-208. doi:10.1016/j.engstruct.2019.02.054.

[14] Lu, Y., Liu, Z., Li, S., & Li, N. (2018). Bond behavior of steel fibers reinforced self-stressing and self-compacting concrete filled steel tube columns. Construction and Building Materials, 158, 894–909. doi:10.1016/j.conbuildmat.2017.10.085.

[15] Wang, L., Chen, H., Zhong, J., Chen, H., Xuan, W., Mi, S., & Yang, H. (2018). Study on the Bond-Slip Performance of CFSSTs Based on Push-Out Tests. Advances in Materials Science and Engineering, 2018, 1–13. doi:10.1155/2018/2959827.

[16] Chen, Z., Tang, J., Zhou, X., Zhou, J., & Chen, J. (2020). Interfacial bond behavior of high strength concrete filled steel tube after exposure to elevated temperatures and cooled by fire hydrant. Materials, 13(1). doi:10.3390/ma13010150.

[17] Almasaeid, H. H., Salman, D. G., Abendeh, R. M., Allouzi, R. A., & Rabayah, H. S. (2024). Interfacial bond capacity prediction of concrete-filled steel tubes utilizing artificial neural network. Cogent Engineering, 11(1), 2297501. doi:10.1080/23311916.2023.2297501.

[18] Guo, Y.-L., Geng, Y., Richard Liew, J. Y., Wang, Y.-Y., & Hong, Z.-H. (2023). Compressive behaviour of circular steel tube confined reinforced concrete (STCRC) columns considering shrinkage and creep. Thin-Walled Structures, 192, 111127. doi:10.1016/j.tws.2023.111127.

[19] Zhang, J., Meng, X., Song, J., Cao, X., & Ma, K. (2023). Push-out tests of interfacial bond slip between H-shaped steel and ultra-high performance concrete. Structures, 57, 105268. doi:10.1016/j.istruc.2023.105268.

[20] Chen, Z., Jia, H., & Li, S. (2022). Bond behavior of recycled aggregate concrete-filled steel tube after elevated temperatures. Construction and Building Materials, 325, 126683. doi:10.1016/j.conbuildmat.2022.126683.

[21] Bahrami, A., & Nematzadeh, M. (2021). Bond behavior of lightweight concrete-filled steel tubes containing rock wool waste after exposure to high temperatures. Construction and Building Materials, 300, 124039. doi:10.1016/j.conbuildmat.2021.124039.

[22] Song, T. Y., Wang, C. H., Liu, X. L., Xiang, K., & Zhou, H. (2023). Post-fire bond behaviour in elliptical concrete filled steel tubes: Experiment and simulation. Journal of Constructional Steel Research, 201, 107725. doi:10.1016/j.jcsr.2022.107725.

[23] Zhao, H., Li, J., Wang, R., Lam, D., & Zhang, Y. (2021). Study on interfacial bond behavior of recycled aggregate concrete filled stainless steel tubes (RAC-FSST). Construction and Building Materials, 313, 125532. doi:10.1016/j.conbuildmat.2021.125532.

[24] Dai, P., Yang, L., Wang, J., Lin, M., & Fan, J. (2022). Bond stress-slip relationship in concrete-filled square stainless steel tubes. Construction and Building Materials, 326, 127001. doi:10.1016/j.conbuildmat.2022.127001.

[25] Parsa-Sharif, M., Nematzadeh, M., & Bahrami, A. (2023). Post-fire load-reversed push-out performance of normal and lightweight concrete-filled steel tube columns: Experiments and predictions. Structures, 51, 1414–1437. doi:10.1016/j.istruc.2023.03.091.

[26] Li, W., Chen, B., Han, L. H., & Packer, J. A. (2022). Pushout tests for concrete-filled double skin steel tubes after exposure to fire. Thin-Walled Structures, 176, 109274. doi:10.1016/j.tws.2022.109274.

[27] Han, L. H., Chen, F., Liao, F. Y., Tao, Z., & Uy, B. (2013). Fire performance of concrete filled stainless steel tubular columns. Engineering Structures, 56, 165–181. doi:10.1016/j.engstruct.2013.05.005.

[28] Ergün, A., Kürklü, G., Serhat Başpnar, M., & Mansour, M. Y. (2013). The effect of cement dosage on mechanical properties of concrete exposed to high temperatures. Fire Safety Journal, 55, 160–167. doi:10.1016/j.firesaf.2012.10.016.

[29] Chan, Y. N., Peng, G. F., & Anson, M. (1999). Residual strength and pore structure of high-strength concrete and normal strength concrete after exposure to high temperatures. Cement and Concrete Composites, 21(1), 23–27. doi:10.1016/S0958-9465(98)00034-1.

[30] Gardner, L., Insausti, A., Ng, K. T., & Ashraf, M. (2010). Elevated temperature material properties of stainless steel alloys. Journal of Constructional Steel Research, 66(5), 634–647. doi:10.1016/j.jcsr.2009.12.016.

[31] Kosmač, A. (2012). Stainless steels at high temperatures. Material and Applications Series, Euro Inox, Brussels, Belgium.

[32] Wang, F.-C., Xie, W.-Q., Li, B., & Han, L.-H. (2022). Experimental study and design of bond behavior in concrete-filled steel tubes (CFST). Engineering Structures, 268, 114750. doi:10.1016/j.engstruct.2022.114750.

[33] Dai, P., Yang, L., Wang, J., Fan, J., & Lin, M. (2021). Experimental study on the steel–concrete bond behaviour of circular concrete-filled stainless steel tubes. Thin-Walled Structures, 169, 108506. doi:10.1016/j.tws.2021.108506.
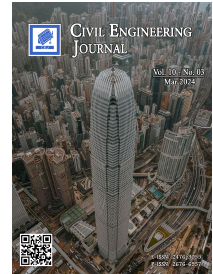
An In-Depth Review on the Eccentric Compression Performance of Engineered Bamboo Columns

Franklyn F. Manggapis [1, 2]*, Orlean G. Dela Cruz [2]

[1] Department of Civil Engineering, Technological Institute of the Philippines, Aurora Blvd, Quezon City 1109, Philippines.

[2] Graduate School, Polytechnic University of the Philippines, Valencia St. Sta. Mesa, Manila City 1016, Philippines.

Abstract

This review paper delves into the eccentric compression performance of engineered bamboo columns, focusing on objectives like evaluating methodologies, influential parameters, and testing techniques for eccentric compression behavior. It employs a systematic literature review adhering to PRISMA 2020 guidelines to synthesize data from various studies on material properties, design parameters, and construction methods. The findings reveal challenges in predicting failure modes under eccentric compression and the need for a unified model to assess the impact of eccentricity and slenderness ratios on performance. It introduces novel insights into the standardization and testing of engineered bamboo for structural applications. It addresses a significant gap in current research by offering a comprehensive predictive framework for eccentrically loaded, engineered bamboo columns.

Keywords: Bamboo; Columns; Slenderness Ratio; Eccentric Compression; Review.

1. Introduction

In the context of the rapid evolution of modern society, there has been a noticeable increase in the favorability of structures constructed from materials derived from sustainable materials such as crumb rubber tires [1], used facial masks [2], and bamboo [3]. The inclination toward exploring sustainable building materials arises from a growing need for an enhanced human living environment. Bamboo, among the materials under scholarly investigation, has attracted increasing attention within the research community [4–7]. The modern construction industry widely uses bamboo [8–10] due to its commendable mechanical and physical properties, comparable to conventional materials such as steel [11–12]. Moreover, bamboo's environmentally friendly characteristics fuel its increasing popularity [13, 14]. These factors collectively elevate bamboo to a leading position among sustainable construction materials, warranting its comprehensive exploration and analysis in an academic context. This combination of factors has propelled bamboo to the forefront of sustainable construction materials, making it a compelling subject for thorough exploration and analysis.

Despite their potential as a sustainable and abundant resource, bamboo culms present challenges that preclude their direct use in conventional structural applications within the built environment. The wide inherent variation in geometric properties among bamboo culms complicates the establishment of a consistent grading system suitable for structural purposes [15]. Furthermore, the mechanical properties of bamboo culms exhibit significant variations influenced by factors such as species, age, and height, necessitating a comprehensive understanding of these dynamics to enable effective utilization [16–19]. Moreover, the organic nature of bamboo culms introduces compatibility issues with

contemporary design and construction procedures, impeding their formal integration into structural applications [7]. Engineered bamboo emerges as a viable solution to overcome these challenges, as it involves the meticulous processing and treatment of bamboo culms to yield a more uniform and predictable set of material properties. Such treatment methods encompass processes like densification, delignification, and lamination, all aimed at enhancing [20]. Notably, engineered bamboo composites garner attention due to their standardized shape and relatively low variability in material properties [21]. These composites boast mechanical properties comparable to timber, rendering them suitable for diverse structural applications, including beams [22], trusses [23], frames [24], wall panels [25], and columns [26].

A column represents a vertical structural element engineered to endure compressive loads within a building or structure. Its primary function involves the transmission of loads from the superstructure to the foundation, thereby playing a pivotal role in upholding the stability and overall integrity of the construction [27]. Engineered bamboo has found application in column construction, with ongoing research focusing on its mechanical properties, connections, and standardization. This underscores its potential to significantly contribute to developing sustainable and resilient structural systems [28].

Numerous studies have investigated the performance of engineered bamboo in column applications, particularly under axial loading conditions [29–34]. However, to the best of the author's knowledge, limited attention has been directed toward understanding the performance of eccentrically loaded, engineered bamboo columns. Several pivotal challenges and research gaps have been identified, warranting further investigation to enhance the structural application of engineered bamboo. One of the foremost challenges lies in understanding and characterizing failure modes under eccentric compression. Li et al. (2020) [32] identified three characteristic failure modes for laminated bamboo lumber columns under eccentric compression, necessitating the development of predictive models that accurately reflect these behaviors across various engineered bamboo types. However, a comprehensive predictive framework that encompasses the myriad of failure behaviors, particularly for laminated bamboo lumber and parallel bamboo strand lumber, remains elusive, highlighting a significant gap in the literature.

Moreover, the influence of the eccentricity ratio and the slenderness of columns on their performance under eccentric compression is another area that demands rigorous scrutiny. Studies, such as those conducted by Li et al. (2015) [35], have shed light on the degradation of ultimate load capacity and deformation characteristics with varying eccentricity ratios and slenderness. Despite these insights, the field lacks a unified model that can predict the impact of slenderness ratio, especially for chamfered and hollow columns, underscoring a critical research void.

The variability in material properties of bamboo, including its tensile and compression strengths, further complicates the standardization of engineered bamboo for structural applications. This variability presents a considerable challenge in achieving consistent ultimate bearing capacity and structural performance under eccentric loads. Researchers have made strides towards engineering bamboo with uniform material properties, yet the effort to establish standardized grading and testing methodologies continues to fall short. Su et al. (2022) [36] emphasize the need for more focused research efforts in this domain to enable reliable predictions of engineered bamboo's performance.

This paper embarks on a comprehensive literature review to delve into the eccentric compression behavior of engineered bamboo columns. The objectives encompass the analysis of methodologies, the synthesis of influential parameters, and the evaluation of testing techniques. The study systematically explores critical factors, including material properties, design parameters, and construction methods, with a specific focus on the impact of slenderness ratio, ultimate bearing capacity, eccentricity distance, column height, and failure modes, drawing insights from the existing literature and studies.

2. Review Methodology

A systematic literature review (SLR) was employed to comprehensively assess the eccentric compression performance of engineered bamboo, drawing upon an extensive body of literature and research. The methodology adopted in this paper aligns with the principles outlined in the Preferred Reporting Items for Systematic Reviews and Meta-Analyses 2020 (PRISMA 2020) guidelines [37]. PRISMA 2020 is a structured reporting framework designed to enhance the transparency and quality of systematic reviews and meta-analyses. Its comprehensive 27-item checklist provides detailed reporting recommendations for various sections of the systematic review, including the title, abstract, introduction, methods, results, discussion, and conclusion [38]. This framework represents a significant advancement in the methodologies for identifying, selecting, appraising, and synthesizing studies, thereby serving the interests of authors, editors, peer reviewers, and diverse users of reviews.

The review process employed in this study adheres to the PRISMA 2020 guidelines, as depicted in Figure 1. Initially, researchers utilized two primary research databases, Google Scholar and ScienceDirect/Scopus.com, known for their ability to discern pertinent literature. These platforms offer sophisticated Boolean syntax functions, allowing users to execute searches using AND, NOT, and OR operators. The researchers meticulously chose and inputted keywords such as "bamboo," "eccentric compression," and "slenderness ratio" into the search fields of these databases. Subsequently, the initial phase identified 132 papers from Google Scholar and 19 from ScienceDirect.
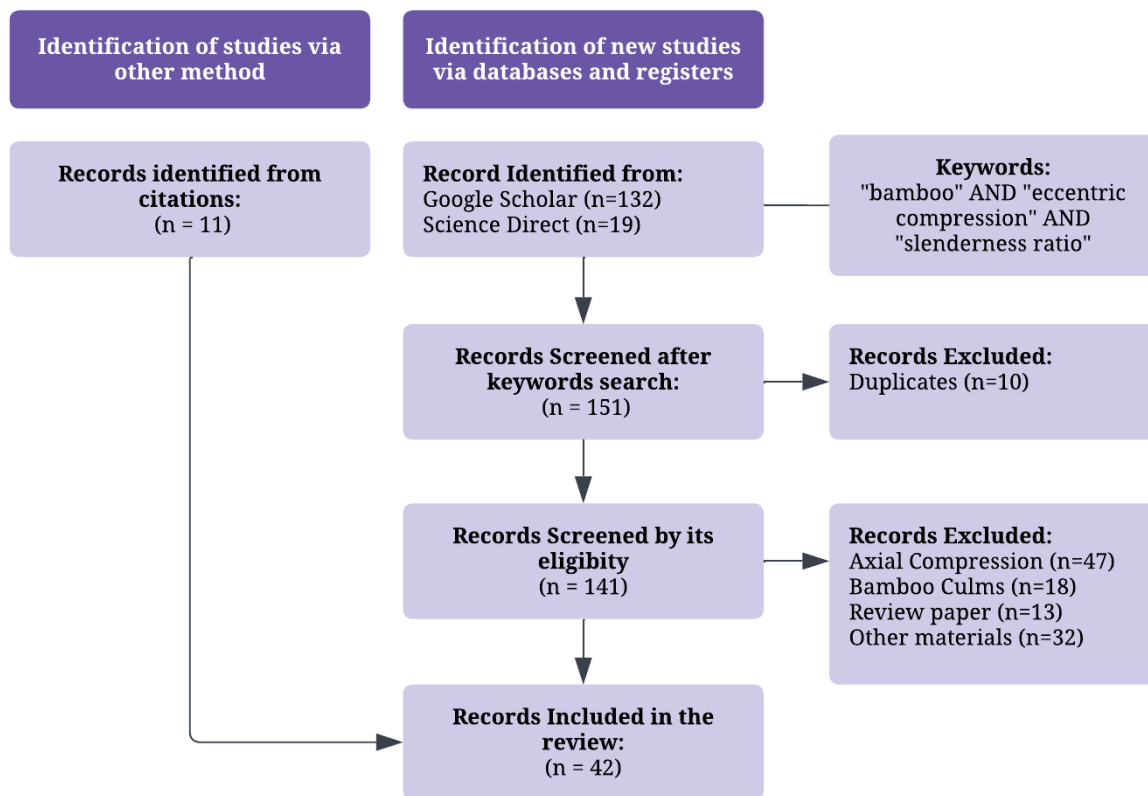
Figure 1. Review process flowchart

Following this, the identified records underwent a screening process to eliminate duplicates, extracting 10 papers. The subsequent stage involved scrutinizing the papers based on their title, abstract, content, and conclusion. The exclusion of papers followed predefined eligibility criteria: firstly, focusing on the performance of engineered bamboo in eccentric compression led to the exclusion of 47 papers concentrated solely on axial compression. Secondly, the emphasis on engineered bamboo as the primary material of interest resulted in removing 18 papers centered on bamboo culms. Thirdly, the researchers excluded all review papers and other materials, totaling 13 and 32 papers respectively. Lastly, a snowballing approach was employed, tracing relevant papers through citation trails and identifying 11 additional papers. Ultimately, a rigorous selection process yielded 42 papers that met the inclusion criteria for this comprehensive review. Upon the culmination of the review process and to achieve the main objective of this paper, the researcher is anticipated to address the following research question:

- What are the physical and mechanical properties of different engineered bamboo types used in structures?

- What are the properties of engineered bamboo columns under eccentric loads?

- What configurations define the theoretical framework and the practical test set-ups employed in assessing the eccentric compression performance of engineered bamboo columns?

- How does the eccentric compression performance of engineered bamboo columns vary, and what are the influencing factors on its outcomes?

3. Engineered Bamboo

Engineered bamboo refers to bamboo-based materials that have undergone processing and manufacturing techniques to enhance their mechanical and structural properties for various applications, especially in construction and engineering. Engineering bamboo aims to make it a more reliable and versatile material with improved strength, durability, and other desirable characteristics [39]. Engineered bamboo's uniform and stable mechanical properties make it an attractive alternative to traditional construction materials such as steel, concrete, and timber [40]. Additionally, researchers have observed that engineered bamboo products exhibit outstanding physical and mechanical properties with a minimal carbon footprint, affirming their environmental sustainability.

3.1. Types of Engineered Bamboo Products

Engineered bamboo encompasses various types of composite materials developed to enhance natural bamboo's mechanical and physical properties for engineering applications. These types include (1) *Bamboo Scrimber* (B.S.); (2) *Parallel Strand Bamboo* (PSB); (3) *Laminated Bamboo Lumber* (LBL); and (4) *Glue-Laminated Bamboo* (Glubam).

Bamboo scrimber, also known as recombinant lumber, reconstructed lumber, or bamboo zephyr board, is made from small-diameter bamboo culms used to create a reconstructed structural material. The manufacturing process for bamboo scrimber initially involved truncation and splitting, softening, removal of the bamboo outer skin, defibering, drying, sizing, assembly, and hot-pressing. As technology has advanced, specific steps have been eliminated in the large-scale production of bamboo scrimber. In the current process, key stages include truncation and splitting, defibering, drying, dipping, assembly, cold-pressing, and heat curing or hot-pressing [41]. Parallel Strand Bamboo (PSB), on the other hand, is a composite material created through the high-pressure adhesive bonding of bamboo strands [42]. The initial step involves cutting bamboo culms into strips of approximately 2 meters in length, with dimensions of roughly 15 mm in width and 3 mm in thickness. These strips undergo a drying process at a temperature of around 80 °C until the moisture content decreases to below 11%. Following this step, the manufacturing process involves flattening the strips into thin strands through crushing, then saturating them with phenolic resin. Subsequently, the process aligns the strands in parallel by bonding them under elevated pressure. This technique, which orients bamboo strands parallel to the longitudinal axis and distributes them evenly in the transverse direction, effectively eliminates the raw fibers' density gradient. Consequently, the produced Parallel Strand Bamboo exhibits superior structural characteristics [43]. The difference in cross-section of these two engineered bamboos is shown in Figures 2-a, and 2-b.

|(a)|(b)|
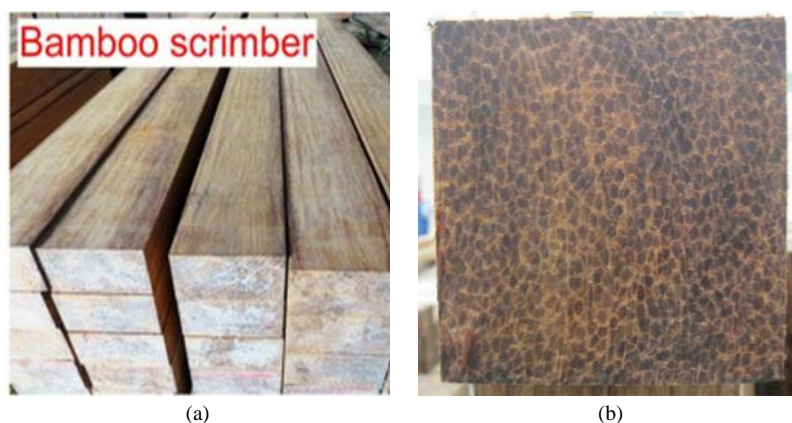
Figure 2. Cross-section view of (a) Bamboo Scrimber [44], and (b) Parallel Strand Bamboo Lumber [26]

The distinction between glue-laminated bamboo and laminated bamboo lumber lies in their manufacturing processes and structural properties. Glue-laminated bamboo, also known as engineered structural bamboo products (SBPs), is similar to engineered wood products such as plywood and glue-laminated timber [45]. It involves using adhesive to bond bamboo strips, allowing for large sections and spans, straight or curved, and continuous, providing excellent plastic properties for its application in structural elements [46]. On the other hand, manufacturers produce laminated bamboo lumber (LBL) using shorter and smaller strips of bamboo, butt-jointing them at sections to form longer and wider lumber or boards [47]. Figures 3-a, and 3-b show the cross-sectional views of glue-laminated and laminated bamboo lumber, respectively.

|(a)|(b)|
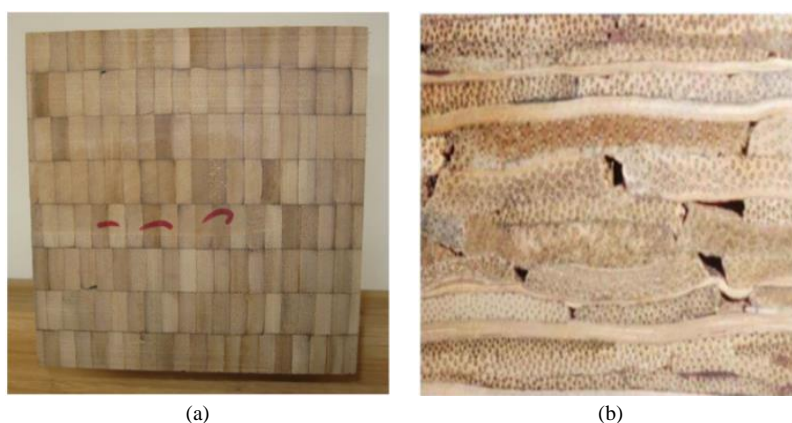
Figure 3. Cross-section view of (a) Glue-Laminated Bamboo and (b) Lumber Laminated Bamboo [44]

3.2. Physical Properties of Engineered Bamboo Products

Determining the physical properties of engineered bamboo is crucial for several reasons. The design of engineered bamboo products aims to reduce the variability of natural bamboo, making understanding their physical properties essential to ensure compliance with the required standards for structural applications [48]. Engineered bamboo strives

to offer a more uniform and stable material than natural bamboo, with the physical properties playing a significant role in achieving this objective [49]. The density and moisture content significantly influence the performance of engineered bamboo as a structural member. For example, bamboo scrimber, a type of engineered bamboo, can exhibit densities ranging from 980 to 1,160 kg/m³, nearly twice that of raw bamboo [50]. This increased density correlates with enhanced mechanical properties, including higher compressive strength and improved dimensional stability, making it more suitable for structural applications [20]. Moisture content's impact on the mechanical properties of bamboo is clear, as fluctuations in moisture content cause substantial dimensional changes that compromise the material's mechanical performance [51]. Additionally, the compressive strength parallel to the grain of bamboo elements decreases notably with increasing moisture content until it reaches the saturation point, highlighting the adverse effects of excessive moisture on mechanical properties [20]. Moreover, moisture content critically influences the dimensional stability of bamboo, which is essential for maintaining the structural integrity of engineered bamboo products [48].

Table 1 presents a comprehensive compilation of information concerning different types of engineered bamboo. The dataset encompasses a range of attributes, including bamboo species, geographical sources, moisture content, and density. This compilation serves as a fundamental reference, fostering a nuanced comprehension of the diverse physical properties inherent in engineered bamboo. Table 1 indicates the moisture content of various engineered bamboo types fluctuates between 5.13% and 11.9%. The control of this percentage is crucial, as it significantly impacts the mechanical properties of engineered bamboo [51]. Notably, researchers observe inconsistencies in the density values of each engineered bamboo. These variations can be attributed to several factors, including the bamboo species, the age at which harvesters collect it, and the location of the sample within bamboo culms. Consequently, further research is imperative to elucidate the factors influencing the properties of engineered bamboo.

Table 1. Comparison of Physical Properties of various Engineered Bamboo based on gathered literature

Engineered Bamboo	Bamboo Species	Source	Moisture Content (%)	Density (kg/m³)	Authors
BS	*Gigantochloa atroviolacea*	Indonesia	8.14	980	Sylvayanti et al (2023). [52]
BS	*Phyllostachys pubescens*)	China	7.00	1,215	Kumar et al. (2016). [53]
BS	*Phyllostachys pubescens*	China	7.00	1,160	Sharma et al. (2015). [54]
Glubam	*Guadua angustifolia*	Colombia	11.9	740.8	Correal et al. (2014). [55]
Glubam	*Phyllostachys pubescens*	China	7.00	880	Xiao et al. (2013). [56]
LBL	*Phyllostachys pubescens*	China	10.60	686	Chen et al. (2020). [57]
LBL	*Phyllostachys pubescens*	China	6.00	783	Kumar et al. (2016). [53]
PSB	*Dendrocalamus strictus*	India	11.00	1,030	Ahmad et al. (2011). [58]
PSB	*Phyllostachys pubescens*	China	7.22	11,515	Li et al. (2019). [59]
PSB	*Phyllostachys bambusodies*	Turkey	5.13	21,210	Çavuş et al. (2023). [60]

3.3. Mechanical Properties of Engineered Bamboo Products

The evaluation of mechanical characteristics in engineered bamboo is necessary for its effective utilization in structural engineering. Engineered bamboo variants, such as laminated composites and bamboo scrimber, have been conceptualized to present sustainable and high-performance alternatives to conventional construction materials. A comprehensive examination of the mechanical attributes of engineered bamboo proves essential in ensuring its structural soundness, load-bearing capacity, and sustained efficacy [45, 61] The mechanical traits of engineered bamboo, encompassing tensile strength, compressive strength, and modulus of elasticity, play a pivotal role in appraising its appropriateness for structural purposes. These characteristics dictate the material's ability to endure external forces like tension, compression, and bending, pivotal considerations in structural design and engineering [62, 63]. Additionally, the mechanical performance of engineered bamboo assumes critical significance in meeting the structural requisites of diverse applications, ranging from building structures and trusses to beams [49, 64].

Researchers have conducted several studies to characterize the mechanical properties of various engineered bamboo products adequately. The designation of each nomenclature is as follows: compression strength parallel to grain ($f_{c_\parallel}$), tension strength parallel to grain ($f_{t_\parallel}$), shear strength parallel to grain ($f_{v_\parallel}$), bending strength parallel to grain ($f_{b_\parallel}$), and static modulus of elasticity ($E_\parallel$). The absence of standardized testing protocols for the mechanical characteristics of engineered bamboo products in civil engineering has impeded their widespread adoption. Additionally, Sharma et al. [48] investigated the impact of processing methods on the mechanical attributes of engineered bamboo, underscoring the imperative for standardized testing approaches. Furthermore, the research conducted by Sharma & Vegte [20] underscored the potential of engineered bamboo for structural applications, emphasizing the need for standardized testing to address its mechanical properties. Hong et al. [49] also stressed the necessity of standardizing structural bamboo products and connections, signaling the importance of establishing testing methods to ensure the reliability and applicability of engineered bamboo in civil engineering. Previous researchers have employed established methods,

including those based on the American Society for Testing and Materials (ASTM), Czech Technical Standards (CSN), and British Standards (B.S.), to assess the mechanical properties of engineered bamboo, as delineated in Table 2.

Table 2. Comparison of Mechanical Properties of various Engineered Bamboo based on gathered literature

Engineered Bamboo	$f_{c_\parallel}$ (MPa)	$f_{t_\parallel}$ (MPa)	$f_{v_\parallel}$ (MPa)	$f_{b_\parallel}$ (MPa)	$E_\parallel$ (MPa)	Author
BS	64.85	34.27	11.15	-	8,525	Sylvayanti et al (2023). [52]
BS	115.70	144.75	17	166.5	14,020	Kumar et al. (2016). [53]
BS	86.00	120	15	-	13,000	Sharma et al. (2015). [54]
Glubam	62.00	143.1	9.5	122.4	32,271	Correal et al. (2014). [55]
Glubam	51.00	82	7.2	99	10,400	Xiao et al. (2013). [56]
LBL	56.30	107.7	17.5	111.5	11,143	Chen et al. (2020). [57]
LBL	77.00	90	16	-	12,000	Kumar et al. (2016). [53]
PSB	65.80	-	-	58.3	11,700	Ahmad et al. (2011). [58]
PSB	66.90	-	-	-	11,515	Li et al. (2019). [59]

Researchers have conducted several studies to characterize the mechanical properties of various engineered bamboo products adequately. The designation of each nomenclature is as follows: compression strength parallel to grain ($f_{c_\parallel}$), tension strength parallel to grain ($f_{t_\parallel}$), shear strength parallel to grain ($f_{v_\parallel}$), bending strength parallel to grain ($f_{b_\parallel}$), and static modulus of elasticity ($E_\parallel$). The absence of standardized testing protocols for the mechanical characteristics of engineered bamboo products in civil engineering has impeded their widespread adoption. Additionally, Sharma et al. [48] investigated the impact of processing methods on the mechanical attributes of engineered bamboo, underscoring the imperative for standardized testing approaches. Furthermore, the research conducted by Sharma & Vegte [20] underscored the potential of engineered bamboo for structural applications, emphasizing the need for standardized testing to address its mechanical properties. Hong et al. [49] also stressed the necessity of standardizing structural bamboo products and connections, signaling the importance of establishing testing methods to ensure the reliability and applicability of engineered bamboo in civil engineering. Previous researchers have employed established methods, including those based on the American Society for Testing and Materials (ASTM), Czech Technical Standards (CSN), and British Standards (B.S.), to assess the mechanical properties of engineered bamboo, as delineated in Table 3.

Table 3. Various Standard Test Methods in determining the Mechanical Properties of Engineered Bamboo

Author	Mechanical Properties	Standard Test Method
Sylvayanti et al. (2023) [52], Correal et al. (2014) [55], Xiao et al. (2013) [56], Chen et al. (2020) [57]	Compressive, Tensile, Shear, Flexural and Modulus of Elasticity	ASTM D143 - Standard Test Methods for Small Clear Specimens of Timber
Kumar et al. (2016) [53]	Compressive Strength	CSN 49 0110 - Timber – ultimate compression strength parallel to the grain.
	Tensile Strength	CSN 49 0114 - Determination method of tensile strength perpendicular to the grain
	Flexural Strength	CSN 49 0115 - Determination method of the ultimate strength in the static bending.
	Shear Strength	CSN 49 0118 - Timber – ultimate shear strength parallel to the grain
	Modulus of Elasticity	CSN 49 0111 - Determination method of modulus in compression parallel to the grain
Sharma et al. (2015) [54]	Compressive Strength	BS 373 - Methods of testing small clear specimens of timber
	Tensile Strength	ASTM D143 - Standard Test Methods for Small Clear Specimens of Timber
	Flexural Strength	BS EN 408 - Timber structures – Structural timber and glue-laminated timber
	Shear Strength	BS 373 - Methods of testing small clear specimens of timber

Previous testing methods for assessing the eccentric compression performance of engineered bamboo exhibit several limitations, necessitating the establishment of a standardized testing protocol. These limitations encompass the inherent variability in both geometric and mechanical properties of bamboo [48] the absence of comprehensive investigations focused solely on the compression of natural bamboo culms [50] and the imperative to scrutinize the impact of

parameters such as slenderness ratio, eccentric distances, and wall thicknesses on the ultimate bearing capacity of bamboo columns subjected to eccentric compression [36]. Moreover, there is a need for further exploration into the influence of eccentricity ratio on the behavior of bamboo columns under eccentric compression [35]. Furthermore, additional research is warranted to investigate the mechanical properties of bamboo under off-axis compression and the influence of length and compression directions on the behavior of bamboo specimens [65, 66]. Examining parameters such as the diameter–thickness ratio, cross-sectional area, and slenderness ratio on the axial compression behavior of original bamboo columns also merits attention [29]. Additionally, it is crucial to explore the mechanical properties of bamboo products and the effects of various processing methods on their mechanical characteristics [67].

Lastly, a comprehensive analysis of parameters such as slenderness ratio, eccentricity, and net cross-sectional area on the compression performance of bamboo composite columns is essential [68, 69]. This multifaceted exploration will provide valuable insights into the structural behavior and performance of bamboo-based materials under eccentric compression, contributing to developing more robust and reliable engineering practices in this domain.

4. Engineered Bamboo Columns Under Eccentric Load

Designers must consider several factors to ensure structural integrity and performance in designing columns. The column's response to various loading conditions, including wind, eccentricity, and buckling scenarios, requires a thorough design approach. Two primary scenarios arise from load application in columns: (1) concentric loading and (2) eccentric loading. Understanding the distinction between these loading conditions is vital for comprehending how columns respond to axial forces. A column under concentric loading experiences an axial load applied at its center or along the central axis, aligning with the column's geometric centerline. This alignment simplifies the analysis, as the load uniformly distributes across the cross-sectional area's centroid. Conversely, applying the axial load away from the centerline in an eccentrically loaded column generates a moment due to eccentricity—the horizontal distance between the load's line of action and the column's centroidal axis. Moreover, moisture content significantly influences the dimensional stability of bamboo, an essential factor in preserving the structural integrity of engineered bamboo products. The existing body of research primarily focuses on exploring the response of engineered bamboo columns to concentric loads [29, 30, 70]. Most columns experience uniaxial or even biaxial loading conditions. Consequently, there is a necessity for investigations into the performance of engineered bamboo under eccentric compression. Understanding the behavior of engineered bamboo under eccentric compression requires acquiring specific properties. Euler's critical buckling load theory, a cornerstone of structural engineering, provides a theoretical basis for determining the critical load that leads to instability and buckling in slender columns. Known as Euler's buckling theory, it assumes that the column is perfectly straight, homogeneous, and lacks initial imperfections. The critical buckling load, P_{cr}, is given in Equation 1.

$$P_{cr} = \frac{\pi^2 EI}{L^2} \qquad\qquad\qquad (1)$$

where P_{cr} is Euler critical buckling load, E is the modulus of elasticity, and L is the column length. This theory is widely used in structural design to assess the stability of columns and other slender structural members. It provides a fundamental understanding of the behavior of columns under compressive loads and is essential for predicting the load at which buckling, a form of structural failure, may occur [71]. Table 4 shows the properties of engineered bamboo columns from several studies identified by this paper to be subjected to evaluation of eccentric compression performance.

Table 4. Engineered Bamboo Properties under Eccentric Loadings

Engineered Bamboo	Cross-section dimension (mm)	Height (mm)	Eccentricity (mm)	Modulus of Elasticity (MPa)	Author
LBL	80×80	850-1,700	37	9,694	Li et al. (2019) [26]
PSB	96×96	570-1,900	20	11,515	Li et al. (2019) [59]
LBL	100×100	600-3,000	30	-	Zhou et al. (2021) [72]
LBL	100×100	1,100	0-120	-	Hong et al. (2021) [73]
LBL	100×100	1,200	0-120	8,200	Li et al. (2020) [32]
PSB	100×100	1,100-1,850	0-100	11,000	Huang et al. (2015) [43]
PSB	100×100	925-1,650	-	11,151	Wang et al. (2017) [74]
LBL	73×73	1,000	0-120	9,643	Li et al. (2016) [75]
LBL	100×100	1,200	0-120	9,694.3	Li et al. (2016) [76]
Glubam	Hollow column	1,350-1,950	40-120	11,613	Su et al. (2022) [36]
LBL	100×100	1,100	30-120	6,324	Jian et al. (2019) [77]
PSB	100×100	1,200	0-120	11,028	Li et al. (2015) [35]

Table 4 presents a comprehensive overview of studies primarily conducted in China, focusing on engineered bamboo properties under eccentric loadings. The predominant bamboo species investigated across these studies is Moso bamboo. Specifically, Laminated Bamboo Lumber (LBL) emerges as a recurrent subject in eccentric loading assessments. The

modulus of elasticity, a critical mechanical property, exhibits a considerable range in the gathered literature, from 6,324 MPa to 11,613 MPa. This variability underscores the diverse mechanical behaviors observed across different studies, emphasizing the need for a nuanced understanding of the material's response under eccentric loading conditions. Exploring the independent variables employed in these studies reveals a range of methodologies aimed at comprehensively assessing engineered bamboo's eccentric compression performance. Variations in column height and eccentricity distance are prominent among the selected studies, as indicated in Table 4. Some investigations focus on altering column heights to determine the ultimate load at which the columns fail, while others manipulate eccentricity distances varying from 0 to 120 mm. These chosen parameters play a pivotal role in evaluating engineered bamboo's eccentric compression behavior, providing valuable insights into its structural performance. The subsequent section of this paper will elaborate on the theoretical and actual test setup employed in these studies, offering a more detailed exploration of the experimental methodologies applied to ascertain the material's response under eccentric loading conditions.

## 5. Actual Test Setup to Evaluate the Eccentric Compression Performance

In exploring engineered bamboo's eccentric compression performance, numerous considerations extend beyond the determination of physical and mechanical properties, as expounded upon in the preceding section. A crucial aspect involves delineating how the load is applied, necessitating a meticulous identification process. Engineered bamboo varieties, exemplified by Laminated Bamboo Lumber (LBL), exhibit three primary directions: (1) longitudinal, aligning parallel to the grain's length in bamboo strips; (2) tangential, running parallel to the longer side of bamboo strips; and (3) radial, oriented parallel to the shorter side of bamboo strips. This geometric arrangement is visually illustrated in Figure 4-a.
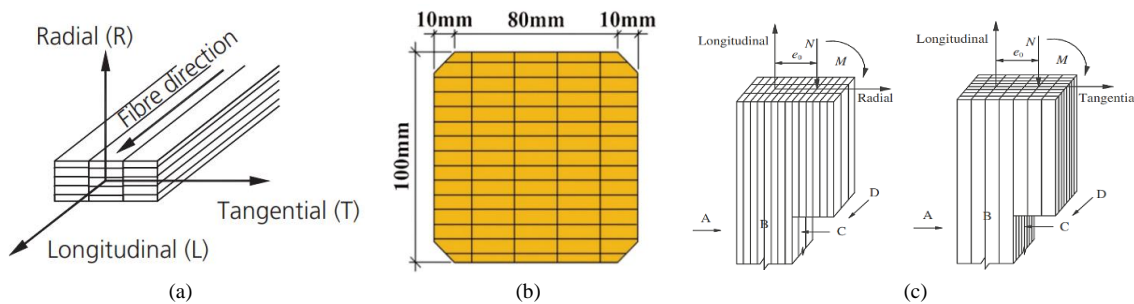
Figure 4. Visual representation of (a) three main directions of engineered bamboo [26]; (b) typical cross-section of engineered bamboo [72]; and (c) load application along radial and tangential direction [76]

For instance, Zhou et al. [72] delved into the behavior of LBL columns subjected to eccentric compression loads. Bamboo strips, measuring 7 mm × 21 mm, were intricately bonded together using resin adhesive, forming a composite of 100 mm × 100 mm, as illustrated in Figure 4-b. The researcher directed the load application along the radial axis. Analogous methodologies were subsequently adopted in studies by [75, 76]. Notably, diverse studies explored load applications in the tangential direction [72–73, 76], with Figure 4-c providing a visual representation of this specific loading orientation. Furthermore, scenarios arise where the eccentric load is simultaneously applied along both radial and tangential directions, as depicted in Figure 5, detailing the parameters of eccentricity and the skew angle as studied by Wang et al. [74]. The skew angle (β), defined as the inverse tangent of the eccentricity distance along the y-direction (e_y) over the eccentricity distance along the x-direction (e_x), is mathematically shown in Equation 2. This intricate exploration underscores the multifaceted nature of load application in assessing the eccentric compression performance of engineered bamboo, serving as a pivotal element in the comprehensive understanding of the material's structural response.

$$\beta = \tan^{-1} \frac{e_y}{e_x} \tag{2}$$
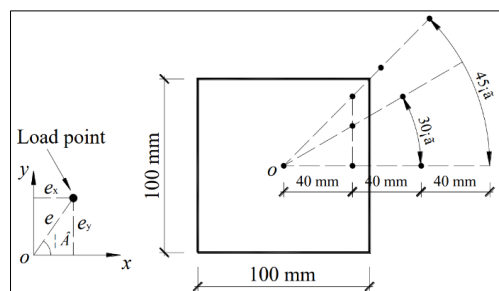
Figure 5. Load application points at the end of each engineered bamboo specimen [74]

The subsequent procedural phase involves the meticulous arrangement of the engineered bamboo under investigation, with a pivotal focus on ensuring the precise application of eccentric loads. This critical step is

operationalized by affixing bamboo brackets strategically at both the upper and lower sections of the engineered bamboo, employing screw connections as shown in Figure 6-a. This methodology mirrors the approach implemented in the study conducted by Hong et al. [73], showcasing the viability and effectiveness of this setup. A comprehensive elucidation of the bamboo bracket's cross-sectional dimensions and bolt diameter is visually presented in Figure 6-b, alongside a depiction of varying eccentricity distances depicted in Figure 6-c, providing a thorough understanding of the experimental apparatus. In augmentation of this methodology, Su et al. [36] introduced an additional reinforcement layer in their study. Beyond the affixed bamboo bracket, the setup incorporates a gusset steel plate with a thickness of 10 mm. This strategic inclusion serves two purposes: it fortifies the integrity of the engineered bamboo and ensures the precision of load application, thereby minimizing the risk of inadvertent misplacement.

(a)　　　　　　　　　　(b)　　　　　　　　　　(c)
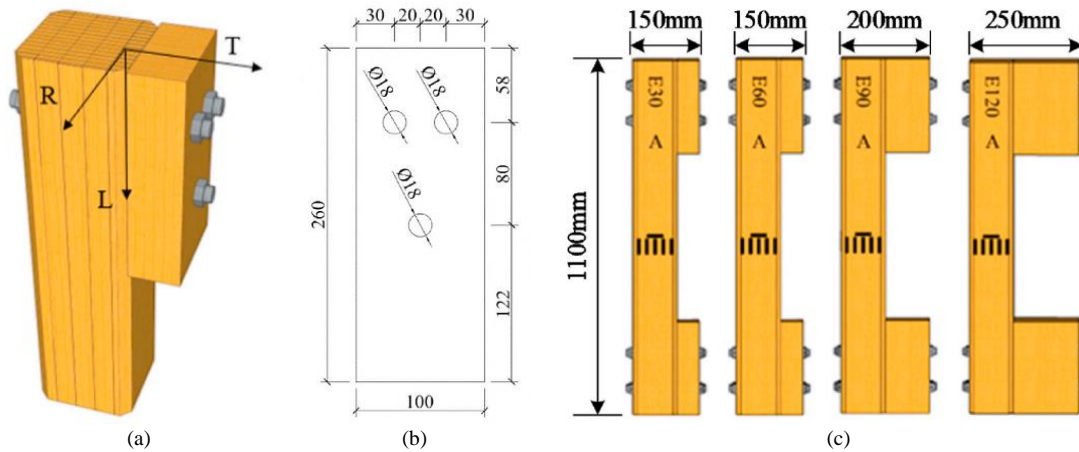
Figure 6. Visual representation of (a) engineered bamboo specimen with bamboo bracket screw at its end; (b) cross-sectional dimension of bamboo bracket; and (c) bamboo bracket varying distances to the specimen [73]

This augmenting gusset plate's meticulous details and dimensions are meticulously delineated in Figure 6-b, contributing to a nuanced comprehension of the sophisticated experimental configuration. These meticulously devised setups not only adhere to established protocols within the field but also underscore the paramount importance of precision and robustness in investigating eccentric compression performance in engineered bamboo.

Most studies follow the testing setup, arrangement of strain gauges, and test configurations as those demonstrated in the works of [70-77]. To prepare the engineered bamboo specimen surfaces, researchers used a rough-textured cloth to polish the surface, which they later cleaned with alcohol [75]. They applied a strain gauge to each face of the engineered bamboo, as Figure 7-b shows; a 3-laser displacement sensor was utilized to measure displacement. They then placed the bamboo on the testing machine, affixing the upper and lower ends to unidirectional hinge supports. This setup ensures the specimen can rotate freely in the eccentric direction and avoid accidental deformation outside the eccentric plane. Figures 7-a, and 7-c display the schematic diagram and the actual test setup, respectively. The comparison of actual test methods across several studies appears in Table 5. Notably, most of these studies adhere to the test standard for timber structures (GB/ T 50329–2012), adjusting the eccentricity distance of axial loads for the test setup.

(a)　　　　　　　　　　(b)　　　　　　　　　　(c)

Figure 7. Eccentric compressive set-up for engineered bamboo columns: (a) schematic diagram of the test setup [76]; (b) arrangement of strain gauge at the surface of specimen [76]; and (c) actual test set-up [76]

Table 5. Summary of the Test Set-up in Evaluating the Eccentric Compression Performance of Specimen

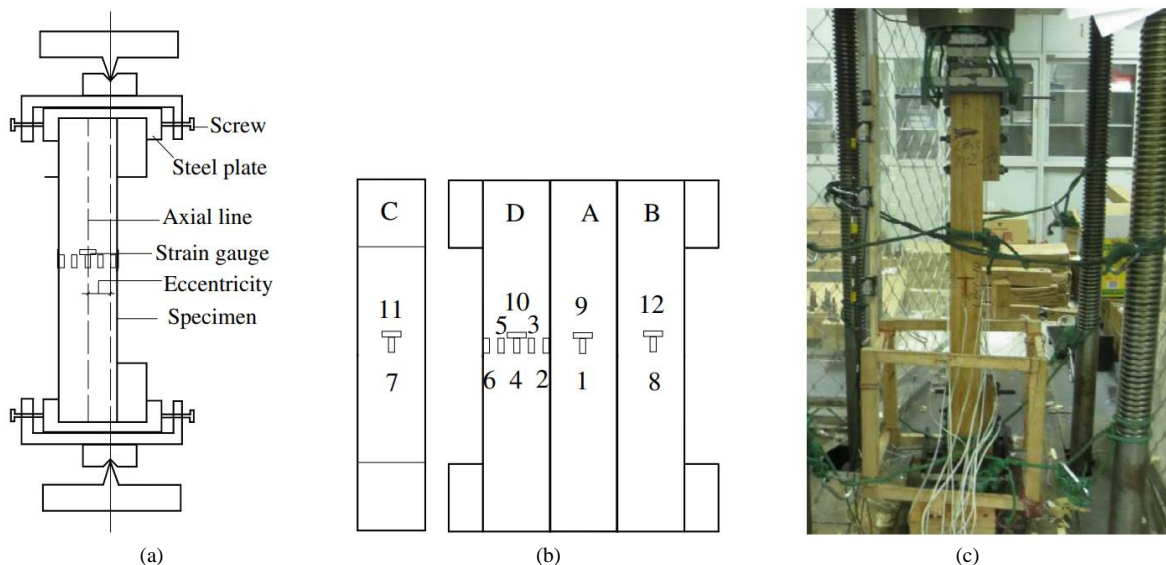| Engineered Bamboo	No. of Test Specimen	Displacement measuring tools	Machine	Load duration	Application of eccentric load	Authors
LBL	20	Strain gauge and Laser Displacement Sensor (LDS)		8-12 min	Along radial direction	Li et al. (2019) [26]
PSB	27	Strain gauge and LDS		8-12 min	Along radial direction	Li et al. (2019) [59]
LBL	15	Strain gauge and LDS	1000 kN microcomputer-controlled electro-hydraulic servo universal with TDS data acquisition system	6-10 min	Along tangential direction	Hong et al. (2021) [73]
PSB	24	Strain gauge and deformation sensors		2 mm/min	Biaxial load	Wang et al. (2017) [74]
LBL	35	Strain gauge and deformation sensors		8-12 min	Along radial direction	Li et al. (2016) [75]
LBL	80	Strain Gauge and LVDT		8-12 min	Both radial and tangential	Li et al. (2016) [76]

6. Eccentric Compression Performance of Engineered Bamboo

The eccentric compression performance of engineered bamboo pertains to the material's behavior under compressive loads applied away from its central axis. Several factors influence this performance, including the bamboo species, moisture content, culm age, and wall thickness. Different species exhibit variations in mechanical properties, while elevated moisture levels can reduce compressive strength. The age of the bamboo culm and the thickness of its walls also play a significant role, with younger bamboo potentially displaying different mechanical properties. Treatments, such as drying, chemical, or heat treatment, are commonly applied to enhance durability and mechanical properties. Critical considerations include joint and connection details, grain orientation, defects, and overall bamboo quality. The orientation of bamboo fibers concerning the applied load, the presence of defects, and adherence to engineering design standards also impact performance. The aforementioned factors arise from bamboo culms' inherent qualities and the manufacturing process's intricacies. However, this section of the paper focuses on exploring independent variables that impact the eccentric compression performance of engineered bamboo, drawing insights from existing literature and studies. The influential parameters, in this case, are the independent variables as follows: (1) eccentricity distance and (2) slenderness ratio. All these influential parameters will affect the dependent variables: (1) Failure modes; and (2) ultimate load-bearing capacity of engineered bamboo. This systematic investigation aims to shed light on the subtle interplay of these variables in influencing the eccentric compression behavior of engineered bamboo, thereby contributing valuable insights to the broader field of bamboo engineering.

6.1. Eccentricity Distance

The effects of eccentricity distance on the eccentric compression performance of engineered bamboo have been explored in various studies, highlighting how this factor influences the structural integrity, load-bearing capacity, and deformation characteristics of engineered bamboo columns. Table 6 provides findings from five relevant studies focusing on the type of engineered bamboo, eccentricity distance, and critical findings.

Table 6. Key Findings on the Effect of Eccentricity Distance on Engineered Bamboo based on literature

Authors	Eccentricity Distance (mm)	Engineered Bamboo	Key findings
Li et al. (2020) [32]	10-120	LBL	Increasing the eccentricity distance reduces the ultimate load-bearing capacity and an alteration in failure modes, from elastic to elastic-plastic, and finally to plastic failure as eccentricity increases.
Su et al. (2022) [36]	40-120	Glubam	The study examines the effects of slenderness ratios, eccentric distances, and wall thicknesses on GLBHC's ultimate bearing capacity, highlighting the significant impact of eccentricity distance on structural performance.
Hong et al. (2021) [73]	30-120	PBSL	Eccentricity distance impacts ultimate bearing capacity and strain distribution, decreasing as eccentricity increases. The strain distribution across the cross-section becomes more non-uniform with higher eccentricity.

The collection of studies consistently observes that the eccentricity distance affects the structural performance of various types of engineered bamboo, including Laminated Bamboo Lumber (LBL), Parallel Bamboo Strand Lumber (PBSL), Chamfered Laminated Bamboo Lumber (LBL) Columns, and Glued Laminated Bamboo Hollow Columns (GLBHC). Notably, an increase in eccentricity distance consistently reduces the ultimate load-bearing capacity and alters the failure modes of these materials. Furthermore, these effects become more pronounced with deformation characteristics and strain distribution changes across the columns' cross-section. Looking back, one can attribute the observed phenomena to the inherent mechanical properties of bamboo as a construction material and the geometric considerations of column design. The increase in eccentricity distance introduces higher bending moments and shear forces, which, in turn, exacerbate material stresses and lead to an earlier onset of failure mechanisms. This insight

highlights the critical nature of eccentricity in the structural design and analysis of engineered bamboo, suggesting that minimizing eccentricity could enhance the structural integrity and performance of bamboo-based construction elements.

The underlying mechanism for the observed reduction in load-bearing capacity and alteration in failure modes with increased eccentricity can be explained through material mechanics and structural engineering principles [78-80]. As eccentricity increases, the bending moment experienced by the column increases, leading to higher stress concentrations on one side of the column [81]. This uneven stress distribution causes the material to transition from elastic behavior to elastic-plastic and eventually to plastic failure more rapidly than it would under a concentric load application [82, 83]. Additionally, the alteration in deformation characteristics and non-uniform strain distribution across the cross-section with increased eccentricity further exemplifies the sensitivity of engineered bamboo's structural performance to load application eccentricity. This sensitivity indicates the critical need to account for eccentric loading conditions in the design, analysis, and application of engineered bamboo in structural applications, ensuring safety, reliability, and optimal performance of bamboo-based construction projects.

6.2. Slenderness Ratio

Recent years have seen extensive studies on the effect of the slenderness ratio on the eccentric compression performance of engineered bamboo, with Table 7 presenting critical insights into this effect. Researchers define the slenderness ratio as the height to least lateral dimension ratio of a column, and it plays a pivotal role in determining the buckling behavior and load-bearing capacity under eccentric loading conditions.

Table 7. Key Findings on the Effect of Slenderness Ratio on Engineered Bamboo based on literature

Authors	Slenderness Ratio Range	Engineered Bamboo	Key findings
Zhou et al. (2021) [72]	21.14, 38.75, 59.89, 81.01, and 105.66	LBL	Good ductility observed in most specimens, highlighting the impact of the slenderness ratio on deformation characteristics and ultimate bearing capacity.
Hong et al. (2021) [73]	38.75	LBL	Eccentricity and slenderness ratio significantly influence ultimate bearing capacity and strain distribution.
Huang et al. (2018) [84]	45 and 57	LBL	Developed an inelastic analysis model for intermediately slender EBWC columns, highlighting how slenderness ratio affects nonlinear responses.
Chen et al. (2020) [85]	5.20, 6.93, 10.39, 11.55, 20.78, 27.71, 41.57 and 83.14	B.S.	The slenderness ratio significantly affects failure modes and load-bearing capacity, with larger ratios leading to instability failure.

Studies by Zhou et al. (2021) [72] and Hong et al. (2021) [73] have shown that with an increase in slenderness ratio, engineered bamboo columns exhibit a decrease in ultimate load-bearing capacity and a transition in failure modes from primarily compression failure in shorter columns to buckling failure in taller columns. This phenomenon is attributed to the increased propensity for lateral deflection and instability as the column's height increases relative to its cross-sectional dimensions [72, 73]. Similarly, Li et al. (2015) [35] observed that the eccentricity ratio, closely related to the slenderness ratio, significantly impacts the bearing capacity, where an increase in eccentricity leads to a reduction in the ultimate load values. This underscores the influence of slenderness on the structural efficiency of bamboo columns under eccentric loads. Furthermore, Su et al. (2022) [36] have demonstrated that the slenderness ratio affects the failure modes and the deformation characteristics of engineered bamboo columns. Columns with higher slenderness ratios showed larger lateral displacements and reduced stiffness, which significantly impacts their practical load-bearing capacity and necessitates careful consideration in design and analysis for structural applications.

In addition, the work by Huang et al. (2018) [84] on inelastic analysis models for engineered bamboo/wood composites under biaxial bending and compression has highlighted the asymmetric stress-strain relationship due to varying slenderness ratios. This asymmetry can complicate the prediction of load-bearing capacities and necessitates advanced analytical and numerical models to capture the behavior of slender columns under eccentric loading.

The observed trends can be elucidated through slender column behavior's fundamental mechanics. As the slenderness ratio of a column increases, it experiences higher susceptibility to buckling, resulting in reduced load-carrying capacity and increased deflection under compressive loads. This phenomenon is exacerbated by eccentric loading conditions, which introduce additional bending moments, further compromising the structural stability of the column. Consequently, the findings underscore the importance of considering the slenderness ratio in designing and assessing engineered bamboo structures, emphasizing the need for appropriate geometric configurations to ensure adequate structural performance and resilience against compression-induced failures.

6.3. Failure Modes

In this section of the review, three distinct studies, namely [26, 59, 72], have been identified, delving into the intricate correlation between mechanical properties and slenderness ratio. These investigations aim to elucidate the calculation

of the laminated bamboo lumber's (LBL) ultimate load capacity, a pivotal determinant before structural failure occurs. The unanimous consensus among these studies underscores the recognition of two primary failure modes when subjecting engineered bamboo to axial loads. The initial mode, termed "failure mode I," manifests as the specimen initially splits around the midpoint of the columns, gradually progressing towards the inner layers as the load intensifies. Conversely, "failure mode II" is characterized by cracks exclusively appearing on the tension side of a singular main layer. These failure modes' visualizations are depicted in Figure 8 for mode I and Figure 9 for mode II. Table 8 summarizes the categorization of failure modes I and II, corresponding to different specimen heights given the variable eccentricity distance.

(a)   (b)   (c)
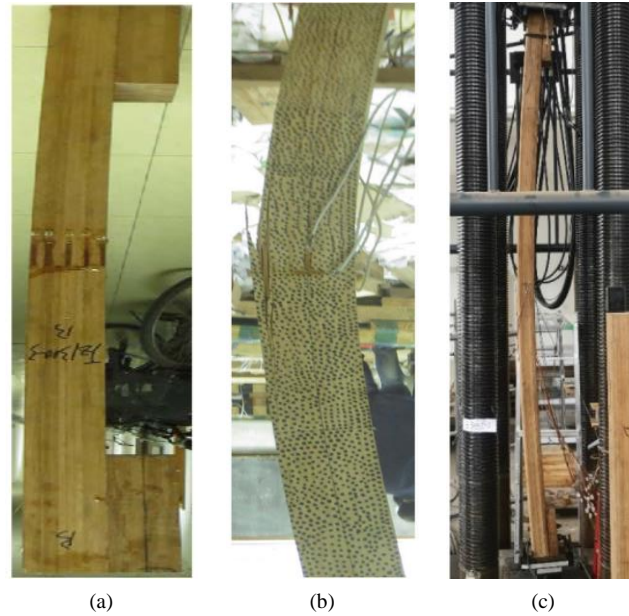
Figure 8. Failure mode I: (a) Li et al (2019) [26]; (b) Li et al. (2019) [59]; and (c) Zhou et al. (2021) [72]

(a)   (b)   (c)
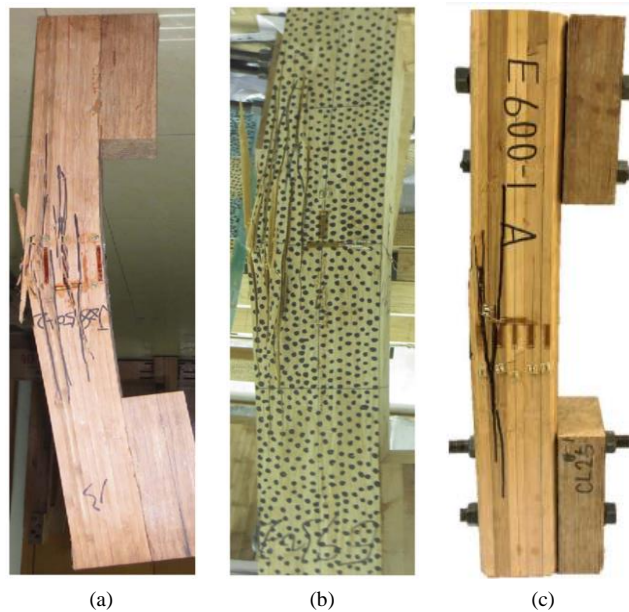
Figure 9. Failure mode II: (a) Li et al (2019) [26]; (b) Li et al. (2019) [59]; and (c) Zhou et al. (2021) [72]

Table 8. Mode of failure and the height specimen designation

Authors	Engineered Bamboo product	Eccentricity (mm)	Specimen height (mm) and its mode of failure	
			Mode I	Mode II
Li et al. (2019) [26]	LBL	37	850, 1,100, and 1,500	1,700
Li et al. (2019) [59]	PSB	20	570, 760, 950, and 1,140	1,330, 1,520, 1,710, and 1,900
Zhou et al. (2021) [72]	LBL	30	600, and 1,100	1,700, 2,300 and 3,000

The collective findings from previous studies, as shown in Table 9, into the eccentric compression performance of engineered bamboo, specifically laminated bamboo lumber (LBL) and parallel bamboo strand lumber (PBSL), illuminate the nuanced and complex failure mechanisms inherent to these materials under load. Li et al. (2020) [32] meticulously analyzed LBL columns, unveiling three distinct failure modes: Mode I, characterized by the initiation of failure from glue or brackets with bamboo fibers remaining elastic; Mode II, where failure is precipitated by the outermost compression fiber reaching the elastic-plastic stage; and Mode III, distinguished by the outermost compression fiber achieving plastic capacity prior to failure. This study underscores the intricate interplay between material composition and failure, advocating for advanced analytical formulations to accurately predict column resistance under eccentric loads.

Table 9. Failure modes as described in other previous studies

Authors	Engineered Bamboo	Failure Modes Description
Li et al. (2020) [32]	LBL	Mode I: Failure initiates from glue or bracket while bamboo fibers remain elastic. Mode II: Outermost compression fiber reaches the elastic-plastic stage.
Li et al. (2016) [63]	LBL	Bamboo nodes and drill holes were the primary causes of failure, with mechanical properties and failure modes significantly differing based on the direction of eccentric compression.
Hong et al. (2021) [73]	LBL	Failure modes remained consistent across different eccentricities, belonging to brittle tension failure.
Li et al. (2016) [76]	LBL	Failure modes are influenced by natural defects such as bamboo joints and mechanical connectors Interaction between compression and bending in determining failure modes.

In a similar study, Li et al. (2016) [63] explored LBL column specimens subjected to radial eccentric compression, discovering failure modes significantly influenced by inherent natural defects such as bamboo joints and mechanical connectors. This research emphasizes the critical role of compression-bending interaction in determining failure, highlighting the material's variability in response to eccentric loads. Another study by Li et al. (2015) [35] on PBSL columns found that the eccentricity ratio markedly impacts bearing capacity, with an increase in eccentricity ratio correlating to a decrease in ultimate load values. This investigation offers vital insights into PBSL columns' design and application, revealing detailed failure modes across specimens.

Further contributing to the body of knowledge, Hong et al. (2021) [73] investigated the behavior of LBL columns with chamfered sections under eccentric compression. Their findings reveal that failure modes remain consistent across varying eccentricities, predominantly manifesting as brittle tension failures. This consistency across eccentricities provides a foundation for developing predictive models for LBL columns under varied load conditions. Lastly, an additional study by Li et al. (2016) [75] evaluated the mechanical performance of LBL columns under two directions of eccentric compression, identifying bamboo nodes and drill holes as primary causes of failure. This study suggests that mechanical properties and failure modes can significantly differ based on the direction of eccentric compression, introducing an essential consideration for designing and applying engineered bamboo columns.

These studies collectively enrich the understanding of engineered bamboo's mechanical behavior under eccentric compression, revealing intricate failure modes that challenge conventional design paradigms. The nuanced failure mechanisms, influenced by material composition, inherent defects, and load directionality, underscore the need for comprehensive analytical models that can accurately predict behavior and optimize the use of engineered bamboo in structural applications.

6.4. Ultimate Load Bearing Capacity

The ultimate load-bearing capacity under eccentric compression in engineered bamboo is a critical measure that directly influences the design and application of bamboo in structural engineering. Many factors affect the ultimate load-bearing capacity of engineered bamboo, which is subjected to eccentric compression as explained in the subsequent section. The convergence towards a standard theory prompts the formulation of equations by various researchers to calculate the ultimate load capacity of engineered bamboo. These equations, encapsulating the influence of mechanical properties and slenderness ratio, are succinctly presented in Table 10. Furthermore, Table 11 offers a comparative analysis, contrasting the outcomes of applying these formulas from different authors against actual test results. Key nomenclatures for equations and tables include ultimate load-bearing capacity. (N_{ult}), slenderness ratio (λ), eccentricity distance (e_o), the height of the column (h), ultimate load-bearing capacity obtained from actual test results (N_{ul}^t), and ultimate load-bearing capacity obtained from proposed calculations (N_{ul}^c).

Table 10. Comparison of Proposed ultimate load calculation based on gathered literature

Authors	Formulated ultimate load-bearing capacity	R-squared value (R^2)	Equation
Li et al. (2019) [26]	$N_{ul} = 0.029\lambda^2 - 4.72\lambda + 244.37$	0.97	(3)
Li et al. (2019) [59]	$N_{ul} = 0.0786\lambda^2 - 10.828\lambda + 493.29$	-	(4)
Zhou et al. (2021) [72]	$N_{ul} = 1.25\lambda^{\left(-0.2016\frac{e_o}{h} - 0.3263\right)}\left(\frac{e_o}{h}\right)^{(0.00776\lambda - 0.4069)} f_{cu}A$	0.90	(5)

Table 11. Comparison of actual test results and calculated results

Authors	Height + Eccentricity	λ	N_{ul}^t (kN)	N_{ul}^c (kN)	Error (%)
	850+37	36.8	111.1	110.7	0.4
	1100+37	47.6	82.8	84.3	1.8
Li et al. (2019) [26]	1300+37	56.3	70.7	70.8	0.1
	1500+37	65.0	63.0	61.0	-3.2
	1700+37	73.6	52.7	53.6	1.7
	570+20	20.6	293.3	310.5	5.9
	760+20	27.4	275	248.9	-9.5
	950+20	34.3	212.4	207.7	-2.2
Li et al. (2019) [59]	1140+20	41.1	185.7	178.2	-4.0
	1330+20	48	144.2	156.0	8.2
	1520+20	54.8	134.3	138.7	3.3
	1710+20	61.7	129.5	124.9	-3.6
	1900+20	68.6	99	113.6	14.7
	600+30	21.1	199.5	217.7	9.1
	1100+30	38.6	128.9	136.8	6.2
Zhou et al. (2021) [72]	1700+30	59.9	83.5	90.5	8.4
	2300+30	81.0	61.2	64.0	4.5
	3000+30	105.7	43.8	44.6	1.8

7. Gaps and Challenges

Challenges and research gaps represent fundamental concepts in the academic and scientific community. Challenges describe the obstacles or difficulties faced in a particular field of study, while research gaps indicate the areas within a specific topic or discipline lacking sufficient knowledge or understanding [86]. The eccentric compression performance of engineered bamboo, being relatively new in bamboo research, encapsulates all the necessary research gaps and challenges, as summarized in Table 12. Researchers have extensively explored the eccentric compression performance of engineered bamboo, demonstrating considerable effort. However, critical analysis uncovers a series of challenges, gaps, and limitations throughout these studies. The main research gaps and challenges in this topic include.

Table 12. Research gaps and challenges based on the gathered literature

Gaps and Challenges	Description	Authors
1. Standards and design codes	a. Lack of international standards for fully characterizing bamboo culms. b. Need for standardization of design codes for engineered bamboo.	a. Li et al. (2019) [26], Hong et al. (2021) [73]; b. Hong et al. (2021) [73].
2. Material characterization and other influencing factors	a. Limited number of studies on eccentric compression performance of engineered bamboo. b. Short length of bamboo specimens with scattered strain values. c. Lack of comprehensive studies on the mechanical performance of engineered bamboo under different loading conditions. d. A lack of comparative analysis of the result to traditional building materials such as wood, concrete, and steel. e. Study other influencing factors to be incorporated in the proposed calculations.	a. Li et al. (2019) [26]; b. Li et al. (2019) [59]; c. Li et al. (2016) [76]; d. Hong et al. (2021) [73], Wang et al. (2017) [74], Li et al. (2016) [76], Jian et al. (2023) [77]; e. Li et al. (2019) [26], Li et al. (2019) [59], Zhou et al. (2021) [72], Hong et al. (2021) [73], Li et al. (2016) [75].

3. Ultimate state behavior and failure analysis	a. Need for understanding the ultimate state of engineered bamboo. b. Limited investigation into failure mechanism.	a. Chen et al. (2021) [44], Wang et al. (2017) [74]; b. Chen et al. (2021) [44].
4. Models	a. Needs for better analytical and theoretical models.	Su et al. (2022) [36], Wang et al. (2017) [74], Jian et al. (2023) [77].
5. Bonding and Manufacturing	a. Further investigation needed on the bonding between bamboo strips. b. Inadequate consideration of the manufacturing process.	a. Li et al. (2016) [76]; b. Hong et al. (2021) [73].
6. Cost and Durability Analysis	a. Needs to study the cost analysis of engineered bamboo in building applications. b. Lack of consideration for long-term performance and durability.	a. Jian et al. (2023) [77]; b. Li et al. (2020) [32], Zhou et al. (2021) [72], Hong et al. (2021) [73], Wang et al. (2017) [74], Li et al. (2016) [75], Li et al. (2016) [76], Jian et al. (2023) [77], Li et al. (2015) [35].
7. Structural Exploration	a. Limited exploration of composite structure. b. Variability in lamination techniques and adhesive types.	a. Hong et al. (2021) [73]; b. Li et al. (2019) [26], Li et al. (2020) [32], Li et al. (2019) [59], Zhou et al. (2021) [72].
8. Slenderness Ratio	a. Insufficient exploration of slenderness ratio range. b. Neglect of interaction between slenderness ratio and other factors.	a. Li et al. (2019) [26], Li et al. (2019) [59], Zhou et al. (2021) [72]; b. Li et al. (2019) [26], Li et al. (2019) [59], Zhou et al. (2021) [72].

- ***Inadequate Comparative Analyses and Lack of Standardization:*** The studies by Li et al. (2019) [59], Zhou et al. (2021) [72], and the experimental and numerical study on laminated bamboo columns emphasize the insufficient comparison with other building materials and the absence of standardized practices or design codes for bamboo structures. Addressing these issues would contribute to a more comprehensive understanding of the unique properties of engineered bamboo and facilitate its widespread adoption in construction.

- ***Limited Scope of Research and Need for Long-Term Studies:*** The experimental and numerical study on laminated bamboo columns Li et al. (2020) [32], and Li et al. (2016) [76] underscored the limited scope of research, advocating for investigations beyond mechanical properties. These studies also emphasized the importance of long-term studies to assess the environmental impact, fire resistance, and durability of engineered bamboo, providing a more holistic understanding of its performance over time.

- ***Insufficient Consideration of Manufacturing Processes and Economic Feasibility:*** Li et al. (2019) [59], Zhou et al. (2021) [72], and Li and Su (2020) [32] identified gaps related to the lack of in-depth analysis of manufacturing processes and insufficient discussions on the economic feasibility and scalability of using bamboo in construction. A thorough exploration of manufacturing technology, cost-effectiveness, and energy consumption is essential for sustainable bamboo applications in construction.

- ***Failure to Address Environmental Impact and Sustainability:*** Li et al. (2019) [59], and Li et al (2016) [75] highlighted the need for a more extensive discussion on the environmental impact, sustainability aspects, and life cycle assessment of engineered bamboo. Evaluating bamboo's ecological footprint and considering its long-term behavior in real-world applications are crucial for ensuring its sustainability and promoting environmentally friendly construction practices.

- ***Challenges in Model Development and Standardization:*** Huang et al. (2015) [43], Wang et al. (2017) [74], and Su et al. (2022) [36] underscored challenges related to model development, including considerations of material nonlinearities, equilibrium equations, and ultimate loading-carry capacity. Additionally, Su et al. (2022) [36] emphasizes the need for addressing the changeable bamboo properties and discussing challenges encountered during the research process. These studies collectively call for improved models and standardized approaches in bamboo structural analysis.

- ***Neglect of Comparative Analysis and Environmental Impact Assessment:*** Li et al. (2016) [76] and Jian et al. (2023) [77] identified common gaps related to the neglect of comprehensive comparative analyses with other materials and the absence of thorough environmental impact assessments. These studies stress the importance of evaluating different reinforcement materials, conducting long-term performance analyses, and considering the environmental implications of reinforcement methods.

8. Conclusions

This review aims to identify gaps and challenges in current research on bamboo, offering a comprehensive overview of the eccentric compression behavior of engineered bamboo columns. Effectively addressing the research question, this paper aligns with the introduction by emphasizing the importance of tackling identified gaps and challenges to fully understand and utilize bamboo in construction.

Several gaps and challenges in the current research on the application of engineered bamboo as a column were highlighted, including the lack of standards and design codes, issues in material characterization, insufficient understanding of ultimate state behavior and failure analysis, outdated models, a need for further investigation into bonding and manufacturing, lack of cost and durability analysis studies, limited exploration in structural aspects, and insufficient understanding of slenderness ratio. To address these gaps and challenges, future researchers could consider exploring the following solutions:

- *Establish International Standards:* Collaborate with international organizations and researchers to develop standardized testing protocols for fully characterizing bamboo culms, providing a common foundation for evaluating eccentric compression performance.

- *Develop Comprehensive Design Codes:* Invest in research to establish design codes specifically tailored for engineered bamboo, considering material characteristics and loading conditions to provide clear guidelines for designing bamboo columns.

- *Expand Experimental Studies:* Conduct extensive experiments to investigate engineered bamboo eccentric compression performance under various loading conditions, including studies with longer specimens for a more accurate representation of real-world scenarios.

- *Incorporate Influencing Factors:* Explore and incorporate additional influencing factors into calculations and design considerations, studying the effects of environmental conditions, treatment methods, and other variables on the eccentric compression behavior of engineered bamboo columns.

- *Comprehensive Slenderness Ratio Studies:* Conduct a systematic and comprehensive exploration of the slenderness ratio range for engineered bamboo columns, testing specimens with varying ratios to understand how different proportions impact eccentric compression performance.

- *Integration of Interaction Effects:* Investigate the interaction between slenderness ratio and other relevant factors influencing the performance of engineered bamboo columns, including material properties, loading conditions, and environmental influences. Understanding these interactions will aid in developing more accurate predictive models and design guidelines.

9. Declarations

9.1. Author Contributions

Conceptualization, F.F.M.; review methodology, F.F.M. and O.G.D.; validation, O.G.D.; writing—original draft preparation, F.F.M.; writing—review and editing, F.F.M. and O.G.D.; supervision, O.G.D. All authors have read and agreed to the published version of the manuscript.

9.2. Data Availability Statement

Data sharing is not applicable to this article.

9.3. Funding

9.4. Acknowledgements

9.5. Conflicts of Interest

The authors declare no conflict of interest.

10. References

[1] Manggapis, F. F., Kumar. S. D. A., Lucena J. P. R. G., Carabbacan, A. P. I., & Dela Cruz, O. G. D. (2023). Advancements in Concrete Incorporation: Harnessing the Potential of Crumb Rubber Tires as Sustainable Alternatives to Fine Aggregates. Environmental Science and Engineering, 195-205. doi:10.1007/978-3-031-42588-2_16.

[2] Carabbacan, A. P. I., & Amatosa, T. A. (2023). Effects of Polypropylene Fibers from Single-Use Facemasks on the Microstructure of Normal Cementitious Composites. Environmental Science and Engineering, 183–193. doi:10.1007/978-3-031-42588-2_15.

[3] Zhang, X., Yin, H., Zhao, E., Li, S., & Liu, Q. (2023). Experimental investigation on embedment strength of bamboo-based composite prepared with the inorganic adhesive. Journal of Building Engineering, 76, 107323. doi:10.1016/j.jobe.2023.107323.

[4] Kumar, R., Ganguly, A., & Purohit, R. (2023). Properties and applications of bamboo and bamboo fibre composites. Materials Today: Proceedings. doi:10.1016/j.matpr.2023.08.162.

[5] Sánchez Vivas, L., Costello, K., Mobley, S., Mihelcic, J. R., & Mullins, G. (2022). Determination of safety factors for structural bamboo design applications. Architectural Engineering and Design Management, 18(1), 26–37. doi:10.1080/17452007.2020.1781589.

[6] Wang, X., & Song, B. (2022). Application of bionic design inspired by bamboo structures in collapse resistance of thin-walled cylindrical shell steel tower. Thin-Walled Structures, 171, 108666. doi:10.1016/j.tws.2021.108666.

[7] Mimendi, L., Lorenzo, R., & Li, H. (2022). An innovative digital workflow to design, build and manage bamboo structures. Sustainable Structures, 2(1), 11. doi:10.54113/j.sust.2022.000011.

[8] Chung, K. F., & Yu, W. K. (2002). Mechanical properties of structural bamboo for bamboo scaffoldings. Engineering Structures, 24(4), 429–442. doi:10.1016/S0141-0296(01)00110-9.

[9] Wei, X., Zhou, H., Chen, F., & Wang, G. (2019). Bending flexibility of Moso Bamboo (Phyllostachys Edulis) with functionally graded structure. Materials, 12(12), 7. doi:10.3390/ma12122007.

[10] Moran, R., & García, J. J. (2019). Bamboo joints with steel clamps capable of transmitting moment. Construction and Building Materials, 216, 249–260. doi:10.1016/j.conbuildmat.2019.05.025.

[11] Adier, M. F. V., Sevilla, M. E. P., Valerio, D. N. R., & Ongpeng, J. M. C. (2023). Bamboo as Sustainable Building Materials: A Systematic Review of Properties, Treatment Methods, and Standards. Buildings, 13(10), 2449. doi:10.3390/buildings13102449.

[12] Cayanan, F., Gabriel, J. R. D., Pantalunan, C. H., Dela Cruz, O. G. D., & Roque, I. R. (2024). A Review on Processing Techniques and Building Methods of Engineered Bamboo. Lecture Notes in Civil Engineering, 374, 137–149. doi:10.1007/978-981-99-4229-9_13.

[13] Amada, S., & Untao, S. (2001). Fracture properties of bamboo. Composites Part B: Engineering, 32(5), 451–459. doi:10.1016/S1359-8368(01)00022-1.

[14] Zhou, A., Huang, D., Li, H., & Su, Y. (2012). Hybrid approach to determine the mechanical parameters of fibers and matrixes of bamboo. Construction and Building Materials, 35, 191–196. doi:10.1016/j.conbuildmat.2012.03.011.

[15] Lorenzo, R., Mimendi, L., Godina, M., & Li, H. (2020). Digital analysis of the geometric variability of Guadua, Moso and Oldhamii bamboo. Construction and Building Materials, 236, 117535. doi:10.1016/j.conbuildmat.2019.117535.

[16] Rini, D. S., Ishiguri, F., Nezu, I., Ngadianto, A., Irawati, D., Otani, N., Ohshima, J., & Yokota, S. (2023). Geographic and longitudinal variations of anatomical characteristics and mechanical properties in three bamboo species naturally grown in Lombok Island, Indonesia. Scientific Reports, 13(1), 2265. doi:10.1038/s41598-023-29288-3.

[17] Deng, J., Chen, F., Wang, G., & Zhang, W. (2016). Variation of Parallel-to-Grain Compression and Shearing Properties in Moso Bamboo Culm (Phyllostachys pubescens). BioResources, 11(1), 1784–1795. doi:10.15376/BIORES.11.1.1784-1795.

[18] Correal, D. J. F., & Juliana Arbeláez, C. (2010). Influence of age and height position on colombian Guadua angustifolia bamboo mechanical properties. Maderas: Ciencia y Tecnologia, 12(2), 105–113. doi:10.4067/S0718-221X2010000200005.

[19] Dessalegn, Y., Singh, B., & van Vuure, A. W. (2021). Analyze the Significance of Age and Height on the Physical and Chemical Properties of Ethiopian Giant Timber Bamboo. American Journal of Engineering and Applied Sciences, 14(2), 185–197. doi:10.3844/ajeassp.2021.185.197.

[20] Sharma, B., & Van Der Vegte, A. (2019). Engineered bamboo for structural applications. Nonconventional and Vernacular Construction Materials: Characterisation, Properties and Applications, 597–623. doi:10.1016/B978-0-08-102704-2.00021-4.

[21] Wang, Y. Y., Li, Y. Q., Xue, S. S., Zhu, W. Bin, Wang, X. Q., Huang, P., & Fu, S. Y. (2022). Superstrong, Lightweight, and Exceptional Environmentally Stable SiO2@GO/Bamboo Composites. ACS Applied Materials and Interfaces, 14(5), 7311–7320. doi:10.1021/acsami.1c22503.

[22] Qaiser, S., Hameed, A., Alyousef, R., Aslam, F., & Alabduljabbar, H. (2020). Flexural strength improvement in bamboo reinforced concrete beams subjected to pure bending. Journal of Building Engineering, 31, 101289. doi:10.1016/j.jobe.2020.101289.

[23] Lucena, J. R. P. G., & Dela Cruz, O. G. D. (2023). A Literature Review on the Use of Bamboo as a Truss Member and Fiber-Reinforced Polymer as a Truss Jointing Material. International Journal of Integrated Engineering, 15(2), 172–185. doi:10.30880/ijie.2023.15.02.017.

[24] Mofidi, A., Abila, J., & Ng, J. T. M. (2020). Novel advanced composite bamboo structural members with bio-based and synthetic matrices for sustainable construction. Sustainability (Switzerland), 12(6), 2485. doi:10.3390/su12062485.

[25] Tri Puspitasari, E. (2023). Experimental Study of Flexural Capacity Strength In-Plane Load On Wall Panels Using Autoclaved Aerated Concrete Block and Bamboo Reinforcement. International Journal of GEOMATE, 24(103), 17-25. doi:10.21660/2023.103.3325.

[26] Li, H. T., Liu, R., Lorenzo, R., Wu, G., & Wang, L. Bin. (2019). Eccentric compression properties of laminated bamboo columns with different slenderness ratios. Proceedings of the Institution of Civil Engineers: Structures and Buildings, 172(5), 315–326. doi:10.1680/jstbu.18.00007.

[27] Cook, D. J., Pama, R. P., & Singh, R. V. (1978). The behaviour of bamboo-reinforced concrete columns subjected to eccentric loads. Magazine of Concrete Research, 30(104), 145–151. doi:10.1680/macr.1978.30.104.145.

[28] Richardson, C., & Mofidi, A. (2021). Non-Linear Numerical Modelling of Sustainable Advanced Composite Columns Made from Bamboo Culms. Construction Materials, 1(3), 169–187. doi:10.3390/constrmater1030011.

[29] Nie, Y., Wei, Y., Huang, L., Liu, Y., & Dong, F. (2021). Influence of slenderness ratio and sectional geometry on the axial compression behavior of original bamboo columns. Journal of Wood Science, 67(1), 36. doi:10.1186/s10086-021-01968-6.

[30] Tan, C., Li, H., Wei, D., Lorenzo, R., & Yuan, C. (2020). Mechanical performance of parallel bamboo strand lumber columns under axial compression: Experimental and numerical investigation. Construction and Building Materials, 231, 117168. doi:10.1016/j.conbuildmat.2019.117168.

[31] Tan, C., Li, H., Ashraf, M., Corbi, I., Corbi, O., & Lorenzo, R. (2021). Evaluation of axial capacity of engineered bamboo columns. Journal of Building Engineering, 34, 102039. doi:10.1016/j.jobe.2020.102039.

[32] Li, H., Su, J., Xiong, Z., Ashraf, M., Corbi, I., & Corbi, O. (2020). Evaluation on the ultimate bearing capacity for laminated bamboo lumber columns under eccentric compression. Structures, 28, 1572–1579. doi:10.1016/j.istruc.2020.10.004.

[33] Liu, S., Gao, D., Xie, Y., & Chen, B. (2022). Experimental Study and Theoretical Analysis of Side-Pressure Laminated Bamboo Lumber Columns under Axial Compression. Sustainability (Switzerland), 14(18), 11360. doi:10.3390/su141811360.

[34] Su, Y., Zou, J., & Lu, W. (2022). A macroscopic shear angle model for ultimate bearing capacity of glued laminated bamboo hollow columns under axial compression. Structures, 45, 560–571. doi:10.1016/j.istruc.2022.09.017.

[35] Li, H., Su, J., Deeks, A. J., Zhang, Q., Wei, D., & Yuan, C. (2015). Eccentric Compression Performance of Parallel Bamboo Strand Lumber Columns. BioResources, 10(4), 7065-7080. doi:10.15376/biores.10.4.7065-7080.

[36] Su, Y., Zou, J., & Lu, W. (2022). Evaluating the Ultimate Bearing Capacity of Glued Laminated Bamboo Hollow Columns under Eccentric Compression. BioResources, 17(3), 5372–5392. doi:10.15376/biores.17.3.5372-5392.

[37] Page, M. J., McKenzie, J. E., Bossuyt, P. M., Boutron, I., Hoffmann, T. C., Mulrow, C. D., Shamseer, L., Tetzlaff, J. M., Akl, E. A., Brennan, S. E., Chou, R., Glanville, J., Grimshaw, J. M., Hróbjartsson, A., Lalu, M. M., Li, T., Loder, E. W., Mayo-Wilson, E., McDonald, S., … Moher, D. (2021). The PRISMA 2020 statement: An updated guideline for reporting systematic reviews. The BMJ, 372, 71. doi:10.1136/bmj.n71.

[38] Moher, D., Liberati, A., Tetzlaff, J., & Altman, D. G. (2009). Preferred Reporting Items for Systematic Reviews and Meta-Analyses: The PRISMA Statement. PLoS Medicine, 6(7), e1000097. doi:10.1371/journal.pmed.1000097.

[39] Tang, S., Zhou, A., & Li, J. (2021). Mechanical Properties and Strength Grading of Engineered Bamboo Composites in China. Advances in Civil Engineering, 2021, 1–13. doi:10.1155/2021/6666059.

[40] Harelimana, V., Zhu, J., Yuan, J., & Uwitonze, C. (2022). Investigating the bamboo as alternative partial replacement of steel bars in concrete reinforcement members. Structural Design of Tall and Special Buildings, 31(6), e1921. doi:10.1002/tal.1921.

[41] Huang, Y., Ji, Y., & Yu, W. (2019). Development of bamboo scrimber: a literature review. Journal of Wood Science, 65(1), 25. doi:10.1186/s10086-019-1806-4.

[42] Huang, D., Bian, Y., Zhou, A., & Sheng, B. (2015). Experimental study on stress-strain relationships and failure mechanisms of parallel strand bamboo made from phyllostachys. Construction and Building Materials, 77, 130–138. doi:10.1016/j.conbuildmat.2014.12.012.

[43] Huang, D., Bian, Y., Huang, D., Zhou, A., & Sheng, B. (2015). An ultimate-state-based-model for inelastic analysis of intermediate slenderness PSB columns under eccentrically compressive load. Construction and Building Materials, 94, 306–314. doi:10.1016/j.conbuildmat.2015.06.059.

[44] Chen, J., Guagliano, M., Shi, M., Jiang, X., & Zhou, H. (2021). A comprehensive overview of bamboo scrimber and its new development in China. European Journal of Wood and Wood Products, 79(2), 363–379. doi:10.1007/s00107-020-01622-w.

[45] Dixon, P. G., & Gibson, L. J. (2014). The structure and mechanics of Moso bamboo material. Journal of the Royal Society Interface, 11(99), 20140321. doi:10.1098/rsif.2014.0321.

[46] Zhan, Y., Huang, W., Si, R., Xiang, T., & Hao, L. (2023). Shear Behavior of Notched Connection for Glubam-Geopolymer Concrete Composite Structures: Experimental Investigation. BioResources, 18(1), 701–719. doi:10.15376/biores.18.1.701-719.

[47] Zhang, H., Gharavi, N., Wong, S. H. F., Deng, Y., Bahadori-Jahromi, A., Limkatanyu, S., Qiao, Y., & Kuang, J. S. (2022). Effect of concentrated Butt-Joints on flexural properties of laminated Bamboo-Timber flitch beams. Journal of Sandwich Structures and Materials, 24(2), 1226–1244. doi:10.1177/10996362211040103.

[48] Sharma, B., Gatoo, A., Bock, M., Mulligan, H., & Ramage, M. (2015). Engineered bamboo: State of the art. Proceedings of Institution of Civil Engineers: Construction Materials, 168(2), 57–67. doi:10.1680/coma.14.00020.

[49] Hong, C., Li, H., Xiong, Z., Lorenzo, R., Corbi, I., Corbi, O., Wei, D., Yuan, C., Yang, D., & Zhang, H. (2020). Review of connections for engineered bamboo structures. Journal of Building Engineering, 30, 101324. doi:10.1016/j.jobe.2020.101324.

[50] Kadivar, M., Gauss, C., Ghavami, K., & Savastano, H. (2020). Densification of bamboo: State of the art. Materials, 13(19), 1–25. doi:10.3390/ma13194346.

[51] Sánchez Cruz, M. L., & Morales, L. Y. (2019). Influence of moisture content on the mechanical properties of Guadua Culms. Inge Cuc, 15(1), 99–108. doi:10.17981/ingecuc.15.1.2019.09.

[52] Sylvayanti, S. P., Nugroho, N., & Bahtiar, E. T. (2023). Bamboo Scrimber's Physical and Mechanical Properties in Comparison to Four Structural Timber Species. Forests, 14(1), 146. doi:10.3390/f14010146.

[53] Kumar, A., Vlach, T., Laiblova, L., Hrouda, M., Kasal, B., Tywoniak, J., & Hajek, P. (2016). Engineered bamboo scrimber: Influence of density on the mechanical and water absorption properties. Construction and Building Materials, 127, 815–827. doi:10.1016/j.conbuildmat.2016.10.069.

[54] Sharma, B., Gatóo, A., Bock, M., & Ramage, M. (2015). Engineered bamboo for structural applications. Construction and Building Materials, 81, 66–73. doi:10.1016/j.conbuildmat.2015.01.077.

[55] Correal, J. F., Echeverry, J. S., Ramírez, F., & Yamín, L. E. (2014). Experimental evaluation of physical and mechanical properties of Glued Laminated Guadua angustifolia Kunth. Construction and Building Materials, 73, 105–112. doi:10.1016/j.conbuildmat.2014.09.056.

[56] Xiao, Y., Yang, R. Z., & Shan, B. (2013). Production, environmental impact and mechanical properties of Glubam. Construction and Building Materials, 44, 765–773. doi:10.1016/j.conbuildmat.2013.03.087.

[57] Chen, G., Yu, Y., Li, X., & He, B. (2020). Mechanical behavior of laminated bamboo lumber for structural application: an experimental investigation. European Journal of Wood and Wood Products, 78(1), 53–63. doi:10.1007/s00107-019-01486-9.

[58] Ahmad, M., & Kamke, F. A. (2011). Properties of parallel strand lumber from Calcutta bamboo (Dendrocalamus strictus). Wood Science and Technology, 45(1), 63–72. doi:10.1007/s00226-010-0308-8.

[59] Li, H., Qiu, Z., Wu, G., Corbi, O., Wei, D., Wang, L., Corbi, I., & Yuan, C. (2019). Slenderness Ratio Effect on Eccentric Compression Properties of Parallel Bamboo Strand Lumber Columns. Journal of Structural Engineering, 145(8). doi:10.1061/(asce)st.1943-541x.0002372.

[60] Çavuş, V., & Ersin, İ. (2023). Determination of Some Physical and Mechanical Properties of Parallel-strand Lumber Manufactured with Bamboo (Phyllostachys bambusoides). BioResources, 18(4), 6802–6814. doi:10.15376/biores.18.4.6802-6814.

[61] Wang, Y. Y., Wang, X. Q., Li, Y. Q., Huang, P., Yang, B., Hu, N., & Fu, S. Y. (2021). High-Performance Bamboo Steel Derived from Natural Bamboo. ACS Applied Materials and Interfaces, 13(1), 1431–1440. doi:10.1021/acsami.0c18239.

[62] Han, S., Chen, F., Ye, H., Zheng, Z., Chen, L., & Wang, G. (2023). Bamboo-Inspired Renewable, High-Strength, Vibration-Damping Composites for Structural Applications. ACS Sustainable Chemistry and Engineering, 11(3), 1146–1156. doi:10.1021/acssuschemeng.2c06490.

[63] Sewar, Y. Y., Zhang, Z., Meng, X., Wahan, M. Y., Qi, H., Al-Shami, Q. M., & Luo, S. (2022). Mechanical properties and constitutive relationship of the high-durable parallel strand bamboo. Journal of Renewable Materials, 10(1), 219–235. doi:10.32604/jrm.2021.016013.

[64] Sharma, B., Gatóo, A., & Ramage, M. H. (2015). Effect of processing methods on the mechanical properties of engineered bamboo. Construction and Building Materials, 83, 95–101. doi:10.1016/j.conbuildmat.2015.02.048.

[65] Yang, D., Li, H., Xiong, Z., Mimendi, L., Lorenzo, R., Corbi, I., Corbi, O., & Hong, C. (2020). Mechanical properties of laminated bamboo under off-axis compression. Composites Part A: Applied Science and Manufacturing, 138, 106042. doi:10.1016/j.compositesa.2020.106042.

[66] Li, H., Qiu, Z., Wu, G., Wei, D., Lorenzo, R., Yuan, C., Zhang, H., & Liu, R. (2019). Compression behaviors of parallel bamboo strand lumber under static loading. Journal of Renewable Materials, 7(7), 583–600. doi:10.32604/jrm.2019.07592.

[67] Shangguan, W., Gong, Y., Zhao, R., & Ren, H. (2016). Effects of heat treatment on the properties of bamboo scrimber. Journal of Wood Science, 62(5), 383–391. doi:10.1007/s10086-016-1574-3.

[68] Zhao, W., Zhou, J., Long, Z., & Peng, W. (2018). Compression performance of thin-walled square steel tube/bamboo plywood composite hollow columns with binding bars. Advances in Structural Engineering, 21(3), 347–364. doi:10.1177/1369433217718982.

[69] Zhao, W., Zhou, J., & Long, Z. (2016). Compression tests on square, thin-walled steel tube/bamboo-plywood composite hollow columns. Science and Engineering of Composite Materials, 23(5), 511–522. doi:10.1515/secm-2014-0117.

[70] Lei, M., Wang, Z., Li, P., Zeng, L., Liu, H., Zhang, Z., & Su, H. (2020). Experimental Investigation on Short Concrete Columns Reinforced by Bamboo Scrimber under Axial Compression Loads. Advances in Civil Engineering, 2020, 1–12. doi:10.1155/2020/8886384.

[71] Jiang, Y., Zhou, H., Beer, M., Wang, L., Zhang, J., & Zhao, L. (2017). Robustness of Load and Resistance Design Factors for RC Columns with Wind-Dominated Combination Considering Random Eccentricity. Journal of Structural Engineering, 143(4), 04016221. doi:10.1061/(asce)st.1943-541x.0001720.

[72] Zhou, K., Li, H., Dauletbek, A., Yang, D., Xiong, Z., Lorenzo, R., Zhou, K., Corbi, I., & Corbi, O. (2022). Slenderness ratio effect on the eccentric compression performance of chamfered laminated bamboo lumber columns. Journal of Renewable Materials, 10(1), 165–182. doi:10.32604/jrm.2021.017223.

[73] Hong, C., Li, H., Xiong, Z., Lorenzo, R., Corbi, I., & Corbi, O. (2021). Experimental and numerical study on eccentric compression properties of laminated bamboo columns with a chamfered section. Journal of Building Engineering, 43, 102901. doi:10.1016/j.jobe.2021.102901.

[74] Wang, X., Zhou, A., & Chui, Y. H. (2018). Load-carrying capacity of intermediately slender parallel strand bamboo columns with a rectangular cross section under biaxial eccentric compression. BioResources, 13(1), 313–330. doi:10.15376/biores.13.1.313-330.

[75] Li, H. T., Chen, G., Zhang, Q., Ashraf, M., Xu, B., & Li, Y. (2016). Mechanical properties of laminated bamboo lumber column under radial eccentric compression. Construction and Building Materials, 121, 644–652. doi:10.1016/j.conbuildmat.2016.06.031.

[76] Li, H. tao, Wu, G., Zhang, Q. sheng, & Su, J. W. (2016). Mechanical evaluation for laminated bamboo lumber along two eccentric compression directions. Journal of Wood Science, 62(6), 503–517. doi:10.1007/s10086-016-1584-1.

[77] Jian, B., Li, H., Zhou, K., Ashraf, M., Xiong, Z., & Zheng, X. (2023). Mechanical evaluation on BFRP laminated bamboo lumber columns under eccentric compression. Advances in Structural Engineering, 26(5), 809–823. doi:10.1177/13694332221138312.

[78] Beer, F., Johnston, E., & DeWolf, J. (2019). Mechanics of materials (8th Ed.). Tata McGraw Hill, New York, United States.

[79] Hibbeler, R. (2017). Structural Analysis (10th Ed.). Pearson Education Limited, Harlow, United Kingdom.

[80] Gere, J. M., & Goodno, B. J. (2015). Mechanics of materials. Langara College, Vancouver, Canada.

[81] Hibbeler, R. (2022). Mechanics of Materials (11th Ed.). Pearson Education Limited, Harlow, United Kingdom.

[82] Callister, W. D., Rethwisch, D. G., Blicblau, A., Bruggeman, K., Cortie, M., Long, J., ... & Mitchell, R. (2007). Materials science and engineering: an introduction. John Wiley & Sons, Hoboken, United States.

[83] Dowling, N. E. (2013). Mechanical Behavior of Materials eBook: International Edition. Pearson Higher Education, London, United Kingdom.

[84] Huang, Z., Chen, Z., Huang, D., Chui, Y. H., & Bian, Y. (2018). An inelastic model for analyzing intermediately slender engineered bamboo/wood columns subjected to biaxial bending and compression. BioResources, 13(2), 2814–2833. doi:10.15376/biores.13.2.2814-2833.

[85] Chen, S., Wei, Y., Hu, Y., Zhai, Z., & Wang, L. (2020). Behavior and strength of rectangular bamboo scrimber columns with shape and slenderness effects. Materials Today Communications, 25, 101392. doi:10.1016/j.mtcomm.2020.101392.

[86] Guenther, L., & Joubert, M. (2017). Science communication as a field of research: Identifying trends, challenges and gaps by analysing research papers. Journal of Science Communication, 16(2), 2. doi:10.22323/2.16020202.